U.S. Department of Energy • Office of Fossil Energy
National Energy Technology Laboratory

2007
Office of Fossil Energy
Fuel Cell Program Annual Report

SECA

Solid State Energy Conversion Alliance

DOE/NETL-2007/1288

2007
OFFICE OF FOSSIL ENERGY
FUEL CELL PROGRAM ANNUAL REPORT

August 2007

Table of Contents

IV. SECA RESEARCH & DEVELOPMENT

I. INTRODUCTION

I. INTRODUCTION

Competitive Innovation: Accelerating Technology Development

The U.S. Department of Energy (DOE) Office of Fossil Energy, through the National Energy Technology Laboratory (NETL) and in collaboration with the Pacific Northwest National Laboratory, is forging government/industry partnerships under the Solid State Energy Conversion Alliance (SECA) to reduce the cost of fuel cells and to develop fuel cell coal-based systems for clean and efficient central power generation. These goals equate to removing environmental and climate change concerns associated with fossil fuel use while simultaneously establishing a foundation for a hydrogen-based economy and a secure energy future in the United States. With the successful completion of the first phase of the Cost Reduction program, SECA is one step closer to realizing its vision of cost-effective, near-zero-emission fuel cell technology for commercial applications.

The Administration's Office of Management and Budget previously cited the SECA program as leading the way in government-industry partnerships.

"The SECA program leverages private-sector ingenuity by providing Government funding to Industry Teams developing fuel cells, as long as the Teams continue to exceed a series of stringent technical performance hurdles. This novel incentive structure has generated a high level of competition between the Teams and an impressive array of technical approaches. The SECA program also develops certain core technologies that can be used by all the Industry Teams to avoid duplication of effort. The program exceeded its 2005 performance targets, and it is on track to meet its goal for an economically competitive technology by 2010."

The SECA fuel cell program is a critical element of the DOE's Office of Fossil Energy technology portfolio. From an energy security perspective, coal is a primary resource for reducing dependence on imported oil and natural gas. More than half of the nation's electricity supply is generated from coal, and developing technology to ensure that the use of coal is environmentally clean and climate friendly is of crucial national importance. SECA technology offers greater than 90 percent carbon capture with less than 0.5 ppm NOx emission and with a coal to electricity efficiency exceeding 50 percent on a higher heating value (HHV) basis. The SECA cost goal of $400/kW will ensure that the cost of electricity to the user will not exceed what is typical today. Concurrently, SECA coal-based systems will scale and integrate SECA solid oxide fuel cell (SOFC) technology for delivery to FutureGen or an equivalent demonstration site. SECA has three program elements that are currently in progress: (a) cost reduction, (b) coal systems, and (c) manufacturing. Cross-cutting research and development and testing support is provided by SECA's Core Technology program.

SECA Targets: Fuel Cell Performance and Cost

	Cost Reduction Targets		
	2008	**2010**	
Power Rating	3 to 10 kW	3 to 10 kW	
Cost	—	$400/kW	
Efficiency (LHV)	40 to 60%	40 to 60%	
	Coal-Based Fuel Cell System Targets		
	2008	**2010**	**2015**
Power Rating*	500 kW	2 MW	50 MW
Cost	—	$400/kW	$400/kW
Efficiency (HHV)**	45%	50%	50%

* Estimated cumulative capacity for three Industry Teams
** Coal plant efficiency

SECA is comprised of three groups: Industry Teams, Core Technology program participants, and federal government management. The Industry Teams design the fuel cells and handle most hardware and market penetration issues. The Core Technology program is made up of universities, national laboratories, small businesses, and other research and development (R&D) organizations and addresses applied technological issues common to all Industry Teams. Findings and inventions under the Core Technology program are made available to all Industry Teams under unique intellectual property provisions that serve to accelerate development. The federal government management facilitates interaction between Industry Teams and the Core Technology program as well as establishes technical priorities and approaches.

2007 CORE TECHNOLOGY & OTHER PARTNERS

Across the United States, SECA Core Technology participants are working on dozens of fuel cell projects, led by the brightest minds from leading universities, national laboratories and businesses. These competitively selected projects work together to provide vital R&D and testing in support to the Industry Teams.

In the same spirit of healthy competition, the Industry Teams leverage the collective ingenuity of the Core Technology participants to independently pursue innovations in fuel cell design that can be mass-produced at lower cost. Focusing on Cost Reduction and Coal-Based Systems, the Industry Teams are working to solve the challenges of fuel cell technology, each using different design and manufacturing approaches. As a result, the SECA program is rich in innovation, allowing it to reach its goals much faster.

Fuel Cell Research and Development

The Office of Fossil Energy and NETL are pleased to present this FY 2007 Office of Fossil Energy Fuel Cell Program Annual Report, a compilation of abstracts from the fuel cell projects managed through these offices. These abstracts are divided into subsections as detailed below.

SECA Fuel Cell Coal-Based Systems: Through its Coal-Based Systems program, SECA seeks to leverage successes in Cost Reduction and technology for the scale-up of SOFCs to sizes appropriate for central generation applications and to integrate the SOFC and associated balance of plant with coal gasification technology. Industry Teams will focus on developing large MW-scale systems while continuing SECA Cost Reduction activities through 2010. It is anticipated that the best technology from any Industry Team will be available for incorporation into one or more of the SECA Coal-Based Systems projects in preparation for operation at FutureGen or an equivalent demonstration site. Key R&D topics include coal contaminants, pressurization, failure analysis, system integration, balance of plant, materials, manufacturing, and controls and instrumentation.

SECA Cost Reduction: To achieve cost targets, Industry Teams are engaged in refining technology and validating this advanced technology in 3-10 kW SOFC modules that can be mass produced, aggregated, and scaled to meet a broad range of applications. This development activity is blending established manufacturing processes with state-of-the-art fuel cell technology advancements in order to leverage the advantages of economies of production (high-volume mass production) and scale. It requires reaching a full spectrum of markets, including large markets such as auxiliary power units (APUs) for trucks and recreational vehicles, and other markets such as residential-commercial-industrial power, a wide range of distributed generation, and specialized applications for the military. Producing a common module for these vast markets will create the opportunity for the high-volume production required to reduce cost to the necessary level.

Delphi SOFC Module

SECA R&D: The Core Technology program provides comprehensive applied research support in five focus areas. This structure and the provisions in place reduce cost by leveraging resources so that all Industry Teams do not engage in separate applied research programs paying multiple times for the same research done once in the Core program. This approach also ensures that only major issues are addressed. SECA R&D's goal is to raise the technology bar in large strides rather than small steps. Core program areas are also funded by special topics under Science Initiatives, Small Business Innovative Research, Basic Energy Sciences, University Coal Research, and Historically Black Colleges and Universities. The Core Technology focus areas include the following:

- **Materials and Manufacturing** – Research focuses on improved reliability, improved performance, ability to tolerate any fuel or air contaminants, and cost reductions;
- **Fuel Processing** – Develop fuel processing technologies that will meet application requirements such as zero water, space and volume, and transient capability;
- **Power Electronics** – Optimizes fuel cell power system efficiency and cost in conversion of fuel cell output to usable DC (direct current) and AC (alternating current) power;
- **Modeling and Simulation** – Creates design models to determine a reliable operating space and guide manufacturing; and
- **Balance of Plant** – Focuses on high temperature heat exchangers and blowers to enable achieving high efficiency, low cost, and a simple system.

Advanced Research: The SECA Advanced Research program provides crosscutting, multidisciplinary research that leads to advanced electrochemical technologies minimizing the environmental consequences of using fossil fuels in energy generation. This program supports future advances in the SECA and Office of Fossil Energy Coal and Power programs by developing novel electrochemical energy-conversion and integrated technologies that advance the efficiency, reliability, and cost goals of fuel cell systems.

Key Program Accomplishments

SECA Transitions to Coal-Based Systems: To address the issues of fuel cell scalability and incorporation into IGCC plants, DOE integrated SECA's Cost Reduction activities into its coal-based systems projects. The goal of these projects is to develop and demonstrate fuel cell technologies that will improve coal-based central power stations and provide a 10–50 megawatt power block for inclusion with FutureGen or equivalent demonstrations. Three Industry Teams– Siemens Power Generation of Pittsburgh, PA, General Electric Hybrid Power Generation of Torrance, CA, and FuelCell Energy Inc. of Danbury, CT–transitioned their Cost Reduction projects into Coal-Based Systems and are working to develop fuel cell systems for an IGCC plant with capacities of 100 megawatts or greater. All SECA Industry Teams will continue their Cost Reduction activities through 2010 with the best fuel cell stacks available for development.

SECA Cost Reduction - The Power of a Goal: The six SECA Industry Teams – Acumentrics, Cummins Power Generation, Delphi Automotive Systems, FuelCell Energy, General Electric, and Siemens Power Generation – designed and manufactured SOFC electrical power generators in the 3-10 kilowatt range that were then subjected to a series of rigorous tests to evaluate system performance with respect to efficiency, endurance, availability, and production cost. To verify results, the prototype tests and system cost analyses were subjected to independent audits, with additional validation testing performed at NETL's fuel cell test facility. General Electric kicked off Phase I testing in June 2005, and tests concluded with Cummins in December 2006.

The Industry Teams' prototypes surpassed the DOE Phase I targets and represent giant leaps made toward fuel cell commercialization. The prototypes demonstrated the following:

- Average efficiency of 38.5 percent and a high of 41 percent, exceeding the DOE target of 35 percent. The demonstrated superior efficiency in this small size confirms the ability to achieve much higher efficiencies in larger systems.
- Average steady-state power degradation of 2 percent per 1,000 hours, beating the DOE target of 4 percent per 1,000 hours.
- System availabilities averaging 97 percent, topping the 80 percent DOE target across the board.
- Projected system costs ranging from $724 to $775 per kilowatt, which eclipsed the DOE intermediate target for an annual production of 250 megawatts and positions the teams to meet the 2010 target of $400 per kilowatt.

Fuel Cell Power Density Improved: One of SECA's primary goals is to enable fuel cells to produce more watts of electric power from smaller volumes of materials. This improved power density is needed to make fuel cells economically competitive with gas turbines and diesel electric generation. Several of SECA's Industry Teams are developing high-power density SOFC prototypes with a net power output of 3–10 kilowatts and the potential for mass production. The following are some examples of the power density improvements that SECA's Industry Teams have realized:

- Siemens Power Generation's new corrugated design increased surface density by 40 percent, and its new fuel cell stack design increases power density by as much as 52 percent.
- General Electric's prototype SOFC reduced system volume by 75 percent, enabling the power density of the SOFC system to increase by 37 percent.

Research Team Develops and Demonstrates Commercial SOFC Interconnect Material: Allegheny Technologies Inc. of Pittsburgh, PA, Pacific Northwest National Laboratory, and NETL have identified and successfully tested a cost-effective interconnect material based on ferritic stainless steels for applications in coal-based SOFC systems. The team's development goal was to use an inexpensive metal alloy to eliminate the negative effects of metallic interconnects on electrical conductivity in SOFCs. With funding and direction from the SECA Core Technology program, Pacific Northwest National Laboratory achieved success in laboratory tests with a commercial alloy from Allegheny Ludlum Corporation of Pittsburgh, PA. More extensive investigations are in progress to determine whether, with appropriate surface treatment, an alloy of this type can fully satisfy stringent SOFC interconnect requirements.

Crack-Resistant Compliant Glass Seal Identified: SOFC systems are more robust if their seals can accommodate motion in cell components and recover from stress-induced cracking. The University of Cincinnati has identified a glass composition that does not crystallize at SOFC operating temperatures and remains soft, so that cracks flow shut as the stack cools to room temperature. University of Missouri-Rolla is now working to improve the chemical compatibility of this class of flowable glass, and Sandia National Laboratories is examining composites in which ceramic filler particles improve the resiliency of the soft glass seal. Engineered materials systems that utilize novel glass formulations and composite structures hold promise for successful seal solutions.

Cathode Poisoning from Interconnect Chromium Mitigated: Chromium is a common element in cost effective fuel cell metal interconnects. However, it often migrates from the fuel cell's interconnect to its cathode material, forming compounds that may decrease cell performance. The SECA Core Technology program has developed a "chromium poisoning" mitigation strategy through work performed at Argonne National Laboratory, Pacific Northwest National Laboratory, and Carnegie Mellon University. The approach allows SECA's Industry Teams to slow chromium transport with applied coatings, remove it via airflow, and capture it in cathode structures—all without significant loss in cell performance.

High-Temperature Blowers Developed for SOFC Systems: Phoenix Analysis & Design Technologies Inc. of Tempe, AZ, and R&D Dynamics Corporation of Bloomfield, CT, have successfully demonstrated two distinctly different high-temperature pumps and blowers for SOFC systems. Each of the novel technologies successfully separates hot fuel cell gases from temperature-sensitive pump components, such as bearings, magnets, electronics, and motor windings. This work is key to improving SOFC efficiencies, and it supports the achievement of fuel cell systems that can adapt to diverse fuels. The efforts were conducted for SECA under a series of Small Business Innovation Research grants.

2007 Annual SECA Workshop in San Antonio, Texas: The SECA program will hold its 8th annual workshop during August 7-9, 2007, in San Antonio, Texas. Principal investigators of 29 projects will provide presentations. The findings and recommendations will be used by the DOE project managers to guide their future work and by the Technology Managers at DOE to make programmatic and funding decisions for the upcoming fiscal years. The workshop proceedings will be found on the program's website at http://www.netl.doe.gov/seca/.

Summary

SECA has surpassed its first set of Cost Reduction targets providing strong confidence in the 2010 $400/kW goal. By developing fuel cells to operate cost effectively on coal gas as well as natural gas, bio-fuels, diesel, and hydrogen, it is building a bridge to the hydrogen economy while solving today's environmental, climate change, fuel availability, and energy security issues. The once distant vision of using clean, low-cost fuel cell technology for everyday applications is now within reach.

II. SECA FUEL CELL COAL-BASED SYSTEMS

II.1 Coal-Based Solid Oxide Fuel Cell Power Plant Development

Jody Doyon
Vice President, Government Programs Administration
Fuel Cell Energy, Inc.
3 Great Pasture Road
Danbury, CT 06813
Phone: (203) 825-6125
E-mail: jdoyon@fce.com; Website: www.fce.com

DOE Project Manager: Travis Shultz
Phone: (304) 285-1370
E-mail: Travis.Shultz@netl.doe.gov

Subcontractors:
- Versa Power Systems, Inc., Littleton, CO
- Gas Technology Institute, Des Plaines, IL
- Worley Parsons, Inc., Reading, PA
- Nexant, Inc., San Francisco, CA
- SatCon Power Systems Inc., Burlington, ON, Canada
- Pacific Northwest National Laboratory, Richland, WA

Objectives

The overall objective of this three-phase coal-based solid oxide fuel cell (SOFC) power plant development project is to develop a cost-competitive, highly efficient, multi-MW solid oxide fuel cell power system using coal-derived synthesis gas with near zero emissions. Specific project technical objectives are as follows:

- Scale-up existing SOFC cell area and stack size (number of cells) for large scale, multi-MW power plant systems.
- Increase SOFC cell and stack performance to maximize power and efficiency operating on coal-derived fuels. Achieve a minimum 50% overall system efficiency (higher heating value [HHV]) from coal.
- Design, build and test a proof-of-concept, multi-MW SOFC power plant system (>1 MW) for high efficiency with 90% CO_2 separation for carbon sequestration. This testing will be conducted at FutureGen or another suitable DOE Solid State Energy Conversion Alliance (SECA) selected site.
- System cost to be <$400/kW for a multi-MW power plant, exclusive of coal gasification and CO_2 separation subsystem costs.

Accomplishments

- Planar SOFC cell area manufacturing scale-up from the baseline 121 cm^2 to over 1,000 cm^2 has been successfully demonstrated using the Versa Power Systems, Inc. (VPS) TSC II process.
- Cell performance repeatability of cell active area scaled-up to 350 cm^2 has been validated with several single cell repeat unit tests. These results indicate that there is no major electrochemical performance loss due to cell scale-up from an active area of 81 cm^2 to 350 cm^2.
- Pilot production manufacturing scale-up analysis is in progress. 500 kW to 1 MW production capacity by the end of the year is planned.
- Review of commercially-available gasification technologies for integration with SOFC power block has been conducted. One prime candidate has been selected for further study.
- Review of acid gas removal processes for dual purpose of sulfur and carbon dioxide removal from coal syngas has been conducted. Selexol process has been identified as a prime candidate for acid gas removal.
- Three system design options are being developed for consideration with various integration schemes for reliability and cost. Further engineering analysis and down select planned.

Introduction

FuelCell Energy (FCE) has been selected by the Department of Energy (DOE) to participate in a multi-phase project for development of very efficient coal-to-electricity power plants with near-zero emissions. The primary objective of the project is to develop an affordable, multi-MW-size SOFC-based power plant system for utilization of synthesis gas (syngas) from a coal gasifier with near-zero emissions. Some of the key project objectives are the development of SOFC technologies, cell and stack size scale-up, SOFC performance optimization, increased stack manufacturing capacity development and MW-class module engineering design. FCE will use the VPS planar SOFC cell and stack technology for this project. VPS has well established processes, quality control procedures and equipment for the manufacture of small to intermediate size cells and stacks. This serves as a solid basis for cell area and stack size scale-up. The other key objective is implementation of an innovative system concept in design of a multi-MW power plant with anticipated efficiencies approaching 50% of the HHV of coal. Combined with existing carbon dioxide separation technologies, the power plant is expected to achieve 50% overall efficiency while emitting near-zero levels of emissions of SOx, NOx, and greenhouse gases to the environment. Power block and balance of plant

cost reduction, performance enhancement and efficiency improvements will be required to achieve the project cost objectives. A ~10 MW proof-of-concept power plant demonstration will be conducted at FutureGen or another suitable SECA selected site. Successful development will provide low-cost, highly efficient multi-MW SOFC power plants that operate on coal syngas with near-zero emissions to help reduce the nation's dependence on foreign fuel sources. FCE is ideally suited for this project based on their experience in various DOE managed projects to develop commercial large-scale, MW-size fuel cell power plants, high-efficiency hybrid fuel cell–turbine systems and SOFC cell and stack development with their SOFC technology partner, VPS.

Approach

The project is organized in three phases according to schedule and technical objectives:

- Phase I of the project will focus on cell and stack development. This will include the scale-up of existing SOFC cell area and stack size (number of cells) and performance improvements. Preliminary engineering design and analysis for multi-MW power plant systems will also be conducted. The Phase I deliverable will be test demonstration of a SOFC stack building block unit that is representative of a MW class module on simulated coal syngas.
- Upon successful completion of Phase I and selection by DOE to continue, Phase II of the project will focus on modularization of the Phase I stack building block units into a MW-size module. Detailed design engineering and analysis for multi-MW power plant systems will also be conducted. The Phase II deliverable will be the test demonstration of a MW-size representative SOFC stack module on simulated coal syngas.
- Upon successful completion of Phase II and selection by DOE to continue, Phase III of the project will focus on the design and fabrication of a proof-of-concept multi-MW power plant. The Phase III deliverable will be tested for at least three years at FutureGen or another suitable SECA selected site.

Results

FCE has recently successfully completed a DOE-managed SECA Phase I SOFC cost reduction project to develop a 3-10 kW SOFC power plant system using the VPS planar cell and stack technology. Two major objectives of the Phase I development effort were to demonstrate the performance of a 3 to 10 kW prototype SOFC system and to develop factory cost estimates showing such systems could be manufactured on a cost-effective basis. Based on tests conducted over a 2,100-hour operational period, the prototype successfully met all DOE-specified targets. These areas included power output, system efficiency, system availability and overall system endurance. System cost calculations also surpassed the DOE metric target. Both the initial system performance tests and the factory cost estimate were audited and confirmed by independent third party consultants approved by the DOE. This VPS cell and stack technology serves as the basis for further development and scale-up in this multi-MW, coal-based system SECA Phase I project. To date, VPS has successfully scaled up its **T**ape casting, **S**creen-printing and **C**o-firing (TSC) manufacturing process from the baseline 121 cm^2 to over 1,000 cm^2 as shown in Figure 1. Cell testing performance repeatability of cell area scaled-up to 400 cm^2 (350 cm^2 active area) has been validated with several repeat single cell tests as shown in Figure 2. These results indicate that there is no major electrochemical performance loss due to cell scale-up from an active area of 81 cm^2 to 350 cm^2. New test facilities are being fabricated to enable cell testing of larger area cells. Figure 3 presents a simplified overview

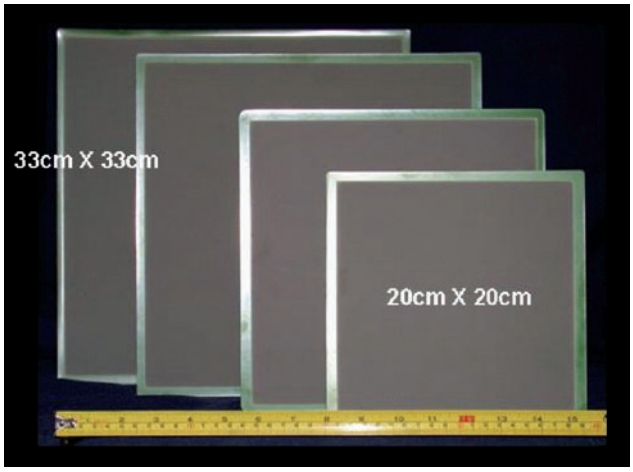

FIGURE 1. Planar SOFC Cell Area Scale-Up

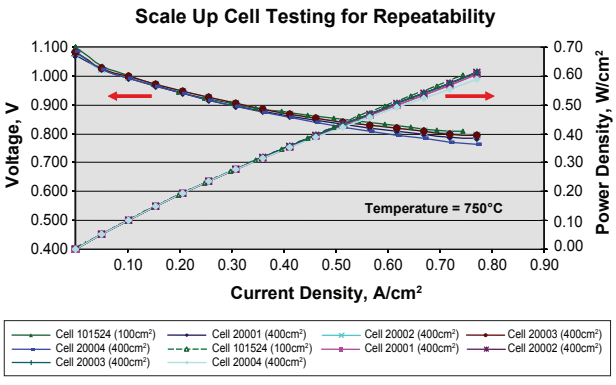

FIGURE 2. Test Performance of Scaled-Up Area SOFC Cells

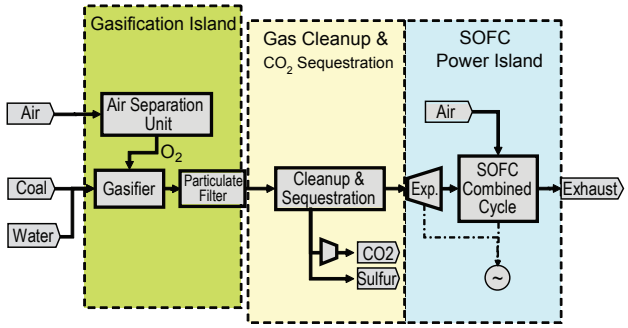

FIGURE 3. Coal-Based Integrated Gasification SOFC Fuel Cell (IGFC) Power Plant Overview

of the planned SOFC coal-based power plant system. Much progress has been made in detailed engineering design analysis with special attention to the coal-gas clean-up system and turbine combined cycle technology for maximum efficiency with minimum cost.

Conclusions and Future Directions

To date, significant progress has been made in the following areas:

- Planar SOFC cell area manufacturing scale-up from the baseline 121 cm^2 to over 1,000 cm^2 has been successfully demonstrated using the VPS TSC II process.
- Cell testing performance repeatability of cell active area scaled-up to 350 cm^2 has been validated with several repeat single cell tests.
- Pilot production manufacturing scale-up analysis is in progress. A production capacity of 0.5 MW to 1 MW is planned by the end of the year.
- Detailed engineering design analysis for the proof-of-concept (10 MW) and baseline (100+ MW) power plant systems are in progress with special attention to the coal-gas clean-up system and combined cycle technology for maximum efficiency with minimum cost.

FY 2007 Publications/Presentations

1. "Coal Based Large SOFC/T Systems", H. Ghezel-Ayagh, J. Doyon, Fuel Cell Energy Inc.; Paper presented at the 2006 Fuel Cell Seminar on November 13–17, Honolulu, Hawaii.

2. "Development of Solid Oxide Fuel Cells at Versa Power Systems", B. Borglum, E. Tang, M. Pastula, R. Petri, Versa Power Systems; Paper and presentation at the 2006 Fuel Cell Seminar on November 13–17, Honolulu, Hawaii.

3. "SOFC Development Status at Versa Power Systems, Inc." B. Borglum, Presentation at the 2006 Lucerne Fuel Cell Forum, July 4, 2006.

II.2 Solid Oxide Fuel Cell Coal-Based Systems

Matthew Alinger (Primary Contact) and Jim Powers
GE Global Research
1 Research Circle, MB277
Niskayuna, NY 12309
Phone: (518) 387-5124; Fax: (518) 387-5576
E-mail: alinger@research.ge.com

DOE Project Manager: Travis Shultz
Phone: (304) 285-1370
E-mail: Travis.Shultz@netl.doe.gov

Objectives

- Develop and optimize a design of an integrated gasification fuel cell (IGFC) power plant incorporating a solid oxide fuel cell (SOFC)/gas turbine (GT) hybrid system that will produce highly efficient, environmentally benign and cost-effective electrical power from coal.
- Design and analyze an IGFC plant operating at both pressurized and ambient pressure conditions.
- Perform component gap analysis to identify performance requirements that exceed current capabilities.

Accomplishments

- Developed a design for an IGFC power plant capable of producing ~500 MW of power from Pittsburgh No. 8 coal at an efficiency of 50% relative to the higher heating value (HHV) of the coal, while isolating 90+% of the carbon in the coal.
- Designed and analyzed two different versions of the IGFC plant.
  - The "baseline" system uses an SOFC operating at ambient (1 atm) pressure producing 67% of plant gross power, a heat recovery steam generator and steam turbine system (HRSG/ST) producing another 30%, and an expansion turbine providing the balance. At GE's baseline SOFC performance targets, this system achieves 44% efficiency.
  - The pressurized system, where the SOFC operates at 15 atm, dispenses with the expansion turbine (as the syngas pressure does not need to be reduced before the SOFC) and adds a GT. In this configuration, the SOFC produces 62% of the gross power, with the rest divided evenly between the GT and ST. This system achieves 50% HHV efficiency at baseline SOFC performance targets.
- Performed SOFC performance sensitivity analysis on baseline system. Results of analysis indicate 50% HHV efficiency can be achieved by improving SOFC performance. SOFC requirements that yield 50% efficiency are extremely challenging, but not inherently impossible.
- Identified component performance requirements that are beyond today's capability.

Introduction

A high-level conceptual design and analysis of IGFC power plants of ~500 MW capacity was performed with two different plant architectures:

1. The "baseline" system, in which the SOFC operates at ambient pressure. This system contains no gas turbine; excess heat from the fuel cell cycle is used to generate steam in a HRSG for a ST.
2. The "pressurized" system, which contains a SOFC and GT, both operating at ~15 atm pressure, in addition to the HRSG/ST.

Both systems use a coal gasification system based on GE's gasification technology. In all cases, the systems were designed and component performance targets set in order to meet or exceed the Department of Energy's (DOE's) program requirements, as shown in Table 1. In the analysis, the Phase III requirements of 50% HHV efficiency and 90% CO_2 isolation were targeted.

TABLE 1. DOE Coal-Based Hybrid Minimum Requirements

	Phase I	Phase II	Phase III
End Date	**FY 2008**	**FY 2010**	**FY 2015**
Fuel	**Coal-Derived Hydrogen or Syngas**		
Cost (Power Blocks)	$600/kW	$400/kW	$400/kW
Efficiency (Coal HHV)	40%	45%	50%
CO_2 Isolated	90%	90%	90%
Validate Test (hours)	1,500	1,500	>25,000
Degradation (/1,000 hrs)	≤ 4.0%	≤ 2.0%	≤ 0.2%

As the Phase III targets are aggressive and will not be realized in hardware for several years, the performance targets of several system components (most notably the SOFC stack) have been set beyond current capabilities. Therefore, there are significant technology gaps that must be closed in order to achieve the results described here.

Approach

In a previous GE study, an IGFC plant design capable of 90% CO_2 isolation was developed and analyzed [1]. The down-selected design from that study, with CO_2 separation taking place downstream of a pressurized SOFC, was chosen as the original baseline concept for the present study. Several alternative approaches were proposed and considered [2]. Eventually, a single design was selected as the most promising for detailed analysis. This design is the "pressurized system" referred to in the Introduction. During the course of this work, DOE requested a study of an unpressurized system. The system selected for this study, the "baseline" system of this report, is very similar to (and simpler than) the pressurized system.

The IGFC concepts were modeled to identify component performance levels required to meet the 50% efficiency requirement. The goals of the analysis were as follows:

- Define the potential of the concept to meet the 50% goal
- Identify key technical gaps
- Perform sensitivity analysis on the effect of key performance assumptions on the system efficiency
- Flow down performance requirements to the SOFC development team

A general approach adopted at the start of the project was to limit technical risk to the SOFC subsystem, using conventional technology for all other parts of the system. However, this approach proved untenable, particularly for the baseline system, because the performance required of the SOFC was deemed unreasonably aggressive, even considering substantial technology development. Therefore, several system components have performance targets beyond current capabilities, including the SOFC stack, coal gasifier, CO shift, inverter, and steam turbine. In some cases, the performance cannot be achieved today because of purely technical limitations. In others, the performance can be achieved only at prohibitive cost. Regardless, technology advances are required to realize the full set of requirements.

Results

System Performance Summary

The performance for each system analyzed is shown in Table 2. Note that all cases shown include 90+% CO_2 isolation, as required. With baseline stack performance targets, the pressurized system is capable of achieving the 50% HHV efficiency target. The baseline system, however, has an efficiency of only 44.9% at these conditions. While this performance is adequate to meet Phase I and Phase II requirements (40% and 45%, respectively), significant improvement is required to reach 50%. This target can be achieved by increasing the SOFC performance requirements, using a "Super" SOFC.

TABLE 2. Performance Summary for Baseline and Pressurized Systems

Power Summary, MW			
	Baseline System	**Baseline System with "Super" SOFC**	**Pressurized System**
Coal Feed, HHV	1047.1	1047.1	1047.1
Total Gross Generated Power	542.5	592.9	585.8
Total Parasitic Power	71.9	69.7	64.9
Net System Power	470.6	523.2	520.9
System Efficiency	44.9%	50.0%	49.7%

Key Technology Gaps

The analysis described requires several system components to provide performance that represents advancement over current technology capability or that requires verification beyond that performed to date. These parameters, therefore, represent the technology risks (and in some cases, the cost risks) associated with achieving 50% HHV efficiency in an ambient-pressure IGFC system. Several of these key technology gaps will be discussed further here.

Coal

As specified by the DOE minimum requirements, this study has been based on a high-rank bituminous coal, Pittsburgh No. 8, which meets these criteria. Using other, lower-rank coals, will invariably result in a lower system efficiency. This is not a technology risk per se, but a factor that must be considered during development (and one that integrated gasification combined cycle developers are beginning to struggle with currently).

Gasifier

The quantity of oxygen required from the air separation unit (ASU) for gasification is a significant efficiency driver. In current systems, the oxygen-to-carbon ratio in the gasifier is ~0.96. An improvement of approximately 10% is assumed in this analysis. Such an improvement will likely require advances in gasifier design and slurry mixing. More detailed study of the issues involved here is needed, but the technical risk is deemed high.

Syngas Coolers

The conventional radiant syngas cooler (RSC) used in today's gasification systems produces saturated steam with an exit temperature of ~650°F. In the IGFC system described in this report, the RSC generates superheated steam with an exit temperature of 850°F. As a result, the convection syngas cooler (CSC) will also see superheated steam and higher temperatures. The modification is not believed to represent a major gap in technology. However, the higher operating temperatures will likely require a change in materials sets and represents a cost challenge. New high-temperature materials may need development; alternatively, cost reductions in current materials may enable achieving these targets. Thus, the risk is considered moderate.

High Temperature CO Shift

Today's CO shift reactors commonly operate with excess steam to avoid forming methane and other carbon-containing byproducts. In this analysis, no such byproducts are produced despite a steam-to-carbon near the equilibrium stoichiometry and much lower than the values >2 typically used. Realizing such capability will require either major advances in catalyst capability or a change to new shift methods, such as the separation membrane approaches under development at GE and elsewhere. This is a high-risk technology gap.

SOFC

Unsurprisingly, most of the gap separating current technology from 50% efficient IGFC systems will need to be filled by SOFC development. The SOFC parameters required to achieve the target efficiency are all extremely challenging. Given the reasonable assumption that power densities >0.5 W/cm^2 are required to make IGFC systems economically viable, the cell voltage and fuel utilization requirements are extremely challenging. GE has made good progress toward these targets recently. Recent tests in simulated high-hydrogen syngas have achieved 0.480 W/cm^2 at 0.80 V and 84% fuel utilization, which could lead one to believe that success is near. However, these results were achieved in a single cell at a uniform temperature of 800°C, while the IGFC air temperature rise means that the average cell operating temperature must drop (or methods of controlling degradation at temperatures >800°C must be developed). Also, achieving high fuel utilization in a large stack comprising 100+ cells is at the very least a major engineering challenge, as design and manufacturing specifications must be set to ensure that cell-to-cell flow variation is almost nonexistent. The risk of achieving the SOFC performance targets is still extremely high.

SOFC Recycle

The IGFC design calls for ~50% recycle of the SOFC air. The recycle fraction is a huge driver on efficiency as it dramatically reduces the fresh air flow requirement and therefore the main compressor parasite. Blowers for the required temperatures (800+°C) do not exist at present and will need development. This is largely a reliability and cost challenge as opposed to a technology challenge, since rotating machinery operating at these temperatures does exist. However, the reliability and cost risks are significant.

Conclusions and Future Directions

SOFC power plants operating on coal have the potential to achieve up to 50% HHV efficiency while isolating the carbon from the coal for later sequestration or transport. This performance represents a 25% efficiency improvement over today's planned IGCC systems as well as a significant emissions advantage.

A highly efficient IGFC system that does not require SOFC pressurization or integration between the SOFC and a GT has been analyzed. It seems likely that a system such as this could be demonstrated far earlier than a pressurized system with a GT, since the former avoids a number of engineering and operational challenges. The results indicate that such ambient-pressure systems would be valuable not just for demonstration purposes, but have the potential to be economically viable in their own right.

Realizing the benefits of these plants will require significant technology development over the next decade. By far the most important developments needed are in the SOFC itself. The dramatic performance improvements of the last several years must continue and be joined by similar advances in cost reduction and degradation minimization.

References

1. Balan, C., Dey, D., Eker, S.-U., Peter, M., Sokolov, P., Wotzak, G., "Coal Integrated Gasification Fuel Cell System Study – Final Report", performed under DOE/NETL Cooperative Agreement DE-FC26-01NT40779, submitted January 2004.

2. Powers, J., Renou, S., Campbell, A., Minh, N., "Solid Oxide Fuel Cell Coal-Based Power Systems Program – Semi-Annual Report", performed under DOE/NETL Cooperative Agreement DE-FC26-05NT42614, submitted March 2006.

II.3 Coal Gas Fueled SOFC Hybrid Power Systems with CO_2 Separation

Joseph F. Pierre
Manager, Government Programs
Siemens Power Generation
Stationary Fuel Cells (SFC)
1310 Beulah Road
Pittsburgh, PA 15235
Phone: (412) 256-5313; Fax: (412) 256-2012
E-mail: joseph.pierre@siemens.com

DOE Project Manager: Travis Shultz
Phone: (304) 285-1370
E-mail: Travis.Shultz@netl.doe.gov

Objectives

- Optimization of the Siemens DELTA-N solid oxide fuel cell (SOFC) and scale-up of its dimensions.
- Verification by test of cell, stack, and module on coal-derived syngas.
- Corroboration of the technical and economic feasibility of a >50% efficient SOFC-based large capacity (>100 MWe) coal-fueled baseline power plant.
- Test on coal syngas of a fully functional 50% efficient proof-of-concept (POC) of lesser multi-MWe capacity.

Approach

- Analytical modeling to optimize the DELTA-N cell geometry.
- Develop a viable cell manufacturing process and fabricate cells.
- Verify by parametric testing cell performance and durability.
- Analyze, design, and develop a fuel cell stack.
- Prepare the preliminary design of a module aggregating fuel cell stacks.
- Test a thermally self-sustaining fuel cell stack on simulated coal syngas at the power system operating pressure.
- Identify and analyze cycle concepts.
- Select a baseline system cycle.
- Prepare the conceptual design for the baseline system.
- Corroborate via independent audit the technical and economic feasibility of the baseline system.
- Develop the conceptual design, performance analysis, and cost analysis for the POC system.

Accomplishments

- Evaluated multiple proof-of-concept and baseline system candidate cycle concepts.
- Developed a figure-of-merit system with which the candidate systems are to be compared.
- Redefined the reference cycle concept for the baseline power system to a less complex technology basis that should provide for more reliable implementation.
- Identified a preferred cycle configuration for the proof-of-concept system.
- Optimized the high power density (HPD) DELTA-N cell geometry for the air feed tube and axial fuel flow configuration.
- Successfully extruded and sintered HPD DELTA-N tubes.
- Completed the conceptual design of the most critical stack components.
- Completed shakedown of the pressurized cell test facility.

Future Directions

- Optimize baseline cycle configuration.
- Update and initiate conceptual design of proof-of-concept system based on optimized baseline system configuration.
- Execute cell and stack performance test.
- Optimize atmospheric plasma spray (APS) operating parameters.
- Continue the conceptual design for the module.

Introduction

Siemens Power Generation SFC will develop a MWe-class solid oxide fuel cell power system to operate on coal-derived synthesis gas and demonstrate operation at greater than 50% electrical efficiency (basis higher heating value [HHV] coal) with greater that 90% CO_2 capture. The system will be scalable to sizes greater than 100 MWe output and, when offered in commercial quantities, will have a target cost of $400/kWe including any extraordinary costs of integration to the balance of plant. Corroboration of the technical and economic feasibility of the SOFC power system will be achieved through the conceptual design of a large [>100 MWe] baseline power plant and the subsequent design, development, fabrication, and test of a proof-of-concept system. The POC will have an identical cycle, be of

multi-MWe capacity, and demonstrate an electrical efficiency >50% (coal HHV).

The proposed cycle concept was redeveloped as the gas turbine and the ion transport membrane (ITM), respectively, were removed from the cycle, the SOFC system is now at atmospheric pressure, and a steam turbine bottoming cycle has been integrated into the heat recovery system. The reference cycle includes an oxygen-blown gasification system with conventional cleanup and scrubbing to produce a syngas rich in hydrogen and carbon monoxide. After shifting, the CO_2 is removed from the syngas via a low-temperature polymer membrane. Oxygen for the gasification process is supplied by a cryogenic air separation unit.

This reference cycle SOFC/steam turbine (ST) configuration is less complex than its predecessor and should provide for more reliable implementation at the POC level. Operating at ambient pressure, the SOFC system is composed of multiple, identical SOFC modules that receive preheated air from the heat recovery system. The SOFC modules are based upon the high power density DELTA-N cell geometry, developed within this project. Cell and stack performance and durability will be verified via performance testing of single and multiple cells (bundles).

Approach

The baseline SOFC/ST power system is fueled by coal-derived syngas. The overall objectives are high electrical efficiency and CO_2 separation capability. The baseline system power capacity is to exceed 100 MWe whereas the proof-of-concept system is to be in the 10 MWe-class range. Several candidate cycle configurations were identified that could be implemented at the >100 MWe level. These configurations were modeled to estimate electrical efficiency of the system and values of key operating parameters (e.g. mass flow rate, temperature, and pressure) for major components. Also to be considered in addition to system efficiency are cost as reflected by system complexity and the potential for POC testing at the 10 MWe-class capacity. The efficiency target for the POC is 50% (net AC/coal HHV).

SFC is developing a new cell and stack design that combines the seal-less stack feature and a cell with a flattened multi-connected tubular cathode with integral ribs. This new design has a closed end similar to the Siemens circular tubular design. Analytical modeling will be utilized to optimize the number and dimensions of ribs for maximum power, the distribution of fuel flow and air flow, and structural stability against thermal stresses during operation from atmospheric to elevated pressure. Additionally, active length and width will be optimized based on practical limitations for cell fabrication and generator utility. The optimized DELTA-N cells will be bundled into an array or bundle (stack) of electrically connected fuel cells forming a monolithic structure. A typical stack will consist of bundles connected in series arranged in parallel rows. The proposed SOFC stack concept is based on technology that has been developed and proven as part of previous generator design and testing programs, a series of atmospheric and pressurized bundle tests, and the 220 kWe pressurized SOFC generator designed, built and operated in the pressurized SOFC/gas turbine (PSOFC/GT) hybrid power system. Further innovation will be required, particularly in development of low-cost ceramic materials, net shape component fabrication, and a high power density stack configuration to reduce the overall cost of the system. Cell and stack performance will be characterized via a series of single and multi-cell tests.

Results

A number of cycle configurations for the baseline system have been identified and evaluated. A figure-of-merit system for selecting the preferred candidate was developed and employed in a rigorous down selection process. A preferred baseline system configuration was identified. The preferred baseline system, shown in Figure 1, meets the efficiency objective, employs the seal-less SOFC cell and module configuration, and has the potential to use a low temperature, low complexity polymer membrane CO_2 separation system.

A seal-less module configuration that features an air feed tube and an axial fuel flow was developed, a result of an investigation evaluating numerous stack configurations. Also, as a result of numerous finite element analyses (FEA), the dimensions of the DELTA-N cell were optimized. Based on these dimensions, an optimization of the various layers of the cell to minimize electrical performance losses and internal stresses was initiated. The validation of the optimized cell geometry commenced via the successful extrusion and sintering of a number of DELTA-N tubes. These tubes are now being used to optimize the APS operating parameters.

Conclusions

Systems analysis indicate the performance objectives (>50% electrical efficiency, net AC/coal HHV) can be achieved and exceeded with the successful implementation of improvements in SOFC module and balance-of-plant component technologies, in cell and module efficiencies, and advanced materials and fabrication processes for the DELTA-N cell.

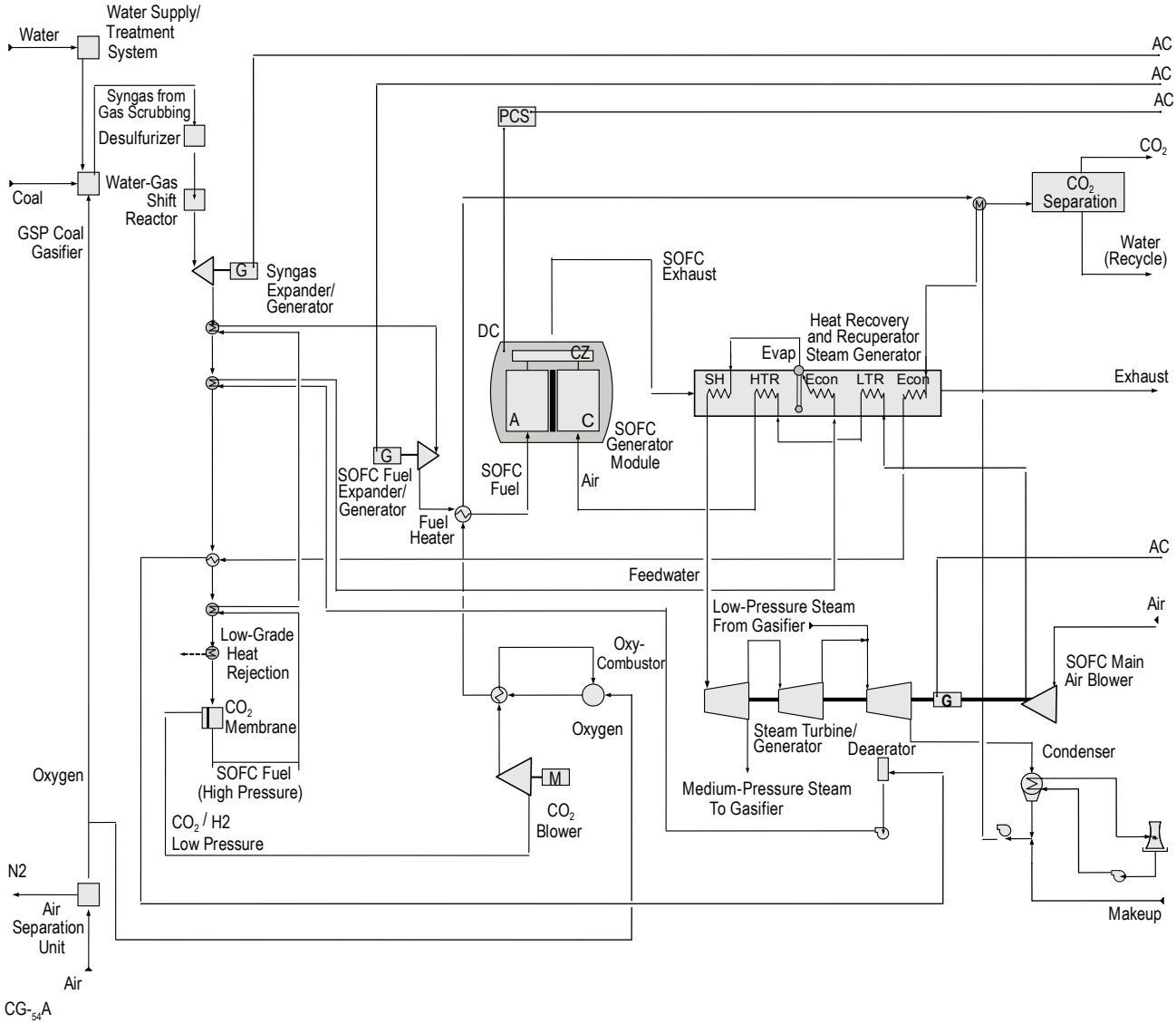

FIGURE 1. Baseline SOFC/ST Power System, Reference Cycle

III. SECA COST REDUCTION

III.1 Development of a Low Cost 10 kW Tubular SOFC Power System

Norman Bessette
Acumentrics Corporation
20 Southwest Park
Westwood, MA 02090
Phone: (781) 461-8251; Fax: (781) 461-8033
E-mail: nbessette@acumentrics.com

DOE Project Manager: Heather Quedenfeld
Phone: (412) 386-5781
E-mail: Heather.Quedenfeld@netl.doe.gov

Objectives

- Adapting the generator design for integration of the next generation higher power multiple connection chromite cells
- Development of an anode supported tubular cell capable of further doubling the power density presently achieved
- Improving cell and stack design to further reduce the stack cost

Approach

- Increase the current collection points per tube to increase cell power
- Improve material conductivity and stability to allow a higher power, longer lasting fuel cell tube
- Decrease solid oxide fuel cell (SOFC) generator component costs through advanced manufacturing techniques
- Perform preliminary testing on simulated coal gas to determine critical operating parameters

Accomplishments

Key Accomplishments in FY 2007 include:

- **Exceeded 350 mW/cm^2 on multiple interconnection cells:** Multiple interconnection cells have been manufactured achieving >350 mW/cm^2. This increases the average value from 120 mW/cm^2 thereby cutting the required number of cells and cost for a desired power level.
- **Demonstrated a tubular SOFC achieving >60 W/tube:** Further advancements in larger diameter tube technology and multiple take-off connections have been integrated into a single cell design. Previous advancements in isopressing technology have also been incorporated. These advancements take the single cell power from 5 W/tube at the start of the Solid State Energy Conversion Alliance (SECA) program to >60 W at this point.
- **Achieved 1,500 hours operation and completed SECA Phase I testing at Acumentrics:** Acumentrics successfully completed the SECA Phase I testing achieving over 6.1 kW output and greater than 35% efficiency and 97%+ availability with no degradation.
- **Achieved 800 hours validation testing at DOE-NETL:** Acumentrics shipped the unit to the validation site at the National Energy Technology Laboratory (NETL) in Morgantown, West Virginia and operated the unit for an additional 800 plus hours running a scaled down test of the version run in the first test. On this test, the power achieved was higher at 6.4 kW with slightly higher efficiency, near 37%, with similar availability and degradation. This unit has been returned to Acumentrics and has now run for over 3,500 total hours with no noticeable degradation.

Future Directions

- **Demonstrate tubular SOFC performance achieving 100 W/cell for scale up to MW-class coal systems:** Work will commence into scaling the individual tube power to 100 W/cell to show a scaled version of a 600-800 W cell for MW-class coal systems by adjusting tube size as well as current collection points.
- **Demonstrate high power density over a wider temperature range:** Work will focus on opening the cell temperature window while achieving high power density. Under this task, this operating temperature will ideally be opened up to a low range of 700°C from 800°C with no detriment to power density.
- **Perform cost study achieving lower stack cost:** Work will focus on furthering the cost study done during Phase I of the SECA program to verify cost at high volume. Advancements in cell power density and generator component design will be integrated into the model. This cost estimate will focus on the stack itself as the building block for MW-class systems.

Introduction

The Acumentrics SECA program has focused on the design and manufacture of micro-tubular SOFC power systems approaching twice the power density now

achieved from state of the art anode supported tubular designs. Based upon DOE funding and a focused research effort, these cells have achieved this goal and the path forward is to again double the power density. These units will be capable of entry into the residential and military markets initially followed by central station power operational on coal gas in the longer term.

Approach

To achieve the reduced stack cost goal, work will focus on increasing cell power thereby decreasing the number of cells per kilowatt or decreasing the cost of each component. With such an aggressive goal, work must focus on both paths. To increase cell power, work is centered on improved materials as well as enhancements in geometry. Cells with increased anode conductivities to decrease electrical bus losses are being investigated. Improved conductivity of cathodes is also being investigated to decrease the potential loss associated with the electrochemical reaction on the airside. Increases in cell tube diameter as well as multiple contact points along the length are also being studied.

Results

Cell and Stack Performance and Power Density

The culmination of three years of cell and stack advancements during Phase I of SECA resulted in the successful completion of the required end of phase test. The Phase I machine achieved practically no voltage degradation over the entire 2,300 hours of testing while achieving a peak power of 6.4 kW on a 5 kW class machine. The machine had an electrical efficiency near 37% while achieving over 97% availability. Figure 1 shows the performance stability of this machine while testing at NETL's site in Morgantown, West Virginia.

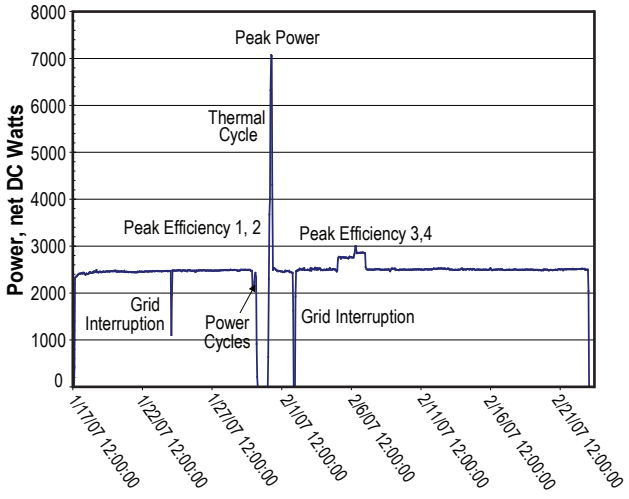

FIGURE 1. Performance Testing at NETL

In addition to major achievements in cell and stack stability, substantial strides in stack power density have been achieved. Figure 2 shows the resulting advancements in stack power density over the entire Phase I SECA program. For a 1.25 kW stack, the cell count has been decreased from 126 cells to 45 cells. Weight has been reduced by 75% from 92 lbs to 23 lbs. Volume has been reduced from 1.55 cubic feet to less than 0.3 cubic feet or by 82%. This results in the desired stack configuration for MW-class systems and now work will focus on cell power density as well as cell size/power increases.

Generator Design

Work has continued in cost reduction of the generator design as well as scale up for larger MW sub-systems. Progress has been made in advancing both metallic and ceramic recuperators for thermal recovery on the SOFC stack side. Figure 3 shows the resulting reductions in size, weight, and cost of the recuperators used for heat recovery. Figure 4 shows the

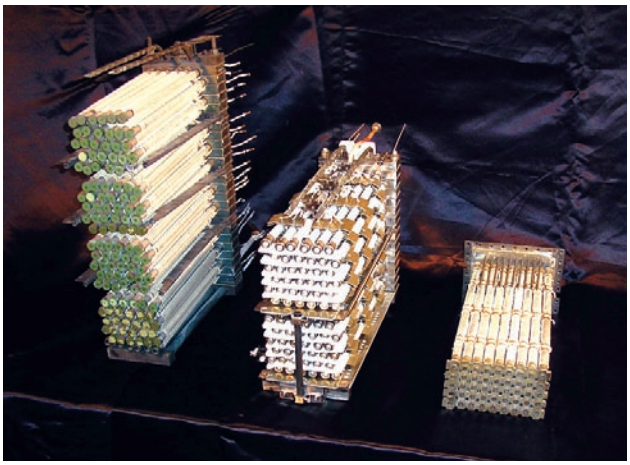

FIGURE 2. Progress in Stack Size and Weight Reduction

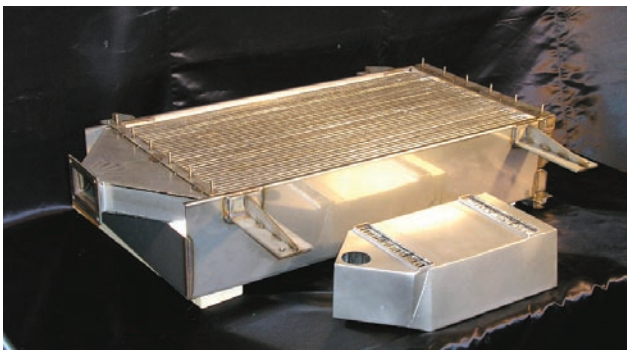

FIGURE 3. Recuperator Advancements

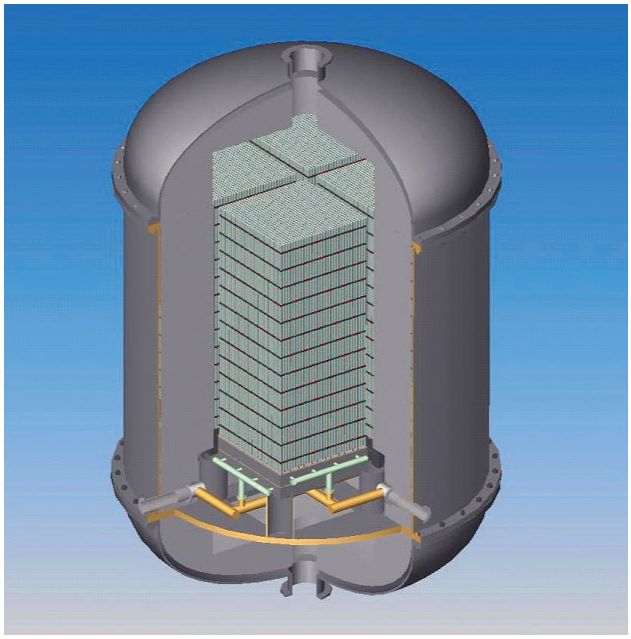

FIGURE 4. 1 MW SOFC Module

resulting preliminary model for a MW-class sub-system incorporating larger tubes with the developed cell power densities previously described.

Conclusions

Continual advancements have been made toward the SECA cost and performance targets in the Acumentrics' SOFC program. These advancements can be summed as:

- Successful completion of all Phase I SECA performance testing and cost analysis
- Cell power densities exceeding 350 mW/cm^2 or 3x greater than previous technology
- Generator design with significant size and weight reductions over pre-SECA designs well suited for mass production

FY 2007 Publications/Presentations

1. "Status of the Acumentrics SOFC Program", N.F. Bessette, Presented at the 2006 SECA Annual Workshop, Philadelphia, PA, September, 2006.

2. "Status of the Acumentrics SOFC Program", N.F. Bessette & D.S. Schmidt, Presented at the 2006 Fuel Cell Seminar, Honolulu, HI, November, 2006.

III.2 10 kW Solid Oxide Fuel Cell Power System Commercialization

Daniel Norrick
Cummins Power Generation
1400 73rd Avenue NE
Minneapolis, MN 55432
Phone: (763) 574-5301; Fax: (763) 528-7229
E-mail: daniel.a.norrick@cummins.com

DOE Project Manager: Heather Quedenfeld
Phone: (412) 386-5781
E-mail: Heather.Quedenfeld@netl.doe.gov

Subcontractor:
Versa Power Systems, Inc., Littleton, CO

Objectives

- Demonstrate solid oxide fuel cell (SOFC) stacks that achieve target performance, stability, and cost.
- Design and develop a SOFC system balance of plant (BOP), including air and fuel supply systems, meeting cost and reliability targets.
- Demonstrate a control system to manage the SOFC power system, including regulation of fuel and air flows and control of key system temperatures.
- Demonstrate an efficient electrical power conditioning system to convert stack output to inverter input DC voltages and regulate stack output current.

Accomplishments

- Constructed and tested a complete SOFC system satisfying the SECA Phase I targets, including an audited manufacturing cost of $742/kW.
- SOFC stacks that achieved target performance, stability, and cost were successfully demonstrated in the tested deliverable prototype.
- The Phase I cold balance of plant (cBOP), including air and fuel supply systems, was completed and successfully demonstrated to meet SECA objectives in the deliverable prototype.
- Control hardware and software providing steady-state and transient control of a SOFC system were successfully demonstrated in the deliverable prototype.
- Identified, characterized, and applied cost-effective cBOP components incorporating low cost, high volume, mass production components from industrial and automotive sources.

Introduction

Solid oxide fuel cell power systems offer the potential to generate electrical power from hydrogen or hydrocarbon fuels cleanly, quietly, and efficiently. The objective of the Cummins Power Generation-Versa Power Systems, Inc. (CPG-VPS) project is to design and develop a 3-10 kW SOFC-based power system that can be competitive with existing small diesel generating systems in terms of cost and package size, but offer significant benefits in efficiency, emissions, lower noise and vibration. Achieving these objectives requires advancement in six major areas:

1. Cell, interconnect, and SOFC stack performance and robustness including operation on low methane content reformate and tolerance to sulfur levels associated with commercially available on-highway diesel fuels.
2. Optimized manufacturing processes for production of cells, interconnects, and stack assemblies.
3. Cost-effective system and BOP design, thermal integration, and packaging of the hot components and sub-systems including stacks, fuel reformer, heat exchangers, and insulation system.
4. Reformation of ultra-low-sulfur diesel fuel to provide a reformate stream compatible with carbon-free operation of SOFC BOP and stacks.
5. Control system for regulating air and fuel flows to the stacks in proportion to electrical load and operating temperatures, and for managing stack electrical load through current regulation compatible with load sharing between the fuel cell and batteries during steady-state and transient loading.
6. Electrical power conditioning, including DC voltage boosts (converters), efficient DC power inversion to AC, and load sharing with batteries.

The team has demonstrated satisfaction of SECA Phase I objectives with progress in all areas during 2007, and has successfully completed Phase I of the SECA program.

Of particular note, the demonstrated system improved on a key SECA objective of manufacturing cost with an audited cost estimate of $742/kW, which was below the Phase I target.

Approach

The CPG-VPS approach coordinated development in a number of major areas including the development of planar solid oxide fuel cells, metallic interconnects, and stacks as well as parallel development in planar SOFC manufacturing and scale-up for economic manufacturing. Parallel work focused on development of a diesel fuel reforming system compatible with application requirements, fuel cell BOP, fuel cell and power electronics system controls, and electronic power conditioning.

Specifically, the CPG-VPS team conducted work to develop and evaluate advanced solid oxide fuel cells that provide the required performance and durability. Part of that development required conducting a progressive sequence of SOFC stack tests to validate development of materials and assembly methods for useable stacks that can achieve high fuel utilization and low degradation rates. The team integrated the BOP components, hot box subsystem, and controls into a working deliverable prototype, initiated prototype operation to shakedown the system, and successfully conducted operation of the full prototype through the SECA Phase 1 test sequence, successfully meeting or exceeding the SECA Phase 1 minimum requirements.

Results

Development work continued to improve cell performance, primarily through the development of sulfur tolerant electrodes and cells with good performance at reduced methane levels.

CPG demonstrated a high-efficiency inductor-based DC-DC boost system which was used to control current flow at constant regulated voltage to the test system load.

The team successfully completed the Phase I testing protocol to demonstrate substantial compliance with SECA Phase I minimum requirements.

TABLE 1. CPG-VPS Results Compared to Seca Phase I Minimum Requirements

	TARGET		ACTUAL	
Power Rating (Net DC @ NOC)	3 – 10	kW	3.2	kW
Cost	$800	/ kW	$742	/ kW
Efficiency Mobile (DC net / LHV)	25	%	37	%
Steady State Degradation	2.0	% / 500 hrs	1.7	% / 500 hrs
Transient Degradation	1.0	% / 10	1.1	% / 10
Total Degradation (1,500 hrs steady state + transients)	7.0	%	6.3	%
Availability	>80	%	99	%
Peak Power (Net DC)	N/A	kW	4.6	kW
Fuel Type	Comm'l	Commodity	NG	Pipeline

Conclusions and Future Directions

1. 2007 work culminated with successful completion of the SECA Phase I evaluation test including steady-state and transient evaluations and reporting results to NETL.

III.3 Solid State Energy Conversion Alliance Delphi SOFC

Steven Shaffer (Primary Contact),
Gary Blake, Sean Kelly, Karl Haltiner,
Subhasish Mukerjee, David Schumann,
Gail Geiger, Larry Chick, Ellen Sun

Delphi Automotive Systems LLC
5725 Delphi Drive
Troy, MI 48098
Phone: (585) 359-6615; Fax: (585) 359-6061
E-mail: steven.shaffer@delphi.com

DOE Project Manager: Heather Quedenfeld
Phone: (412) 386-5781
E-mail: Heather.Quedenfeld@netl.doe.gov

Subcontractors:

- Battelle/Pacific Northwest National Laboratory, Richland, WA
- Electricore, Inc., Valencia, CA
- United Technologies Research Center, East Hartford, CT

Objectives

- Develop a 3-5 kW solid oxide fuel cell (SOFC) power system for a range of fuels and applications (see Figure 1).
- Develop and demonstrate technology transfer efforts on a 3-5 kW stationary distributed power generation system that incorporates reforming of methane and then natural gas.
- Develop a 3-5 kW auxiliary power unit (APU) for heavy-duty trucks and military power applications.
- Develop system modeling, stack design and cell evaluation for a high-efficiency coal-based solid oxide fuel cell gas turbine hybrid system.

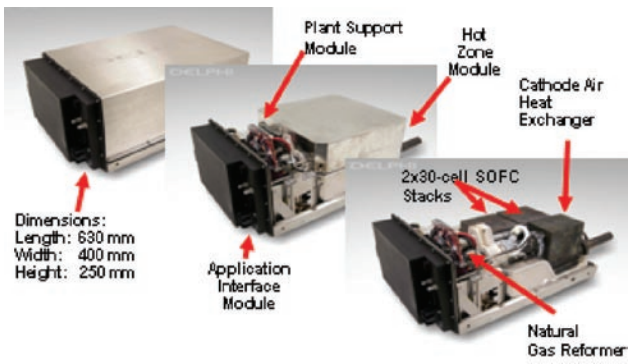

FIGURE 1. Generation 3 SOFC System

Accomplishments

Systems

- A Delphi SOFC system durability test was conducted using utility-supplied natural gas and a TDA Research Inc. sorbent desulfurizer. This system logged over 2,400 hours of testing with a stack degradation rate of less than 1% per 500 hours.
- A Delphi SOFC system was run to full power, and it produced 2.2 kW net and 36% efficiency on methane with full internal reforming. This system was then run for 470 hours at high load (50 amps, 1,800 W net) with 75% internal reforming. The measured degradation on the stacks was 1.1% per 500 hours.

Stack

- Generation 3.2 cassettes were successfully fabricated. Based on the experience gained by producing Generation 3.1 cassettes, the new design was developed to reduce stresses within the cassette, allowing for a more robust cassette.
- An improved cassette-to-cassette seal was developed. Current seals allow only 5 thermal cycles per stack. A new seal was developed that demonstrated 16 thermal cycles in the stack lab without leaks or degradation in power.
- A low-cost coating solution (coupon level test) for interconnects was demonstrated. A new coating was developed which has low resistivity, blocks Cr effectively and, most importantly, can be processed by high-volume manufacturing processes. This will allow for a cost-effective solution for coatings for interconnects.
- An effort is underway to design, develop and fabricate large-footprint cells to enable the eventual design of a MW-class coal-based solid oxide fuel cell gas turbine hybrid system.

Reformer/Catalyst

- An endothermic reformer design was modified for use with US07 diesel fuel and evaluated with recycle-based reforming. The benefit of this type of reforming is the recovery of unspent fuel energy in the anode tail gas.
- A liquid fuel vaporizer was developed to vaporize US07 diesel fuel and demonstrated durability to 500 hours. This is a key development for designing a diesel fuel delivery and catalyst system.

- Natural gas pre-reforming has been demonstrated with ~100% conversion of higher hydrocarbons and no selectivity to ethylene formation, yielding a high-methane-content product suitable for use in internal reforming.
- An improved surface- and gas-phase chemical reaction rate model has enabled chemical kinetics modeling to accurately predict experimental observations of partial oxidation reactions.

Balance-of-Plant

- The cast integrated component manifold (ICM) tooling fabrication and casting process development was completed with the supplier, and three upper and lower ICM manifolds were successfully completed. This will enable high-volume, low-cost manufacturing.
- A test was developed and implemented for studying Cr vaporization in balance-of-plant components. This will enable Delphi to determine the level of chromium being released from completed assemblies and thereby understand the system degradation mechanism.

Introduction

Delphi has been developing SOFC systems since 1999. After demonstrating its first-generation SOFC power system in 2001, Delphi teamed with Battelle under the Solid State Energy Conversion Alliance (SECA) program to improve the basic cell and stack technology, while Delphi developed the system integration, system packaging and assembly, heat exchanger, fuel reformer, and power conditioning and control electronics, along with other component technologies. Compared to its first-generation system in 2001, the Delphi-led team has reduced system volume and mass by 75 percent. By January 2005, the Delphi team was able to demonstrate test cells with power density greater than that required to meet the SECA 2011 goals.

In addition to its compactness, another key advantage of the SOFC is its high system fuel efficiency, particularly when its high-temperature co-product heat can be used in combination with its electrical output. For example, SOFCs can be teamed with gas turbines driven by the SOFC's co-product heat to potentially generate power at 55 percent to 80 percent thermal efficiency (depending on scale and fuel used). This is significantly more efficient than today's typical coal-fueled power plant, which has a thermal efficiency of 35 percent to 40 percent. By co-generating power on-site at industrial facilities, commercial businesses, or even residences, the SOFC's high-grade co-product heat will enable up to 90 percent efficiency in distributed, combined heat and electrical power generation. Similarly, heavy-duty trucks will be able to utilize SOFC auxiliary power systems for both heat and electrical power when parked to save 85 percent of the fuel that they consume when idling the main engine, and likewise reduce idling emissions.

While size and efficiency advantages are important for many potential applications, the SOFC's most significant advantage overall is its very broad applicability due to its inherent fuel-flexibility. With relatively small changes, SOFC systems can potentially operate on a full range of conventional and alternative fuels. This includes natural gas and conventional petroleum-based fuels like low-sulfur gasoline, diesel and propane; high-sulfur military fuels like JP-8 and jet fuel; low-CO_2 renewable fuels from biomass like ethanol, methanol and bio-diesel; synthetic fuels from coal and natural gas; and non-hydrocarbon fuels such as hydrogen and ammonia.

Approach

Delphi utilized a staged approach to develop a modular SOFC system for a range of fuels and applications.

- Develop and test major subsystems and individual components as building blocks for applications in targeted markets.
- Integrate major subsystems and individual components into a "close-coupled" architecture for integrated bench testing.
- Integrate major subsystems and individual components into a stationary power unit for the stationary market.
- Integrate major subsystems and individual components into an APU for the transportation market.
- Leverage previous work for modeling of a MW-scale hybrid power system and development of a hybrid stack module that can operate on simulated coal gas.

Results

SECA Phase II is a continuation of the core hardware development activities begun in Phase I. The systems efforts in Phase II are more application-driven as Delphi moves this technology closer to pilot and production releases. The Phase II project will support and address two market opportunities. The stationary market and the transportation market have unique demands, and development tasks must address specific values that are economic drivers of the design and application.

Delphi has continued to build and test 30-cell Gen 3.1 stack modules. Key lessons have been learned from the performance of these modules and their post-test autopsy analysis. The Gen 3.2 design is complete, and prototype parts are being validated. Fundamental development has focused on low-cost coatings for interconnects, robust seals, sulfur-tolerant anodes and understanding the failure mechanisms within the cell and stack during thermal cycling and long-term continuous durability tests. Process development and improvements include development of more robust and cost-effective formulations and processes for cell manufacturing, and optimization of cassette fabrication and stack assembly processes to improve first-time quality of stacks.

Focused work on diesel (US07) endothermic reforming was conducted this period. The benefit of anode tail recycle as a reactant to diminish inlet coking was demonstrated. A comprehensive comparison of non contact vaporizer versus contact vaporizer was conducted. The endothermic tubular reactor continues to be evaluated. Initial enthalpy balances and heat exchange analysis revealed areas for improvement in heat management. These deficiencies are being addressed via a brazed core design and a more substantial re-design for the next-generation endothermic reactor. A natural gas cracking reactor has been developed to crack or reform C2s to make possible the benefits of internal reforming of natural gas.

A new six-valve process air module assembly was designed, fabricated and assembled along with new modular control valve blocks. Cast Inconel ICMs were received from the supplier, and process development for brazing the castings has been initiated. Recycle pump robustness has been improved by re-orienting the pump, changing pump bearings, and modifying a recycle cooler. Prototype natural gas desulfurizers were specified, purchased, and placed on test. This completed one of the Phase II milestones: running a system on line natural gas. A designed experiment/robust engineering test of sorbents for a hot reformate desulfurizer continued and resulted in sorbent selection for a non-regenerating desulfurizer.

A system study was initiated to investigate SOFC system configurations utilizing gasified coal and to evaluate a modified Delphi SOFC cell. The primary objective of the system study is to formulate highly efficient SOFC-based hybrid system configurations and establish an optimized conceptual design of the SOFC stack and stack-module. The objective of the cell evaluation effort is to determine the compatibility between Delphi's cell and a modified stack design, identifying gaps between the current Delphi cell technology and the stack requirements for a MW-scale hybrid power system.

Conclusions

- Delphi's Phase II SECA project is focused on two markets, stationary and transportation, with additional emphasis on developing the system and stack requirements for a coal-gas-based MW-scale hybrid power system.
- Product and process improvements were initiated for the current Gen 3 stack design with the initial requirements and development for the next-generation stack design.
- A tubular diesel endothermic reformer was initiated and developed. In addition, a natural gas cracking reactor was developed.
- A cast Inconel integrated component manifold was developed and fabricated. A natural gas desulfurizer was specified, purchased, and validated in an SOFC stationary power unit system. Engineering began on a hot reformate desulfurizer.

Future Directions

- Demonstrate SOFC system on varying loads using the natural gas-fueled APU during Q4 2007.
- Demonstrate the next-generation stack during Q4 2007.
- Design and release the next-generation SOFC system during Q1 2008.
- Complete initial test on next-generation SOFC system during Q3 2008.

FY 2007 Publications/Presentations

1. September 2006: SECA Core Technology Workshop and Peer Review, Philadelphia, PA: Presentation by Steven Shaffer, Delphi Corporation, "Development Update on Delphi's Solid Oxide Fuel Cell System".

2. November 2006: 2006 Fuel Cell Seminar in Honolulu, HI: Presentation by Steven Shaffer, Delphi Corporation, "Update on Delphi's Development of a SOFC Power System".

Special Recognitions & Awards/Patents Issued

1. US Patent Office Grant Numbers: 7094486, 7144644, 7147953, 7179558, 7201984, 7217300.

III.4 SECA Solid Oxide Fuel Cell Power Plant System Cost Reduction

Jody Doyon
Vice President, Government Programs Administration
Fuel Cell Energy, Inc.
3 Great Pasture Road
Danbury, CT 06813
Phone: (203) 825-6125
E-mail: jdoyon@fce.com; Website: www.fce.com

DOE Project Manager: Travis Shultz
Phone: (304) 285-1370
E-mail: Travis.Shultz@netl.doe.gov

Subcontractors:
- Versa Power Systems, Inc., Littleton, CO
- Pacific Northwest National Laboratory, Richland, WA

Objectives

FuelCell Energy Corporation (FCE) has been engaged in a Department of Energy (DOE) managed, Solid State Energy Conversion Alliance (SECA) project to develop a 3-10 kW solid oxide fuel cell (SOFC) power plant system since April, 2003. The FCE team recently successfully completed Phase I of the project, surpassing all DOE specified metrics for performance and cost. FCE utilizes the planar cell and stack technology of its SOFC provider, Versa Power Systems, Inc. (VPS), for all its SOFC development programs. Two major objectives of the Phase I Cost Reduction project development effort were to demonstrate the performance of a 3 to 10 kW prototype SOFC system and to develop factory cost estimates showing such systems could be manufactured on a cost-effective basis. FCE has recently been selected through a competitive process by DOE to participate in a multi-phase project for development of very efficient, large-scale (multi-MW) coal-to-electricity power plants with near zero-emissions. The new project's technical objectives will be merged with the existing SECA Phase I SOFC Cost Reduction project technical objectives based on the similarities for cell and stack development in both projects. One of the key project objectives is the development of fuel cell technologies, fabrication processes, manufacturing infrastructure and capabilities for scale-up of SOFC stacks that are cost competitive with existing commercial competing power generation technologies. Specific Cost Reduction related objectives for these projects are:

- Scale-up existing SOFC cell area and stack size (number of cells) within a building block unit and stack tower to minimize cost.
- Scale-up existing manufacturing infrastructure and capabilities for SOFC cell and stacks production on a cost effective basis.
- Increase SOFC cell and stack performance to maximize power and efficiency for reduced cost on a per kilowatt basis.
- Power block unit system cost goal is to be <$400/kW.

Accomplishments

Two major objectives of the Phase I Cost Reduction project development efforts were to demonstrate the performance of a 3 to 10 kW prototype SOFC system and to develop factory cost estimates showing such systems could be manufactured on a cost-effective basis. Following are milestone accomplishments related to these objectives:

- A 3 kW prototype SOFC system (3-1) was tested as a project requirement at VPS Ltd. (Calgary) for over a 2,100-hour operational period. Test results successfully surpassed all DOE-specified Phase I SECA program performance metric targets that included power output, system efficiency, system availability and overall system endurance.
- Following the metric test mentioned above, the prototype 3 kW SOFC system was shipped to the DOE's National Energy Technology Laboratory (NETL) in Morgantown, West Virginia, and re-tested for another 1,600 hours validating the performance of the metric test conducted at VPS.
- A detail factory cost estimate analysis was conducted indicating the total 3-10 kW system cost to be $776/kW based upon an annual production rate of 50,000 units and a peak power rating of 5.1 kW. This surpasses (less than) the SECA Phase I metric of $800/kW using the same assumptions.
- Both the metric system performance tests and the factory cost estimate were audited and confirmed by independent third party consultants approved by the DOE.

Introduction

FCE has been engaged in a DOE managed, SECA project to develop a 3-10 kW SOFC power plant system since April, 2003. FCE has recently been selected by DOE to participate in a multi-phase project for development of very efficient coal to electricity, large scale (multi-MW) power plants with near zero-emissions. The new project's technical objectives will be merged with the existing 3-10 kW program

Phase I technical objectives based on similarities for cell and stack development. The primary objectives of these projects are to develop affordable, SOFC-based power plant systems with high efficiency that are cost competitive with other power generating technologies of similar capacity without incentive funding support. In order to be cost competitive with other power generating technologies of similar capacity without the need for incentive funding programs, significant SOFC stack and system cost reduction must occur from the current low volume development level to high volume, mass production prices. The achievement of the project cost targets is a key facet of the SECA projects. FCE is ideally suited for these projects based on experience with cost reduction successes for their commercial fuel cell power plants now being installed worldwide. FCE will use the cell and stack design of their SOFC technology partner, VPS, as the basis for these projects. VPS has been actively engaged in cost-effective SOFC manufacturing process research and development since 1998 and has well establish processes, quality procedures and equipment for the manufacture of small to intermediate size cells and stacks. The DOE specified metric for the final project (Phase III) system cost that is determined to be competitive with other power generating technologies of similar capacity without incentive funding is <$400/kW for a multi-MW power plant, exclusive of coal gasification and CO_2 separation subsystem costs.

Approach

The SOFC Cost Reduction project is organized in three phases according to schedule, technical and cost objectives. Following is a short description of the approach as it relates to the SOFC Cost Reduction project:

- Phase I will focus on cell and stack development activities. This will include scale-up of existing SOFC cell area, stack size (number of cells) and performance improvements. Phase I deliverable for the 3-10 kW SOFC Cost Reduction development project will be test demonstration of a 3 kW power block system that meets all DOE performance and cost metrics. This includes demonstration of system peak power performance that will be used as the basis for cost. The DOE specified metric for the Phase I 10 kW system factory cost must be less than $800/kWe.
- Upon successful completion of Phase I and notice by DOE to continue, Phase II of the SOFC Cost Reduction project will verify the robustness of the 3-10 kW SOFC stack design (10,000 hours life, 50 thermal cycles) and validate the ability to meet the Phase II cost target of $600/kWe.
- Upon successful completion of Phase II and notice by DOE to continue, during Phase III of the SOFC Cost Reduction project, the overall work plan shall be to continue manufacturing process development for the 3-10 kW module and to meet the $400/kWe cost target and to conduct tests on opportunity fuels.

Results

FCE has been engaged in a DOE managed SECA Phase I project to develop a 3-10 kW SOFC power plant system since April, 2003. Much progress has been made in the SECA Phase I project on cell and stack scale-up, increased performance and cost reduction. VPS has successfully scaled up its **T**ape casting, **S**creen-printing and **C**o-firing (TSC) manufacturing process from the baseline 81 cm^2 to 121 cm^2 in this project. This defined the cell area that was tested in the 3-1 SOFC prototype system as a program deliverable. The 3-1 system as shown in Figure 1 was tested at VPS Ltd. to demonstrate the DOE specified performance metrics for power output, system efficiency, system availability and overall system endurance. Figure 2 and Table 1 summarize the test performance and results. The 3-1 SOFC system test results surpassed all the DOE Phase I SECA program performance targets. The performance test set-up, measurement equipment and results for the metric test were audited and confirmed by an independent third party consultant approved by the DOE. Following the metric test mentioned above, the prototype 3 kW SOFC system was shipped to the DOE's NETL in Morgantown, West Virginia, and re-tested for another 1,600 hours validating the performance of the metric test conducted

FIGURE 1. Packaged 3 kW SOFC System

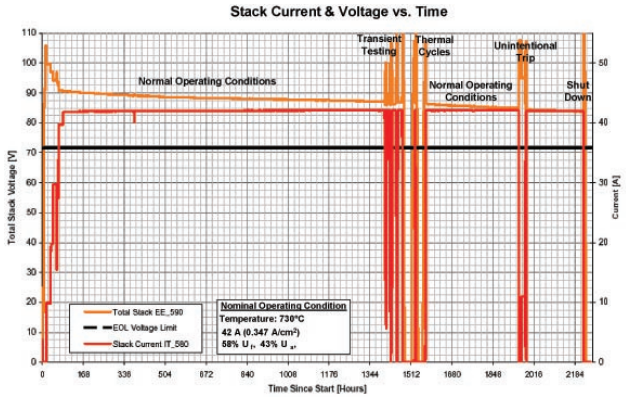

FIGURE 2. SECA 3 kW SOFC System Performance

TABLE 1. SECA Cost Reduction Project Phase I Metric Test Results

	Steady State Operation (BOT)	Steady State Operation (EOT)	Peak Power Operation	SECA Metric	
Net DC Electrical Power	3.39 kW	3.13 kW	5.26 kW	3 to 10 kW	✔
Net DC Electrical Efficiency	38.7%	36.4%	33.3%	>35% (Steady State)	✔
Stack Power Density	280 mW/cm^2	260 mW/cm^2	430 mW/cm^2	N/A	
Steady State Degradation		1.2% / 500 hours	N/A	<2% / 500 hours	✔
Transient Degradation (7 load interruptions, 3 thermal cycles)		0.7%	N/A	<1.0%	✔
Availability		98.6%	N/A	<80%	✔

✔ All SECA 3 kW Phase I Cost Reduction Program performance metrics have been successfully demonstrated!

at VPS. A detail factory cost estimate analysis was conducted indicating the total 3-10 kW system cost to be $776/kW based upon an annual production rate of 50,000 units and a peak power rating of 5.1 kW. This surpasses (is less than) the SECA Phase I metric of $800/kW using the same assumptions. As shown in Figure 3, the stack accounts for ~17% of the total system cost, while the balance of plant (BOP) components account for ~70% of the cost. The remainder of the system cost (~13%) is associated with building, commissioning and testing (BC&T) of the power block unit. The low cost associated with the stack reflects the many years of process development and cost reduction activities at VPS. Greater than 75% of the BOP costs are procured components. Once a design configuration

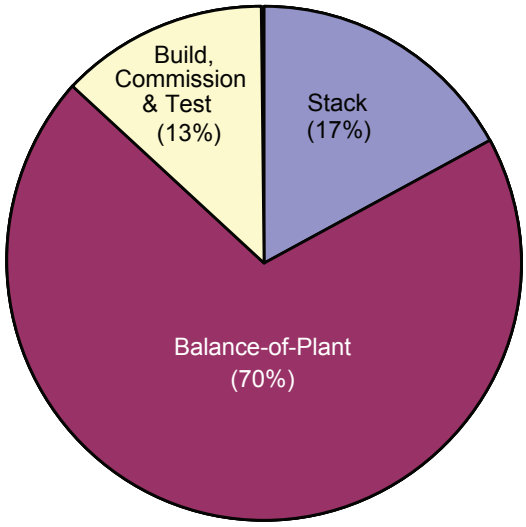

FIGURE 3. Packaged 3 kW SOFC System Costs

is stabilized to enable volume pricing, multiple vendor sourcing is established and value-engineering programs are in play, it is anticipated that significant cost savings (>50%) will be realized. As the power plant size becomes larger, the BOP and associated costs will also diminish proportionally on a cost-per-kilowatt basis. This provides the greatest cost reduction opportunity for the coal-based, large scale, multi-MW sized power plants to be developed in FCE's new SECA project. The methodology and results from the factory cost estimate analysis were audited and confirmed by an independent third party consultant approved by the DOE.

Conclusion and Future Directions

- FCE has been engaged in a DOE managed SECA Phase I SOFC Cost Reduction project to develop a 3-10 kW SOFC power plant system since April, 2003. The FCE team recently successfully completed Phase I of the project, surpassing all DOE specified metrics for performance and cost.
- A 3 kW prototype SOFC system (3-1) was tested as a project requirement at VPS for over a 2,100-hour operational period. Test results successfully surpassed all DOE specified Phase I SECA program performance metric targets that included power output, system efficiency, system availability and overall system endurance.
- Following the metric test mentioned above, the prototype 3 kW SOFC system was shipped to the DOE's NETL in Morgantown, West Virginia, and re-tested for another 1,600 hours validating the performance of the metric test conducted at VPS.
- A detailed factory cost estimate based on a commercial production output of 50,000 units per year was conducted on the 3-1 SOFC system

tested in the above bullets. System factory cost calculations surpassed the DOE Phase I program cost metric target being less than $800/kW.

- Both the metric system performance tests and the factory cost estimate were audited and confirmed by independent third party consultants approved by the DOE.
- The FCE SECA team has now been redirected to participate in a multi-phase SECA project for development of very efficient coal-to-electricity power plants with near-zero emissions. The primary objective of the project is to develop an affordable, multi-MW size SOFC-based power plant system for utilization of synthesis gas (syngas) from a coal gasifier with near-zero emissions to help reduce the nation's dependence on foreign fuel sources. The final Phase III project deliverable will be a ~10 MW proof-of-concept power plant demonstration at FutureGen or another suitable SECA selected site.

FY 2007 Publications/Presentations

1. "Coal Based Large SOFC/T Systems", H. Ghezel-Ayagh, J. Doyon, Fuel Cell Energy Inc; Paper presented at the 2006 Fuel Cell Seminar on November 13–17, Honolulu, Hawaii.

2. "Development of Solid Oxide Fuel Cells at Versa Power Systems", B. Borglum, E. Tang, M. Pastula, R. Petri, Versa Power Systems; Paper and presentation at the 2006 Fuel Cell Seminar on November 13–17, Honolulu, Hawaii.

3. "SOFC Development Status at Versa Power Systems, Inc.", B. Borglum, Presentation at the 2006 Lucerne Fuel Cell Forum, July 4, 2006.

III.5 Solid State Energy Conversion Alliance (SECA) Solid Oxide Fuel Cell Program

Matthew Alinger
GE Global Research
1 Research Circle, MB277
Niskayuna, NY 12309
Phone: (518) 387-5124; Fax: (518) 387-5576
E-mail: alinger@research.ge.com

DOE Project Manager: Travis Shultz
Phone: (304) 285-1370
E-mail: Travis.Shultz@netl.doe.gov

Subcontractors:
- Pacific Northwest National Laboratory, Richland, WA
- University of South Carolina, Columbia, SC

Objectives

- Develop and optimize the design of a >100 MWe integrated gasification fuel cell (IGFC) power plant.
- Resolve identified barrier issues concerning the long-term economic performance of solid oxide fuel cells (SOFCs).

Accomplishments

- Evaluated competing design features for a hybridized coal gas SOFC stack including internal vs. external manifolding.
- Demonstrated fabrication of SOFCs of 45 cm in diameter (~1,600 cm^2 in area).
- Evaluated two cell manufacturing techniques, sintering and air plasma spray, for impact on cell performance and manufacturing cost.
- Determined, through the manufacturing down-select study, that the economic feasibility of SOFCs is primarily dependent upon improving long-term stability of cell performance rather than choice of manufacturing process.
- Verified moisture-assisted vapor phase transport of Cr-species to the cathode is dominant over bulk/surface diffusion.
- Demonstrated effectiveness of Co,Mn spinel coated interconnect with lanthanum strontium manganate (LSM) cathodes at reducing degradation rates from ~100 to ~25 mΩ-cm^2/1,000 h.
- Demonstrated Co,Mn spinel coated interconnect with lanthanum strontium cobalt ferrite (LSCF) cathodes is effective at reducing degradation rates.
- Validated effectiveness of Co,Mn spinel interconnect coating at impeding Cr bulk diffusion.
- Identified 'free' silicon in interconnect alloy as likely contributor to high performance degradation.

Introduction

SOFCs represent an important opportunity to utilize fossil fuels in an efficient and environmentally friendly manner. Simple cycle fuel cells have obtained efficiencies to AC power as high as 45-50% with NOx production less than 0.5 ppm. Power producing systems containing fuel cells in combination with other power producing components such gas turbines, known as combined-cycle or hybrid systems, have the potential for even higher efficiencies in converting fossil fuels to AC electricity. SOFC/gas turbine hybrid systems utilizing coal synthesis gas (from a gasifier) as a fuel will provide environmentally friendly, inexpensive and dependable central power from an abundant fuel source (coal) and will make an important contribution to improving U.S. energy security.

This project aims at developing a highly efficient, environmentally benign, and cost-effective multi-MW SOFC-based power system operating on coal. The project will be a critical step towards the overall goal of realizing large (>100 MW) fuel cell power systems that will produce electrical power at greater than 50% overall efficiency from coal higher heating value (HHV) to AC power, including CO_2 separation preparatory to sequestration. The overall approach for this project is to integrate the SOFC with a gas turbine (GT) in a SOFC/GT hybrid power island, providing system efficiency greater than that achievable by either a simple cycle SOFC IGFC or an integrated gasification combined cycle (IGCC). Currently, commercial success of SOFC technology lies in minimizing the overall cost and dramatically reducing performance degradation over time.

Approach

The project focuses on designing and cost estimating the IGFC system and resolving technical and economic barrier issues relating to SOFCs. In doing so, manufacturing options for SOFC cells are evaluated, options for constructing stacks based upon various cell configurations are identified, and key

performance characteristics are identified. Key factors affecting SOFC performance degradation for cells in contact with metallic interconnects will be studied and a fundamental understanding of associated mechanisms will be developed. Experiments and modeling will be carried out to identify key processes/steps affecting cell performance degradation under SOFC operating conditions. Interfacial microstructural and elemental changes will be characterized, and their relationships to observed degradation will be identified. Mitigation strategies, including innovative coatings and bond layers, will be developed, evaluated and down-selected to improve degradation rates. Focus will be on microstructural stabilization and minimization of the area specific resistance (ASR) contribution from Cr_2O_3 scale growth and other interactions at electrode/interconnect interfaces evaluated during electrochemical testing and advanced microstructural characterization. Novel long-term and accelerated testing techniques will be developed and conducted under standard operating conditions to demonstrate capability to meet targeted performance degradation rates (<0.2%/1,000 h).

Results

Manufacturing options for SOFC cells have been evaluated, and options for constructing stacks based upon various cell configurations identified and key performance characteristics have been established. These evaluations were based on a detailed cost model. Ultimately, the key challenge of meeting the long-term cost requirement is heavily driven by the materials content of the cells, hence the need to focus on planar cells with "simple" materials. This project has evaluated two cell manufacturing techniques, sintering and air plasma spray, for impact on cell performance and manufacturing cost. Both manufacturing approaches present risks of achieving a technical level compatible with business and commercial goals. In both cases, if the success of the technical project is assumed, no significant differentiation can be identified from a "should-cost" perspective under high volume assumptions (>500 MW/year). Air plasma spray appeared to have some cost advantages at smaller production volumes given its inherent scaling advantage. However, the major risks related to SOFC technology development are not related to cell fabrication but in the capability of the technology to meet degradation and performance metrics compatible with the cost targets. It was determined, through the manufacturing down-select study, that the economic feasibility of SOFCs are primarily dependent upon improving long-term stability of cell performance rather than choice of manufacturing process. Therefore, key factors affecting performance degradation for SOFCs using ferritic stainless steel interconnects are currently being studied and a fundamental understanding of the associated mechanisms is evolving.

To this end, performance stability, in the presence of chromia, has been characterized with electrolyte-supported cells using sintered 8YSZ (yttrium-stabilized zirconia) electrolyte with symmetrically positioned electrodes comprised of LSM/YSZ and gold mesh current collectors as shown schematically in Figure 1. In this figure, the distance of the chromium source from the electrolyte can be varied (0-100 mm). The tests were performed at 800°C, in air at open cell voltage (OCV) and 0.1 A/cm^2 conditions. No effect on degradation rate was observed from either the current density or humidification investigated in absence of the ferritic steel. With the introduction of the chromium source, the resulting cell ASR is shown in Figure 2. The events labeled in the figure are 1) Cr-source brought into contact with the cathode; 2) humid air started; 3) dry air started; 4) humid air started; 5) cell left at OCV;

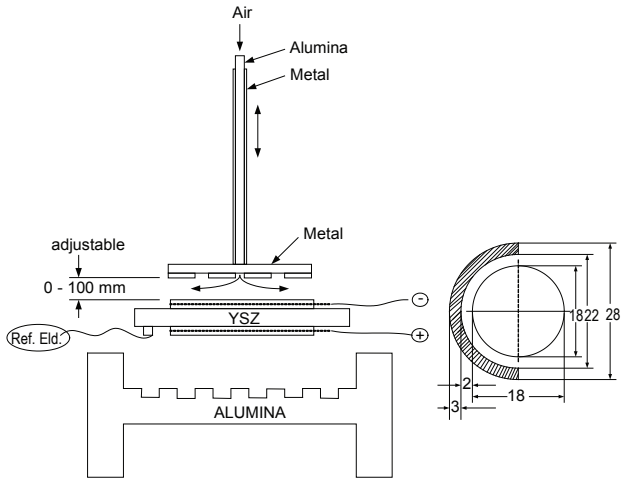

FIGURE 1. Schematic of the Experimental Setup and the Cell to Study Cr-Contamination of SOFC Cathodes; Dimensions Are in Millimeters

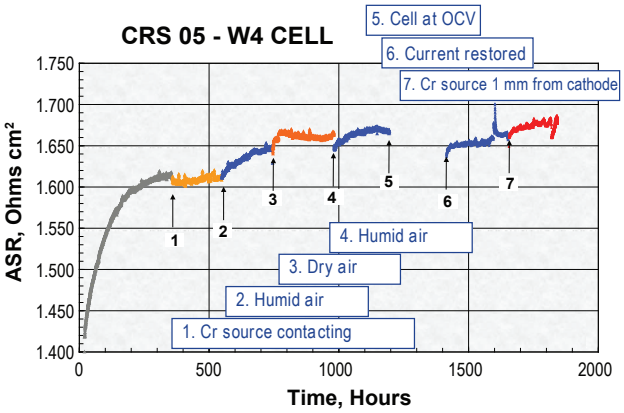

FIGURE 2. Total ASR of Electrolyte-Supported Cell with LSM/YSZ Electrodes as a Function of Time at 800°C in the Presence of a Ferritic Steel at 0.1 A/cm^2 and OCV in Dry and Humid Air Conditions

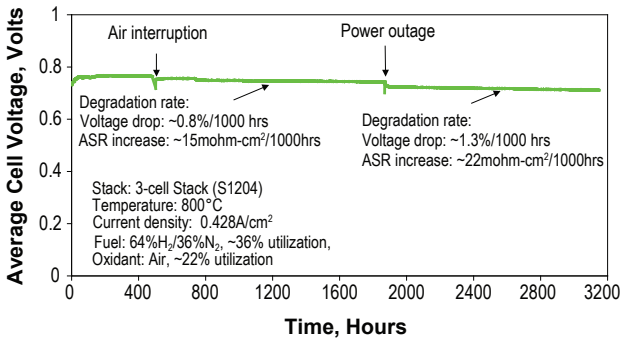

FIGURE 3. Average Cell Performance of 3-Cell Stack with the Protective Coating

6) current turned back on; and 7) Cr-source lift up to ~1 mm away from the cathode. The continued degradation when the Cr source was not in direct contact with the cathode indicated a gas transport and interaction mechanism in the presence of water vapor. Cr poisoning to the cathode was accelerated with moisture in air. Thus, these results support the claim that moisture-assisted vapor phase transport of Cr-species to cathode is dominant over bulk/surface diffusion. From these results, it is evident that Cr volatilization must be prevented to maintain high performance SOFCs, a fundamental goal of multi-MW SOFC power plants.

In order to mitigate the detrimental effects of chromium poisoning, protective coatings can be applied to the ferritic steel interconnects. This work uses Co,Mn spinel coatings. Shown in Figure 3 is the average performance of a 3-cell stack having the protective coating on the cathode interconnect surface. All three cells performed close to each other; the degradation rate was in the range of 11-16 mohm-cm^2/1,000 hours with average being ~15 mohm-cm^2/1,000 hours before a power outage. Even after the power outage, the stack maintained very good performance with an average degradation rate of ~22 mohm-cm^2/1,000 hours. In comparison, the typical degradation rate for LSM-based cells without coating was about 100 mohm-cm^2/1,000 hours.

The formation of thin, electrically insulating phases on the SOFC interconnect can contribute to significant cell performance degradation. Detailed characterization studies of the chromia/steel interface, after long-term electrochemical testing, reveals appreciable (100 nm thick) amorphous silica scale formation between the E-BRITE® interconnect and the chromia scale. Evidence of this is shown in the transmission electron microscope (TEM) micrograph shown in Figure 4. This continuous, electrically insulating silica scale is formed as a result of silicon impurities present in the alloy. Experiments are currently underway to understand the specific degradation impact of this layer.

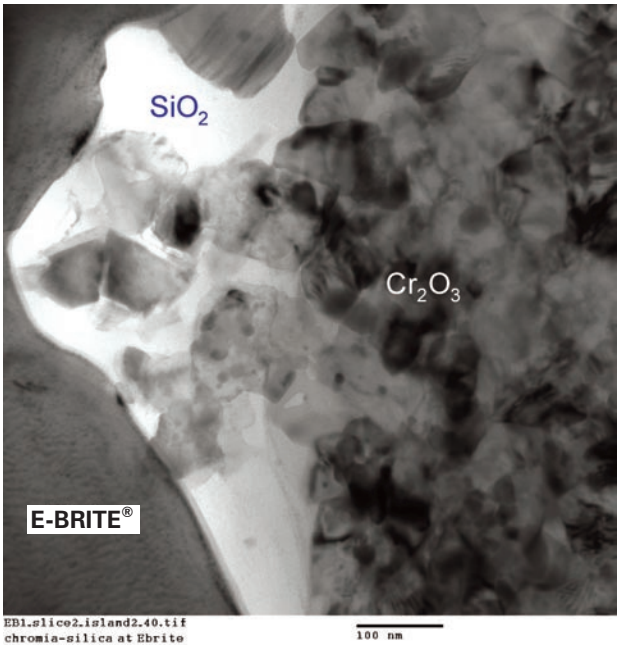

FIGURE 4. TEM Micrograph of Amorphous Layer of Silica at Interconnect/Chromia Interface

Conclusions and Future Directions

As a result of the findings from the manufacturing down-select, project scope is focused on mitigating performance degradation without increasing the cost.

To study and address the issues of performance degradation, a small-scale ceramic test vehicle will be developed to be used for evaluation of performance and degradation entitlement for gold and steel interconnects under high fuel utilization conditions. The data collected from this test, along with additional testing, will be used to construct a Pareto of cathode-side degradation mechanism impact to determine the dominant mechanism(s). This information will be used in the evaluation of the ASR stack-up from data collected through contact resistance testing and ceramic test vehicle data on the baseline materials set. Ultimately, a degradation mitigation solution for high performance SOFCs with ferritic steel interconnects, having a performance degradation of less than 25 mΩ-cm^2/1,000 hours (i.e. chromia growth dominated), will be demonstrated.

FY 2007 Publications/Presentations

1. M. Alinger, J. Guan, S. Zecevic, R. Klug, S. Taylor, S. Gaunt and P. Lam, "Performance degradation of SOFCs with metallic interconnects", Presentation at SOFC X, Nara, JP, 2007.

2. J. Guan, S. Zecevic, Y. Liu, P. Lam, R. Klug, M. Alinger S. Taylor, B. Ramamurthi, R. Sarrafi-Nour and S. Renou,

"Performance degradation of SOFCs with metallic interconnects", ECS Transactions, V7N1, pp. 405-412, 2007.

3. T. Striker, J.A. Ruud, W.J. Heward, Y. Gao and C. Steinbruchel, "A-site deficiency and phase purity of lanthanum strontium ferrite powders", ECS Transactions, V7N1, pp. 1207-1216, 2007.

III.6 Small-Scale Low Cost Solid Oxide Fuel Cell Power Systems

Shailesh D. Vora
Siemens Power Generation
1310 Beulah Road
Pittsburgh, PA 15235
Phone: (412) 256-1682; Fax: (412) 256-1233
E-mail: Shailesh.vora@siemens.com

DOE Project Manager: Travis Shultz
Phone: (304) 285-1370
E-mail: Travis.Shultz@netl.doe.gov

Objective

To develop a commercially viable 5-10 kWe solid oxide fuel cell (SOFC) power generation system that achieves a factory cost goal of $400 per kWe.

Accomplishments

- Completed testing of Phase 1 prototype meeting or exceeding all objectives.
- Developed the design of next generation cell.
- Fabricated next generation cells.

Introduction

The objective of this project is to develop a standard high performance, low cost SOFC system that can be manufactured in high volume for application in a number of different end uses including residential and as auxiliary power units (APUs) in commercial and military transportation applications. The proposed project is a 10-year, three-phase project with prototype SOFC systems being tested at the end of every phase. Performance and cost improvements made during each phase will be incorporated in each prototype, and products based on each prototype will be made ready for market entry, as they become available.

Approach

We have identified key technical issues that must be resolved to achieve low cost commercial SOFC systems. We will focus on cost reductions and performance improvements to transform today's SOFC technology into one suitable for low cost mass production of small systems for multi-market applications. The key advances identified are:

- Improved cell performance through design and materials innovations to more than double the power and thus reduced cost/kWe.
- On-cell reformation of natural gas fuel to eliminate high cost internal reformer components.
- Use of low cost insulation and containment vessels by lowering the system operating temperature.
- Use of net shape cast components to reduce machining costs.
- Simplification of stack and balance of plant (BOP) designs to lower parts count.
- High efficiency (95%) power conditioning systems to improve overall system electrical efficiency.

In addition to the key advances noted above, adoption of more automated, mass production techniques for cell, module and BOP manufacturing will ensure overall SOFC system cost effectiveness.

Results

Prior to the start of the project, it was recognized that Siemens' seal-less tubular cell design would not be able to meet the cost and performance targets of the project. A need to develop a cell with higher power density and compact design was identified. A new design that combined the seal-less feature and a flattened cathode with integral ribs was chosen. This new design referred to as high power density (HPD) cell has a closed end similar to the tubular design. The ribs reduce the current path length by acting as bridges for current flow. The ribs also form air channels that eliminate the need for air feed tubes. This cell design, due to shorter current path has lower cell resistance and hence higher power output than tubular cells. In addition, a variation of the HPD design, Delta, has a corrugated surface which significantly increases the active area of the cell yielding higher power per cell.

During FY 2007, a prototype system for residential applications was tested. The primary objective of this system was to demonstrate operation of HPD cells in a generator environment. The system ran on internally reformed pipeline natural gas fuel. The test duration was approximately 6,300 hours without any voltage degradation. Table 1 shows system targets versus actual performance. It met or exceeded all DOE targets for a Phase 1 prototype.

TABLE 1. Phase 1 System Performance

Performance Parameter	Requirements	Results
Net DC Efficiency	35%	38%
DC Peak Power (kW)	3-10	5.9
Steady State Degradation	<2% per 500 hrs	0 (2% Power Enhancement)
Thermal Cycle	1	1
Power Cycle	9	9
Availability	80%	100%
Test Duration (hrs)	1,500	6,300

Also during FY 2007, a next generation cell was optimized as the Delta8 design, based on net system power. Several Delta8 cells were fabricated for electrical testing. This cell has an active area of approximately 2,000 cm^2. Figures 1a and 1b show different views of a Delta8 cell.

Computational modeling of thermal and electrical fields to optimize the cell and stack design for maximum power and mechanical stability from thermal stresses during stack operation continued during FY 2007. Efforts were also directed towards the development of cell-to-cell connections to bundle cells.

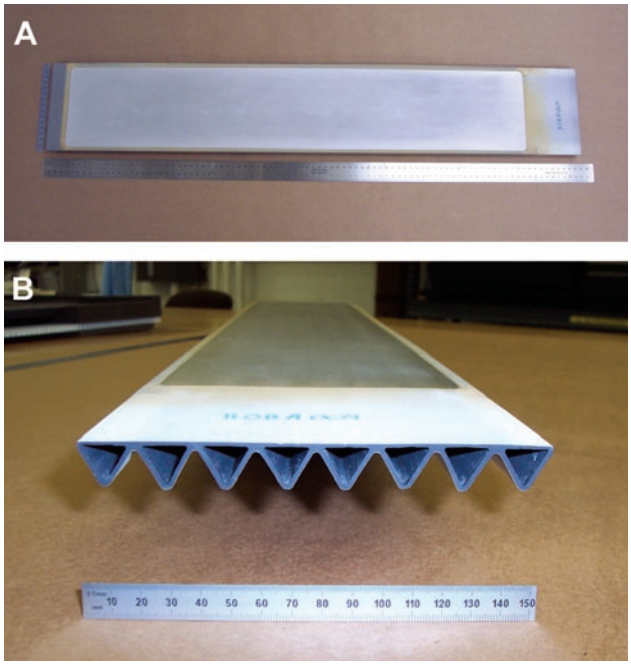

FIGURE 1. (a) Delta8 Cell Top View and (b) Delta8 Open End View

Conclusions and Future Directions

- Completed testing of Phase 1 prototype.
- Fabricated next generation cells.
- Electrically test next generation cells.
- Optimize cell and stack design for maximum power and reliability.
- Evaluate and develop automated mass production processes for cell, module and BOP components.

FY 2007 Publications/Presentations

1. S. D. Vora, "SECA Program at Siemens", Presented at Seventh Annual SECA Meeting, September 12–14, 2006, Philadelphia, PA.

2. S. D. Vora, "Development of High Power Density Seal-less SOFCs", Presented at the 2006 Fuel Cell Seminar, November 13–17, 2006, Honolulu, Hawaii.

3. S. D. Vora, "Development of High Power Density Seal-less SOFCs", to be presented at SOFC-X Symposium, June 3–8, Nara, Japan.

IV. SECA RESEARCH & DEVELOPMENT

A. Materials & Manufacturing

IV.A.1 Evaluation of a Functional Interconnect System for SOFCs

James M. Rakowski
Allegheny Technologies, Inc. (ATI Wah Chang)
Allegheny Ludlum Corp.
Technical and Commercial Center
1300 Pacific Avenue
Natrona Heights, PA 15065
Phone: (724) 226-6383; Fax: (724) 226-6452
E-mail: jrakowski@alleghenyludlum.com

DOE Project Manager: Ayyakkannu Manivannan
Phone: (304) 285-2078
E-mail: Ayyakkannu.Manivannan@netl.doe.gov

Objectives

- Identify and/or develop a metal substrate for a low-cost, high-performance mass production interconnect through environmental exposures and electrical property evaluation.
- Optimize methods for solid-state processing of ferritic stainless steels to remove elements which play a role in degrading electrical performance (primarily silicon).

Accomplishments

- An initial set of novel ferritic stainless steel compositions were melted and processed to thin strip. These were tested for oxidation resistance.
- A second set of ferritic stainless steel compositions have been melted, based on the results of the first iteration and a complementary review of the literature. These are currently being processed to thin strip.
- A novel process was developed to remove silicon from commercially available ferritic stainless steel in the solid state. This process was applied to common ferritic stainless steels, which resulted in the desired effect and improved area specific resistance (ASR) by up to 75% in initial testing.
- Cladding was used to produce multi-layered interconnect structures. These were tested in simulated anode gas (hydrogen-base and methane base) and in dual atmosphere exposures.
- Equipment has been installed for long-term ASR testing and evaluation.

Introduction

The interconnect is a critical part of planar solid oxide fuel cells (SOFCs). The interconnect serves to separate the fuel and oxidant gas streams, and also collects the electrical output of the SOFC. A shift from relatively inert ceramic interconnects to metallic structures has been driven primarily by cost and manufacturing considerations. Interconnect alloy selection has been defined as an important issue impeding the commercialization of SOFCs, with the focus being the use of inexpensive substrates in conjunction with special processing and/or coatings [1]. High temperature degradation has been and remains a significant issue in the application of metallic alloys for interconnect substrates. Oxides in general have reduced electrical conductivity, leading to increased contact resistance as they increase in thickness. These oxides can also react with the surrounding ceramic components, resulting in reduced electrical functionality. The cumulative result is degradation of stack performance over time [2].

Successful metallic alloy-based interconnects will have to address these concerns while minimizing the installed component cost. This may be possible through the use of specially formulated alloys, particularly at lower operating temperatures. Higher operating temperatures may be attainable through the use of more heat-resistant alloys, or notably by the application of oxidation-resistant, electrically conductive coatings [3].

Approach

Commercially available, low-cost stainless steels will be evaluated for suitability as SOFC interconnect substrates. Testing will focus on alloys with moderate chromium contents (16-18%) such as Types 430, 439, and 441HP. Testing and evaluation will focus on general oxidation behavior (notably resistance to accelerated oxidation, in simulated anode gas, cathode air, and dual atmosphere environments) and the evolution of ASR with time for both bare and coated metal substrates using controlled laboratory conditions and in button cell test systems. The effect of silicon removal via post-processing will remain a critical area of investigation, as most inexpensive commercially available alloys inevitably contain a moderate amount of residual silicon (typically 0.4% by weight).

Alloy development will proceed in parallel for applications which call for increased resistance to environmental and electrical degradation. Focus areas

will be the effect of low-cost reactive element additions, moderate control of residual silicon, and slightly higher chromium contents. Initial testing will be on laboratory-scale heats melted to custom compositions and processed to thin strip via hot and cold rolling.

Results

Clad panels were produced using a variety of alloys which are expected to be inert in the anode environment, notably nickel 201 (UNS N02201), oxygen-free copper (UNS C10100), and a commercially produced Ni-32Cu alloy (UNS N04400). Some panels were also clad on the cathode side with oxidation-resistant nickel-base superalloys.

- Testing of clad samples in both hydrogen- and methane-based simulated anode gas atmospheres at 800°C resulted in a significant reduction in weight gain as compared to a Type 430 stainless steel control sample. This is attributable to the clad face exhibiting only minor surface oxidation. However, some internal attack was noted for both the copper and the copper-nickel alloy-clad samples (Figure 1).
- The sample clad with nickel exhibited considerably less degradation under the same exposure conditions (Figure 2).

Post-process thermal and chemical treatments are being investigated in an attempt to improve the performance of typical ferritic stainless steels in the SOFC environment by mitigating the formation of electrically resistive silica at the scale/alloy interface. Samples of Type 430 stainless steel (Fe-16.5Cr-0.3Si) were exposed in wet hydrogen in an attempt to pre-form a thick silica layer at the surface without oxidizing other elements, notably chromium. The initial results were successful, resulting in the formation of a 0.2 micron thick silica layer during a relatively short-term exposure. The expected effect on a ferritic stainless steel substrate is shown in Figure 3. This treatment can be very efficient in removing silicon, particularly for thin (0.1 mm or less) substrates, but the effect becomes marginal for thicker substrates. This is likely to be counteracted somewhat due to the presence of a silicon depletion gradient, but this is difficult to measure quantitatively.

Current work is focused on optimizing this treatment and extending its applicability. Test panels of various commercially available stainless steels (Types 430, 439HP and 441) have been processed and are being characterized using surface science and ASR measurements to determine the effect of processing variables. Larger panels (200 mm on a side) have been prepared and have been sent to researchers at the National Energy Technology Laboratory (NETL) for in-cell testing.

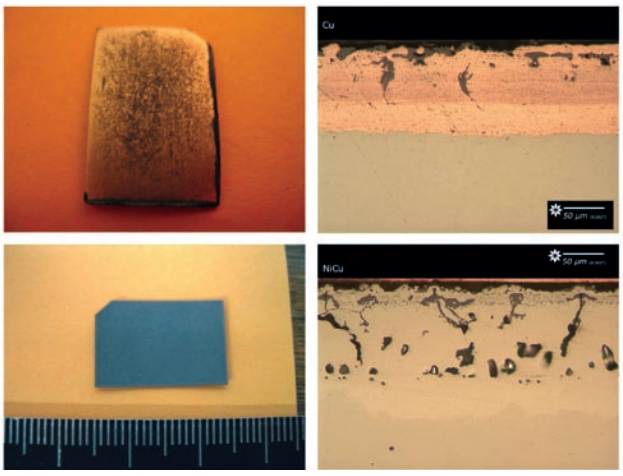

FIGURE 1. Post-exposure images of samples exposed in Ar-4% H_2-3%H_2O at 800°C for 1,371 hrs. (top left) macrophotograph of the Cu-clad surface; (top right) light optical micrograph of the Cu-clad sample cross-section; (bottom left) macrophotograph of the Ni-32Cu-clad surface; (bottom right) light optical micrograph of the Ni-32Cu-clad sample cross-section.

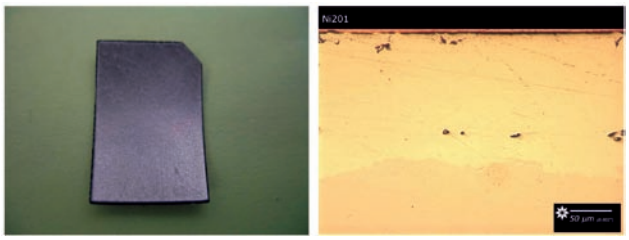

FIGURE 2. Post-exposure images of samples exposed in Ar-4% H_2-10%H_2O at 800°C for 1,221 hrs (left) macrophotograph of the Ni-clad surface; (right) light optical micrograph of the Ni-clad sample cross-section.

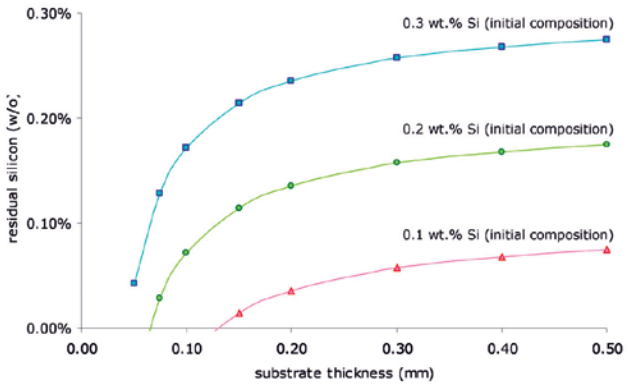

FIGURE 3. Calculated Effect of Silicon Removal Treatment on Ferritic Stainless Steels (Nominally Fe-18Cr) with Different Starting Silicon Levels as a Function of Substrate Thickness

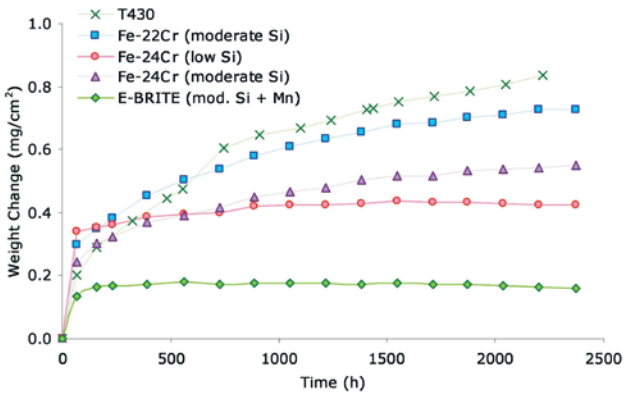

FIGURE 4. Oxidation Test Results for Various Ferritic Stainless Steels Exposed in Air Containing 10 Percent (by Volume) Water Vapor at 800°C

Substrate alloy development continues, based on the results obtained from an initial set of laboratory-scale vacuum induction melting (VIM) heats. Initial heats results of novel and modified stainless steels have been produced and tested in simulated cathode environments (humidified air). Selected results are presented in Figure 4 and are summarized below.

- A heat of T430 with a relatively low silicon content (nominally 0.1%) exhibited good oxidation resistance, but a heat with very low silicon content (nominally 0.03%) exhibited rapid breakaway oxidation.
- A series of alloys with increasing chromium content (18-24%) with relatively low silicon content exhibited a general trend towards decreasing oxidation rate with increasing chromium content.
- Modified E-BRITE®-type alloys containing low silicon and small (0.1%) to moderate (0.4%) manganese additions exhibited low oxidation rates and increased resistance to oxide scale evaporation.

A set of five refined compositions have been melted, cast, and are being processed to light-gauge strip. Two primary alloy families are being investigated, based on the test results from the first set of compositions.

- A superferritic stainless steel based on a modified E-BRITE® composition. The goal is to produce an alloy with the beneficial qualities of E-BRITE® alloy (e.g. very low oxidation rate), while improving the resistance to oxide scale evaporation, resistive oxide formation, and intermetallic phase evolution.
- A specialty ferritic stainless steel, resembling commercially available 16-18Cr alloys but with significant modifications to improve SOFC-specific properties.

Conclusions and Future Directions

- Cladding has been identified as a potential method for improving the performance of the anode-side of a solid oxide fuel cell by eliminating the resistive oxide layer entirely. Commercially pure nickel (Ni201 alloy) in particular appears to be resistant to degradation and also appears to be relatively mechanically and chemically compatible with a ferritic stainless steel substrate when applied as a thin surface layer. No further work is planned for clad structures in the future.
- A post-process, solid-state method for removing silicon from the surface of a ferritic stainless steel has been identified. Process parameters will be refined and the long-term efficacy of the technique will be tested using ASR evaluation.
- Two general compositional ranges for ferritic stainless steel substrates have been identified based on the initial work for this project. A set of five heats has been melted and is currently being processed. The resulting strip material will be extensively tested for oxidation resistance in both anode and cathode environments and for ASR evolution with time. Electrically conductive oxidation-resistant coatings will also be explored as a means for enhancing performance.

Special Recognitions & Awards/Patents Issued

1. U.S. Patent Application filed March 6, 2007 for *Method For Reducing Formation Of Electrically Resistive Layer On Ferritic Stainless Steels*, Serial No. 60/905,219.

FY 2007 Publications/Presentations

1. Quarterly Report for 1st calendar quarter 2007, April 26, 2007.

2. Quarterly Report for 4th calendar quarter 2006, February 27, 2007.

3. Quarterly Report for 3rd calendar quarter 2006, October 31, 2006.

4. Quarterly Report for 2nd calendar quarter 2006, July 27, 2006.

5. *Metallic SOFC Interconnect Systems*, presented at the 7th Annual SECA Workshop and Peer Review, Philadelphia, PA, September 12-14, 2006.

6. Project Fact Sheet Update, August 31, 2006.

References

1. *U.S. DOE Fossil Energy Fuel Cell Program*, W. Surdoval, presented at the 7th Annual SECA Workshop and Peer Review, Philadelphia, PA, September 12-14, 2006.

2. Fuel Cell Handbook, 7th Edition, EG&G Technical Services, Inc. p. 7-6.

3. *SOFC Interconnects and Coatings*, J.W. Stevenson et. al., presented at the 7th Annual SECA Workshop and Peer Review, Philadelphia, PA, September 12-14, 2006.

IV.A.2 Oxidation Resistant, Cr Retaining, Electrically Conductive Coatings on Metallic Alloys for SOFC Interconnects

Dr. Vladimir Gorokhovsky
Arcomac Surface Engineering, LLC
151 Evergreen, Suite D
Bozeman, MT 59715
Phone: (406)522-7620; Fax: (406) 522-7617
E-mail: vgorokhovsky@arcomac.com

DOE Project Manager: Ayyakkannu Manivannan
Phone: (304) 285-2078; Fax: (406)285-4638
E-mail: Ayyakkannu.Manivannan@netl.doe.gov

Objectives

- Enable the use of inexpensive ferritic stainless steels (FSSs) as planar solid oxide fuel cell (SOFC) interconnects (ICs) via advanced physical vapor deposition protective coatings.
- Develop and demonstrate novel, cost-effective coating deposition processes to establish dense and uniform protective and functional coatings on FSS SOFC-IC substrates.
- Evaluate protective coatings during SOFC-IC relevant exposures.
- Optimize coating deposition process parameters to maximize SOFC-IC performance and ultimately reduce cost.

Accomplishments

- Developed and tested novel, hybrid surface engineering technologies combing large area filtered arc deposition (LAFAD), electron beam physical vapor deposition (EBPVD), unbalanced magnetron (UBM) and thermal evaporation to deposit dense, protective coatings in an economical manner.
- Engineered LAFAD coatings to combine favorable electronic conductivity and transport barrier characteristics. Diffusion-barrier amorphous Al and Cr oxide coatings were embedded with electronically conductive Co and/or Mn-containing spinel oxide crystallites.
- Achieved low, stable area specific resistance (ASR) of <50 Ohm•cm^2 for >1,000 hours in 800°C air in contact with porous lanthanum strontium manganate (LSM).
- Significantly reduced Cr volatility. 430 FSS with ~2 µm LAFAD nanocomposite TiCrAlY oxide coating exhibited negligible Cr volatility compared with uncoated counterparts, in spite of the coating containing ~12 at% Cr.
- Demonstrated protective, stable amorphous coatings for sealing areas with high ASR values and negligible chemical or physical changes after >1,000 hours in 800°C air.
- Developed thermochemical modeling of multi-elemental high temperature oxicermet coatings.

Introduction

To achieve Solid State Energy Conversion Alliance (SECA) cost and performance goals, attention has been directed toward inexpensive FSSs as SOFC-ICs. Currently, the SOFC-IC in planar SOFC systems accounts for a dominant portion of the overall stack cost. Inexpensive FSSs meet many SOFC-IC functional requirements; however, during operation, FSSs form blanketing thermally-grown chromium oxide (TGO) scales, which dramatically degrade SOFC stack performance and limit device life-time. To date, deleterious issues with Cr volatility, electrical resistance and thermal-chemical incompatibilities with adjoining components have restricted the use of FSSs as SOFC-ICs. Since 2004, Arcomac Surface Engineering, LLC (ASE) has been engaged in the development of protective and functional coatings on FSSs as SOFC-ICs. ASE has developed advanced coating deposition technologies, which show promise for resolving both SOFC-IC performance requirements in an economically-feasible manner.

Approach

ASE is developing hybrid, filtered arc plasma deposition technologies to establish protective, functional coatings on commercially available FSSs. Coating design is aimed at inhibiting ionic transport and Cr volatility, while retaining low and stable ASR at ~800ºC in air during long-term exposures. Desired coating compositions and architectures are determined through thermodynamic and transport modeling in addition to prior art. Appropriate deposition materials are acquired and deposition processes are designed and performed using ASE patented equipment and technologies. Coated samples are exposed to conditions simulating SOFC-IC operation, and complimentary surface analyses are conducted to evaluate performance. Results are employed to assist in developing new coating deposition process formulations. Promising coating systems from preliminary testing are then subjected to more prototypical SOFC interconnect conditions

for further assessments. Concurrently, economic evaluations of coating process and SOFC-IC fabrication are ongoing.

Results

The patented filtered arc plasma source ion deposition (FAPSID) system developed by ASE utilizes two dual filtered cathodic arc LAFAD sources in conjunction with two UBM sputtering sources, two EBPVD evaporators and a thermal resistance evaporation source in one, universal vacuum chamber layout (as illustrated in Figure 1) [1-4]. This system has demonstrated the capability to deposit nanocomposite, nanolayered coatings with a wide-variety of compositions and architectures. Photographs of uncoated and LAFAD coated (~2 µm TiCoMnCrAlYO) FSS sheets of typical SOFC-IC geometry are shown in Figure 2. The FSS sheets show laser cut specimen tabs used for specific SOFC-IC testing.

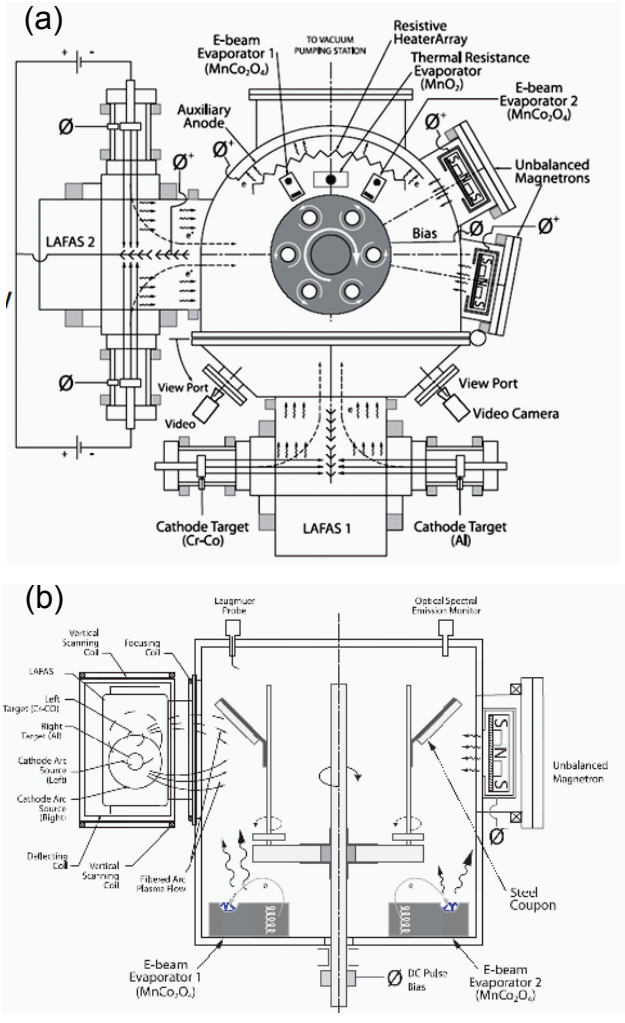

FIGURE 1. Schematic Illustration of the FAPSID Surface Engineering System, Showing (a) Top View; and (b) Side View

The most promising ASE coatings yet identified are LAFAD nanostructured coatings from the MCrAlYO system (where M = Co, Ti, and/or Mn). These coatings are designed to function as effective barriers, blocking both inward and outward ionic diffusion, while providing adequate electronic conductivity through the coating thickness. The transition metal dopants are selected to increase high-temperature electronic conductivity by forming nanocomposite thermistor-like oxicermets. Thermochemical modeling, using the advanced "TERRA" thermodynamic equilibrium calculation code with solid solution considerations, is being used to estimate phase composition of multielemental oxicermet coatings and their interactions with SOFC-IC operating environments. An extensive matrix of LAFAD coatings have been successfully deposited with excellent adhesion to various FSS substrates under consideration for SOFC-ICs. Other hybrid coating deposition methods, employing filtered arc assisted thermal resistance evaporation and filtered arc assisted electron beam evaporation are also being explored.

SOFC IC-relevant behavior of coated and uncoated samples, i.e. high temperature oxidation, ASR, and Cr volatility have been investigated in collaboration with researchers at Montana State University, Pacific Northwest National Laboratory (PNNL), Lawrence Berkeley National Laboratory (LBNL) and NASA-Glenn Research Center. Summary ASR data from FSS uncoated and with four different LAFAD coatings is shown in Figure 3. The ASR of the uncoated FSS continues to increase due to the growth of the chromia-based TGO scale. The ASR of the coated specimens generally decreases and stabilizes. The decrease is attributed to the restructuring of the as-deposited amorphous coating into a polycrystalline film. The stability is attributed to the transport-barrier properties of the coatings, whose thicknesses and chemical composition do not change appreciably during the 1,000 hour ASR test. LAFAD coatings with Co and/or

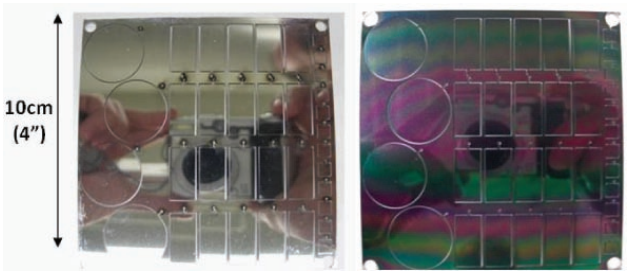

FIGURE 2. Photographs of Uncoated (left) and Coated (right) FSS Sheets (100 x 100 x 1 mm) with Laser Cut Specimen Tabs of Various Testing Geometries

Mn exhibit significantly lower initial ASR than those without. The TiCrAlYO and CrAlYO coatings are permeable to the high-oxygen-affinity Mn from the FSS, and evolve percolating networks of conductive Mn-containing oxides, thus lowering the ASR over time.

Figure 4 displays a summary of Cr volatility results from uncoated and LAFAD TiCrAlYO coated FSS. The graph displays the cumulative amount of Cr collected during the test. The uncoated FSS continues to volatilize Cr throughout the test, while the coated specimen demonstrates negligible Cr volatility after the first 24 hours. This coating contains ~12 at% Cr; however, the Cr is apparently sequestered in a solid solution with complex Al-containing oxides, which agrees well with thermochemical modeling.

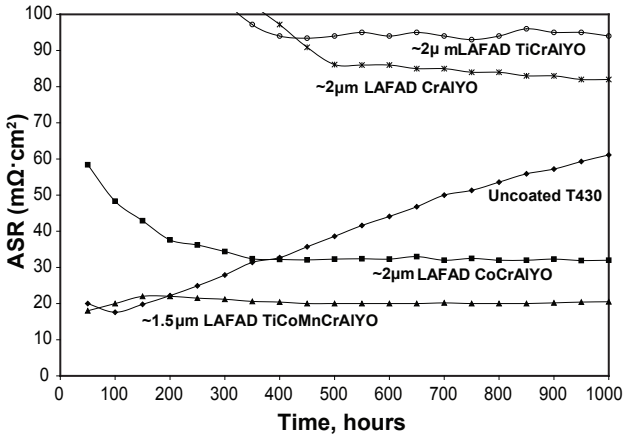

FIGURE 3. Summary ASR Data for Uncoated and Three Different LAFAD MCrAlYO Coated FSS

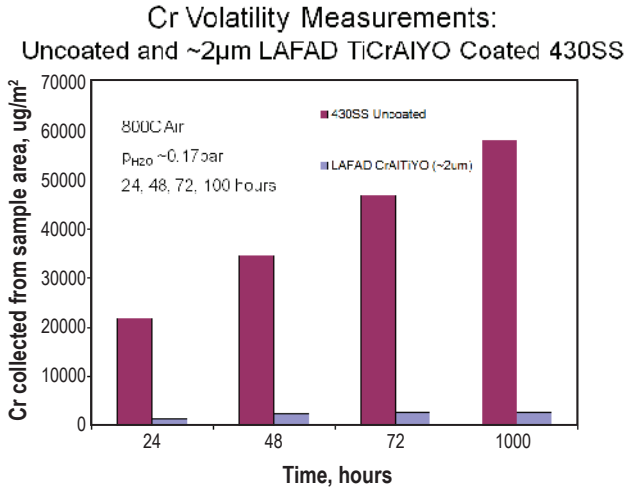

FIGURE 4. Cumulative, Time-Dependant Cr Volatility Data for Uncoated and TiCrAlYO Coated FSS

Conclusions and Future Directions

ASE has developed advanced coating deposition processes, which may enable the use of inexpensive metallic alloys as interconnect components in planar SOFC systems. Nanostructured oxicermet coatings, deposited by hybrid filtered arc assisted techniques are being investigated to meet SECA SOFC-IC performance and cost requirements. A large-scale FAPSID surface engineering process, offering favorable economics through high yield and advanced hybrid design, is under investigation for deposition of protective coatings on SOFC-ICs. Based upon success with similar physical vapor deposition (PVD) processes, cost estimates for this process at full-scale production reach ~$0.10 per SOFC-IC. Future work will focus on cross comparison with other coatings on identical FSS samples and testing in short SOFC stacks. Coating composition and architecture will be continually optimized to further improve thermal-chemical and mechanical stability, transport barrier properties and low ASR during long-term operation.

FY 2007 Publications/Presentations

1. "Deposition and evaluation of protective PVD coatings on ferritic stainless-steel SOFC interconnects" V.I. Gorokhovsky, P.E. Gannon, M.C. Deibert, R.J. Smith, A. Kayani, M. Kopczyk, D. VanVorous, Zhenguo Yang, J.W. Stevenson, S. Visco, C. Jacobson, H. Kurokawa, and S.W. Sofie, *Journal of Electrochemical Society* 153 (10) A1886-A1893 2006.

2. "Enabling inexpensive alloys as SOFC interconnects: an investigation into hybrid coating technologies to deposit nanocomposite functional coatings on ferritic stainless steels" P.E. Gannon, V.I. Gorokhovsky, M.C. Deibert, R.J. Smith, A. Kayani, P.T. White, Z. Gary Yang, D. McCready, S. Visco, C. Jacobson, and H. Kurokawa, *International Journal of Hydrogen Energy* In-press.

3. "Oxidation resistance of magnetron-sputtered CrAlN coatings on 430 steel at 800°C" A. Kayani, T.L. Buchanan, M. Kopczyk, C. Collins, J. Lucas, K. Lund, R. Hutchison, P.E. Gannon, M.C. Deibert, R.J. Smith, D.-S. Choi, and V.I. Gorokhovsky, *Surface and Coatings Technology* 201, n. 7 SPEC. ISS., December 20, 2006, p. 4460–4466.

4. "Chromium volatility of coated and uncoated steel interconnects for SOFCs" C. Collins, J. Lucas, T.L. Buchanan, M. Kopczyk, A. Kayani, P.E. Gannon, M.C. Deibert, R.J. Smith, D.-S. Choi, and V.I. Gorokhovsky, *Surface and Coatings Technology*, v. 201, n. 7 SPEC. ISS., December 20, 2006, p. 4467–4470.

5. "Oxidation studies of CrAlON nanolayered coatings on steel plates" A. Kayani, R.J. Smith, S. Teintze, M. Kopczyk, P.E. Gannon, M.C. Deibert, V.I. Gorokhovsky,

V. Shutthanandan, *Surface and Coatings Technology* 201, n. 3–4, October 5, 2006, p. 1685–1694.

6. "Overview of current trends in SOFC materials" in New Developments in Advanced Functional Ceramics Massimo Viviani, Paolo Piccardo, Antonio Barbucci, Daria Vladikova, Zdravko Stoynov, Vladimir Gorokhovsky and Paul Gannon, 2007: ISBN: 81-7895-248-3 Editor: Liliana Mitoseriu.

7. "Advanced PVD Nanocomposite Protective Coatings for SOFC Metallic Interconnects" Invited Presentation - TMS Annual Meeting; February 25 – March 1, 2007; Orlando, FL.

References

1. V.Gorokhovsky, US Pat. No. 6,663,755 B2.

2. V.Gorokhovsky, US Pat. Application No. 20040168637A1.

3. V.I. Gorokhovsky, P.E. Gannon, M.C. Deibert, R.J. Smith, A. Kayani, M. Kopczyk, D. VanVorous, Zhenguo Yang, J.W. Stevenson, S. Visco, C. Jacobson, H. Kurokawa, and S.W. Sofie, *Journal of Electrochemical Society* 153 (10) A1886-A1893 2006.

4. http://www.arcomac.com

IV.A.3 SOFC Research and Development in Support of SECA

Michael Krumpelt (Primary Contact), Terry A. Cruse and Brian D. Ingram
Argonne National Laboratory
Argonne, IL 60439
Phone: (630) 252-8520; Fax: (630) 252-4176
E-mail: krumpelt@cmt.anl.gov

DOE Project Manager: Lane Wilson
Phone: (304) 285-1336
E-mail: Lane.Wilson@netl.doe.gov

Objectives

- Explore the effects and mechanisms of chromium migration in solid oxide fuel cells (SOFCs).
- Explore cathode formulations that mitigate the effects of chromium.

Accomplishments

- The effects of temperature and current density on the chromium oxide deposition rates were determined.
- A cathode material with 20% improved maximum power density was found.

Introduction

Chromium contamination of SOFC cathodes has been observed by several groups of researchers developing cells with metallic bipolar plates. Hilpert et al have attributed the chromium transport to the formation of a volatile oxyhydroxide species that forms when chromium-containing steels are exposed to oxygen and water at elevated temperatures [1, 2]. The volatile oxyhydroxide, $CrO_2(OH)_2$, can form either by reaction of the surface oxide with oxygen and water, or by direct reaction of metallic chromium [3]. It has also been shown that $CrO_2(OH)_2$ is the dominant species in the gas phase when water is present [4], and that the cathode acts as a nucleation site for the deposition of chromium [5]. Quadakkers et al provide an overview of this and other issues related to metallic-based interconnects [6]. There is also work that indicates that both the cathode and electrolyte composition can play a role in chromium poisoning [7, 8].

As discussed by Hilpert and others [9, 10] the chromium oxyhydroxide is presumed to be reduced to chromium trioxide at the triple phase boundaries in the cathode as shown:

$$2CrO_2(OH)_2 + 6e^- + 3V_o^{\bullet\bullet} = Cr_2O_3 + 2H_2O + 3O^{2-}$$

The oxide deposits block the access of oxygen to the electrochemically active sites and cause the performance decay of the cell. However, the magnitude of the effect varies greatly between cells and stacks from various organizations. In last year's work, we showed that a steady state cell performance degradation of 5% in 1,000 hours occurs in cells with E-BRITE® interconnects at 800°C [11]. We unequivocally identified chromium oxide deposits near the electrolyte interface and manganese chromium spinel near the metal interface. Only the first is responsible for the cell potential decline. In the present work, the effects of temperature and current density on the chromium oxide deposition are quantified and results with an improved cathode are presented.

Approach

The same experimental apparatus as discussed last year was used. Briefly, the fuel cell housing is a two-piece circular structure made of alumina (last year Macor® was used initially but proved to be unsuitable) that contains a 2.5-cm^2 metal current collector with five flow channels. Under the channels is a fuel cell consisting of a lanthanum manganite cathode, a zirconia electrolyte and a nickel/zirconia anode. These cells were purchased from InDEC. To define the effects of current density four cells were run at 0, 184, 367 and 735 mA/cm^2, respectively. All cells had an air flow of 160 standard cubic centimeters per second and a temperature of 700°C for 500 hours; another series was tested at 800°C.

As a follow-up of last year's work, showing chromium oxide deposits at the triple phase boundaries, we tested cathodes that had various amounts of chromium added deliberately to the lanthanum manganite. Up to 22% of the manganese was substituted with chromium and the powder was screen printed onto anode supported substrates, sintered and tested.

Results

The effects of current density at 800°C are shown in Figure 1. Without any applied current, the cell potential held steady, but when current was flowing, the potentials decline asymptotically to a steady state rate, which clearly increases with current density. Although not shown here, the effect is linear.

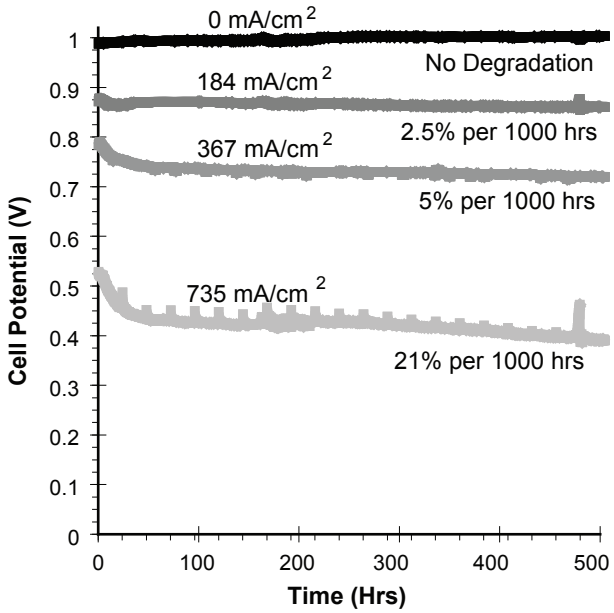

FIGURE 1. Effects of Current Density on Cell Potentials

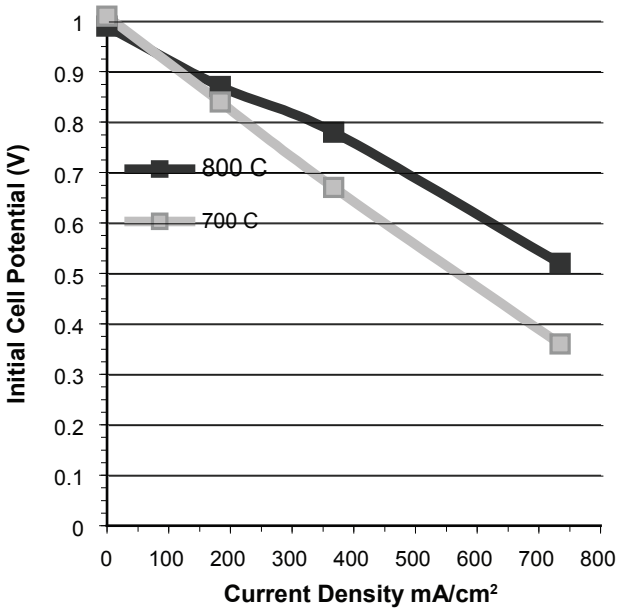

FIGURE 3. Initial Cell Potentials before Degradation

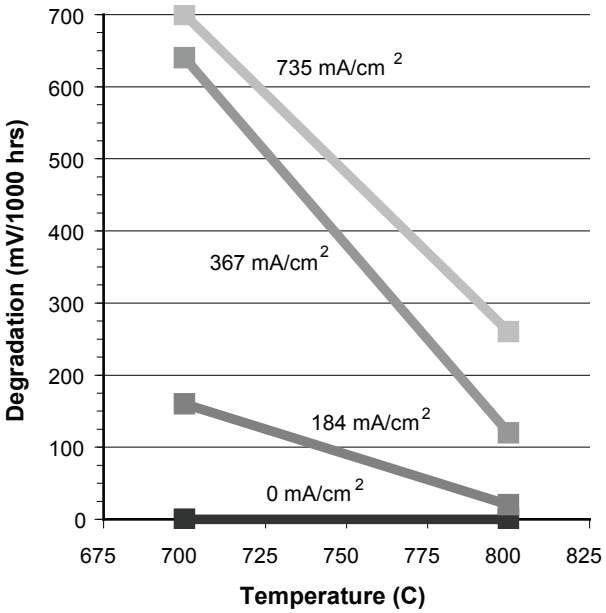

FIGURE 2. Degradation Rates at 800 and 700°C

Figure 2 gives the steady state degradation rates at 800 and 700°C. The degradation rates increase as the temperature is lowered, but the change is more dramatic than one would anticipate from the thermodynamics of the chromium oxyhydroxide formation.

An indication for the reasons can be inferred from Figure 3. Here, the initial cell potential before chromium poisoning sets in is plotted versus current density at 700 and 800°C. Consistent with thermodynamics, the cell potential is slightly higher at 700 than at 800°C at the open circuit potential. With current flowing, the cell potentials are much lower at 700 than at 800°C, indicating that the polarization resistance is much higher because the strontium doped lanthanum manganite (LSM) cathodes are considerably less active.

These effects are discussed below, but a surprising and encouraging result was obtained from testing the chromium substituted cathodes. As shown in Figure 4, the cell performance improved by 18%.

Discussion

Current density is clearly a major factor in the deposition of chromium oxide and one needs to ask why? Either the rate of deposition of Cr_2O_3 is dependent on the cell potential which changes with current density, or it is controlled by transport of the oxyhydroxide. There would appear to be at least four independent transport mechanisms for the chromium oxyhydroxide in an operating SOFC. First, it desorbs from the metal surface where it forms. Second, it diffuses through the streaming gas in the flow channel. Third, it diffuses through the pores of the inactive cathode, and forth it diffuses to the surface of the triple phase boundaries.

The first is not current density dependent since formation is not an electrochemical process. The second is largely influenced by fluid dynamics in the channel and again not significantly affected by the current density. The fourth mechanism would be expected to follow Buttler-Volmer kinetics and increase with overpotential, but since the concentration of the oxyhydroxide is extremely low, at only one molecule per

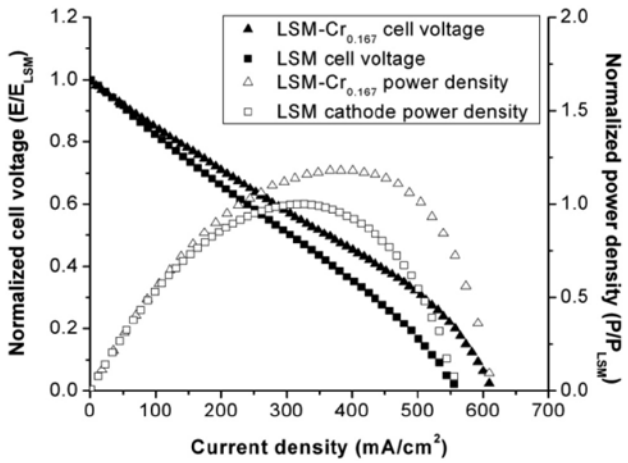

FIGURE 4. Voltage and power density values as a function of current density for a cell operated at 800°C after 500 hours. Typical cells were used with cathodes of LSM and LSM-$Cr_{0.167}$ (i.e., $(La_{0.8}Sr_{0.2})_{0.99}Mn_{0.883}Cr_{0.167}O_{3-\delta}$). Values are normalized to LSM results.

ten million oxygen molecules, it will be diffusion limited and not potential driven.

Since the experimental evidence shows a linear correlation with current density, it appears that the oxyhydroxide flux is coupled to the flux of oxygen to the triple phase boundaries or though the pores of the cathode.

The effect of temperature on the chromium deposition as shown in Figure 2 is equally dramatic. Hilpert had looked at the thermodynamics of the oxyhydroxide formation and found only minor differences between 700 and 800°C. However, it is well known that lanthanum manganite cathodes lose a significant amount of there activity when the temperature is decreased below 800°C as is also evident in Figure 3. Since the effect of chromium tracts more closely with the decline in initial cell potentials rather than the thermodynamics of oxyhydroxide formation, it stands to reason that the diminished triple phase boundary area at the lower temperature is blocked more fully by the chromium oxide.

The results in Figure 4 are an exiting and unexpected finding. Since chromium oxide can react chemically with the cathode material, we were initially concerned that chromium on the surface of the manganite might adversely influence the charge transfer reaction of the oxygen. The opposite appears to be the case.

Conclusions and Future Directions

The results presented in this report seem to raise concerns about the effects of chromium at lower temperature and higher current densities. However, we need to remember that these results were obtained with uncoated E-BRITE® and coated material would have two orders of magnitude lower formation rates of the oxyhydroxide. More importantly, the dramatic effects of the chromium precipitation at lower temperature point to the solution to the problem. We need more active cathodes.

The results with the chromium doped manganite show already that the currently preferred cathode material can still be improved, and ferrites or mixed manganese/iron cathode would be much less affected because of the higher oxide ion vacancy concentration and mobility.

References

1. Hilpert, K., D. Das, M. Miller, D. H. Peck, and R. Wei, *J. Electrochem. Soc*., **143**, 3642, (1996).

2. Gindorf, C., L. Singheiser, and K. Hilpert, *Steel Research*, **72**, 528 (2001).

3. Fryburg, G., F. Kohl, and C. Stearns, *J. Electrochem. Soc.*, **121,** 952 (1974).

4. Ebbinghaus, B. B., *Combustion and Flame*, **93**, 119 (1993).

5. Jiang, S. P., et al., *J. European Ceramic Society*, **22**, 361 (2002).

6. Quadakkers, W. J., J. Piron-Abellan, V. Shemet, and L Singheiser, *Materials at High Temperatures*, **20**,115 (2003).

7. Matsuzaki, Y., and I. Yasuda, *J. Electrochem. Soc*., **148**, A126 (2001).

8. Kaun, T. D., T. A. Cruse, and M. Krumpelt, *Ceramic Engineering and Science Proceedings*, **25** (2004).

9. Jiang, S. P., *J. Power Sources*, **124**, 390 (2003).

10. Matsuzaki,Y. and I. Yasuda, *J. Electrochem. Soc.,* **148**, A126 (2001).

11. T.A. Cruse, B. J. Ingram, Di-Jia Liu, M. Krumpelt, ECS Transactions, 5 (1) 355-346 (2007).

FY 2007 Publications/Presentations

1. M. Krumpelt, T. A. Cruse, B. J. Ingram, Chromium volatility and transport in SOFCs, 2006 Fuel Cell Seminar, Honolulu, November 19, 2006.

2. B. J. Ingram, T. A. Cruse, M. Tetenbaum, and M. Krumpelt, "Effects of chromium interactions with LSM-based cathodes in solid oxide fuel cells" Materials Science and Technology Meeting and Exposition, Cincinnati, OH, October 15-19, 2006.

3. T. A. Cruse, B. J. Ingram, D. -J. Liu and M. Krumpelt, "Chromium reaction and transport in solid oxide fuel cells," *ECS Transactions*, **5**(1), 335 (2007).

4. M. Krumpelt, T. A. Cruse, and B. J. Ingram, "Chromium Volatility and Deposition in SOFCs," American Ceramic Society, Cocoa Beach, FL, January 22-27, 2006.

IV.A.4 SOFC Cathode Surface Chemistry and Optimization Studies

Prof. Paul A. Salvador (Primary Contact), Joanna Meador, Balasubramaniam Kavaipatti
Carnegie Mellon University
Department of Materials Science and Engineering
Pittsburgh, PA 15213
Phone: (412) 268-2702; Fax: (412) 268-7596
E-mail: paul7@andrew.cmu.edu

DOE Project Manager: Lane Wilson
Phone: (304) 285-1336; Fax: (304)285-4638
E-mail: Lane.Wilson@netl.doe.gov

Collaborators: Drs. Paul Fuoss, Jeff Eastman, Dillon Fong, and Peter Baldo
Argonne National Laboratory (ANL)
9700 South Cass Avenue
Argonne, IL 60439-4837
Phone: (630) 252-3289; Fax: (630) 252-9595
E-mail: fuoss@anl.gov

Objectives

- To determine the key correlations between surface features and electrochemical performance for solid oxide fuel cell (SOFC) cathodes.
- To develop and to employ a high throughput chemical screening methodology that provides a sensitive measure of activity/stability in operational conditions.
- To develop thin film samples having specific surface structures and chemistries using thin film preparation methods.
- To determine the stability of engineered surface chemistries as a function of thermodynamic parameters (temperature [T], pressure [P], ε, and electrochemical parameters).
- To determine the effects of engineered surface chemistries on oxygen uptake kinetics in thin film samples.

Accomplishments

- Epitaxial thin films of $LaMnO_3$, $SrMnO_3$, $La_{0.7}Sr_{0.3}MnO_3$ (LSM) were grown on various substrates, both with and without different surface layers and with and without epitaxial strain. These serve as the basis for providing samples to other tasks and collaborators.
- Epitaxial thin films were investigated with X-rays using the Advanced Photon Source (APS) at ANL and both the bulk structure of the films and their surface chemical compositions were determined as a function of T and P. These provide the initial understanding of the physicochemical response of LSM to various thermodynamic parameters.
- Showed that films exhibited superstructures consistent with unit cells doubled in all three dimensions (as compared to the simple perovskite) and exhibiting a complex microtwinning; the superstructure/microtwins persisted from room temperature to 700°C.
- Demonstrated that the surface of LSM films are Sr-rich and that Sr surface segregation is a function of P. Sr segregation was observed to increase with decreasing P.

Introduction

The cathode in SOFCs is responsible for the reduction of O_2 gas and its incorporation into the electrolyte. To accomplish this, most SOFCs use a three-phase composite for the active cathode region. The three phases are commonly: LSM and yttria-stabilized zirconia (YSZ) as solid phases and O_2 as a gas in pores. When SOFCs are operated at specific current densities/voltages, the oxygen incorporation (or uptake) process can contribute significantly to the losses of the cell, thereby limiting the performance of the SOFC system. Two major options exist for improving the cathode performance by specifically targeting the oxygen incorporation process: changing the component solid materials or adding yet another material (a catalyst) to the existing frameworks. We aim to address both approaches in this work by: (1) developing an experimental program that allows us to probe the nature of atomic scale surface chemistry and its role in oxygen incorporation in LSM and related cathode materials, and (2) determining the optimal catalyst chemistry from both an activity and stability perspective. Realizing these goals will lead to improved cathode performance in SOFCs and an acceleration of introduction of new materials into SOFCs to allow for the DOE Solid State Energy Conversion Alliance (SECA) program to meet performance metrics.

Generally speaking, the limitations in designing highly active cathodes for oxygen incorporation arise from the general lack of direct correlations between surface/interface chemistry/structure and performance of SOFC cathode materials. In other words, very little is quantitatively known about why specific materials/surfaces behave the way they do in SOFC operating conditions. To fill this gap, one must probe the nature of atomic scale surface chemistry or interface

crystallography in fuel cell operating conditions. In this work we aim to realize this by: (1) developing a high throughput screening methodology that will provide a sensitive measure of activity/stability in operational conditions, and (2) determining key correlations between structure (solid state atomic, electronic, crystallographic, and chemical) and electrochemical performance (mass and charge transfer) parameters in surface engineered samples. Several important collaborations have been developed to realize these goals, including that between Carnegie Mellon University (CMU) and ANL, where thin film samples developed at CMU are investigated using high-energy synchrotron X-ray techniques at the APS. This project began in May 2007 and, since it is only a few months old, we will describe in some detail the experiments that are being developed as well as initial observations. Results from detailed structural investigations carried out at CMU and ANL will be highlighted in this initial report.

Approach

A key part of an experimental program that can address the above stated goals is the development of samples that allow both for controlled changes in surface chemistry and for screening experiments to be carried out upon them. Epitaxial and textured thin films are ideal samples for these experiments. To screen for structure-performance correlations, we will produce single-crystal and textured thin film samples using pulsed laser deposition (PLD) and hybrid (laser or standard) molecular beam epitaxy (MBE) approaches to produce thin, flat films having surfaces of specific terminations. Figure 1a shows a schematic of a surface engineered thin film sample. The green inner layer represents the bulk of the thin film or, in oxygen uptake experiments, the reservoir to be filled. The red outer layer represents the surface of the thin film or, in oxygen uptake experiments, the active surface being investigated. By systematically depositing various surface (red) layers on specific bulk (green) layers, we can achieve the goals listed above - determining key correlations between surface structure and electrochemical performance. Figure 1b is a structurally-engineered sample of related composition to LSM: praseodymium strontium manganate (PSM) where the sample is separated into layers of praseodymium manganese oxide (PMO) and strontium manganese oxide (SMO) two unit cells thick [1], demonstrating that such engineering is stable for a length of time to make structural and physical property measurements. In the future, we will develop several physical property measurement techniques that monitor the kinetics of oxygen uptake for a specific reservoir layer as a function of the composition of the surface-active layer. By combining such observations with detailed structural analyses we will develop the above-described key correlations. By generating a large number of

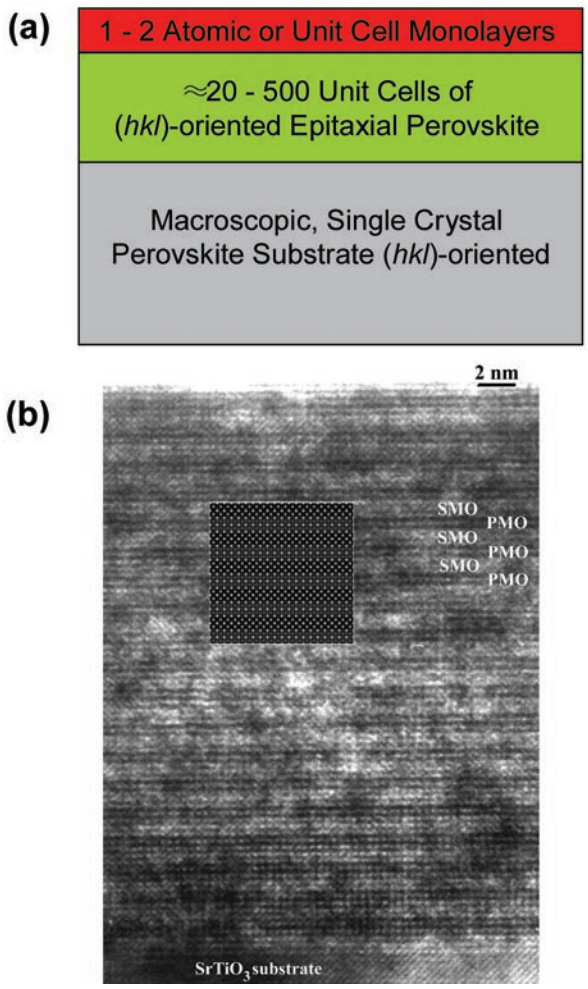

FIGURE 1. Engineered thin film samples of (a) a schematic of a surface engineered thin film cathode material, where the red layer is the surface active layer a few unit cells thick and the green layer is the bulk reservoir in which the oxygen concentration is being altered. (b) A TEM image of a PMO/SMO engineered film [1] made with PLD-MBE having spatially separated regions only two unit cells thick.

well-controlled thin film samples, we will have a high-throughput screening process that probes the identified key correlation.

To establish a baseline in understanding the bulk and surface structure of LSM, epitaxial LSM samples were grown using PLD on different single crystal perovskite substrates ($SrTiO_3$, $NdGaO_3$, YSZ, and $DyScO_3$). The films were characterized for their growth rate, surface roughness, and structural nature at CMU using X-ray techniques and atomic force microscopy (AFM). Certain representative samples were sent to ANL and were characterized at the APS using *in situ* X-ray scattering observations, while the films were exposed to various T and P environments. An environmental chamber was used that allowed for grazing incidence X-ray scattering and depth sensitive

X-ray fluorescence measurements to be made over a T range from room temperature (RT) to 700°C and a P range from 0.01 to 100 Torr. The observations made on these epitaxial films provide a basic scientific understanding for how LSM behaves and provide important structural information that will enable a better understanding to interpret physical property observations.

Results

Figure 2 shows the calibration experiments carried out at CMU that demonstrate the high quality of the films; this film is an LSM film deposited on $SrTiO_3$(100) at 700°C in 50 mTorr O_2 and cooled in 300 Torr O_2; it has a thickness of 310 Å. Figure 2a shows an AFM image of the film which has an rms roughness of 4.4 Å, or about one unit cell. This image indicates that unit-cell rough films can easily be obtained for the bulk of the film. It also implies that, by depositing two or more unit cells atop the bulk, the surface chemistry can be easily modified (as also shown in Figure 1b). It should be noted that small particulates are sometimes observed in the films, as is well known for PLD produced films. These can be removed by optimizing processing; in the future we will explore their effects on the results and remove them as necessary. Figure 2b shows the X-ray reflectivity scan and a refined fit to the scan. The excellent agreement between fit and data allows for structural parameters to be established with confidence: the thickness of this film was 310 Å and the X-ray roughness was 3.1 Å, in agreement with the AFM roughness. The growth rate was determined to be 0.115 Å/pulse, and this allows us to design specific thicknesses of the bulk-layer and surface layers in engineered thin films. Finally, Figure 2c shows the Θ-2Θ X-ray diffraction scan for this film, demonstrating that a single out-of-plane orientation exists, corresponding nominally to the expected cube-on-cube epitaxy considering both the substrate and the film are perovskites. Such observations provide the routine information that ensure films used in the high-throughput screening experiments, and other physical property measurements, are of high-quality and are similar to other samples.

It should be noted that similar results have been obtained on other substrates (high quality film growth with flat surfaces and cube-on-cube arrangements) for $LaAlO_3$, $NdGaO_3$, and $DyScO_3$. The latter two are of extreme interest because they have very high crystal qualities (much lower dislocation densities than $SrTiO_3$) and contain no similar elements to the targeted cathode materials, both of which improve our ability to understand the native surface activity of materials. Films of different thicknesses had different levels of strain states and phi scans are also routinely carried out to quantify the strain state of the films. Nevertheless, it is challenging to obtain a full X-ray data set that allows for the determination of the detailed structure of our films using this type of X-ray source.

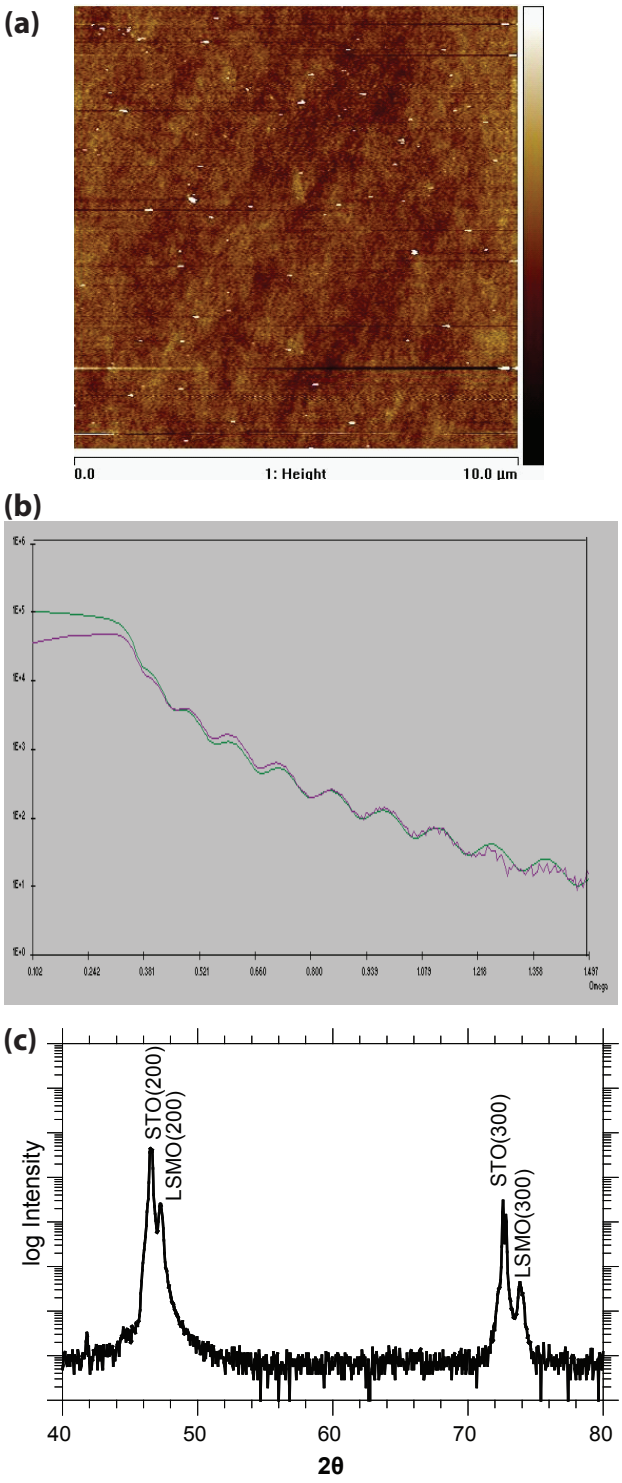

FIGURE 2. Standard calibration measurements of LSM films on $SrTiO_3$(100). (a) An AFM scan, (b) an X-ray reflectivity scan, and (c) a Θ=2Θ X-ray scan.

As a starting point for understanding the structures of surface engineered thin film samples, we explored

the nature of the bulk crystallography and surface chemistry of pure LSM single crystal epitaxial films with thicknesses of 5 to 75 nm grown by PLD on $SrTiO_3$ (001) substrates using X-ray scattering at the APS. Two important observations have been made that are relevant to our goals. First, a stable structural distortion (with respect to the basic perovskite sub-cell) was observed in the epitaxial films that was not observed in bulk powders and, second, Sr-segregation to the film surface was observed, and it was dependent on P. The former observation is of interest in determining the structural behavior of bulk layers in different thermodynamic conditions (T, P, ε) which represent the reservoir to be filled with O_2 during oxygen incorporation experiments. For epitaxial films, the strain state can be further engineered, which allows us to explore this parameter in a systematic fashion. LSM grains in active cathodes experience a range of thermal stresses and may have significant local strains. The latter observation is of interest since it implies that even pure LSM films have some spatial inhomogeneities similar to that shown in Figure 1a. In other words, the surface-active layer in LSM is of a different chemistry than the bulk of the film, and this is a function of P.

Half-order Bragg reflections (*e.g.*, 3/2, 1/2, 1/2), were observed that indicate the unit cell periodicity is double that of the normal unit cell in all three dimensions. We have also found evidence of satellites to the half-order peaks indicating another periodic long-ranged structural modulations in LSM thin films. Figure 3 shows the intensity of one such half-order peak (3/2 -1/2 1/2) as a function of temperature during cooling; satellites are also observed adjacent to these half-order peaks. Both the satellites and the half-order peak intensify as room temperature is approached. While we have not yet fully determined the atomic structure associated with these features, the unit cell doubling is consistent with an antiferrodistortive orbital ordering (albeit at much higher temperatures than typically observed in LSM) and the satellites are consistent with microtwinning (albeit exhibiting a slightly more complex domain pattern than previously reported). Figures 3b and 3c demonstrate that the symmetry of satellite distributions varies for different 1/2-order peaks, indicating a three-dimensionally-complex domain structure to the microtwins.

We also observe Sr segregation to the surface of these epitaxial single crystal LSM (001)-oriented films. Moreover, surface segregation increases with decreasing oxygen partial pressure. The near surface chemical signatures are shown in Figure 4 and one can observe that while the Sr signal increases on decreasing P, the La and Mn signals decrease. Interestingly, the structural modulations described above persist after this rearrangement takes place, implying that the surface crystal structure remains the same on changing P but that the surface chemistry does not. This type of P-dependant segregation is important to understanding both surface activity and surface stability in cathodes, both of which are essential in obtaining highly active and stable cathode materials. In the future we will correlate the surface chemistry to activity using our engineered thin film samples and explore their stabilities using the APS and other techniques, such as Auger electron spectroscopy (AES) and X-ray photoelectron spectroscopy (XPS).

Conclusions and Future Directions

We have demonstrated that surface engineered films of cathode materials can be produced and characterized in detail for the structural and chemical properties. Even for pure epitaxial LSM films, surface segregation occurs that is a strong function of the thermodynamic variables, although the crystal structure does not appear to be strongly perturbed. As this project only began in

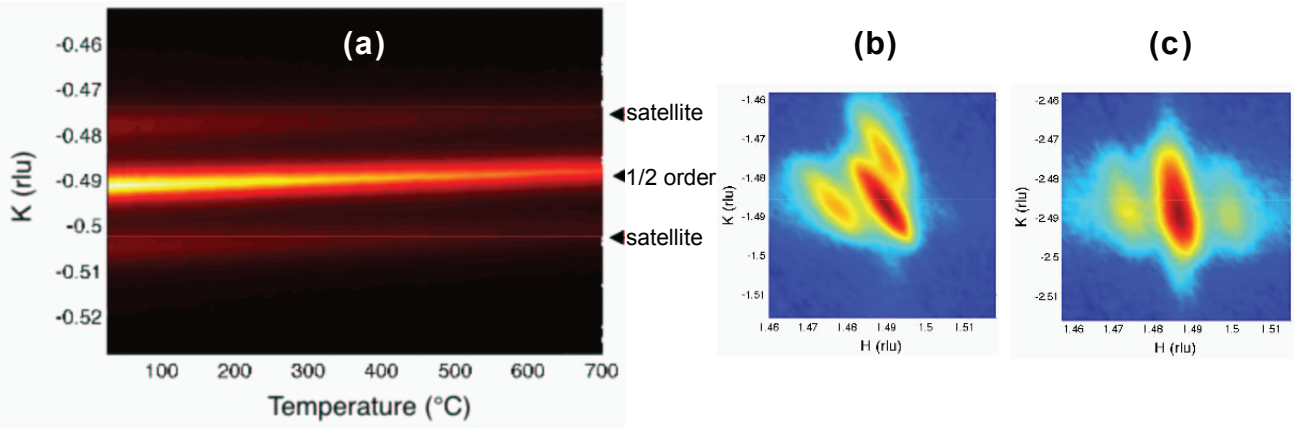

FIGURE 3. X-ray scattering data of a 5.8 nm thick LSM film grown epitaxially on $SrTiO_3$(001). (a) Temperature dependence of the 3/2 -1/2 1/2 peak and satellites. (b) and (c) In-plane reciprocal space maps centered on the 3/2 -3/2 1/2 and 3/2 -5/2 3/2 peaks.

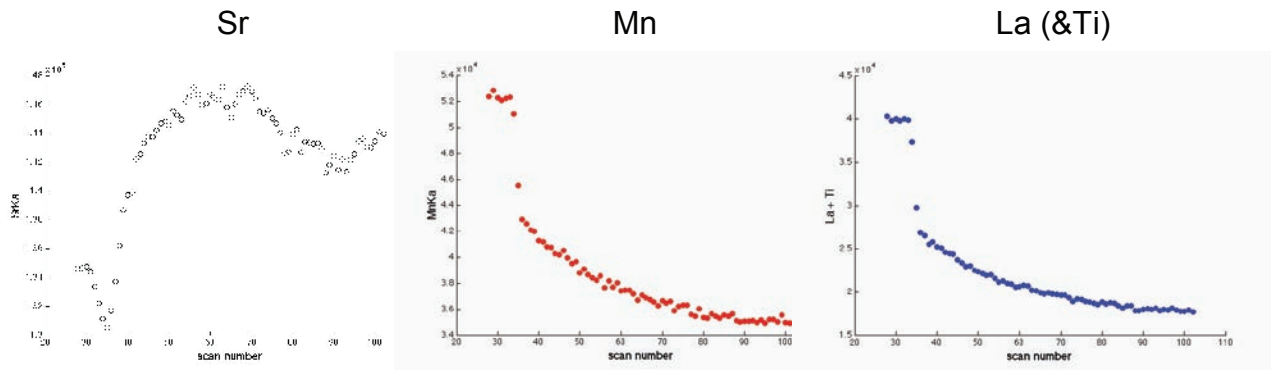

FIGURE 4. Chemical signatures using X-ray fluorescence of the near surface region on changing pO_2 from 100 Torr to 0.01 Torr. The count number is related to time. The kinetics are likely associated with the time to equilibrate the atmosphere, which was changed near count ≈30.

May 2007, significant portions of the goals remain to be realized. We will produce a series of surface engineered films and will investigate: (1) their structural properties, (2) their stabilities, (3) their oxygen uptake kinetics using specially designed crystal microbalances and electronic conductivity rigs, and (4) will investigate how electrochemical parameters affect segregation/activity. By fabricating a matrix of related materials and carrying out these measurements, we will be able to provide a large amount of data to determine the key parameters that correlate surface structure to surface activity.

Reference

1. B. Mercey *et al.*, *Journal of Applied Physics*, 94(4), 2716-2724 (2003).

IV.A.5 Investigations of Cr Contamination in SOFC Cathodes Using TEM

Prof. Paul A. Salvador (Primary Contact)
and Dr. Shanling Wang
Carnegie Mellon University
Department of Materials Science and Engineering,
5000 Forbes Ave.
Pittsburgh, PA 15213
Phone: (412) 268-2702; Fax: (412) 268-7596
E-mail: paul7@andrew.cmu.edu

DOE Project Manager: Lane Wilson
Phone: (304) 285-1336
E-mail: Lane.Wilson@netl.doe.gov

Collaborators:
Dr. Michael Krumpelt and Dr. Terry A. Cruse
Argonne National Laboratory (ANL)
9700 South Cass Avenue
Argonne, IL 60439-4837
Phone: (630) 252-8520; Fax: (630) 252-4176
E-mail: krumpelt@cmt.anl.gov

Objectives

- To develop a straightforward sample preparation method using a focused ion beam (FIB) to produce transmission electron microscopy (TEM) specimens from specific regions of solid oxide fuel cells (SOFCs) exposed to different operating conditions.
- To carry out TEM investigations on SOFCs provided by ANL collaborators to determine the local microstructure/chemistry associated with Cr contamination.
- To understand better the mechanism of Cr contamination in the active (mixed) cathode region of SOFCs.

Accomplishments

- Developed FIB technique to reliably produce TEM specimens from the mixed lanthanum strontium manganate/yttria-stabilized zirconia (LSM/YSZ) (or active) cathode region of SOFCs, either under the flow channel or under the contact (landing) in ribbed interconnects.
- Determined the local microstructures and Cr-containing phases in various regions of six different fuel cells, each run for 500 hours but each run under different operating conditions (temperature and current density).
- Analyzed chemical composition and crystal structures of Cr-containing phases using energy dispersive spectroscopy (EDS), electron energy loss spectroscopy (EELS), selected area electron diffraction (SAED), and scanning transmission electron microscopy (STEM).
- Demonstrated that the highest contamination points were directly under the interconnect contact and near the electrolyte; evidence of contamination decreased quickly away from these areas.
- Established the signature of degradation as the existence of nanoparticles ($d<100$ nm) on solid surfaces (YSZ and/or LSM); the local number density, size, and chemical composition of such nanoparticles are factors of location, temperature, and current density.
- Clarified the mechanism of Cr contamination for SOFCs run at 700°C.

Introduction

Ferritic stainless steel alloys have been considered as interconnect materials in SOFCs whose operating temperature is in the 600-800°C range, since steels are relatively inexpensive and are stable in these conditions. However, in hydrated oxidizing atmospheres at these temperatures, Cr is volatile and forms several vapor species, such as $CrO_2(OH)_2$. It is well known that, without the use of effective protective coatings on the steel, the gaseous Cr species can react with cathode components (in LSM/YSZ cathodes) and can cause rapid degradation of SOFC performance. While coatings may effectively reduce the vapor pressure of Cr species, it is still important to understand the mechanism by which Cr contamination occurs in the SOFC cathode and to establish operating conditions in which the degradation levels are acceptable for a given vapor pressure. There are considerable disagreements on the mechanism(s) by which Cr species react with the cathode components.

This work aims to determine the precise mechanism of Cr contamination. To do so, we have carried out TEM investigations of SOFCs operated (at ANL) under different conditions to better understand the nanoscale microstructural/chemical properties at different stages of Cr contamination. This project is part of a larger effort led by the group at ANL to understand SOFC degradation as a function of operating conditions. At ANL, cells were operated in various fuel cell conditions and were characterized electrochemically as well as microstructurally using scanning electron microscopy (SEM), EDS, and high-energy X-rays at the Advanced Photon Source (APS). TEM complements these spatially averaging techniques by allowing us to locate nanosized

grains and interrogate their precise chemistry/structure; for low levels or the initial stages of contamination, TEM allows us to identify the location and nature of Cr contamination. The results will ultimately allow us to determine how SOFC interconnects/cathodes can be optimized to meet DOE program goals.

Approach

Anode (Ni/YSZ) supported single cells (8YSZ electrolyte and LSM/8YSZ active [mixed] cathode) were purchased from InDEC and operated under various conditions: 700°C and 800°C at several current densities. E-BRITE® interconnects were used for current collection on the cathode, and provided the source of chromium. Between the interconnect and the active cathode, an LSM contact paste was applied. In some cases, Au foil was wrapped around regions of the E-BRITE® interconnect to block Cr migration pathways. Such single cell SOFCs were run for 500 hours each and the operating conditions, such as temperature and current density, were varied between cells.

To determine the local nature of Cr-poisoning in these cells, we developed a cross-sectional TEM specimen fabrication method using a FIB that enables us to locate and later image precise positions in the LSM/YSZ active cathode. TEM, STEM, EDS, chemical mapping, EELS, and SAED techniques were used to analyze chemical composition and crystal structures of the Cr-containing phases and to investigate how degradation occurred under the given operating conditions.

Results

TEM specimens from different locations in the active (mixed) cathode of different fuel cells were studied. In this report, based on the observations made of many cells using TEM, we define degradation as the observation of changes from the original cathode microstructure, the observation of nanoparticles ($d<100$ nm), and the observation of Cr in solid phases. Figure 1 gives examples of a degradation-free cell (1a) and a severely degraded cell (1b), which are discussed more below.

Cell numbers ANL-35, 36, and 37 were each operated at 700°C under the "standard" current density (1.15 A), but with different types of interconnects. For the interconnect, ANL-35 had E-BRITE®, ANL-36 had E-BRITE® that was Au-wrapped in a manner where the landings were covered but the flow channels were exposed, and ANL-37 had E-BRITE® that was Au-wrapped in a manner where such that no E-BRITE® was exposed. No degradation was observed under regions that were protected with Au foil (i.e., in the landing region of ANL-36 or anywhere in ANL-37).

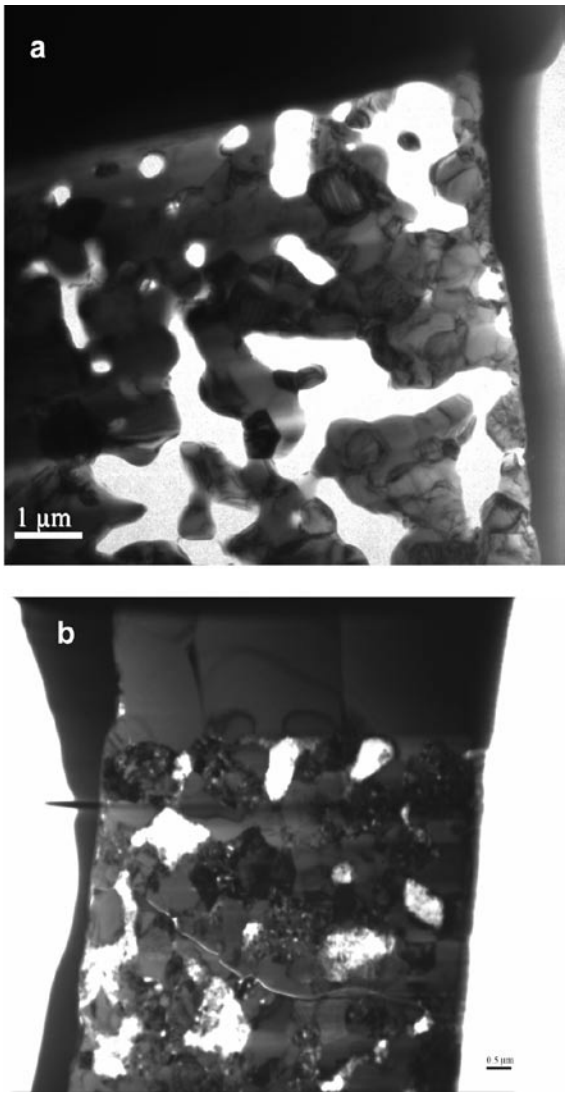

FIGURE 1. Bright-Field TEM Images Showing Active LSM/YSZ Cathode Microstructures for Different Fuel Cells: (a) ANL-36 with No Degradation and (b) ANL-35 with Massive Degradation Under the Interconnect Landing

Furthermore, no degradation was observed in ANL-36 under the exposed channel (as seen in Figure 1a), implying that the Au on the landing sufficiently protected the cell under these conditions. For other ANL fuel cells with exposed E-BRITE® interconnect landings, including ANL-35, degradation was observed throughout the cell. Figure 1b shows the massive degradation below the landing in ANL-35 (discussed further below), in which the pores are largely filled with nanoparticles and some pre-existing grains of LSM have decomposed. It should be noted that no microstructural degradation was observed in the porous-LSM contact paste region of the cathode, and the extent of degradation in the active LSM/YSZ region depended strongly on the location (landing or channel

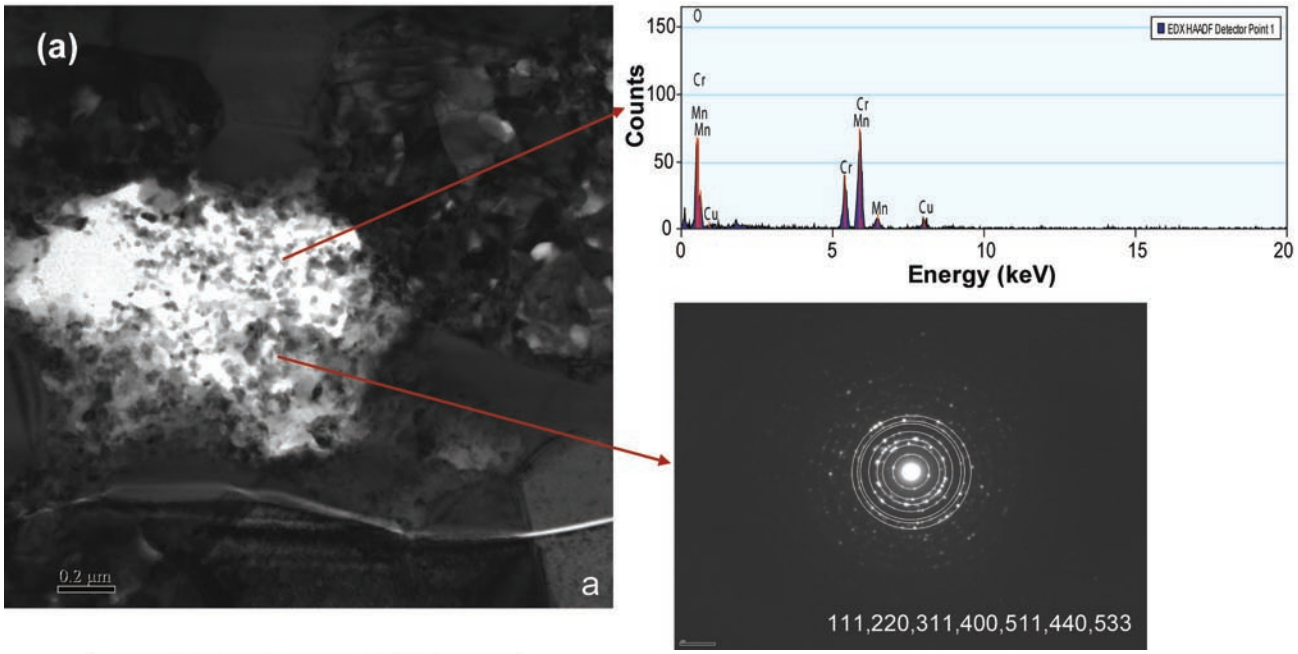

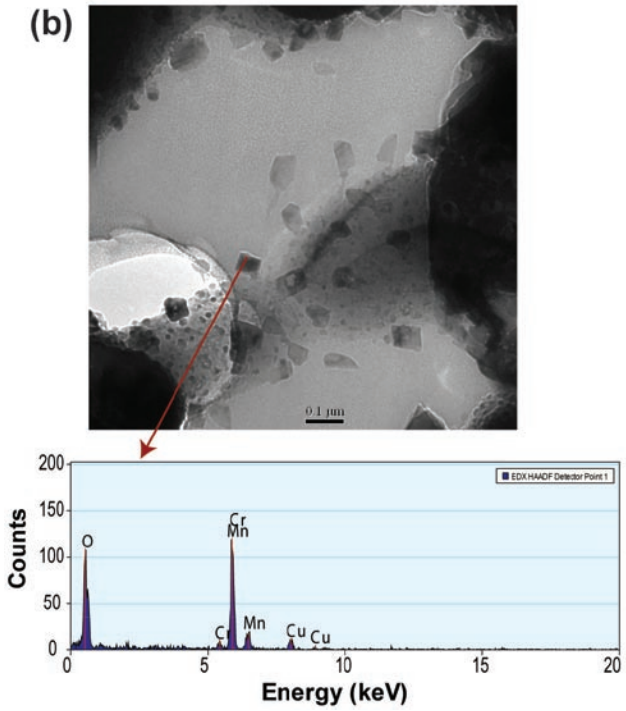

FIGURE 2. (a) Bright-field TEM image, EDS spectrum, and SAED showing degradation microstructures for ANL-35 under the landing. The EDS and SAED pattern of nanoparticles correspond to $(Cr, Mn)_3O_4$. (b) Similar images for ANL-35 under the channel.

and proximity to electrolyte), temperature, and current density.

For fuel cell ANL-35, two different degradation rates were observed under the landing and channel (Figure 2), respectively. Under the landing (Figure 1b and Figure 2a), nanoparticles filled the pores of LSM/YSZ region and LSM was almost completely decomposed. SAED in TEM demonstrated that the nanosized materials in the pores were crystalline and their diffraction pattern was consistent with the spinel structure ($Mn_xCr_{3-x}O_4$) (Figure 2a). Under the flow channel, Cr-poisoning was observed to a much less extent than in the similar region under the interconnect landing, owing to the fact that the Cr-containing vapor species appear to be removed by oxidant flow in the channels (similar to the lack of degradation in ANL-36 under the flow channels). A significant number of individual nanoparticles were observed to occur on the YSZ-pore boundaries (under the flow channel), with no obvious LSM in contact with them. These particles contained Cr and Mn, but no Y or Zr. The solids that most of the nanoparticles decorated contained Y and Zr, but no Cr or Mn. This strongly indicates that the YSZ surfaces are prone to coverage by $(Cr,Mn)_xO_y$ solids at low levels of degradation (see Figure 2b).

SOFC ANL-43 was operated in conditions similar to ANL-35 but using half the standard current density, or 0.575 A. Electrochemically, the cell experienced little degradation and one expects that the levels of Cr contamination under the landing and flow channel will decrease as well. In fact, the degradation observed under the landing of ANL-43 was similar to that observed under the flow channel of ANL-35, in line with expectations. As shown in Figure 3, a significant amount of Cr and Mn was found on the surface of the YSZ particle. At the boundary between YSZ and LSM, there are some phases that contain less Mn (the black spots) and, more importantly, there were no Cr-containing phases observed across the boundary on the LSM particle. These results imply that the initial stages of the

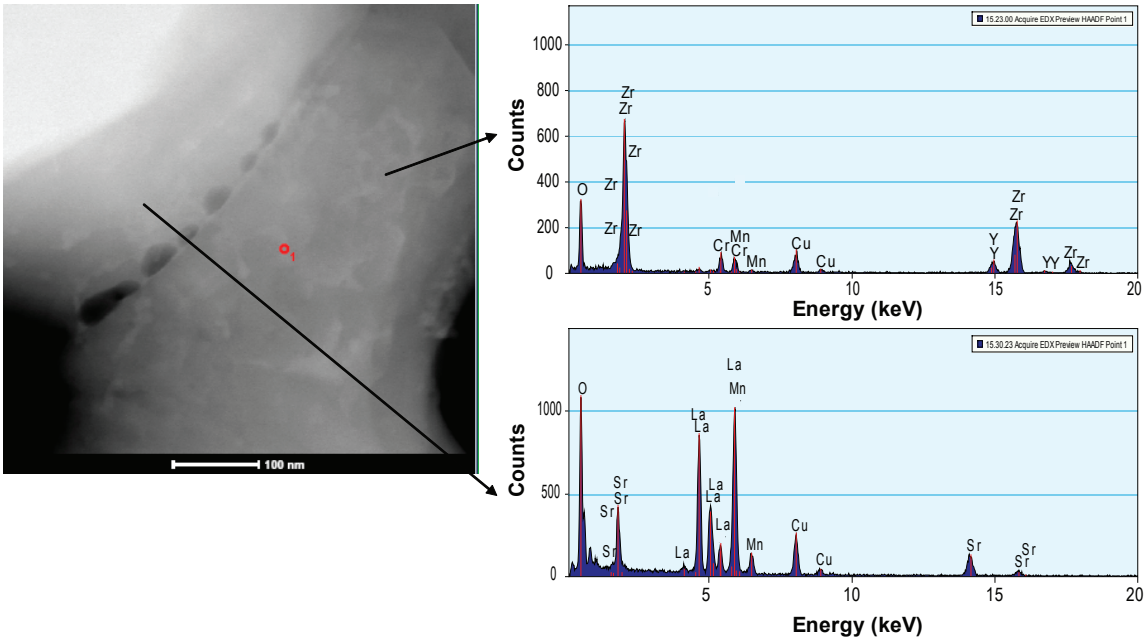

FIGURE 3. STEM Image (Left Panel) Showing Active LSM/YSZ Cathode Boundary Microstructures for ANL-43, with Two EDS Patterns from the Marked Regions (Above a YSZ Grain for the Top Right Panel and Above a LSM Grain for the Lower Right Panel)

deposition of gaseous Cr species occur on YSZ surfaces that contain Mn species (generated under cathodic polarization and high temperatures) as Cr-Mn-O nuclei. This is likely followed by LSM decomposition that begins at LSM/YSZ boundaries having YSZ coated with Cr-containing solids. Other images showed that YSZ particles that had Cr-containing solids had some regions with Mn containing solids, but also had local regions that appeared Mn-free. This implies that Mn plays a role in nucleation but growth can occur without Mn present.

Figure 4 shows the nanoparticles' microstructures for ANL-31. This cell was similar to ANL-35 (having exposed to E-BRITE® and operated at 1.15 A), but ANL-31 was run at 800°C instead of 700°C. ANL-31 exhibited a different structural degradation and a lower electrochemical degradation. The structural degradation occurred in the active LSM/YSZ region of the cathode. Three different types of particles were found; MnO_x (on LSM), Cr_2O_3, and $(Cr, Mn)_3O_4$ particles were all found. SAED showed that the most of the particles (which covered most of the regions) are of the Cr_2O_3 type. These results imply that the mechanism of Cr-contamination is different at these two temperatures.

Conclusions and Future Directions

The microstructures of LSM/YSZ active cathode region of ANL fuel cells under different operating conditions were studied by analytical TEM, and the local position, chemical composition and crystal structure of Cr-containing nanoparticle phases were determined. All results were consistent with earlier observations made

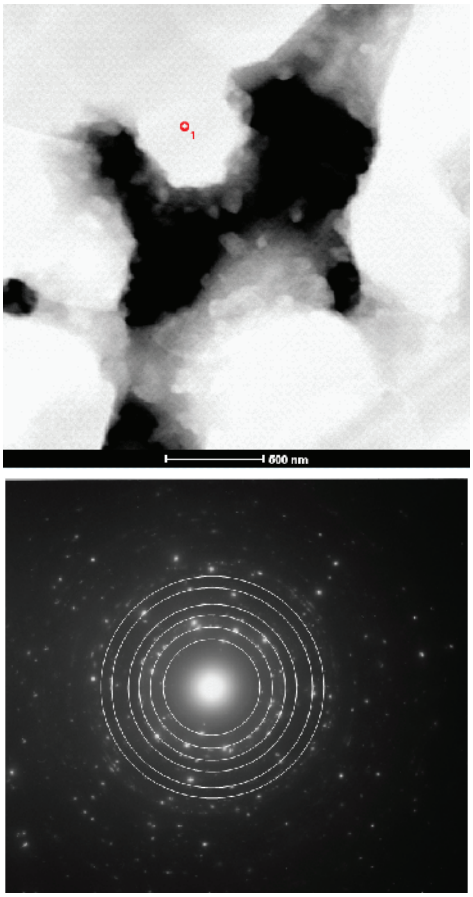

FIGURE 4. Bright-field image showing the active LSM/YSZ cathode microstructures for ANL-31 under the landing. The SAED pattern and EDS spectrum of the nanoparticles correspond to Cr_2O_3 type.

at ANL but these allowed for the local distribution of phases on individual particles to be ascertained. The Cr-poisoning mechanism was established for cells operated at 700°C; which demonstrated that Mn-species covered YSZ and participated in the early stages of Cr-deposition. Later stages were likely more complex, but included the complete decomposition of LSM grains. Future work will further confirm this model and will explore the degradation mechanisms at other temperatures and using other electrochemical operational parameters.

FY 2007 Publications/Presentations

1. Contributed images to: "Degradation of SOFCs in Contact with EBrite," T. A. Cruse*, M. Krumpelt, B. Ingram, and D. Liu, presented at "4th International Symposium on Solid Oxide Fuel Cells (SOFC)," at 31st International Cocoa Beach Conference & Exposition on Advanced Ceramics & Composites, Daytona Beach, January 21-26, 2007.

2. Contributed images to: "Microtexture of SOFC Cathodes Subjected to Thermal and Electrochemical Loads," Y. Cao, H. M. Miller, C. Johnson, L. Wilson, P. Salvador, and G. S. Rohrer*, presented at "4th International Symposium on Solid Oxide Fuel Cells (SOFC)," at 31st International Cocoa Beach Conference & Exposition on Advanced Ceramics & Composites, Daytona Beach, January 21-26, 2007.

IV.A.6 Intermediate Temperature Solid Oxide Fuel Cell Development

S. (Elango) Elangovan (Primary Contact), Brian Heck and Mark Timper
Ceramatec, Inc.
2425 South 900 West
Salt Lake City, UT 84119-1517
Phone: (801) 978-2162; Fax: (801) 972-1925
E-mail: Elango@ceramatec.com
Website: www.ceramatec.com

DOE Project Manager: Lane Wilson
Phone: (304) 285-1336
E-mail: Lane.Wilson@netl.doe.gov

Subcontractors:
- Dr. Sossina Haile, Caltech, Pasadena, CA
- Dr. Scott Barnett, Northwestern University, Evanston, IL

Objectives

- Fabricate and test a thin, supported lanthanum gallate electrolyte-based solid oxide fuel cell (SOFC) stack.
- Determine operating characteristics of the stack in the intermediate temperature range.

Approach

- Develop fabrication process for thin, supported lanthanum gallate electrolyte.
- Verify performance of thin cells in button cell configuration.
- Evaluate low temperature cathode materials using symmetric cells.
- Test the new cathode material in short stacks.

Accomplishments

- Button cells were fabricated using the tape lamination technique.
- Preliminary cathode half-cell evaluation was conducted using new cathode compositions.
- Process for infiltration of electrode material has been developed.

Future Directions

- Select promising cathode compositions and develop cathode application process.
- Fabricate and test short stacks.

Introduction

Reducing the operating temperature of SOFCs offers several benefits: improvement in long-term stability by slowing physical and chemical changes in the cell materials; lower cost systems by the use of less expensive balance of plant components; compatibility with hydrocarbon reformation allowing partial internal reformation which in turn reduces the heat exchanger duty; and finally, the potential to improve thermal cycle capability. In addition, the use of stainless steel interconnects is also facilitated by lower operating temperatures. A temperature range of 600 to 700°C is ideally suited to derive the performance stability, system integration and cost benefits.

In order to derive the advantages of the lower operating temperature, two factors that limit the cell performance, namely the electrolyte resistance and electrode polarization, must be addressed. Lanthanum gallate compositions have shown high oxygen ion conductivity when doped with Sr and Mg. Unlike other oxygen ion conductors such as ceria and bismuth oxide that are potential candidates for lowering cell operating temperature, the Sr and Mg doped lanthanum gallate (LSGM) compositions are stable over the oxygen partial pressure range of interest. The combination of stability in a fuel gas environment and the high oxygen ion conductivity makes the LSGM material a potential choice for intermediate temperature SOFCs. However, challenges in the development of electrode materials and thin cell fabrication processes need to be overcome to make use of the potential of the LSGM electrolyte.

Approach

Tape cast process development was performed to cast LSGM tape of various thicknesses to provide sintered electrolyte thicknesses ranging from 50 to 200 microns. The process variables included: powder surface area, organic content in the tape slip, and sintering temperature. The primary objectives of the activity were to achieve sintered electrolyte density and flatness required for stacking. Single cells and symmetric cells with 2.5 cm^2 active area were tested for performance characteristics.

While a lanthanum cobaltite cathode has good intermediate temperature catalytic activity, the primary issues related to the use of cobaltite cathodes are excessive diffusion of Co into LSGM causing phase destabilization of the electrolyte, and the high coefficient of thermal expansion (CTE) of cobaltite compositions.

Two alternative cathode compositions were evaluated in half-cell tests at the two universities.

Results

Thin electrolyte single cells were fabricated using the tape lamination technique. Both anode and cathode porous structures were evaluated as the support for the electrolyte. At least one electrode material was infiltrated into the porous structure. The performance of a cathode-supported cell is shown in Figure 1. The thin, 75 micron LSGM electrolyte cells showed an area specific resistance of 0.5 ohm-cm^2 at an operating temperature of 700°C. The long-term performance of selected cells is shown in Figure 2. Similar performance and stability results were also obtained using cells with the anode-support configurations. A modified infiltration technique was developed in order to achieve a more uniform distribution of electrode material into the porous structure. Micrographs of the cathode infiltrated structure are shown in Figure 3. Button cell tests using the new infiltration technique showed (Figure 4) an improvement in cell performance.

Cathode symmetric cells using cobalt-ferrite compositions were tested at the two universities. The cathode polarization losses were measured to be 0.06 ohm-cm^2 at 650°C.

Sintering process development for fabricating 10 x 10 cm electrolyte was conducted. Initial trials with thick electrolyte defined the sintering process to achieve flat, dense electrolyte. Fabrication development of a thin 10 x 10 cm cell structure has been initiated.

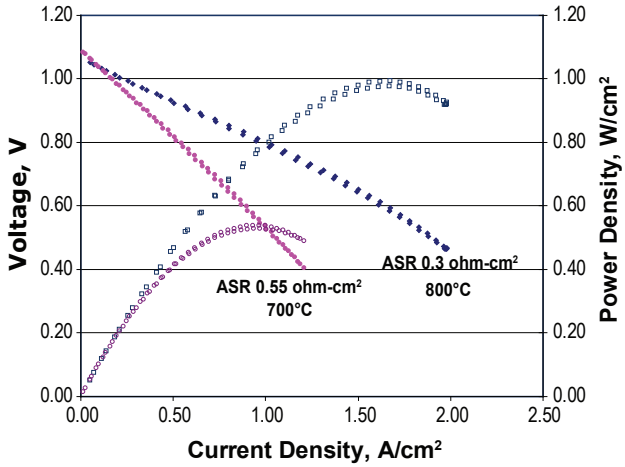

FIGURE 1. Performance of a Cathode Supported LSGM Cell; Electrolyte Thickness of 75 Microns Was Used

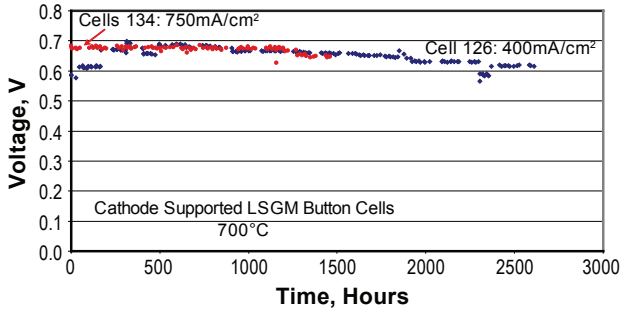

FIGURE 2. Long-Term Stability of Cathode Supported Cells at an Operating Temperature of 700°C

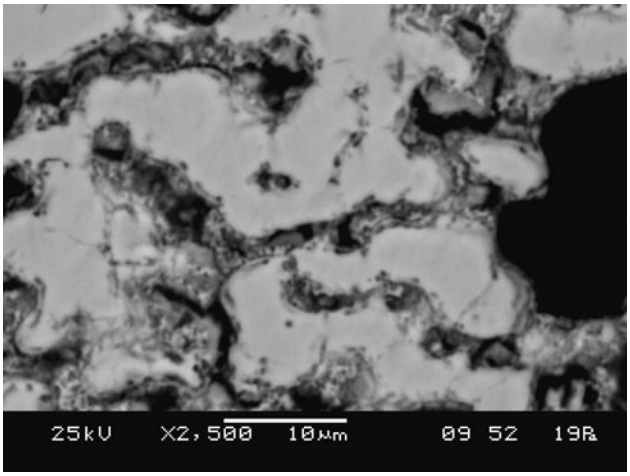

FIGURE 3. Micrograph of Infiltrated Cathode

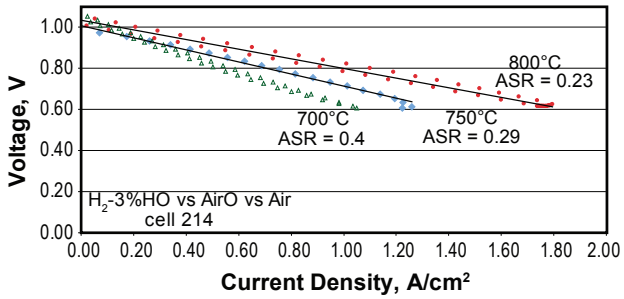

FIGURE 4. Button Cell Performance with Infiltrated Cathode

Conclusions

- Thin, supported cells meet the performance target of 0.5 ohm-cm^2 resistance at 700°C.
- Long-term tests of single cells show stable performance.
- Alternative cathode materials show low cathode polarization at temperatures <700°C.

IV.A.7 Characterization of Atomic and Electronic Structure of Electrochemically Active SOFC Cathode Surfaces

Meilin Liu (Primary Contact), YongMan Choi, Robert Williams, Jr.
Georgia Institute of Technology
771 Ferst Drive NW
Atlanta, GA 30332
Phone: (404) 894-6114; Fax: (404) 894-9140
E-mail: meilin.liu@mse.gatech.edu

DOE Project Manager: Lane Wilson
Phone: (304) 285-1336
E-mail: Lane.Wilson@netl.doe.gov

Objectives

- Elucidate oxygen reduction mechanisms on $LaMnO_3$–based cathode materials using quantum chemical calculations
- Simulate the interactions between O_2 and $LaMnO_3$–based cathode materials under solid oxide fuel cell (SOFC) operating conditions using quantum molecular dynamics (QMD) methods
- Fabricate, characterize, and model dense $La_{0.85}Sr_{0.15}MnO_3$(LSM)-$Ce_{0.9}Gd_{0.1}O_{1.95}$ (GDC) composite electrodes, which will be used as a platform for characterization of surface catalytic properties of other cathode materials

Accomplishments

- Quantum chemical calculations showed that the oxygen reduction reaction on $LaMnO_3$-based cathode materials may occur via a stepwise elementary reaction sequence.
- QMD simulations predict that defective $LaMnO_3$ exhibits faster O_2 dissociation kinetics than perfect $LaMnO_3$ at 800°C, suggesting that oxygen vacancies play a critical role in oxygen reduction reactions.
- Fabricated and characterized dense LSM-GDC composite electrodes with various composition and microstructures. The amount of triple-phase boundaries (TPBs) was determined using stereological methods.

Introduction

Understanding the detailed oxygen reduction mechanism is critical to achieving a rational design of new cathode materials for SOFCs [1,2,3]. Because of the complexity of the involved charge and mass transfer processes, however, it is extremely difficult to probe the mechanistic details using experimental tools. Here we report our findings on the application of periodic density functional theory (DFT) calculations, containing the exploration of the molecular processes involved in oxygen reduction on $LaMnO_3$–based cathode surfaces. We aim to predict the most probable oxygen reaction pathway as well as the vibrational frequencies of the adsorbed surface oxygen species. To develop a reliable experimental approach for the determination of the surface catalytic properties of various cathode materials, we have designed, fabricated, and characterized dense LSM-GDC composite electrodes.

Approach

Periodic DFT calculations [4,5] and molecular dynamics (MD) simulations have been used to examine oxygen reduction reactions and ionic transport of cathode materials for SOFCs. The details of the computational methods are as described elsewhere [2,3,6].

A dense LSM-GDC composite electrode is typically fabricated with a GDC electrolyte layer to form a bi-layer structure using a co-pressing and co-firing process. LSM (Rhodia, average particle size: 1.1 μm) and GDC (Rhodia, average particle size: 0.3 μm) powders with various volume ratios ranging from 40:60 to 70:30 were mixed in a mortar further reducing particle sizes. The co-pressing consisted of several successive steps: the as-prepared mixture powder was added to a die (diameter of 10 mm) and tapped smooth using a pestle. Next, GDC powder was loaded into the die. The whole body was cold-pressed under 200 MPa into cylindrical pellets using a uniaxial die-press. After firing the samples at 1,450°C for 5 h in air, dense GDC/LSM-GDC wafers were attained. The thicknesses of GDC and LSM-GDC composite were ~0.5 mm and ~0.15 mm, respectively.

Results

Shown in Figure 1a are the optimized geometries, O-O bonds, and their vibrational frequencies of the adsorbed oxygen species on a defective $LaMnO_3$ (with an oxygen vacancy). Those intermediates on the defective $LaMnO_3$ surface are energetically more favorable compared to those on a perfect surface (without oxygen vacancy). We carried out a mechanistic study for the molecular adsorption pathway at the defective $LaMnO_3$ surface. Since we were unable to locate peroxo-like species at the La cation site, we

considered only the Mn cation pathway. As depicted in Figure 1b, the first step is the formation of either superoxo-like **Mn-super** or peroxo-like **Mn-per** with exothermicities of 1.82 or 2.70 eV, respectively. As summarized in Figure 1a, they have distinct vibrational frequencies of 1265 or 861 cm^{-1}, respectively. Because of the further charge transfer from the surface to the adsorbate, superoxo-like **Mn-super** can also isomerize to the peroxo-like **Mn-per** intermediate after overcoming a 0.1 eV reaction barrier of **TS**, leading to a lengthening of the O-O bond distance from 1.301 to 1.445 Å (see Figure 1a). Then, one of the oxygen atoms of the peroxo-like **Mn-per** species is incorporated into the oxygen vacancy ($V_O^{\bullet\bullet}$), while breaking the O-O bond without a well-defined transition state, producing **P-V** with an exothermicity of 6.99 eV. The highly exothermic process validates the good catalytic activity for oxygen dissociation on $LaMnO_3$-based cathode materials. The monatomic oxygen species absorbed at the Mn cation diffuses to a more stable site (labeled as Products in Figure 1), which is 2.32 eV more stable than **P-V**. In order to simulate SOFC conditions on the LaMnO-terminated $LaMnO_3$ surface models, MD simulations at 800°C were carried out. To simulate a reactant gas-phase oxygen, the distance between an O_2 molecule and the surface was kept at approximately 4 Å and fully optimized. The defective $LaMnO_3$ surface was modeled to verify our minimum-energy paths (MEPs) shown in Figure 1b. For the MD simulations, $\Delta t = 2$ femtoseconds (fs) was applied and the calculations were iterated until they reached an equilibrium state. As illustrated in Figure 2, in 100 fs, the molecular adsorption of a superoxo-like species occurs. Then, one of the oxygen atoms of the adsorbed species moves toward the oxygen vacancy with energy stabilization and charge transfer, which takes place in approximately 130 fs. After the incorporation process in an additional 30 fs, the adsorbed oxygen monatomic species at Mn cations diffuses to a more stable site. The time from adsorption to dissociation (with incorporation) was 220 fs. Even though MEP calculations (Figure 1b) determined two pathways via superoxo- and peroxo-like species without a reaction barrier, the MD simulations with our surface models suggested that the most probable reaction pathway is the formation of superoxo-like species, and then conversion to peroxo-like species with a small reaction barrier. Thus, we can write a possible route with oxygen vacancies on the $LaMnO_3$-based surfaces. We summarize the most probable pathway for the oxygen-reduction mechanism based on the DFT/MD modeling

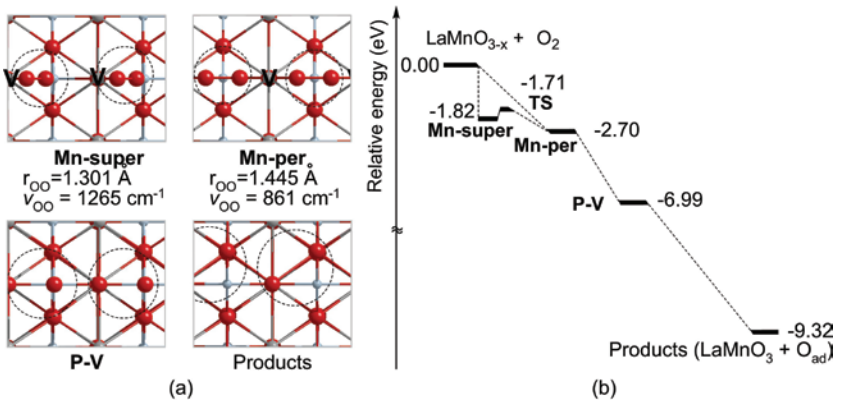

FIGURE 1. (a) Geometrical information of adsorbed oxygen species on a defective $LaMnO_3$ surface. **V** and dashed circles denote an oxygen vacancy and adsorbed oxygen species on the surface, respectively. (b) Potential energy profiles at 0 K for the oxygen reduction reaction on a defective $LaMnO_3$ surface.

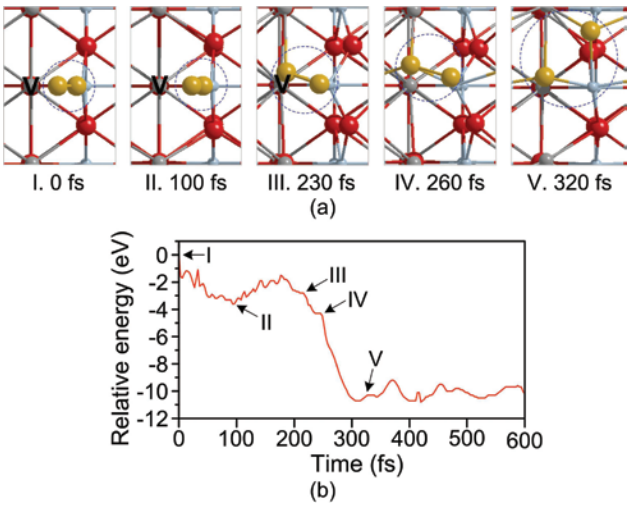

FIGURE 2. MD results simulated at 800°C. **V** and dashed circles denote an oxygen vacancy and adsorbed oxygen species on the surface, respectively.

in Figure 3, where (g), (ad), (super), (per), and (lc) represent gas, molecular adsorption, superoxo-like species, peroxo-like species, and lattice, respectively.

Shown in Figure 4a is a typical scanning electron microscope (SEM) micrograph of the dense composite layer. After performing energy dispersive X-ray (EDX) characterization on hundreds of small particles, it was found that particles with a terrace structure on their surface corresponded to LSM, while those with small dents on their surface corresponded to GDC. In this manner, the two phases were able to be differentiated. To quantify the TPB length for the various sample sets, established stereographic techniques were employed. Micrographs of the sample surfaces were taken using SEM and test lines were overlaid on the image. Using the known magnification of the micrograph, the

actual total length of the test lines was determined. The number of intersections between the test lines and the LSM-GDC grain boundaries (which represents a TPB line), P_L, were counted. This process was repeated at different locales on the surfaces of several samples for a minimum of thirty fields of view, and an average value of the number of intersections per test line, $\langle P_L \rangle$, was calculated. The average value of the total boundary length per unit area, $\langle L_A \rangle$, is related to $\langle P_L \rangle$ through the simple expression, $\langle L_A \rangle = \pi/2 \langle P_L \rangle$. Figure 4b shows a plot of inverse polarization resistance versus TPB lengths. The plot is expected to be linear but shows significant scatter, specifically from the low volume percentages of LSM samples. The main cause of this nonlinearity is due most likely to not all of the TPBs for each sample being active. For the TPB around each LSM particle to be considered active, it must contact a GDC particle that is part of a percolating cluster through to the electrolyte. The likelihood of percolation for the GDC particles becomes increasingly smaller as the volume percentage of LSM increases. It is expected that once site percolation is taken into account and the amount of active TPB length is calculated, better linearity will be achieved.

FIGURE 3. A Stepwise Reaction Mechanism of Oxygen Reduction on a Defective LMO Surface

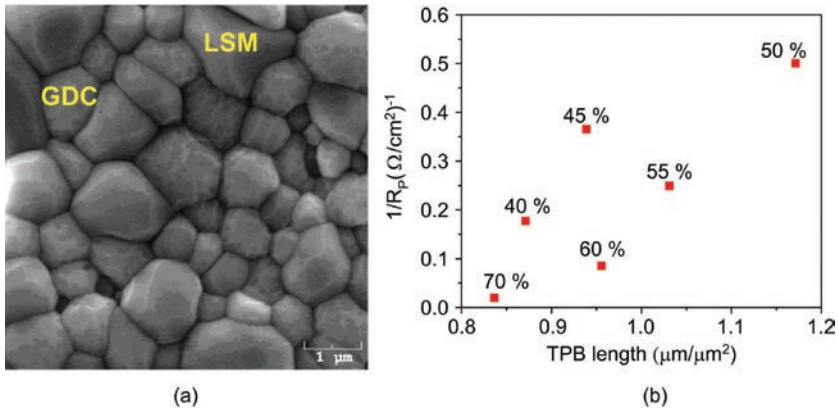

FIGURE 4. (a) SEM image of a dense LSM-GDC composite cathode fabricated by a co-pressing and co-sintering method. (b) Inverse polarization resistance versus TPB length. The values next to the data points are LSM volume percentages for the samples.

Conclusions and Future Directions

In the past year, we have made important progress in elucidation of the mechanisms of oxygen reduction of perovkite-type cathode materials for SOFCs using quantum chemical calculations. Dense LSM-GDC composite electrodes have been developed using a co-pressing and co-firing technique. The amount of TPB length for samples of varying volume percentages was determined using stereographic methods. It was found that the volume percentage of 50% LSM to 50% GDC produced the largest amount of TPB length. In correlating the cell performance with the TPB length, a large amount of scatter in the data was observed. Future studies are briefly outlined as follows:

- The computational framework will be used to predict new cathode material with fast O_2 reduction kinetics and rapid ionic transport. Once a candidate material is identified, we will use experimental methods to characterize the catalytic and transport properties.
- Computer simulations on percolation for samples with various volume percentages will be performed to obtain a more complete picture of the amount of active TPB in order to better correlate with cell performance.
- Once the performance of the LSM-GDC composite electrode is well characterized, a thin film of another cathode material will be deposited on the composite cathode to determine its surface catalytic properties.

FY 2007 Publications/Presentations

Publications

1. Y. M. Choi, D. S. Mebane, M. C. Lin, M. Liu, "Oxygen Reduction on $LaMnO_3$-based Cathode Materials in Solid Oxide Fuel Cells," *Chemistry of Materials*, 19, 1690, 2007.

2. D. S. Mebane, Y. Liu, M. Liu, "A Two-Dimensional Model and Numerical Treatment for Mixed-Conducting Thin Films: The Effect of Sheet Resistance," *Journal of the Electrochemical Society*, 154, A421, 2007.

3. R. Williams Jr., S. Zha, M. Liu, "Fabrication and Characterization of Dense $La_{0.85}Sr_{0.15}MnO_3$-$Ce_{0.9}Gd_{0.1}O_{1.95}$ Composite Electrodes," *Ceramic Engineering and Science Proceedings*, 2007.

4. Y. M. Choi, M. C. Lin, M. Liu, "Computational Study of Catalytic Mechanism toward Oxygen Reduction on $La_{0.5}Sr_{0.5}MnO_3$(110) in Solid Oxide Fuel Cells," *Angewandte Chemie, International Edition*, in press.

5. Y. M. Choi, D. S. Mebane, J. H. Wang, M. Liu, "Continuum and Quantum-Chemical Modeling of Oxygen Reduction on the Cathode in a Solid Oxide Fuel Cell," *Topics in catalysis (Invited)*, in press.

Presentations

1. R. Williams Jr., S. Zha, M. Liu, "Fabrication and Characterization of Dense $La_{0.85}Sr_{0.15}MnO_3$-$Ce_{0.9}Gd_{0.1}O_{1.95}$ Composite Electrodes," 31st International Conference on Advanced Ceramics and Composites (ACerS), 2007.

2. Y. M. Choi, M. C. Lin, M. Liu "First-principles Investigation on Gas-Electrode Interactions in Solid Oxide Fuel Cells: Sulfur Tolerance and Oxygen Reduction Reaction," Exploratory Workshop-I/UCRC for Fuel Cells at USC-GT, Georgia, 2007.

3. Y. M. Choi, M. C. Lin, M. Liu "Computational Studies of the Oxygen Reduction Reaction on Cathode Materials for Solid Oxide Fuel Cells using Quantum-Chemical Calculations," 2nd Korea-USA Fuel Cell Symposium, South Carolina, 2007.

References

1. Y. M. Choi, D. S. Mebane, J. H. Wang, M. Liu, "Continuum and Quantum-Chemical Modeling of Oxygen Reduction on the Cathode in a Solid Oxide Fuel Cell," *Topics in Catalysis (Invited)*, in press.

2. Y. M. Choi, D. S. Mebane, M. C. Lin, M. Liu, "Oxygen Reduction on $LaMnO_3$-based Cathode Materials in Solid Oxide Fuel Cells," *Chemistry of Materials*, 19, 1690, 2007.

3. Y. M. Choi, M. C. Lin, M. Liu, "Computational Study of Catalytic Mechanism toward Oxygen Reduction on $La_{0.5}Sr_{0.5}MnO_3$(110) in Solid Oxide Fuel Cells," *Angewandte Chemie, International Edition*, in press.

4. G. Kresse, J. Hafner, "Ab initio molecular dynamics for liquid metals," *Physical Review B*, 47, 558, 1993.

5. G. Kresse, J. Furthmüller, "Efficient iterative schemes for ab initio total-energy calculations using a plane-wave basis set," *Physical Review B,* 54, 11169, 1996.

6. E. A. Kotomin, R. A. Evarestov, Y. A. Mastrikov, J. Maier, "DFT plane wave calculations of the atomic and electronic structure of $LaMnO_3$ (001) surface," *Phys. Chem. Chem. Phys.* **7,** 2346, 2005.

IV.A.8 Functionally Graded Cathodes for Solid Oxide Fuel Cells

Meilin Liu (Primary Contact), David S. Mebane
Georgia Institute of Technology
School of Materials Science and Engineering
771 Ferst Drive NW
Atlanta, GA 30332-0245
Phone: (404) 894-6114; Fax: (404) 894-9140
E-mail: meilin.liu@mse.gatech.edu

DOE Project Manager: Briggs White
Phone: (304) 285-5437
E-mail: Briggs.White@netl.doe.gov

Objectives

- Qualitatively evaluate the importance of sheet resistance of thin-film electrodes in fundamental studies of electrode properties.
- Quantitatively estimate the bulk defect structure of the cathode material $La_xSr_{1-x}MnO_{3\pm\delta}$ (LSM) at low temperatures in order to better determine thermodynamic and transport properties of LSM.

Accomplishments

- Achieved qualitative correspondence between continuum models featuring sheet resistance in thin films of LSM and experimental studies.
- Developed a new model for bulk defects in LSM at low temperatures, quantitatively validated the model against experimental nonstoichiometry data, and attained quantitative estimates for model parameters.

Introduction

The cathode reaction in solid oxide fuel cells (SOFCs) is the largest single source of polarization resistance in the cell at low temperatures. Optimization of cathode microstructure – likely in the form of functionally graded electrodes, wherein the composition of the cathode changes through its thickness in order to best facilitate the overall oxygen reduction process – is therefore paramount to achieving better performing fuel cells at lower operating temperatures and lower cost. However, optimization is hindered by a lack of quantitative and qualitative knowledge regarding the oxygen reduction process in SOFC cathodes. LSM is the most widely used cathode material in SOFCs. Our work this year has focused on acquiring knowledge about two aspects of oxygen reduction on LSM cathodes that are important for optimization of the microstructure. The first is the propensity to encounter power losses due to sheet resistance – or losses due to transport of electrons and electron holes through LSM, as opposed to losses due to transport of oxygen ions or that due to slow chemical reactions – for certain cathode geometries. The second is the quantitative bulk defect structure of LSM at low temperatures. Bulk defects influence the rate of transport of oxygen ions as well as the rate of chemical reactions on the electrode. Existing defect models for LSM were derived and applied for high-temperature situations, and are not appropriate for low-temperature operation [1-5].

Approach

For the sheet resistance study, we developed a continuum model based on the well-known Nernst-Planck equation, but we could not use the approximations typically employed for high electronic conductivity mixed ionic electronic conductors (MIECs) that preclude any consideration of electronic resistance. We were therefore forced to develop computational simulation methods, which we applied to two-dimensional renderings of thin-film LSM cathodes. We used the best available literature data to estimate model parameters. We then compared our results with experiments on dense, thin-film LSM cathodes.

For the determination of bulk defect structure, we developed a computational method for quantitatively comparing bulk defect models with nonstoichiometry experiments. These experiments are designed to investigate defect structure by comparing the weight change of the material as the atmosphere in contact with the material changes composition. The computational methods we developed allow for validation of the model as well as quantitative parameter estimation.

Results

Qualitative comparisons to electrochemical experiments on LSM thin films show that these films very likely experience significant sheet resistance effects. The model successfully replicated these effects, as shown in Figure 1. The plot shows both the current density and the utilization of the electrode versus applied potential. Utilization is the total fraction of the electrode that is active; it is 1.0 when there is zero sheet resistance but drops as sheet resistance becomes more prominent. Note that the current density curve, plotted logarithmically versus potential, consists of two approximately straight-line regions, and that the point

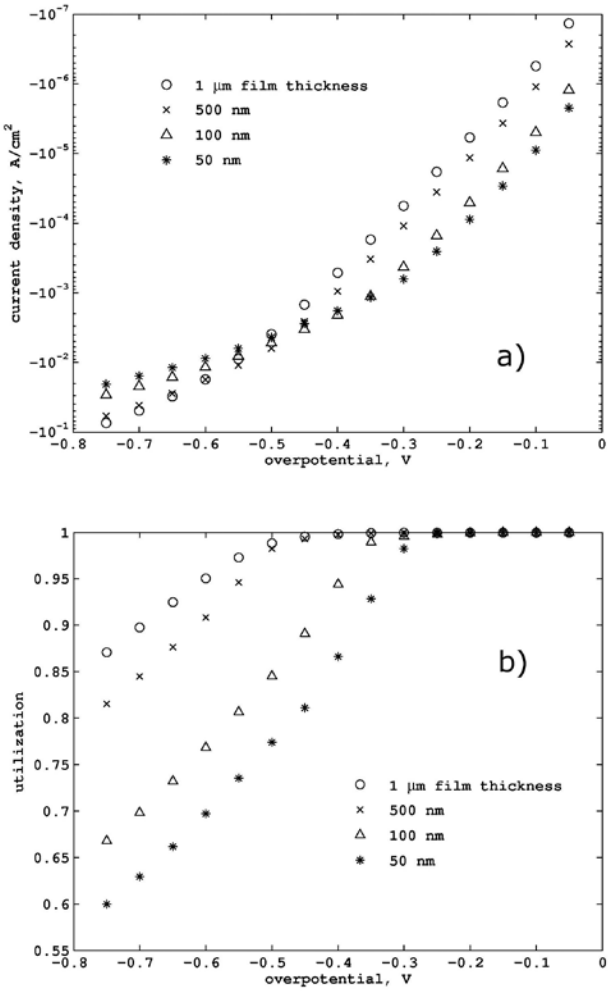

FIGURE 1. a) Current-Voltage and b) Total Film Utilization for Model LSM Thin Films of Different Thicknesses

of inflection between these regions occurs at the point where the utilization curve drops significantly below 1. The existence of a similar shape in current-potential curves reported for thin films in the literature is a strong indication that sheet resistance is an issue in these thin films.

Using the procedures we developed for rigorous, quantitative comparison between experiment and model, we definitively showed that the best existing model for bulk defects in LSM failed to adequately describe the behavior of nonstoichiometry experiments at temperatures below 800°C, a temperature that is now generally considered to be too high for economical operation of SOFCs. We modified the model and used our techniques to show the resulting good correspondence between the model and experiment at temperatures as low as 600°C (see Figure 2).

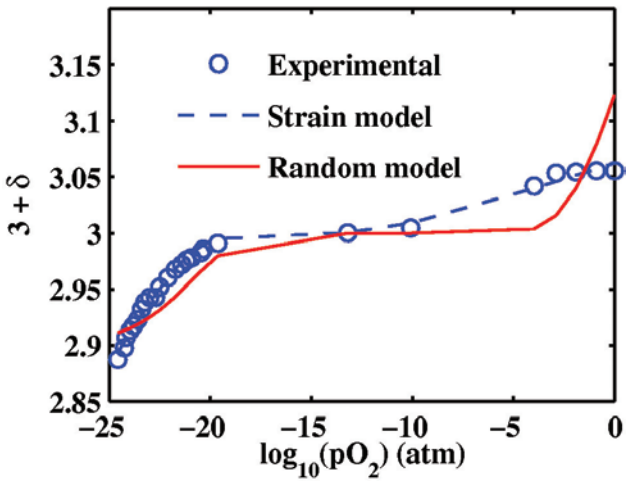

FIGURE 2. Fits to LSM nonstoichiometry data for the previous bulk defect model (Random) and a new model including strain interaction between cation defects developed by the authors. The ordinate indicates a measure of the ratio between oxygen and manganese in LSM.

We additionally estimated the well-defined parameters of the model, enabling straightforward calculation of the defect structure of LSM at any temperature.

Conclusions and Future Directions

The analysis of sheet resistance clearly shows that designers of LSM cathodes must take sheet resistance into account. This becomes especially important as structures become finer in scale, as is anticipated in terms of the development of nanostructured morphologies. We have an approximate idea of the types of morphologies that will encounter sheet resistance effects, and we are using this knowledge in the development of new cathode designs. We are also endeavoring to gain a more quantitative understanding of sheet resistance in LSM.

Since the bulk defect structure critically influences many aspects of cathode operation, the work in bulk defects provides a foundation for more quantitative investigation of LSM using the same computational parameter estimation methods that we have developed in the past year. We are currently turning our sights on quantitatively estimating bulk oxygen transport properties in LSM along with rate constants for some of the key chemical-electrochemical reactions taking place in the material. Our objective is to produce cathode microstructures that display higher performance than current state-of-the-art composite cathodes at low temperatures (600-750°C). Both microstructure and composition of the composite cathodes will be optimized to achieve better performance.

FY 2007 Publications/Presentations

Publications

1. E. Koep, C. Jin, M. Haluska, R. Das, R. Narayan, K. Sandhage, R. Snyder, M. Liu, "Microstructure and electrochemical properties of cathode materials for SOFCs prepared via pulsed laser deposition," Journal of Power Sources, 161, 250, 2006.

2. Mebane, D. S., Liu, Y. J. and Liu, M. L. "A two-dimensional model and numerical treatment for mixed conducting thin films: the effect of sheet resistance," *Journal of the Electrochemical Society* 154 (5) A421–A426, 2007.

3. R. Das, D. Mebane, E. Koep, M. Liu, "Modeling of Patterned Mixed-Conducting Electrodes and the importance of sheet resistance at small feature sizes," *Solid State Ionics*, 178(3–4), 249, 2007.

4. D. Mebane and M. Liu, "Modeling of MIEC Cathodes: Effect of Sheet Resistance", in *Advances in Solid Oxide Fuel Cells II, Ceramic Engineering and Science Proceedings, Cocoa Beach*, **27** (4) 2006.

5. Mebane, D. S., Liu, Y. J. and Liu, M. L. "Refinement of the Bulk Defect Model for $La_xSr_{1-x}MnO_{3\pm\delta}$," *Solid State Ionics*, submitted.

Presentations

1. Mebane, D. S., Liu, Y. J. and Liu, M. L., "Quantitative Understanding of Oxygen Reduction on LSM," Exploratory Workshop-I/UCRC for Fuel Cells at USC-GT, Georgia, February 2007.

2. Lynch, M., Mebane, D. S. and Liu, M. L., "Modeling of Porous SOFC Cathodes," Exploratory Workshop-I/UCRC for Fuel Cells at USC-GT, Georgia, February 2007.

References

1. Kuo, J. H., Anderson, H. U. and Sparlin, D. M., "Oxidation-Reduction Behavior of Undoped and Sr-doped $LaMnO_3$: Nonstoichiometry and Defect Structure," *Journal of Solid State Chemistry* **83** (1989) 52-60.

2. vanRoosmalen, J. A. M. and Cordfunke, E. H. P., "Defect Chemistry of $LaMnO_{3\pm\delta}$ 4. Defect Model for $LaMnO_{3\pm\delta}$," *Journal of Solid State Chemistry* **110** (1994) 109-112.

3. Nowotny, J. and Rekas, M., "Defect Chemistry of $(La,Sr)MnO_3$," *Journal of the American Ceramic Society* **81** (1998) 67-80.

4. Mizusaki, J., Mori, N., Takai, H., Yonemura, Y., Minamiue, H., Tagawa, H., Dokiya, M., Inaba, H., Naraya, K., Sasamoto, T. and Hashimoto, T., "Oxygen Nonstoichiometry and Defect Equilibrium in the Perovskite-Type Oxides $La_{1-x}Sr_xMnO_{3\pm\delta}$," *Solid State Ionics* **129** (2000) 163–177.

5. Poulsen, F. W., "Defect Cheimstry Modelling of Oxygen-Sooichiometry, Vacancy Concentrations, and Conductivity of $La_{1-x}Sr_xMnO_{3\pm\delta}$," *Solid State Ionics* **129** (2000) 145-162.

IV.A.9 Novel Sulfur-Tolerant Anodes for Solid Oxide Fuel Cells

Meilin Liu (Primary Contact), Jeng-Han Wang, Songho Choi, Zhe Cheng
Georgia Institute of Technology
School of Materials Science and Engineering
771 Ferst Drive NW
Atlanta, GA 30332-0245
Phone: (404) 894-6114; Fax: (404) 894-9140
E-mail: meilin.liu@mse.gatech.edu

DOE Project Manager: Briggs White
Phone: (304) 285-5437
E-mail: Briggs.White@netl.doe.gov

Objectives

- Characterize the sulfur-poisoning effect on anode-supported solid oxide fuel cells (SOFCs) under practical operation conditions
- Investigate the sulfur-anode interaction mechanism in H_2S contaminated fuels at elevated temperatures
- Establish an effective operational window that allows SOFCs to reach lifetime targets in commercially viable power generation environments
- Modify Ni-YSZ (yttria-stabilized zirconia) anode surface to achieve enhanced sulfur tolerance

Accomplishments

- Revealed sulfur poisoning mechanism and the effects of cell operating conditions (including temperature and H_2S concentration) on sulfur poisoning and recovery of nickel-based anodes in SOFCs.
- Predicted a new S-Ni phase diagram with a region of sulfur adsorption on Ni surfaces, corresponding to sulfur poisoning of Ni-YSZ anodes under typical SOFC operating conditions.
- Established the "standard" Raman spectra for several nickel sulfides commonly observed in sulfur poisoning of Ni-based anodes and verified the characteristic Raman shifts using density functional theory (DFT) calculations.
- Designed and constructed a multi-cell testing system capable of simultaneously performing electrochemical tests of 12 button cells in fuels with four different concentrations of H_2S.
- Achieved modification of the Ni-YSZ anode surface using a thin coating of Nb_2O_5 to enhance sulfur tolerance.

Introduction

SOFCs have a great potential to be one of the cleanest, most efficient and versatile systems that convert chemical energy to electrical energy. One of the unique advantages of SOFCs over other types of fuel cells is the capability of direct utilization (sometimes through internal reforming) of hydrocarbon fuels. Unfortunately, many hydrocarbon fuels contain sulfur, which may dramatically degrade SOFC performance even at very low levels. Low concentrations of sulfur are difficult to remove efficiently and cost-effectively. Therefore, knowing the exact poisoning process for state-of-the-art cells with Ni-YSZ supporting anodes, understanding the detailed anode poisoning mechanism, and developing new sulfur-tolerant anodes are essential for the promotion of SOFCs that run on hydrocarbon fuels.

The current project focuses on (i) characterizing both the short-term and long-term sulfur poisoning process for state-of-the-art SOFC button cells with a anode-supported structure, (ii) investigating the sulfur poisoning mechanism for the Ni-based anode via experiments and theoretical calculations, and (iii) developing new anode materials and/or architectures that provide enhanced sulfur tolerance.

Approach

In theoretical analysis, quantum chemical calculations with thermodynamic correction were used to predict the interactions between H_2S-contaminated hydrogen fuel and Ni surfaces under SOFC operation conditions. The vibrational frequencies and modes of several nickel sulfides were computed using finite displacement approach to assist the interpretation of Raman spectra obtained from experiments. The electronic structures of these sulfides were also calculated and correlated with the poisoning behavior.

On the experiment side, a multi-cell testing system was designed and constructed in our lab, consisting of a high temperature furnace, a gas distribution system, and a 12-channel electrochemical testing station. Meanwhile, the surfaces of Ni-YSZ anodes were modified with a thin film of other materials to improve the sulfur tolerance. Fuel cells with dense Ni-YSZ anodes were fabricated using a co-sintering method in a reducing atmosphere. A thin film of Nb_2O_5 was then deposited on the anode surface by sputtering. The power output and the interfacial impedance response were recorded as a function of time upon exposure to hydrogen with or without 50 ppm H_2S.

Results

Shown in Figure 1 is a new S-Ni phase diagram constructed from quantum chemical calculations with thermodynamic corrections. This phase diagram suggests that a clean Ni surface (in the white region) will first adsorb sulfur atoms when exposed to a small amount of H_2S, crossing the blue line and entering the blue (middle) region. The surface coverage of nickel by sulfur increases as the temperature is reduced until the surface is completely covered by sulfur (approaching the red line between the blue and the yellow region) before the formation of Ni_3S_2 (in the yellow region). The blue region can not be predicted directly from the classical thermodynamic database and, thus, is missing from the existing S-Ni phase diagram [1]. The important implication of the calculated phase diagram is that it can be used to accurately predict the conditions to avoid sulfur poisoning (in the white region) and to explain existing measurements [2]. These results also suggest that sulfur poisoning is due to the adsorption of sulfur atoms on the nickel surface, which blocks active sites for fuel oxidation.

Listed in Table 1 are the Raman frequencies of four nickel sulfide species (i.e., Ni_3S_2, NiS, Ni_3S_4, and NiS_2) determined from DFT calculations as well as

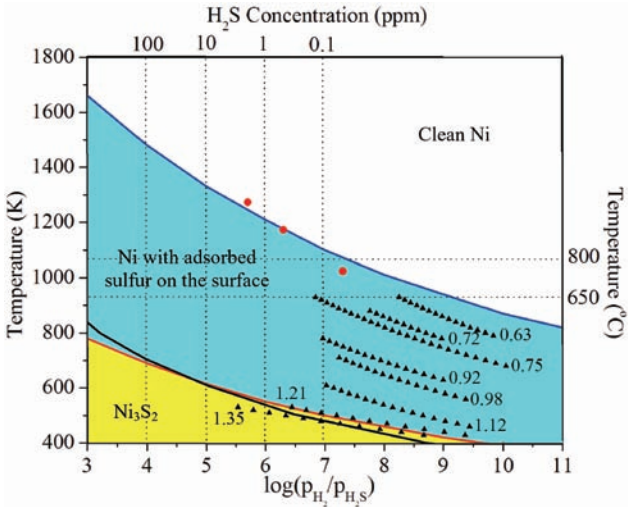

FIGURE 1. Calculated phase diagram for the S-Ni system in H_2S/H_2 fuel mixtures. The white, blue, and yellow regions represent clean Ni phase without adsorbed sulfur on the surface, Ni phase with adsorbed sulfur on the surface, and Ni_3S_2 bulk phase, respectively. The blue line is the calculated phase boundary between clean Ni surface and Ni surface with adsorbed sulfur; the red line is the calculated phase boundary between Ni surface with adsorbed sulfur and Ni_3S_2 bulk phase; the black line is phase boundary between bulk nickel and Ni_3S_2 determined by experiments [1]. The black triangles are data points for the sulfur chemisorption isosteres on Ni surface with different surface coverage [3]. The red circles represent the experimentally determined critical H_2S concentration values above which the sulfur poisoning of fuel cell anode became significant [2].

TABLE 1. The Raman Vibrational Frequencies (cm^{-1}) Determined by Theoretical Calculations and Experiments for Ni_3S_2, NiS, Ni_3S_4 and NiS_2

Material	Modes	Calculated	Experiment
Ni_3S_2	E(1)	367, 367	351
	A_1(1)	320	325
	E(2)	317, 316	303
	E(3)	241, 241	223
	E(4)	204, 203	201
	A_1(2)	201	189
NiS	A_1(1)	356	370
	E(1)	341, 341	349
	A_1(2)	290	300
	A_1(3)	254	
	E(2)	252, 251	246
	E(3)	231, 230	
	E(4)	201, 201	
	E(5)	148, 148	
Ni_3S_4	A_{1g}(1)	388	375
	T_{2g}(1)	339, 338, 338	335
	T_{2g}(2)	284, 284, 283	285
	E_g(1)	208, 207	222
	T_{2g}(3)	206, 206, 205	
NiS_2	T_g(1)	462, 462, 461	489
	A_g(1)	446	479
	T_g(2)	342, 341, 341	
	E_g(1)	285, 285	285
	T_g(3)	278, 278, 277	273

from Raman measurements. The computed vibrational frequencies are generally in good agreement with Raman spectra obtained by experiments (with deviation of less than <10%) and can be used to identify nickel sulfides in our sulfur poisoning studies. The significance of the theoretical calculations is that previous studies on the nickel sulfide Raman spectra often contradicts one another, which makes it impossible to use any of them as a reliable reference.

Shown in Figure 2 is a picture of the multi-cell testing system built in our lab. The multi-cell system is capable of simultaneously testing 12 button cells under various electrochemical conditions (e.g., potentiostatic, galvanostatic, or potentiodynamic conditions) at a temperature up to 1,050°C. The gas distribution system can delivery gas mixtures from humidified inert gas (e.g., N_2), fuel (e.g., H_2), and H_2S containing fuels. It can supply up to four different fuel mixtures with H_2S concentration varying from 0.05 to 100 ppm.

FIGURE 2. The Multi-Cell Testing System Consisting of a High Temperature Furnace, a Gas Distribution System, and a 12-Channel Electrochemical Testing System

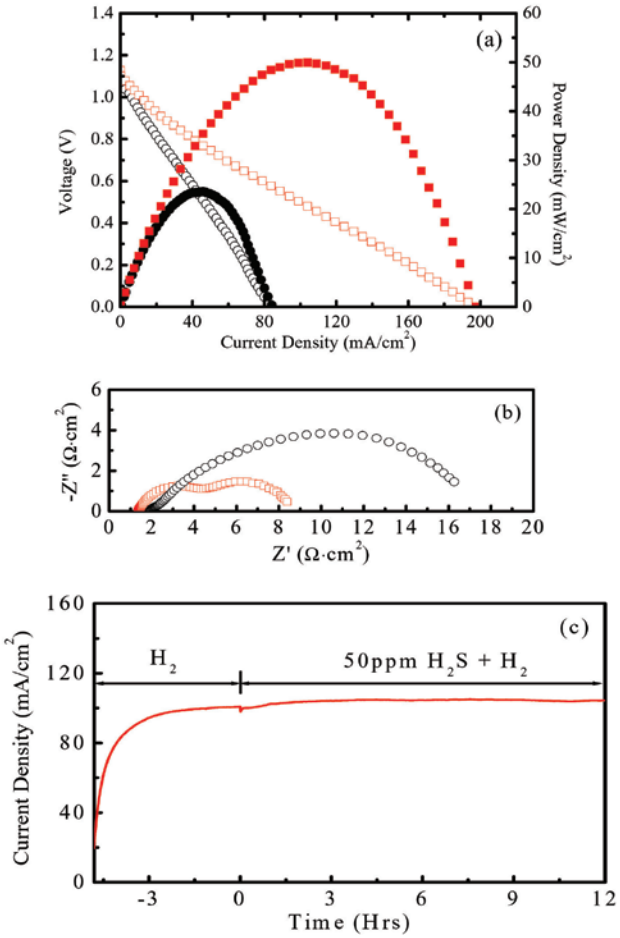

FIGURE 3. (a) Current-voltage relationship and power output and (b) impedance spectra for cells (Pt/YSZ/dense Ni-YSZ tri-layer structure) with (squares in red) and without (circles in black) Nb_2O_5 coating in dry H_2 at 700°C, and (c) the change in current density for the cell with a Nb_2O_5 coating over the dense Ni-YSZ anode in dry 50 ppm H_2S balanced with H_2 at 700°C.

Shown in Figure 3 are the electrochemical measurements on cells having a structure of Pt/YSZ/dense Ni-YSZ with or without Nb_2O_5 coating in dry H_2 at 700ºC. In Figure 3(a), the increased power density (from 23 to 49 mW/cm^2 for the cell with a Nb_2O_5 coating) indicates that Nb_2O_5 enhanced cell performance after (partially) reduced in H_2. This is also supported by the impedance data shown in Figure 3(b); the interfacial resistance decreased from 15 for the cell without Nb_2O_5 coating to 7 Ω·cm^2 for the cell with a Nb_2O_5 coating. Shown in Figure 3(c) is the stability of the cell with a Nb_2O_5 coated anode exposed to 50 ppm H_2S at 700°C. The current density dropped slightly as H_2S was first introduced, but quickly recovered to the same value as in H_2 fuel. The cell with Nb_2O_5 coating showed stable performance in fuel with 50 ppm H_2S for 12 h.

Conclusions and Future Directions

The effective operational windows have been identified from the computed Ni-S phase diagram, which can distinguish the clean Ni surface, the Ni surfaces partially covered with adsorbed sulfur atoms, and bulk nickel sulfide Ni_3S_2. A multi-cell testing system has been built: it enables simultaneous testing of up to 12 cells and can greatly increase the experiment output. The vibrations at the Γ-point of the sulfides are computed and confirmed with Raman measurements. Finally, the Nb_2O_5 coated Ni-YSZ anode showed promising sulfur tolerance in 50 ppm H_2S contaminated fuels.

Future work is briefly outlined as follows:

- Characterize both the short-term and long-term sulfur-poisoning effect for anode-supported SOFC button cells under various current density and H_2S concentrations.
- Optimize the surface modification process to achieve enhanced sulfur tolerance while maintaining reasonable cell performance and stability.

FY 2007 Publications/Presentations

1. Z. Cheng, S. Zha, and M. Liu, "Stability of Materials as Candidates for Suflur-Resistant Anodes of Solid Oxide Fuel Cells," *Journal of The Electrochemical Society*, **153**, A1302-A1309 (2006).

2. Y. M. Choi, C. Compson, Charles, M. C. Lin, M. Liu, "A mechanistic study of H_2S decomposition on Ni- and Cu-based anode surfaces in a solid oxide fuel cell," *Chemical Physics Letters*, **421**, 179-183 (2006).

3. J. Dong, Z. Cheng, S. Zha, and M. Liu, "Identification of Nickel Sulfides on Ni-YSZ Cermet Exposed to H_2 Fuel Containing H_2S Using Raman Spectroscopy," *Journal of Power Sources*, **156**, 461-465 (2006).

4. Y. M. Choi, C. Compson, M.C. Lin, and M. Liu, "Ab initio analysis of sulfur tolerance of Ni, Cu, and Ni–Cu alloys for solid oxide fuel cells," *Journal of Alloys and Compounds*, **427**, 25 (2007).

5. S. Zha, Z. Cheng, and M. Liu, "Sulfur Poisoning and Regeneration of Ni-based Anodes in Solid Oxide Fuel Cells", *Journal of The Electrochemical Society*, **154**, B201 (2007).

6. Z. Cheng, M. Liu, "Characterization of Sulfur Poisoning of Ni-YSZ Anodes for Solid Oxide Fuel Cells Using *in situ* Raman Microspectroscopy," *Solid State Ionics*, 178, 925, 2007.

7. J. H. Wang, M. Liu, "Prediction of Ni-S Phase Diagram using DFT Calculations and Thermodynamic Corrections," *Electrochemistry Communications*, in press.

8. J. H. Wang, Z. Cheng, J.-L. Bredas, M. Liu, " Electronic and Vibrational Properties of Nickel Sulfides: A Density Functional Theory Study," *Journal of Physical Chemistry C*, submitted.

9. J. H. Wang, M. Liu, "Computational Study of Surface Regeneration of Sulfur-Poisoned Ni surface under SOFC Operation Conditions by First-Principles and Thermodynamic Calculations," *Journal of Physical Chemistry C*, submitted.

References

1. T Rosenqvist: J. Iron Steel Inst. 176 (1954) 37.

2. Y Matsuzaki, I Yasuda: The poisoning effect of sulfur-containing impurity gas on a SOFC anode: Part I. Dependence on temperature, time and impurity concentration. Solid State Ionics 132 (2000) 261.

3. JG McCarty, H Wise: Thermodynamics of sulfur chemisorption on metals. I. Alumina-supported nickel. J. Chem. Phys. 72 (1980) 6332.

IV.A.10 Development of Inexpensive Metal Alloy Electrodes for Cost-Competitive Solid Oxide Fuel Cells

Steven J. Visco (Primary Contact),
Craig Jacobson and Lutgard De Jonghe
Lawrence Berkeley National Laboratory (LBNL)
Materials Science Division
Berkeley, CA 94720
Phone: (510) 486-5821; Fax: (510) 486-4881
E-mail: sjvisco@lbl.gov

DOE Project Manager: Lane Wilson
Phone: (304) 285-1336; Fax: (304) 285-4638
E-mail: Lane.Wilson@netl.doe.gov

Objectives

- Improve the low temperature performance of electrodes using catalyst infiltration technology developed at LBNL. Three approaches are currently under development:
  - **Type 1:** Infiltration of ionically conductive network (non-functional) with nanoparticles to yield a functional (ionically and electronically interconnected) electrode structure.
  - **Type 2:** Infiltration of functional cathodes with mixed ionic-electronic conductors (MIECs) to improve electrode performance (e.g., ceria nanoparticles on $La_{0.6}Sr_{0.3}Co_{0.8}Fe_{0.2}O_3MnO_{3-\gamma}$ [LSCF] network).
  - **Type 3:** Infiltration of functional composite electrodes with nanoparticles (e.g., $La_{0.65}Sr_{0.3}MnO_{3-\gamma}$ [LSM] or ceria nanoparticles into a composite yttria-stabilized zirconia [YSZ]-LSM network) to improve low temperature performance.
- Standardized testing.
  - Design and fabrication of pressure-contact rigs.
  - Design and fabrication of a standard 5 x 5 cm solid oxide fuel cell (SOFC) stack.
  - Determination of performance and degradation rate in a standard stack.
  - Determination of degradation rate of commercial SOFC plates with and without catalyst infiltration.
- Engineer performance of interconnect alloys through control of oxide scale growth and conductivity.
- Mechanistic studies of Cr contamination of air electrode structures.
- Assist potential U.S. manufacturers of SOFC components through collaborative efforts.
- Technology transfer (through in-house training and instructional DVD production).

Approach

- Develop low-cost metal salt infiltration technology to boost the performance of the air electrode, particularly at temperatures below 700°C. The LBNL technology involves the use of simple catalyst impregnation to yield dispersed nano-particles, or a viscous catalyst precursor is vacuum impregnated into porous structures to yield a connected catalyst network. Vacuum impregnation can be accomplished with a porous electrolyte structure or and electrode/electrolyte (LSM/YSZ) network.
- Design and fabricate a standardized 2-cell SOFC stack to be used as a platform for comparative studies between universities, national labs, and industry.
- Measure the baseline performance and long-term stability of commercially produced air electrodes with and without an infiltrated catalyst.
- Determine the mechanism for Cr migration from steel-based interconnects into the air electrode and devise strategies to mitigate or minimize degradation behavior due to Cr poisoning.

Accomplishments

- **Refinement of infiltration technology:** The LBNL infiltration technology has undergone continual refinement over the past 24 months, and we are now able to infiltrate a variety of complex microstructures including conventional air electrodes and porous electrolyte networks. In one approach the LBNL team infiltrated a dispersed catalyst using simple nitrate precursors. We are now collecting data on commercial air electrodes with and without infiltration to see the effect of instantaneous performance and long-term degradation. In another approach, we impregnate a wide variety of microstructures with electrode catalysts using vacuum infiltration.
- **Completed design and fabrication of a standard SOFC stack:** The LBNL group worked with McAllister Technical Services to design the first standard 2-cell SOFC stack for 5 x 5 cm SOFC plates; the team also worked with Lane Wilson of the National Energy Technology Laboratory

(NETL) to refine the design and considered input from Argonne and Pacific Northwest National Laboratories in the final phases of the design.

- **Sulfur tolerance:** The LBNL team infiltrated a variety of anode structures with nanoparticulate ceria and demonstrated excellent tolerance to sulfur (as H_2S); LBNL is also working with industrial team members to determine if this technique can be used with their specific anode structures.

Future Directions

- **Optimize infiltration technology:** The LBNL team is continually refining the technology for catalyst infiltration to accommodate a wide range of air electrode (or anode) compositions and microstructures. This capability allows industrial teams to adapt the LBNL approach to their specific needs. The LBNL group has also begun to test its infiltration technology on industrial team structures and will continue to do so as part of the technology transfer process.
- **Determine long-term stability of infiltrated electrodes:** The LBNL team has redesigned its cell test rig for long-term testing and has placed an order with H.C. Starck/InDec for 3 cm SOFC discs and 5 cm x 5 cm SOFC plates. LBNL will use these for baseline testing and then compare degradation rates for infiltrated and non-infiltrated SOFC electrodes.
- **Short-term and long-term testing in a standard SOFC stack:** The LBNL team completed the design of the 5 x 5 cm standard stack and has received the machined parts for assembly. In the next contract period we will begin testing in the 2-cell stack. Initial studies will be focused on contact pastes and seals to assure reliable operation, followed by long-term testing for comparison to single-cell tests of infiltrated and non-infiltrated SOFC electrodes.
- **Elucidate the interplay of electrode composition and microstructure on cell performance:** As we continue to improve infiltration technology and understand its relationship to electrode performance and longevity, we will continue our limited work in transmission electron microscopy of electrode/electrolyte interfaces to elucidate the role of impurities and reaction products in limitations to cell life.
- **Technology transfer:** The LBNL team initiated technology transfer in FY 2007 through collaboration with industrial team members and by the hosting of an infiltration workshop at LBNL; the LBNL group also provided an instructional DVD to interested Solid State Energy Conversion Alliance (SECA) members.

Introduction

Among the most challenging hurdles to the commercialization of solid oxide fuel cell technology is the need to manage cost such that SOFCs are competitive with entrenched power generation technologies. The LBNL group has long maintained that the key to a cost-effective SOFC solution is to develop systems operating in the 650 to 700°C range. A number of SECA industrial teams are now pursuing that goal as well. In order to achieve the 40,000 hour life needed for distributed generation, it is clear that stainless steel interconnects will have to be maintained at temperatures below 800°C. Since electrode kinetics (and electrolyte conductivity) are thermally activated, it is not a trivial task to maintain SOFC performance as the operating temperature is lowered. The LBNL group has developed several infiltration techniques whereby standard LSM electrodes can be modified to perform well at temperatures as low as 650°C. Electrode modification can be as simple as infiltrating a metal nitrate such as $Co(NO_3)_2$, involve a mixture of precursors to form a known electrocatalyst such as $Sm_{0.6}Sr_{0.4}CoO_{3-\delta}$ (SSC), or use the newly developed LBNL technique of vacuum impregnation of porous structures with connected nano-particle architectures. The LBNL group has also performed extensive investigations into high temperature corrosion of stainless steel alloys for interconnects, determined the Cr vaporization rates for steels in humidified air, and developed low-cost coating technologies that reduce Cr vaporization to negligible levels while simultaneously improving oxidation behavior. The LBNL team has initiated measurement of degradation rates of infiltrated and non-infiltrated air electrodes produced in-house and by commercial suppliers. We are also conducting focused ion beam (FIB) and transmission electron microscopy (TEM) studies to aid in the elucidation of fundamental mechanisms for air electrode degradation and failure.

Approach

In order to achieve SECA commercialization targets, a number of SOFC developers are targeting reduced operating temperatures as a means of controlling cost. The LBNL effort is aligned with that goal through the use of electrode infiltration technology to boost the performance of the air electrode. The LBNL team has now focused its infiltration technology to cover three basic types of infiltration: 1) infiltration of ionically conductive network (non-functional) with nanoparticles to yield a functional (ionically and electronically interconnected) electrode structure; 2) infiltration of functional cathodes with MIECs to improve electrode performance (e.g., ceria nanoparticles

on LSCF network); and 3) infiltration of functional composite electrodes with nanoparticles (e.g., LSM or ceria nanoparticles into a composite YSZ-LSM network) to improve low-temperature performance. The LBNL team has also designed long-term test rigs and standardized stacks to verify the persistence of the performance boost afforded by infiltration technology. LBNL also works directly with industrial team members to determine whether or not the existing infiltration technology is compatible with vertical team SOFC structures or needs to be modified to suit their needs. We are also investigating the mechanism of Cr transport in a variety of cathode compositions and microstructures in order to generate strategies to minimize or eliminate air electrode performance degradation due to Cr poisoning.

Results

The infiltration (impregnation) of nanoscale particles, forming connected networks, into solid oxide fuel cell electrodes, has been shown to lead to considerable benefit in performance. Porous electrode skeletons (backbones), consisting of electrolyte material such as YSZ, when infiltrated, delivered results comparable to those of the standard Ni-YSZ and LSM-YSZ electrode configurations. Additionally, the performances of both single component mixed ionic electron conductor and of composite electrodes have been significantly enhanced by the connected nanoscale particle networks formed by infiltration.

Nanoscale materials (<100 nm) are receiving increased interest for application in devices where their unusual properties may possibly be exploited. In SOFCs they can be added as catalyst, where it has been theorized that the advantageous catalytic properties of nanosized oxides relate to an enhanced surface vacancy concentration and increased ionic and electronic conductivities. However, due to the elevated operating temperatures found in modern SOFCs, 500-750°C, the use of entirely nanostructured components would undoubtedly lead to structural instability. Hence, nanoparticles have been incorporated in conjunction with more stable micrometer-sized supporting functional architectures.

To enhance electrode performance at the lower operating temperatures, nanoparticulates are added to the internal surfaces of the porous electrodes to enhance some aspect of the electrode processes. The nanoparticulates are typically added through processes that involve the precipitation of a metal salt in the pores of the electrodes, and their subsequent decomposition, to generate the desired nanoparticulate metallic or oxide catalyst. This method of electrode enhancement has proved reasonably successful. Additionally, it has been found that higher electrode loading of nanoparticulate catalysts further increases performance. Unfortunately, the particle distribution produced by typical infiltration methods necessitates a large number of repetitions to produce a connected network of nanoparticulates, causing pore filling besides the intended coating of pore walls. Progressive filling of the pores has the drawback of causing gas diffusion limitations within the electrodes, which in turn limit performance at higher current densities. It would therefore be advantageous to engineer a uniform networked nanoparticulate layer within the electrodes, involving a minimal number of processing steps. Previously, uniform and continuous networks of nanoparticulates were incorporated into porous electrodes by infiltration. Importantly, the infiltration could be completed in a single processing step on both electrodes. Additionally, since the method is independent of all other processing steps, it can be preformed at lower temperatures, allowing for the use of otherwise reactive nanoparticulate catalysts. The engineering of enhanced SOFC electrodes through the incorporation of networked nanoparticulate layers is more generally elaborated below. Advances in infiltration methods as well as their application to three SOFC electrode classes will be discussed. A single-step method is demonstrated, which not only improves performance in both fuel and air electrodes but additionally decreases the rate-limiting step in the cathode's oxygen reduction reaction at intermediate temperatures. The engineering of electrodes to such a level has broad implications for the improvement of SOFC performance.

In Figure 1, schematic illustrations of both a general and a nanostructured SOFC electrode are shown. The schematic can be used to describe the three classes of SOFC electrodes: (a) porous electrolyte backbones with infiltrated electrocatalyst; (b) single-component MIEC backbones; and (c) composite electrodes backbones. Both the nanoscale component of the electrode and the micronscale backbone grains, which

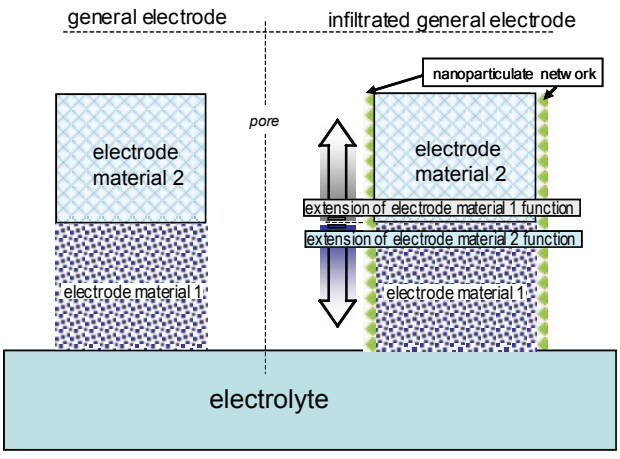

FIGURE 1. Cross-Sectional Illustration of Nanoparticulate Infiltration into a General Composite Electrode

TABLE 1. Function of Backbone and Nanoparticles within Each Electrode Class

Porous Electrode Class	Backbone Function	Nanoparticle Functions
Single Component Electrolyte Composition	oxygen ion conduction	global electron supply -electrocatalyst
MIEC	oxygen ion and electron conduction -electrocatalyst	local oxygen ion conductivity -electrocatalyst
Composite	global oxygen ion and electron conductivity -electrocatalyst	local oxygen ion and electron conductivity -electrocatalyst

they are built on, serve a distinct purpose within each of the SOFC electrode classes. These functions are listed in Table 1 and will be further described in the following sections. An important advance in the single-step infiltration procedure involved the modification of the chain length of the surfactant, Triton X, from n~10 for Triton X-100 to n~5 for Triton X-45. Assuming that micelles form in the precursor solutions and that the contents of the micelles are similar, a switch to a shorter chain length would yield a considerable increase in material deposited by the infiltration. This decrease in surfactant chain length has facilitated the formation of well-connected nanoparticulate networks in a single step within less open electrodes. A conventional LSM/YSZ composite air electrode infiltrated with this improved method is shown in Figure 2, showing nearly complete coverage in a single step as compared to earlier efforts where the infiltrated electrodes were of highly porous electrodes. With the ability to form well-connected nanoparticulate networks in a single processing step within conventional electrodes, focus can be shifted to decreasing the size of the nanonparticles, so as to exploit further the distinct properties that can be achieved at the nanoscale. For example, changes in infiltration procedure such as decreasing the concentration of the precursor solution, altering reaction rates, modifying the pH, or exploring other surfactants can yield micelles of the proper constitution to synthesize smaller nanoparticles within the porous electrodes.

(A) Infiltrated Porous Electrolyte Backbone Electrodes. Infiltration of porous electrodes is used to avoid solid-state reaction between the electrolyte and electrode materials that may otherwise occur at the elevated processing temperatures (~1,100-1,300°C) needed to sinter such structures. One type of backbone for such electrodes, as can be visualized using Figure 1, would consist of the backbone grains being composed of the same material as the electrolyte. However, since electrolyte material usually serves no catalytic purpose and only provides an ion-conducting pathway, it is necessary to infiltrate a second material, which can form the electron pathways as well as the electrocatalytic sites within the electrode. The main advantage in this case is the ability to infiltrate superior electrocatalysts. As is shown in Figure 3, an LSM-infiltrated electrocatalyst is compared to a superior LSF infiltrated electrocatalyst. LSM has been the material of choice in composite air electrodes because of its minimal interactions with YSZ at the elevated processing temperatures; however, it is a relatively poor electrocatalyst at intermediate operating temperatures. Therefore, since the infiltration procedure only requires low-temperature sintering, 600-1,000°C, a reactive but otherwise effective electrocatalyst such as LSF can

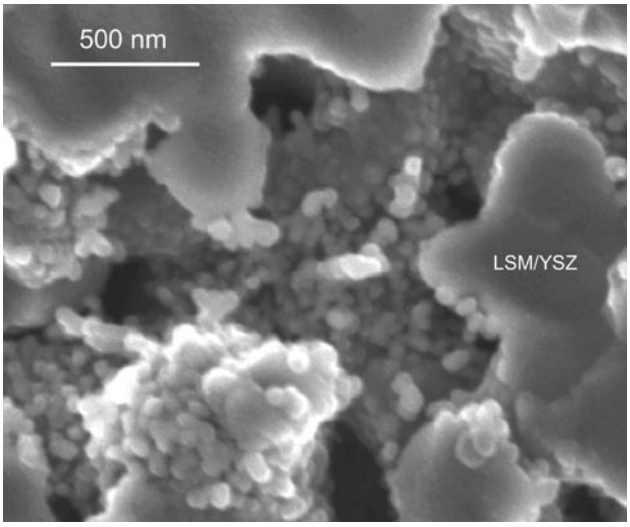

FIGURE 2. Secondary Electron Micrograph of Conventional LSM-YSZ Cermet Air Electrode Infiltrated with YDC

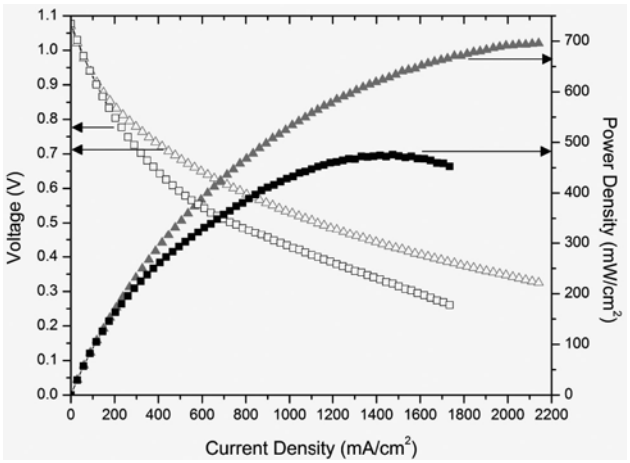

FIGURE 3. 700°C performance of anode supported cell with porous YSZ air electrode infiltrated with LSM (■) or LSF (▲). The power density at 0.7 V is about 15% higher for LSF compared to LSM infiltrated backbones.

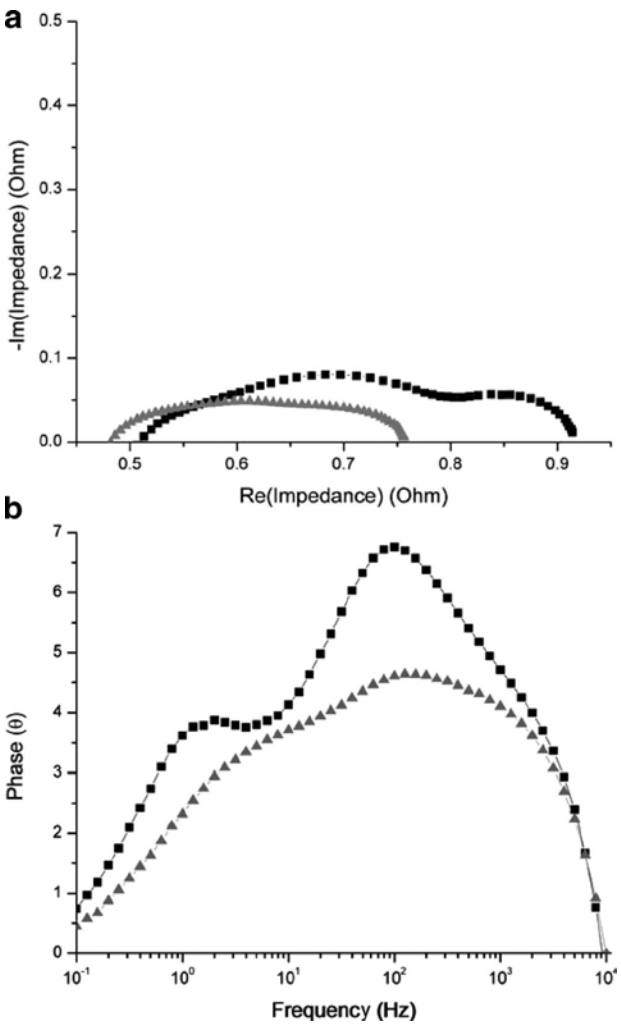

FIGURE 4. 700°C AC Impedance Characteristics of Electrolyte Supported LSCF Symmetric Cell at OCV, a) Nyquist and b) Bode Plots for Cathode Before (■) and After (▲) Infiltrating with YDC

be used. In the I-V cure in Figure 3, the enhanced electrocatalytic activity is illustrated by both the decreased overvoltage and the lower slope of the porous YSZ electrode activated by LSF infiltration.

(B) Infiltrated MIEC Backbone Electrodes. A major reason for LSF's superior electrocatalyic activity at lower operating temperatures is its mixed conductivity. The ability of MIECs to provide both electron and oxygen ion conduction pathways through an electrode, allows them to be utilized as single-component electrodes. To visualize these electrodes, consider both electrode grains to be composed of the MIEC in Figure 1. Even though MIEC electrodes are better electrocatalysts than LSM at intermediate temperatures, they can be improved by infiltration, as seen in Figure 4. Alternating current impedance characteristics of a LaSrCoFe (LSCF) symmetric cell provided by H.C. Stark are shown before and after the infiltration with nanoparticulate $Y_{0.2}Ce_{0.8}O_{1.9}$ (YDC). Since LSCF already provides sufficient electronic conductivity, it only stands to benefit from the ionic conductivity of the infiltrated YDC and possibly from additional catalysis. The enhanced ionic conductivity in the electrode away from the electrolyte surface can be seen by the decrease in ohmic resistance in the Nyquist plot, Figure 4a, and by the decrease in the maximum phase shift of the high frequency arc of the Bode plot (~102 Hz), Figure 4b. Additionally, there is a decrease in the phase angle (θ) of the low frequency arc of the Bode plot (~1 Hz), Figure 4b, indicating that even LSFC, a good electrocatalyst at intermediate operating temperatures, can be catalytically enhanced by infiltrated nanoparticles.

(C) Composite Backbone Electrodes. As for MIEC electrodes, the incorporation of nanoparticulate networks into working electrodes can produce added electrocatalysis, but more importantly in the case of composite electrodes, it can expand the strict triple phase boundary (TPB) reaction area typical for composite electrodes. Following Figure 1, the electrode is now composed of both electrode and electrolyte grains, providing percolative networks for both electronic and ionic conduction, respectively. The nanoparticulate chosen for infiltration was YDC. YDC has a high ionic conductivity as well as sufficient electronic conductivity, especially in nanoparticulate form as has been demonstrated in the case of ceria, allowing for both ionic and electronic extension of the TPBs. Because composite electrodes already possess built-in electronic and ionic percolation networks through the electrode, the nanoparticulate YDC network layer does not need to be continuous throughout the electrode, since only short-range extension at the grain level dimension is needed. This significantly decreases the dependence of the cell on the morphological stability of the nanonparticulate networks, because a structurally stable backbone is already present.

Air Electrodes. Dramatic improvements in performance of a standard LSM-YSZ cathode are directly evident in the AC impedance characteristics, Figure 5. After infiltration with YDC, the Nyquist plot, Figure 5a, reduced in size to less than 50% of its original form. The lowering in overall cell impedance is more readily seen in the Bode plot which explicitly shows frequency information, Figure 5b. There is an overall decrease in the phase angle (θ) after infiltration, for both the intermediate ~10 Hz and high ~104 Hz frequency peaks, with the intermediate frequency peak at ~10 Hz most drastically reduced. This intermediate frequency peak is usually associated with slow surface kinetics on the LSM-YSZ air electrode. The strong decrease in the phase angle and in the overall impedance at

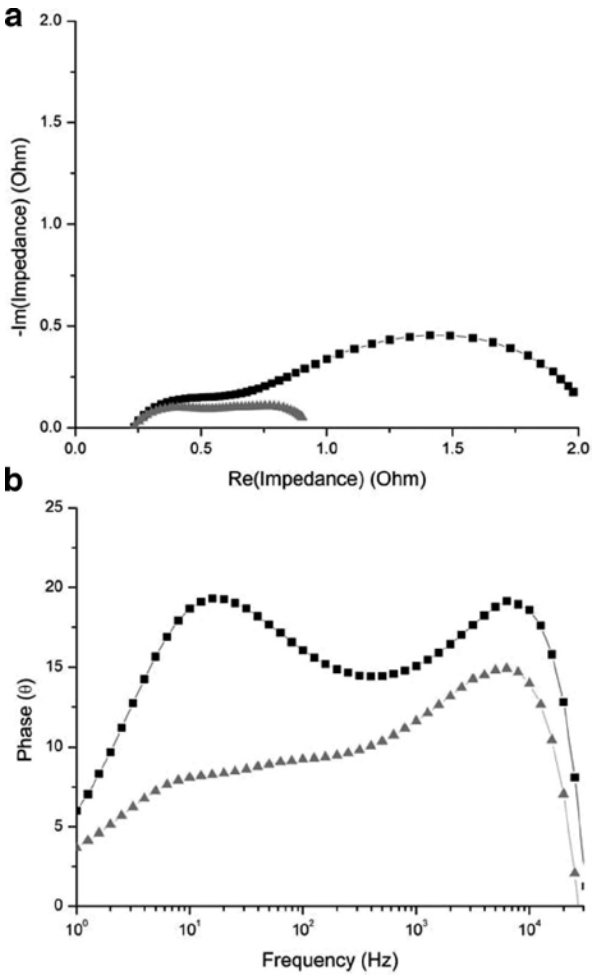

FIGURE 5. 700°C ac impedance characteristics of anode-supported cell with LSM-YSZ cathode: (a) Nyquist and (b) Bode plots before and after (2) infiltration of YDC.

this frequency following infiltration suggests that the enhanced microstructure minimizes the rate-limiting step in the reduction reaction within LSM-YSZ cathodes.

The result of the infiltration is a dramatic increase in cell performance, Figure 6. Even though the increase in peak power density from 208 to 519 mW/cm^2 before and after infiltration, respectively, is impressive, the most significant result of the infiltration is a dramatic increase in the power densities at low overpotentials. The cell shows a drastic enhancement of power density at 0.7 V from ~135 mW/cm^2 before infiltration to ~370 mW/cm^2 after infiltration. This decrease in "activation" losses is a marked improvement compared to infiltrated systems with isolated nanoparticulates.

Fuel Electrode. Though the largest improvements in performance at intermediate operating temperatures stand to be made within air electrodes, significant improvement in fuel electrode AC impedance

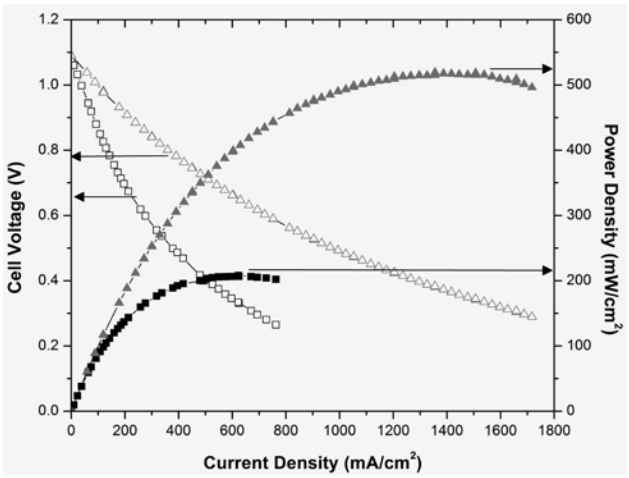

FIGURE 6. Enhancement of Anode Supported LSM-YSZ Cathode Before (■) and After (▲) Infiltration of YDC, at 700°C

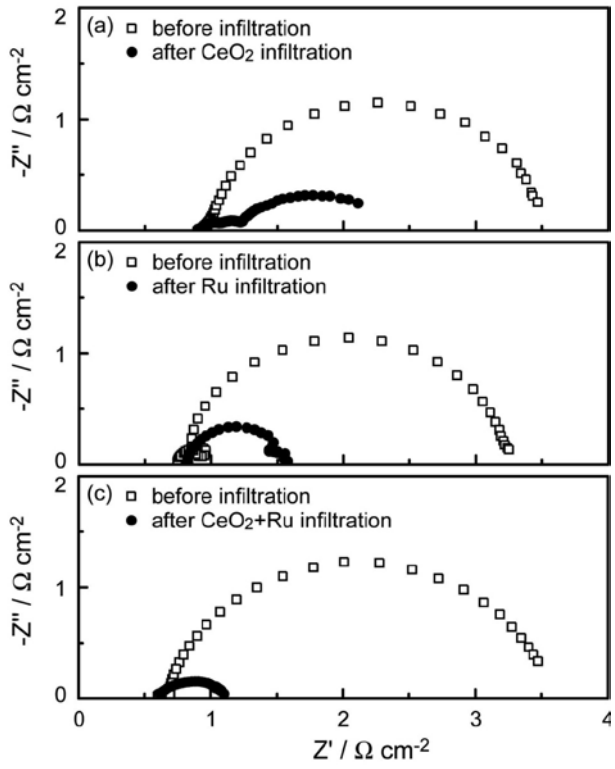

FIGURE 7. Impedance Spectra at 1,073 K for the Cells: (a) Before and After the Ceria Infiltration, (b) Before and After the Ru Infiltration, (c) Before and After the Ceria and Ru Infiltration

characteristics at open circuit voltage (OCV) are evident following infiltration of $Sm_{0.2}Ce_{0.8}O_{1.9}$ (SDC), Figure 7. Unlike for the air electrodes, it is the high-frequency peak at ~104 Hz that correlates with the pronounced decrease in the overall cell impedance seen in the Nyquist plot, Figure 7a. A decrease in phase angle (θ) at high frequencies is common to both air, Figure 5b, and

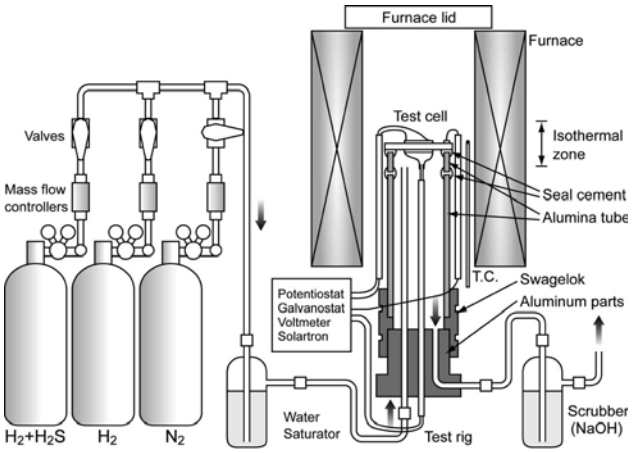

FIGURE 8. Schematic Diagram of Experimental Apparatus for Sulfur-Tolerant Anode Test

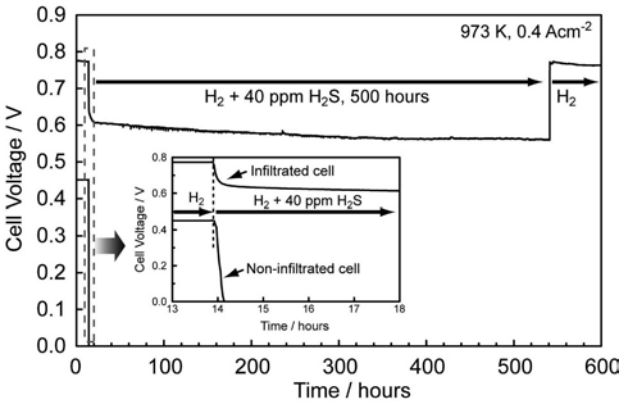

FIGURE 9. Cell Voltage as a Function of Time for Cells Exposed to 40 ppm H_2S at 973 K

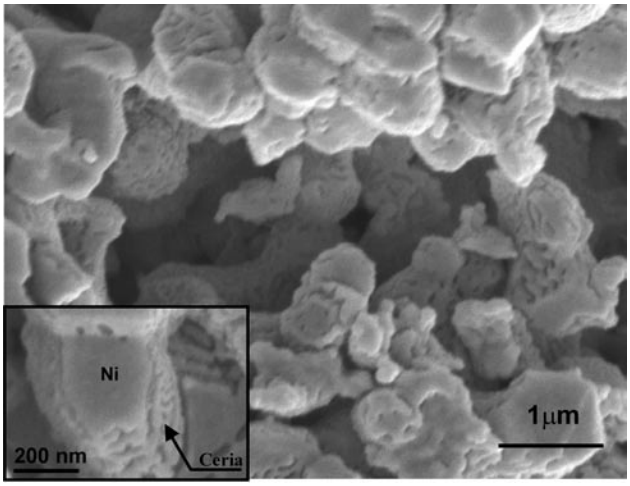

FIGURE 10. Scanning Electron Micrographs of Ceria Infiltrated Cathode Supported Cell After Exposure to 40 ppm H_2S for 500 Hours

fuel electrodes, Figure 7b, suggesting a common origin. While a number of electrode-specific processes have been associated with this high-frequency peak, they can be broadly grouped into the category of charge-transfer processes within the electrodes. As described earlier, the enhanced microstructure produced by the infiltration method will provide additional pathways through the electrodes, in essence minimizing the pathway for charge transfer, producing an increase in overall cell reaction area. While the improvement was seen in the cell's AC impedance characteristics at OCV after infiltration, it does not translate into significant improvement in cell performance at low overvoltages, Figure 7. However, the infiltration produces a measurable increase in peak power density, from ~348 to ~403 mW/cm^2.

While the increase in fuel electrode performance is the most immediate benefit of the SDC infiltration, a more vital result is the significant increase in sulfur tolerance that is obtained. A number of cells have been tested (see Figure 8 test apparatus) and have shown sustained sulfur tolerance up to 40 ppm H_2S using the conventional Ni-YSZ material set infiltrated with doped and undoped ceria. These preliminary tests indicate that it is possible to allow for the use of any commercial natural gas and promises that with further optimization of the anode microstructure and infiltration composition, stable sulfur tolerant anodes can be achieved using the conventional composite Ni-YSZ anodes. Additionally, the infiltration of ceria can aid the stability of Ni-YSZ fuel electrodes by preventing sintering, grain growth and agglomeration of the Ni phase, as well as providing the ability to directly reform hydrocarbons. Therefore, because doped ceria infiltration can enhance both the air and the fuel electrodes performance, it should be the preferred choice for single-step infiltration of both SOFC electrodes, while at the same time decreasing manufacturing time and cost.

The stability of the nanostructured SOFC electrodes under the fuel cell operating conditions is of potential concern. However, extended stability has been demonstrated for several systems: LSM-infiltrated porous electrolyte backbones have shown over 500 hours of continued performance enhancements at 650°C; ceria-infiltrated Ni-YSZ fuel electrodes, in humidified hydrogen containing significant concentrations of sulfur, were stable for over 500 hours at 700°C; and doped ceria-infiltrated LSM-YSZ air electrodes have been stable at 700°C in the 100+ hour tests conducted to date (see Figures 9 and 10).

Conclusion

A single-step infiltration method, producing connected nanoparticulate networks in porous SOFC backbone electrodes, improves both air and fuel electrode performance. The nanoscale nature of the

infiltrated material has shown advantages in enhancing all three electrode classes and is expected to yield further benefits with progress in decreasing infiltrated nanoparticle size.

FY 2007 Publications/Presentations

1. Tucker, M. C.; Kurokawa, H.; Jacobson, C. P.; De Jonghe, L. C.; Visco, S. J., "A fundamental study of chromium deposition on solid oxide fuel cell cathode materials," **Journal of Power Sources** 2006, 160, (1), 130. Publisher: Elsevier, Netherlands.

2. Sholklapper, T. Z.; Lu, C.; Jacobson, C. P.; Visco, S. J.; De Jonghe, L. C., "LSM-Infiltrated Solid Oxide Fuel Cell Cathodes," **Electrochemical and Solid-State Letters** 2006, 9, (8), A376. Publisher: The Electrochemical Society, USA.

3. Sholklapper, T. Z.; Radmilovic, V.; Jacobson, C. P.; Visco, S. J.; De Jonghe, L. C., "Synthesis and stability of a nanoparticle-infiltrated solid oxide fuel cell electrode," **Electrochemical and Solid-State Letters** 2007, 10, (4), 74–76. Publisher: The Electrochemical Society, USA.

4. Kurokawa, H.; Jacobson, C. P.; DeJonghe, L. C.; Visco, S. J., "Chromium vaporization of bare and of coated iron-chromium alloys at 1073 K," **Solid State Ionics** 2007, 178, (3-4), 287. Publisher: Elsevier, Netherlands.

5. Kurokawa, H.; Yang, L.; Jacobson, C. P.; De Jonghe, L. C.; Visco, S. J., "Y-doped SrTiO3 based sulfur tolerant anode for solid oxide fuel cells," **Journal of Power Sources** 2007, 164, (2), 510. Publisher: Elsevier, Netherlands.

6. Kurokawa, H.; Lau, G. Y.; Jacobson, C. P.; De Jonghe, L. C.; Visco, S. J., "Water-based binder system for SOFC porous steel substrates," **Journal of Materials Processing Technology** 2007, 182, (1-3), 469. Publisher: Elsevier, Netherlands.

7. Sholklapper, T.; Kurokawa, H.; Jacobson, C. P.; Visco, S. J.; De Jonghe, L. C., "Enhancing Cathode Performance and Anode Sulfur/Carbon Tolerance of SOFCs by Nano-Infiltration," **ECS Transactions** 2007, 7, (1), 837. Publisher: The Electrochemical Society, USA.

8. Sholklapper, T. Z.; Kurokawa, H.; Jacobson, C. P.; Visco, S. J.; DeJonghe, L. C., "Nanostructured Solid Oxide Fuel Cell Electrodes," **Nano Letters** 2007. in press. (available online June 9, 2007). Publisher: American Chemical Society, USA.

9. Kurokawa, H.; Sholklapper, T. Z.; Jacobson, C. P.; Visco, S. J.; De Jonghe, L. C., "Ceria Nanocoating for Sulfur Tolerant Ni-Based Anodes of Solid Oxide Fuel Cell," **Electrochemical and Solid-State Letters** 2007, 10, (9), in press. Publisher: The Electrochemical Society, USA.

10. Steve Visco, Hideto Kurokawa, Mike Tucker, Tal Sholklapper, Xuan Chen, Ken Lux, Craig Jacobson, Lutgard De Jonghe, "Cathode Infiltration," presentation at **7th Annual SECA Workshop and Peer Review**, Philadelphia, PA, September 13, 2006.

11. Steve Visco, Hideto Kurokawa, Mike Tucker, Inna Belogolovsky, Grace Lau, Craig Jacobson,

12. Peggy Hou, Lutgard De Jonghe, "Interconnects," presentation at **7th Annual SECA Workshop and Peer Review,** Philadelphia, PA, September 13, 2006.

13. Hideto Kurokawa, Craig Jacobson, Peggy Hou, Steve Visco and Lutgard De Jonghe, "The effect of protective coatings for alloy interconnect on oxidation and Cr vaporization," presentation at **Materials Science and Technology 2006**, Cincinnati, OH, October 15–19, 2006.

14. Mike Tucker, Craig Jacobson, Lutgard De Jonghe, and Steve Visco, "Metal-Supported Thin Film Electrolyte SOFCs," presentation at **Materials Science and Technology 2006**, Cincinnati, OH, October 15–19, 2006.

15. Tal Zvi Sholklapper, Craig Jacobson, Steve Visco, and Lutgard De Jonghe, "Advances in Single Step Electrode Infiltration," presentation at **Materials Science and Technology 2006**, Cincinnati, OH, October 15–19, 2006.

16. Michael Tucker, Craig Jacobson, Hideto Kurokawa, Tal Sholklapper, Lutgard DeJonghe, Steve Visco, "SOFC Designed for Rapid Thermal Cycling", presentation at **Fuel Cell Seminar**, Honolulu, HI, November 13–17, 2006.

17. Tal Sholklapper, Craig Jacobson, Steven Visco, Lutgard De Jonghe, "Stable Nanoparticulate SOFC Electrodes," presentation at **American Ceramic Society's 31st International Conference & Exposition on Advanced Ceramics and Composites**, Daytona Beach, FL, January 21–26, 2007.

18. Grace Lau, Michael Tucker, Hideto Kurokawa, Craig Jacobson, Steven Visco, and Lutgard DeJonghe, "Mechanism of Chromium Transport during Solid-State Diffusion on Cathode Materials of Solid Oxide Fuel Cells," presentation at **American Ceramic Society's 31st International Conference & Exposition on Advanced Ceramics and Composites**, Daytona Beach, FL, January 21–26, 2007.

19. Michael Tucker, Grace Lau, Craig Jacobson, Steven Visco, and Lutgard DeJonghe, "Advances in Metal-Supported SOFCs," presentation at **American Ceramic Society's 31st International Conference & Exposition on Advanced Ceramics and Composites**, Daytona Beach, FL, January 21–26, 2007.

20. Michael Tucker, Grace Lau, Craig Jacobson, Lutgard DeJonghe, and Steven Visco, "Metal Supported SOFCs," presentation at **Electrochemical Society's Tenth International Symposium on Solid Oxide Fuel Cells (SOFC X),** Nara, Japan, June 3–8, 2007.

Workshops & Instructional Videos

1. LBNL Infiltration Workshop, February 16, 2007, Berkeley, CA.

2. LBNL Infiltration Workshop DVD (available by request).

Special Recognitions & Awards/Patents Issued

1. United States Patent 7,163,713; Craig Jacobson, Steven J Visco, Lutgard C. DeJonghe, "Method for making dense crack free thin films", issued January 16, 2007.

2. United States Patent 7,118,777; Steven J Visco, Craig Jacobson, Lutgard C. DeJonghe, "Structures and fabrication techniques for solid state electrochemical devices", issued October 10, 2006.

3. Tal Sholklapper: Dr. Bernard S. Baker Award for Fuel Cell Research: 2nd Place Winner, Presented by the Fuel Cell Seminar and FuelCell Enegry, Inc., 2006.

IV.A.11 Reliability and Durability of Materials and Components for Solid Oxide Fuel Cells

Edgar Lara-Curzio (Primary Contact), Ke An, Rosa Trejo, and Randy Parten
Oak Ridge National Laboratory
1 Bethel Valley Rd.
Building 4515, MS-6062
Oak Ridge, TN 37831-6062
Phone: (865) 574-1749; Fax: (865) 574-4913
E-mail: laracurzioe@ornl.gov

DOE Project Manager: Travis Shultz
Phone: (304) 285-1370
E-mail: Travis.Shultz@netl.doe.gov

Objectives

- To support the Solid State Energy Conversional Alliance (SECA) industrial teams towards the development of reliable and durable solid oxide fuel cells (SOFCs).
- To support SECA Core Technology Program (CTP) modeling efforts by establishing material property databases.
- To establish failure criteria for SOFC materials and components associated with thermal fatigue and other degradation mechanisms.
- To determine the fracture behavior of SOFC materials and their interfaces.

Accomplishments

- Developed a test procedure to quantify the fracture toughness of interfaces between cathode contact paste and metallic interconnects.
- Assessed the effect of sintering temperature and sintering time on the fracture toughness of interfaces between cathode contact paste and metallic interconnects.
- Contributed to the preparation of a design guide for solid oxide fuel cells.

Introduction

The steady decrease in performance, as determined by steady decreases in voltage with time, exhibited by some planar SOFCs has been associated with processes that occur on the cathode side of the cell. Some of these processes result from the interaction between the cathode and the interconnect material [1].

Interconnect materials for SOFC fall into two categories: conductive ceramics for operation at high temperature (900 to 1,000°C) and metallic alloys for lower temperature operation. Metallic interconnects have the advantage of higher electronic and thermal conductivity, higher ductility, and better workability [2]. However, even at lower operating temperatures, design requirements for metallic interconnects are challenging because they must maintain uniform contact (usually requiring some pressure) with the electrodes and in the case of the cathode, preserve low contact resistance while exposed to oxidizing conditions [3].

To reduce interfacial resistance, electrical contact layers are often applied between the cathode and the metallic interconnect during assembly of SOFC stacks. The contact material must be chemically compatible in oxidizing conditions with both the interconnect material and the cathode because reactions could result in the formation of phases that could lead to an increase in contact resistance or thermal expansion mismatches that could lead to delamination. It is common to sinter the contact layer during the first heating cycle of the stack in which case it is important that the contact material possesses appropriate sintering activity to increase contact area and thus decrease contact resistance. However, excessive sintering could eliminate porosity in the contact layer and block airflow to the cathode/electrolyte interface, thus affecting cell performance [4].

The objective of this study is to identify and utilize test techniques to determine the physical and mechanical properties of cathode contact paste materials and the mechanical properties of the interfaces that exist among the cathode, the contact paste and metallic interconnects or coated metallic interconnects in SOFCs. The properties obtained in this study will support ongoing efforts to develop models of the thermomechanical and electrochemical behavior of SOFCs. This study will also provide insight into the mechanisms responsible for the degradation of SOFCs and in turn, strategies to overcome these limitations, particularly when SOFCs are subjected to service conditions for long periods of time, including cyclic operation.

Approach

Test specimens were prepared by cutting strips of the metallic alloy Crofer 22 APU (ThyssenKrupp VDM) by electric discharge machining followed by grinding using 1200 grit silicon carbide sand paper to obtain beams with dimensions of 30 mm x 2.5 mm x 0.2 mm and 15 mm x 2.5 mm x 0.2 mm. One end of the short beams was impregnated with a solution of 97% BN, 1% MgO

and 2% SiO_2 to prevent wetting in subsequent steps and to facilitate the initiation of a delamination crack. A layer of lanthanum strontium manganate (LSM) contact paste (LSM-20 Ink, FuelCellMaterials) was applied on one side of a 30-mm long beam and the two 15-mm long beams were placed on top of the coated beam. A fixture was fabricated to ensure the alignment of the beams and to control the thickness of the LSM contact paste. Test specimens were allowed to dry in air followed by heating at a rate of 3°C/min to various sintering temperatures and for various periods of time. A sharp blade was used to introduce a notch between the two 15-mm long beams. The edges of some test specimens were polished according to standard metallographic techniques to facilitate microstructural observations after the test. Figure 1 illustrates the sequence of steps followed to prepare the test specimens.

The test specimens were evaluated in four-point bending following a modified version of the test method of Charalambides et al., which allows the determination of the critical energy release rate at bi-material interfaces by means of four-point bending under approximately equal shear and normal displacement conditions [5-6]. This test method is attractive for this application because it uses a relatively simple sample geometry and a well-established testing procedure. The sample geometry consists of a sandwich structure comprised of metallic interconnect layers bonded by a layer of contact paste as described above. The top metallic interconnect layer suppresses the segmentation of the brittle contact paste and increases the stored energy in the layer and therefore the driving force for delamination [7].

The tests were carried out at a constant crosshead displacement rate of 0.1 µm/second using an electromechanical testing machine and a four-point bending fixture with a support span of 20 millimeters and a loading span of 10 millimeters. The load versus displacement data were collected during the test to subsequently calculate the energy release rate. Test specimens with different sintering temperatures and sintering times were evaluated. Also, the effect of the thickness of the LSM contact paste was investigated.

The energy release rate was determined according to Equation (1):

$$G = \frac{(1 - v^2)M^2}{2E}\left(\frac{1}{I_2} - \frac{1}{I_c}\right) \quad (1)$$

$$M = \frac{Pl}{2b} \quad (2)$$

$$I_c = \frac{h_1^3}{12} + \frac{h_2^3}{12} + \frac{h_1 h_2 (h_1 + h_2)}{4} \quad (3)$$

$$I_2 = \frac{h_2^3}{12} \quad (4)$$

where G is the energy release rate, P is the applied load, b is the width of the bars (2.5 mm), h_1 and h_2 are the thickness of the top and bottom bars (0.2 mm), l is the distance between the inner and outer pins (see Figure 2), M is the applied bending moment and E and v are the elastic constants of the metallic interconnect material.

Results

Figure 3 illustrates a typical load versus crosshead displacement curve obtained from one of these tests. In all cases the load increases linearly until a vertical crack forms in the LSM paste at the root of the notch introduced with a sharp blade. That event is followed by a sudden load drop, which corresponds to the growth of a crack across the LSM layer and its deflection into one of the interfaces between the LSM layer and the Crofer 22 APU layers. The load plateau in the load versus

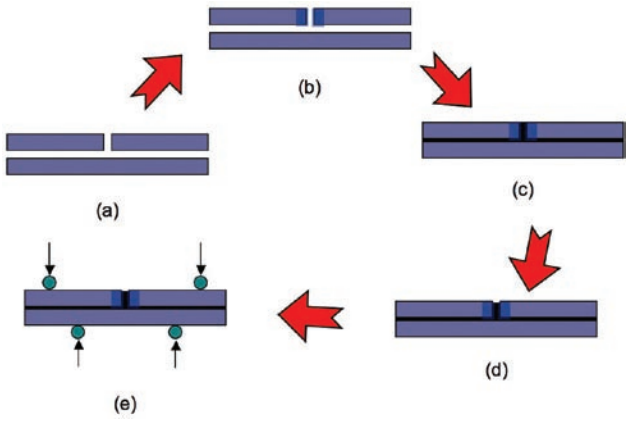

FIGURE 1. (a) Crofer 22 Beams; (b) Application of BN to Facilitate Crack Initiation; (c) Application of LSM Contact Paste Followed by Sintering; (d) Introduction of Notch in LSM Contact Paste; (e) 4-point Bend Testing of Test Specimen

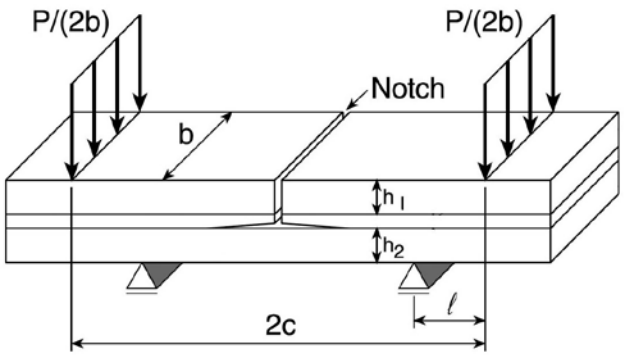

FIGURE 2. Schematic of Test Configuration [5-6]

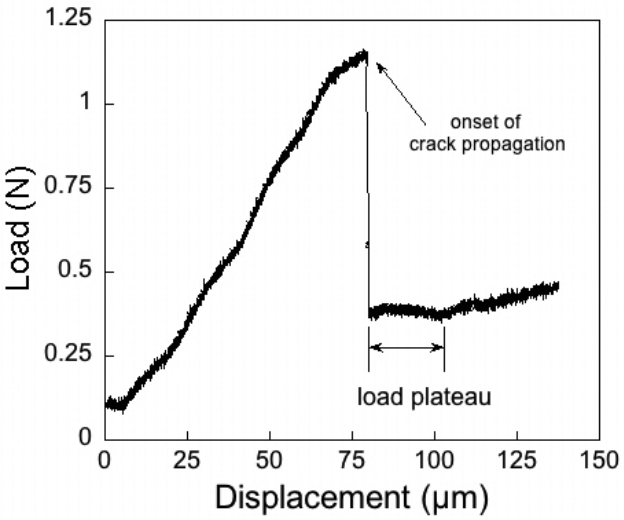

FIGURE 3. Typical Load Versus Displacement Curve Obtained from the Interfacial Evaluation of a Test Specimen Comprised of Crofer 22 APU Interconnects and LSM Contact Paste Sintered at 900°C for 1 Hour

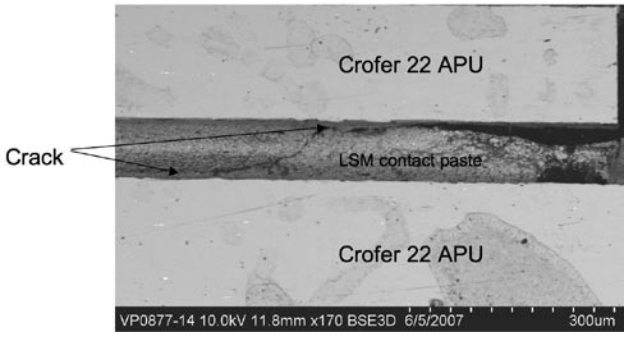

FIGURE 4. Scanning Electron Micrograph of Test Specimen Illustrating Path of Crack Propagation

displacement curve corresponds to the stable growth of the interfacial crack and that is the value of the load used for the calculation of the energy release rate. Upon further machine crosshead displacement, the crack reaches the loading points and is arrested.

The test specimens were examined after the mechanical tests using optical and scanning electron microscopy. It was found that cracks propagated through the LSM contact paste layer and were deflected to the interface between the LSM contact paste and the Crofer 22 APU layers as illustrated in Figure 4. Similar observations were obtained from the analysis of the two halves of test specimens after complete separation, which revealed regions of bare metal and islands of LSM contact paste.

It was found that the interfacial energy release rate increased with both the LSM contact paste sintering temperature and sintering time as shown in the plot in

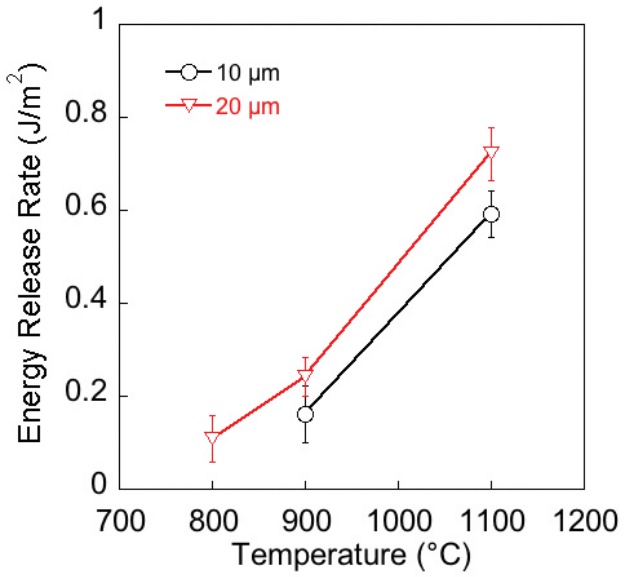

FIGURE 5. Effect of Sintering Temperature on the Interfacial Energy Release Rate Test Specimens Comprised of Crofer 22 APU Interconnects and LSM Contact Paste

Figure 5. These results are consistent with the fact that the density, and hence the strength, of the LSM contact paste increase with sintering time and temperature. It was also found that the energy release rate increased with the thickness of the LSM contact paste layer. This result was unexpected but work is in progress to prepare and evaluate test specimens with a wider range of LSM contact paste thickness values to further understand these trends.

Current work in collaboration with researchers at Pacific Northwest National Laboratory (PNNL) is focused on the characterization of systems that include metallic interconnects that have been coated with $(Mn,Co)_3O_4$ spinel to prevent Cr volatilization. These measurements are being complemented with *in situ* impedance measurements and observations of the cracking processes.

Conclusions and Future Directions

A technique was developed to determine the energy release rate of interfaces between LSM contact paste and Crofer 22 APU metallic interconnects. Results were obtained for test specimens that were processed at different sintering temperatures and for different periods of time. It was found that the interfacial energy release rate increases with both sintering temperature and sintering time. It was also found that cracks initiated in the LSM contact paste and were deflected to the interface between the contact paste and the metallic interconnect. Current and future work is focused on using these techniques and analysis to characterize

the interfacial properties of other systems that include $(Mn,Co)_3O_4$ spinel coated metallic interconnects and other contact paste compositions.

FY 2007 Publications/Presentations

1. E. Lara-Curzio, R. M. Trejo, C. Cofer , "Dimensional Stability of Ni-YSZ at Elevated Temperatures," Presented at the 31st International Conference & Exposition on Advanced Ceramics and Composites, Daytona Beach, FL, January 22–26, 2007.

References

1. Y. S. Taniguchi, M. Kadowaki, H. Kawamura, T. Yasuo, Y. Akiyama, and Y. Miyake, "Degradation phenomena in the cathode of a solid oxide fuel cell with an alloy separator," *J. Power Sources*, **55** (1995) pp. 73-79.

2. W.J. Quadakkers, H. Greiner, M. Hansel, A. Pattanaik, A.S. Khanna, W. Mallener, "Compatibility of Perovskite Contact Layers Between Cathode and Metallic Interconnector Plates of SOFCs," *Solid State Ionics* **91** (1996) pp. 55-67.

3. Fuel Cell Handbook (Seventh Edition). National Energy Technology Laboratory, Morgantown, West Virginia 26507-0880, November 2004.

4. Z. Yang, G. Xia, P. Singh and J. W. Stevenson, "Electrical contacts between cathodes and metallic interconnects in solid oxide fuel cells," *Journal of Power Sources* **155** (2006) 246–252.

5. H. C. Cao and A. G. Evans, "An Experimental Study of the Fracture Resistance of Bimaterial Interfaces," *Mechanics of Materials* **7** (1989) pp. 295-304.

6. P. G. Charalambides, H. C. Cao, J. Lund and A. G. Evans, "Development of a Test Method for Measuring the Mixed Mode Fracture Resistance of Bimaterial Interfaces," *Mechanics of Materials* **8** (1989) pp. 269-283.

7. I. Hofinger, M. Oechsner, H-A. Bahr and M. V. Swain, "Modified four-point bending specimen for determining the interface fracture energy for thin, brittle layers" *International Journal of Fracture*, **92** (1998) pp. 213–220.

IV.A.12 Combined Theoretical and Experimental Investigation and Design of H_2S Tolerant Anode for Solid Oxide Fuel Cells

Madhivanan Muthuvel, Andres Marquez, Gerardine Botte (Primary Contact)
Department of Chemical and Biomolecular Engineering, Ohio University
183 Stocker Center
Athens, OH 45701
Phone: (740) 593-9670; Fax: (740) 593-0873
E-mail: botte@ohio.edu

DOE Project Manager: Briggs White
Phone: (304) 285-5437
E-mail: Briggs.White@netl.doe.gov

Objectives

- Determine the mechanism for solid oxide fuel cell (SOFC) anode deterioration by H_2S gas found in coal syngas.
- Employ molecular modeling to study the interaction of the anode with chemical species.
- Confirm the theoretical model with experiments and surface analysis.

Accomplishments

- Established the detrimental influence of H_2S on H_2 oxidation at the nickel oxide in yttria-stabilized zirconia (Ni-YSZ) anode from quantum chemistry calculations – binding energies for pure H_2 were reduced from -89.5 to -23.2 kcal/mol in the presence of H_2S.
- Confirmed the need of moisture for gas mixtures containing CO – binding energy for pure CO was increased from -26.9 to -76.6 kcal/mol with H_2O molecule.
- Predicted infrared and Raman spectra from quantum chemistry calculations.
- Molecular dynamics calculations confirmed the slow diffusion of H_2 in Ni-YSZ interface is due to the presence of H_2S gas molecules.
- Built a new solid oxide fuel cell testing station.

Introduction

The SOFC is a high temperature fuel cell which operates at 850-1,000°C. The SOFC is a viable option for a high temperature hydrogen fuel source. One of the high temperature hydrogen sources is coal syngas. Burning coal produces a gas known as coal syngas, which contains hydrogen along with other chemical species such as CO and CO_2. Since a SOFC operates at high temperature, the presence of CO and CO_2 in coal syngas will not affect its performance. However, coal syngas also contains H_2S at high concentrations (between 0.5-5%) depending on where the coal is mined [1]. A commonly used anode material for SOFCs is Ni-YSZ. When H_2S containing gas comes in contact with a Ni-based anode, deterioration of the anode is inevitable. Most of the experimental research in the area of SOFCs has been focused on development of new anode materials for sustaining H_2S attack. In this project, we concentrate on understanding the mechanism of anode (Ni-YSZ) deterioration by H_2S gas, present in the coal syngas, using molecular modeling. We also want to establish validity for the predicated theoretical models by performing experiments. Hence, objectives for this project are to determine the mechanism for H_2S interaction with the Ni-YSZ anode and recommend either preventive measures for the Ni-YSZ anode or a new sulfur tolerant anode material.

Approach

This investigation is aimed at covering both theoretical and experimental aspects of H_2S interaction with the Ni-YSZ anode material. Theoretical study was based on molecular modeling of all the gaseous species (H_2, H_2S, CO) involved with Ni-YSZ. Molecular modeling comprises both quantum chemistry (QC) and molecular dynamics (MD) calculations for the proposed system. QC calculation was performed using Gaussian 03 software involving the density functional theory (DFT) method and LANL2DZ basis set. In addition to optimizing the structures of the anode material and other gas molecules, the QC calculations can also predict infrared and Raman spectra for each system. Physical properties of these systems were predicted in MD calculations using Cerius2 (v. 4.8) software. The parameters predicted include diffusion coefficient of gas species interacting with the Ni-YSZ surface and the packing and orientation of the chemical species at the surface of the anode material. A detailed explanation of the steps involved in molecular modeling is described in our publication [2]. Using the information from theoretical studies, experiments will be carried out to confirm the predications from the molecular models. A set-up will be constructed to perform various SOFC experiments comprising different gas compositions as well as to perform surface analysis of the SOFC anode to validate the mathematical models.

Results

The initial studies about the construction of the anode molecule and performing QC calculations to optimize the anode and various systems along with MD studies have been explained in our last year's annual report [3]. QC calculations of the different systems with the Ni-YSZ anode have been listed in Table 1. We have included moisture or the H_2O molecule in the gas stream for modeling because experimentally, the Ni-YSZ anode is known to get clogged with carbon deposits from the presence of CO in the gas stream. When H_2, H_2S and CO are present individually, the binding energies indicate an oxidation trend of H_2 (-89.5 kcal/mol) > CO (-26.9 kcal/mol) > H_2S (-24.2 kcal/mol), but with the addition of moisture to the pure gas components all the binding energies are changed.

Presence of H_2O with H_2 drops the binding energy from -89.5 to -39.9 kcal/mol whereas moisture with CO increases its oxidation from -26.9 to -76.6 kcal/mol, which confirms the experimental observation to add moisture for CO containing gas streams. On combining H_2S with H_2, we get a binding energy of -23.2 kcal/mol, which is less than the -51.1 kcal/mol binding energy found from adding the H_2O molecule to H_2 and the H_2S system. For the systems devoid of moisture, H_2 oxidation on the anode surface was most favorable when pure H_2 gas (-89.5 kcal/mol) was used and least favorable with the $H_2 + H_2S$ system (-23.2 kcal/mol). Presence of CO in H_2 gas helped oxidation of H_2 (-40.3 kcal/mol) as compared to the $H_2 + H_2S$ system, which was evident in the anode + H_2 + H_2S + CO system (-58.5 kcal/mol) where CO helped H_2 oxidation by hindering H_2S attack on anode surface.

Continuing on the first principle calculations, we have predicted spectroscopic data (infrared and Raman) for all the systems, which will be very useful information for comparison with experimental analysis. Raman spectrum gives information about the chemical species present on the surface of the anode material; it is more like a signature for each chemical molecule. In Figure 1, we have shown a few Raman spectra from different systems we have studied over a frequency range where chemical species which adsorbed to the anode surface can be identified. Each system has at least one distinguishable peak. For example, the anode + H_2 + H_2S has two peaks near 200 Hz, and a high, intense peak very close to 600 Hz was found if CO was mixed with the H_2 and H_2S gas mixture. We are expecting similar results from the Ni-YSZ anode surface after performing SOFC testing experiments.

MD calculations were performed on a system, anode + H_2 + CO (1%) + H_2O (1%), to determine the effect of moisture in CO containing gas mixture. The radial distribution function (RDF) plots provide information on the packing and orientation of the chemical species on the anode surface. The RDF plot for this system at 850°C illustrates a similar trend as other RDF plots; the Ni atom on the anode surface was the active site for H_2 oxidation but at the same time carbon from CO also displayed affinity towards the Ni atom. Interatomic distance between Ni and H atoms was 2 Å as compared to 3.2 Å for the Ni-C pair, which suggests CO could to some extent hinder H_2 oxidation at Ni sites. In addition to the RDF plots, an MD calculation also predicts the diffusion coefficient for the gas molecules at the interface of the anode surface. A pure H_2 over Ni-YSZ anode has a diffusion coefficient of 1.35×10^{-4} cm^2/s and with the addition of 2% CO, H_2 diffusivity drops down to 5×10^{-6} cm^2/s because of CO interference with Ni active sites. For the anode + H_2 + CO (1%) + H_2O (1%) system, H_2 has a much lower diffusion coefficient (4.9×10^{-7} cm^2/s), almost one order lower than the anode + H_2 + CO (2%) gas mixture because moisture at a very high temperature of 850°C can easily affect H_2 diffusion through the anode material. Moisture had not only affected H_2 transport but also the diffusion coefficient of CO by dropping it to 6.4×10^{-8} from 3×10^{-7} cm^2/s.

TABLE 1. Binding Energies for Various Gas Compositions with and without Moisture

Systems	Binding Energy (kcal/mol)	
	Without H_2O	With H_2O
Anode (Ni-YSZ)	-128.3	-40.8
Anode + H_2	-89.5	-39.9
Anode + H_2S	-24.2	-48.9
Anode + CO	-26.9	-76.6
Anode + H_2 + H_2S	-23.2	-51.1
Anode + H_2S + CO	-61.5	-56.0
Anode + H_2 + CO	-40.3	Computing
Anode + H_2 + H_2S + CO	-58.5	Computing

The data obtained from mathematical calculations has to be verified experimentally before concluding the theoretical models as the mechanism for anode destruction or a tool to understand the interaction of H_2, H_2S and CO molecules with the Ni-YSZ anode. The experimental phase started after half of the theoretical studies have begun. A new design for SOFC testing was developed over the last year. This design was primarily focused on studying the anode electrode in a SOFC. In Figure 2a, the quartz tube assembly is illustrated, which is different from the commonly used long tubular ceramic SOFC testing set up. The quartz tube assembly consists of two quartz tubes with the outer tube used for sealing the cathode side of the SOFC. The inner quartz tube consists of four ports and one of the ports extends spirally inside the tube to provide the gas stream to the anode material. The purpose of the windings for the gas inlet is to provide more residence time for the gas mixture to reach 850°C. Of the other ports, two are used

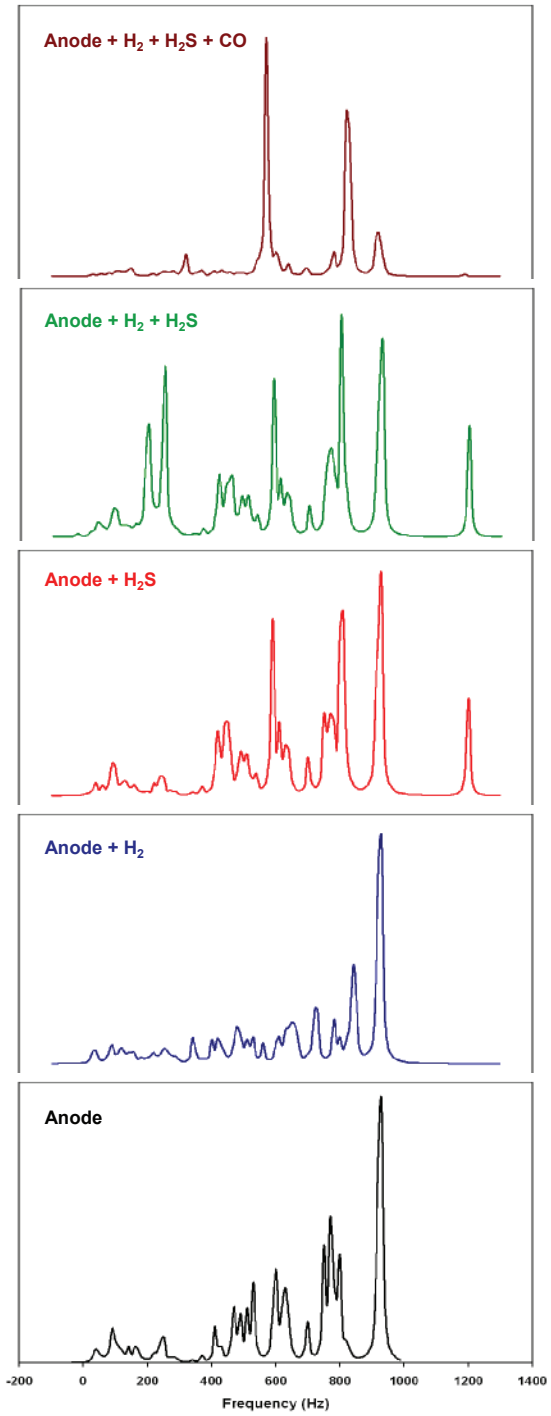

FIGURE 1. Raman Spectra for H_2, H_2S and CO Gas Components with Ni-YSZ Anode

for electrical contact wires from the anode and one for a gas outlet.

The solid oxide fuel cell was fabricated as an electrolyte supported cell. The electrolyte for the cell is YSZ with a thickness of 270 µm and 30 mm in diameter

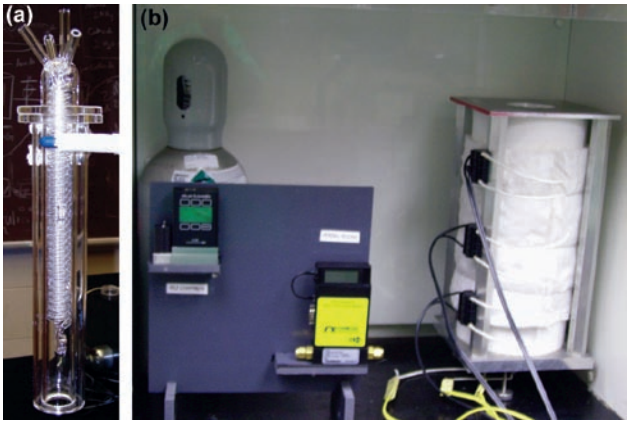

FIGURE 2. SOFC Testing System: (a) Quartz Tube Assembly, (b) Furnace in Fume Hood

(Nextech Materials, Inc.). This kind of cell is known as a button cell. It is planned to have three electrodes on the YSZ electrolyte, the anode is Ni-YSZ, and the cathode and reference will be Pt. Dimensions for these electrodes are 10 mm in diameter for both the anode and cathode, but the diameter for the reference electrode will be 3 mm. Thickness for all the electrodes will be 50 µm. The anode is designed to face the inside of the inner quartz tube and the cathode as well as the reference electrode will be on the other side. We want to study the behavior of the anode when exposed to gas mixtures; we only have the reference electrode to measure anode potential during the experiment. Electrodes are screen printed and sintered using Ohio Coal Research Center (OCRC) facilities.

Once the button cells are ready to be tested, they will be placed inside the quartz tube. The quartz tube assembly will be mounted on a three zone furnaces; three individual furnaces are mounted over each other to maintain a uniform temperature profile. The furnace stand, temperature controllers, flow controllers and gas cylinders are displayed in the schematic diagram (Figure 3). During experiments gas mixtures of either pure H_2 or gas mixtures of H_2 and H_2S will be passed through the inner quartz tube for the anode side, were as in the cathode side air will be supplied from the bottom of the furnace. The concentration of H_2S in the gas mixture will be 1, 10 and 100 ppm, which will be supplied to the Ni-YSZ anode for a period of 6 hours exposure. Electrochemical data collected during the experiment will include cell voltage, anode potential as well as impedance spectroscopy. We are planning to analyze the anode surface with scanning electron microscopy (SEM), energy dispersive X-ray spectroscopy (EDX), Fourier transform infrared spectroscopy (FT-IR) and Raman spectroscopy for surface morphology and chemical identification on the surface.

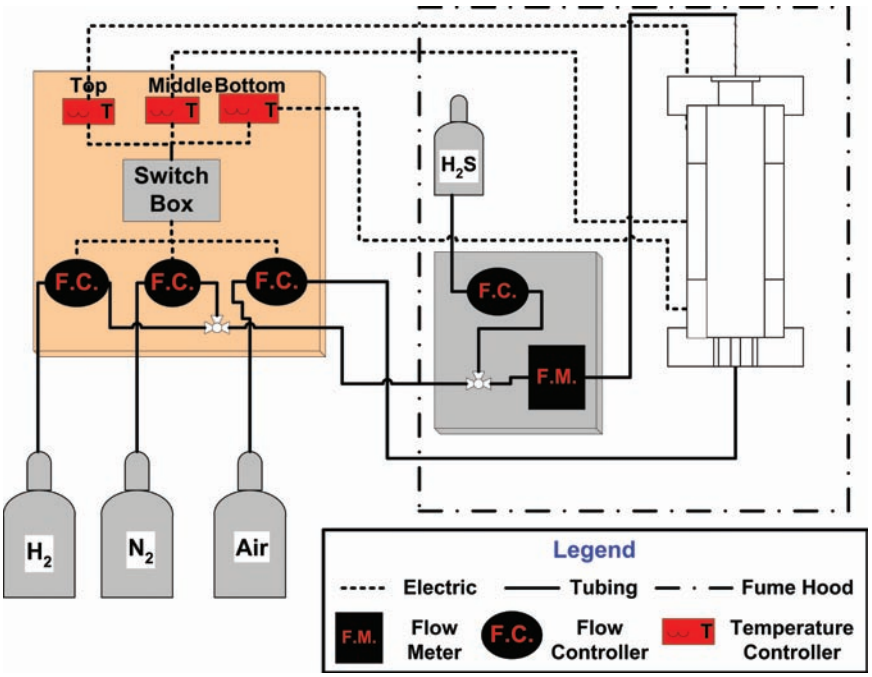

FIGURE 3. Schematic Diagram for SOFC Testing Station

Conclusions and Future Directions

- Oxidation of pure H_2 is more favorable than pure H_2S and CO on a Ni-YSZ surface is proven by quantum chemistry calculations.
- With the addition of the H_2O molecule to a CO gas mixture, the binding energy of pure CO increases from -26.9 to -76.6 kcal/mol, which helps CO oxidation on the Ni-YSZ surface.
- Quantum chemistry calculation predicts both infrared and Raman spectra for all the systems, which provides useful information to compare with experimental results.
- In the future, we want to perform SOFC testing with various gas compositions and characterize the anode material with analytical and electrochemical tools.
- Extend the modeling study to other anode materials (ceria-based) and different fuel sources such as natural gas and jet fuel.

Special Recognitions & Awards/Patents Issued

1. Third Prize (Poster) at Eastern Regional Chemical and Materials Engineering Graduate Symposium, October 2006, Lexington, KY.

2. First Prize (Poster) in Chemical and Biomolecular Engineering Session at 6th Annual Student Research and Creative Activity Fair, May 2007, Ohio University, Athens, OH.

FY 2007 Publications/Presentations

1. Daramola, D., Muthuvel, M., Marquez, A., and Botte, G. G., *Theoretical Investigation of Solid Oxide Fuel Cell Anode Materials in the presence of H_2, H_2S and CO*, Eastern Regional Chemical and Materials Engineering Graduate Symposium, October 2006, Lexington, KY.

2. Daramola, D., Muthuvel, M., Marquez, A., and Botte, G. G., *Theoretical Study of Solid Oxide Fuel Cell Anodes in the Presence of H_2S*, General Student Poster Session, 211th Electrochemical Society (ECS) Meeting, May 6 – 10, 2007, Chicago, IL.

References

1. G. Y. Lai, *High Temperature Corrosion of Engineering Alloys*, ASM International, Materials Park, OH (1990) p. 117.

2. A. Marquez, Y. De Abreu, and G. G. Botte, Theoretical Investigation of NiYSZ in the Presence of H_2S, *Electrochemical and Solid-State Letters*, 9 **(3)** A163-A166 (2006).

3. M. Muthuvel, A. Marquez, and G. G. Botte, Combined Theoretical and Experimental Investigation and Design of H_2S Tolerant Anode for Solid Oxide Fuel Cells, *FY 2006 Fuel Cell Annual Report*, DOE Office of Fossil Energy Fuel Cell Program, July 2006.

IV.A.13 Cost Effective, Efficient Materials for Solid Oxide Fuel Cells

Paul E. King, PhD (Primary Contact),
Paul D. Jablonski, PhD, Omer Dogan, PhD,
and David E. Alman, PhD.
National Energy Technology Laboratory (NETL)
1450 Queen Ave. SW
Albany, OR 97321
Phone: (541) 967-5948; Fax: (541) 967-5958
E-mail: Paul.King@netl.doe.gov

DOE Project Manager: Paul Turner
Phone: (541) 967-5863
E-mail: Paul.Turner@netl.doe.gov

Objectives

- **Task 1:** Determine the mechanisms used in surface infusion treatments, including CeOx, for improved oxidation resistance.
- **Task 2:** Melt and fabricate 430ss-related alloys with low Si and Al.
- **Task 3:** Evaluate the effect of syngas on 430-related alloys with low Si and Al.

Accomplishments

- The mechanism of oxidation resistance found by surface treating candidate materials for interconnects and other balance-of-plant applications has been studied. The mechanism, which is the preferential pre-oxidation of the surface of the material, is enhanced by the fact that the rare earth treatment modifies the scale that is formed which, in turn enhances oxidation resistance and slows scale growth. The mechanism of oxidation resistance by rare earth surface infusion, specifically cerium, will be published in peer reviewed journals during the second half of this year.
- A series of experimental alloys with controlled low levels of Si and Al were melted, fabricated and provided for further evaluation. The majority of the material utilized for producing commercial 430ss is from scrap which necessarily contains Si and Al. Methodologies of removing the Si and/or Al during the melting of cheap, low grade scrap have been postulated and may be the focus of future efforts. All experimental alloys have been made available to any interested parties who wish to evaluate the materials for their specific solid oxide fuel cell (SOFC) environment or application.
- Single environment testing for oxidation (cathode side) has been completed on the experimental low Si/Al 430ss alloys with and without the rare earth surface infusion treatment. The maximum amount of Si tolerable with respect to area specific resistance (ASR) measurements has not yet been determined, however an upper limit has been developed. Single environment testing on the anode side as well as dual environment testing are currently underway.

Introduction

Fuel cells are energy conversion devices that generate electricity and heat by electrochemically combining a gaseous fuel and an oxidizing gas via an ion-conducting electrolyte. The chief characteristic of fuel cells is their ability to convert chemical energy to electrical energy without the need for combustion, thereby giving much higher conversion efficiencies than conventional methods, such as steam turbines. Cost remains the final obstacle that must be overcome for fuel cells to realize their full commercial potential. Many of these costs can be attributed to components in the "balance-of-plant." Advances in solid-state material manufacturing shows promise for making SOFCs applicable in any power application. Cost reduction can be achieved in component fabrication, materials used, and cell and stack designs. However, balance of plant issues also present problems in the commercialization of fuel cell technology. Specifically for SOFCs, air and fuel need to be heated and cooled at some stage of the process. This requires pumps, piping, heat exchangers, etc. in order to deliver useable electrical power. This project explores materials of construction as a means of developing low cost, high temperature components for SOFC systems.

Approach

The approach to reaching the goals of this project is three fold. First, it has been shown that rare earth infusion of the base material alloys can enhance the oxidation resistance while maintaining favorable electrical characteristics where required. However, a determination of why the rare earth treatment works has not yet been made. Task 1 of this project looks at determining this mechanism with the goal of determining whether the candidate rare earth (cerium) is the best fit for the lowest cost. The second task looks at the silicon and aluminum levels in 430-like stainless steels. It is well known that silicon forms a protective layer on the surface of the alloy in oxidizing environments. However, this protective layer is electrically insulative, an

undesirable characteristic for interconnect applications. This task looks to minimize the silicon levels while maintaining the operational integrity of the alloy. Finally, Task 3 looks at single and dual environment corrosion mechanisms in the experimental alloys, as well as other commercially available alloys, with and with the rare earth treatment, in order to determine the different corrosion characteristics. Moreover, the task looks at determining what, if any, deleterious effects can be seen across a metallic material in the case that there are different (hot) gases flowing on either side of the material.

Results

Task 1 – Determine the mechanisms used in surface infusion treatments, including CeOx, for improved oxidation resistance.

Progress – A number of alloys have been treated with the NETL-Albany surface infusion process including the NETL-Albany 430 family of alloys (Task 2) and Crofer 22APU, which is used for baseline studies. After surface treatment, $CeCrO_3$-type and Cr-Mn oxides formed on the surface of the Fe-22Cr-Mn current collectors, as determined by the X-ray diffraction scans obtained from the surface of the sample cross sectioned in Figure 1. $CeCrO_3$-type oxides have been found to form in chromia forming alloys doped with rare earths [1, 2]. The X-ray diffraction results also show that subjecting the alloy to only the thermal portion of the treatment, without the presence of CeO_2, does not result in pre-oxidation. As previously reported, coupons subjected to only the thermal portion of the treatment oxidized in an identical manner as polished samples [3]. Only in the presence of CeO_2 does pre-oxidation occur during treatment, biasing the surface to form a more slowly growing, and hence, a more protective oxide scale during subsequent exposure.

Examination of the oxide scales through scanning electron microscopy-wavelength dispersive X-ray (SEM-WDX) analysis has shown that the outer Cr-Mn spinel scale contains Ce (Figure 2). The addition of rare earth modifies Cr_2O_3 formation, from cation (metal) controlled to (oxygen) anion controlled. This inversion has been found to be accompanied by modification in Cr_2O_3 structures from large columnar grains in the undoped scale to small grain structure in the doped scale. Consequently, diffusion of oxygen inward is slowed, resulting in slower scale growth and less internal oxidation.

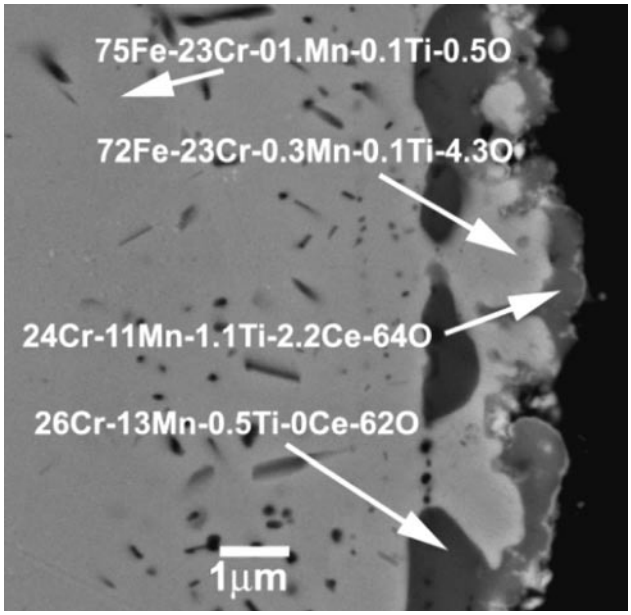

FIGURE 1. Cross section of Crofer 22APU after Ce-surface treatment. Compositions for Cr, Mn, Ti, Fe, Ce are in atomic percent and were determined by WDX analyses in a field emission SEM.

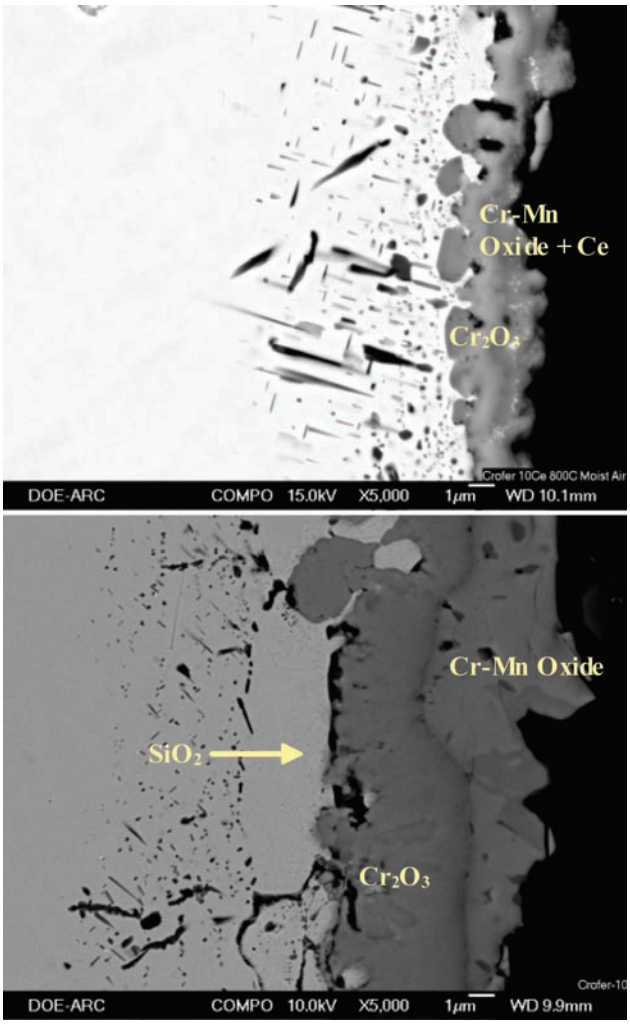

FIGURE 2. Comparison of Scale that Formed on: (a) Ce Surface Treated Crofer-22APU and (b) Untreated Crofer 22APU after 2,000 Hours Exposure at 800°C to Moist Air

A. Oxidation of Ce-treated 430 Alloys

Figure 3 illustrates the influence of Si content on the oxidation behavior (800°C in moist air) of custom Type-430 alloys melted and reduced to sheet at NETL-Albany. In Figure 3, the behavior of 430 is compared with Crofer 22APU. These results clearly demonstrate the effect of high Si content on the oxidation resistance. The commercial 430 alloy, with almost 0.4 wt% Si, has the lowest mass gain during testing, implying it is the most oxidation resistant alloy. However, it should be mentioned that previous testing at NETL-Albany has shown that commercial 430 with high Si levels can spall during oxidation, leading to variability in mass change results and the appearance of superior performance (oxidation resistance). The mass gain of the low-Si 430 alloys is similar in magnitude to Crofer 22APU. It is interesting to note that a trend is emerging that indicates Crofer 22APU is more oxidation resistant, that is, after about 2,500 hours of exposure Crofer 22APU consistently shows a slightly lower mass gain than the low Si 430 alloys. However, this is not surprising since Crofer has a higher Cr content than 430 (22 wt% compared to 17 wt%).

Figure 4 illustrates the effect of the Ce surface treatment on the oxidation behavior on the alloys. It is clear that at 800°C the surface treatment enhances oxidation resistance of all the alloys. The mass gain during oxidation of the low Si-430 alloys has been reduced by a factor of three to four with the Ce treatment, and is equivalent to the commercial high Si 430 alloy. Although not clearly shown on the figure, the Ce-treated commercial 430 alloy had a slightly higher mass gain than the alloy in the untreated condition. However, as mentioned above the apparent superior oxidation resistance of the untreated 430 is due to oxide scale spallation. The Ce treated samples do not spall during oxidation.

Note: These tests are on going and are part of an experiment to assess the long term effectiveness of the Ce-treatment on the behavior of alloys.

B. Influence of Temperature on Oxidation Behavior of Ce-treated Alloys

Figure 5 summarizes the effect of temperature on the oxidation behavior for alloy 430-A while Table 1 summarizes the scales that formed on this alloy as a function of test temperature (as determined by X-ray diffraction [XRD]). Of note is that at 950°C, Chromia and Cr-Mn oxide formed on the surface of the Ce-treated alloy, although Fe_2O_3 was also detected. The formation of Fe_2O_3 leads to the accelerated behavior displayed by the alloys after a few hundred hours of exposure. Furthermore, it is noteworthy that this alloy is two phase (ferrite plus austenite) at 950°C while it is single phase ferrite below about 875°C. At 800°C, a Cr_2O_3 scale and Cr-Mn oxide formed on the surface of the alloy in both conditions. Interestingly, at 650°C, only Fe_2O_3 was detected on the untreated and treated alloys. The base Fe-Cr (bcc) metal phase is the primary phase detected on the surface of the 430-A in the untreated condition. This is not surprising, based on the extremely small weight gain (hence expected thin oxide layer) on this alloy (650°C, 250 hours). Hematite was the major phase detected on the surface of the 430-A+Ce, again not surprising based on relatively low weight gain. Of note is the fact that CeO_2 was not detected on the

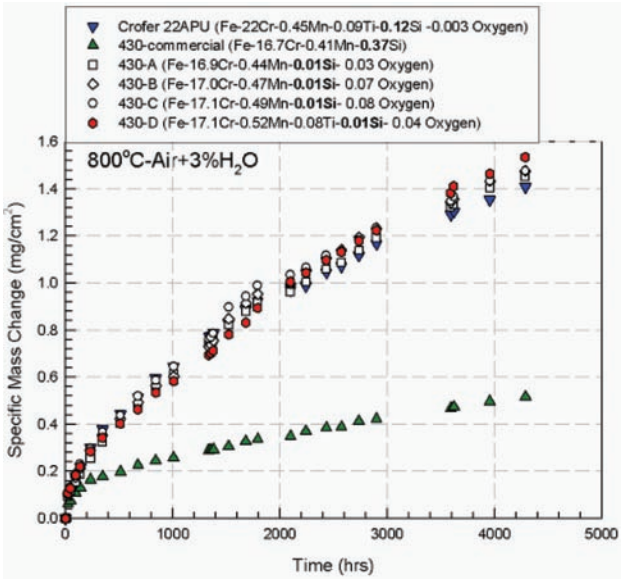

FIGURE 3. Comparison of the Oxidation Behavior of Low-Si Type 430 to Commercial Type-430 (high-Si) and Crofer 22APU

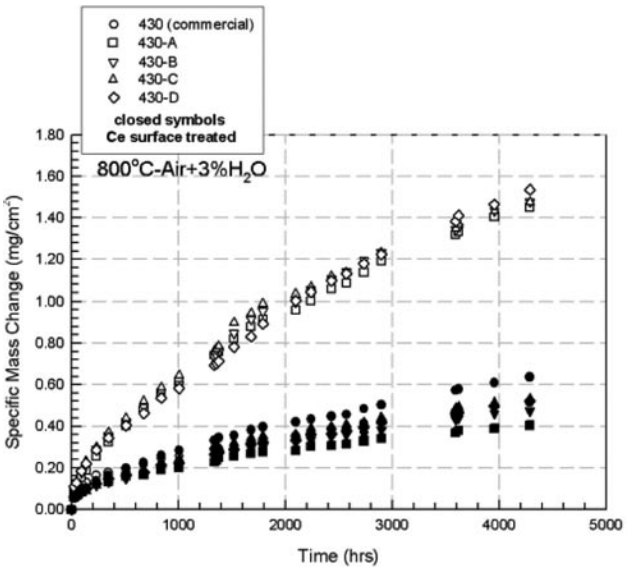

FIGURE 4. Effect of the Ce Surface Treatment on the Oxidation Behavior of Type-430

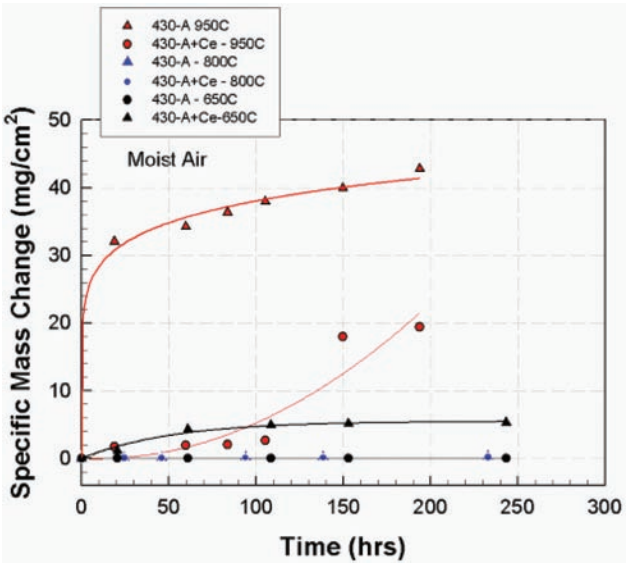

FIGURE 5. The Effect of Temperature on the Oxidation Behavior of Low-Si Alloy 430-A

surface of this sample. In any event, SEM analysis is required to confirm scale formation.

TABLE 1. Oxide Phase Formation as a Function Exposure Temperature as Determined by XRD

	Alloy 430-A	Alloy 430-A+Ce
650°C-250 hrs	Fe-Cr alloy (major) Fe_2O_3 (trace)	Fe_2O_3 (major) Fe-Cr alloy trace
800°C-500 hrs	Cr_2O_3 $Mn_{1.5}Cr_{1.5}O_4$	Cr_2O_3 $Mn_{1.5}Cr_{1.5}O_4$ CeO_2
950°C-200 hrs	Fe_2O_3	Cr_2O_3 $Mn_{1.5}Cr_{1.5}O_4$ CeO_2 Fe_2O_3

Task 2 – Melt and fabricate 430ss-related alloys with low Si and Al.

Progress – A number of 430ss-related alloys with low Si and Al have been developed, fabricated, rolled and samples supplied to various groups for testing (including scientists in Tasks 1 and 3). The samples were formulated to study the effects of varying such quantities as C or Ti. Table 2 gives the composition of the alloys as fabricated as well as the 430 baseline.

Alloys NETL-430-a-c were designed as a low Si, low Al alloy with varying amounts of carbon in order to be able to investigate the effects of the variability of carbon in commercially available 430 stainless steel; NETL-430-d was designed with moderate amounts of carbon and addition of titanium for investigations of the effects of a de-oxidizer other then Si and Al with results presented in Task 1; NETL-430-e-g was designed with a minimal level of carbon and varying the silicon to investigate a tolerable silicon level for commercially produced alloys that will meet the service requirements within the fuel cell environment. That is, if the majority of the material utilized for producing the modified 430 is from scrap, then it will necessarily contain Si and Al. Methodologies of removing the Si and/or Al during the melting of cheap, low grade scrap have been postulated. If these prove acceptable, then a production question is at what levels do the Si and Al have to be before the alloy produced becomes unacceptable? This question is being addressed by the NETL-430-e-g series in combination with Task 1. All experimental alloys have been made available to any interested parties who wish to evaluate the materials for their specific SOFC environment or application.

TABLE 2. NETL-430 Stainless Steel Compositions

	Al	Cr	Mn	Ti	C	Si	Fe
Commercial 430	--	17	1.00	--	0.12	1.00	Bal.
NETL-430-a	0.011	16.85	0.44	n.d.	0.0054	n.d.	Bal.
NETL-430-b	0.011	17.03	0.47	n.d.	0.0482	n.d.	Bal.
NETL-430-c	0.011	17.13	0.49	n.d.	0.1180	n.d.	Bal.
NETL-430-d	0.010	17.11	0.52	0.080	0.0123	n.d.	Bal.
NETL-430-e	0.009	16.98	0.38	n.d.	0.0045	n.d.	Bal.
NETL-430-f	0.011	17.02	0.40	0.018	0.0014	0.024	Bal.
NETL-430-g	0.010	17.28	0.45	n.d.	0.0013	0.057	Bal.

Task 3 – Evaluate the effect of syngas on 430-related alloys with low Si and Al.

Progress – The NETL-430 stainless steel samples have been received as per Task 2. These samples have been prepared and are ready for exposure in the single and dual environments identified for testing. A new sample preparation and polishing procedure was developed due to the fact that traditional polishing methodologies have the potential for introducing silicon or aluminum in low amounts to the sample. Because NETL alloys have little or no Si or Al, it was deemed necessary to find a new way of preparing the samples.

The following chemical composition of the coal syngas without H_2S has been selected for the corrosion experiments: 46.6% CO + 38.5% H_2 + 12.7% CO_2 + 0.01% H_2O + 0.1% CH_4 + 1.1% Ar + 0.89% N_2. This environment was based upon publications on the syngas compositions from various gasification processes and through private consultations with gasifier manufacturers. Meanwhile, late in FY 2006, the furnace utilized in the dual environment testing failed. A new furnace has been purchased and installation is

proceeding with an expected completion date of March 31, 2007. At this time, a series of dual environment tests will be conducted on the NETL alloys.

Corrosion experiments on NETL low Si low Al 430-A, NETL-430-1, 430 – commercial, Crofer 22APU, NETL J5, J1, Haynes 230, and Haynes 242, in a single environment of 45 vol% CO+12 vol% CO_2+0.01 vol% H_2O+4.19 vol% N_2 at 800°C was initiated.

Oxidation kinetics of Crofer 22APU in simulated air at 800 °C using thermogravimetric analysis (TGA) is being determined.

Conclusions and Future Directions

Task 1 – NETL-430 Stainless Steel Compositions

Determine the mechanisms used in surface infusion treatments, including CeOx, for improved oxidation resistance.

The mechanism of improved oxidation resistance by surface treating candidate materials for interconnects and other balance-of-plant applications has been studied. The mechanism was determined to be the preferential pre-oxidation of the surface to form a Ce-modified oxide. The incorporation of the rare earth metal in turn slows the scale growth, and thus, enhances oxidation resistance through the well known reactive (rare) element effect. The NETL-430 family of alloys (Task 2) were tested with and without the CeOx treatment with interesting results. Briefly, the CeOx treatment enhances the oxidation resistance at the operating temperature of the fuel cells. Interestingly, though, this does not appear to be as prevalent at lower temperatures. Crofer 22APU was also tested, both as a baseline for the 430 family of alloys and for comparison with other rare earth treatments, specifically lanthanum. The lanthanum treatment shows similar characteristics with respect to oxidation resistance that the cerium treatment has. It is expected that the ASR of the La treated samples will be decreased slightly in comparison to the Ce treated samples due to the overall cleaner state that the La treatment gives. The mechanism of oxidation resistance by rare earth surface infusion, specifically cerium, will be published in peer reviewed journals during the second half of this year. Meanwhile, once an invention disclosure is complete, the lanthanum treatment will be published as well. Future work will include measuring the ASR of lanthanum treated steels at SOFC operational temperatures and comparing behavior to cerium treated steels and untreated steels.

Task 2 – Melt and fabricate 430ss-related alloys with low Si and Al.

One result from the controlled, low Si 430 melts is that they end up with about half of the designed amount of Si. The melts were poured with little superheat (about at the liquidus temperature) so there was a heavy skull left in the crucible. The thermodynamic analysis (ThermoCalc) suggests that the liquid was enriched with Si at this temp rather than the first solid to form at that temperature; interestingly, this is opposite of the results and may require further investigations.

A second way to reduce the Si in commercial 430, which, for cost purposes, will be made with recycled material (which includes high amounts of Si) would be to utilize a slagging process which scavenges the Si from the molten metal. Initial studies and "back of the envelope" calculations indicate that this can be done if it is determined that NETL should pursue this topic further.

Task 3 – Evaluate the effect of syngas on 430-related alloys with low Si and Al.

This task is ongoing. Single environment testing for oxidation (cathode side) has been completed (Task 1) while single environment testing on the anode side is underway. Preliminary results will be available shortly with long term results at the end of the fiscal year.

FY 2007 Publications/Presentations

Publications

1. D.E. Alman, C.D. Johnson, W.K. Collins and P.D. Jablonski, "The Effect of Cerium Surface Treated Ferritic Stainless Steel Current Collectors on the Performance of Solid Oxide Fuel Cells (SOFC), accepted for publication in J. Power Sources, 2007 (in press).

2. M. Ziomek-Moroz, T.A. Adler, K-S. Kwong, G.R. Holcomb, L. Penner, "Corrosion performance of metallic materials in carbon oxide – containing atmosphere for solid oxide fuel applications," submitted to the 32nd International Technical Conference on Coal Utilization and Fuel Systems, Session: Coal Compatible Fuel Cells.

3. M. Ziomek-Moroz, B.S Covino, G.R. Holcomb, S.J Bullard, "Chemical Stability of Ferritic Steel in Carbon-containing Atmosphere for SOFC Applications," Proceedings of the Materials Science & Technology 2006 Conference and Exhibition, Cincinnati, OH, October 15-19, 2006.

4. M. Ziomek-Moroz, T. Adler, P. King , "Materials Performance of Ferritic Steel in Combustion Gases for Heat Exchanger Applications in Solid Oxide Fuel Cell Systems" M. Ziomek-Moroz, T. Adler, P. King to appear in proceedings, CORROSION 2008.

5. M. Ziomek-Moroz, T. Adler, D. E. Alman, P.D. Jablonski, J. Clark, L.R Penner, "Materials Performance of Modified 430 Stainless Steel in Simulated SOFC Stack Environments for Integrated Gasification Fuel Cell System Applications" to appear in proceedings of the Fuel Cell Seminar, 2007.

Presentations

1. M. Ziomek-Moroz, B.S Covino, G.R. Holcomb, S.J Bullard, "Chemical Stability of Ferritic Steel in Carbon-containing Atmosphere for SOFC Applications," presented at Materials Science & Technology 2006 Conference and Exhibition, Cincinnati, OH, October 15-19, 2006.

2. D.E. Alman and P.D. Jablonski, "Influence of a Ce-Surface Treatment on the Oxidation Behavior of Commercial Fe- and Ni- Based Alloys" at MST'2006 Symposium on High Temperature Degradation of Fe-, Ni-, and Co- Based Alloys Including Metal Dusting: Alloying Elements and Corrosive Environments, October 15-19, 2006.

3. P.D. Jablonski and D.E. Alman, "Evaluation of Experimental Ni-Base and Fe-Base Alloys Containing Lower Chrome," at MST'2006 Symposium on Fuel Cells and Energy Storage Systems: Materials, Processing Manufacturing and Power Management Technologies: Interconnection and Metallic Materials in SOFCs, October 15-19, 2006, Cincinnati, OH.

4. G.R. Holcomb and D.E. Alman, "Oxidation of Interconnect Alloys in an Electric Field," at MST'2006 on Symposium Fuel Cells and Energy Storage Systems: Materials, Processing Manufacturing and Power Management Technologies: Interconnection and Metallic Materials in SOFCs, October 15-19, 2006, Cincinnati, OH.

5. D.E. Alman, C.D. Johnson, and P.D. Jablonski, "Evaluation of a Surface Treatment on the Performance of Crofer 22APU," at TMS-2007, Symposium on Materials in Clean Power Systems II, Solar and Hydrogen Based Technologies: SOFC," February 25 – March 1, 2007, Orlando, FL.

Invited Talks

1. P.D. Jablonski and, D.E. Alman "Evaluation of Model 6-22 Cr Ferritic Alloys For Interconnect Applications," at TMS-2007, Symposium on Materials in Clean Power Systems II, Solar and Hydrogen Based Technologies: SOFC," February 25- March 1, 2007, Orlando, FL.

2. R.D. Wilson, O.N. Dogan, P. King, "Welding of Dissimilar Alloys for High Temperature Heat Exchangers for SOFC", Materials Science and Technology 2006, Cincinnati, OH, October 15-19, 2006.

3. M. Ziomek-Moroz, T. Adler, P. King , "Materials Performance of Ferritic Steel in Combustion Gases for Heat Exchanger Applications in Solid Oxide Fuel Cell Systems" M. Ziomek-Moroz, T. Adler, P. King to appear in proceedings, CORROSION 2008.

4. M. Ziomek-Moroz, T. Adler, D. E. Alman, P.D. Jablonski, J. Clark, L.R Penner, "Materials Performance of Modified 430 Stainless Steel in Simulated SOFC Stack Environments for Integrated Gasification Fuel Cell System Applications" to appear in proceedings of the Fuel Cell Seminar, 2007.

References

1. D.A Downham and S.B. Shendye, Oxidation of Metals, Vol. 43, Nos5/6, 1995, p. 411.

2. S. Chevalier et al, Surf. Coat. Tech., Vol. 100–101, 1998, p. 208.

3. D.E. Alman, P. D. Jablonski and S. C. Kung, in Ceram. Engr. Sci. Proc., Vol. 27, Issue 4, ed N.Bansal, Amer. Ceram. Soc., Westerville, OH, 2006. p. 253.

IV.A.14 SOFC Glass Seal Development at PNNL

Yeong-Shyung (Matt) Chou (Primary Contact), Jeff Stevenson and Prabhakar Singh
Pacific Northwest National Laboratory (PNNL)
K2-44, P.O. Box 999
Richland, WA 99354
Phone: (509) 943-5233; Fax: (509) 375-2186
E-mail: yeong-shyung.chou@pnl.gov

DOE Project Manager: Travis Shultz
Phone: (304) 285-1370
E-mail: Travis.Shultz@netl.doe.gov

Objectives

- To develop and validate devitrifying sealing glasses for intermediate temperature solid oxide fuel cells (SOFCs).
- To study the interfacial chemical compatibility and mechanical integrity of interconnect alloys with candidate sealing glasses.

Accomplishments

- Completed interfacial compatibility and mechanical integrity studies of $(Mn,Co)_3O_4$ spinel-coated Crofer22APU with candidate sealing glasses.
- Completed interfacial compatibility and mechanical integrity studies of aluminized Crofer22APU with candidate sealing glasses.
- Demonstrated the electrical stability of refractory sealing glasses in a simulated SOFC environment under DC loading over 1,200 hours at 850°C. (Due to space limitations, results of electrical testing are not included in this report.)

Introduction

Glasses are considered promising candidates for SOFC seals because of their good wetting behavior, tailorable coefficient of thermal expansion (CTE), electrically insulating behavior, ease of processing, and low cost. Seal development at PNNL is primarily focused on "refractory" devitrifying sealing glasses with relatively high sealing temperatures (e.g., ≥950°C). The major potential advantages of refractory sealing glasses include stable thermal properties (including CTE), reduced interfacial reactivity, and lower volatility. In addition, the higher sealing temperature may enhance sintering and bonding of electrical contact pastes to mating surfaces, and hence, improve mechanical strength and electrical conductance. PNNL has developed "refractory" sealing glasses in the Sr-Ca-Y-B-Si-O system, which exhibit stable CTE in the range of 11.5-12.5 ppm/°C. Microstructural analysis by X-ray diffraction (XRD) and volatility studies confirmed the desired stability in terms of crystallization products and weight loss, but the analysis also revealed the formation of $SrCrO_4$ at alloy interconnect/glass interfaces, near sealing edges. The formation of these chromates at metal interfaces presents a technical challenge that must be dealt with, due to their very high CTE (~22 ppm/°C), which can result in micro-cracking during thermal cycling.

To minimize the formation of undesirable chromate phases, two approaches were evaluated in FY 2007 to prevent direct contact between the Cr-containing interconnect alloy and the sealing glass. The first approach involves aluminization of the alloy, followed by oxidation to form a dense alumina layer. The second approach uses $(Mn,Co)_3O_4$ spinel coatings to prevent the alloy/glass interaction. Use of the spinel coating offers potential advantages over the aluminizing process in that the spinel has a better CTE match, and the metal interconnect would need one coating process, instead of two processes; the same coating could be used for both sealing areas, and active cathode areas. However, reaction of $(Mn,Co)_3O_4$ spinel with the sealing glass, and its limited phase stability in reducing environments are potential challenges for this approach. In FY 2007, the seal (joint) strength of a candidate refractory sealing glass (YSO75) with Crofer22APU coated with either alumina or spinel was evaluated.

Approach

A commercial vendor performed the aluminizing using vapor phase or pack cementation processes, followed by oxidation in air, to form the alumina layer. The $(Mn,Co)_3O_4$ spinel coatings were fabricated in-house using PNNL's slurry-based process. Test samples were prepared by applying glass powder paste between two coated Crofer22APU coupons (1/2"x1/2" squares), followed by sealing at 950°C/2h, and short-term crystallization at 800°C/4h in air. In some cases, samples were aged for longer periods. For comparison, as-received Crofer22APU was evaluated in seal strength tests. The strength was tested in uni-axial tension, at room temperature. After testing, the samples were examined with optical and scanning electron microscopy, to identify failure origins.

Results

Initially, we evaluated the baseline strength of glass seals with uncoated Crofer22APU. Alloy coupons were pre-oxidized in air, at three conditions (800°C/2h, 1,000°C/2h, and 1,200°C/2h) to promote mild to severe oxidation. The oxide scales were approximately <0.5, 1, and 5-6 microns thick after heat treatment at 800, 1,000, and 1,200°C. Figure 1 shows the seal (joint) strength of samples for as-received and pre-oxidized samples. It is evident that the strength degraded substantially when Crofer22APU was pre-oxidized at 1,000 or 1,200°C. The as-received or 800°C pre-oxidized samples showed seal strength of ~6.3 MPa, while the higher temperature pre-oxidation resulted in strengths of 2.6-2.9 MPa with large standard deviation (0.81 to 0.44 MPa). In post-test analysis, fracture surfaces of the higher pre-oxidation temperature samples (1,000°C/2h and 1,200°C/2h) showed substantial amounts of yellowish color, suggesting fracture through $SrCrO_4$ or at the $SrCrO_4/Cr_2O_3$ interface. Thus, the results supported the assumption that chromate formation negatively affects the strength of the glass seals.

The effects of aging in different environments were also studied. Sealed coupons were tested at 850°C, either in air for 500 hours, or in 30% H_2O / 70% dilute hydrogen (2.7%H_2/Ar) for 250 hours. The joint strengths are plotted in Figure 2 along with those of the as-sealed samples. Aging in air degraded the strength from an initial value of ~6.3 MPa to ~0.5 MPa. The yellowish color observed on the fracture surfaces indicated the formation of $SrCrO_4$. Overall, these tests suggest that a protective coating is required to prevent chromate formation on the airside of interconnect seals. Aging in the wet reducing environment did not result in degradation of strength. This is not surprising, since chromate formation is thermodynamically unfavorable under reducing conditions typical of the SOFC fuel environment.

Results of strength tests for seals to aluminized Crofer22APU are plotted in Figure 3. Two pre-oxidation conditions (in air) for the aluminized alloy were evaluated: 1,000°C/2h and 1,200°C/2h. Overall, the seal strength for the aluminized Crofer22APU was similar to that of the uncoated alloy. For the aluminized samples, the fracture mode was primary through the glass, rather than the alumina/glass interface. This is consistent with the CTE of the constituents; alumina has the lowest CTE and, therefore is likely to be in compression after cooling

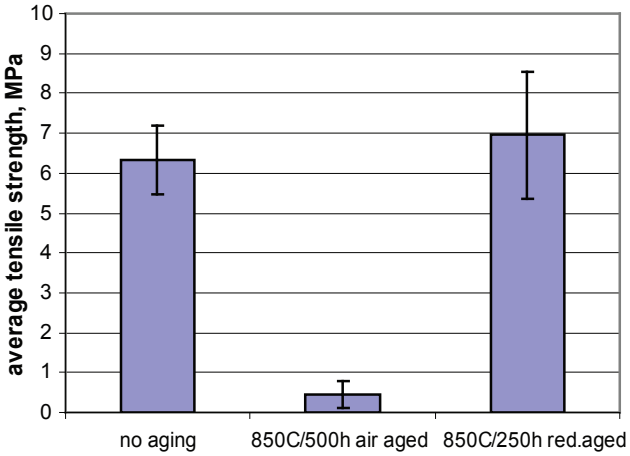

FIGURE 2. Room Temperature Seal (Joint) Strength of As-Received Crofer22APU with Refractory Sealing Glass (YSO75) after Aging in Different Atmospheres

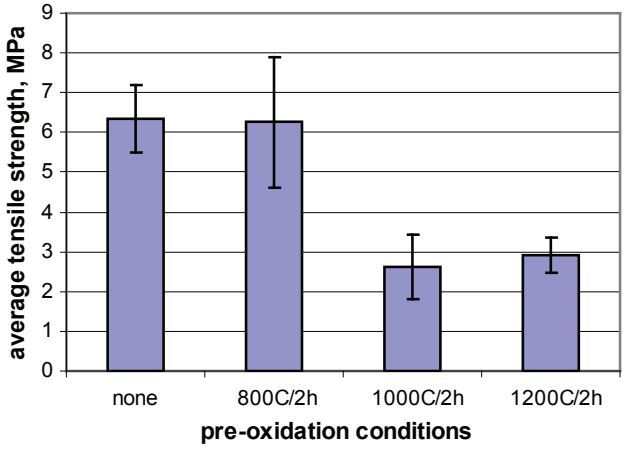

FIGURE 1. Room Temperature Seal (Joint) Strength of Uncoated Crofer22APU and Refractory Glass (YSO75) as a Function of Pre-Oxidation Temperature

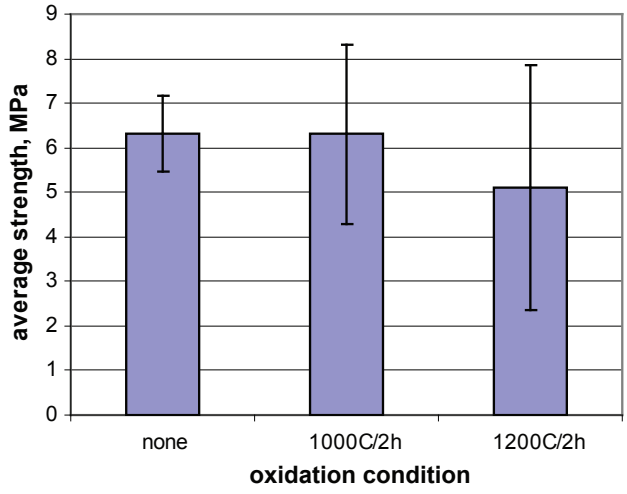

FIGURE 3. Room Temperature Seal (Joint) Strength of Aluminized Crofer22APU with Refractory Sealing Glass (YSO75)

while the glass was in tension. As a result, the fracture propagated through the glass. Earlier reports showed that a dense alumina layer was effective in suppressing the chromate formation (at least in the short term) and therefore, one might expect to have seen improvement in joint strength, since no high CTE chromate should have been present along the interfaces. The reason for the observed similar strength of aluminized Crofer22APU to the uncoated Crofer22APU (either as-received or 800°C oxidized) is not clear. One possible cause is that the edge defects were larger for the aluminized alloy (which had a relatively rough surface) than the uncoated alloy (with a smoother surface). Another possible cause could be residual tensile stress induced by the low CTE alumina layer (CTE ~8.8). The tests will be repeated using a second batch of aluminized Crofer22APU, which has a smoother surface due to improvements in the aluminization process.

Seal strength tests were also performed using spinel-coated Crofer22APU. The measured strengths of the as-sealed, air-aged, and reducing environment-aged samples are shown in Figure 4. The as-sealed tensile strength was 5.5 ± 0.7 MPa, slightly lower than the strength of the uncoated Crofer22APU (6.3 ± 0.8 MPa). The air-aged spinel-coated samples, however, were much stronger than the air-aged uncoated samples (4.6 ± 1.1 MPa vs. 0.5 ± 0.3 MPa). The reducing environment-aged samples had similar strengths to the as-sealed samples (5.4 ± 0.8 MPa). Overall, the current tests indicated that the initial seal (joint) strength was relatively independent of the presence/absence or type of coating. However, while the seal strength of uncoated samples degraded substantially during aging in air, the spinel-coated samples retained much of their initial strength after aging in either air or a wet, reducing environment.

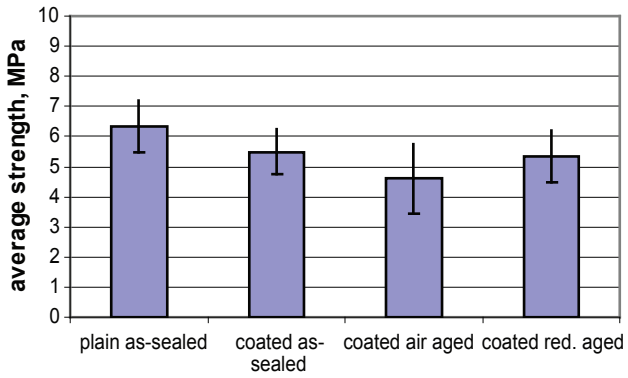

FIGURE 4. Room Temperature Seal (Joint) Strength of Spinel-coated Crofer22APU before and after Aging with Refractory Sealing Glass (YSO75)

Conclusions and Future Directions

Room temperature strength testing of sealed Crofer22APU/glass/Crofer22APU coupons showed similar strengths for samples in the as-sealed state, with or without protective coatings. Without the coatings, the strength degraded substantially, after aging in air for 500 hours at 850°C. With the coatings however, strength showed significantly less degradation during aging in air. During aging in a wet, reducing environment, no strength degradation was observed. Future directions of glass seal development will include continued electrical stability testing of coated Crofer22APU (aluminized and spinel coating) in SOFC environments, and interfacial microstructure analysis after the DC loading tests. Strength and short-term thermal cycling tests will also be performed on these electrically aged samples. In addition, optimization of coating microstructure (thickness and porosity) will be performed for several refractory sealing glasses covering a sealing temperature range of ~950 to ~1,050°C in air. Concerning glass microstructure development, a study of glass, particle size effects, as well as fine-tuning of glass compositions will be performed to yield better wetting (sealing) and dense microstructure. In addition to the current Crofer22APU, a low-cost interconnect candidate stainless steel (441) will be evaluated in terms of chemical compatibility, seal strength, and coating adhesion. Finally, the performance of candidate refractory seals glasses will be tested in a 2" x 2" single cell stack.

FY 2007 Publications/Presentations

1. Y-S Chou, J. W. Stevenson, R. N. Gow, "Novel alkaline earth silicate sealing glass for SOFC, Part I: the effect of nickel oxide on the thermal and mechanical properties," J. Power Sources, 168, 426 (2007).

2. Y-S Chou, J. W. Stevenson, P. Singh, "Novel refractory alkaline earth silicate sealing glasses for planar solid oxide fuel cells," J. Electrochemical Society, 154, B644 (2007).

3. Y-S Chou, J. W. Stevenson, and P. Singh, "Effect of pre-oxidation of a metallic interconnect on the bonding strength of a SOFC sealing glass," Presented at 31st International Conference on Advanced Ceramics & Composites, January 21–26, 2007, Daytona Beach, FL.

4. Y-S Chou, J. W. Stevenson, and P. Singh, "Effect of ageing on the thermal and electrical properties of a novel SOFC sealing glass," Presented at 31st International Conference on Advanced Ceramics & Composites, January 21 – 26, 2007, Daytona Beach, FL.

5. Y-S Chou, J. W. Stevenson, and P. Singh, "Glass seal development at PNNL," presented at Glass & Optical Materials Meting and 18th University Conference on Glass, The American Ceramic Society, May 20–23, 2007, Rochester, NY.

6. Y-S Chou, J. W. Stevenson, and P. Singh, "SOFC seal development at PNNL," presented at TMS 2007 Annual Meeting and Exhibition: Materials in Clean Power System: Fuel Cells, Solar and Hydrogen Based Technologies, February 25 – March 1, 2007, Orlando, FL.

IV.A.15 SOFC Cathode Materials Development at PNNL

Steve Simner, Mike Anderson and
Jeff Stevenson (Primary Contact)
Pacific Northwest National Laboratory (PNNL)
P.O. Box 999, MS K2-44
Richland, WA 99352
Phone: (509) 372-4697; Fax: (509) 375-2186
E-mail: jeff.stevenson@pnl.gov

DOE Project Manager: Travis Shultz
Phone: (304) 285-1370
Email: Travis.Shultz@netl.doe.gov

Objectives

- Develop and optimize solid oxide fuel cell (SOFC) cathode materials and microstructures offering low polarization losses and long-term stability at intermediate SOFC operating temperatures (650-850ºC).
- Improve understanding of mechanisms affecting cathode performance, including both intrinsic factors (e.g., composition, microstructure) and extrinsic factors (e.g., Cr poisoning).

Accomplishments

- Performed baseline testing on Sr-doped lanthanum manganite (LSM), LSM/yttria-stabilized zirconia (LSM/YSZ), and LSM/samarium-doped ceria (LSM/SDC) cathodes.
- Initiated development of composite cathodes prepared using mechanofusion process.

Introduction

Minimization of cathodic polarization losses represents one of the greatest challenges to be overcome in obtaining high, stable power densities from SOFCs. Cathodic polarization typically exhibits high activation energy relative to other internal power losses, so the need to improve cathode performance becomes increasingly important as the targeted SOFC operating temperature is reduced. For high-temperature SOFCs operating at around 1,000ºC, the preferred cathode material is doped lanthanum manganite, which offers adequate electrical conductivity and electrocatalytic activity, reasonable thermal expansion, and stability in the SOFC cathode operating environment. For SOFCs operating at substantially lower temperatures, modified or alternative cathode materials may be required. For example, alternative perovskite compositions containing La on the A site and transition metals such as Co, Fe, and/or Ni on the B site have received attention. In general, they offer higher oxygen ion diffusion rates and exhibit faster oxygen reduction kinetics at the electrode/electrolyte interface than lanthanum manganite, but tend to exhibit significant degradation of performance over time. During FY 2007, PNNL's cathode development work was focused on development of LSM-based composite cathodes intended to provide improved performance in the 650-850ºC temperature range.

Approach

Cathode performance was measured by screen-printing and sintering the cathode material onto anode-supported YSZ membranes. In some cases, an SDC interlayer was included between the cathode and YSZ. After attachment of current collectors, the resulting cells were placed into test fixtures, and their current-voltage characteristics were evaluated using DC and impedance spectroscopy measurements. Cells were tested in air vs. moist (~3% H_2O) hydrogen at low fuel utilizations. After cell tests were completed, the cells were analyzed by scanning electron microscopy/energy dispersive spectroscopy (SEM/EDS) and other techniques as appropriate.

Results

Cathode compositions under study were $(La_{0.8}Sr_{0.2})_{0.98}MnO_3$ (LSM), LSM/YSZ (50/50 vol% mixture of LSM and 8YSZ), and LSM/SDC (50/50 vol% mixture of LSM and $Ce_{0.8}Sm_{0.2}O_2$). For each cathode composition, a range of sintering temperatures was evaluated in order to determine effects of sintering temperature of cathode performance. All of the cells were tested at 750ºC and at 0.7 V, with periodic current-voltage and impedance spectroscopic analysis. Although this study is still in progress, results to date are summarized in this report.

LSM Cathodes. For LSM cathodes sintered directly onto anode-supported YSZ electrolyte membranes, cell power densities were relatively low and quite variable even for nominally identical cathodes sintered at the same temperature. This result suggests that the performance of the LSM cathode may be highly dependent on slight changes in the cathode microstructure. In general, somewhat higher cell power densities were observed for LSM cathodes sintered onto SDC interlayers (Figure 1), but again the results for nominally identical cells showed considerable

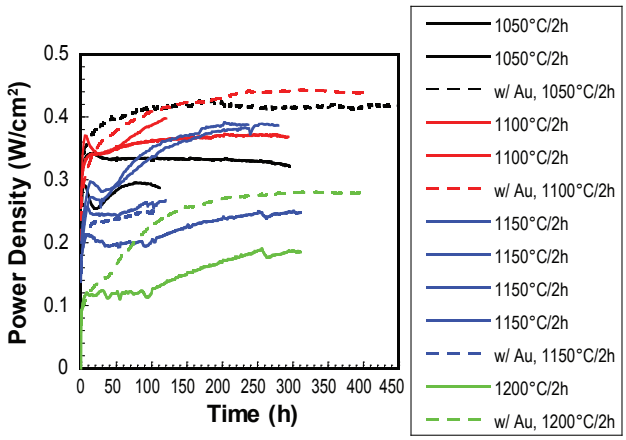

FIGURE 1. Anode-supported button cell test results for LSM cathodes sintered onto SDC interlayers at the indicated temperatures and tested at 0.7 V and 750°C. LSM contact paste was used except where Au is indicated.

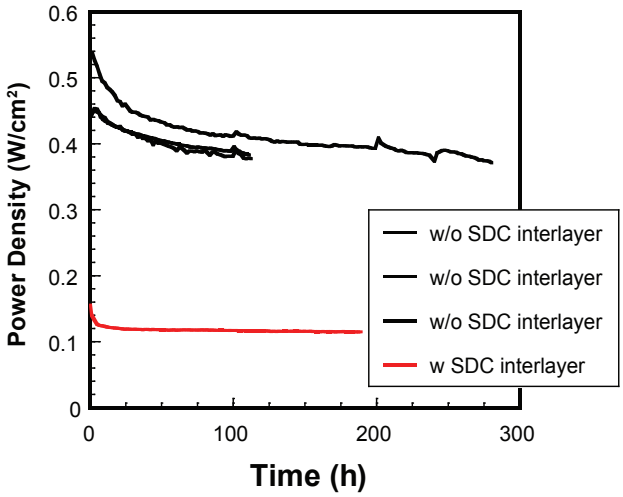

FIGURE 2. Anode-Supported Button Cell Test Results for LSM/YSZ Cathodes Sintered at 1,150°C and Tested at 0.7 V and 750°C

variability. Nyquist plots from impedance spectroscopic analysis indicated that, for cells with or without the SDC electrolyte interlayer, higher sintering temperatures tended to result in lower initial power densities, presumably due to increased densification and therefore reduction in triple phase boundary (TPB) length at the cathode/electrolyte interface. It will be noted that the ohmic resistance of samples with the SDC interlayer was higher than those sintered directly onto YSZ, which suggests that insulating zirconate phases were not formed at the cathode/YSZ interface during cell fabrication.

It was observed that, for a given sintering temperature, cathodes sintered directly onto YSZ tended to be denser than cathodes sintered onto an SDC interlayer. The enhanced densification of the cathodes on YSZ may be related to diffusion of Ni (from the NiO/YSZ anode) through the YSZ electrolyte into the LSM cathode. It has been established by SEM/EDS analysis that Ni diffusion from the anode into the YSZ during anode/electrolyte co-sintering at 1,375ºC results in a Ni content of ~2-3 at% in the YSZ membrane. Similarly, SEM/EDS analysis on as-fabricated cells indicated that ~1-2 at% of Ni was present in an LSM cathode sintered at 1,150ºC, and ~2-3 at% was present in an LSM cathode sintered at 1,250ºC. In contrast, no Ni was detected in LSM cathodes sintered at those temperatures onto an SDC interlayer, suggesting that the SDC substantially blocks diffusion of Ni out of the YSM electrolyte into the cathode. The mechanism behind the enhanced sinterability of the LSM cathode containing Ni is not clear, but may be related to presence of free manganese oxide formed when Mn was displaced by Ni from B-sites in the LSM perovskite lattice.

LSM/YSZ Cathodes. Results for LSM/YSZ cathodes sintered at 1,150ºC (with and without the SDC interlayer) are shown in Figure 2. LSM-YSZ on an SDC interlayer exhibited very poor performance, while LSM/YSZ sintered directly onto YSZ (no SDC interlayer) gave high initial performance followed by significant degradation. Overall the LSM/YSZ cathodes without the SDC layer demonstrated better consistency in performance, suggesting that a performance of a mixture of electronically conducting LSM and ionically conducting YSZ is less sensitive to subtle changes in microstructure compared to cathodes consisting of the electronically conducting LSM alone. The higher initial performance of the LSM/YSZ cathodes (compared to LSM) is probably associated with an expanded active region for oxygen reduction due to the mixed-conducting nature of the composite, but a more porous microstructure for the composite compared to LSM alone may also contribute. Figure 3 shows the difference in microstructure for LSM and LSM/YSZ cathodes sintered under identical conditions (1,200ºC for 2 hours). It is frequently observed that, under identical conditions, and in the absence of liquid phase formation, multi-phase mixtures of oxide powders exhibit reduced densification relative to the single phase components on their own. Results from impedance spectroscopy analysis of the cells with LSM/YSZ cathodes revealed that the decrease in performance over time was predominantly associated with an increase in the ohmic resistance of the cell. It is possible that the increased resistance is a result of the formation of an insulating phase such as lanthanum zirconate during cell operation.

LSM/SDC Cathodes. Results for cells with SDC interlayer and LSM/SDC cathodes, sintered at the indicated temperatures, are shown in Figure 4. The cells typically showed some performance conditioning which was associated with a decrease in the non-ohmic component of the cell impedance. Ohmic resistance was relatively high, but remained stable over time. Similar

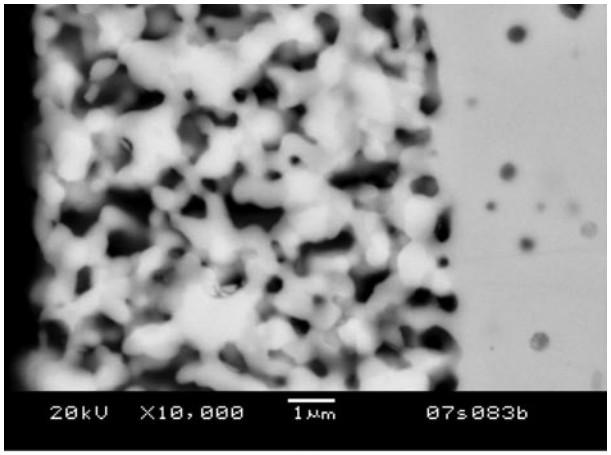

(a)

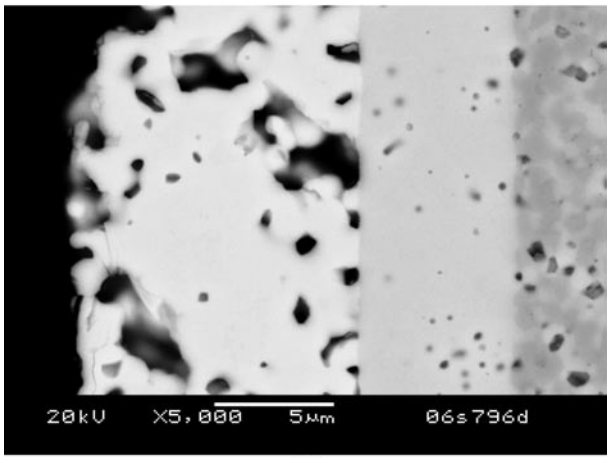

(b)

FIGURE 3. SEM Micrographs of a) LSM/YSZ and b) LSM Cathodes after Sintering at 1,200ºC for 2 Hours

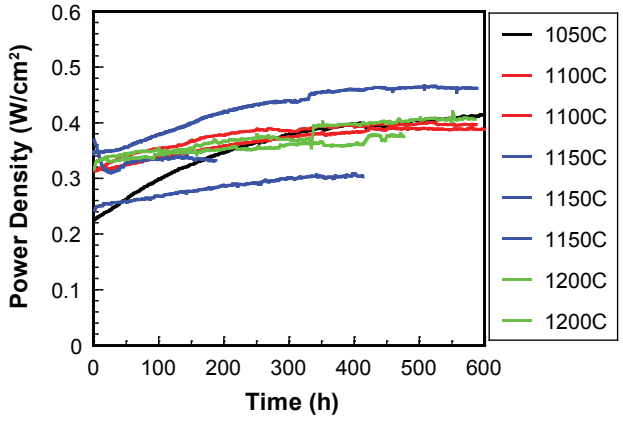

FIGURE 4. Anode-Supported Button Cell Test Results for LSM/SDC Cathodes Sintered onto SDC Interlayers at the Indicated Temperatures and Tested at 0.7 V and 750°C

to the LSM/YSZ cells, the LSM/SDC cells showed better performance consistency than the LSM-only cells. Overall, performance of the LSM/SDC cells was more stable than that of the LSM/YSZ cells. It is anticipated that future work directed towards a) optimizing the LSM/SDC microstructure via mechanofusion, and/or b) increasing cathode activity by insertion of electrocatalytic materials via infiltration may result in improved, stable performance for anode-supported cells with LSM/SDC or LSM/YSZ cathodes.

Conclusions and Future Directions

- LSM cathodes exhibited relatively poor performance and low reproducibility compared to composite (LSM/YSZ, LSM/SDC) cathodes.
- LSM/YSZ cathodes exhibited relatively high initial performance but the performance degraded over time, possibly due to the formation of insulating phases.
- LSM/SDC cathodes exhibited improved stability compared to LSM or LSM/YSZ cathodes.
- Future work will focus on optimizing LSM-based composite cathode microstructures via mechanofusion and/or other techniques to obtain improved, stable cathode performance at intermediate SOFC operating temperatures.

FY 2007 Publications/Presentations

Publications

1. S.P. Simner, M.D. Anderson, J.W. Templeton, and J.W. Stevenson, "Silver-Perovskite Composite SOFC Cathodes Processed via Mechanofusion," J. Power Sources, 168, 236 (2007).

Presentations

1. S.P. Simner, M.D. Anderson, and J.W. Stevenson, "Performance of a Novel La(Sr)Fe(Co)O_3-Ag SOFC Cathode," MS&T 2006, Cincinnati, OH, October 15–19, 2006.

2. S.P. Simner, M.D. Anderson, and J.W. Stevenson, "SOFC Cathode Degradation Mechanisms", MS&T 2006, Cincinnati, OH, October 15–19, 2006.

3. S.P. Simner, M.D. Anderson, and J.W. Stevenson, "SOFC Cathode Development at Pacific Northwest National Laboratory," 31st Int. Conference on Advanced Ceramics & Composites (American Ceramic Society), Daytona Beach, FL, January 21–26, 2007.

IV.A.16 SECA Core Technology Program Activities—PNNL

Prabhakar Singh
Pacific Northwest National Laboratory (PNNL)
P.O. Box 999, MS K2-44
Richland, WA 99354
Phone: (509) 375-5945; Fax: (509) 375-2186
E-mail: Prabhakar.Singh@pnl.gov

DOE Project Manager: Travis Shultz
Phone: (304) 285-1370
E-mail: Travis.Shultz@netl.doe.gov

Objectives

- Direct Solid State Energy Conversion Alliance (SECA) core technology programs.
- Identify and prioritize technology development needs that meet the cost and performance targets of SECA.
- Develop and execute experimental plans, summarize technical findings, and prepare topical reports; disseminate technical information and assist in technology transfer to SECA industrial teams.
- Develop materials, design and fuel processing technologies for large coal-based solid oxide fuel cell (SOFC) systems.
- Participate, organize technical and topical meetings and workshops, and exchange technical information with industrial and academic experts.
- Hold technical and program reviews and meetings to present the results of on-going technical work.
- Provide leadership and organization to technical societies and outreach programs.

Accomplishments

- Identified key cell component materials cost reduction, thermal management, design scale-up approaches, and methodologies. Established a collaborative program with Allegheny Technologies, Inc. (ATI) for the development and testing of low-cost, bulk interconnect materials produced, using conventional melt and ladle metallurgical processes.
- Initiated a low-cost surface coatings development program to mitigate multi-step heat treatment process.
- Conducted modeling workshop and provided simulation tools to SECA industrial teams.
- Provided technical reports and materials samples of advanced coatings and seals to facilitate technology transfer.
- Published quarterly progress and topical reports. Peer reviewed journal papers were also published.
- Presented invited technical lectures at technical societies, universities, and industries.
- Organized American Society for Metals and Materials Science & Technology 2007, and American Ceramic Society, Cocoa Beach meetings on SOFC technology.

Introduction

The SECA Core Technology Program (CTP) at PNNL conducts, and coordinates research towards the development and implementation of advanced cell and stack materials, systems design, simulation and performance optimization, along with the utilization of hydrocarbons and coal-derived fuels, in SOFC power systems. The PNNL program also collaborates with academic institutions, national laboratories, and industries towards the identification of technology gaps and prioritization of development needs. Research programs are focused on the development of cost effective materials and fabrication processes, electrical performance optimization and long-term stability, stack and systems design, and optimization along with thermal and structural analysis, and utilization of hydrocarbons and coal-derived fuels.

The CTP facilitates the exchange and dissemination of technical information to SECA participants in a timely manner. Technical workshops, topical reports, peer reviewed publications in technical journals, and presentations at technical meetings facilitate the information exchange. Quarterly and topical progress reports are prepared, and provided to SECA participants. The CTP also interacts with other government agencies, to gather and disseminate technical information related to SOFCs.

Approach

The CTP conducts and coordinates research to meet the cost and performance targets of SECA. The program disseminates the research findings through workshops, technical and topical reports, and journal publications.

- Meet with SECA industrial participants, discuss technology status, and identify technology needs.
- Hold technical and program reviews and meetings to present the results of on-going technical work.
- Organize topical area workshops and exchange technical information with industrial and academic experts.

- Identify and transfer key technologies to industries.
- Publish technical findings in quarterly, annual, and topical technical reports, after completion of the task.
- Provide leadership and organization to technical societies and outreach programs.
- Organize and participate in the Annual SECA Program Review Meeting.
- Co-ordinate with the National Energy Technology Laboratory (NETL) on all aspects of the SECA-CTP.
- Organize technical society meetings.
- Foster university interactions, student exchange and training.

Results

The SECA CTP has developed low-cost, interconnect materials and coatings, and provided the technical details to industrial teams. Mechanistic understanding of corrosion processes has also been developed. Advanced refractory glass formulations were developed, and are currently being tested, under SOFC exposure conditions. Thermal and structural models for large cell stacks were developed. The role of on anode reforming on temperature distribution was studied. Technical meetings with industrial teams were held and technical information related to cell materials, design and performance, were provided. Technical findings were presented at technical society meetings (MST 06-Cincinnatti and ACerSoc Cocoa Beach meeting). Numerous peer-reviewed journal articles were published, based on the core technology research.

Cell and stack component materials development activity focused on the development of lower cost, bulk interconnect alloy and surface coatings for improved corrosion resistance under bi-polar exposure conditions and mitigation of chromia poisoning of cathode electrodes exposed to ambient air. Evaluation of glass formulations also continued for applications in seals. Alloy metallurgy developed utilizing conventional melt processing, and ladle metallurgy techniques are currently being investigated, in collaboration with Allegheny Technologies Inc., for the development of modified ferritic stainless steels. This approach eliminates the use of expensive vacuum melt treatment techniques. Use of selected alloy additives to the melt also allow for localized segregation of Si. Although the spinel-based coatings have proven successful in reducing the alloy scaling, elimination of chromia evaporation and poisoning of the cathode electrode, the coating technique requires multiples of controlled heat treatment steps. Our current focus is on the development of low-cost electroplating or electrophoretic deposition processes for the fabrication of near net shape surface coating on stamped or formed interconnects. Several glass modifications were developed for seal applications, and are currently being examined for structural and chemical stability. Issues related to glass interaction with adjoining chromia scale, resulting in the dissolution of chromia and interface separation, have been studied. An aluminizing surface treatment of the steel has been developed for the elimination of chromia interaction with the glass. The aluminizing process is a commercial, low-cost process and can be scaled-up for coating large volume and large area current collectors. Another advantage of the aluminizing process is that it results in the formation of electrically insulating surface oxide.

Cell and stack design, performance simulation and long-term reliability studies at PNNL have focused on in-depth structural and thermal analysis of SOFC stacks. Glass seals stability, metal interconnection deformation, electrode-electrolyte interface stability, on-anode reforming, etc. have been investigated using computational simulation tools developed at PNNL. Training was conducted for the efficient utilization of modeling tools to SECA industrial partners. Utilization of hydrocarbon on the anode was found highly effective in controlling the stack temperature distribution more effectively for large size cells and stacks. We found that the reformation rate for methane remained very high, resulting in significant endotherm and cooling, at the cell inlet. Anode modification was developed and found to be effective in controlling the reformation rate and inlet cooling. We studied morphological changes in the bulk anode, due to subsequent reduction during the initial reduction or long-term operation. Phase changes in the zirconia present in the anode bulk were investigated, and results were disseminated to all SECA industry teams and to appropriate CTP participants. Topical reports covering the results and mechanistic understanding has been prepared and provided to SECA participants. Technical specifications, materials formulations, processing techniques, etc. have been documented in technical reports and provided to industrial partners as part of the technology transfer. PNNL provides topical and technology development status reports to SECA participants.

Topical and technical workshops to gather and disseminate technical information were conducted. PNNL participated in a joint meeting with ATI and NETL to develop a low-cost interconnection bulk alloy utilizing conventional metallurgical processes. A seal workshop was held at NETL to develop and test refractory glass seals. Use of refractory glass in the cell stack has the potential to reduce interactions with interconnect scale, along with increasing the glass sealing operational window. PNNL, along with the University of Cincinnati, is developing a comparative assessment of rigid and viscoelastic glass seals during nominal and transient cell operating conditions. The core technology management interacted with

Delphi, Siemens, General Electric and Fuel Cell Energy, and presented the technical status of research conducted in cell materials, simulation and fuel processing. A technical meeting with Delphi was held in Rochester to present the results of on-going work on interconnection corrosion, coatings, seal, anode reforming and simulation and modeling. Issues related to performance and performance stability, materials interaction, cell to cell interconnection and processing of liquid and gaseous hydrocarbons were identified and approaches for mitigation were developed. Because of the workshop, white papers in the areas of liquid fuel processing and catalyst stability have been prepared. Meetings with SECA industrial teams help identify and prioritize technical issues and promote technology transfer. PNNL works closely with the NETL Project Management Team and provides technology status reports.

Conclusions

The SECA CTP at PNNL conducts research to meet the cost, performance and performance stability requirements of SECA. PNNL also coordinates the research activities with universities, national laboratories and industries for the development of advanced materials, electrodes, fuels and fuel processing, and modeling and design tools. Technical findings are presented at workshops and technical society meetings, as well as published in technical journals.

Future Directions

- Continue technology development and collaborative programs with industries. Identify technology gaps and development needs at the stack and systems levels to meet the cost and performance targets.
- Prioritize technology needs for SOFC operation on coal-derived fuels. Assist industries in developing and optimizing cell, stack and systems design and configurations for scale-up.
- Develop and implement cost effective materials and fabrication processes to meet the SECA cost and life targets.
- Identify long-term performance degradation mechanisms.
- Accelerate technology transfer to industries.
- Provide technical and topical progress reports to SECA participants.
- Organize technical society meetings to exchange technical information.
- Conduct CTP meetings and topical workshops.

Publications/Presentations

1. P. Singh and Z. Gary Yang "Corrosion in Fuel cells" ASM Handbook, Volume 13C.

2. Xiaodong Zhou and Prabhakar Singh, "Electrolytes for solid Oxide Fuel cells" Book Chapter.

3. J.W. Stevenson, L. A. Chick, M. A. Khaleel, D. L. King, L. R. Pederson, and P. Singh, "Recent Advances in Solid Oxide Fuel Cell Technology at Pacific Northwest National Laboratory" Fuel Cell Seminar, 2006.

IV.A.17 SOFC Interconnect Materials Development at PNNL

Zhenguo "Gary" Yang (Primary Contact), Guanguang Xia, Jeff Stevenson and Prabhakar Singh
Pacific Northwest National Laboratory (PNNL)
P.O. Box 999, MS K2-44
Richland, WA 99352
Phone: (509) 375-3756; Fax: (509) 375-2186
Email: zgary.yang@pnl.gov

DOE Project Manager: Travis Shultz
Phone: (304) 285-1370
E-mail: Travis.Shultz@netl.doe.gov

Objectives

- Develop cost-effective, optimized materials for intermediate temperature solid oxide fuel cell (SOFC) interconnects and interconnect/electrode interfaces applications.
- Identify and understand degradation processes in interconnects and at interconnect/electrode interfaces.

Accomplishments

- Evaluated ferritic stainless steels based on AISI430 for interconnect applications.
- Completed isothermal kinetics study on bare and spinel-coated Crofer22APU, AISI430, and T-441.
- Completed one-year stability tests on bare and spinel-coated Crofer22APU.
- Investigated and developed conductive oxides and cermets for cathode-side contact layer applications.

Introduction

With the reduction in SOFC operating temperatures, low-cost high temperature oxidation resistant alloys have become promising candidates to replace lanthanum chromite, a ceramic that can withstand operating temperatures in the 1,000°C range. However, the metallic materials face challenges including chromia scale evaporation, scale electrical resistivity, oxidation/corrosion under interconnect dual exposure conditions, and scale adherence and compatibility with adjacent components, such as seals, electrodes and/or electrical contact materials. To improve the understanding of the advantages and limitations of alloy interconnects, PNNL has been engaged in systematic evaluation and development of candidate materials for interconnects and their interfaces with electrodes.

Approach

Oxidation/corrosion behavior of candidate alloys has been investigated in air, air/hydrogen and air/simulated reformate environments, typical of SOFC interconnect operation conditions. Alloys evaluated include traditional compositions, newly developed alloys, and recently ferritic stainless steels with a relative low Cr content, but a unique alloy chemistry. Candidate alloys are surface-modified by application of conductive oxide protection layers to improve surface, chemical, and electrical stability. Conductive oxides have been investigated and optimized for application as contact layers between electrodes and interconnects. Novel processing approaches have been designed and optimized for fabrication of the electrical contact layers or interfaces between electrodes and metallic interconnects.

Results

Due to space limitations, this report will focus on: i) evaluation and identification of ferritic stainless steels that are more cost-effective than the state-of-the-art compositions, but potentially offer comparable or improved performance, and ii) development and long-term evaluation of $(Mn,Co)_3O_4$ spinel protection layers.

The first task is a collaborative effort between PNNL and Allegheny Technologies, with a goal to identify and develop a ferritic stainless steel that is more cost-effective than recently developed compositions such as Crofer22APU, while demonstrating at least comparable performance for interconnect applications. The current approach focuses on evaluation and modification of ferritic stainless steels that have a similar level of Cr to AISI430, but are alloyed with minor additions so that the formation of an insulating silica layer at the scale/metal interface during high temperature exposures can be avoided. In other words, potential negative effects of residual Si on the electrical stability of metallic interconnects are avoided by an inexpensive alloying approach, instead of high cost vacuum refining that is commonly used for the state-of-the-art compositions such as Crofer22APU. Preliminary evaluation of one alloy in particular, T-441, has been encouraging. Minor additions of Ti and Nb appear to prevent the build-up of silica, an insulating phase, along the scale/metal interface (see Figure 1), even though the stainless steel contains ~0.5% residual Si. The presence of residual Mn (~0.5%) led to growth of a scale on T-441 similar to that on Crofer22APU, consisting

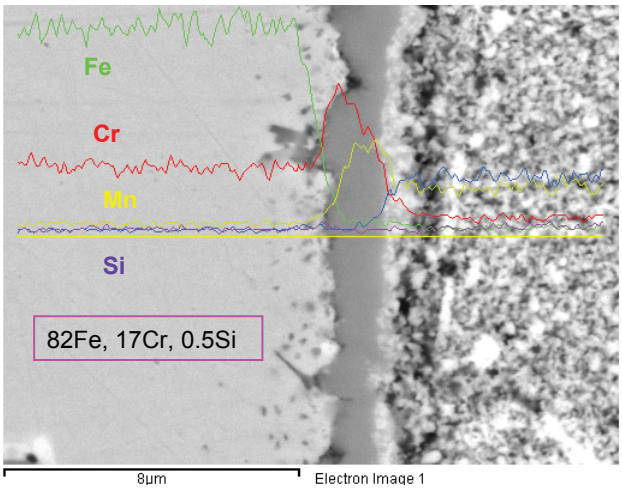

FIGURE 1. Cross-Section Scanning Electron Microscopy/Energy Dispersive Spectoscopy (SEM/EDS) of 441 with LSM Contact Paste after 500 hours of Oxidation at 800°C in Air

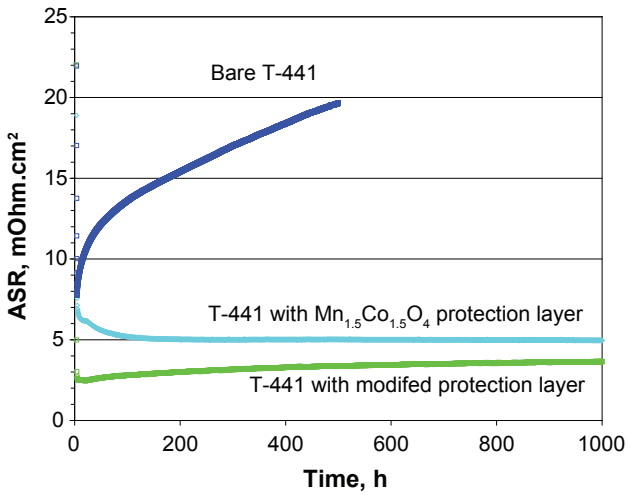

FIGURE 2. Contact area specific resistance (ASR) of uncoated T-441 and T-441 with two versions of the spinel protection layer. The tests were carried out in air at 800°C.

of a dual layer structure: a $(Mn,Cr)_3O_4$ top layer and a Cr_2O_3 sub-layer. The absence of the silica interfacial layer and formation of the dual layer scale structure resulted in low scale electrical resistance (see Figure 2). Application of $Mn_{1.5}Co_{1.5}O_4$ spinel protection layers on T-441 significantly improved its oxidation resistance. Further investigations are in progress to develop a more extensive understanding of the properties and performance of uncoated and coated T-441.

Spinel protection layers developed at PNNL are intended to: i) protect metallic interconnects from environmental attack and improve the metallic interconnect surface stability; ii) serve as a barrier to Cr migration from the chromia-forming alloy interconnect; and iii) minimize the interfacial contact resistance. Following previous success in fabrication of the protection layers on ferritic steel substrates and short- and mid-term evaluation of their performance, a year-long isothermal evaluation was completed in this fiscal year. After ~9,000 hours in air at 800°C, the oxide scale grown on Crofer22APU beneath a spinel protection layer fabricated via a slurry coating approach was much thinner (~4 µm) than the scale (~14-15 µm) grown on uncoated Crofer22APU. Importantly, there was no evidence of Cr penetration through the spinel protection layer after one year. Thus, the spinel protection layer acted as an effective barrier to both oxygen inward and chromium outward diffusion. Also, the high conductivity of the spinel protection layer may have helped to minimize the interfacial contact resistance, as indicated by data presented in Figure 2. The average thickness of the scale grown on coated and uncoated Crofer22APU during numerous oxidation and electrical resistance tests is shown in Figure 3. Overall, it appears that protective coatings or other surface modifications

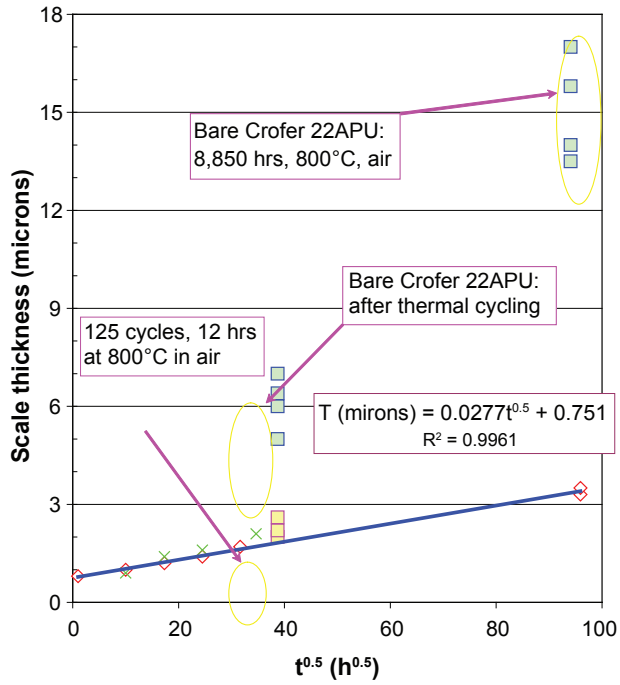

FIGURE 3. Thickness of Scales on Uncoated and Spinel-coated Crofer22APU, as a Function of Time during Oxidation in Air at 800°C

will be required for ferritic stainless steel interconnects operating at ~800°C.

Conclusions

Preliminary evaluation of T-441, a ferritic stainless steel with ~17% Cr and minor additions of Nb and Ti, proved the feasibility of using an alloying approach to

avoid the formation of insulating silica layers along the scale/metal substrate. Thermally grown spinel protection layers fabricated via a slurry approach demonstrated long-term benefits, including improved surface stability, reduction of Cr outward migration, and reduction of electrical resistance of ferritic stainless steel interconnects.

Future Directions

- Continue to evaluate and modify cost-effective ferritic stainless steels for SOFC interconnect applications.
- Modify $(Mn,Co)_3O_4$ spinel protection layers and optimize coating processes for further performance improvement and cost reduction of ferritic stainless steel interconnects.
- Develop and optimize materials and processing approaches for contact layer applications.

FY 2007 Publications/Presentations

Publications

1. "Investigation of Modified Ni-Cr-Mn Base Alloys for SOFC Interconnect Applications," Z.G. Yang, P. Singh, J.W. Stevenson, G.-G. Xia, *Journal of the Electrochemical Society,* 153, A1873, 2006.

2. "Evaluation of Ni-Cr-Base Alloys for SOFC Interconnect Applications," Z.G. Yang, G.G. Xia, J.W. Stevenson, *Journal of Power Sources,* 160, 1104, 2006.

3. "Conductive Protection Layers on Oxidation Resistant Alloys for SOFC Interconnect Applications," Z.G. Yang, G.G. Xia, G.D. Maupin, J.W. Stevenson, *Surface & Coatings Technology,* 201, 4476 (2007).

4. "Evaluation of Perovskite Overlay Coatings on Ferritic Stainless Steels for SOFC Interconnect Applications," *Journal of the Electrochemical Society,* Z.G. Yang, G.-G. Xia, G.D. Maupin, J.W. Stevenson, 153, A1852, 2006.

5. "High Temperature Corrosion Behavior of Oxidation Resisitant Alloys under SOFC Interconnect Dual Exposures," Z.G. Yang, G.-G. Xia, J.W. Stevenson, P. Singh, *Ceram. Eng. & Sci. Pro.,* 27, 211, 2007.

6. "Properties of $(Mn,Co)_3O_4$ Spinel Protection Layers for SOFC Interconnects," Z.G. Yang, X.S. Li, G.D. Maupin, P. Singh, J.W. Stevenson, G.-G. Xia, X.D. Xhou, *Ceram. Eng. & Sci. Proc.,* 27, 231, 2007.

7. "Advanced Interconnect Development at PNNL," Z.G. Yang, G.-G. Xia, G.P. Maupin, S. Simner, X. Li, J.W. Stevenson, P. Singh, Fuel Cell Seminar Abstracts, Courtesy Associates, 2006.

Presentations

1. "Volatilization of Cr Vapor Species from Coated and Uncoated SOFC Interconnects," J.W. Stevenson, G.D. Maupin, P. Singh, Z.G. Yang, G.-G. Xia, Int. Conf. Metal. Coatings & Thin Films (ICMCTF 2007), San Diego, CA, 2007.

2. "Corrosion Behavior of Metals and Alloys under SOFC Interconnect Exposure Conditions,"Z.G. Yang, G.-G. Xia, J.W. Stevenson, P. Singh, Advanced Ceramics and Composites Meeting, Daytona Beach, FL, 2007.

3. "Properties of $(Mn,Co)_3O_4$ Spinel Protection Layers for SOFC Interconnect Applications," Z.G. Yang, G.-G. Xia, X.S. Li, G.D. Maupin, S.P. Simner, C.M. Wang, X.D. Xhou, Y.S. Chou, J.W. Stevenson, Advanced Ceramics and Composites Meeting, Daytona Beach, FL, 2007.

4. "Metallic Interconnect and Its Degradation in SOFCs," Z.G. Yang, P. Singh, J.W. Stevenson, M.S. Walker, G.-G. Xia, 136th TMS Conference, Orlando, FL, 2007.

5. "Electrical Contacts and Interfacial Resistance between Electrodes and Metallic Interconnects in SOFCs," G.-G. Xia, Z.G. Yang, Z. Nie, J.F. Bonnet, S.P. Simner, J.W. Stevenson, 136th TMS Annual Conference, Orlando, FL, 2007.

IV.A.18 Reliable Seals for Solid Oxide Fuel Cells

Ronald E. Loehman (Primary Contact),
Erica Corral and Marlene Chavez
Sandia National Laboratories
MS 1349
Albuquerque, NM 87185-1349
Phone: (505) 272-7601; Fax: (505) 272-7304
E-mail: loehman@sandia.gov

DOE Project Manager: Ayyakkannu Manivannan
Phone: (304) 285-2078
E-mail: Ayyakkannu.Manivannan@netl.doe.gov

Objectives

- Develop reliable, cost-effective sealing techniques for solid oxide fuel cells (SOFCs).
- Determine performance-limiting features of sealing methods.
- Optimize seal properties.
- Determine seal degradation mechanisms and predict useful seal lifetimes.

Approach

- We are making composite seals comprising a glass matrix and powder filler that exhibit a wide range of chemical and mechanical properties.
- The composite approach allows glass and filler properties to be optimized independently.
- Seal thermal and mechanical strains are reduced by selecting glass compositions with glass transition temperatures (Tg) below the SOFC operating temperature.
- Viscosity, coefficient of thermal expansion (CTE), and other seal characteristics can be tailored by adding unreactive powder.
- The volume fraction of the glass phase can be reduced to a minimum for the seal, which reduces reactivity with fuel cell materials.

Accomplishments

- We selected two glasses with properties suitable for further seal development and testing after making extensive measurements on over 30 different custom glass compositions.
- We used the high temperature optical dimension measuring instrument (TOMMI), which allows *in situ* video recording of specimens at elevated temperatures (T<1,700°C), to determine the additive powder composition, particle size, and aspect ratio that optimize composite seal flow and adhesion for the selected glasses.
- A completed series of 2,000-hour tests in air at 750°C of two composite seal compositions on ferritic stainless steal (SS) alloys and yttria-stabilized zirconia (YSZ) electrolyte showed the seal materials are unreactive.
- We measured weight losses with time at 750°C of the pure and powder filled glasses in simulated steam for 2,000 hours and found the extrapolated 40,000-hour weight losses to be less than 5% for both linear and parabolic weight loss mechanisms.
- We developed an apparatus for testing seal adherence and bond strengths at room temperature under 2 atm of internal gas pressure. The best seals survived nine thermal cycles from room temperature to 750°C and back. Those that leaked could be resealed by heating them above 850°C.

Future Directions

- Continue long-term tests of stability of seals and seal materials under realistic environmental conditions. Model weight loss data to predict 40,000-hour performance.
- Modify the pressure test apparatus to allow seal strength measurements at 750°C.
- Use a combination of X-ray photoelectron spectroscopy (XPS), Auger spectroscopy, time of flight secondary ion mass spectrometry (SIMS), and wet chemical analysis to identify the species responsible for the observed (small) weight loss from the sealing glasses when they are heated at 750°C.
- Begin tests of operating button cells sealed with these composite sealing glasses.

Introduction

Seals for SOFC stacks face the most challenging set of performance requirements in the entire field of ceramic joining. The industry teams in the Solid State Energy Conversion Alliance (SECA) program have consistently identified seal development as one of their highest priorities.

Approach

As we have written in previous annual reports, we are using Department of Energy (DOE) support to develop techniques for sealing SOFCs that can be

tailored to the specific requirements of the vertical teams in the DOE/SECA program. The approach is based on our many years of seal development for other applications as applied to the special requirements for SOFC seals. It is evident to us that relief of thermal expansion mismatch stresses will require SOFC seals to incorporate either a ductile metal or a high-viscosity glass that can relieve stresses through viscous creep. Accommodating mismatch stresses, as well as other SOFC design and operational constraints that frequently are in conflict, severely restrict the options for seal materials. Based on our prior experience in ceramic joining and on results obtained on this project, we believe we have the greatest design flexibility using ceramic-filled glasses and metal-filled glass composites. We have demonstrated control of properties such as glass transition temperature and thermal expansion coefficient by varying the compositions, amounts, and microstructures of the different phases. The choices are guided by thermochemical and composite microstructural models that allow us to target specific seal properties for a given design. Our seals are showing great promise in functional and 2,000-hour lifetime tests with results that extrapolate very favorably to 40,000-hour operation.

Results

In this past year we concentrated our efforts on making seals using the two best glass compositions and determining properties necessary to control processing and to demonstrate functionality.

Seal material properties: We have made many measurements of composite viscosities using the parallel plate method in our TOMMI apparatus (thermooptical mechanical measuring instrument, Fraunhofer Gesellschaft, Wurtsburg, Germany). Data on variation of viscosity as a function of composition, relative volume fraction of glass and filler, and temperature allow us to assess the performance of different composites and to choose the best combination of joining material for the specific use conditions. Viscosity controls the flow of seal materials at temperature. If the viscosity is too high the sealant will not flow enough to make the seal and it also will not be able to dissipate thermal expansion mismatch stresses. If the viscosity is too low, the sealant will not stay in the joint and the seal may leak and be too weak. We also measure spreading rates and contact angles of composite sealants on different SOFC materials at temperature in the TOMMI. These properties depend on both viscosities and surface energies of the seal constituents and the data are complementary to the viscosity measurements. Contact angles and spreading rates are needed to specify heating schedules for seal formation and to determine adhesion and compatibility of the seal materials with different substrates.

Seal strengths: It is difficult to measure the absolute strengths of joints in brittle materials such as ceramics. One common technique is to make butt seals in test bars (typically 3x4x40 mm with the seal in the 3x4 mm plane at the 20 mm point) that are then loaded in four point flexure. The load at failure is recorded and the fracture surface is analyzed to determine the fracture origin and to assess whether the failure should be counted as a good data point. Because brittle fracture is stochastic, data on 30 specimens of each condition are typically necessary to evaluate the statistics. Using the measured flexure strength to predict failure in some other geometry requires computational modeling such as the finite element method. The technique can give reliable results but it is labor intensive and it is not a very efficient method for screening a lot of different process variables.

The other approach to determining seal strengths is proof tests either of samples of the actual device or simplified versions that are deemed to embody the essential features. The data are not absolute materials properties in any sense, but they provide relative levels of performance. We have followed this latter method in designing a strength test apparatus in which an annular seal creates a volume that can be pressurized with air. Discs and washers of the desired materials are sealed with different composite sealants to create a small interior volume as shown in Figure 1. The assembly is immersed in water and the pressure is slowly increased until either the seal leaks and air bubbles are detected or 2 atm pressure is reached. Two atmospheres of over pressure is much greater than any pressure differential that has ever been suggested for SOFC operation. Leakers are resealed at the normal process temperature

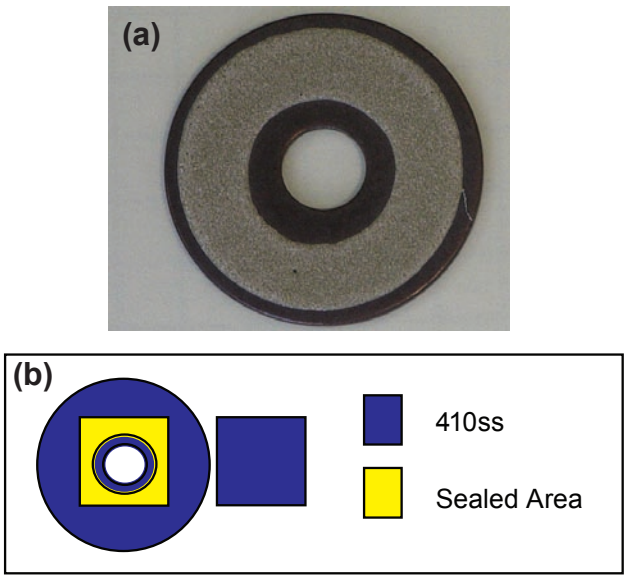

FIGURE 1. (a) Result of a Wetting Experiment for a 14a Glass Composite Sealed to a 410 SS Substrate and (b) the Test Geometry for Measuring Seal Strength/Leak Properties

and retested. Seals that do not leak are heated to 750-850°C, typical of SOFC operating temperature, cooled to room temperature, and retested in the pressure apparatus. We record the number of cycles to seal failure as a function of materials variables and process conditions and determine if the leakers can be resealed. Note that testing strengths at room temperature is not a drawback since any leaks at high temperature will likely be worse at room temperature.

For the strength tests we used a 14a glass-Ag composite sealing composition that was formulated as a matched CTE seal to 410 SS. The rule of mixtures was used to calculate the volume fraction of Ag needed in the glass to adjust its CTE to that of the 410 SS. Composite preforms were made using conventional tape casting techniques. Wetting studies on 410 SS showed the optimum sealing temperature to be 900°C. Seal strengths were determined using a 410 SS to 410 SS sandwich geometry as shown in Figure 1. The crosshatched area in the figure is the actual sealed area tested.

Strength and leak tests were performed at room temperature. As stated above, we assumed that flaws at higher temperatures will likely persist at room temperature and therefore should be detected in our tests. Strength data from the first round of tests are presented in Table 1.

We examined the effects of differences in the tape cast performs on seal strengths. For example, we found that tapes made with finer powders gave higher seal strengths. For the initial experiments we made and tested 15 seals, of which four failed under pressure, giving an average fracture strength of 5.58 N/mm^2. Those fractured specimens were then resealed, retested and gave similar strengths. Other sealed specimens did not fail after as many as nine resealing and testing cycles. Table 2 shows the strength results for seal specimens that never failed. We believe that variations in the seal strengths listed in Table 1 are likely due to defects in the tape. The results in Table 2 show that tapes made with finer powders may give slightly stronger seals, although the strength distributions overlap.

TABLE 1. Seal Strength Values for Specimens that Failed after Pressure Testing

Specimens [#/total]	Seal Material	Initial Fracture Strength [N/mm^2] *10^{-2}	Strength after *n*th Sealing Cycle [N/mm^2] *10^{-2}
2/5 failed	14A Š Ag (coarse powder)	10.16 ± 9.34	8.35 ± 5.53 (3^{rd})
4/15 failed	14A Š Ag (fine powder)	5.68 ± 2.34	6.84 ± 1.93 (1^{st})

TABLE 2. Seal Strength Values for Specimens that Never Failed in Pressure Testing

Specimens [#/total]	Seal Material	Minimum Fracture Strength [N/mm^2] *10^{-2}	Strength after *n*th Thermal Cycle [N/mm^2] *10^{-2}
3/5 did not fail	14A Š Ag (coarse powder)	9.68 ± 1.78	>9.68 ± 1.78 (7^{th})
9/15 did not fail	14A Š Ag (fine powder)	9.83 ± 1.65	>9.83 ± 1.65 (9^{th})

Long-term tests: We have set up a number of furnaces to test seal stability for extended times at temperature. We have investigated both the pure seal materials and seal materials in combination with different substrates. The test rigs comprise airtight ceramic muffle tubes inside resistance-heated tube furnaces. The ceramic tubes are sealed with end caps that allow gas to be passed through them at temperature. For the steam tests Ar-3%H_2 is bubbled through a 62°C water bath to create a 30% simulated steam atmosphere. Weighed samples are heated in the center of the hot zone under flowing wet hydrogen or air, depending on the specific test. Standard tests last 2,000 hours with the specimens cooled to room temperature at intervals and then weighed. For tests of stability of the seal materials by themselves, specimens are supported on alumina wafers that contribute no weight change since they are inert to the test conditions. For tests of stability of sealants on component materials, which are just getting underway, the seals are placed on coupons of the specific material, e.g. 410 stainless steel or YSZ, and then tested as described. The measured weight changes are plotted as a function of time at temperature.

Concern about vaporization of glass constituents in long-term use of glass sealants has been voiced at various SECA reviews and workshops. Possible preferential loss of boron from borate glasses in different SOFC atmospheres has been a particular issue. The SECA design lifetime is 40,000 hours, which is too long an interval to test in an iterative materials development program. Therefore we have calculated upper and lower bounds to weight loss for both linear and parabolic loss mechanisms assuming a weight loss of 5% at 40,000 hours as a conservative, tolerable level. We made most of our long-term weight loss measurements on two glass compositions, one of which contains almost twice the boron of the other. Comparison of our measured weight losses for times up to 2,000 hours with the predictions of the two weight loss models shows the sealing glass weight losses track the lower parabolic limit pretty well, which strongly suggests that loss of boron or other glass constituents is not an issue for borate glass seals in typical SOFC operating environments. Thus, the weight loss data so far are showing that our borate-based glasses

are stable over long times at the representative SOFC operating temperature of 750°C in both simulated steam and air.

The seal stability experiments have concentrated on Glass 14a and Glass 17, whose as-cast compositions contain 40 mol% B_2O_3 and 25 mol% B_2O_3, respectively. Bulk sections of glass cast from the melt were cut to pieces large enough to give measurable weight losses in our experiments. Both the 14a and 17 glasses were tested with and without a pre-crystallization heat treatment. Pre-crystallized specimens were heated up to 900°C, which is well above the glass T_g (T_g of Glass 14a = 576°C, T_g of Glass 17 = 632°C) and the targeted SOFC operating temperature of 750°C.

Figure 2 shows the 2,000-hour weight loss measurements for Glasses 14a and 17 in air at 750°C. The glass with less boron gave a lower weight loss. The observed weight loss in air for both glass compositions was not affected by the pre-crystallization heat treatment. The maximum weight loss for Glass 14a was found near the end of the 2,000-hour experiment to be about 0.2 wt%. Glass 17 was even more stable with less than 0.05% weight loss over the entire 2,000-hour heating period. After a higher rate of loss for an initial 200 hours at 750°C, Glass 14a settled down to a long period of linear weight loss with time. The weight loss for Glass 17 also increased for the first 200 hours and then maintained a constant weight loss for the rest of the 2,000 hours. However, all the weight losses were very low, so these differences in rates are small.

Figure 3 shows the data from our first measurements of long-term weight loss for Glasses 14a and 17 in a wet-H_2, simulated steam environment. Unlike the results for heating in air, the data for simulated steam did not give smooth weight loss curves for heat treatments longer than 500 hours. We are not sure if the data are accurate or whether there may have been some error in the measurements, so we currently repeating this experiment. Figure 4 is a plot of the data in Figure 3 for only the first 500 hours of heating where the data appear well behaved. During this initial 500-hour period both glasses exhibit a constant weight loss over time, independent of glass composition or pre-crystallization treatment. The pre-crystallized glasses appear to be more stable than the as-cast glass specimens once they have been heated for 300 hours.

Our experiments show that there is higher weight loss in air than in simulated steam initially, as shown in Figure 5. If long-term results in simulated steam are confirmed in our current experiments, then we can conclude that our borate sealing glasses will experience only negligible weight loss in typical SOFC operating conditions. Because we want to know what is evaporating from the sealing glasses we presently are implementing a furnace setup that allows us to capture the evolved species for analysis using atomic absorption-inductively coupled plasma spectroscopic techniques.

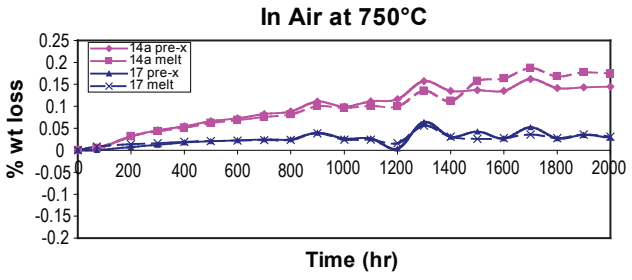

FIGURE 2. Long-Term Weight Loss for Glasses 14a and 17 in Air at 750°C

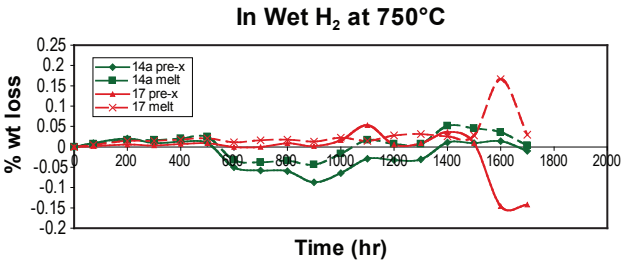

FIGURE 3. Weight Loss for 1,800 Hours for Glasses 14a and 17 in Wet-H_2, Simulated Steam at 750°C

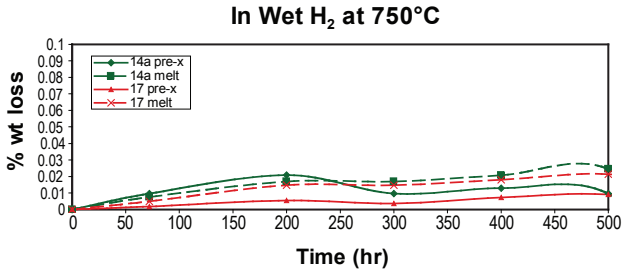

FIGURE 4. Weight Loss Over 500 Hours for Glasses 14a and 17 in Wet-H_2, Simulated Steam at 750°C

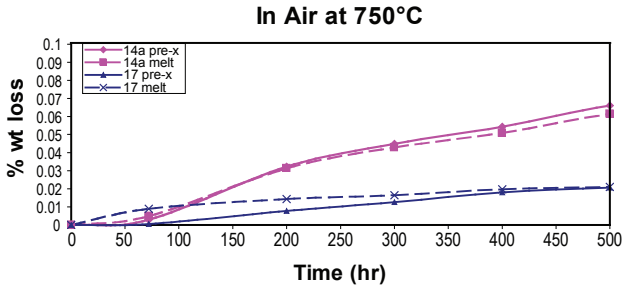

FIGURE 5. Early Stage Weight Losses in Air of Glasses 14a and 17 Show that Glass 17 is More Stable than Glass 14a in Air at 750°C

Summary of Specific Accomplishments

1. We measured viscosities of glass composites with different types and volume fractions of filler powders and as a function of temperature up to 850°C and selected two compositions with the best properties for further SOFC seal development.
2. We developed a test rig for measuring strengths of seals cycled between room temperature and typical SOFC operating temperatures. Our measurements showed many of the 410 SS to 410 SS seals were hermetic at 2 atm of pressure. Seals that leaked could be resealed by briefly heating them to 900°C.
3. Long-term testing of glass compositions in air and simulated steam, coupled with weight loss projections according to two models, lead us to predict that none of our glass composite sealing compositions would experience more than 5% mass loss in 40,000 hours of operation in typical SOFCs.

Conclusions and Future Directions

Our results to date show that the borate glasses are stable in air and simulated steam for long times at 750°C. The largest weight loss in all the experiments was only 0.2 wt%, observed in air towards the end of a 750°C, 2,000-hour test. The highest weight loss measured in simulated steam was 0.03 wt%. The replication of experiments that is underway should allow us to confirm these low weight losses. The identity of the evaporating species will be revealed by analysis of the captured condensates. We also are planning to analyze surfaces of composite seal materials that have been heated under different test conditions using XPS or SIMS to determine depletion or buildup of constituents in the first few atomic layers. Although these results will not give information on bulk compositional changes, they should show changes in surface compositions with heating.

We have demonstrated that our glasses can be made into composite seals with a wide range of CTEs. Pressure tests to 2 atm of composite seals with CTEs matched to 410 SS showed high strengths after multiple pressure cycles. Seals that did leak could be resealed. The long-term stability, reliability and strength of the glass composite seals demonstrate the versatility of the glass composite seals.

FY 2007 Publications/Presentations

Presentations

1. E. Corral, B. Gauntt and R. Loehman, "Sealing SOFCs with Glass Matrix Composites," SECA Glass Sealing Workshop, National Energy Technology Laboratory, Morgantown, WV, September 20–21, 2006.

2. E. Corral, B. Gauntt and R. Loehman, "Glass Composites for Sealing Solid Oxide Fuel Cells: A Science Based Engineering Approach," Rio Grande Symposium on Advanced Materials, October 10, 2006, Embassy Suites Hotel, Albuquerque, NM.

3. E. Corral, A. Ayala, B. Gauntt, and R. Loehman, "Long-Term Evaluation of Engineered Glass-Ceramic Composites for Solid Oxide Fuel Cell Applications," Materials Science & Technology 2006 Conference and Exhibition (MS&T 06), October 15–19, 2006, Cincinnati, OH.

4. E. Corral, A. Ayala, B. Gauntt, and R. Loehman, "Properties of Engineering Glass Composites for Sealing Solid Oxide Fuel Cells," Materials Science & Technology 2006 Conference and Exhibition (MS&T 06), October 15–19, 2006, Cincinnati, OH.

5. E. Corral, B. Gauntt, R. Loehman, "Glass Composites as Sealing Materials for Solid Oxide Fuel Cells", The American Ceramic Society's 2007 Glass & Optical Materials Division Meeting & 18th University Conference on Glass, May 20–23, 2007, Rochester, New York (invited).

Papers

1. E. Corral, B. Gauntt, R. Loehman, "Controlling Seal Material Properties for Reliable Seal Performance Using Glass-Ceramic Composites," 30th International Conference on Advanced Ceramics and Composites, Daytona Beach, FL, January 21-26, 2007 (invited).

IV.A.19 Novel Composite Materials for SOFC Cathode-Interconnect Contact

Jiahong Zhu (Primary Contact), Zigui Lu, Jacky Shoulders, and David Ballard
Department of Mechanical Engineering
Tennessee Technological University
115 W. 10th St., Box 5014
Cookeville, TN 38505
Phone: (931) 372-3186; Fax: (931) 372-6340
E-mail: jzhu@tntech.edu

DOE Project Manager: Briggs White
Phone: (304) 285-5437
E-mail: Briggs.White@netl.doe.gov

Objectives

- Elucidation of the mechanism of Ag evaporation at elevated temperatures.
- Alloy design and development of new Ag-based alloys with significantly reduced Ag evaporation/migration.
- Optimization of the processing and the microstructures of Ag alloy/perovskite composites.
- Demonstration/assessment of performance of the new contact materials in the solid oxide fuel cell (SOFC) operating conditions.

Accomplishments

- A number of Ag-base alloys have been prepared using both the arc-melting/drop-casting technique and the powder metallurgical route. These alloys were pressed into 1-mm sheets for Ag evaporation testing.
- Pd, Pt, and Au have been found to be effective in reducing the Ag evaporation rate; however, these elements are too expensive. The effects of other low-cost alloying additions on the Ag evaporation are being studied.
- The perovskite-containing composite contact layer has been demonstrated to effectively reduce the Cr migration from the interconnect to the porous cathode.
- With the increase of Ag in the composite contact layer, both the area specific resistance (ASR) of and thermal cycling-induced damage in the interconnect/contact/cathode test cells decreased.

Introduction

To reduce the electrode/interconnect interfacial resistance in SOFC stacks, electrical contact layers are often applied between the interconnect and electrodes during construction of an SOFC stack by compensating for the corrugations present on their respective surfaces. Some of the major criteria for SOFC contact materials are (1) sufficiently high electrical conductivity over the SOFC lifetime; (2) chemical stability under high current conditions and compatibility with other cell components, especially negligible effects on the formation of protective oxides on interconnect alloy; and (3) reasonable match in coefficient of thermal expansion (CTE) with other cell components. In addition, it is highly desirable for the contact materials to have some damage tolerance (possible self-healing if thermal cycle-induced cracking occurs in the contact layer) and to act as a Cr "sponge" by absorbing the Cr species migrating from the interconnect to the cathode and therefore reducing the Cr "poisoning" of the cathode. Because of the stringent criteria, finding a suitable material for the interconnect-cathode contact is very challenging.

The materials currently under consideration for cathode/interconnect contact application include low melting-point ceramics (such as doped $LaCoO_3$), noble metals (e.g. Ag or Pt), and their composites [1-2]. Pt, Au, and Pd are not desirable for this application because of their high raw material cost. However, Ag is an exception due to its relatively low price. An Ag-ceramic composite is one of the very promising candidates for a SOFC contact due to the inherent properties of Ag, such as high chemical stability, high electrical conductivity, high ductility, and relatively low melting point. The perovskite component in the composite is expected to provide a more desirable CTE match and potentially act as a Cr absorbent and/or a barrier for Cr migration to the cathode. One major drawback of Ag as a SOFC interconnect/cathode contact material is its tendency to evaporate at the SOFC operating temperatures, while for the perovskite material, thermal cycle-induced cracking and damage accumulation might be an issue.

Approach

Ag would be a wonderful contact material if its evaporation/migration can be reduced. Since Ag evaporation is determined by the bonding of Ag atoms, alloy design should focus on identifying suitable alloying elements that drastically affect the bonding in Ag or finding surface-active elements that segregate to and thus block the Ag sites on the Ag surface. What is desired

of the alloying elements is to effectively reduce Ag evaporation/migration without significantly altering the overall properties of Ag. A number of alloying additions have been selected based on these considerations and the Ag evaporation rate of each of these alloys is being determined using the optimized evaporation parameters identified last year. Another approach to reduce the Ag evaporation rate as well as improve the other properties of the contact material is to form a Ag/perovskite composites. By selecting the right perovskite material and optimizing the Ag-to-perovskite ratio, a composite material might address all the issues facing the interconnect-cathode contact material development.

The Ag-base alloys were prepared using both the arc-melting/drop-casting technique and the powder metallurgical route. These alloys were pressed into 1-mm sheets for Ag evaporation testing. The composite materials with different Ag-to-perovskite ratios were also synthesized and the performance of the composite materials as interconnect/cathode contact was assessed using a special testing rig.

Results

The effects of a number of alloying additions on Ag evaporation were investigated. The noble metals such as Pt, Pd, and Au noticeably reduced the Ag evaporation rate. Figure 1 shows the weight losses of the Ag-Pd alloys after exposure at 850°C for 40 hours in flowing air with a flow rate of 1.5 cm/s. It can be seen that the weight loss due to Ag evaporation decreased significantly as the content of Pd in the alloys increased. The weight loss of Ag decreased from about 0.28 mg/cm^2 for pure Ag to 0.08 mg/cm^2, less than one third of that of pure Ag, with a Pd content of 25 wt.% after exposure. Similar results were obtained for Ag-Au and Ag-Pt alloys. Obviously, the noble metal additions can reduce the evaporation rate of Ag. However, the reduction was more significant when the Pt, Pd, or Au additions were higher than 50%. Considering the cost of these elements, they are not suitable choices as alloying additions. Low-cost alloying additions with similar or further improved performance should be identified. Initial work indicates that micro-alloying with non-noble elements Cu, Ce, and Y had very little effect on the evaporation of Ag. The Ag alloys with Ce and Y additions even showed a slightly larger weight loss than pure Ag. A systematic study on the effects of other elements on Ag evaporation is currently underway.

Two types of Ag-perovskite composites are being evaluated, with the Ag contents of 0, 25, 50, 75, and 100% (in volume) in the composites. The first type is with $La_{0.6}Sr_{0.4}Co_{0.2}Fe_{0.8}O_3$ (LSCF-6428) as the perovskite, while the second type is with $La_{0.6}Sr_{0.4}Co_{0.8}Fe_{0.2}O_3$ (LSCF-6482). Both Ag and the perovskite had very fine particle size of around 1 µm. The powders with the desired Ag-to-perovskite ratio were thoroughly mixed before pastes were made for screen printing. To evaluate the performance of various contact materials in a simulated SOFC environment, a special interconnect/contact/cathode test cell was constructed. Analysis with energy-dispersive spectroscopy (EDS) indicates that the amount of perovskite in the composite contact materials had a significant effect on chromium migration to the cathode from the interconnect alloy. Figure 2 shows that the amount of Cr detected in the center of the porous cathode layer as a function of the volume % of Ag in the Ag-(LSCF-6428) composite contact layer after the test cells were thermally exposed to air for 300 hours at 800ºC. The increase of the LSCF content (and therefore the reduction of silver) in the contact material led to a significant decrease in chromium migration, as more Cr was absorbed by the perovskite phase.

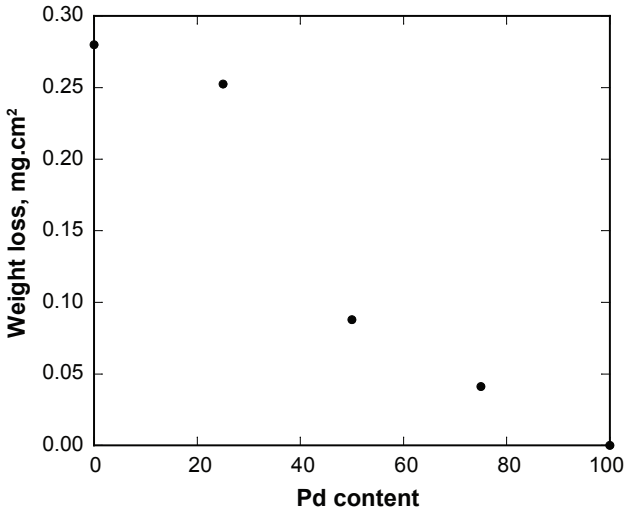

FIGURE 1. Weight Losses of Various Ag-Pd Alloys after Thermal Exposure at 850°C for 40 Hours in Air with a Flow Rate of 1.5 cm.s^{-1}

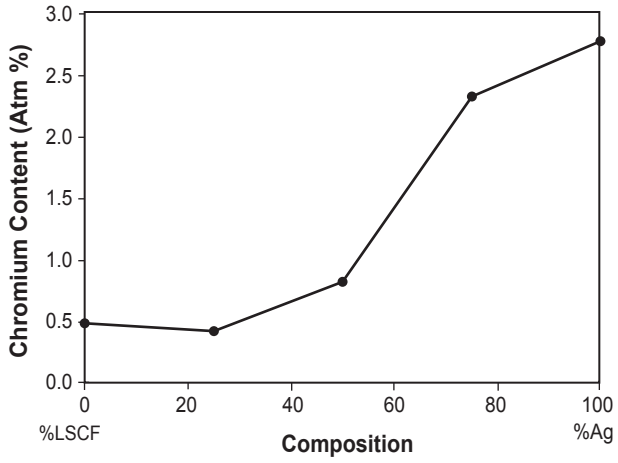

FIGURE 2. Chromium Content in the Porous LSM Cathode Layer vs. Volume % of Ag in the Ag-LSCF-6428 Composites

The ASR of the test cells with different Ag-LSCF contact materials as a function of exposure time and thermal cycling is shown in Figure 3. The data clearly indicate that the amount of perovskite in the composite contact materials had a significant effect on the ASR stability of the test cell as well as the cell resistance to thermal cycle-induced damage. For the pure perovskite contact material, after the initial "break-in" period, the ASR increased significantly during thermal cycling. This implies the damage was introduced in the contact layer during the cycling due to the brittleness of the perovskite material, leading to the jump in the ASR curve. Interestingly, the contact layer seemed to undergo a "self-healing" process during additional isothermal holding at 800°C, as the ASR value dropped continuously in this period of time. Nevertheless, the recovery in ASR was not complete; the accumulation of the residual damage led to a significant rise in ASR value, over 50 mΩ·cm^2, which is the targeted ASR limit for SOFC. From these results, it appears that pure LSCF contact materials are not adequate for interconnect-cathode contact application. With the increase in Ag content in the contact material, the ASR dropped continuously, as shown in Figure 3. The ASR value dropped from about 75 mΩ·cm^2 for the pure perovskite contact material to about 6 mΩ·cm^2 for the pure Ag contact material after 450 hours of thermal exposure at 800°C. Furthermore, the increase in ASR with thermal cycling was much lower for the Ag-containing contact materials. The Ag-containing contact materials are less prone to thermal cycle-induced damage, which might be a result of good ductility of the metal Ag. While pure Ag contact material exhibited the best performance with regard to ASR stability and damage tolerance, it alone is not considered a good contact material, due to its high evaporation rate as well as ineffectiveness in blocking the Cr migration from the interconnect to the cathode. Based on these results, it seems that a Ag-composite material with about 50 vol% Ag and 50 vol% LSCF might be a good contact material that deserves further investigation.

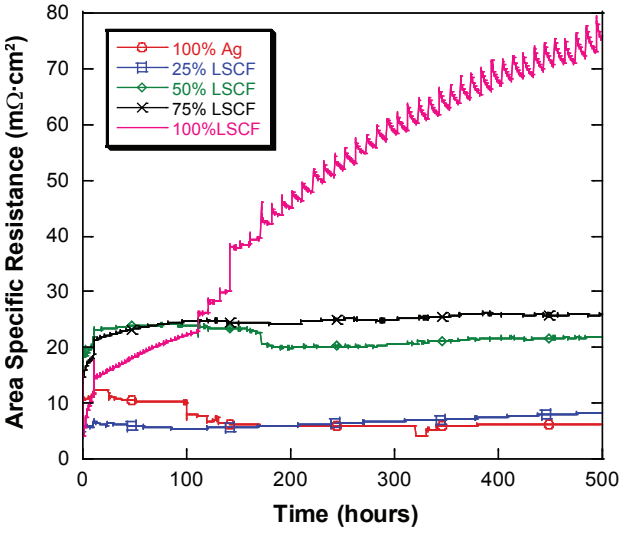

FIGURE 3. ASR of the Test Cell during Thermal Cycling for the Cells with Different Amounts of LSCF in the Contact Material (initial firing of 850°C x 10 h; "break-in" of 800°C x 100 h; 40 cycles with 800°C x 10 h holding plus furnace cooling to 250°C)

Conclusions and Future Directions

The following conclusions can be drawn based on this study:

- Noble metals Pd, Pt, and Au were effective in reducing the evaporation rate of Ag. Micro-alloying with Y, Ce, or Cu had little effect on the evaporation of Ag.
- The perovskite in the contact material decreased the Cr migration from the interconnect to the porous cathode.
- While the pure perovskite LSCF is prone to thermal cycle-induced damage and ASR increase during thermal exposure, the addition of Ag to form a Ag-LSCF composite is effective in reducing the thermal cycling effect.

The future directions for this project are listed below:

- The evaporation rate of a number of binary and ternary Ag alloys with various alloying additions will be measured and potential alloying elements which can significantly reduce the Ag evaporation will be identified.
- The evaporation behavior of Ag+perovskite composites with different Ag-to-perovskite ratios will be studied.
- Electrical characterization and thermal cycling of the interconnect/contact/cathode test cells will be continued to identify the desired Ag-to-perovskite ratio as well as the best perovskite materials for achieving stable electrical conductivity of the cells.

FY 2007 Publications/Presentations

1. "Thermal Evaporation of Pure Ag in SOFC-Relevant Environments", *Electrochemical and Solid-State Letters*, in press, 2007.

2. "Evaporation of Pure Ag under SOFC Operation Conditions", Presented at the Symposium Fuel Cells and Energy Storage Systems: Materials, Processing, Manufacturing and Power Management Technologies, MS&T 06, Cincinnati, Ohio, October 15-19, 2006.

3. "Development and Characterization of Ag-LSCF Composite Contact Material for SOFC", Presented at the Symposium Fuel Cells and Energy Storage Systems: Materials, Processing, Manufacturing and Power Management Technologies, MS&T 06, Cincinnati, Ohio, October 15–19, 2006.

References

1. S. Koch, and P.V. Hendriksen, Solid State Ionics, 168, 1 (2004).

2. Z. Yang, G. Xia, P. Singh, J.W. Stevenson, J. Power Sources, 155, 246 (2006).

IV.A.20 Developing Low-Cr Fe-Ni Based Alloys for Intermediate Temperature SOFC Interconnect Application

Jiahong Zhu (Primary Contact), Shujiang Geng, David Ballard, Xiaochuan Lu, Zigui Lu
Department of Mechanical Engineering
Tennessee Technological University
115 W. 10th St., Box 5014, Cookeville, TN 38505
Phone: (931) 372-3186; Fax: (931) 372-6340
E-mail: jzhu@tntech.edu

DOE Project Manager: Ayyakkannu Manivannan
Phone: (304) 285-2078
E-mail: Ayyakkannu.Manivannan@netl.doe.gov

Subcontractors:
- Oak Ridge National Laboratory, Oak Ridge, TN
- Harlan U. Anderson, Consultant, Rolla, MI

Objectives

- Develop a series of new Fe-Ni-based alloys without Cr or with low Cr for intermediate temperature solid oxide fuel cell (SOFC) interconnect application
- Demonstrate suitable oxidation resistance, oxide scale area specific resistance (ASR), and coefficient of thermal expansion (CTE) for these new alloys
- Achieve low Cr evaporation rate and good compatibility with the cathode materials for these alloys without surface coatings

Accomplishments

- The composition of the new low-Cr Fe-Ni-based alloy has been optimized and several promising alloying elements have been identified, which are effective in reducing the oxidation rate of this alloy system. Stable, low oxide scale ASR during thermal oxidation has been demonstrated for the new developmental low-Cr Fe-Ni-based alloy.
- Adequate oxidation performance in the SOFC anode environment has been demonstrated for this new alloy. Furthermore, the alloy surface is conductive even at room temperature after oxidation in such an environment.
- The alloying elements that are effective in improving the oxidation resistance of these new alloys does not negatively affect the thermal expansion behavior of these alloys.

Introduction

With the reduction of the SOFC operating temperatures to 700-800°C, Cr_2O_3-forming ferritic alloys are widely used as interconnect materials in the SOFC stacks being developed by the Solid State Energy Conversion Alliance (SECA) Industrial Teams. These ferritic alloys, including Crofer 22 APU, SS 430, SS 441, Ebrite, etc., posses an overall combination of properties desirable as SOFC interconnect materials such as low cost, excellent manufacturability, adequate match in CTE with other cell components, high electronic conductivity and thermal conductivity. Two of the major concerns (or problems) with these ferritic interconnect alloys are (1) their long-term oxidation resistance and oxide scale electrical conductivity, and (2) Cr evaporation and associated "poisoning" of the cathode under the operating environments of SOFC [1]. This SECA project has focused on the development of new low-Cr Fe-Ni-based interconnect alloys with low CTE and scale ASR, suitable oxidation resistance, and reduced Cr evaporation which is expected to resolve the Cr poisoning issue for SOFC stacks.

Approach

Using alloy-design principles, a series of new low-Cr Fe-Ni-based alloys have been developed. Upon thermal exposure, these low-Cr Fe-Ni-based alloys with 6 wt% Cr maximum develops a double-layer oxide scale consisting of a Cr-free, electrically-conductive $(Fe,Ni,Co)_3O_4$ spinel outer layer that acts as a surface seal for blocking Cr evaporation from the alloy surface atop a protective, electrically-conductive Cr_2O_3 inner layer [2].

The feasibility of thermally growing the double-layer oxide structure on the low-Cr Fe-Ni-based alloys was demonstrated last year and this year we have been focusing on compositional optimization of the new alloys for further fine-tuning and improving their performance for SOFC interconnect application. We have also studied their long-term oxidation resistance in air and oxidation behavior in the SOFC anode environment, the stability of the oxide scale ASR during thermal exposure, and thermal expansion coefficients of these low-Cr Fe-Ni-based alloys.

Results

Through an extensive alloy design effort, a low-Cr Fe-Ni-Co-based alloy with optimal performance as a SOFC interconnect has been developed. Several alloying additions have been found effective in further improving the oxidation resistance of this alloy system. While the detailed alloy compositions will not be disclosed in this report, the effect of one specific element, denoted as X, on the oxidation resistance of this alloy system is given in Figure 1. Obviously, the mass gain of the alloy without X increased significantly with the oxidation time. The second alloy with 0.75% X (all the alloying additions were given in wt.% in this report) exhibited a decreased oxidation rate compared to the alloy without X. However, its weight gains were higher than those of the alloys with 1.5% and 3.5% of X, respectively. For the alloy with 1.5% X, the mass gain increased noticeably during the first week, which remained relatively constant afterwards. The weight gain of the alloy with 3.5% X was the lowest among the four alloys, and increased only slightly with the oxidation time. Clearly, the oxidation resistance of the alloy could be improved by the addition of X.

Based on the oxidation results, 1.5% X is needed to significantly reduce the oxidation rate of this alloy system. On the other hand, if the X content is too high (e.g. 3.5% X), a protective Cr_2O_3 scale was developed upon thermal exposure and the formation of the Cr-retaining spinel outer-layer is suppressed, based on the cross-sectional observation of the oxidized samples. Therefore, it is concluded that the 1.5% X alloy is the most suitable for a SOFC interconnect application with regard to oxidation resistance and Cr evaporation. Furthermore, thermal expansion measurements indicate that the X level in the alloy did not drastically affect the CTE of the alloy. Also, Figure 2 shows ASR values measured at 800°C in air for the alloy with 1.5% X and Crofer 22 APU after oxidation for different times at 800°C in air. While Crofer 22 APU exhibited a continuous increase in ASR as the exposure time increased due to continued oxidation, the ASR of our new alloy was relatively constant, implying that no continuous insulating layer was formed between the oxide scale and alloy substrate.

Figure 3 compared the weight gain of the new alloy in air and the reducing environment of $Ar+5\%H_2+3\%H_2O$. The new alloy exhibited lower mass gain in the reducing environment ($Ar+5\%H_2+3\%H_2O$)

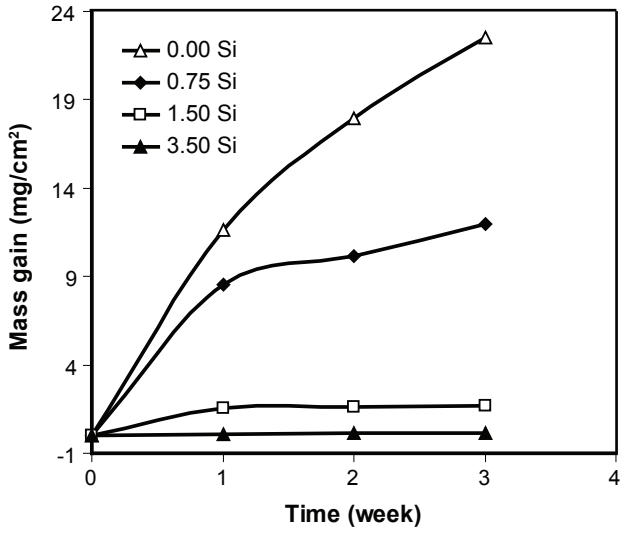

FIGURE 1. Oxidation Kinetics of the Low-Cr Fe-Ni-Co Alloy with Different X Levels in Air at 800°C

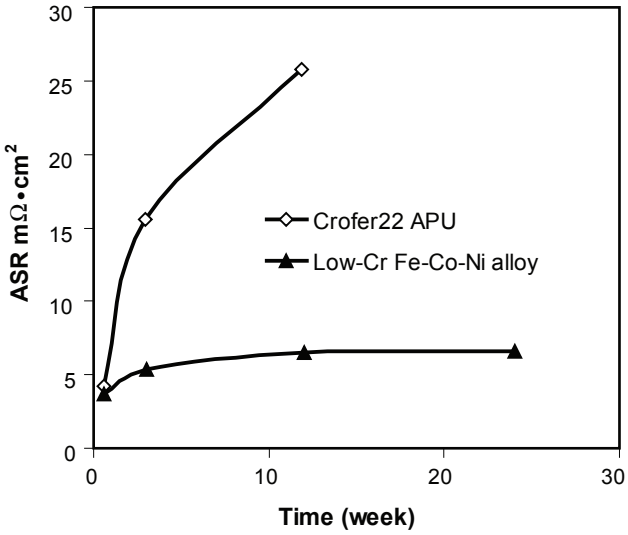

FIGURE 2. ASR Values Measured at 800°C in Air for the New Alloy and Crofer 22 APU as a Function of Oxidation Time at 800°C in Air

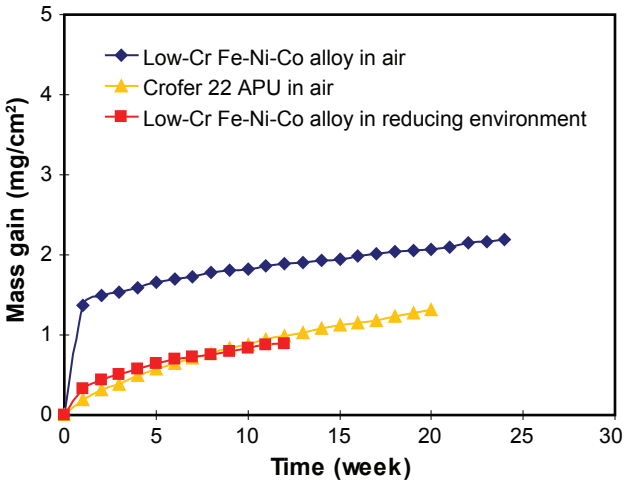

FIGURE 3. Oxidation Kinetics of the Low-Cr Fe-Ni-Co Alloy at 800°C in Air and $Ar+5\%H_2+3\%H_2O$

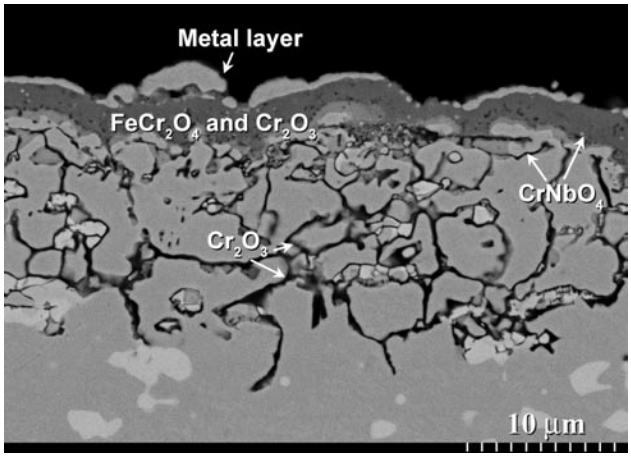

FIGURE 4. Cross-Sectional View of the Low-Cr Fe-Ni-Co Alloy after Thermal Exposure in Ar+5%H_2+3%H_2O at 800°C for 12 Weeks

than that in air after similar exposure. The cross-sectional view of the low-Cr alloy after thermal exposure for 12 weeks in the reducing environment is shown in Figure 4. The surface metallic layer consisted mainly of Fe, Co and Ni, which was followed by the oxide layer in contact with an internal oxidation zone. The oxide layer comprised mainly the Fe, Cr and Nb oxides, which according to the X-ray diffraction (XRD) results were $FeCr_2O_4$, Cr_2O_3 and $CrNbO_4$. After thermal exposure in the reducing atmosphere, electrical resistance of the coupon was measured using a multimeter at room temperature, which was similar to that of metal, as the electron passed through the surface metal layer.

The thermal expansion behaviors of the low-Cr Fe-Ni-Co alloys with different levels of Co, Nb and W additions were close to one another, indicating that the effect of the Co, Nb and W additions on the thermal expansion behaviors of this alloy system was insignificant.

Conclusions and Future Directions

The design and development of new alloys, which upon thermal exposure form an electrically conductive Cr-free spinel outer layer atop a protective, electrically conductive oxide inner layer, is highly desirable to mitigate the Cr poisoning problem in the SOFC stack as well as reduce the overall interconnect material cost. Several alloying additions have been identified that effectively improved the oxidation resistance of the alloys without negatively impacting their other properties. The optimized alloys exhibited drastically improved oxidation resistance, low and stable scale ASR, and CTE match with other cell components. Furthermore, this alloy system showed a lower oxidation rate in the reducing environment and the surface remained electrically conductive after thermal exposure in the reducing environment due to the presence of the surface metallic layer. The alloying additions of Co, Nb, W, etc. did not noticeably change the thermal expansion behaviors of this alloy system.

Future directions for this project are listed below:

- **Compatibility and in-cell performance evaluation.** The interaction and compatibility of the new interconnect alloys with the contact and cathode materials are being conducted using screen-printed interconnect/contact/cathode couples. After thermal exposure of the couple, ASR measurement will be conducted to get the overall resistance of the couple. The effect of the new interconnect alloys on the cell performance will be conducted with a SOFC test stand, which will be compared with that of the ferritic interconnect steels.
- **Characterization of the mechanical properties of the new interconnect alloys.** The mechanical properties of the optimized alloy sheets will be determined, including hardness test for the annealed alloy sheets, as well the alloy sheets aged at 800°C for various durations. Additionally, tensile testing in air at different temperatures to determine the effect of test temperature as well as the aging treatment on the yield strength, tensile strength, and ductility of the alloys will be determined.
- **Electroplating of the new Fe-Ni-Co alloy on low-cost ferritic steels.** By combining the attributes of the new Fe-Ni-Co alloy and the ferritic steels, a new interconnect material with superior performance may be achieved. The Fe-Ni-Co alloys will be codeposited onto the ferritic steels using electroplating techniques; upon thermal oxidation, the deposited alloy layer will be converted into a Cr-free, electrically-conductive $(Fe,Ni,Co)_3O_4$ spinel layer that blocks the Cr evaporation as well as reduces the oxygen penetration into the steel substrate.

Special Recognitions & Awards/Patents Issued

1. An invention disclosure on the new low-Cr Fe-Ni alloys has been completed.

FY 2007 Publications/Presentations

1. "Evaluation of Several Low Thermal Expansion Fe-Co-Ni Alloys as Interconnect for Reduced-Temperature Solid Oxide Fuel Cell", *International Journal of Hydrogen Energy*, in press, 2007.

2. "A low-Cr Metallic Interconnect for Intermediate-Temperature Solid Oxide Fuel Cells", *Journal of Power Sources*, in press, 2007.

3. "Evaluation of Binary Fe-Ni Alloys as Intermediate-Temperature SOFC Interconnect", manuscript under internal review, to be submitted to *Journal of the Electrochemical Society*, 2007.

4. "Evaluation of Several Commercial Alloys as SOFC Interconnect in the Reducing Environment", presented at the Symposium "Fuel Cells and Energy Storage Systems: Materials, Processing, Manufacturing and Power Management Technologies" as part of MS&T 06, Cincinnati, OH (October 15–19, 2006).

5. "Evaluation of Several Low Thermal Expansion Alloys as Interconnect for IT SOFC", presented at the symposium "Fuel Cells and Energy Storage Systems: Materials, Processing, Manufacturing and Power Management Technologies" as part of MS&T 06, Cincinnati, OH (October 15-19, 2006).

6. "Some Issues Related to the Measurement of Area Specific Resistance of Interconnect Alloys", Presented at the Symposium Materials in Clean Power Systems II: Fuel Cells, Solar, and Hydrogen-Based Technologies, TMS Annual Meeting, Orlando, FL (February 26 - March 1, 2007).

References

1. Gindorf, C., Singheiser, L & Hilpert, K., Chromium vaporisation from Fe,Cr base alloys used as interconnect in fuel cells. Steel Research 72 (11-12), 528-533 (2001).

2. Geng, S.J., Zhu, J.H., Brady, M.P., Anderson H.U., Zhou X.D. & Yang, Z.G., "A low-Cr Metallic Interconnect for Intermediate-Temperature Solid Oxide Fuel Cells", *Journal of Power Sources*, in press, 2007.

IV.A.21 Innovative Seals for Solid Oxide Fuel Cells

Professor Raj N. Singh
University of Cincinnati
Department of Chemical and Materials Engineering
Cincinnati, OH 45221-0012
Phone: (513) 556-5172, Fax: (513) 556-3773
E-mail: Raj.Singh@uc.edu

DOE Project Manager: Ayyakkannu Manivannan
Phone: (304) 285-2078
E-mail: Ayyakkannu.Manivannan@netl.doe.gov

Objectives

- Further develop the self-healing glasses with long-term durability through compositional modifications and seal testing.
- Develop toughened glasses by fiber and filler reinforcements for enhancing toughness.
- Characterize long-term stability of the self-healing and toughened glasses through ex-situ and *in situ* seal testing. Work with the Solid State Energy Conversion Alliance (SECA) industry teams to help transition some of the technologies developed in Phase II through collaborative efforts.

Accomplishments

- Self-healing glasses were developed for making seals for solid oxide fuel cells (SOFCs). The seals were tested for leakage at 800°C and demonstrated self-healing ability for tests performed for 3,000 hours and 300 thermal cycles in a variety of test environments typical of a SOFC.
- Self-healing glasses have shown stability against crystallization in seal tests for 3,000 hours, and in thermal annealing tests in moist fuel and air at 800°C for 1,500 and 2,500 hours, respectively.
- *In situ* X-ray diffraction of glasses at temperatures from 25°C to 800°C displayed no crystal phases in tests performed at the National Energy Technology Laboratory.
- The weight loss experiments performed in moist fuel environment at 800°C for 500 hours yielded insignificant weight loss. A weight loss of 0.53% over 40,000 hours is calculated from the extrapolated data.
- These results show great promise towards meeting SECA goals for seals for SOFCs.

Introduction

A functioning SOFC requires seals that prevent electrode leakage and internal gas manifold leakage if internal gas manifolds are utilized. The seals must prevent the mixing of fuel and oxidant streams as well as prevent reactant escape to the surrounding environment. The seal material must be electrically isolating as well as mechanically and chemically stable in contact with interfacing cell components in humid duel reducing and oxidizing conditions. Particularly important is the ability to seal between metallic and ceramic components with differing coefficients of thermal expansion (CTE), and to do so while exposed to temperature transients over a range from room temperature up to SOFC operating temperature (800ºC). This project is developing innovative sealing concepts for both short- and long-term functionality of SOFCs, addressing the aforementioned issues.

Approach

A novel concept of *in situ* crack healing by glasses was pursued in Phase I of the project and is continued in Phase II of the project. The fundamental idea underlying this concept is based on the fact that a glass with suitable low viscosity can heal cracks created by thermal expansion mismatch between materials that are being joined by a glass seal in a SOFC. The functionality of this innovative sealing approach based on *in situ* crack healing by a glass was demonstrated and quantified. Toughening and strengthening of the glass by fibers/particulates was pursued to minimize or eliminate bulk cracking of the seals. These concepts are pursued further in Phase II to address sealing capabilities and durability issues related to a functioning seal for a SOFC. In particular, exposure of the self-healing glasses over an extended time period is being pursued to determine long-term stability of the self-healing and reinforced glasses when exposed to environments simulating fuel and air at 800°C. These results are expected to provide inputs towards meeting SECA goals of 40,000 hours of seal life for a SOFC.

Results

The object of work performed for this project is to select glasses that show self-healing behavior and long-term stability in SOFC environments. Some of the glasses from Phase I are being used and modified by changes to their composition to achieve stability over long times in SOFC conditions. The purpose

of the compositional modifications is also to achieve optimum expansion behavior in contact with Crofer and Ni-YSZ (nickel-yttria-stabilized zirconia), glass transition and softening temperatures over a range of temperatures between 600 and 800°C without adversely affecting stability. Fillers are being used to modify glass properties to achieve some of these goals as well. The stability of the glasses selected above is determined by annealing glass samples in air and simulated fuel (Ar-4%H_2-6%H_2O) environments at 800°C; the glasses have accumulated >1,500 hours in these tests. The weight change is monitored to observe any loss, which will be related to changes in the composition of the glass by techniques such as energy-dispersive X-ray (EDAX), secondary ion mass spectrometry (SIMS), or electron spectroscopy for chemical analysis (ESCA). Species being lost will be identified by mass spectroscopy and other analytical approaches.

The weight loss for a self-healing glass annealed at 800°C in humid fuel environment consisting of Ar-4%H_2-6%H_2O over a time period of 500 hours was measured. From the preliminary data on weight loss, a total loss in weight of the glass of 0.53% in 40,000 hours is estimated, which is insignificant. A new set of samples was prepared, and weight loss measurements are continuing for up to 500 hours. Subsequent to this, the samples will be characterized by EDAX, SIMS, and X-ray photoelectron spectroscopy (XPS) for surface and depth profiles in order to identify species responsible for the small weight loss observed.

Glass samples alone and those containing 5-10% (wt) YSZ powder were annealed in air and Ar-4%H_2-6%H_2O atmospheres at 800°C over a range of times up to 1,500 hours to determine long-term stability, crystallization behavior, and weight loss. Figure 1 shows an example of the effect of annealing in Ar-4%H_2-6%H_2O atmosphere on the expansion behavior of a glass containing 5% (by weight) YSZ powder as a filler.

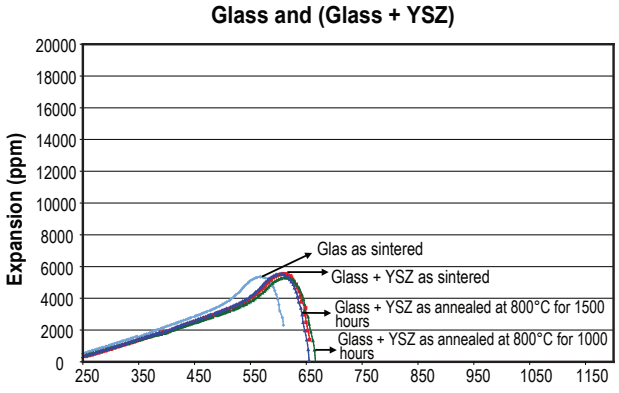

FIGURE 1. Effect of Annealing at 800°C in Ar-4%H_2-6% H_2O Moist Fuel Environment on the Thermal Expansion Behavior of the Glass Containing 5% YSZ Filler Annealed for 1500 Hours

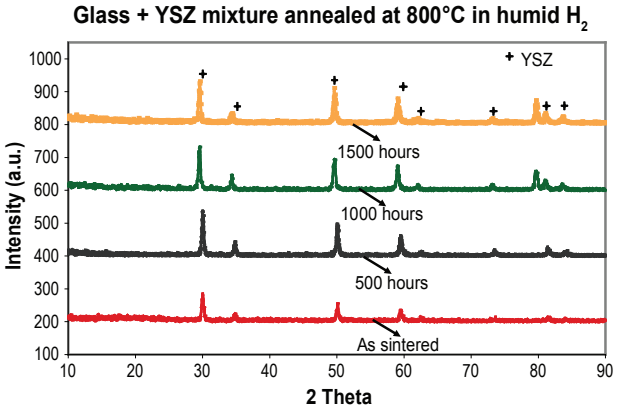

FIGURE 2. Effect of annealing at 800°C in Ar-4%H_2-6% H_2O moist fuel environment on the X-ray diffraction behavior of the glass containing 5% YSZ filler annealed for 1,500 hours. Note a lack of crystallization of the glass-5%YSZ upon annealing for 1,500 hours.

The data on the pure glass is also shown. The addition of 5% YSZ in the glass increased the glass transition and softening temperatures. However, annealing of the glass-YSZ mixture for 1,500 hours in moist fuel did not change the expansion behavior. The X-ray diffraction patterns from the glass-5% YSZ taken at different times of annealing are shown in Figure 2, which indicates that the glass did not show any evidence of crystallization due to the 5% YSZ over the annealing time of 1,500 hours at 800°C in moist air. This test is being continued to accumulate more annealing time to assess long-term stability of the glass and glass with YSZ filler. Towards this goal, glass and glass containing YSZ as fillers were also prepared and annealed in air to assess any changes in crystallization behavior over a longer period of time because of the annealing in air. In addition, electrical resistivity of the glass under direct current applied electric field is being measured between 25 and 800°C.

A sample of the glass was also prepared for high-temperature X-ray diffraction studies at the National Energy Technology Laboratory in collaboration with Dr. Chris Johnson. The glass sample was run at 400, 500, 600, 700, and 800°C in a high temperature diffractometer. It was heated in air between 25 and 800°C in steps and held at 400, 600, 700, and 800°C for 1 hour each, and the X-ray pattern was taken at each temperature. The X-ray patterns were also collected while cooling from 800°C to 25°C by holding for 1 hour each at 700, 600, 400, and 25°C. The results show no evidence of crystalline phases in the high temperature X-ray patterns. These results confirm stability of the glass at high temperature against crystallization.

These results on stability of the self-healing glass with and without fillers show excellent stability over extended time periods of annealing and are quite promising for developing seals to meet the SECA goals for SOFCs.

Conclusions and Future Directions

- Seals incorporating self-healing glasses were fabricated. The effect of up to ~300 thermal cycles between 25 and 800°C and ~3,000 hours at 800°C on hermeticity of the seals was demonstrated. Self-healing behaviors of the leaking seals were also demonstrated. These results are important for achieving SECA goals for SOFC sealing systems.
- Long-term stability of the self-healing glasses with and without fillers was studied. The glasses demonstrated stability against crystallization in annealing tests performed over 1,500 hours in fuel and air environments at 800°C.
- Insignificant weight loss of 0.53% over 40,000 hours was estimated for self-healing glasses when annealed in moist fuel at 800°C over 500 hours.
- High temperature X-ray diffraction runs on self-healing glasses to 800°C showed no evidence of crystallization.
- Plans are to further pursue long-term stability of the self-healing glasses, reinforced glasses, and seals made thereof to further demonstrate long-term performance, stability, and applicability of the self-healing glass seals to SOFCs.

FY 2007 Publications/Presentations

1. Program Quarterly Reports Between July 2006 and June 2007.

2. Phase-I Annual Report (July, 2006).

3. R.N. Singh, "High-Temperature Seals for Solid Oxide Fuel Cells (SOFC)," J. Mater. Eng. Per. 15[4] 422-426 (2006).

4. R.N. Singh and S.S. Parihar, "Performance of Self-Healing Seals for Solid Oxide Fuel Cells," Ceram Eng. Sci. Proc. 27(2-8), (2006).

5. R.N. Singh and S.S. Parihar, "Performance of Self-Healing Seals for Solid Oxide Fuel Cells," 30th Annual Cocoa Beach Conference and Exposition on Composites, Advanced Ceramic Materials, and Structures, January 23–26, Cocoa Beach, FL (2006).

6. R.N. Singh, "Approaches to High Temperature Seals for Solid Oxide Fuel Cells," **Invited Presentation**, MS&T Conference, October 15-19, Cincinnati, OH (2006).

7. S.S. Parihar and R.N. Singh, "Crack Healing Behavior of Glasses for Solid Oxide Fuel Cell," **Invited Presentation**, MS&T Conference, October 15–19, Cincinnati, OH (2006).

IV.A.22 Resilient Sealing Materials for Solid Oxide Fuel Cells

Richard K. Brow (Primary Contact),
Signo T. Reis, Teng Zhang
University of Missouri-Rolla
Department of Materials Science & Engineering
222 McNutt Hall
Rolla, MO 65409-0330
Phone: (573) 341-4401; Fax: (573) 341-6934
E-mail: brow@umr.edu

DOE Project Manager: Ayyakkannu Manivannan
Phone: (304) 285-2078
E-mail: Ayyakkannu.Manivannan@netl.doe.gov

Objectives

- Develop silicate-based glasses with requisite properties to be used for hermetic seals for solid oxide fuel cells (SOFCs).
- Evaluate thermo-mechanical and thermo-chemical properties of the glass-ceramics under SOFC operational conditions.
- Demonstrate hermeticity and materials compatibility of SOFC seals.

Accomplishments

- Formulated new alkaline earth silicate glass-ceramic compositions with requisite thermal properties, including sealing temperatures at or below 900ºC and coefficients of thermal expansion (CTE) in the range 11-12 ppm/ºC.
- Produced hermetic seals between interconnect alloys and SOFC components, including Y-stabilized zirconia (YSZ) electrolytes and Ni-YSZ anodes, that pass He-leak tests after at least 55 thermal cycles between 800ºC and room temperature.

Introduction

Reliable hermetic sealing technologies must be developed to achieve the high power densities possible for SOFC stacks. For the past decade, considerable effort has gone into the development of glasses and glass-ceramics that are suitable for these seals [1]. Compositions with the requisite thermal properties for seals have been developed (see, for example, reference [2] for a recent survey), but questions about long-term property stability, deleterious interfacial reactivity, and component volatility make the development of new, reliable sealing materials a priority.

Approach

The glasses developed at University of Missouri-Rolla (UMR) have relatively low silica contents (<45 mole%) with molecular-level structures that are much less connected than conventional silicate glasses, allowing the melts to readily flow at relatively low temperatures before crystallizing to form glass-ceramic phases with the desired thermal properties. Some compositions were designed to fully-crystallize to form rigid glass-ceramic seals, and others were designed to retain a significant fraction of a glassy phase after crystallization to allow viscous relaxation of thermal stresses.

Results

Nearly eighty glass compositions have been prepared and evaluated. Many of the compositions have the requisite thermal properties required for SOFC seals (e.g., CTE match to SOFC components and sealing temperatures at or below 900ºC) and have received closer examination for their suitability as potential sealing materials. Figure 1 shows how one compositional variation affects the CTE of crystallized sealing glasses. In this case, increasing the relative ZnO-content of the base glass decreases the CTE of the crystallized material, through the formation of lower expansion Zn-silicate phases, including Zn_2SiO_4.

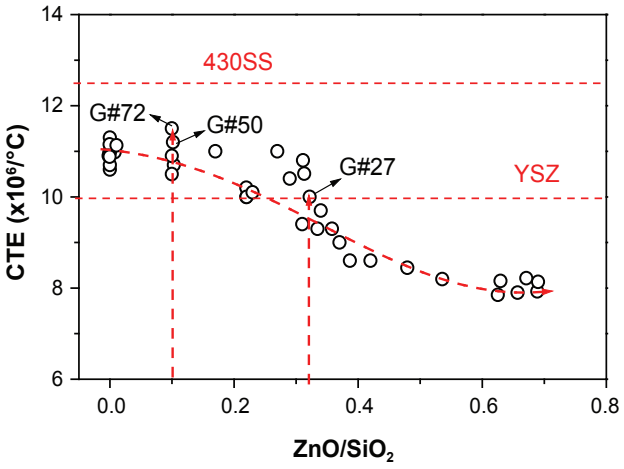

FIGURE 1. The effect of the ZnO/SiO_2 molar ratio on the CTE of crystallized "invert" silicate glass-ceramics. The CTE values for YSZ and 430SS are shown for comparison.

Compositions with relatively large ZnO contents, like G#27, produce glass-ceramics that have thermal expansion coefficients that are good matches to YSZ (~10ppm/°C), whereas compositions like G#50 or G#72, with a lower ZnO-content, have CTE values that are closer matches to 430SS.

An important consideration for long-term SOFC applications is the thermal stability of the CTE of the sealing material. Figure 2 shows the average CTE (between 200 and 700°C) for four crystallized sealing glasses as a function of time at 800ºC. Three of the compositions, G#27, G#50, and G#72 have relatively stable values of CTE, whereas G#36 shows significant decreases in CTE, particularly after the first two weeks on test. X-ray diffraction (XRD) analyses, shown elsewhere [1], indicate that glasses with stable CTEs exhibit no significant changes with time in their crystalline phase assemblages, whereas those materials with decreasing CTEs have crystalline compositions that change with time. For example, the decrease in CTE for G#36 results from the formation of a low expansion phase ($CaSiO_3$) with heat-treatment time. G#50 retains a relatively high CTE ($11.4x10^{-6}$/°C) after 112 days at 800°C (Figure 2). The XRD patterns collected from these samples reveal no discernible changes in the distributions of the crystalline phases, $(Ca,Sr)SiO_3$, $Sr_2Al_2SiO_7$ and $CaSrSiO_4$, over the course of the long-term heat treatments.

A series of simple seals have been fabricated using G#50 and 430 stainless steel, a possible SOFC interconnect material, and with either YSZ electrolytes or Ni/YSZ anode substrates. The seals were fabricated using glass tapes (PVB binder, 2.3 μm glass particles) fired in air to 850-900°C. These test samples were heated to 800°C at 2°C/minute in different atmospheres, held for 24 hours, then cooled to room temperature (-2°C/minute) where they were tested for hermeticity using helium gas at 2 psig. Samples that did not leak (hold 2 psig pressure for four hours) were reheated for another 800°C/24 hour heat treatment, and cycled back to room temperature for another hermeticity measurement. Table 1 summarizes the results of some of these tests. Post-mortem analyses of these test samples reveal good chemical compatibilities between the glasses and the various SOFC materials.

TABLE 1. Summary of thermal cycling/hermeticity tests on sealed components. All tests were done using helium at room temperature, following the thermal treatment indicated.

Sealing Materials	Test Conditions	Number of Cycles	Notes
430SS/ glass 50/YSZ	800°C, 24 hours, wet forming gas	31	Failed after 31 cycles due to the break of YSZ
430SS/glass 50/YSZ	800°C, 24 hours, air	60	Failed after 60 cycles due to the break of YSZ
430SS/glass 50/Ni-YSZ	800°C, 24 hours, air	30	Failed after 30 cycles due to the break of Ni-YSZ
430SS/glass 50/Ni-YSZ	800°C, 24 hours, wet forming gas	36	Failed after 60 cycles due to the break of Ni-YSZ

The seal failures after 30+ thermal cycles may be related to defects in the glass seals related to the rapid crystallization of the glass powders used to fabricate the tapes. The effects of glass particle size on the crystallization kinetics have been studied using differential thermal analytical techniques developed at UMR [3]. Figure 3 summarizes those effects. Particles that have diameters of ~10 μm fully crystallize in less

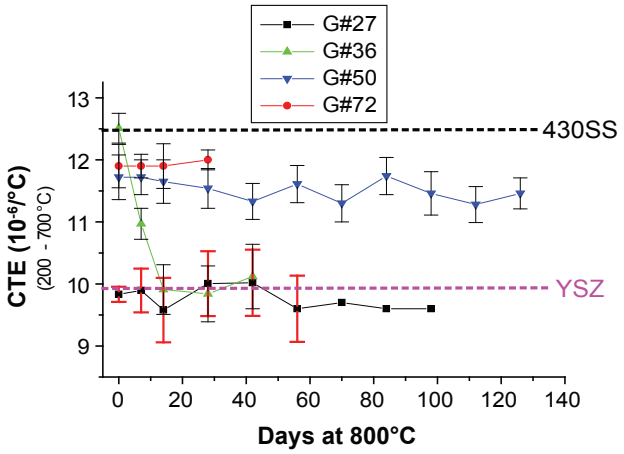

FIGURE 2. CTE data for crystallized glasses #27, and #50 held at 800°C in air for up to 120 days. The 'as received' CTE values for YSZ and 430SS are shown for comparison.

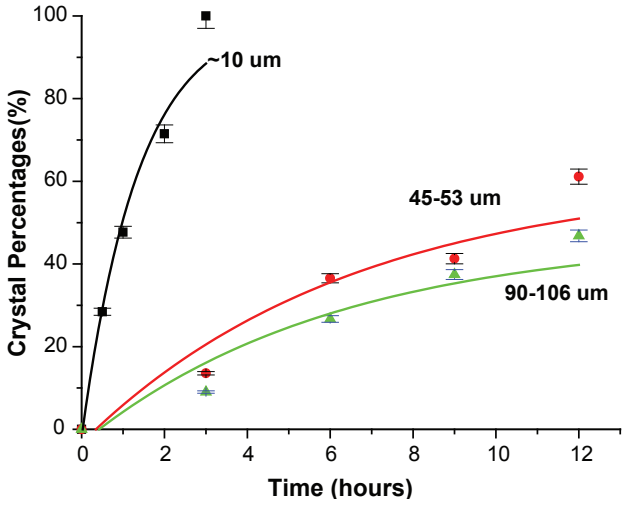

FIGURE 3. Crystallization Kinetics for Glass#27 with Different Particle Sizes at 800°C in Air, as Determined by Differential Thermal Analysis

than two hours, whereas larger particles crystallize much more slowly. These results are typical for glasses that crystallize predominantly from their surfaces, and this indicates that care must be taken in developing sealing cycles that account for this behavior.

Conclusions and Future Directions

- Promising sealing glass compositions have been developed and evaluated.
- Hermetic seals have been fabricated and tested at room temperature after thermal treatments at 750-800°C, in oxidizing and reducing environments.
- The effects of ZnO on the thermo-mechanical and thermo-chemical stability of new glass systems under SOFC operational conditions are under investigation. In particular, we wish to understand what effect (if any) ZnO has on the formation of deleterious interfacial chromate phases.
- The influence of the B_2O_3 content on the residual glass of glass-ceramic under SOFC conditions is under investigation. The presence of residual glass could be potentially positive since the glass relaxation would help relieve some stresses that would otherwise develop because of CTE-mismatches among the cell materials.

Special Recognitions & Awards/Patents Issued

1. R.K. Brow, S. T. Reis, G. M. Benson, "Glass and glass-ceramics for solid oxide fuel cell hermetic seals," US Patent Application, UM Disclosure No. 04UMR023 entitled "Glass and Glass-Ceramic Sealant Compositions," filed January 2005.

FY 2007 Publications/Presentations

1. C. S. Ray, T. Zhang, S. T. Reis, and R. K. Brow, "Determining Kinetic Parameters for Isothermal Crystallization of Glasses," *Journal of the American Ceramic Society*, **90**[3], 769 – 773 (2007).

2. S. T. Reis*, Teng Zhang, and R. K. Brow, "Development of thermochemically stable sealing glasses for solid oxide fuel cells" 4th International Symposium on Solid Oxide Fuel Cells: Materials and Technology, Daytona Beach, Florida, January 22–27, 2007.

3. S.T. Reis, R.K. Brow, "Designing Sealing Glasses for Solid Oxide Fuel Cells," Journal of Materials Engineering and Performance, **15** 410 – 413 (2006).

References

1. S.T. Reis, R.K. Brow, "Designing Sealing Glasses for Solid Oxide Fuel Cells," Journal of Materials Engineering and Performance, **15** 410 – 413 (2006).

2. N. Q. Minh, "Ceramic fuel cells", *J. Am. Ceram. Soc.*, **76,** 563 – 588 (1993).

3. T. Zhang, C.S. Ray, S.T.Reis, and R.K. Brow, "Isothermal Crystallization of Solid Oxide Fuel Cell Sealing glass by Differential Thermal Analysis," J. Amer. Ceram. Soc. (in preparation).

IV.A.23 Thermochemically Stable Sealing Materials for Solid Oxide Fuel Cells

Richard K. Brow (Primary Contact),
Signo T. Reis, Teng Zhang
University of Missouri-Rolla
Department of Materials Science & Engineering
222 McNutt Hall
Rolla, MO 65409-0330
Phone: (573) 341-4401; Fax: (573) 341-6934
E-mail: brow@umr.edu

DOE Project Manager: Ayyakkannu Manivannan
Phone: (304) 285-2078
E-mail: Ayyakkannu.Manivannan@netl.doe.gov

Objectives

- Develop 'invert' glasses with requisite properties and chemical stability for hermetic seals for solid oxide fuel cells (SOFCs).
- Develop processing techniques to fabricate hermetic seals for SOFC components, including understanding the crystallization behavior of sealing glass.
- Demonstrate hermeticity and materials compatibility under SOFC operational conditions.

Accomplishments

- Developed alkaline earth/zinc silicate glasses that form glass-ceramics with requisite thermal properties, including sealing temperatures at or below 900ºC and coefficients of thermal expansion (CTE) in the range 10-12x10^{-6}/ºC.
- Demonstrated the effect of B_2O_3 on the volatility of promising sealing materials under SOFC operational conditions at temperatures up to 800ºC, for up to 28 days in wet forming gas; identified new sealing glasses compositions with weight loss in wet forming gas/or air at 800°C over 500 hours in the range 0.01-0.1 g/m^2 (under 0.001-0.0001 wt%).
- Studied the effects of glass composition on the formation of deleterious chromate phases at glass-steel interfaces.

Introduction

SOFCs require seals to prevent the mixing of fuel/oxidant within the stack, prevent leaking of fuel/oxidant from the stack, electrically isolate cells in the stack and also provide mechanical bonding of components. There have been many reports on the development of a variety of compositional systems to form suitable glass and glass-ceramics seals for SOFCs, including silicates, aluminosilicates, borosilicates, and aluminophosphates, i.e. see reference [1]. Many of these sealing materials have property or performance shortcomings. Some fail to remain thermomechanically stable under SOFC operational conditions, and others undergo deleterious interfacial reactions with other SOFC components. One such reaction occurs between BaO-containing sealants and the Cr-oxide scale that forms on interconnect alloys, resulting in the formation of a $BaCrO_4$ interfacial phase that can adversely affect the mechanical integrity of the seal [2,3]. The materials developed in the present project have unusual structural characteristics that contribute to a desirable set of thermal and chemical properties required for SOFC seals.

Approach

The glasses developed at the University of Missouri-Rolla (UMR) are based on alkaline earth silicate compositions modified by ZnO. They possess relatively low silica contents (45 mole%) and rapidly crystallize to form silicate crystals with the desirable thermomechanical properties, including long-term stability of the CTE. The glasses are designed to be thermochemically stable, both against volatilization under SOFC conditions, and against the formation of deleterious interfacial reaction products in seals to SOFC materials.

Results

Figure 1 shows that glasses with greater concentrations of B_2O_3 exhibit greater weight losses under simulated SOFC operational conditions; e.g., wet forming gas at 800°C. Thermochemical calculations have been performed to determine the equilibrium reactions that might contribute to this weight loss, and it was shown that B_2O_3 is the least stable of the oxides that constitute these sealing glasses. Figure 2 shows which B-species will have the greatest partial pressures at 800ºC in a wet, reducing environment.

X-ray diffraction (XRD) analyses (not shown here) reveal no boron-containing crystalline phase in the glass-ceramics, suggesting that the borate components are to be found in residual glassy phases. Borate species in a liquid state (glassy or amorphous phase) are more likely to volatilize than those in solid state (crystal). Increasing the B_2O_3 content of the base composition increases the fraction of residual glass in the glass-ceramic, which in turn leads to greater weight lost under SOFC operational conditions. More detailed

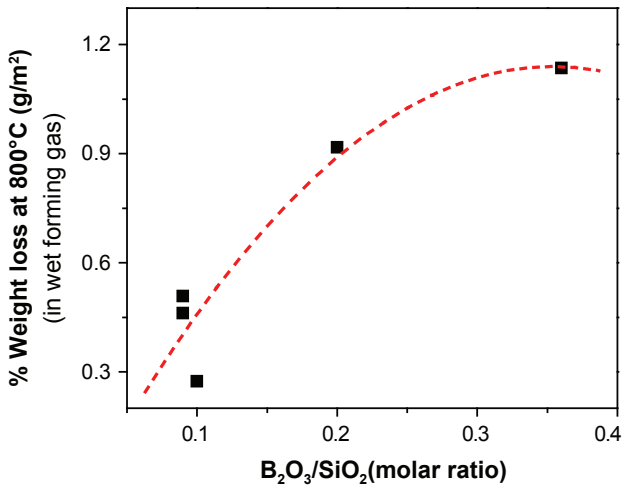

FIGURE 1. The Effect of B_2O_3/SiO_2 Molar Ratio on the Cumulative Weight Lost after 28 Days at 800°C in Wet Forming Gas

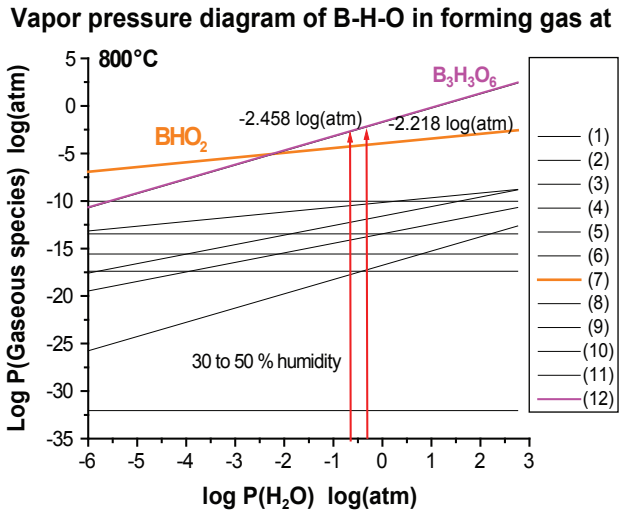

FIGURE 2. Thermochemical Predictions of the Effect of Atmosphere at 800°C on the Stability of B_2O_3

experiments are currently underway to characterize volatilization behavior and its effect on the glass-ceramic sealing materials.

Glass ID	ZnO (mole%)	SrO (mole%)	$SrCrO_4$
27	13.0	18.5	4 wt%
50	5.0	25.5	11 wt%
36	0.0	26.5	14 wt%

A second issue related to thermo-chemical stability involves the reaction in oxidizing environments between alkaline earth oxides in the sealing glass and chromium in the steel interconnects. The reaction leads to the formation of chromates like $SrCrO_4$ and $BaCrO_4$, high expansion phases that could adversely affect the thermo-mechanical integrity of the seal [2]. One simple experiment to test relative stability of a composition against chromate formation is to mix glass powder with 10 wt% Cr_2O_3 in air for 24 hours at 800°C, and then to characterize the resulting reaction products using quantitative x-ray diffraction techniques. Table I summarizes experiments done with glasses with a range of SrO and ZnO contents, and shows that glasses with greater ZnO content produce relatively lower amounts of $SrCrO_4$. The effects of composition on the relative reactivity of glasses is illustrated in Figure 3, which shows an optical micrograph of the surfaces of G#27 (13.0 mol% ZnO, left) and G#50 (5.0 mole% ZnO, right) coatings bonded to a 430SS substrate, then held in air at 800ºC for 60 days. The Glass #27 coating retains the white color of the original glass ceramic, whereas the Glass #50 coating has turned yellow, an indication of the formation of $SrCrO_4$. The mechanism for the reduced reactivity of the ZnO-containing glasses is unknown but is the focus of current research.

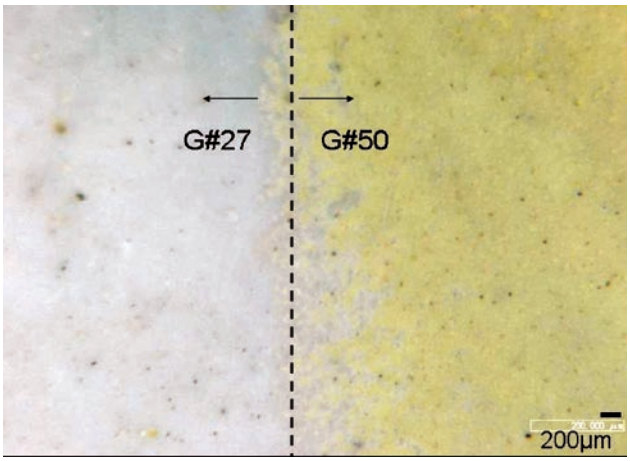

FIGURE 3. Optical micrograph of SOFC glass coatings bonded to 430SS, then held in air for 60 days at 800°C. The G#27 coating (left) retains its original color, whereas the G#50 coating (right) has turned yellow because of the formation of $SrCrO_4$.

Conclusions and Future Directions

- Both B-O and Zn-O species are more volatile in wet conditions than in dry conditions at 800°C.
  - $B_3H_3O_6$ (gas) has the highest vapor pressures in wet conditions at 800°C.
  - Zn (gas) has the highest vapor pressures in dry and wet conditions at 800°C.
- The addition of ZnO appears to impede the formation of $SrCrO_4$ when glasses react with chromium in air.
- There is a size dependence on the crystallization behavior of the 'invert' sealing glasses.

  - For G#50, particle sizes of 45-53µm exhibit desirable thermal stability against crystallization.
- The volatility calculations will be correlated with weight-loss measurements from glasses with different compositions.
  - Volatile species collected from reacted glasses will be analyzed.
- The effect of ZnO on the formation of $SrCrO_4$ will be modeled using thermodynamic calculations like those used to study the volatility conditions.
- The study of the effects of glass particle size on crystallization behavior will be completed and the results will be applied to optimize processing conditions for SOFC seals.

Special Recognitions & Awards/Patents Issued

1. R.K. Brow, S. T. Reis, G. M. Benson, "Glass and glass-ceramics for solid oxide fuel cell hermetic seals," US Patent Application, UM Disclosure No. 04UMR023 entitled "Glass and Glass-Ceramic Sealant Compositions," filed January 2005.

FY 2007 Publications/Presentations

1. C. S. Ray, T. Zhang, S. T. Reis, and R. K. Brow, "Determining Kinetic Parameters for Isothermal Crystallization of Glasses," *Journal of the American Ceramic Society*, **90**[3], 769–773 (2007).

2. S. T. Reis*, Teng Zhang, and R. K. Brow, "Development of thermochemically stable sealing glasses for solid oxide fuel cells" 4th International Symposium on Solid Oxide Fuel Cells: Materials and Technology, Daytona Beach, Florida, January 22–27, 2007.

3. S.T. Reis, R.K. Brow, "Designing Sealing Glasses for Solid Oxide Fuel Cells," Journal of Materials Engineering and Performance, **15** 410–413 (2006).

References

1. J.W. Fergus, *J. Power Sources*, **147** 46-57 (2005).

2. Z. Yang , J. W. Stevenson, and K. D. Meinhardt, *Solid State Ionics*, **160** 213–222, (2003).

IV.A.24 Novel Low Temperature Solid State Fuel Cells

Dr. Chonglin Chen (Primary Contact), Jian Liu, Greg Collins, Jennifer Weaver, and Dr. Patrick Nash
University of Texas at San Antonio
Department of Physics and Astronomy
UTSA Road One
San Antonio, TX 78249
Phone: (210) 458-6427; Fax: (210) 458-4919
E-mail: cl.chen@utsa.edu

DOE Project Manager: Patricia Rawls
Phone: (412) 386-5882
E-mail: Patricia.Rawls@netl.doe.gov

Objectives

The objective of this research is to use advanced nanostructured material synthesis via optimally fabricating and fundamentally understanding the physical properties and chemical stability of multilayered structures for development of an intermediate temperature solid oxide fuel cell (IT-SOFC), and to demonstrate their advantages and unique qualities for energy device applications.

Accomplishments

- Fabricated highly mixed (ionic and electronic) conductive $PrBaCo_2O_{5+x}$ (PBCO) thin films on various substrate materials such as $SrTiO_3$ (STO), $LaAlO_3$ (LAO), $NdGaO_3$ (NGO), and MgO.
- Studied the electrical conductivities of the as-grown films on various substrates and simulated the nature of the conductivity.
- Investigated the interface strain effect on the film properties, in which with the increase of the temperature, the conductivity exponentially increases due to thermal activation and becomes steady around 400°C (or 670 K) probably owing to the lost of oxygen.
- Discovered that the PBCO films tensile strain on LAO and NGO substrates have excellent electrical conductivity, ~10^2 S/cm^2, over a very broad temperature region of 300 to 1,000 K, and the films with relaxed strain on STO and MgO have relative lower electrical conductivity. In the high temperature range (higher than 400°C), tensile strained films show much better conductivity.
- Compared with the traditional electrode materials such as $(La,Sr)MnO_3$ or $(La,Sr)(Co,Fe)O_3$, PBCO thin films have much better electrical conductivity especially in the low temperature region.

Introduction

Perovskite oxides with high ionic conductivity have practical applications in solid oxide fuel cells, chemical membranes, and gas sensors. Among the many possible compositions with the perovskite structure, systems containing cobalt are particularly attractive systems for the electrodes due to their low electrical resistivity and high ionic conductivity. This family of cobalt containing perovskite oxides also displays many interesting physical phenomena. The oxygen-deficient ordered double perovskites $RBaM_2O_{5-\delta}$ (where R is a rare earth element and M = Mn, Fe, Co) have been the subject of a number of investigations because of their wide ranges of stoichiometry and concomitant variable transition metal oxidation states. The low temperature structural properties of these compounds have been studied in detail and some data are available on their high temperature oxygen chemistry. Recently, with the collaboration of Professor A. Jacobson at the University of Houston, rapid surface exchange kinetics have been successfully fabricated and studied on the PBCO thin films. The epitaxial single crystalline PBCO thin films were grown on single crystal $SrTiO_3$ (STO) substrates and shown to have two types of domain and spin-glass interaction behavior in magneto-resistance studies.

Approach

To fabricate highly epitaxial PBCO on various oxide substrates, a KrF excimer pulsed laser deposition (PLD) system with a wavelength of 248 nm was employed to deposit the PBCO thin films on different substrate materials such as (001) STO and (001) MgO substrates. By controlling and optimizing the deposition conditions, single crystalline PBCO thin films have been achieved on the as-selected substrates and the microstructural studies from X-ray diffraction θ-2θ scan, high-resolution synchrotron X-ray diffraction, and transmission electron microscopy (TEM) indicate that the as-growth films have good epitaxial quality. The transport properties of both the as-grown and after-annealing samples were measured by resistance measurements in the temperature range from 50 K to 450 K using the four probe method (low temperature [T] range) and impedance measurements (high T range).

Results

To understand the physical properties of materials for cathode, electrolyte, and anode applications, the focus of this study has been on the systematical characterizations of the new cathode candidate,

(Pr,Ba)CoO_3 (PBCO). Highly mixed conductive PBCO thin films have been fabricated on various substrate materials such as $SrTiO_3$ (STO), $LaAlO_3$ (LAO), $NdGaO_3$ (NGO), and MgO. For instance, Figure 1 is an X-ray θ-2θ diffraction contour plot of an as-grown PBCO thin film showing that the as-grown films are predominantly *a*-oriented. The rocking curve measurement of the (200) reflection has a full width at half maximum of 0.1 deg, compared to a resolution-limited width of the STO (200) of 0.007 deg, indicating that the film on STO substrate has excellent single crystallinity and epitaxial behavior. More precise radial scan synchrotron studies performed along the STO [200] in plane direction showed that the interface relationship to be $(100)_{PBCO}//(001)_{STO}$ and $[001]_{PBCO}//[100]_{STO}$. Both PBCO (200) and (004) peaks were observed, indicating that the as-grown PBCO films are a-axis oriented with two different domain structures in the directions parallel to the substrate surface.

The crystallinity and epitaxial quality of the as-grown films were further investigated by transmission electron microscopy. A dark field cross sectional TEM image (Figure 2 top) shows that two types of domain structures exist on the interface, which agrees with the synchrotron studies. The selected area electron diffraction (SAED) pattern taken in the area only covering the film is shown in Figure 2 (top inset). The sharp electron diffraction spots with no satellites indicate that the films have good single crystallinity. The electron diffraction pattern also confirms that the film is *a*-axis oriented with c-axis along the interface. High resolution cross sectional TEM studies have demonstrated that as-grown films have excellent epitaxial behavior and a sharp atomic interface, as seen in Figure 2 (bottom).

The impedance measurements on the as-grown PBCO thin films suggest that the electrical conductivities of the PBCO thin films are highly dependent upon the measuring temperature and the interface strain which induce from the lattice mismatch of the films and substrates. The lattice mismatches between the PBCO films and substrates can be simply estimated by the standard crystal lattice parameters. It is easy to find that the PBCO films are tensile on both NGO and LAO but become strain on both MGO and STO. As seen from the Figure 3, the electrical conductivities of PBCO films on these substrates in air have been measured to determine the high temperature transport properties. With the increase of the temperature, the conductivity exponentially increases due to thermal activation and

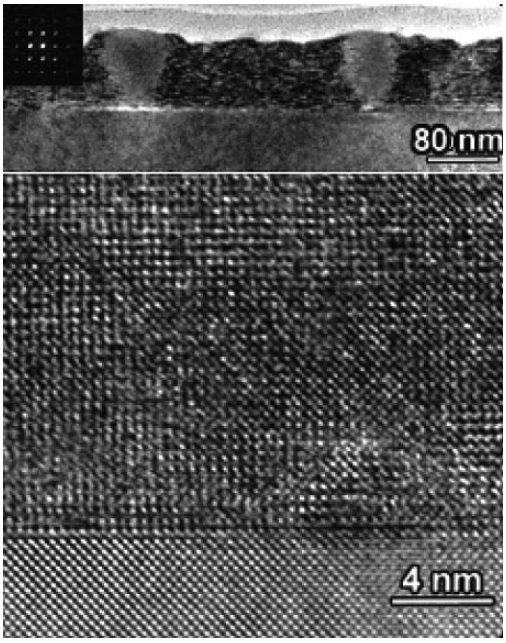

FIGURE 2. Cross Sectional TEM Studies Show the Crystallinity and Pitaxial Behavior of the As-Grown PBCO Thin Film on STO (top) and the Interface Structures of PBCO/STO

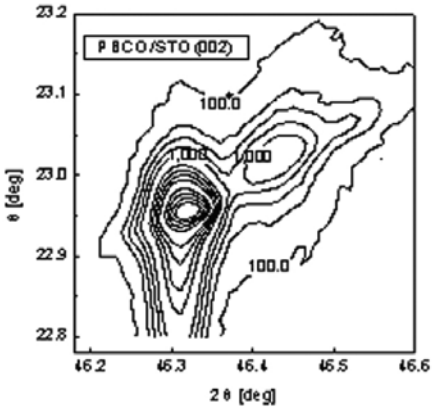

FIGURE 1. The X-ray Diffraction θ-2θ Scans of As-Grown PBCO/STO Thin Film

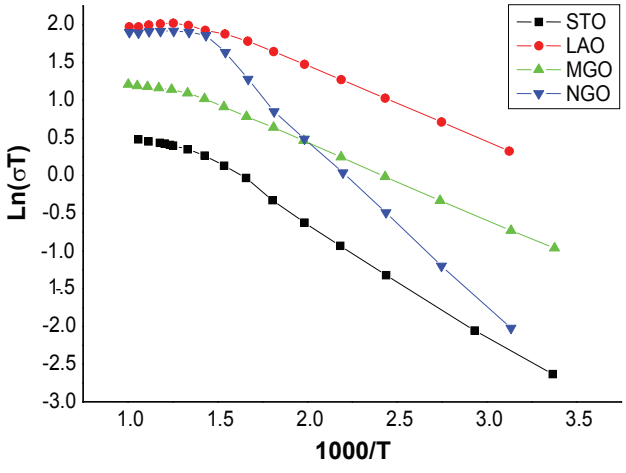

FIGURE 3. The Impedance Measurement for the PBCO Films on Various Substrates

becomes steady around 400°C (or 670 K) probably owing to the lost of oxygen. It is interesting to note that the PBCO films tensile strain on LAO and NGO substrates have excellent electrical conductivity, ~10^2 S/cm^2, over a very broad temperature region of 300 to 1,000 K. In contrast, the films with relaxed strain on STO and Mg, have relative lower electrical conductivity. In the high temperature range (higher than 400°C), tensile strained films show much better conductivity. Also, compared with the traditional electrode materials such as (La,Sr)MnO_3 or (La,Sr)(Co,Fe)O_3, PBCO thin films have much better electrical conductivity especially in the low temperature region.

To understand the mechanisms of the electrical conductivity and the strain effect on the physical properties, the co-PI (Professor P. Nash) has formulated a point defect model in which mobile electrons and electron holes are assumed to be localized on specific Co-site ions. Electrons localize on $Co^{2+} = Co' = Co'_{Co}$ sites and holes (small polarons) on $Co^{4+} = Co^{\cdot} = Co^{\cdot}_{Co}$. The substitution of $Ba^{2+} = Ba' = Ba'_{Pr}$ for $Pr^{3+} = Pr^{\times} = Pr^{\times}_{Pr}$ in the $PrCoO_3$ perovskite lattice requires charge compensation. Electroneutrality can be maintained in two ways: either by a valence change of the Co-site cation $= Co^{3+} = Co^{\times} = Co^{\times}_{Co}$ (creation of holes, electronic compensation) or by the formation of oxygen vacancies $V^{\cdot\cdot}_O$ (ionic compensation). In general, both processes occur and compete with each other, depending on composition, oxygen partial pressure and temperature. It is assumed that the defect chemistry of $PrBaCo_2O_{6-2\delta}$ can be described by the following three reactions:

$$2BaO + 2\,Pr^{\times}_{Pr} + O^{\times}_O \rightarrow 2Ba'_{Pr} + V^{\cdot\cdot}_O + Pr_2\,O_3 \qquad [1]$$

$$2Co^{\times}_{Co} \qquad Co'_{Co} + Co^{\bullet}_{Co} \quad \text{(charge disproportionation)} \qquad [2]$$

$$O^{\times}_O + 2Co^{\bullet}_{Co} \qquad \frac{1}{2}O_2 + V^{\cdot\cdot}_O + 2Co^{\times}_{Co} \qquad [3]$$

Here the oxide lattice site anion is denoted $O^{2-} = O^{\times}_O$. This system of equations provides a partial mathematical expression that substitution of Ba^{2+} for Pr^{3+} in the $PrCoO_3$ lattice is electronically compensated by the oxidation of $Co^{\times} = Co^{3+}$ cations to Co^{4+} and the formation of oxygen vacancies $V^{\cdot\cdot}_O$. This system of equations is completed by overall electroneutrality conditions, which can be represented by

$$\left[Ba'_{Pr}\right] + \left[Co'_{Co}\right] = \left[Co^{\bullet}_{Co}\right] + 2\left[V^{\cdot\cdot}_O\right] \qquad [4]$$

$$\left[Co^{\times}_{Co}\right] + \left[Co'_{Co}\right] + \left[Co^{\bullet}_{Co}\right] = 1 \qquad [5]$$

$$\left[O^{\times}_O\right] + \delta = 3 \qquad [6]$$

It is expected that when the temperature increases or the pO_2 (O_2 pressure) decreases, the equilibrium of Equation [3] shifts to the right. As a result, oxygen vacancies $V^{\cdot\cdot}_O$ are formed, at the expense of two holes for each $V^{\cdot\cdot}_O$. Therefore, a loss of lattice oxygen takes occurs when the temperature increases. This can be experimentally measured using thermogravimetry (TGA).

Conclusions and Future Directions

The focus of this study continues to be on the investigation of the physical property of PBCO on various substrate materials. The understanding of the interface behavior and ionic transport dynamics of oxygen in this new material is extremely important for the development of the fuel cell devices. Another part of the on-going research includes that the multilayered Gd:CeO_2 (GCO) and yttria stabilized zirconia (YSZ) will be fabricated (once the ordered targets arrival). The various thickness combinations of GCO and YSZ will be synthesized, and the ionic transport properties of these multilayered structures and the interface effect on the physical properties will be systematically investigated. The purpose of the YSZ layer in the multilayered structures is to block the electronic conduction to enhance the quality of the electrolyte materials and lower down the operation temperature from 800°C to 600°C. On the other hand, the fabrication and characterizations of half-cell structure from PBCO/YSZ and PBCO/GCO will be the next focusing topic to determine the best interface structures for the cathode/electrolyte interface. The fabrication and characterization of the advanced proton conductive $Y_xBaCe_{1-x}O_3$ (YBCO) for the anode is also planned. The physical properties and ionic transport behavior of each material (YBCO, PBCO, and multilayered GCO/YSZ structures) will be systematically studied. Various crystal structures and different crystal grain sizes will be fabricated, and the physical properties and interface phenomena of each material and the effects from interface, size, and strain will be comprehensively analyzed. The model will be used to calculate the concentrations of holes and mobile electrons, [$Co^{\cdot}_{Co}$] and [Co'_{Co}], respectively, from TGA data from Frontera, et al. Then, the interface phenomena in each half-cell combination can be experimentally studied and simulated by computer. The ultimate goal is to build the foundation for development of intermediate temperature SSFCs devices based on these new materials.

Acknowledgements

The authors thank Prof. Alan Jacobson at University of Houston for his support, suggestions, and helpful discussion and Prof. W. Donner and Dr. D. X. Huang for the microstructural characterizations.

IV.A.25 Electrically Conductive, Corrosion-Resistant Coatings through Defect Chemistry for Metallic Interconnects

Anil V. Virkar
University of Utah
Department of Materials Science & Engineering
122 S. Central Campus Drive
Salt Lake City, UT 84112
Phone: (801) 581-5396; Fax: (801) 581-4816
E-mail: anil.virkar@m.cc.utah.edu

DOE Project Manager: Ayyakkannu Manivannan
Phone: (304) 285-2078
E-mail: Ayyakkannu.Manivannan@netl.doe.gov

Objectives

- To synthesize and characterize coating materials with ultra-low oxygen diffusion coefficient, that are electronically conducive using site-specific doping and through fundamental understanding of defect chemistry, for application as coatings for metallic interconnects in intermediate temperature (800°C) solid oxide fuel cells (SOFCs).
- To apply the coatings on low thermal expansion, relatively inexpensive stainless steels and other alloys, and investigate oxidation kinetics in air and fuel atmospheres.
- To conduct preliminary short stack (4-cell) test, using 5 cm x 5 cm active area cells to validate ex-situ results.
- To initiate work on the development of low-cost processes for the deposition of coatings on metallic interconnects.
- To offer coated interconnect foils to Solid State Energy Conversion Alliance (SECA) vertical teams under suitable confidentiality agreements.

Approach

- To conduct literature search on the identification of suitable perovskite and non-perovskite materials exhibiting high electronic conductivity but very low oxygen ion conductivity. Non-perovskite materials of interest include spinels and bronzes.
- To synthesize perovskite oxides with transition elements on the B-site, with site-specific doping to suppress oxygen vacancy concentration.
- To fabricate sintered bars and discs of the materials. Sintered bars are to be used for the measurement of total conductivity as a function of temperature. Discs are to be used for measuring ionic conductivity using electron blocking electrodes.
- To deposit thin coatings of the materials on stainless steels and nickel-based alloy foils, and investigate oxidation kinetics.
- To conduct theoretical analysis of oxidation kinetics of coated and pristine alloys.
- To develop a method for the measurement of area specific resistance (ASR), and apply it to the foils oxidized under various conditions.

Accomplishments

- Identified a number of materials with low oxygen ion conductivity (possibly lower than 10^{-7} S/cm at 800°C) by taking into account ionic size effect.
- Fabricated $LaMnO_3$ (LM) and $LaCrO_3$-based materials with dopant levels as high as 20% on the B-site to suppress oxygen ion conductivity.
- Measured the total conductivity over a temperature range from room temperature to 800°C; measured oxygen ion conductivity at 800°C using different sample designs.
- Sputter-deposited 1 and 3-micron coatings of various materials on Haynes 230 (H230), Inconel 718, and SS430.
- Conducted oxidation in flowing air up to 180 days at 800°C for samples having $LaMnO_3$-based coating.
- Conducted oxidation studies in flowing 10%H_2/ 90%N_2 gas with 5% humidity up to 90 days for samples having $LaCrO_3$ (LC) and Nb-doped $LaCrO_3$ (LNC) coating.
- Examined the oxide scale formed and measured its thickness on coated and pristine materials.
- Developed a theoretical model for oxidation kinetics and verified experimental oxide scale thickness data with this model.
- Measured the total ASR of the coated and pristine samples after oxidation for 45 days at 800°C. It was observed that the pristine samples exhibited significant oxidation. However, even samples with as small as 1 micron coating were highly resistant to oxidation.
- Dip-coated $LaMnO_3$ and $LaCrO_3$-based compositions on SS430 foils.

Future Directions

- Conduct pressure assisted heat treatment on dip-coated perovskite coatings on SS430 foils.

- Conduct a short stack test with the best coating material, as determined by ex-situ oxidation studies.

Introduction

Planar SOFC stacks are preferred over their tubular counterpart due to compact design, higher power and energy density, and projected lower cost. However, planar SOFC stacks require interconnect or bipolar plates which keep fuel and oxidants separate, and electrically connect adjacent cells. From the standpoint of cost and ruggedness, metallic interconnects are preferred. However, metallic interconnects of choice are stainless steels or nickel-chromium-based alloys, which are prone to oxidation. The oxide scale formed increases the ASR, which adversely affects the SOFC performance and efficiency, and thus in balance also adversely affects the cost. The potential remedy is the development of either baseline alloys that are oxidation-resistant, or suitable coating materials which can suppress oxidation kinetics. From the standpoint of cost and practicality, the preferred approach is the development of suitable coating materials.

To date, several coating materials have been tried, with varying degrees of success. The approach, however, has not been systematic, and has relied on trial and error. As a result, most of the coatings used to date were very thick (several or several tens of microns). This increases the potential for spalling, which is undesirable. The approach selected in this work is based on fundamental chemistry of materials, which has the potential to develop coatings that are adherent and very thin (typically less than 5 microns, and may be as thin as 1 micron), and yet can suppress oxidation kinetics to greater than 40,000 hours of operating life.

Approach

Possible coating materials are perovskites with a transition metal, capable of exhibiting multiple valence states. An example is $LaMnO_3$. The approach involves doping a material such as $LaMnO_3$ with suitable elements, which tend to suppress oxygen vacancy concentration, without significantly reducing electronic defect concentration. Powders of various coating materials, doped appropriately, are made. Samples of the materials are made by sintering. Two types of electrical tests are performed: (a) Measurement of total electrical conductivity; and (b) Measurement of oxygen ion conductivity using blocking electrodes. Thin coatings (1 to 5 microns) are then deposited on foils of various alloys. For the initial investigation, Haynes 230, Inconel 718, and SS 430 were the alloys selected. The coated and uncoated foils are subjected to air and fuel, for various periods of time and over a range of temperatures, up to ~800°C. Samples are oxidized for various periods of time, up to a maximum of six months. The oxide scale thickness is measured using scanning electron microscopy (SEM). The observed kinetics of oxidation is compared with the theoretical models developed. The ASR of the samples is also measured as a function of time of oxidation, with measurements conducted over a range of temperatures. Finally, a short stack will be tested using coated interconnects exhibiting the best properties.

Results

1. Experiments were conducted on the measurement of oxygen ion conductivity using blocking electrodes at 800°C. Results showed that the blocking electrodes function successfully. It was decided to use a three electrode configuration (with guard electrode [Figure 1]) to eliminate the effects of surface conductivity. Lower values of conductivity were obtained for the sputter coated yttria-stabilized zirconia (YSZ)/perovskite couple as compared to the co-pressed sandwich structure. This was attributed to better equilibration to steady-state in the thinner (sputter deposited) samples. The lowest value of ionic conductivity measured was 2.0 x 10^{-7} Scm^{-1} and was obtained for Ti-doped $LaMnO_3$ (LMT). Measurements were also conducted on tape-cast YSZ/perovskite/YSZ sandwich structures which had stronger interfaces and thinner YSZ layers as compared to the sputtered samples.

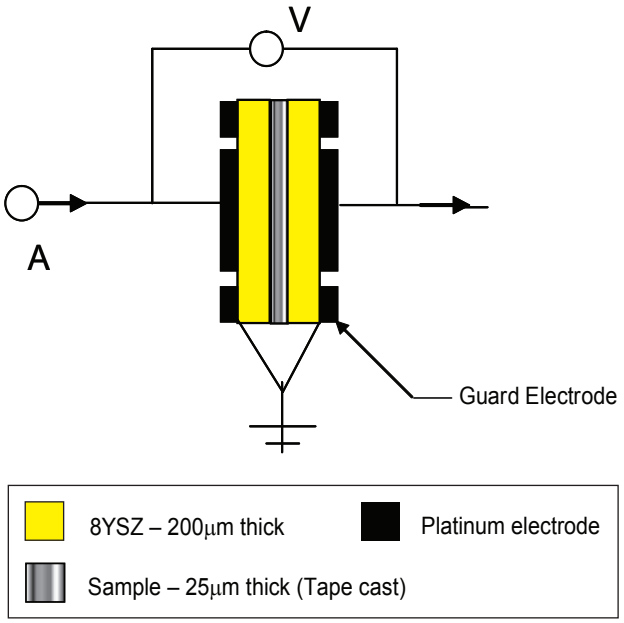

FIGURE 1. Schematic of a Tape Cast Couple for Hebb-Wagner Polarization Measurement with Guard Electrodes

The readings were more consistent but the ionic conductivity values were higher (Table 1).

TABLE 1. Ionic Conductivity Values of Tape-Cast Sandwich Samples

Coating Material	LMT	LM	LSM
Conductivity (S/cm)	4.2 x10^{-7}	7.4 x10^{-7}	9.1 x10^{-7}

2. Oxidation in flowing air was conducted at 800°C on the coated metal foils (LM, LMT and Sr-doped lanthanum manganite (LSM) for durations up to 4,320 hours (180 days). The oxidized samples were characterized by X-ray diffraction (XRD) and SEM. The oxidation products were identified and the oxidation kinetics ascertained by measuring the thickness of the oxide layer as a function of time. The results demonstrated that the LMT coating was the most effective and LSM least effective in suppressing the oxidation kinetics of the alloys. The results were verified by a theoretical model and demonstrated that the LMT coating was the most protective. The data were consolidated and compared with earlier work on spinel (Mn_2CrO_4) coatings on Haynes 230 and it was found that the perovskite coatings are far superior with regard to protection against oxidation.

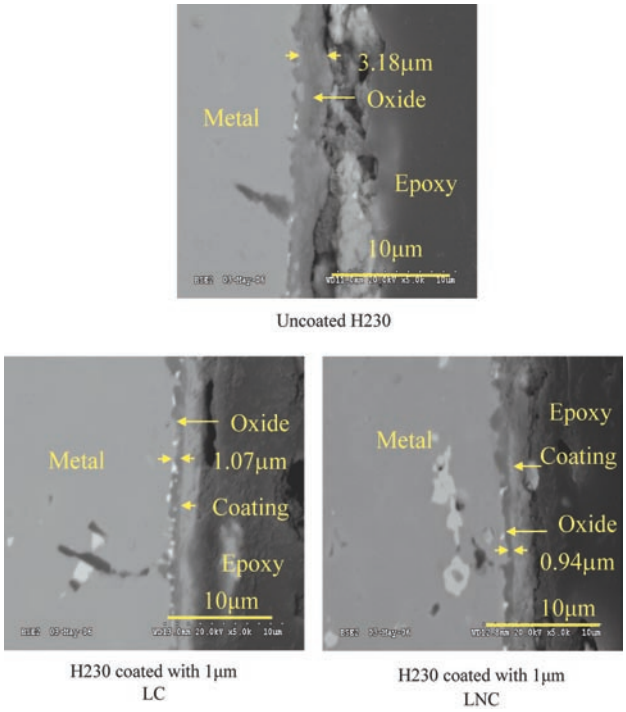

FIGURE 2. SEM Micrographs (Edgewise) of Uncoated, LC-coated (1 μm) and LNC-coated (1 μm) H230 Foils Oxidized for 2,160 Hours in Reducing Atmosphere at 800°C

3) Oxidation in flowing 10%H_2/90%N_2 gas with 5% humidity was conducted on the coated metal foils ($LaCrO_3$ and Nb-doped $LaCrO_3$) for durations up to 2,160 hours (90 days). The oxide layer thickness was determined as a function of time. The perovskite coating significantly slowed down the oxidation kinetics of the metal foil. While an uncoated H230 foil formed an oxide layer of average thickness 3.18 μm after 90 days, a 1 μm coating of $LaCrO_3$ reduced the thickness to 1.07 μm (Figure 2).
4) A spring loaded fixture was used to measure the ASR of the oxidized foils. Conductive paste was not used for these measurements as this could permeate the porous oxide layer and lead to an under-estimation of the ASR value. The ASR on the LMT-coated (1 micron) and uncoated foils showed that after 1,080 hours (45 days) in air at 800°C, the ASR of the coated foils was typically smaller by about half. The ASR for the $LaCrO_3$ and Nb-doped $LaCrO_3$ coated foils were also considerably lower than that for the uncoated foil over the entire temperature range (Figure 3).
5. LSM and LMT were dip coated on to 2" x 2" SS430 foils. The coatings were cured at 1000°C for 1 to 5 hours. The samples were characterized by SEM. The coatings were about 5 to 10 μm thick and showed excellent adherence. In some samples, load was applied on the dip coating by means of a spring at the time of heat curing. The application of load resulted in a more compact and less porous coating (Figure 4).

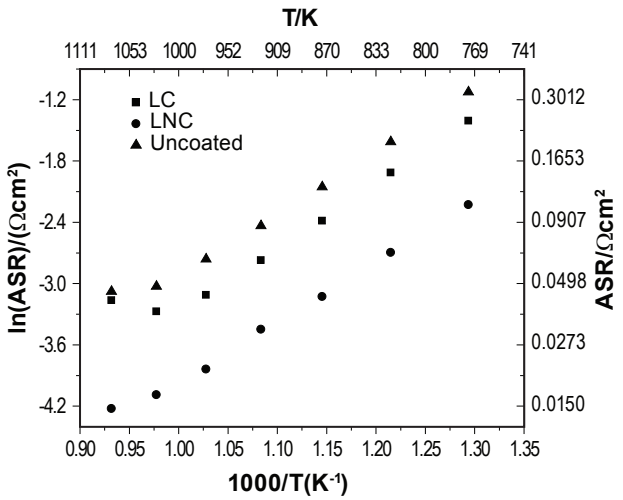

FIGURE 3. Plots of ASR vs. 1000/T for Uncoated and Coated H230 Metal Foils with 1 μm Coatings of LNC and LC, Oxidized in Reducing Atmosphere at 800°C for 336 Hours

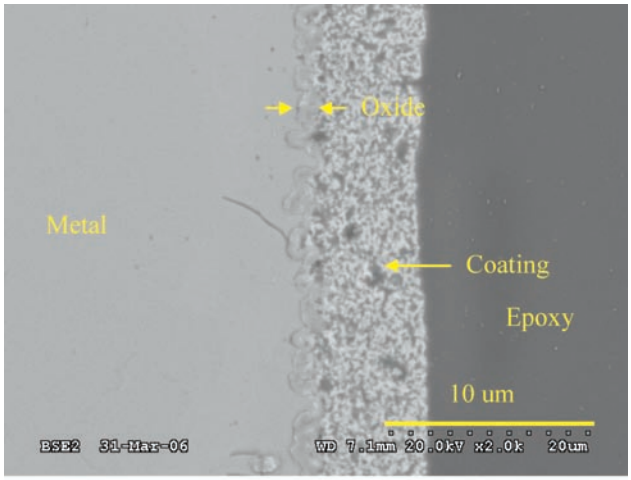

Annealed without application of pressure

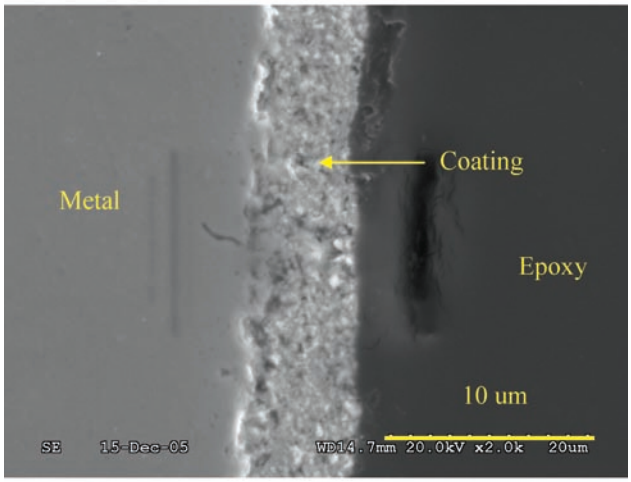

Annealed with application of pressure

FIGURE 4. SEM Micrographs of Dip-coated SS430 Foils with LSM0.85 Coating, Annealed at 1000°C for 2 Hours in Air

Conclusions

Defect chemistry plays a major role in oxygen ion transport through oxides, and thus determines the suitability of a given material as a coating. Coating materials based on $LaMnO_3$ and $LaCrO_3$ were successfully made. It was demonstrated that perovskite coating is an order of magnitude superior to spinel coating.

1. Electronic and ionic conductivities of coating materials are in accord with defect chemistry, and that defect chemistry provides a scientific basis for the design of oxidation-resistant coatings.
2. High quality, strongly adherent coatings can be sputter deposited. The resulting foils exhibit improved oxidation resistance over the baseline foils. Even after 45 days at 800°C, the coating continues to remain well-bonded.
3. Coated foils also exhibit much lower ASR as compared to pristine foils.
4. Initial trials suggest that it is possible to coat larger metal sheets cost effectively by a combination of dip technique and pressure assisted curing at elevated temperature.

IV.A.26 Digital Manufacturing of Gradient Meshed SOFC Sealing Composites with Self-Healing Capabilities

Dr. Kathy Lu (Primary Contact),
Christopher Story, Dr. W. T. Reynolds, Jr.
Virginia Polytechnic Institute and State University
213 Holden Hall, M/C 0237
Blacksburg, VA 24061
Phone: (540) 231-3225; Fax: (540) 231-8919
E-mail: klu@vt.edu

DOE Project Manager: Ayyakkannu Manivannan
Phone: (304) 285-2078
E-mail: Ayyakkannu.Manivannan@netl.doe.gov

Objectives

- Use three dimensional printing (3DP) technique to build a shape memory alloy (SMA) skeleton for the seal on the seal-interconnect side.
- Use glass to fill the meshed SMA structure and transition into pure glass seal on the electrolyte side.
- Provide gradient coefficient of thermal expansion (CTE) to reduce the thermal stress.
- Further reduce the thermal stresses in the seal by SMA phase transformation toughening.
- Provide self-healing of cracks by SMA shape recovery during solid oxide fuel cell (SOFC) thermal cycling.

Accomplishments

- Developed multiple AUTOCAD drawings of wire structure and 3D printed multiple configurations of the wire structure.
- Synthesized new composition TiNiHf alloy by gas atomization method. The new alloy composition has a slightly higher Ni concentration to facilitate a more uniform microstructure.
- Extensive work was carried out for the optimization of the parameters of the three dimensional printing technique. An emulsion binder was developed for the proposed TiNiHf alloy powder.
- SMA/glass composite was produced. Neutron diffraction provided 0.001 Å measurement resolution for the TiNiHf alloy lattice parameter change during thermal cycling. Austenite to martensite phase transformation can be observed in-situ by neutron diffraction.
- SMA alloy demonstrated the ability of reducing the thermal stresses in the seal by SMA phase transformation toughening.
- Dilatometry has been used to measure the thermal expansion coefficient of the commercial cell electrolyte and interconnect. The proposed SMA/glass has the potential to bridge the thermal expansion coefficient mismatch between the cell components.

Introduction

SOFC seals have a demanding set of imposed performance criteria. Of particular importance is the ability to seal between metallic and ceramic components with differing CTEs and do so while being electrically insulating and exposed to temperature transients from room temperature up to ~650-950ºC. A major roadblock to long-term SOFC operation has been gas leakage through the seal caused by multiple heating and cooling cycles (thermal cycling). The gas seal cracks because the metal and ceramic components that are sealed together shrink and expand differently (CTE mismatch), causing high stresses in the seal.

A host of seal materials have been explored, such as FeCrAlY, DuraFoil, Si-C-N polymers, ceramic and metallic fillers, mica, and glass-ceramic fibers (1-6). However, interdiffusion and durability of some of these materials in the oxidizing and reducing environments of SOFC are unknown. Some of these seals require compressive loads or have unknown leakage protection capability. An improved glass matrix should be selected to avoid the above problems. Also, cracking during thermal cycling can be avoided by the integration of a second phase which is a better match to the thermal expansion of the metallic interconnect. An SMA has a CTE close to that of the interconnect and presents the possible benefit of crack healing because of the shape memory behavior when heated.

Approach

We used gas atomization to obtain different size particles and adjusted the SMA composition to a higher Ni content in the process of optimizing the SMA alloy composition. After the SMA is fabricated, the powder was processed to -635 mesh. After that, the SMA alloy was 3D printed into a wire structure. 3D printing allows creating wire diameters of 200-500 µm and printing layers that are 25-100 µm thick. Since the 3DP technique was newly applied to the TiNiHf system, the printing parameters and the binders all need to be re-examined. We have systematically analyzed all the 3DP

parameters and identified three key parameters that need to be optimized: binder type, binder saturation level, and printing layer thickness. The SMARTS system in the Lujan Center at Los Alamos National Laboratory, New Mexico was used for neutron diffraction of glass/SMA composite. Samples were placed free standing on a graphite base in the chamber of a vacuum furnace. They were heated at 15°C/min to 800°C and then cooled at different rates. The glass/SMA sample was cooled first at 5ºC/min to 375°C and then held for approximately 30 minutes to achieve a neutron detection count of 1.5×10^3 Ah. The sample was then cooled in 10°C and 20°C steps at 5ºC/min for more diffraction patterns. The same glass/SMA sample was heated again to 800ºC and then cooled at 30°C/min to a first diffraction temperature of 350°C and cooled in 25°C and 10°C steps. A similar temperature profile was conducted on the SMA slivers without glass, with the exception that the cooling rate was at 15°C/min. For the CTE measurements, a push rod dilatometer (Orton 1600B, Edward Orton, Jr. Ceramic Foundation, Westerville, Ohio) was used. We obtained commercial SOFC electrolyte, Sc-stabilized ZrO_2, from Ceramatec (Salt Lake City, Utah) and the stainless steel interconnect from ATI Allegheny Ludlum (Pittsburgh, Pennsylvania) under the trade name E-BRITE®. The temperature range studied was from room temperature to 800°C to mimic the operation condition of actual SOFCs.

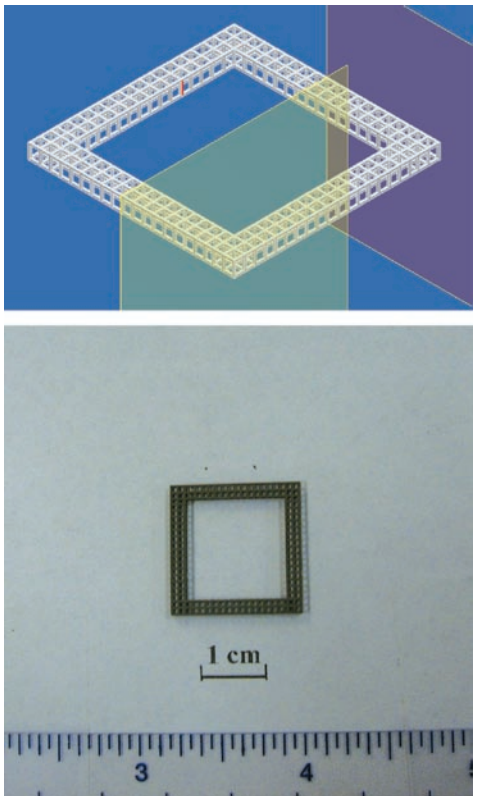

FIGURE 1. AUTOCAD Wire Mesh Design (top) and 3D Printed Wire Mesh (bottom)

Results

New composition TiNiHf alloy powder has been successfully synthesized by gas atomization. As desired, the atomic percent of Ni increased by 1% in comparison to the arc-melted TiNiHf composition reported last year.

Extensive work has been carried out for the 3DP parameter optimization. In an effort to increase the mesh strength, the binder saturation level was increased several times from 55% to 170%. Intricate wire structures were printed as shown in Figure 1. An emulsion binder was developed for the proposed TiNiHf alloy powder. The viscosity of the emulsion binder is much lower than that of the existing binder, making it suitable to be used in the 3D printing machine (Figure 2). The particles bound by the 40 vol% emulsion binder solution could not be broken with tweezers.

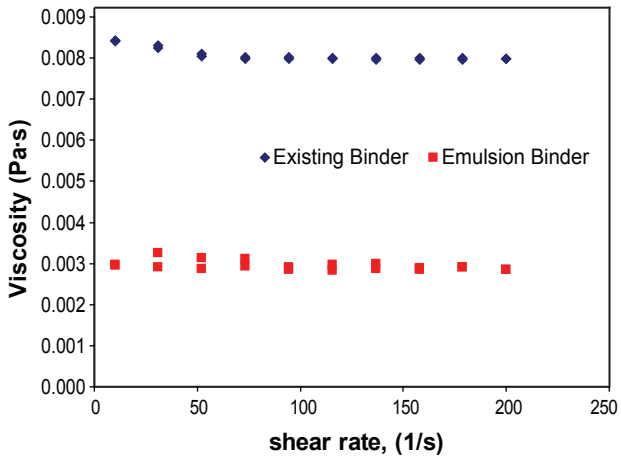

FIGURE 2. Viscosity Comparison of the Existing Binder and the Emulsion Binder

Neutron diffraction provides 0.001 Å measurement resolution for the TiNiHf alloy lattice parameter change. The thermal stress generated from the glass matrix shifts the SMA austenite to martensite phase transformation temperature to a higher temperature during cooling. The thermal expansion coefficient at the lattice level from the neutron diffraction matches well with the CTE measurement from the dilatometry. Figure 3 is a neutron diffraction pattern during the austenite to martensite transition. The thick arrow points to the austenite (110) peak while the dotted arrow points to a martensite double peak. As shown in Figure 3, the martensite peak was barely visible at 180°C. As the temperature was decreased to 162°C and 124°C, the martensitic (101) and (020)/(012) double peak intensity kept increasing, indicating the austenite to martensite

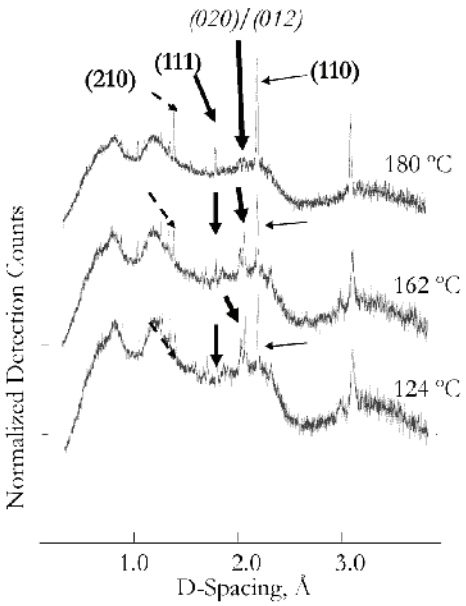

FIGURE 3. Neutron Diffraction Pattern from the Glass/SMA Sample at 180°C, 162°C, and 124°C

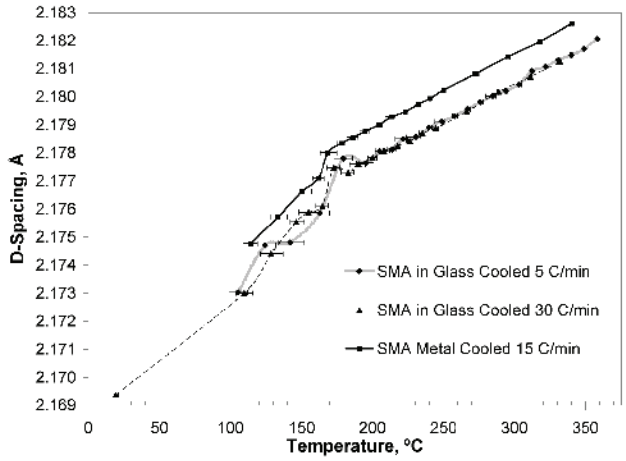

FIGURE 4. D-Spacing of the (110) Austenite Peak during Cooling

phase transformation process ((020) and (012) peaks are located on the right side of the double peak but are too close to be resolved).

D-spacing of the (110) austenite peak is plotted in Figure 4 for the three samples at different temperatures. The (110) d-spacing for the SMA alloy without glass is approximately 0.001 Å higher than that in glass during cooling above the martensitic transition. The curves are identical for the slow cooled and fast cooled SMA/glass samples and are both parallel to that of the SMA sample. The only likely cause is the thermal stress induced phase transformation change. However, there is one aspect that cannot be explained. The thermal stresses from the glass should increase the SMA d-spacing because the metal has a higher CTE and tends to shrink more during cooling. This can be caused by the metastable nature of the glassy phase but needs to be further studied.

Dilatometry has been used to measure the CTEs of the commercial cell electrolyte and interconnect. The CTE of the E-BRITE® stainless steel interconnect is $16.8x10^{-6}$/K. The CTE of the scandia stabilized zirconia is $9.5x10^{-6}$/K. For both stainless steel and ZrO_2, the CTEs are fairly consistent across the measurement temperature range of room temperature to 800°C. The CTE of the glass is $7.02x10^{-6}$/K between 40°C and 500°C, $32.0x10^{-6}$/K between 500°C and 700°C, and $21.4x10^{-6}$/K between 700-800°C; the overall CTE is $13.9x10^{-6}$/K. The CTE of SMA is $12.5x10^{-6}$/K. These measurements confirm the need for CTE match at various temperatures for different SOFC components. These measurements provide quantitative CTE difference comparison for continuing seal composition optimization.

Conclusions

1. TiNiHf alloy has been successfully synthesized by gas atomization with the desired particle size for the 3DP process. This solves the SMA ductility issue encountered during the SMA alloy milling.
2. The parameters for the 3DP process have been evaluated and optimized. A new binder has been identified to match with the specific chemistry of the SMA particles.
3. Neutron diffraction shows to be an extremely useful tool in providing information regarding the austenite to martensite phase transformation, SMA alloy lattice constant change, and the corresponding thermal stress from the glass matrix. It pinpoints regions of SMA phase transformation and the thermal stress effect under simulated SOFC thermal cycles.

Future Directions

- Detailed glass and SMA composition optimization is needed.
- Further understanding of the glass and SMA interaction is needed.
- Composite seal performance should be studied with the optimized seal design.

FY 2007 Publications/Presentations

1. K. Lu, C. Story, and W. T. Reynolds, "Glass/Shape Memory Alloy Composite Study for Solid Oxide Electrolyzer/Fuel Cell Applications," 31st International Cocoa Beach Conference & Exposition on Advanced Ceramics and Composites, January 21-26, 2007, Daytona Beach, FL.

2. C. Story, W. Reynolds, and K. Lu, "Shape Memory Alloy/Glass Composite Gas Seal for Solid Oxide Fuel Cells," 2007 TMS Annual Meeting & Exhibition, February 25, 2007 – March 1, 2007, Orlando, FL.

3. C. Story, K. Yu, K. Lu, and W. T. Reynolds, "Self-Healing Composite Seals for Solid Oxide Electrolyzer/Fuel Cells," Deans' Form on Energy Security and Survivability, October 16, 2006, Blacksburg, VA.

References

1. K. S. Weil, J. Y. Kim and J. S. Hardy, "Reactive Air Brazing: A Novel Method of Sealing SOFCs and Other Solid-State Electrochemical Devices," *Electrochemical and Solid-State Letters*, 8(2), A133-A136, 2005.

2. K. S. Weil and J. S. Hardy, "Development of a Compliant Seal for Use in Planar Solid Oxide Fuel Cells," *28th International Conference on Advanced Ceramics and Composites*, E. Lara-Curzio and M. J. Readey, eds. 25, pp. 321-326, American Ceramic Society, Cocoa Beach, FL, 2004.

3. Y.-S. Chou and J. W. Stevenson, "Long-Term Thermal Cycling of Phlogopite Mica-Based Compressive Seals for Solid Oxide Fuel Cells," *Journal of Power Sources*, 140, 340–345, 2005.

4. M. Bram, S. Reckers, P. Drinovac, J. Monch, R. W. Steinbrech, H. P. Buchkremer and D. Stover, "Deformation Behavior and Leakage Tests of Alternate Sealing Materials for SOFC Stacks," *Journal of Power Sources*, 138, 111–119, 2004.

5. S. Taniguchi, M. Kadowaki, T. Yasuo, Y. Akiyama, Y. Miyake and K. Nishio, "Improvement of Thermal Cycle Characteristics of a Planar-Type Solid Oxide Fuel Cell by Using Ceramic Fiber as Sealing Material," *Journal of Power Sources*, 90, 163–169, 2000.

6. J. W. Fergus, "Sealants for Solid Oxide Fuel Cells," *Journal of Power Sources*, 147, 46-57, 2005.

IV. SECA RESEARCH & DEVELOPMENT

B. Fuel Processing

IV.B.1 An Innovative Injection and Mixing System for Diesel Fuel Reforming

Spencer D. Pack (Primary Contact),
John E. Short, and Nick R. Overman
Goodrich Turbine Fuel Technologies
2200 Delavan Drive
West Des Moines, IA 50265-0100
Phone: (515) 633-3460; Fax: (515) 271-7296
E-mail: spencer.pack@goodrich.com

DOE Project Manager: Charles Alsup
Phone: (304) 285-5432
E-mail: Charles.Alsup@netl.doe.gov

Objectives

- Develop reliable, cost-effective diesel fuel injection and mixing systems for use with an auto-thermal reformer (ATR) or catalytic partial oxidation (CPOX) reformer in solid oxide fuel cell (SOFC) auxiliary power units (APUs), including a fuel preheating concept and a piezoelectric concept
- Determine operation and performance limitations of both injection and mixing concepts for diesel fuel reforming applications
- Optimize both injector/mixers for diesel fuel reformers to operate with no steam/water usage and minimize air and fuel supply pressure
- Test and analyze various anti-carbon formation coatings to improve the preheating injector life by reducing carbon formation in the fuel injector passages

Accomplishments

- Completed the design and fabrication of two different preheating fuel injection concepts and a piezoelectric injection concept, optimized through statistical design of experiment studies utilizing an optical patternater.
- Completed heated air temperature uniformity testing for the preheating fuel injection concepts.
- Conducted a detailed computer analysis and characterization of air flow field of the preheating fuel injector.
- Created a carbon formation test rig and down-selected to three most promising anti-carbon coatings using the statistical design of experiments technique.

Introduction

Fuel reformers are a very important component of SOFC systems, enabling them to compete with conventional auxiliary power units in remote stationary and mobile power generation markets. Currently, liquid fuel processing technology is not yet viable for commercial applications in SOFC systems. One of the major technical barriers for liquid fuel processing is reactor durability. The performance of the reforming catalysts in the reactor quickly deteriorates as a result of carbon deposition, sulfur poisoning and loss of precious metals due to sintering or evaporation at high temperatures. To mitigate these problems, research efforts are being conducted to optimize catalyst materials and to improve fuel reactor design/operation.

Problems associated with liquid fuel reactors could possibly be alleviated by improvement of feed stream preparation. Proper feed stream preparation can significantly improve reactor durability and minimize problems of inadequate fuel atomization, wall impingement, mixture recirculation and non-uniform mixing. These problems can easily lead to local conditions that favor carbon deposition, auto-ignition and formation of hot spots in the reactor. Because liquid fuels are extremely difficult to reform, a proper understanding of injection and mixing systems for feed stream preparation plays an essential role in the development of reliable and durable liquid fuel reformers.

Approach

To achieve a Solid State Energy Conversion Alliance (SECA) goal of improved feed stream preparation, two promising fuel injection and mixing chamber concepts were proposed for a thorough evaluation using both computational and laser diagnostic techniques. The key performance parameters included in the evaluation involved fuel atomization, droplet evaporation, mixing, uniformity of mixture temperature, velocity, concentration, wall impingement, flow recirculation, carbon deposits, feed stream supply pressure, power consumption, complexity, and reliability of injector design/operation.

One obstacle with preheating the fuel before injection into the feed stream is carbon formation in the fuel injector. Carbon can restrict the fuel flow in the injector and reduce atomizer performance. Several anti-carbon coating applications were proposed for

evaluation, to determine their ability to reduce carbon formation within the fuel circuit of the preheating atomizer.

Results

A carbon formation test rig was designed and fabricated to test carbon formation rates on surfaces of various test specimens. This carbon formation test rig has the ability to preheat the fuel to 200°C and heat a test specimen to 600°C inside an N_2 purged oven (fuel is back pressured to reduce fuel boiling). This rig gives the flexibility to test specimens at wetted wall temperatures up to 500°C. Six anti-carbon formation coatings were tested. All six coated specimens and an uncoated baseline were tested at four different test conditions using ultra-low sulfur diesel. The specimens were tested inside the oven at two fuel preheating temperature levels of 150°C and 175°C, while the oven temperature was varied between two temperature levels of 425°C and 480°C. Figure 1 shows a picture of the carbon formed on a specimen tested at a fuel preheat temperature of 175°C, and an oven temperature of 480°C. As seen from Figure 1, the carbon that has formed on the surface is beginning to cover-up the tooling marks on the test specimen. This image was taken using a scanning electron microscope at 1.18K magnification. The coating tested in Figure 1 is AMCX Inertium diffusion bonded to 347 stainless steel base metal. Three coatings from the original six have been selected for further testing (AMCX Inertium, AMCX AMC26, & Restek Silcosteel AC). A final back-to-back test with injector components is planned to select a single preferred coating for use in the preheating injector.

Two preheating fuel injector concepts have been designed, fabricated, and tested. Build 1 utilized large flow recirculation zones to maximize fuel air mixing. This caused some concern since recirculation zones potentially lead to spontaneous ignition of the fuel rich mixture. Also, this work focuses on creating a nozzle that doesn't require H_2O/steam injection, which would be deterrents to auto-ignition. Therefore, Build 2 improved over Build 1 by eliminating these recirculation zones. Computational fluid dynamics (CFD) was utilized to help predict flow rates, pressure drops and flow non-uniformities associated with Build 1 and 2 design modifications. CFD was also utilized to simulate the overall flow-field structure and potential mixing capabilities, providing a qualitative assessment of the injector/mixer performance under the actual reformer operating conditions. The computation domain contains a flow path from the feed stream inlets, through the injector circuits and the diffuser section of the mixing chamber, terminating at the 72 mm diameter diffuser exit. The grid system for the flow path consists of over 1.3 million computational cells, with clustering tailored to regions of expected high gradients. The solutions were obtained using FLUENT 6.2 software to solve the unsteady, Reynolds-averaged Navier-Stokes equations, with the RNG k-ε turbulence model, wall-functions and differential viscosity models. Figure 2 shows a comparison of time-averaged velocity contours of the Build 2 preheating injector. Counter rotating air streams were utilized to produce mixing of the fuel and air. CFD predictions indicated that the preheating injector Build 2 design produces no recirculation zones.

For fuel atomization evaluation of the Build 2 preheating injector, detailed measurements were made at various operating conditions using phase/Doppler interferometry and using a SETscan OP-600 patternator produced by En'Urga Inc. The SETscan OP-600 is a high frequency statistical extinction tomography based optical patternator. The SETscan allows detailed visual and numerical characterization of spray quality in terms of cone angle, asymmetry, streaks, voids, and patternation number. Figure 3 presents SETscan

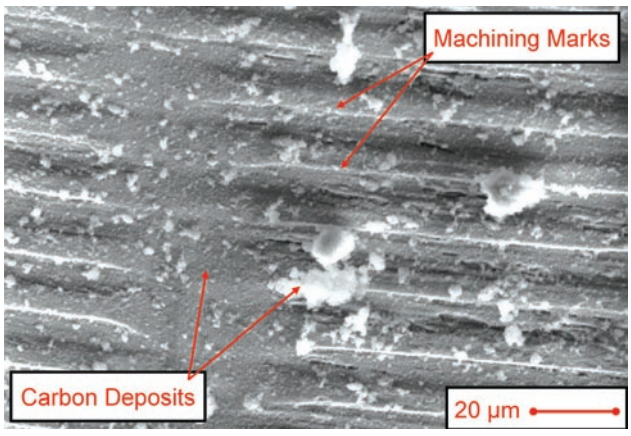

FIGURE 1. Typical carbon formation image via SEM. Anti-carbon formation coating is Inertium at 1.18K magnification.

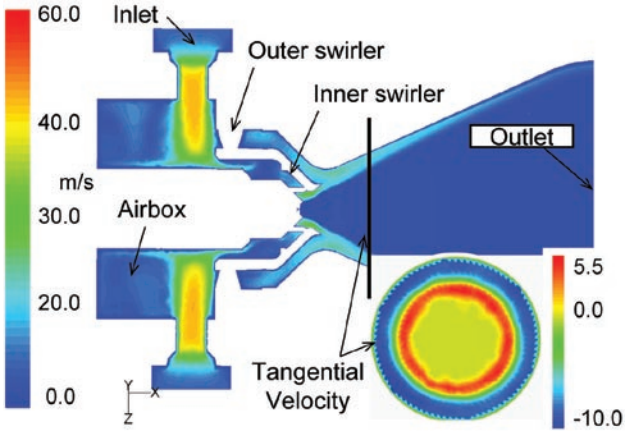

FIGURE 2. CFD Contours of Velocity Magnitude (m/s) of Build 2 Preheating Injector which Avoids Separation (Strong Jets in Air Box Will Be Reduced)

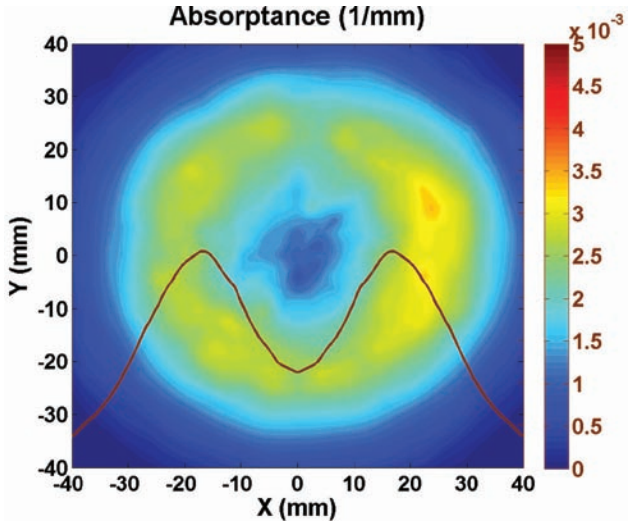

FIGURE 3. Fuel Absorptance Contours and Radial Distribution of Build 2 Preheating Injector 2 Inches Down Stream from Fuel Injection Point

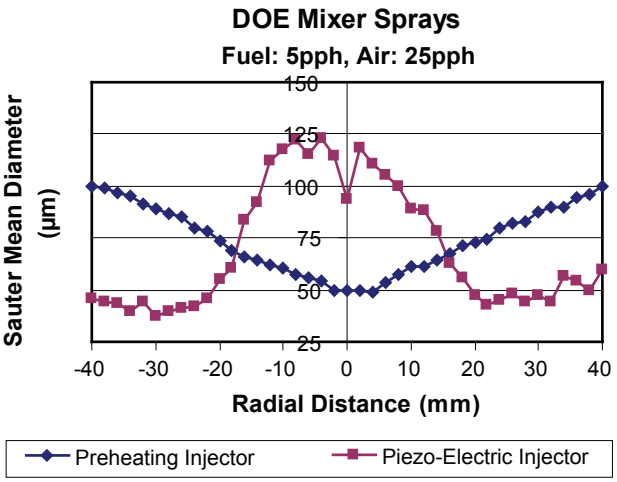

FIGURE 4. A Comparison of the Radial Distribution of Sauter Mean Diameter for the Build 2 Preheating Injector and Piezoelectric Injector at a Simulated 5 Kilowatt Load Condition

contours and radial distribution of absorption (1/mm) for the preheating Build 2 injector at a simulated 5 kilowatt load condition. This contour is taken at the diffuser exit plane (diffuser was not attached during this test). As shown, the fuel air mixture fills the 72 mm exit uniformly and evenly. It is expected that a mixing chamber will be able to capitalize on this optimized injector and further mix the fuel and air to allow complete vaporization of the fuel. Figure 3 test points were performed at ambient conditions with no preheating of the fuel.

A Phase Doppler Particle Analyzer (PDPA) system was used to measure droplet size and velocity. The PDPA was used to collect droplet information via two different methods: a continuous traverse method for global spray measurement and a point-to-point method. The continuous traverse method provides mean droplet diameters that represent the entire spray and the point-to-point method offers detailed local distributions of droplet size, velocity and fuel volume flux. This information is extremely useful in determining the spray dynamic structure and to identify differences between injector concepts. Figure 4 shows point-to-point measurements taken at a location three inches below the preheating injector exit, at a simulated 5 kilowatt load condition. For this test, the fuel pressure was 22 psi and the air pressure was 0.7 in. H_2O, with fuel and air temperatures at ambient conditions. Also shown in Figure 4 are PDPA measurements of the piezo-electric injector described below at the same flow rates.

A single piezo-electric fuel injector concept has been designed, fabricated, and tested. Though only one concept for this injector was created, several variations of sub-components were made. As with the preheating injector design, evaluation of the piezo-electric injector has been performed using both the SETscan OP-600 and the PDPA system. This concept utilizes piezo-electric crystals to induce mechanical vibration for atomizing the fuel, rather than large pressure differentials. Employing piezo-electrics to aid in atomization allows for minimization of air and fuel supply pressures. To date, tests have included a range of operation such that air pressures range between 0.10 in. H_2O – 3.0 in. H_2O, and fuel pressures less than 1 psi for flow rates up to 4.08 kg/hr. This design allows for low pressures, and consequently low velocities, while generating small droplets in the atomization process. When coupled with the high operating temperatures required by SOFCs, the small droplets and low velocities will allow for vaporization of the fuel within a very short distance. Therefore, this design promises to yield a smaller mixing chamber and overall a more compact injector/mixing unit.

Conclusions and Future Directions

- Feed stream preparation and injector selection are extremely important in improving the performance and durability of liquid fuel reformers.
- A preheating simplex injector has been developed into a promising concept for diesel fuel processing which could be used in SOFC APUs in commercial diesel truck applications with diesel fuel flow rate applications between 5 to 20 lb/hr (PPH).
- A piezoelectric injector has been developed into a promising concept for diesel fuel processing which could be used in SOFC APUs in commercial diesel truck applications with diesel fuel flow rate applications up to 5 PPH.

- Three anti-carbon coatings applied to 347 SS have shown reduced carbon formation rates over uncoated 347 SS. A final back-to-back test is pending to determine which coating will be recommended for use in the preheating injector.

Special Recognitions & Awards/Patents Issued

1. "Fuel Injection and Mixing Systems and Methods of Using the Same," Patent Pending, Filed April 12, 2007.

FY 2007 Publications/Presentations

1. "Innovative Fuel Injection and Mixing Systems for Diesel Fuel Reforming," Poster, SECA 7th Annual Workshop & Peer Review, September 12, 2006, Philadelphia, PA.

IV.B.2 Reformer for Conversion of Diesel Fuel into CO and Hydrogen

Michael V. Mundschau (Primary Contact), Christopher G. Burk
Eltron Research and Development Inc.
4600 Nautilus Court South
Boulder, CO 80301-3241
Phone: (303) 530-0263; Fax: (303) 530-0264
E-mail: mmundschau@eltronresearch.com

DOE Project Manager: Ayyakkannu Manivannan
Phone: (304) 285-2078
E-mail: Ayyakkannu.Manivannan@netl.doe.gov

Objectives

- Develop a fuel reformer for converting pump-grade diesel fuel with 15 ppmw sulfur into a mixture of H_2 and CO suitable for use in solid oxide fuel cells (SOFC).
- Demonstrate the use of a self-cleaning reactor wall, which diffuses and effuses oxygen to prevent the formation of carbonaceous layers that could otherwise plug a reformer.
- Synthesize and evaluate low-cost, sulfur tolerant, perovskite-based catalysts for use on the reformer wall and in the hot zone.

Accomplishments

- Designed and built laboratory scale reformer system for testing catalysts and design parameters.
- Commissioned laboratory reactor components (fuel handling lines, air input, seals and fittings, gas chromatograph, etc.).
- Measured permeability of air through porous yttria-stabilized zirconia (YSZ) and found it to meet or exceed minimum design specification.
- Designed and fabricated porous YSZ tubes according to design specifications.
- Analyzed pump-grade low-sulfur diesel fuel for sulfur content and carbon-hydrogen ratio.

Introduction

A fuel reformer is under development for the conversion of pump-grade diesel fuel into a mixture of hydrogen and carbon monoxide which can be utilized in solid oxide fuel cells. The design of the reformer is being driven by the following considerations. Thermodynamic analysis indicates that the desired products will be maximized and overwhelmingly favored if one atom of oxygen is added for each carbon atom in the fuel and if the mixture is brought to equilibrium above about 950°C, and preferentially above 1,000°C [1, 2]. Such temperatures place severe stability requirements on catalysts and reformer wall materials. Components must not melt or significantly evaporate, or form volatile compounds which potentially could contaminate fuel cells downstream. In the strongly reducing, high-temperature environment of the reformer, many common ceramics and oxide catalyst supports are reduced, and these must be avoided. Most common catalysts are sintered and deactivated at such high temperatures. Sulfur in the diesel fuel can also poison common catalysts. The reactor must be almost perfectly insulating if maximum efficiency is to be achieved, because the heat released by the partial oxidation of diesel fuel is just sufficient to heat fuel and air to the reaction temperature.

Thermodynamic and kinetic analyses indicate that formation of elemental carbon is favored in the range of 300–900°C. A major challenge is to bring the diesel fuel from room temperature to the catalytic hot zone without deposition of carbon onto reactor walls. Deposition of carbon is autocatalytic and can rapidly plug reactors. Infrared radiation from the catalyst hot zone can heat reactor walls in cool zones or heat the fuel injector nozzle, cracking diesel fuel to carbon and clogging reactors. Deposition of carbon at lower temperatures is suppressed by addition of extra oxygen, but usually at the expense of efficiency due to formation of deep oxidation products, carbon dioxide and steam. Thermodynamics also indicates that if the reformate is cooled, some hydrogen and carbon monoxide could be lost due to formation of carbon, water, methane and carbon dioxide, which become thermodynamically favored and could form in the exhaust if exhaust line surfaces are catalytic.

Approach

A catalytic membrane reactor is being developed. In such a reactor, oxygen is brought into the system through the reactor walls (see Figure 1). A goal is to form self-cleaning walls which prevent formation of carbon. High local concentration of oxygen near the inner walls, combined with oxidation catalysts having good bulk transport properties for atomic oxygen, suppresses deposition of carbon. Porous yttria-stabilized zirconia is being used as one reactor wall material because of its good thermal and chemical stability, its ability to transport oxygen through the bulk, and because of its good thermal insulating properties. Silver,

is being investigated as an oxidation catalyst on the inner walls of the cool zones of the reactor and at the fuel injector nozzle. Silver has the advantage of high oxygen diffusivity through its bulk, allowing oxygen to attack deposited carbon from beneath. Silver also has the highest reflectivity for infra-red radiation of any element, allowing reflection of radiation, especially from the fuel nozzle, back to the hot zone. Perovskite-based catalysts are being investigated as oxidation catalysts on the walls of the hot zones of the reactor. These materials also readily transport oxygen through their bulk, allowing attack of carbon from beneath. Oxygen transported through the porous zirconia and high local concentration of oxygen near the walls helps stabilize the perovskites and inhibit reduction of these oxides.

Perovskites containing cobalt and iron are being investigated as oxidation catalysts in the hot zone. Such catalysts act as reverse Fischer-Tropsch type catalysts, converting hydrocarbons back into hydrogen and carbon monoxide. These less expensive catalysts are being compared to a platinum-rhodium wire gauze. Molecular oxygen adsorbs and dissociates on the Pt-Rh surface into atomic oxygen. Atomic oxygen is especially reactive with hydrocarbons and is desired for oxidation of the more refractory aromatic compounds in the diesel fuel. Unlike Pt-Rh bimetallic catalysts supported by zirconia, the Pt-Rh gauze does not suffer from sintering. At high temperatures, the gauze is not poisoned by sulfur at levels in commercial diesel fuel (15 ppmw). The high cost of the noble metals will prevent their use in all but military applications but is providing a good baseline for comparison of activity of the less expensive perovskite-based catalysts.

Results

Most of the activity in this reporting period involved the design, construction and commissioning of a laboratory apparatus (Figure 2) for testing of the various components of the catalytic membrane reactor. A schematic of the catalytic membrane reactor is shown in Figure 1. Inner walls are all of yttria-stabilized zirconium

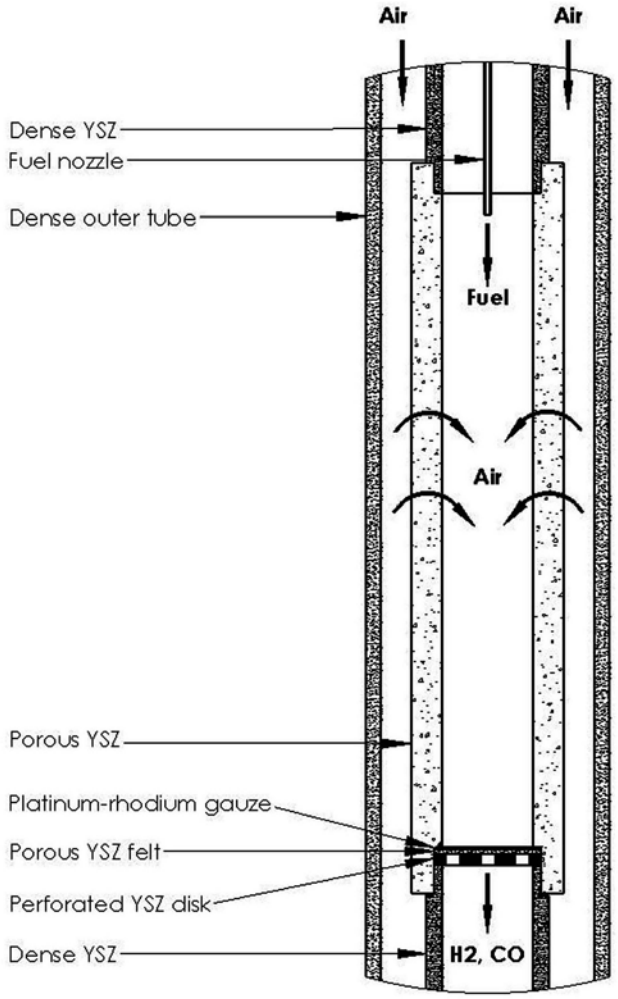

FIGURE 1. Schematic of Catalytic Membrane Reactor Employing Porous Yttria-stabilized Zirconia Inner Walls

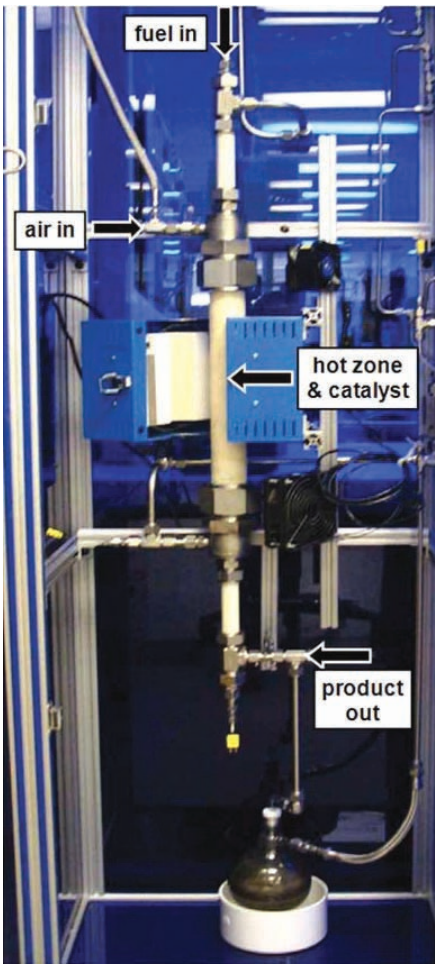

FIGURE 2. Laboratory Test Apparatus

oxide. Dense cylinders of yttria-stabilized zirconia are used surrounding the fuel injector nozzle and in the exhaust. In the exhaust tube, it is desired to use a catalytically inert inner wall material to avoid reaction between H_2 and CO to form H_2O, CH_4, CO_2 and C, which have a significant thermodynamic driving force for formation at temperatures below about 900°C [1].

Air is brought into the system through the walls of a porous yttria-stabilized cylinder (Figure 1). Figure 3 shows one end the porous cylinder, which is ¼ inch (0.635 cm) thick to provide mechanical support and insulation. Flow of air through the porous material is more than adequate for the partial oxidation of the fuel.

The present configuration employs a platinum-rhodium wire gauze as reforming catalyst in the reactor hot zone. The wire gauze is placed atop a porous felt of yttria-stabilized zirconia. The purpose of the porous felt is to promote turbulence and allow longer residence time of the reactive gases near the wire gauze. Figure 4a shows a scanning electron microscope image of the wire gauze. Figure 4b shows an image of the zirconia felt.

Most of the zirconia employs yttria-stabilized material containing quantities of yttria near that of the Nernst Mass (8.8 mole % = 15 mass % Y_2O_3), which maximizes oxygen flux. In the hot zones, however, yttria concentrations above about 9.5 mole % are being considered to ensure that the material remains completely within the cubic fluorite phase of the ZrO_2-Y_2O_3 phase diagram [3] to avoid potential phase transformations at elevated temperatures.

Perovskite catalysts containing cobalt and iron as the catalytic metal [1] have been synthesized. The goal is to replace the expensive Pt-Rh wire gauze with less expensive pellets of perovskite catalysts [4].

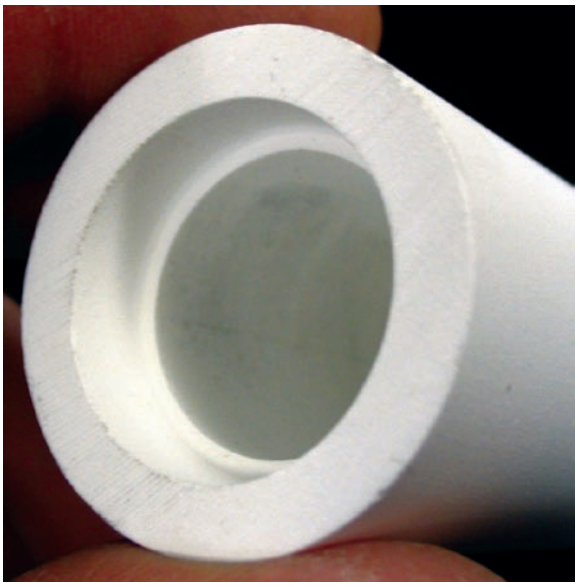

FIGURE 3. Photograph of porous yttria-stabilized zirconia tube used in the catalytic membrane reactor. Walls are ¼ inch (0.635 cm) thick.

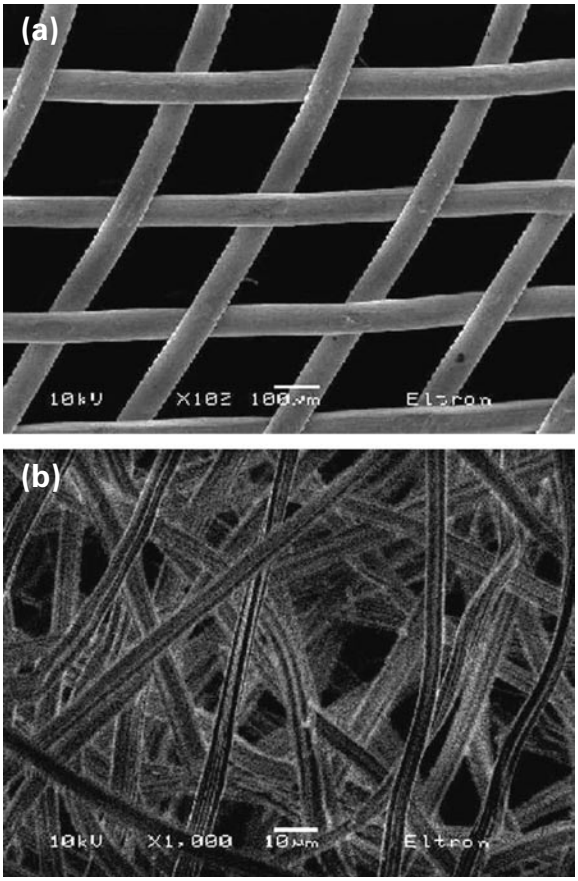

FIGURE 4. (a) Scanning electron microscope image of platinum-rhodium wire gauze used as a diesel fuel reforming catalyst. (b) Image of yttria-stabilized zirconia felt.

Conclusions and Future Directions

- A laboratory test apparatus has been completed and commissioned.
- A catalytic membrane reactor using inner walls of porous zirconia has been fabricated and tested with commercial diesel fuel containing ~15 ppmw sulfur using a Pt-Rh wire gauze as the ideal test catalyst.
- Perovskite catalysts have been synthesized and will be tested.
- Considerable laboratory tests and engineering design remain to produce a viable prototype design with low cost. Considerable effort remains to control carbon deposition on all components.
- Stability of catalysts and components under repeated temperature cycling must be demonstrated. Insulation and thermal efficiency must be improved. Fuel ignition sources must be improved. Parasitic power consumption must be reduced.

Special Recognitions & Awards/Patents Issued

1. Michael V. Mundschau, *Catalytic Membrane Reactor and Method for Production of Synthesis Gas*, U.S. Provisional Patent Application Filed September 8, 2006.

FY 2007 Publications/Presentations

1. M.V. Mundschau and J.A. Benjamin, *Liquid Fuel Processing Using Catalytic Membrane Reactors*, SECA Core Program – Fuel Processing, 7th Annual SECA Workshop and Peer Review, Philadelphia, Pennsylvania, September 13, 2006.

2. D.S. Jack, J.H. White, J.A. Trimboli, C.G. Burk, S.L. Rolfe, D.H. Anderson, M.V. Mundschau, *Liquid Fuel Reforming Using Catalytic Membrane Reactors*, Submitted to and accepted by the Division of Fuel Chemistry for the 234th ACS National Meeting, Boston, MA, August 19–34, 2007.

References

1. Jarrod A. Benjamin and Michael V. Mundschau, Reformer for Conversion of Diesel Fuel into CO and Hydrogen, DOE Hydrogen Program, FY 2006 Annual Report, III.B.4.

2. Dushyant Shekhawat, David A. Berry, Todd H. Gardner and James J. Spivey, Catalytic Reforming of Liquid Hydrocarbon Fuels for Fuel Cell Applications, *Catalysis* **19** (2006) 184–253.

3. H. G. Scott, Phase Relationships in the Zirconia-Yttria System, *J. Mat. Sci.* **10** (1975) 1527–35.

4. Di-Jia Liu and Michael Krumpelt, Activity and Structure of Perovskites as Diesel-Reforming Catalysts for Solid Oxide Fuel Cells, *Int. J. Appl. Ceram. Technol.* **2** [4] (2005) 301–307.

IV.B.3 Hexaaluminate Reforming Catalyst Development

Todd H. Gardner (Primary Contact),
Dushyant Shekhawat and David A. Berry
U. S. Department of Energy
National Energy Technology Laboratory (NETL)
3610 Collins Ferry Road
Morgantown, WV 26507-0880
Phone: (304) 285-4226; Fax: (304) 285-0943
E-mail: Todd.Gardner@netl.doe.gov

Contractor:
Edwin L. Kugler, West Virginia University,
Morgantown, WV

Objectives

- The development of a durable, low-cost catalyst to reform middle distillate fuels.
- Evaluate the activity, selectivity and carbon deposition resistance of transition metal doped hexaaluminate-type catalysts:
  - Evaluate the effect of doping the hexaaluminate lattice with noble metals.
  - Perform extended performance test on diesel fuel.

Accomplishments

- Synthesized numerous hexaaluminate and hexametallate catalyst formulations.
- Demonstrated 150 hours of operation on diesel fuel.
- Performed catalyst characterization by X-ray diffraction (XRD), temperature-programmed reduction (TPR), extended X-ray absorption fine structure (EXAFS), X-ray absorption near edge structure (XANES), temperature-programmed oxidation (TPO) and Brunauer-Emmett-Teller (BET) surface area.
- Evaluated the activity and selectivity of synthesized hexaaluminate samples using methane, n-tetra-decane and diesel fuel.
- Patent disclosure filed for a novel reforming catalyst.

Introduction

The catalytic partial oxidation of diesel fuel is an attractive source of H_2 and CO for fuel cell applications. However, the deposition of carbon onto the surface of the catalyst and the migration and loss of active metals remain the principal issues in the development of a suitable catalyst. The formation of elemental carbon onto the surface of a catalyst has been shown to be related to both the size of the active metal cluster [1] and its coordination [2]. The substitution of a catalytic metal into the lattice of hexaaluminate compounds may serve to reduce the size of active metal clusters and to increase their dispersion thereby reducing their susceptibility toward carbon deposition. Interactions between neighboring substituted metals and the hexaaluminate lattice may serve to suppress active metal mobility. In this project, catalytically active metals are doped directly into the hexaaluminate lattice resulting in an atomically dispersed catalyst system that has been shown to possess carbon deposition resistance [3,4].

Recent work sponsored by the National Energy Technology Laboratory has shown progress toward understanding the structure-activity relationship which exists with solid oxide catalysts. Within this study, the average Ni coordination of a $BaNi_yAl_{12-y}O_{19-\delta}$ series of catalysts was characterized by EXAFS. Catalyst activity and selectivity was assessed by H_2 and CO concentrations obtained from methane and n-tetradecane ($C_{14}H_{30}$) partial oxidation. Post-run characterization of the catalysts was undertaken by TPO to locate and quantify the amount of carbon deposited onto the catalysts. The effect of doping the hexaaluminate lattice with noble metals was also evaluated with a 150 hour partial oxidation experiment on diesel fuel.

Approach

The deposition of carbon onto the surface of a reforming catalyst occurs predominately through pyrolytic and dehydrogenation reactions. The dehydrogenation of hydrocarbons into coke occurs when the relative rate of hydrocarbon adsorption is faster than that of the surface reaction [5]. It is therefore desirable to design catalysts which limit the residence time of the hydrocarbon adsorbate to minimize complete dehydrogenation into coke.

The aim of the present study has been to reduce the formation of large ensembles of active sites that are responsible for forming carbon and also for strongly adsorbing sulfur compounds. This was accomplished by substituting catalytically active metals into the framework lattice of hexaalumina. A series of catalysts based on transition metal doped hexaalumina and compounds with hexaalumina-type structure were prepared by co-precipitation from nitrate salt precursors. The stability of one of these catalysts was assessed over 150 hours of continuous operation. Catalyst activity, selectivity and carbon deposition resistance were

investigated over these catalysts utilizing n-tetradecane and diesel fuel.

Results

n-Tetradecane is used in this investigation as a model diesel fuel compound. Within the reactor, oxygen is preferentially consumed at the reactor inlet resulting in the formation of steam and CO_2. These products then react with the n-tetradecane (and its derivatives) in reforming reactions to produce CO and H_2. To illustrate the structure-activity relationship that exists with Ni substituted hexaaluminate catalysts, n-tetradecane catalytic partial oxidation (CPOx) was used as a probe reaction. The results obtained exemplify the effect of increasing the Ni substitution into the hexaaluminate lattice.

Prior to the experiments, the hexaaluminate catalysts were first reduced in 5 vol% H_2/Ar at 900°C for 1 hour. Experiments were conducted at an O/C = 1.2, a gas hourly space velocity (GHSV) = 50,000 $cm^3h^{-1}g^{-1}$, a pressure of 2 atm, a total inlet gas flow rate of 450 sccm and $C_{14}H_{30}$ and O_2 concentrations of 2.17 and 18.22 vol%, respectively. $C_{14}H_{30}$ conversion was observed to be 100%. Catalyst activity and selectivity were examined by isothermal reaction at 900°C. Carbon deposition was measured by TPO using 5% O_2/N_2 and a ramp rate of 1°C/min. The yield of product A (H_2 and CO) is defined as:

Where, N is the number of moles of hydrogen/mole of hydrocarbon for the H_2 yield and is the number of carbon atoms in the hydrocarbon fuel for CO.

$$\text{Yield of A(\%)} = \frac{\text{moles of A in reactor effluent x 100}}{\text{N x moles of hydrocarbon fed to the reactor}}$$

The EXAFS data for the three catalysts are shown in Table 1. From the data, the average Ni-O bond distance did not vary significantly by increasing the Ni substitution into the lattice, however increasing Ni substitution slightly decreased Ni-O coordination. This suggests that the concentration of Ni present in the lattice remained sufficiently dilute such that these parameters were not significantly affected. The Debye Waller factor was found to be low for all catalysts indicating a well ordered Ni crystalline structure.

TABLE 1. EXAFS Parameters for Ni-O Bonds in $BaNi_yAl_{12-y}O_{19-\delta}$

Catalyst	Avg. Ni-O Coordination	Ni-O Bond Distance (Å)	Debye Waller factor
$BaNi_{0.2}Al_{11.8}O_{19-\delta}$	4.1 ± 0.8	1.935 ± 0.016	0.0020 ± 0.0021
$BaNi_{0.6}Al_{11.4}O_{19-\delta}$	3.0 ± 0.5	1.966 ± 0.008	0.0006 ± 0.0019
$BaNi_{1.0}Al_{11}O_{19-\delta}$	3.0 ± 0.5	1.957 ± 0.013	0.0021 ± 0.0019

The H_2 and CO yields over the $BaNi_yAl_{12-y}O_{19-\delta}$ series of catalysts at 900°C are given in Table 2. The yield indicates that catalyst activity was influenced by the concentration of Ni present. The $BaNi_{0.2}Al_{11.8}O_{19-\delta}$ catalyst exhibited H_2 and CO yields which were 64 and 59% of equilibrium. However, the $BaNi_{0.6}Al_{11.4}O_{19-\delta}$ and $BaNi_{1.0}Al_{11}O_{19-\delta}$ catalysts exhibited near equilibrium H_2 and CO yields. The observed selectivity was significantly lower for the $BaNi_{0.2}Al_{11.8}O_{19-\delta}$ catalyst suggesting that at low Ni substitution the catalyst was not only less active, but also was likely more prone to carbon deposition.

TABLE 2. Product Yields for the CPOx of n-$C_{14}H_{30}$ Over $BaNi_yAl_{12-y}O_{19-\delta}$ at 900°C

Catalyst	H_2 Yield (%)	CO Yield (%)
Equilibrium	89.2	91.5
$BaNi_{0.2}Al_{11.8}O_{19-\delta}$	57.4	54.5
$BaNi_{0.6}Al_{11.4}O_{19-\delta}$	92.7	91.0
$BaNiAl_{11}O_{19-\delta}$	88.3	85.8

The TPO results for the three exposed catalysts are given in Figure 1. The results indicate that increasing the substitution of Ni into the lattice produced distinct differences in both the amount of carbon deposited onto the catalyst and its location. The $BaNi_{0.2}Al_{11.8}O_{19-\delta}$ catalyst exhibited a single asymmetrically shaped burn-off peak located at ~550°C. The asymmetry associated with this peak suggests the presence of two overlapping peaks. The portion of the peak located between 430 and 518°C is, therefore, attributed to carbon located at an interfacial region near, but not on, the Ni surface [6,7]. The portion of the peak located between 518 and 634°C is attributed to carbon located on the support [6,7]. The carbon present on this catalyst is dominated by carbon deposited onto the support. This observation is consistent with a less active catalyst with less Ni metal present on the surface. The relatively high concentration of total carbon deposited onto the catalyst is consistent with the observed poor CO selectivty.

The $BaNi_{0.6}Al_{11.4}O_{19-\delta}$ catalyst exhibited three peaks at various burn-off temperatures. The low temperature peak located at 296°C was attributed to the metal burn-off region [6,7], the peak located at 537°C was identified as carbon located at an interfacial region, and the peak located at 592°C was identified as carbon deposited onto the support [6,7]. A significant decrease in total carbon deposited onto the catalyst was observed at higher Ni substitution. This is consistent with the observed CO selectivity.

The $BaNi_{1.0}Al_{11}O_{19-\delta}$ catalyst exhibited a single broad burn-off peak located at 559°C. The broadness associated with this peak suggests that carbon is located at both interfacial and support regions. This catalyst exhibits the lowest amount of carbon deposited onto the

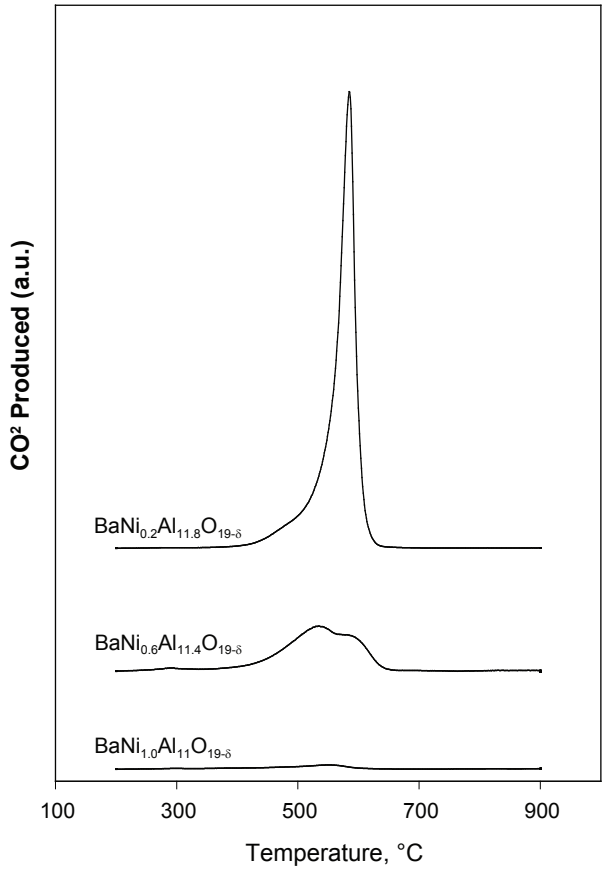

FIGURE 1. TPO Results for $BaNi_yAl_{12-y}O_{19-\delta}$ (y = 0.2, 0.6 and 1.0) Series of Catalysts after the CPOx Experiments with n-Tetradecane

catalyst surface which correlates with the greatest Ni substitution into the lattice.

A performance test run of the NETL-developed fuel atomization/reactor and noble metal doped hexaaluminate catalyst was performed using diesel fuel. The composition of the diesel fuel (DF) is DF #1 given in Table 3. This was the first NETL test to employ both a fuel atomizer and a novel NETL-developed reforming catalyst. The specific test objective was to examine integrated atomizer/catalyst performance and to assess catalyst stability. In this test series, the catalyst was examined at 900°C, at a GHSV = 25,000 $cm^3g^{-1}h^{-1}$, O/C = 1.2. The catalyst exhibited stable performance over the test period (Figure 2).

TABLE 3. Diesel Fuel Compositions

	DF #1	DF #2
Constituent	**Concentration (wt%)**	**Concentration (wt%)**
Sulfur	9 ppm w/w	125 ppm w/w
Aromatic	18	23
Paraffin	38	38
Naphthenes	44	39

A 150-hour test on diesel fuels was performed on the noble metal doped hexaaluminate catalyst to assess stability as a function of time. Continuous operation of 150 hours on diesel fuel was achieved before the inlet preheat lines clogged with carbon deposits. The diesel fuel compositions examined are given in Table 3. The reaction conditions used were a temperature of 900°C, an O/C = 1.2 and a pressure of 14 psig. The performance results from the experiment are given in Figure 3. From this figure, the catalyst exhibits relatively stable performance on DF #1 for 95 hours. After 95 hours, the fuel was switched to DF #2 for 55 hours where a decline in performance was observed. The change in performance was likely due to the higher concentration of sulfur and aromatic compounds present in DF #2 relative to DF #1. The profile of the reactor contents after the partial oxidation reaction revealed carbon build-up at the leading edge of the bed likely due to dehydrogenation and pyrolysis of inlet feed hydrocarbons.

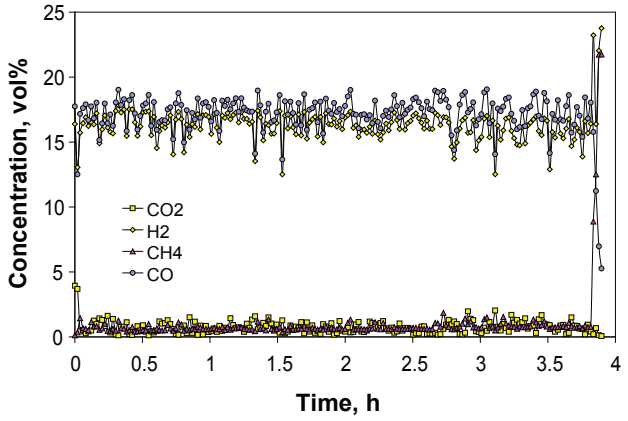

FIGURE 2. Performance of NETL Fuel Atomizer/Reactor and Noble Metal Doped Hexaaluminate Catalyst

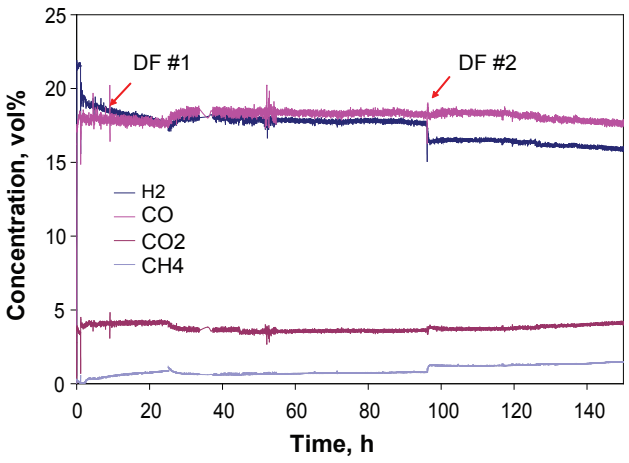

FIGURE 3. 150 Hour Performance Test with Diesel Fuel over a Noble Metal Doped Hexaaluminate Catalyst

Conclusions and Future Directions

EXAFS analysis of the $BaNi_yAl_{12-y}O_{19-\delta}$ catalysts has shown the average Ni-O bond distance to be relatively insensitive to increasing Ni substitution, however increasing Ni substitution decreased Ni-O coordination. Catalyst activity and selectivity was shown to be strongly dependant on the Ni substitution. TPO of the reacted catalysts indicates that carbon deposited onto the surface of the catalysts was directly related to their activity and selectivity. The addition of noble metals to the lattice hexaalumina was effective at producing stability toward deactivation. A 150-hour test with diesel fuel over this catalyst showed good stability.

Future Directions

- Improved catalyst activity and carbon deposition resistance.
- Continue to evaluate the activity and selectivity of platinum group metals doped hexaaluminate catalysts.
- Improved sulfur resistance:
  - Evaluate the effects of high temperature operation on sulfur resistance.

Acknowledgements

EXAFS studies were carried out at LSU's synchrotron facility (Baton Rouge, LA).

Special Recognitions & Awards/Patents Issued

1. "Nano-structured noble metal containing catalysts based on hexametallate architecture for the reforming of hydrocarbon fuels to hydrogen and carbon monoxide and method for making the same," Patent disclosure filed.

FY 2007 Publications/Presentations

1. "Catalytic Partial Oxidation of Hydrocarbon Fuels: Structural Characterization of Ni-Substituted Hexaaluminate Catalysts," *American Chemical Society National Meeting 2007, Division of Fuel Chemistry Preprints,* Boston, MA, August 2007.

2. "Catalytic Partial Oxidation of CH_4 over Ni-Substituted Hexaaluminate Catalysts" *North American Catalysis Society, 20th North American Meeting*, Houston, TX, June 2007.

References

1. Barbier, J.; Marecot, P. J. Catal.102 (1986) 21.

2. Bengaard, H.S.; Norskov, J.K.; Sehested, J.; Clausen, B.S.; Nielsen, L.P.; Molenbroek, A.M.; Rostrup-Nielsen, J.R. J. Catal. 209 (2002) 365.

3. Xu, Z., Zhen, M., Bi, Y. and Zhen, K., Catal. Lett. 64 (2000) 157-161.

4. Gardner, T. H., Shekhawat, D., Berry, D. A., AIChE Fall Meeting, Austin, TX (2004).

5. Rostrup-Nielsen, J. R., Catal. Sci. & Tech., Ed. J. R. Anderson and M. Boudart, Vol. 5, pp. 90-91, Springer-Verlag, NY, 1984.

6. Shekhawat, D., Gardner, T. H., Berry, D. A., Salazar, M., Haynes, D. J., Spivey, J. J., Applied Catalysis A: General 311 (2006) 8.

7. Shamsi, A., Baltrus, J. P., Spivey, J. J., Applied Catalysis A: General 293 (2005) 145.

IV.B.4 Liquid Hydrocarbon Fuel Reforming Studies

Dushyant Shekhawat (Primary Contact), David A. Berry, Todd H. Gardner and Steven A. Mascaro[b]
U.S. Department of Energy
National Energy Technology Laboratory (NETL)
3610 Collins Ferry Road
Morgantown, WV 26507-0880
Phone: (304) 285-4634; Fax: (304) 285-0903
E-mail: Dushyant.Shekhawat@netl.doe.gov
[b]RDS Parsons
3610 Collins Ferry Road
Morgantown, WV 26507-0880

Objectives

- Evaluate the use of plasma energy to reform heavy hydrocarbon fuels (e.g. diesel) into hydrogen-rich synthesis gas for fuel cells for use by high-temperature fuel cells being developed in the Solid State Energy Conversion Alliance (SECA) program.
- Conduct literature survey.
- Assess different liquid fuel introduction/mixing schemes.
- Evaluate effects of operating parameters on reformer quality.
- Complete the reactor setup to use the Drexel Plasma Institute (DPI) Reverse Vortex Plasma Reformer.

Accomplishments

- Design work for the DPI's Reverse Vortex Plasma Reformer is nearly complete with acceptance testing and delivery of the unit from Drexel University in Fall 2007.
- Conducted literature survey of plasma processes relative to plasma reforming. A draft report has been prepared for possible peer-reviewed publication.
- Performed shakedown runs in the catalyst screening unit in order to prepare it for DPI's Reverse Vortex Plasma Reformer. Successfully evaluated an ultrasonic nozzle for the liquid fuel introduction into the reactor. Also, studied several reactor configurations for diesel reforming.

Introduction

The successful deployment of fuel cell technology for many market applications requires the use of hydrocarbon-based fuels. The U.S. Department of Energy is sponsoring development of high temperature fuel cell power systems based on solid oxide technology through its SECA program. The fuel processor is a critical component of these systems and must be able to provide a clean, tailored hydrogen-rich synthesis gas to the fuel cell stack for long-term operation. There are a number of barrier issues that must be overcome in using hydrocarbon fuels. Carbon formation, both during startup and long-term operation, must be minimized to avoid coking of the catalysts in the reformer and downstream fuel cell. Also, most fuels contain some level of sulfur that can poison both the reforming catalysts and the fuel cell anode. Much of the technology development thus far has focused on catalytic systems. Although widely used in high steam commercial processes, most known catalytic-only systems are not capable of sustained reforming operation in low steam concentration (dry) reforming conditions. Oxide-based catalysts show some promise, but are unproven to at this point.

The use of non-catalytic processes such as plasma or thermal reforming needs to be evaluated and considered. Catalytic processes also may be enhanced by use of alternative approaches. For example, it may be possible to pre-treat the fuel in such a way as to saturate the aromatic and double-bonded carbons that are thought to be predominately responsible for carbon formation. In addition, alternative reactor materials, configurations, and schemes may play a significant role in resolving the carbon deposition issues surrounding these reformers. NETL will evaluate internally-generated ideas/concepts as well as selected external efforts.

Approach

Novel approaches or concepts are necessary for the development of robust fuel processors for the fuel cell systems. The use of non-catalytic process such as plasma reforming needs to be evaluated and considered. Low temperature non-thermal plasma can be a viable alternate to catalytic processes because of the absence of any catalyst that can be deactivated in the presence of highly complex diesel-like fuels. There are several articles in the open literature using plasma techniques to reform a simple hydrocarbon such as methane. However, technical as well as economic viability of the reforming of higher hydrocarbons such

as diesel using plasma has yet to be established. Also, a series of different kinds of plasma techniques using different plasma discharge mechanisms are being used for reforming: corona, gliding arc, dielectric barrier, radio frequency and microwaves. Each of them has its advantages as well as disadvantages. However, we will explore the reverse vortex plasma reformer (uses a gliding arc discharge) for the reforming of hydrocarbon fuels such as diesel. This novel type of reactor design has a plasma discharge that is created and contained within a vortical counter-current flow-field. This reformer will be supplied by DPI of Drexel University, Philadelphia, PA.

This plasma reactor is designed to operate at a pressure of 15 psig and utilizes partial oxidation or steam reforming of methane or diesel fuel at different oxygen-to-carbon ratios. Figure 1 gives a general idea of how the central core of the plasma reformer works as well as the locations of the input/output streams.

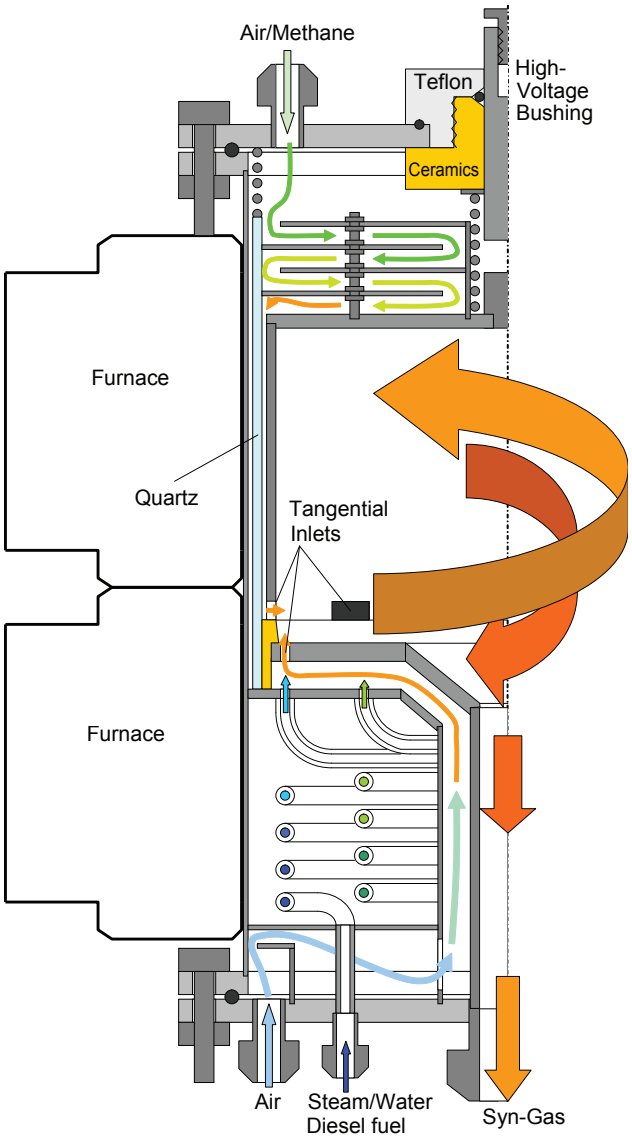

Figure 1. Overview of Plasma Reformer

Results

Recently, in a research project supported by ChevronTexaco, DPI developed and patented plasma technology for methane conversion into syngas [1-3]. A special plasma system, gliding arc in tornado (GAT) reactor was developed for this technology [1-3]. Non-equilibrium plasma generated in the gliding arc has demonstrated the potential of combining the advantages of both thermal and non-thermal plasmas in optimized regimes. GAT is a source of non-equilibrium plasma for plasma-catalytic process of partial oxidation. This means that energy for chemical conversion is taken mostly from the process itself, and only a small portion (about 2%) is supplied by the plasma. The GAT system is especially promising for liquid fuel conversion, as the reverse vortex flow that stabilizes the plasma has a natural place for a second flow injection (for example, diesel fuel). According to the available information, absence of such place in conventional vortex reactors and resulting fuel coking are major reasons for significant delay in commercialization of the technology developed elsewhere.

The reaction vessel and lid of the plasma reformer are being designed to include an external window (in the top flange) which will allow us to view the interior of the plasma reformer. Two windows into the reactor, one on the reactor lid and the other window to be located on the top flange, will provide a view of the state of the discharge and location of reaction the flame. Both windows can be aligned so that it would be possible to see straight down into the reaction vessel when looking from the top of the vessel. This will provide an optical access into the plasma reformer for the plasma characterization measurements such as electron distribution and plasma density.

DPI has conducted some shakedown runs using methane as a fuel at partial oxidation conditions. Photos in Figure 2 are the view of plasma from top down into the reactor: (1) arc elongation and (2) gliding arc zoom. The plasma reformer is expected to be delivered to NETL in Fall of 2007.

Conclusions

Plasma technology provides an interesting and possible alternative for either full or assisted fuel reforming. A facility and reactor system has been established at NETL to allow for parametric evaluation of plasma processes with the DPI unit and/or other plasma developments efforts being undertaken to provide suitable hydrocarbon reforming for fuel cell based systems.

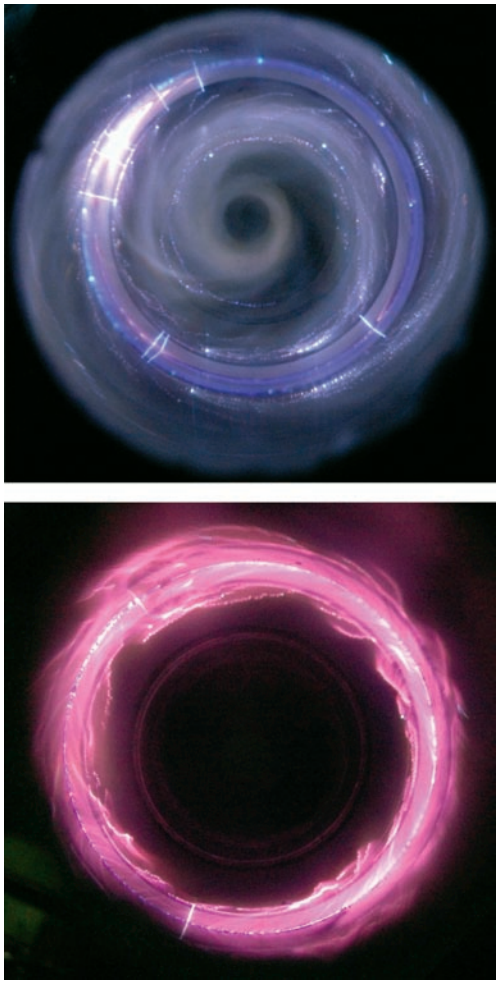

FIGURE 2. View of Plasma from Top Down into the Reactor: (1) Arc Elongation (2) Gliding Arc Zoom

FY 2007 Publications/Presentations

1. D. Shekhawat, D. A. Berry, T. H. Gardner, D. J. Haynes, J. J. Spivey, Effects of fuel cell anode recycle on catalytic fuel reforming, J Power Sources 168 (2007) 477–483.

References

1. C. S. Kalra, Y. I. Cho, A. Gutsol, A. Fridman, T. S. Rufael, V. A. Deshpande, Plasma Catalytic Conversion of Methane in Ultra Rich Flame Using Transient Gliding Arc Combustion Support, Electronic Proceedings of 2004 Technical Meeting, Central States Section, The Combustion Institute, 21–23 March 2004, University of Texas at Austin, Texas.

2. C S Kalra, Y. I. Cho, A Gutsol, A. Fridman, T. S. Rufael, Gliding Arc in Tornado Using a Reverse Vortex Flow, Review of Scientific Instruments 76, 025110 (2005).

3. C. S. Kalra, Y. I. Cho, A. F. Gutsol, A. Fridman, Gliding Arc Discharges as a Source of Intermediate Plasma for Methane Partial Oxidation, IEEE Transactions on Plasma Science, Vol. 33, No. 1, February 2005.

IV.B.5 Facility Development for Fuel Reforming R&D

Dushyant Shekhawat,
David A. Berry (Primary Contact)
and Todd H. Gardner
U.S. Department of Energy
National Energy Technology Laboratory (NETL)
3610 Collins Ferry Road
Morgantown, WV 26507-0880
Phone: (304) 285-4430; Fax: (304) 285-0903
E-mail: David.Berry@netl.doe.gov

Objectives

- Develop a capability for test evaluation of 1-30 kW (thermal) endothermic or exothermic reformer technologies being considered in the NETL Solid State Energy Conversion Alliance (SECA) fuel cell development project. The test stand will be capable of a variety of fuel types (coal-derived fuels, diesel, jet fuels, gasoline, natural gas, etc.) and be capable of variable gas compositions to simulate anode recycle along with other system schemes.
- Modify an existing test rig (catalyst screening unit [CSU]) for multipurpose use in evaluating advanced fuel reforming concepts such as plasma-assisted reforming at a multi-hundred watt scale as technologies progress beyond laboratory scale development.

Accomplishments

- Completed the construction of a test stand capable of evaluating 1-30 kW (thermal) reformers on a continuous 24/7 basis on a variety of gaseous and liquid hydrocarbon fuels.
- Modified a smaller scale test rig to make it flexible to adapt to evaluate any new reforming technique such as plasma reforming, reactor configurations, etc.

Introduction

The U.S. Department of Energy's SECA program is sponsoring the development of high-temperature fuel cell power systems based on solid oxide technology. Many of the market applications for mass manufactured, high volume fuel cells rely on the use of hydrocarbon fuels. Several key characteristics desired for the processor (and the system) include; low cost, high efficiency, maximum thermal integration, low maintenance intervals, and acceptable startup and transient response. In addition, there are also several barrier issues that must be overcome to achieve these characteristics, which are generally applicable to all hydrocarbon fuels (gaseous, liquid, coal-based). Development and demonstration of this critical fuel processing technology is vital for the overall success and commercialization of the fuel cell technology. Therefore, the NETL's fuel processing facilities were established to explore fundamental and applied reforming research and development (R&D) issues that are inherent in catalytic and non-catalytic unit operations present in fuel cell power plants. These issues include: reaction kinetics, development of fundamental reforming activity and selectivity scales, mapping reforming catalyst coking regimes, understanding the mechanism of poisoning, improving sulfur and carbon tolerance of catalytic materials and identifying/developing novel processes that are more resistant to typical degradations. This report discusses the NETL fuel processing facilities in detail.

Approach

By providing a means to evaluate fundamental and applied fuel processing issues, the fuel reforming facility will aid the SECA program to meet its goal of developing cost-effective fuel processors for high temperature fuel cell systems based on solid oxide technology. Prototype reformer test capability (up to 30 kW thermal) will be provided by a new fuel processing unit (FPU) test facility in FY 2007. Technology evaluation/development beyond the laboratory-scale will be provided by modification of an existing facility (the CSU).

Results

The fuel reforming facilities are comprised of four bench-scale reactor systems, two reforming test rigs (catalyst screening unit and fuel processing unit), one Micrometrics catalyst characterization unit, and state-of-the-art analytical capabilities. These facilities were designed as fuel flexible such that natural gas, alcohols, coal-derived fuels, Fischer-Tropsch fuels, diesel, automotive gasoline and their surrogates may be utilized as feedstock.

Bench-Scale Reactor Systems

- Four identical high temperature and high pressure fixed-bed reactor systems. (A schematic of these reactor systems is given in Figure 1.) Two of the reactor systems are designed to operate 24/7 with

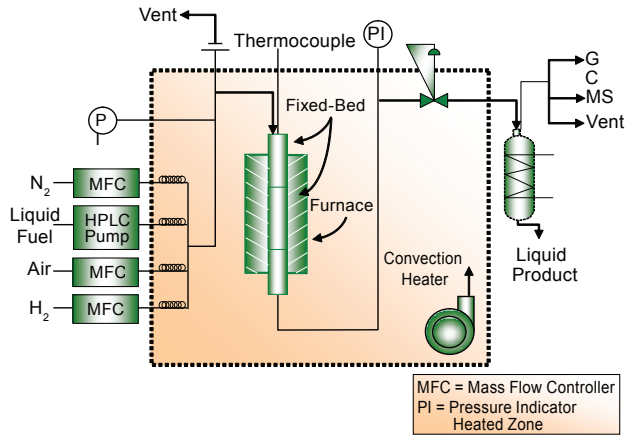

FIGURE 1. Schematic of Bench-Scale Reactors

FIGURE 2. Fuel Processing Laboratory with Twin-performance Reactors, Online Mass Spectrometer and GCs

unattended operation. Figure 2 shows two bench scale reactor systems with online mass spectrometer and gas chromatographs (GCs).

- Capability to run in different reforming modes such as autothermal reforming, partial oxidation, steam reforming and hydrodesulfurization of hydrocarbon compounds and the temperature programmed oxidation and reduction of catalyst samples.
- Reactor outlet streams are analyzed for the permanent gases as well as C1-C7 hydrocarbons using an online mass spectrometer and online gas chromatograph, respectively.

Reforming Test Rigs

- Capability to run in different reforming modes such as autothermal reforming, partial oxidation, steam reforming and hydrodesulfurization of hydrocarbon compounds and the temperature programmed oxidation and reduction of catalyst samples.

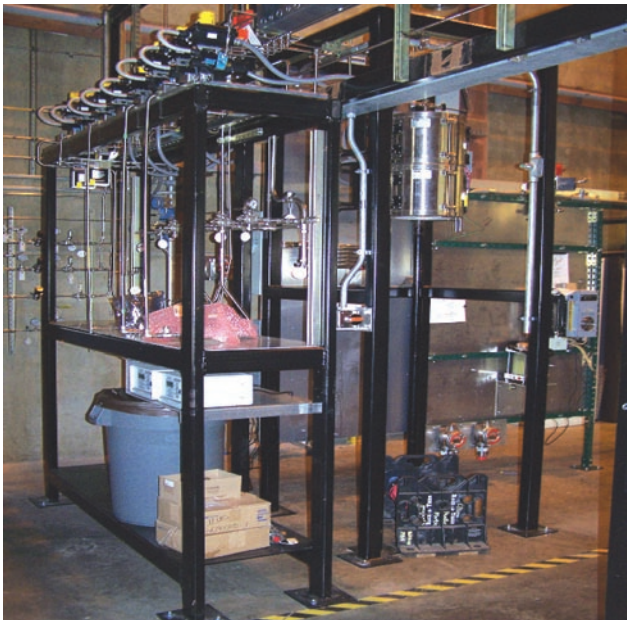

FIGURE 3. Fuel Processing Unit: A Test Stand Capable of Testing 10-28 kW Reformers

- Reactor outlet streams are analyzed for the permanent gases as well as C1-C7 hydrocarbons using an online mass spectrometer and online gas chromatograph, respectively.
- The CSU is a multipurpose and versatile research facility and can easily be modified for evaluating the advanced concepts for fuel reforming such as plasma-assisted reforming, temperature profiling of the catalyst bed during exothermic or endothermic reactions. The facility is rated in the multi-hundred kW range.
- The FPU has been designed and constructed for the purpose of testing 1-30 kW fuel processors developed by the NETL sponsored developers, such as those in the SECA program. The FPU may also be used during collaborations with other industrial developers through Cooperative Research and Development Agreements and is designed for 24/7 unattended operation. Figure 3 shows a side view of the FPU.

Catalyst Characterization Unit

- This unit performs N_2 Brunauer-Emmett-Teller surface area analyses, temperature programmed reduction, temperature programmed oxidation, temperature programmed desorption, surface titrations, and chemisorption experiments.
- Effluent gas can be analyzed using an online mass spectrometer.

Analytical Tools

- Fourier transform infrared spectroscopy and FT-Raman coupled.
- X-ray diffraction equipment.
- Scanning electron microscope.
- Inductively coupled plasma for catalyst composition analysis.
- Mass Spectrometer couple with gas chromatograph (flame ionization detector) (for $< C_{20}$ liquid hydrocarbon analysis).

Conclusions and Future Directions

An array of test and characterization facilities is required to properly evaluate and develop adequate fuel reforming technology. The fuel reforming facilities/capabilities at NETL are well-suited to accomplish the necessary R&D at various scales/stages needed to demonstrate commercial readiness and technology transfer. External developers and collaborators are encouraged to utilize the facilities to the extent possible to accomplish the goals of the program.

IV.B.6 Modification of Nickel-YSZ Anodes for Control of Activity and Stability from Carbon Formation during SOFC Operation

David L. King (Primary Contact) and James J. Strohm
Pacific Northwest National Laboratory
PO Box 999
Richland, WA 99352
Phone: (509) 375-3908; Fax: (509) 375-2186
E-mail: david.king@pnl.gov

DOE Project Manager: Travis Shultz
Phone: (304) 285-1370
E-mail: Travis.Shultz@netl.doe.gov

Objectives

- Quantify and evaluate microstructural evolution as a function of time and pretreatment conditions. Correlate the catalytic activity with Ni microstructure.
- Develop methods to adjust and control Ni-YSZ anode activity to provide good thermal management and efficiency for methane on-anode reforming.
- Determine the activity and thermal profile of Ni-YSZ anode wafers under steam methane reforming and compare results with previous powder test results and computational modeling calculations.
- Determine what factors and conditions influence NiO solubility into yttria-stabilized zirconia (YSZ) and formation of Ni crystallites from the NiO/YSZ solution.

Approach

- Complete construction and installation of plate reactor system.
- Measure thermal profiles and conversion levels over a Ni-YSZ anode plate, under open circuit conditions, i.e., in the absence of electrochemistry.
- Carry out supporting work in catalytic micro-reactor powder testing.
- Utilize surface area measurements, X-ray diffraction, transmission electron microscopy (TEM) and scanning electron microscopy (SEM) microscopy to characterize catalysts before and after reforming.
- Develop understanding of Ni dissolution into/exolution from YSZ.

Accomplishments

- Brought on-line anode plate reactor and measured activity and thermal profiles of Ni-YSZ anode wafers with time at 700°C and 750°C.
- Demonstrated leading edge to back edge migration of endotherm in plate reactor tests, consistent with Ni microstructural sintering, and showed that the magnitude of the endotherm migration decreases as it migrates down the cell.
- Demonstrated that the Ni anode, following initial activity lineout, is sufficient to fully convert methane, but insufficient to generate an endotherm that would lead to destructive thermal gradients during long-term operation.
- Brought on line, and utilized, new powder testing capability to support activity evolution and plate reactor studies of Ni-YSZ anodes.
- Designed, and implemented, a multi-tubular reactor to study effects of steam and hydrogen treatment on evolution of Ni microstructure; obtained and tabulated initial sintering data.
- Identified possible role of NiO dissolution in YSZ on enhancing the presence of the ZrO_2 monoclinic phase.

Introduction

During FY 2007, the Solid State Energy Conversion Alliance (SECA) Core Technology Program in Fuel Reforming at Pacific Northwest National Laboratory (PNNL) moved to completion of its work on Ni/YSZ internal reforming of methane. A major focus was to carry out plate reactor tests and analyze the test results. The focus of this work was on anode activity and activity maintenance, to determine their effect on the magnitude and positioning of any endotherm encountered on the anode. This is of interest because it is believed to be necessary to bring the reforming activity into balance with electrochemical (H_2 and CO oxidation) activity, in order to avoid excessive and damaging thermal gradients, along the anode during reformation.

The activity of the anode toward methane reforming depends substantially on the nickel microstructure that develops. We reported previously that NiO dissolves into YSZ and exolves during the reduction procedure, generating small Ni crystallites at the surface of YSZ. These small crystallites generate high initial catalyst activity, but activity declines as these crystallites sinter.

In our current work, we are investigating the effect of pretreatment procedures and conditions on development of the Ni microstructure, and have seen important differences, depending upon pretreatment. Thus, pretreatment can provide a method to control anode activity, which may be important in operating the overall fuel cell.

Approach

Our approach has been to measure thermal profiles and conversion levels over a Ni-YSZ anode plate under open circuit conditions, i.e., in the absence of electrochemistry. A plate reactor was constructed and described (had not been used) in the previous annual report. In FY 2007, the reactor was brought on line, and several experiments were carried out, under a variety of conditions. Temperatures were measured at various positions on the anode wafer as a function of time, to obtain an estimate of the extent of endotherms and possible thermal gradients. Methane conversion was measured simultaneously to verify that anode activity was sufficient to assure that no unconverted methane could exit the anode compartment of the fuel cell.

In addition to the plate reactor tests, supporting work was carried out through catalytic micro-reactor powder testing, surface area measurements via chemisorption, X-ray diffraction, TEM and SEM, and other methods. These data were used to gain a better understanding of Ni exolution from YSZ, and the fate of the exolved Ni by either sintering or other interaction with the YSZ.

Results

Ni-YSZ Anode Plate Tests

A first catalytic test was carried out for approximately 130 hours, operating the plate reactor at a nominal temperature of 700°C. The conditions of the test were: S/C/H (steam/methane/hydrogen) = 3/1/2; weight hourly space velocity (WHSV) $gCH_4/gNi\text{-}YSZ\text{-}h$ = 0.8; wafer dimensions 10 cm (length) x 5 cm (width) x 0.45 mm (thickness). During the test, temperatures were monitored by thermocouples placed at various locations along the flow axis. Figure 1 provides a visual summary of the thermal profile during the test at the different distances from the front edge of the wafer. There is a sharp endotherm produced immediately at the front edge of the cell and at 2 mm from the leading edge. This indicates that the majority of the reforming is carried out at the leading edge. With time, however, the temperature at those locations increases and a temperature lowering is observed, at progressive distances from the front edge. This behavior is indicative of a "wave" of activity that propagates with time, consistent with progressive sintering of the anode along the flow axis. As the sintering takes place at a given distance from the leading edge, the primary conversion is carried out farther down the anode. We monitored the methane conversion and product distribution during the run, and equilibrium conversion of methane was achieved. However, we were seeing indications that, if the endotherm migration had continued, conversion below equilibrium most likely would have occurred. Post analysis of the anode was carried out to determine Ni surface area. As seen in Table 1 the leading edge had a substantial decrease in Ni surface area, compared with the back edge, indicative of significant sintering occurring at the leading edge.

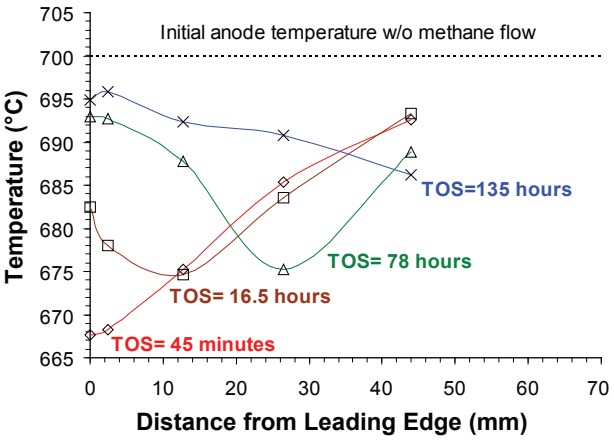

FIGURE 1. Thermal Profile along Anode Wafer as a Function of Time for First Methane Steam Reforming Plate Test at 700°C

TABLE 1. Post analysis of Ni-YSZ wafer following 700°C steam reforming test, indicating significant Ni particle sintering at the leading edge.

	H^2 Uptake (umol/g)	Surface Area $m^2Ni/gcat$	Surface Area $m^2Ni/gcat$	Particle Size (nm)	Active Ni (umol/g)
Leading Edge	1.1	0.086	0.194	3481	2.2
Back Edge	2.7	0.211	0.475	1418	5.4

A second reforming plate reactor test was carried out, this time at 750°C, S/C/H = 3/1/4 and WHSV = 1.12 g CH_4/gcat-h. The temperature profile measured during this test is provided in Figure 2. There is a clear migration of the endotherm maximum down the flow axis with time, and the extent of the endotherm decreased as it migrated down the flow axis. After approximately 50 hours on stream, we saw evidence of CH_4 conversion decreasing below equilibrium values, indicating that under these conditions the anode was insufficiently active to achieve full conversion after the full sintering of the anode occurred. Post analysis showed some mechanical damage to the front edge of

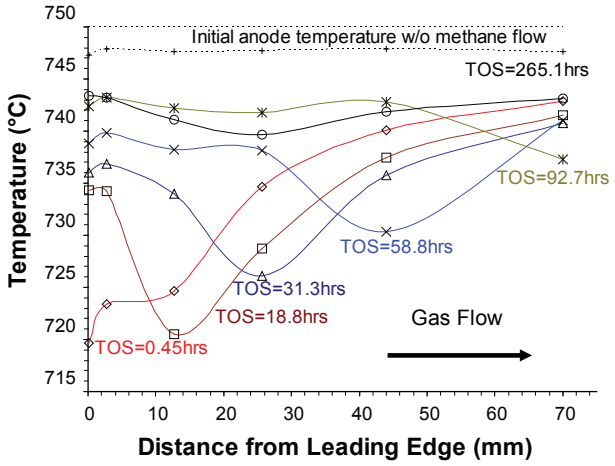

FIGURE 2. Thermal Profile along Anode Wafer as a Function of Time for Second Methane Steam Reforming Plate Test at 750°C

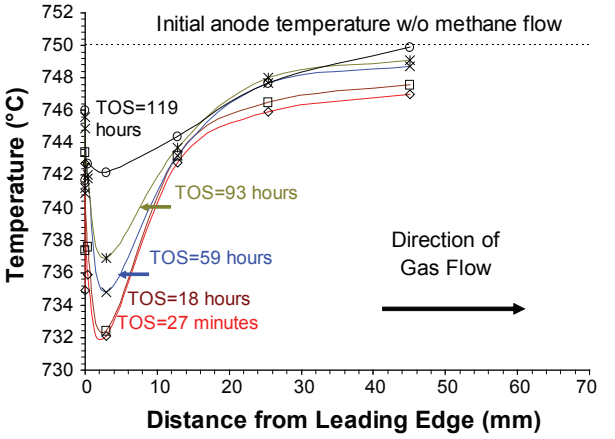

FIGURE 3. Thermal Profile along Anode Wafer as a Function of Time for Third Methane Steam Reforming Plate Test, Also at 750°C

the anode plate because of the rather severe operating conditions. A third run, also carried out at 750°C but at a lower flow rate (more typical of anticipated fuel cell operating conditions) showed very slow migration of the endotherm, although it decreased in intensity with time (Figure 3), and under these conditions we expect full conversion of methane at long reaction times.

Ni Dissolution into and Exolution from YSZ

We previously described the appearance of small Ni crystallites on the surface of YSZ that are generated following a reduction procedure. We have asserted that NiO must be present in the YSZ, possibly because of NiO migration during the sintering procedure (calcination in air at 1,375°C). Supporting evidence and additional information is provided in Figure 4. This shows X-ray diffraction traces of the Ni-YSZ material,

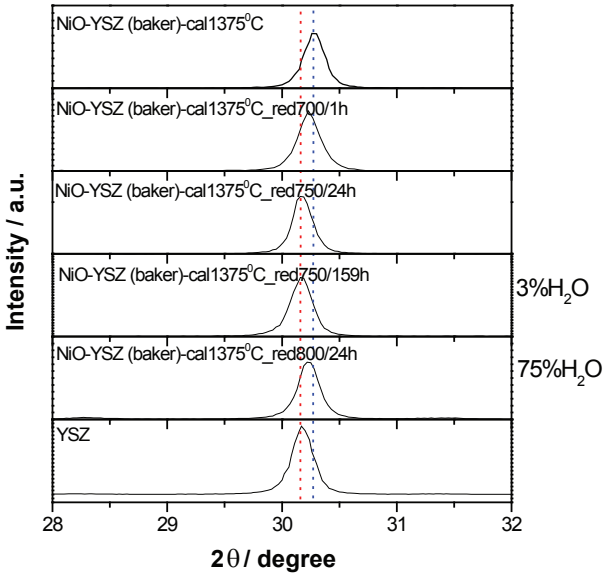

FIGURE 4. X-ray Diffraction Traces of Primary YSZ Peak, Showing Effect of NiO Dissolution into the YSZ Structure and the Effect of Various Pretreatments on Exolution of NiO from the YSZ

following a series of different treatments. The figure focuses on the specific location of a characteristic YSZ line at around 30.15° 2θ. Following sintering, NiO dissolution into YSZ is evidenced by the change in peak location to 30.3°, indicative of a change in lattice spacing caused by NiO. Following reduction in H_2 at 750°C, the peak moves again close to 30.15°, however at 800°C, in high quantities of steam, only partial shift of the peak is observed, indicating that NiO remains in the YSZ. It appears that water vapor plays a role in dictating the ease of reduction and exolution of the Ni from YSZ. Pretreatment, therefore can have a strong effect on Ni-YSZ activity, by modulating the amount of small crystallite Ni available for reaction with CH_4.

Conclusions

Ni-YSZ methane reforming activity is a result of two contributions: the activity from the bulk Ni in the structure, and the activity arising from small Ni crystallites that are contained in the YSZ and migrate to the surface, under reduction pretreatment. Both have been found to sinter during methane steam reforming, the extent a result of several factors, including steam content in the feed and overall flow rate. Our studies have indicated that understanding the pretreatment process allows some flexibility in controlling the anode activity for methane steam reforming. In general, we have found that initial activity of the Ni-YSZ can generate a substantial endotherm and thermal gradients across the anode. However, as the Ni component of the anode undergoes sintering, lined out activity is substantially reduced, and does not appear to be a

danger from strong endotherm, or thermal gradients, under normal operating conditions.

Future Directions

- Evaluate the effect of NiO present within the YSZ on facilitating possible phase changes in the YSZ.
- Begin studies of diesel reforming.

FY 2007 Publications/Presentations

1. Y-H. Chin, D. L. King, H-S. Roh, Y. Wang, and S. M. Heald. Structure and Reactivity Investigations on Supported Bimetallic Au-Ni Catalysts Used for Hydrocarbon Steam Reforming; J. Catalysis 244 (2006) 153-162.

IV.B.7 Sorbents for Desulfurization of Natural Gas and LPG

Gökhan Alptekin
TDA Research, Inc.
12345 W. 52nd Avenue
Wheat Ridge, CO 80033
Phone: (303) 940-2349, Fax: (303) 422-7763
E-mail: galptekin@tda.com

DOE Project Manager: Ayyakkannu Manivannan
Phone: (304) 285-2078
E-mail: Ayyakkannu.Manivannan@netl.doe.gov

Objectives

- Develop a low-cost, high capacity expendable sorbent that can reduce the concentration of organic sulfur species in natural gas and liquified petroleum gas (LPG) to less than ppb levels.
- Develop a regenerable version of the sorbent for large-scale stationary power generation applications.
- Scale-up sorbent production.
- Demonstrate combined operation of the desulfurizer with a solid oxide fuel cell (SOFC).
- Carry out an independent engineering analysis to fully assess the potential of the new desulfurization sorbent.

Approach

- Carry out bench-scale screening tests to identify materials that adsorb organic sulfur species with high capacity.
- Perform parametric experiments with selected sorbents to optimize operating conditions.
- Demonstrate the regeneration potential and long-term durability of the best sorbent through many consecutive adsorption/regeneration cycles.
- Produce larger batches of the new material using high throughput equipment (e.g., spray dryers, screw extruders) representative of commercial production.
- Establish partnerships with SOFC technology developers in the Solid State Energy Conversion Alliance (SECA) to demonstrate the potential of the new desulfurization sorbent in combination with SOFCs.
- Based on the performance results assess the technical and economical impact of the new materials in SOFC-based distributed and stationary power generation systems.

Accomplishments

- TDA developed the SulfaTrap™ sorbent platform for cost-effective desulfurization of different light hydrocarbon streams
  - SulfaTrap™-R3 sorbent, the baseline sorbent material recommended for common natural gas streams could achieve a sulfur capacity greater than 3.12 wt% (lb of sulfur removed per lb of sorbent) provided that the water vapor content of the gas is within the pipeline specifications (7 lb/MMSCF or 154 ppmv).
  - SulfaTrap™-R2 sorbent can treat gas streams with high moisture content (1,000 to 5,000 ppmv H_2O).
  - SulfaTrap™-R5 sorbent is specifically designed for desulfurizing natural gas streams with high concentrations of carbonyl sulfide (COS). The sorbent reduces the COS content to less than 10 ppbv and tolerates the presence of water vapor and CO_2 impurities in the gas.
  - SulfaTrap™-P sorbent is designed for desulfurization of heavier hydrocarbons (LPG or natural gas oil).
- The performance of TDA's SulfaTrap™ sorbents was demonstrated in several field tests at the 1 to 300 kWe range through collaborations with Siemens Power Corporation, Delphi Corporation and FuelCell Energy with successful results.

Future Directions

TDA will identify a commercial partner to scale-up the production of its sorbent well above the current levels (40 kg per batch) to meet the growing demand for its sorbents and to provide a lower cost product.

Introduction

Pipeline natural gas is the fuel of choice for fuel cell-based distributed power generation systems because of its abundant supply and well-developed infrastructure. However, effective utilization of natural gas in fuel cells requires that sulfur impurities (naturally occurring sulfur compounds and sulfur bearing odorants) be removed to prevent them degrading the performance of the fuel cell stacks and poisoning of the catalysts used in the fuel processor. Sulfur removal is important in all types of fuel cells. Even the more sulfur tolerant SOFCs need the sulfur content of the natural gas to be reduced to less

than 0.1 ppmv. TDA is developing a low-cost, high-capacity sorbent that can remove odorants from natural gas and LPG and enable effective utilization of these fuel gases in fuel cells.

Approach

While there are large-scale commercial technologies (e.g., hydrodesulfurization) that can remove organosulfur compounds to levels that fuel cells can tolerate, they are far too complex and expensive for small-scale systems (less than 1 MW). Most of the fuel cell technology developers prefer to remove sulfur from the feed gases using expendable (once-through) sorbents that operate at ambient temperature (a simple addition to the fuel cell fuel processor).

In our work, we first prepared a large number of formulations and carried out bench-scale screening tests to identify materials that adsorb sulfur-bearing odorants with high capacity. We then performed parametric experiments with selected sorbents to optimize the conditions for their operation. We demonstrated the full potential of the new desulfurization sorbents in combination with SOFCs. We scaled-up the sorbent production to be able to provide quantities of samples to support relatively large-scale field trials (up to 300 kW). In the future, we will produce even larger batches of the new material using high throughput equipment (e.g., spray dryers, screw extruders) representative of commercial production. Based on the field performance results, we will assess the technical and economical impact of the new materials in distributed and stationary power generation systems.

Results

We supplied our sorbent to the technology developers in the SECA group to support various demonstrations in combination with the SOFC systems ranging from 1 to 300 kW in size. TDA delivered three 100 kW desulfurizers to Siemens Power Corporation in 2006. Figure 1 shows one of the 100 kW TDA desulfurizer delivered to GTT, Milan, Italy. This particular device, topped with an activated carbon sorbent for COS removal, successfully reduced all the sulfur species to levels tolerable by the SOFC system.

We evaluated the effect of water on the performance of various sorbents. Although the U.S. pipeline natural gas specification requires the water vapor content of the gas reduced below 154 ppmv (~7 lbs of water per million cubic foot of natural gas), in our demonstrations we observed much higher water concentrations (up to 5,000 pmmv) in most of the natural gas used in the demonstration tests. We developed a new sorbent to enhance the water tolerance of our standard sorbent. Figure 2 shows the performance of our SulfaTrap™-R2

FIGURE 1. Pictures of the Two 100 kW TDA Desulfurizers

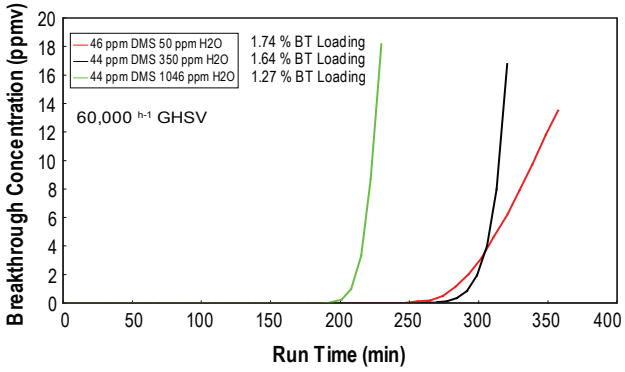

FIGURE 2. The effect of water vapor on the performance of TDA's SulfaTrap™-R2 sorbent at various water vapor concentrations. T= 22°C, P= 5 psig, natural gas with 46 ppmv DMS at 60,000 h^{-1}.

sorbent in natural gas streams with high water vapor content. We used a simulated natural gas with 46 ppmv dimethyl sulfide (DMS); we selected DMS as the sulfur contaminant since it is one of the most difficult to remove organic sulfur species. Our water tolerant sorbent could achieve over 1.27% sulfur capacity on weight basis (lb of sulfur removed per lb of sorbent) even when 1,046 ppmv of water vapor is present in the gas.

Under the SulfaTrap™ sorbent platform, we also developed a sorbent that is effective for the removal of COS. In fact, the sorbent is capable of removing all sulfur species. To maximize its COS capacity it is recommended to be used in combination with our baseline sorbent material, where the SulfaTrap™-R3 and R5 sorbents are placed into the same desulfurizer device in sequential manner, where the former removes all sulfur species with the exception of COS, and the latter removes any COS not captured in the preceding bed. Figure 3 shows the performance of the SulfaTrap™-R5 in comparison with the commercially available adsorbents. In this experiment, we used a simulated natural gas that contains 100 ppbv of COS and 50 ppbv of water vapor. The SulfaTrap™-R5 showed the highest sulfur capacity, while reducing the sulfur level to less than single digit ppb levels (the sulfur detection capability of the analyzer used in this experiment was measured as 4 ppbv). The

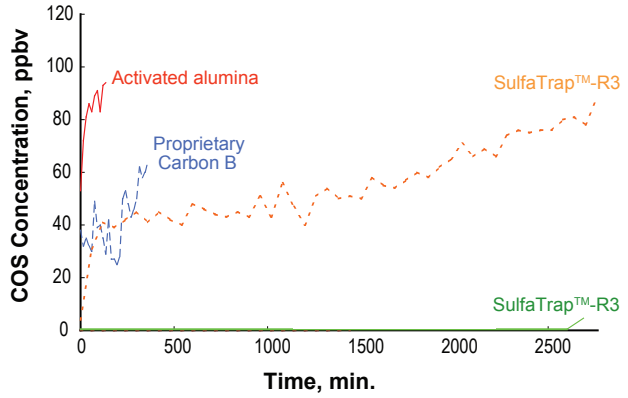

FIGURE 3. COS breakthrough over various commercially available sorbents and SulfaTrap™-R5 sorbent. T= 22°C, P= 5 psig, natural gas with 100 ppbv COS and 50 ppmv H_2O at 6,000 h^{-1}.

FIGURE 4. Picture of Two TDA Desulfurizers using a Mixture of SulfaTrap™-R3 and R5 Sorbents

R5 sorbent could achieve 0.78% wt. sulfur capacity for COS. We also showed that the SulfaTrap™-R5 sorbent could also be regenerated by heating the sorbent bed up to 150°C, using a purge gas of clean humidified natural gas without any signs of degradation in a three-cycle test.

We supplied a number of desulfurizers to Delphi Corporation using a mixture of the two sorbents (Figure 4). These desulfurizers were used as guard beds to support Delphi's SOFC tests using pipeline gas. TDA desulfurizers successfully reduced the sulfur content of the gas, which contained fair quantities of COS to the desired levels.

To meet the growing demand for its sorbents, TDA invested in a small-scale in-house production facility with a capability of supplying finished products at a rate of 200 lb/month.

Conclusions

Low-cost, high capacity, regenerable sorbents were developed for removing sulfur compounds from natural gas at ambient temperature to sub-ppm levels. The sorbent performance was demonstrated not only in bench-scale tests but also in various field trails in combination with the SOFC power generation systems.

FY 2007 Publications/Presentations

1. "Sorbents for Desulfurization of Natural Gas and LPG", G. Alptekin, Presented at the Annual SECA Workshop and Peer Review Meeting, Philadelphia, PA, 2006.

2. "Sorbents for Desulfurization of Hydrocarbons", G. Alptekin, Presented at the Fuel Cell Seminar, Honolulu, HI, 2006.

IV.B.8 Hybrid Experimental/Theoretical Approach Aimed at the Development of Carbon Tolerant Alloy Catalyst

Eranda Nikolla, Johannes Schwank and Suljo Linic (Primary Contact)
University of Michigan
2300 Hayward Street
Ann Arbor, MI 48409
Phone: (734) 764-7469
E-mail: linic@umich.edu

DOE Project Manager: Ayyakkannu Manivannan
Phone: (304) 285-2078
E-mail: Ayyakkannu.Manivannan@netl.doe.gov

Objectives

- Utilize quantum density functional theory (DFT) calculations and various state-of-the-art experimental tools to identify carbon-tolerant hydrocarbon reforming catalysts and solid oxide fuel cell (SOFC) anodes.
- Test the potential carbon-tolerant catalysts in steam reforming of various fuels.
- Implement these catalysts as SOFC anodes.
- Utilize various tools of spectroscopy and microscopy to characterize the tested catalysts.

Accomplishments

- In our first principles DFT calculation, we have established that the carbon-tolerance of Ni can be improved by formulated Ni-containing surface alloys that, compared to Ni, preferentially oxidize C atoms rather than form C-C bonds and/or that have lower thermodynamic driving force associated with carbon nucleation on the low-coordinated sites.
- Based on the molecular insights, we have identified a number of surface alloys that satisfy the above described criteria.
- We have tested these surface alloys in steam reforming of various hydrocarbon fuels.
- We have also utilized the surface alloy as a SOFC anode catalyst.

Introduction

The development of clean, efficient, and environmentally friendly energy generation systems will require major advances in catalysis. Among others, improved hydrocarbon reforming catalysts and electro-catalysts need to be formulated and synthesized. These catalysts need to perform the desired reactions with utmost efficiencies, at reduced costs, and with improved durability.

One of the main issues associated with the catalytic and electro-catalytic reforming of hydrocarbon fuels is that current catalysts, such as Ni supported on oxides, deactivate due to the formation of carbon deposits formed in the process of hydrocarbon activation. In this document we describe a hybrid experimental/theoretical effort aimed towards a bottom-up, knowledge-based formulation of carbon-tolerant reforming alloy catalysts that can be used as potential anode electro-catalysts for SOFCs.

Our objective was to utilize quantum DFT calculations and various state-of-the-art experimental tools to study the factors that govern the stability of Ni-based reforming catalysts. We demonstrate that monometallic Ni deactivates due to the high rates of C-C bond formation and the high thermodynamic driving force associated with the nucleation and growth of extended sp2 carbon structures. We have identified Ni surface alloys as potential carbon tolerant catalysts [1-3]. The utility of these catalysts was demonstrated in multiple reactor tests in the reforming of various fuels.

Approach

We have employed quantum DFT calculations as well as catalyst synthesis, testing, and characterization studies to identify carbon-tolerant alloy catalysts.

DFT calculations allow us to obtain, from first principle and with high accuracy, the ground state geometries and energies of relevant reactants, products, and transition states involved in elementary chemical reactions on catalyst surfaces [4]. Reactor experiments and various characterization techniques were applied to test the predictions of DFT calculations. The alloy catalysts were also tested as potential SOFC anodes.

Results

A critical issue with catalytic hydrocarbon reforming and on-cell reforming in SOFCs is that traditional catalysts, such as Ni supported on oxides, facilitate the formation of extended carbon deposits which deactivate the catalyst or electro-catalyst, see Figure 1a. The formation of carbon deposits can be partially suppressed by an introduction of steam (steam reforming). This approach is problematic for SOFCs since (i) the

presence of steam results in low power densities, (ii) significant energy is required to heat the steam to the desired temperature, and (iii) the storage of steam requires additional cell components, making the cell design more complex. It is imperative to design carbon-tolerant reforming electro-catalysts that can operate with minimal steam concentrations.

The elementary-step mechanism for hydrocarbon reforming on Ni involves the hydrocarbon activation and fragmentation into H and C adsorbates. The strongly bound carbon atoms or fragments are removed from the Ni surface in C-oxidation reactions yielding adsorbed CO, which further reacts in the water-gas shift reaction to form gas-phase CO_2. The oxidizing agents, O and OH, are formed on the catalyst surface in the process of steam activation. In addition to reacting to form CO and CO_2, the C atoms and fragments also react with each other to form extended sp2 carbon networks such as graphene sheets or nanotubes. It has been shown that the extended carbon deposits nucleate at low-coordinated sites on Ni [5]. The formation of extended carbon networks leads to the loss of catalyst activity. Figure 1b shows the DFT-calculated reaction energies for various elementary steps involved in methane steam reforming on Ni(111). The calculations in Figure 1b support the mechanism discussed above.

Figure 1b also suggests that the catalyst lifetime can be prolonged by formulating catalysts that (i) preferentially oxidize C atoms rather than from C-C bonds or (ii) suppress the nucleation and growth of carbon deposits. We have utilized the above discussed molecular mechanistic information to identify Ni-containing surface alloy catalysts that are promising carbon-tolerant alternatives to monometallic Ni [1-3]. For example, our quantum DFT calculations have shown that a small amount of Sn alloyed into the Ni surface layer enhances the rates of C-oxidation compared to the rate of C-C bond formation [1,2]. In addition, our DFT studies also showed that the nucleation of carbon deposits can also be suppressed with the introduction of Sn [3]. This is illustrated in Figure 2b which shows the calculated adsorption energies for various carbon nucleation centers on low-coordinated step sites of Ni and Sn/Ni. The calculated adsorption energies are a measure of the thermodynamic driving force to form these structures on the catalyst surface. Figure 2a shows that the driving force to nucleate the carbon centers on Ni is significantly larger than the driving force on Sn/Ni. For example, the DFT calculated adsorption energies for a C_8 carbon cluster (8 sp2 carbon atoms) and a graphene chain on Ni(211) are by 0.23 eV and 0.15 eV per carbon atom respectively more exothermic than for Sn/Ni(211), see Figure 2a. The reason for the Sn-induced change in the thermodynamic driving force to form the carbon nucleation centers is that Sn disrupts the connectivity of the low-coordinated Ni sites which bind carbon very strongly.

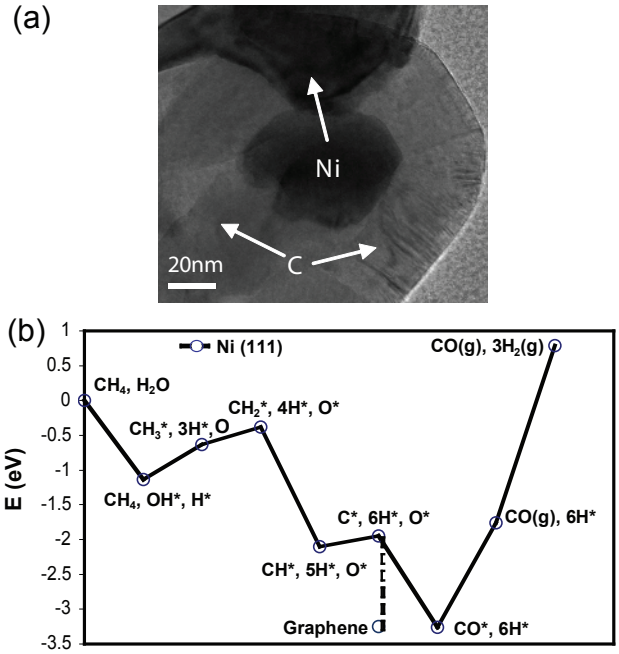

FIGURE 1. a) Transmission electron micrographs of the Ni particles covered by carbon deposits. The carbon deposits are formed in the process of propane steam reforming at 1,073 K and a steam-to-carbon ratio of 1.5. b) Reaction energies for various elementary steps in steam reforming of methane on Ni(111).

In addition to the investigation of the chemistry of carbon on Ni and Ni alloys described above, we have also utilized DFT calculations to asses the thermodynamic stability of Sn/Ni surface alloys [3]. In these studies, we have calculated the formation energies of various Sn/Ni structures including: (i) Sn/Ni surface alloys, (ii) Sn/Ni bulk alloys, (iii) Sn adsorbed on Ni substrate, and (iv) separated Sn and Ni. The calculated formation energies are shown in Figure 2b. Figure 2b demonstrates that Sn/Ni surface alloys have the lowest formation energies out of all examined structures and that the surface alloys should be stable under typical reforming conditions.

To test the predictions of the DFT calculations, we have synthesized and characterized Sn/Ni alloys. Various characterization techniques including scanning electron microscopy (STEM), electron energy loss spectroscopy (EELS), X-ray photoelectron spectroscopy (XPS), and temperature programmed reduction (TPR) demonstrated that the synthesized material was the Sn/Ni surface alloy [3]. The performance of the alloy catalysts was examined in a reactor setup in steam reforming of methane, propane, and iso-octane at moderate steam-to-carbon ratios (between 1 and 2). In all experiments, the Sn/Ni catalyst shows no significant deactivation while the Ni catalyst deactivated rapidly. The characterization studies on used catalysts (SEM, transmission electron microscopy [TEM], X-ray

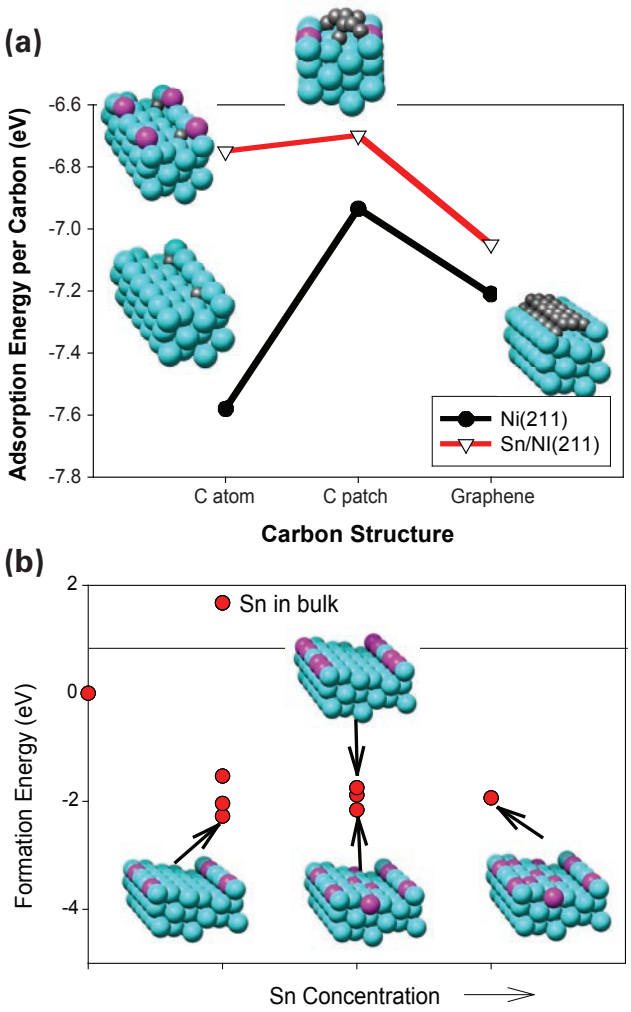

FIGURE 2. a) The DFT calculated adsorption energies per carbon atom for a C atom, C_8 cluster, and a graphene chain adsorbed on Ni(211) and Sn/Ni(211). The surface alloy is characterized by replacing every third Ni atom on the edge by the Sn atoms. b) Formation energy for various Sn/Ni configurations is plotted as a function of Sn concentration. The structure with the lowest energy is the thermodynamically most stable structure for a given Sn concentration.

photoelectron spectroscopy [XPS] and X-ray diffraction [XRD]) showed no signs of carbon formation on Sn/Ni. On the other hand, the Ni catalysts were completely poisoned by graphitic carbon deposits.

We have also implemented the Sn/Ni surface alloy catalyst as a SOFC anode electro-catalyst for on-cell utilization of hydrocarbons. The anode was composed of a mixture of the Sn/Ni catalyst and YSZ. The electrolyte was made of a thin layer (~20 microns) of YSZ and the cathode was composed of a mixture of LSM and YSZ. Our preliminary results indicate that when isooctane is used as a fuel, the Ni/YSZ/LSM SOFC degrades significantly over time due to carbon poisoning which leads to the cell fractures. On the other hand, the Sn/Ni/YSZ/LSM SOFC shows a higher resistance to carbon than the Ni SOFC under identical conditions. One issue worth mentioning is that the formation of carbon deposits in gas-phase (before the fuel comes in contact with the anode) presented a problem for the life span of both the Sn/Ni and Ni electrocatalysts. The formation of these carbon deposits over time puts a significant strain on the seal. The strain results in the fuel cell damage. For example, in the case of the Sn/Ni surface alloy anode, the triple phase boundary was free of carbon, as demonstrated by the elemental mapping of the interface, but the large carbon deposits on the wall of the cell-reactor resulted in the failure of the seal over time.

Conclusions and Future Directions

- We have utilized DFT quantum calculations to develop molecular insights into the mechanism of carbon poisoning of Ni.
- We have determined that the long-term stability of reforming electro-catalysts is governed by their capacity to (1) selectively oxidize carbon atoms, while preventing the formation of C-C bonds and (2) suppress the C nucleation on the low coordinated catalyst sites.
- DFT studies demonstrated that Sn/Ni favored the C-oxidation reaction over C–C bond formation and hindered the nucleation of carbon at the low coordinated sites.
- The reactor studies showed that the Sn/Ni catalyst was more stable than monometallic Ni in steam reforming of various hydrocarbons at moderate steam-to-carbon ratios.
- Sn/Ni alloys also showed promising preliminary results as potential anodes for on-cell utilization of hydrocarbons.

Special Recognitions & Awards/Patents Issued

1. Best Paper Presentation, "Experimental/Theoretical Studies Aimed at the Development of Carbon-Tolerant Catalysts", Michigan Catalysis Society Annual Meeting 2006, Dow Chemicals, Midland, MI, May 2006.

2. Best Poster, "Controlling Carbon Chemistry via alloying: Hybrid Experimental/theoretical Approach", University of Michigan Engineering Competition 2006, Ann Arbor, MI, March 2006.

3. Best Poster Award (Eranda Nikolla, fourth year Ph.D. student), Gordon Research Conference on Catalysis, 2006, New Hampshire. (The poster was selected, along with four others, among >100 posters presented by Ph.D. students and postdoctoral fellows.)

FY 2007 Publications/Presentations

1. Nikolla, E. Schwank, J. Linic, S., "Promotion of the Long-Term Stability of Reforming Catalysts by Surface Alloying", Journal of Catalysis, in press.

2. Nikolla, E. Holowinski, A. Schwank, J. Linic, S., "Controlling Carbon Surface Chemistry by Alloying: Carbon Tolerant Reforming Catalyst", *JACS*, 128 (35), 11354–11355, 2006.

3. Nikolla E., Schwank J., Linic. S, "Development of Carbon Tolerant Anodes for Solid Oxide Fuel Cells", North American Catalysis Society Meeting, Houston, TX, May 2007.

4. Linic. S, Nikolla E., "Controlling Carbon Surface Chemistry on Ni by Alloying: Carbon Tolerant Hydrocarbon Reforming Alloy Catalysts", American Chemical Society National Meeting, Chicago, IL, March 2007.

5. Nikolla E., Schwank J., Linic. S., "Controlling Carbon Chemistry by Surface Alloying", AIChE Annual Meeting, San Francisco, CA, November 2006.

6. Nikolla E., Schwank J., Linic S., "Hybrid Theoretical/ Experimental Approach Aimed at the Development of Carbon Tolerant Alloy Catalysts", Gordon Research Conference on Catalysis, New Hampshire, June 2006 (poster).

7. Nikolla E., Schwank J., Linic S., "Experimental/ Theoretical Studies Aimed at Development of Carbon-Tolerant Catalysts", Michigan Catalysis Society Annual Symposium, Midland, MI, May 2006.

References

1. Nikolla, E. Holowinski, A. Schwank, J. Linic, S., "Controlling Carbon Surface Chemistry by Alloying: Carbon Tolerant Reforming Catalyst", *JACS*, 128 (35), 11354-11355, 2006.

2. Nikolla E., Schwank J., Linic S., "Experimental/ Theoretical Approach Aimed at the Development of a Carbon-Tolerant Alloy Catalyst", *Fossil Fuel Cell Program Annual Review*, June 2006.

3. Nikolla, E. Schwank, J. Linic, S., "Promotion of the Long-Term Stability of Reforming Catalysts by Surface Alloying", Journal of Catalysis, in press.

4. B. Hammer, J.K. Nørskov, "Theory of Adsorption and Surface Reactions" in (eds.) R. Lambert and G. Pacchioni, NATO ASI Series E, Kluwer Academic Publishers, Dordrecht 1997.

5. H. S. Bengaard, J. K. Nørskov, J. Sehested B. S. Clausen L. P. Nielsen, A. M. Molenbroek, and J. R. Rostrup-Nielsen, " Steam Reforming and Graphite Formation on Ni Catalysts", Journal of Catalysis, 2002, 209, 365-384.

IV. SECA RESEARCH & DEVELOPMENT

C. Power Electronics

IV.C.1 DC-AC Inverter with Reactive-Power-Management Functionality

John N. Mandalakas (Primary Contact) and David J. Shero
Mesta Electronics Inc.
11020 Parker Drive
North Huntingdon, PA 15642
Phone: (412) 754-3000; Fax: (412) 754-3016
E-mail: john@mesta.com

DOE Project Manager: Donald Collins
Phone: (304) 285-4156
E-mail: Donald.Collins@netl.doe.gov

Objectives

- Determine the operating specifications for the DC-AC inverter.
- Determine optimum power designs to meet the system specifications derived during the first objective.
- Determine the control components and algorithms needed to optimize the performance of the power hardware, maximizing performance and minimizing power losses and other undesirable byproducts.

Accomplishments

- Compiled and analyzed utility grid interconnection specifications.
- Identified and quantified utility grid conditions that would influence the design of the DC-AC inverter. Also prioritized inverter functions with respect to perceived value to the utility.
- An optimum design approach for the multi-function DC-AC inverter was developed.
- Designed and tested a low leakage isolation transformer to be incorporated as part of the 25 kW/kVA energy converter prototype.
- Designed, built, and successfully tested a 25 kW/kVA prototype DC-AC inverter/energy converter which demonstrates the feasibility of a multi-function system capable of providing real power, reactive power, harmonic cancellation and three-phase line balancing to the utility grid.

Introduction

Presently, many electrical power distribution circuits have areas that are supplied with substandard power. Sections of the electrical distribution system are often heavily loaded to the point that voltage regulation and reliability deteriorate. These problems can be reduced, but not substantially eliminated, by increasing the size of components in the distribution circuit. An alternative to increasing the size of the distribution circuits is to add distributed generation throughout the system. Distributed generation units with the capability of injecting real and reactive power into heavily loaded sections of the distribution system can correct this problem. Highly reliable (99.9% minimum availability), cost-effective (less than $100/kW in quantity) energy converters that convert DC power from a generating source such as a fuel cell, along with providing reactive power, are needed for such distributed generation units.

The energy converter is a key element in distributed power generation and correcting problems with existing electrical distribution systems caused by heavy loading along the system. Its high performance, high efficiency, high reliability, and low cost will be very attractive to utilities, alternative energy sources (fuel cells, solar arrays, windmills, etc.) and other businesses that benefit from adding distributed power generation and power correction. Such benefits include improving the quality of power, thus decreasing financial losses caused by poor power quality; and decreasing power transmission losses and costs, without resorting to much more expensive upgrades to distribution components (transmission wires, transformers, sub-stations, etc.). The energy converter's concept and modular design will also allow future higher power systems to be developed that could be applicable for the proposed Department of Energey (DOE) 100+ MW FutureGen power plants.

Approach

Working with a utility consultant, Mesta has worked towards developing an accurate set of specifications for the energy converter. This set of specifications will be used to guide the design process. The first part of the design is to identify major components that will make up the energy converter. At the heart of the energy converter is a DC to AC converter, commonly referred to as an inverter. The inverter converts DC power originally generated by the fuel cell into 3-phase AC power that is synchronous with the voltage on the electrical distribution circuit. The inverter can pull power from the distribution circuit by producing a voltage slightly lower than the distribution circuit voltage. This power is stored in the capacitance across the DC side of the inverter. If the voltage produced by the inverter is slightly out of phase with the distribution circuit voltage, reactive power is transferred between the energy converter and distribution circuit. The converter

can generate either a leading or lagging reactive power, as needed by the system. In a similar manner, the converter can also produce harmonic currents that "cancel" harmonic currents flowing in the distribution circuit.

During Phase I, Mesta uses portions of several Mesta existing product designs to produce a conceptual design for an energy converter. The transformer that interfaces the energy converter with the distribution circuit is also characterized. The control components and algorithms need to be optimized and the performance of the power hardware is studied. Mesta tests portions of the new conceptual design in a lab environment using actual hardware during Phase I of the project.

Results

During Phase I of the project, a 25 kW/kVA prototype energy converter was developed and tested. This prototype added a DC-DC converter, 480 VDC bank of batteries, and a 3-phase transformer to a 480 VAC, 50 amp (43 kVA) inverter. The inverter and most of the controls were part of a 50 amp standard product DPM (power factor correction equipment incorporating active harmonic filtering, linear power factor correction, and line current balancing) manufactured by Mesta Electronics. The DPM's hardware and software controls were altered to incorporate the additional function of power generation simulated by the bank of batteries. A block diagram of the prototype is shown in Figure 1.

Figure 2 shows the energy converter connected to 480 VAC 3-phase power from the utility. The three utility power lines are powering a simulated load. The simulated load draws current that has a representative amount of harmonics, has inductance to represent a lagging linear power factor, and is unbalanced so that different amounts of current are drawn by the load from each phase. The energy converter is controlled to inject currents into the three power lines to effectively cancel these problems caused by the load. The net result is that balanced, sine wave current is provided by the utility. This results in the utility supplying only "in phase" 60 Hz currents. The magnitudes of these currents are less than what the load draws because the power factor that the utility sees is very close to 1.00, whereas the power factor of the load is less than 0.90. The net benefit is that the distribution network supplying the power for this test network has lower losses (due to the need for less current and due to the absence of harmonics in the supplied current). Also, with the elimination of harmonic currents, the voltage waveform distortion seen by this load, and by other equipment fed by this distribution network, is minimized and the voltage regulation is improved.

In addition to these "reactive" current corrections, the DC source allows "simulated generated power" similar to that generated by a fuel cell, etc. to be injected into the distribution network at the same time that these current corrections are occurring. The energy converter converts the DC power to AC power that is then injected into the network. The AC power from the DC source is almost perfectly sinusoidal and in-phase with the voltage. The powerful control capabilities of the energy converter allow this power injection to occur simultaneously with the "reactive" current corrections. Since the real power derived from the DC source and reactive corrections are out of phase with each other, the total current needed is much less than the amount required if two separate systems performed these tasks.

Figure 3 shows data collected with the energy converter performing reactive power correction only. The first line of Figure 3 shows the line-to-line voltages of the three AC line phases and the rms current from the energy converter (DPM_AMPS) for all three phases. The second line shows the line currents from the utility (LINE_AMPS) and currents drawn by the load (LOAD_AMPS). The third line shows the harmonic current distortion as a percentage of total rms current for the line (LINE_THD%) and the load (LOAD_THD%). The fourth line shows the actual total rms current of the harmonics for the line and load. The fifth line shows the kilowatts, kilovars, and power factor of the line and load. The sixth line shows the frequency of the line and the regulated DC voltage of the energy converter (nominally

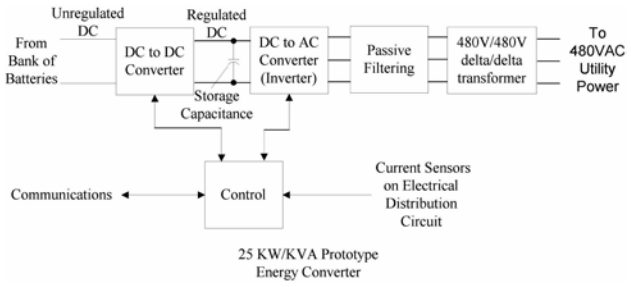

FIGURE 1. 25 kW/kKVA Prototype Energy Converter

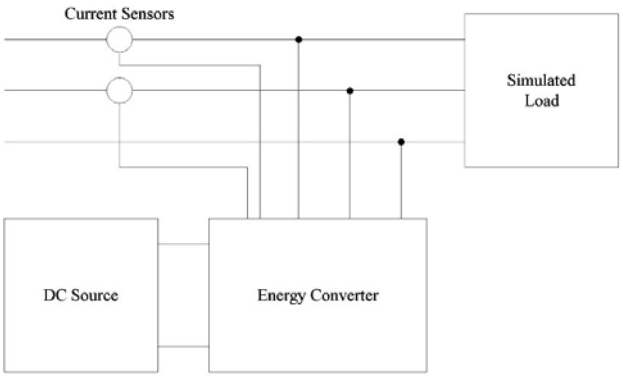

FIGURE 2. Energy Converter Power Test Setup

```
*** MESTA DPM STATUS (04/02/07, 15:52:55) ***

LINE_VOLT AB/BC/CA= 489.3/495.2/490.8   DPM_AMPS  A/ B/ C =  25.6/ 17.0/ 19.8
LINE_AMPS A/ B/ C =  44.7/ 44.1/ 43.7   LOAD_AMPS A/ B/ C =  50.5/ 40.1/ 52.4
LINE_THDR% A/B/ C =   2.1/  1.9/  2.9   LOAD_THDR% A/B/ C =  32.1/ 32.6/ 32.3
LINE_AMPS HARMONIC=   0.9/  0.8/  1.3   LOAD_AMPS HARMONIC=  16.3/ 13.1/ 17.0
LINE_PWR KW/KVA/PF=  37.6/ 37.6/0.999   LOAD_PWR KW/KVA/PF=  36.8/ 40.6/0.904
LINE_FREQUENCY(HZ)=       59.98         DC_VOLT(LO+HI=SUM)= 408.7+410.9=819.7
MODE = ON - INV(S) 1       ENABLED      STATUS = FULLY OPERATIONAL
TEMP PCB/HS1A/HS1B=  25.9/ 26.9/ 27.6   BATTERY V/I/KW    = 501.6/  0.0/  0.0
WREQ/WACT/BATTCHRG=     0/   0/  50%
```

FIGURE 3. Full Reactive Current Correction with No Real Power Component

```
*** MESTA DPM STATUS (04/02/07, 15:59:00) ***

LINE_VOLT AB/BC/CA= 490.9/496.8/492.3   DPM_AMPS  A/ B/ C =  28.8/ 16.9/ 27.2
LINE_AMPS A/ B/ C =  31.3/ 30.8/ 30.3   LOAD_AMPS A/ B/ C =  50.3/ 40.5/ 52.7
LINE_THDR% A/B/ C =   2.7/  3.0/  4.3   LOAD_THDR% A/B/ C =  32.3/ 32.5/ 32.3
LINE_AMPS HARMONIC=   0.9/  0.9/  1.3   LOAD_AMPS HARMONIC=  16.2/ 13.2/ 17.0
LINE_PWR KW/KVA/PF=  26.3/ 26.3/0.999   LOAD_PWR KW/KVA/PF=  36.8/ 40.9/0.901
LINE_FREQUENCY(HZ)=       59.99         DC_VOLT(LO+HI=SUM)= 407.6+410.9=818.6
MODE = ON - INV(S) 1       ENABLED      STATUS = FULLY OPERATIONAL
TEMP PCB/HS1A/HS1B=  26.8/ 33.3/ 38.2   BATTERY V/I/KW    = 447.9/ 25.9/ 11.6
WREQ/WACT/BATTCHRG=    50/  50/   8%
```

FIGURE 4. Full Reactive Current Correction with 11.6 kW of Power Generation

820 volts). The last half of the eighth line shows the battery DC source's voltage (volts), current (amps), and power (kilowatts); where positive current and power indicate that the battery is supplying power and negative values indicate the batteries are being charged by the energy converter. As can be seen in Figure 3, the load currents are unbalanced (50, 40, and 52 amps), the load currents contain substantial harmonics (about 32% each), and the load has a power factor of only about 0.9. On the other hand, the line currents are balanced at about 44 amps each, there is very little harmonic current coming from the utility (only 2-3% of the total current), and the power factor seen by the utility is at 0.999 out of a possible 1.000. The energy converter is making a fairly obnoxious load look like an ideal balanced, purely resistive load to the utility distribution system.

Figure 4 shows data taken under the same conditions as Figure 3 except the DC/DC converter is activated so that 11.6 kW of power is generated to the AC line. The result is that the line amps supplied by the utility drop from about 44 to about 31. Although 11.6 kW would require almost 14 amps of rms current on each phase to be generated by a separate inverter, the energy converter is only outputting slightly higher current on each phase (28.8, 16.9, and 27.2 vs. 25.6, 17.0, and 19.8) than it did when only reactive correction was being performed in the previous case. This illustrates how doing reactive correction and real power generation with the same equipment can be done much more efficiently than using separate pieces of equipment.

In addition to the above referenced work on a prototype energy converter, efforts were coordinated with Mesta's utility consultant, Southern California Edison, to compile detailed information regarding utility grid interconnection specifications, grid operating characteristics, and utility disturbances that would influence the design of the DC-AC inverter/energy converter. Certain portions of the information influenced the design of the prototype energy converter that was tested. A substantial portion of this information will also be utilized during Phase II of the project when a larger scale production quality system is developed for utility grid application.

Conclusions and Future Directions

The data indicates a very successful demonstration of the energy converter's capabilities, albeit at a reduced power level. However, the system is very scalable and can be scaled up to larger systems that would have a much more profound effect on actual power distribution systems. Future work will be dedicated to further analyzing utility grid specifications and moving forward to develop and test a production quality energy converter capable of 600 kW/kVA total of reactive current correction and/or real power generation from a DC source. This size module will be capable of being paralleled to produce higher total power capabilities.

Special Recognitions & Awards/Patents Issued

1. U.S. patent application is in process.

IV.C.2 Advanced Power Conversion System (PCS) Technologies for High-Megawatt Fuel Cell Power Plants

Allen R. Hefner, Jr.
National Institute of Standards and Technology (NIST)
100 Bureau Dr.
Gaithersburg, MD 20899
Phone: (301) 975-2071
E-mail: hefner@nist.gov

DOE Project Manager: Heather Quedenfeld
Phone: (412) 386-5781
E-mail: Heather.Quedenfeld@netl.doe.gov

Objectives

- Identify advanced technologies that may significantly reduce the cost of the power conversion systems (PCS) required for future high-megawatt fuel cell power plants.
- Determine fuel cell power plant PCS performance requirements, including requirements for interfacing to fuel cell modules and for power grid connectivity.
- Develop simulation models for advanced PCS architectures, circuit topologies, and component technologies and perform simulations required to determine overall cost and performance benefits of advanced technologies.
- Coordinate with related industry and federal government programs to enable the development of advanced high-megawatt PCS technologies necessary to meet the Solid State Energy Conversional Alliance (SECA) and FutureGen PCS goals.

Accomplishments

- High-Megawatt Converters Workshop held at NIST in Gaithersburg, MD on January 24, 2007, included 42 invited participants and 21 invited presenters.
- Industry/government/university consensus reached on the process and parameters for the NIST/DOE advanced PCS technology impact analysis.
- Several approaches identified for reducing the fuel cell power plant PCS cost using silicon-carbide (SiC) power semiconductor devices.
- Simulation models developed for 10 kV SiC power metal-oxide-semiconductor field effect transistors (MOSFETs) and 10 kV SiC junction barrier Schottky diodes to be used for validation and refinement of cost reduction and performance impacts.
- Industry/government/university consensus reached on the formation of a roadmapping committee and interagency task group for high-megawatt PCS technology.

Introduction

High-megawatt PCSs are required to convert the low voltage power produced by fuel cell modules in central station scale plants to the very much higher voltage levels required for delivery to the grid. The SECA megawatt power plant PCS cost goal of $40-$100/kW is generally recognized as a difficult stretch goal that cannot be met with today's technology. To address this challenge, DOE and NIST have entered into an interagency agreement to have NIST lead an effort to evaluate various advanced technology options for the PCS and to identify technologies requiring development to meet the cost and efficiency goals of the SECA central station fuel cell power plant.

Approach

This project aims to evaluate advanced PCS architectures, circuit topologies, and component technologies that may significantly reduce the lifecycle cost of the SECA central station fuel cell power plant. Various PCS approaches that focus on the use of advanced technologies for low-voltage, medium-voltage, and high-power architectures are considered. The advanced component technologies being considered include advanced power semiconductor devices made with the SiC material, advanced nano-crystalline magnetic materials for filters and transformers, advanced capacitor technologies, advanced power electronic component cooling systems, and modular power electronic package and interconnect approaches.

Each PCS approach is being evaluated for its ability to meet the performance requirements of the fuel cell power plant including requirements for interfacing to fuel cell modules and for power grid connectivity, as well as the cost of constructing and maintaining the PCS. The cost and performance estimates are made using tabular spreadsheet calculations where detailed circuit simulations are used to verify and refine the component interaction and system performance impacts used in the spreadsheet calculations. The project thus requires the development of simulation models for advanced PCS architectures, circuit topologies, and component technologies.

The evaluation of the overall impact of advanced PCS technologies requires input from, and coordination with, the broad power electronics community. To initiate this interaction and review the approach being used for the advanced technology impact evaluation, a "*High Megawatt Converter Workshop*" [1] was held at NIST headquarters in Gaithersburg, MD on January 24, 2007. The objectives of the workshop were to exchange information focused on state-of-the-art technologies for high-megawatt PCSs, discuss the merits of proposed approaches to achieving significant cost reduction and improved electrical conversion efficiency, discuss how federal resources could potentially be utilized in a coordinated effort to address these issues, and to discuss the merits of establishing an industry-led roadmap committee to offer guidance that could facilitate the achievement of the desired goals.

Results

High-Megawatt Converter Workshop: The High Megawatt Converter Workshop held at NIST on January 24, 2007 included 42 invited participants and 21 invited presenters. Ten of the presentations described specific technologies deemed to have the potential to reduce PCS cost and seven presentations discussed the common needs for high-megawatt PCSs across industry and government agencies. Open discussion sessions were also held to discuss the specific approach being used for the NIST/DOE Advanced PCS Technology Impact Analysis, and to discuss the merits of forming an interagency task group and an industry roadmap effort for high-megawatt PCS technologies.

Interagency Task Group on High-Megawatt PCS: The High Megawatt Converter Workshop participants agreed that a federal interagency task group for high-megawatt power converter technologies could play an important role in this area. It was also suggested that the Interagency Power Group (IAPG) would be a good organization to host such a task group. Subsequently, during the IAPG Strategic Planning Meeting on April 3, 2007, the IAPG agreed that a reinitiated IAPG Electrical Systems Working Group (ESWG) could serve, in part, as an umbrella organization for the High-Megawatt PCS Interagency Task Group.

Industry Roadmap on High-Megawatt PCS: The High Megawatt Converter Workshop participants agreed that a roadmap process should be initiated to offer guidance for further development of PCSs that could meet the requirements for more cost-effective and more efficient power conversion and a number of those present expressed a willingness to serve on such a committee.

Advanced PCS Technology Impact Analysis: During the High Megawatt Converter Workshop, various aspects of the NIST/DOE Advanced PCS Technology Impact Analysis effort were reviewed including: the overall approach of the study, the current and voltage boundary conditions, the grid-connectivity requirements, fuel cell current regulation and ripple requirements, as well as, the topology and component technologies being considered by the study. Various conversion approaches that focus on the use of advanced technologies for low-voltage, medium-voltage, and high-power architectures were outlined.

Consensus on Impact Analysis Approach: A general consensus was reached on the approach and specifications for the NIST/DOE study as described below:

- Methodology for impact study:
  - Classify power converter architectures and component technologies that may reduce cost
  - Perform tabular calculations of cost for each option using estimated advantages of new technologies
  - Use component modeling and circuit and system simulations to verify and refine calculations
- Consider power electronics and/or transformer up to 18 kV AC and assume transformer from 18 kV AC to transmission level voltage.
- Boundary conditions and performance parameters:
  - Fuel cell stack: center tap ~700 VDC, 1,000 A
  - Individual fuel cell stack current control (may be necessary for fuel cell reliability)
  - Fault tolerant and serviceable
- Converter cost components:
  - Semiconductors
  - Module packaging
  - Interconnects
  - Cooling system
  - Magnetics: filter inductors and high frequency voltage isolation transformers
  - Transformer up to 18 kV
  - Breakers

The initial baseline for the study is a center tapped fuel cell (approximately 700 V DC, 0.6 MW) with a DC-DC converter for fuel cell current regulation, a 480 VAC inverter, and a 60 Hz transformer to raise the output voltage to 18 kV AC. This option is chosen as the baseline because it includes the individual functions necessary to expand to a DC common bus and to high-voltage and/or high-power inverter topologies. The "present lowest-cost" option combines the DC-DC regulator and 480 V AC inverter functions into a single converter stage that uses the "present lowest-cost" switching power device, a 1,200 V insulated gate bipolar transistor (IGBT) module.

Low-voltage PCS inverters: For the low voltage inverter options, advanced semiconductor technologies such as SiC power devices enable the use of higher frequencies that may reduce the cost of passive components. The advanced semiconductor devices may also result in lower switching losses resulting in higher power conversion efficiency and lower cost thermal management systems. SiC power semiconductor devices have recently begun to emerge as commercial products where low current SiC junction barrier Schottky diodes are becoming common place in computer server power-factor-correction circuits. Commercial 1,200 V SiC MOSFET switches and 1,200 V hybrid SiC-junction barrier Schottky/Silicon-IGBT modules are also expected in the near future.

Medium voltage inverters: The second class of power converters being evaluated uses a DC-DC converter to step the voltage up to 6 kV and a medium-voltage inverter is used to produce 4,160 VAC, then a transformer is used to raise the voltage to 18 kV AC. In this case, the DC-DC converter can combine the function of increasing voltage with the function of regulating fuel cell current. The advantage of using a medium-voltage inverter is that it reduces the current for a given power processing level so that a single inverter can be used for multiple fuel cell stacks.

Medium-voltage semiconductors: Various semiconductor options exist for medium-voltage inverters including high voltage (HV)-IGBTs, integrated gate commutated thyristor (IGCTs), and high-voltage SiC devices. Recently, commercial HV-IGBT modules have been introduced to increase the voltage and current level to 6.5 kV, 600A, and commercial 6.5 kV, 3,000 A IGCTs have been introduced that provide improved gate turnoff thyristor (GTO) switching speed using a high current, low-inductance gate drive to switch off the full wafer GTO in unity-gain mode. However, these existing semiconductor devices require the use of multilevel inverters for medium voltage applications. This is due to the lack of voltage margin when using a 6.5 kV switch and, also, to the relatively low switching frequency of the high-voltage silicon devices (<1 kHz). On the other hand, the high-voltage, high-frequency (10 kV, 20 kHz) SiC semiconductor devices currently under development by the Defense Advanced Research Projects Agency (DARPA) High Power Electronics program would enable the use of a single level inverter with a much lower part count and lower filter inductance requirements [2].

High-power architectures: Finally, various power converter architecture options are being evaluated for using a single medium-voltage, high-power inverter for multiple 700 V, 0.6 MW fuel cell stacks. Each architecture option imposes different requirements on the DC-DC converter and DC-AC inverter functions and thus realizes different benefits from advanced semiconductors, magnetics, and capacitors. For example, architectures requiring DC-DC converters with high-voltage gain or high voltage-isolation may also benefit from advanced magnetic materials, which, in effect, step-up the voltage using the high-frequency magnetic components rather than a much larger 60 Hz transformer. In each case, the power converter architecture and component technologies must be considered together to determine the overall benefits to the PCS system and to identify a complete set of advanced technologies required for a given approach.

Consensus on specifications: After the briefing on the approach being considered for the impact study and on the individual power converter technologies, the High-Megawatt Converter Workshop participants were asked during an open discussion session to provide feedback on additional specifications and technologies to be included in the study. The questions posed during this session and the consensus for additional considerations to the impact study are summarized below.

Requested inputs from the workshop participants:

- Preferred high-megawatt architectures and topologies.
- Specifications for filter requirements:
  - Harmonics for power generation connectivity (e.g. IEEE1547).
  - Electromagnetic interference (EMI) requirements.
- Other advanced component technologies:
  - Nano-crystalline magnetic materials for high-gain converters or voltage-isolated converters.
  - Packaging and advanced cooling systems.
  - Interconnects and modularity.
  - Capacitors (Dry Q cap: low cost, low maintenance).

The experts at the workshop recommended that the study be based on the following:

- Specifications for filter requirements:
  - Inverter harmonics requirement: IEEE 519.
  - EMI requirements: Mil STD 461 or equivalent.
- Specifications for fuel cell current regulator:
  - Ripple requirement: <3% for frequencies <1kHz.
- Year 2020 fuel cell voltage may be 2,000 V (center-tap).

Of particular importance is the consensus on the power converter performance requirements and applicable standards. It was also recommended that the study be expanded to include the impact of increased fuel cell stack voltage that is expected to occur by the year 2020.

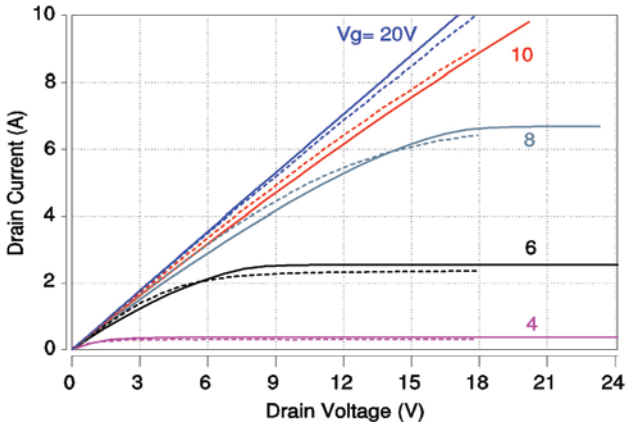

FIGURE 1. Comparison of Measured (Dashed) and Simulated (Solid) Output Characteristics at 125°C for a 5 A, 10 kV SiC MOSFET

Advanced PCS Component Technology Models: Simulation models for advanced PCS architectures, circuit topologies, and component technologies are required for the technology impact evaluation. One of the most potentially revolutionary technologies for high-voltage and high-power conversion systems is power semiconductor devices made with the SiC material. NIST has recently developed models and parameter sets for 1,200 V and 10 kV SiC MOSFETs and junction barrier Schottky diodes to be used in this work. As an example, Figures 1 through 3 show comparisons of the 10 kV SiC power MOSFET and junction barrier Schottky diode models with measured steady-state and transient characteristics [3]. (In general, the high-voltage SiC devices are two orders of magnitude faster than devices made with the conventional silicon material.) The NIST developed models will be used to evaluate the cost and performance advantages of the DC-DC and DC-AC converters identified above [4].

Conclusions and Future Directions

The major effort of this project thus far has been focused on establishing the approach and conditions for the NIST/DOE Advanced PCS Technology Impact Analysis and in initiating the Interagency Task Group on High-Megawatt PCS. The High Megawatt Converter Workshop held at NIST on January 24, 2007, resulted in a consensus on the process and parameters for the NIST/DOE study and the formation of an interagency task group, and on a roadmapping committee for high-megawatt PCSs.

The IAPG Strategic Plan document developed at the IAPG meeting includes plans for reinitiating the ESWG that will host the high-megawatt PCS interagency task group. The points-of-contact and participants from appropriate federal agencies have been identified and

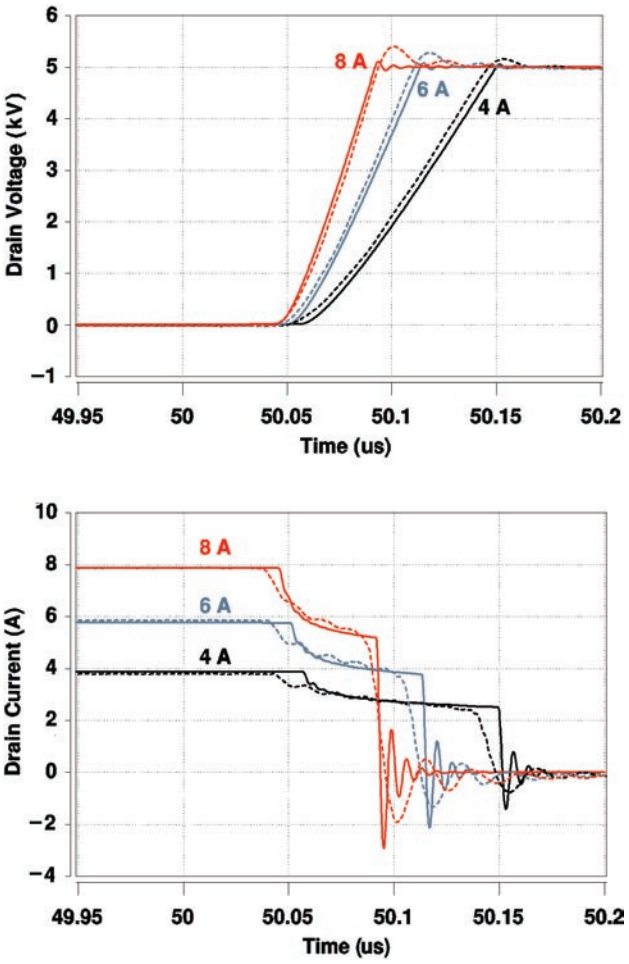

FIGURE 2. Comparison of Measured (Dashed) and Simulated (Solid) Inductive-Load Switching Turn-Off Waveforms at 25°C for a Clamp Voltage of 5 kV and a 5 A, 10 kV SiC MOSFET

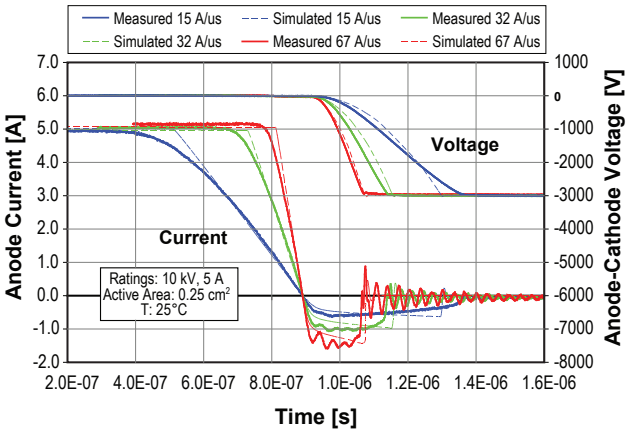

FIGURE 3. Comparison of Measured (Solid) with Simulated (Dashed) Clamped Reverse Recovery Transient Waveforms for a 10 kV, 5 A SiC Junction Barrier Schottky Diode at Three Different Turn-Off Current Ramp Rates (15, 32, and 67 A/us)

a meeting is tentatively planned for September 2007 to begin this activity that will continue in the future.

Simulation models for advanced PCS component technologies and simulation schematics for power DC-DC and DC-AC converters are now under development. Simulations are beginning to be performed and will continue in the future to validate the system impact of the identified advanced PCS component technologies.

FY 2007 Publications/Presentations

1. Proceedings of the High Megawatt Converters Workshop, Jan. 24, 2007, NIST Headquarters, Gaithersburg, MD, www.high-megawatt.nist.gov/workshop-1-24-07/.

2. A. R. Hefner, R. Sei-Hyung, B. A. Hull, D.W. Berning, C. E. Hood, J. M. Ortiz-Rodriguez, A. Rivera-Lopez, T. Duong, A. Akuffo, and M. Hernandez , "Recent Advances in High-Voltage, High-Frequency Silicon-Carbide Power Devices," Proceedings of the 2006 IEEE Industry Applications Society (IAS) Annual Meeting, October 08-12, 2006, Tampa, FL, pp. 330-337.

3. J. M. Ortiz-Rodriguez, T. Duong, A. Rivera-Lopez, and A. R. Hefner, "High-Voltage, High-Frequency SiC Power MOSFETs Model Validation," Proceedings of the 2007 IEEE Power Electronics Specialists Conference (PESC), June 17–21, 2007, Orlando, FL.

4. T. H. Duong, D.W. Berning, A. R. Hefner, and K. M. Smedley, "Long-Term Stability Test System for High-Voltage, High-Frequency SiC Power Devices," Proceedings of the 2007 IEEE Applied Power Electronics Conference (APEC 2007), February 25 – March 1, 2007, Anaheim, CA, pp. 1240-1246.

IV.C.3 A Low-Cost Soft-Switched DC/DC Converter for Solid Oxide Fuel Cells

Jason Lai (Primary Contact), Sung-Yeul Park, Seungryul Moon, and Chien-Liang Chen
Virginia Polytechnic Institute and State University
614 Whittemore Hall
Blacksburg, VA 24061-0111
Phone: (540) 231-4741; Fax: (540) 231-3362
E-mail: laijs@vt.edu

DOE Project Manager: Donald Collins
Phone: (304) 285-4156
E-mail: Donald.Collins@netl.doe.gov

Subcontractor:
Southern California Edison, Los Angeles, CA

Objectives

- Develop a low-cost DC-DC converter for low- to high-voltage power conversion as the standard interface between the solid oxide fuel cell (SOFC) source and the load-side DC-AC inverter.
- Develop a low-cost 5 kW DC-AC inverter with a minimum energy efficiency of 99% operating with >400 VDC input.
- Develop power management control strategies and demonstrate the ability to supply and consume reactive power while simultaneously supplying active power to the utility grid.
- Develop sensory and control logic to enable autonomous/semi-autonomous response to aid supporting grid voltage and frequency needs without nuisance tripping or disconnection of the fuel cell system.

Accomplishments

- Improved the peak efficiency of the 50 V V6 DC-DC converter to 97.3% by reducing the device turn-off loss with a smaller gate-drive resistance.
- Developed a precision power flow controller for a universal power conditioning system by incorporating an admittance compensation loop and advanced digital control technique.
- Developed a hybrid contactor for utility grid connection that allows zero current turn-on by a solid-state relay and zero connection loss by a mechanical contactor.
- Developed a new low-cost TMS320F2808 digital signal processor (DSP) based controller board for faster current loop and power flow control.

Introduction

The DC-DC converter that serves as the interface between the SOFC and the output stage DC-AC inverter has been the focus of the Virginia Tech Solid State Energy Conversion Alliance (SECA) project. The peak efficiency of the V6 DC-DC converter was reported at 96.5% with either 25 V or 50 V fuel cell voltage. Recently the 50 V level peak efficiency at the half-load was further improved to 97.3% by reducing the power metal oxide semiconductor field effect transistor (MOSFET) turn-off loss with a smaller gate-drive resistance. The efficiency at the 5 kW rated load is about 96.5%.

For the DC-AC inverter, the proposed soft-switching inverter shows 99% efficiency for the switching stage. After adding an inductor-capacitor-inductor (LCL) filter, the efficiency remains 98%. The problem is the originally used solid-state relay consumes another 1% loss, and in addition the relay itself requires separate heat sink and cooling. Recently we developed a hybrid contactor that combines the solid-state relay and a mechanical contactor to eliminate the loss and to maintain high efficiency operation.

The utility grid interface adopts an LCL filter that allows universal applications. In other words, it can operate in both standalone and grid-tie modes. In order to control such an LCL filter-based system, an admittance compensation technique was proposed to allow simple control design with well-defined control loop stability. A provisional patent has been filed through the Virginia Tech Intellectual Property office.

Approach

Figure 1 shows the hybrid contactor based grid-tie universal power conditioning system. For standalone mode, the output voltage needs to be filtered by inductor L_{o1} and capacitor C_o. For the grid-tie inverter, additional inductor L_{o2} is needed to reduce the output current ripple content. The hybrid contactor consists of a thyristor based solid-state relay (SSR) and a mechanical contactor. The SSR turns on and off at zero-voltage crossing to avoid any current transient. The mechanical contactor turns on after and off before the SSR turns on to eliminate the loss caused by the thyristor conduction.

Figure 2 shows the block diagram of the proposed admittance compensation method along with a proportional-resonant (PR) controller for the precise power flow control. The state-of-the-art controller design for LCL-based inverters is to make one equivalent

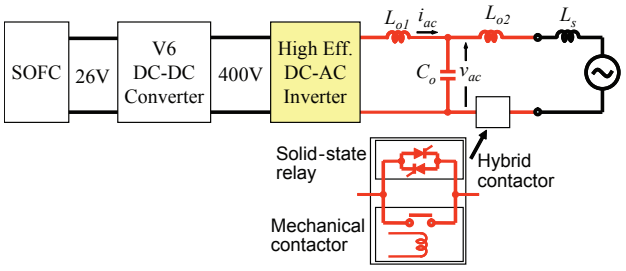

FIGURE 1. A Hybrid Contactor Based Grid-Tie SOFC PCS

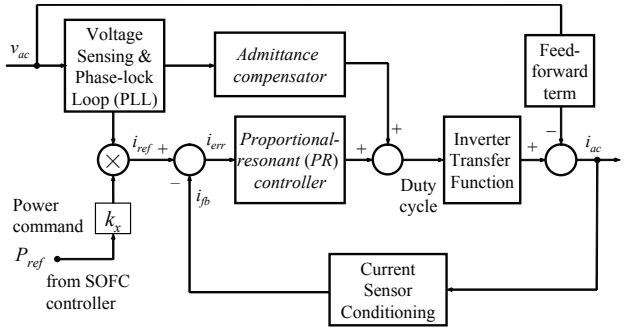

FIGURE 2. Block Diagram of a Grid-Tie SOFC PCS Using Admittance Compensator and PR Controller

circuit, which is a third-order system, and its original physical components, such as inductor current and capacitor voltage, disappear. Without knowing the physical term, the conventional controller cannot precisely control the power flow. The proposed admittance compensation is to solve the control design problem of the conventional LCL filter-based inverter, which has an undesirable feed-forward control term coming from the AC voltage source. The feed-forward term can produce a negative current command that reverses the power flow direction, and in low power commands, it can overcharge the DC bus capacitor voltage and results in catastrophe failure.

The admittance compensation method not only compensates the feed-forward term, but also avoids the use of a high-order filter circuit in controller design; instead, a second-order equivalent circuit can be used as the plant transfer function for standalone mode, and a first-order transfer function can be used for grid-tie mode. As a result, the controller design has well-defined frequency domain response, and the stability margins can be ensured. Additional benefit with the proposed admittance compensation technique is the placement of current and voltage sensors. Both standalone and grid-tie modes share the same sensing signals, thus allowing a potential cost saving on the sensors and their associated conditioning circuits.

The adopted PR controller is to replace the proportional-integral (PI) controller that has been widely used in DC-DC converters. The PI controller can eliminate the steady-state error for DC-DC converters but not for DC-AC inverters because the PI controller gain is not infinity at 60 Hz. With a finite gain at 60 Hz, the output can no longer follow the command, resulting in a significant command error.

For 50 V or higher voltage input V6™ converters, the Virginia Tech SECA team changed the switching device to a higher voltage rating and the transformer turns ratio to test the V6™ converter with a 50 V input. Initially the peak and full-load efficiencies were about the same as that obtained from 25 V level, but it was discovered that high-voltage switching tends to be slower than low-voltage switching, resulting in higher turn-off losses. Therefore, we added a small resistor and a blocking diode in the gate drive circuit to accelerate the turn-off speed. As a result, the switching between upper and lower devices was no longer overlapped, and the efficiency was improved over the entire load range. Without changing the existing circuit layout and design, this simple modification allows significant efficiency gain in a higher voltage system.

Results

In order to implement the proposed admittance compensation and PR controller, a DSP-based board has been developed, and the software program has been coded. As shown in Figure 2, a phase-locked loop (PLL), an admittance compensator, and a PR controller are all included in the DSP controller. The PLL is to obtain the grid synchronization signal and to produce the in-phase or orthogonal sine waves. These sine waves are multiplied with the real power command P_{ref} to obtain the reference control current i_{ref}. The comparison between i_{ref} and the feedback current i_{fb} results in a current error, which serves as the input to the PR controller. The duty cycle produced by the PR controller is compensated with the admittance compensator output to overcome the undesired feed-forward term that comes from the nature of the power circuit. The combination of admittance compensation and PR controller not only eliminates the steady-state error to control the power more precisely, but also avoids the current spike during startup and dynamic load changes [1,2].

Figure 3 compares the PR control results with and without admittance compensation at zero command operation. The PR controller allows elimination of steady-state error between the current command and actual current. Without admittance compensation, the PR controller produces a current spike under startup with zero command condition. Furthermore, the output current at zero command is not true zero. The rms current was measured at 1.34 A, and the output power was found to be –120 W. As mention before, without admittance compensation, such a negative power flow is not avoidable because of the feed-forward term. With the admittance compensation, the startup current spike

no longer exists. The measured power was found to be 4 W, which can be considered within the measurement error. The utility grid voltage for both cases is the same sinusoidal with 208 V rms.

For the DC-DC converter, the experiment is to compare the efficiency with different gate drive turn-off resistances. The turn-off voltage fall time was reduced from 270 ns to 200 ns by reducing the gate-drive turn-off resistor from 4.7 Ω to 2.2 Ω. Figure 4 compares the efficiency profiles with two different turn-off switching speed conditions. With a faster turn-off speed, the full-load (5 kW) efficiency is improved from 95.7% to 96.5%, and the peak efficiency at the half-load (2.5 kW) is improved from 96.5% to 97.3%. At 120% overload condition, the efficiency is improved from 95% to 96%. The total loss at 5 kW is 3.5% or 175 W. Note that the turn-on speed does not affect the efficiency because it is always under either zero voltage or zero current switching condition. A majority of the loss remains in conduction loss. Including the switch and transformer, the conduction loss is responsible for more than two-thirds the total loss. Therefore, it is possible that the V6™ converter efficiency will further go up if the fuel cell voltage goes higher. The question is how high the voltage should be? Because the MOSFET conduction loss is exponentially proportional to the blocking voltage level, and its switching loss is also increased with higher voltages, there should be a sweet spot for the V6™ converter input voltage, which remains a research issue.

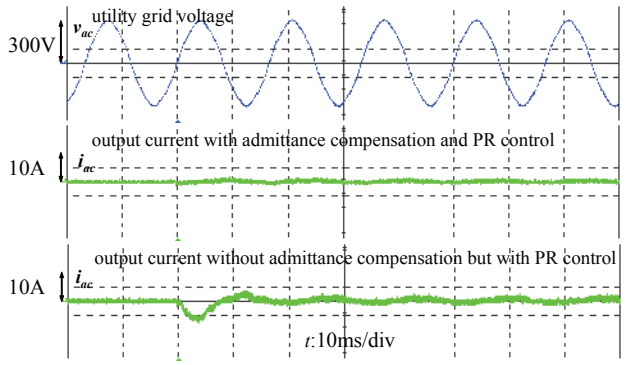

FIGURE 3. Experimental PR Controlled Voltage and Current Waveforms with and without LPAC under Startup with Zero Command Condition

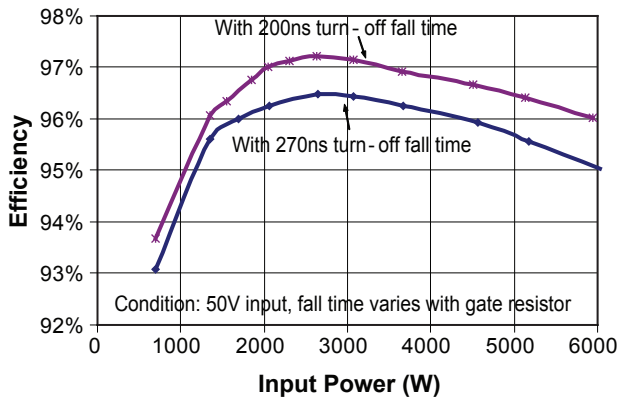

FIGURE 4. V6™ Converter Efficiency Test Results with 50 V Input Voltage

Conclusions and Future Directions

Major efforts have been focused on the precise power flow control and continuing improvement of PCS efficiency. A novel control system was developed to show its superiority to the conventional control methods. A simple modification of the gate drive circuit achieves further efficiency improvement. Major accomplishments are listed as follows.

- Developed a hybrid contactor that incorporates a solid-state relay to avoid switch current spike and a mechanical contactor to eliminate the contact conduction loss.
- Developed a control system that incorporates an admittance compensator and a proportional-resonant controller to precisely control the power flow. Test results indicated that not only the steady-state error is eliminated, but also the startup transient is avoided with the proposed controller.
- Modified and tested the V6™ DC-DC converter at 50 V input voltage with an efficiency gain of nearly 1%.

Future directions are:

- Test the V6™ DC-DC converter at a higher voltage to see if efficiency can increase further.
- Develop control system to comply with IEEE 1547 standard and California Rule 21.
- Test the entire PCS at EPRI-Solutions to show the performance of EMI and power quality under grid-tie control conditions.

Special Recognitions & Awards/Patents Issued

1. A U.S. provisional patent entitled “Control Method for a Universal Power Conditioning System” has been filed.

2. The V6™ converter was licensed to Hydra, Portland, OR and renewing the license to PEMDA Corp., Knoxville, TN.

FY 2007 Publications/Presentations

1. C. Liu, A. Ridenour, and J.-S. Lai, “Modeling and Control of a Novel Six-Leg Three-Phase High-Power Converter for Low-Voltage Fuel Cell Applications,” *IEEE Transactions on Power Electronics*, September 2006, pp. 1292 – 1300.

2. J.-S. Lai, S.-Y. Park, S.-R. Moon, C.-L. Chen, “A High-Efficiency 5-kW Soft-Switched Power Conditioning System

for Low-Voltage Solid Oxide Fuel Cells", in *Proc. of Power Conversion Conference*, Nagoya, April 2007, pp. 463 – 470. Note: This paper received the Best Paper Award from the conference.

3. S.-R. Moon and J.-S. Lai, "Multiphase Isolated DC-DC Converter for Low-Voltage High-Power Fuel Cell Applications," in *Proceedings of IEEE APEC*, Anaheim, CA, February 2007, pp. 654 – 660.

4. S.-Y. Park, J.-S. Lai, C.-L. Chen, S.-R. Moon and T-W. Chun, "Current Loop Control with Admittance Compensation for a Single-Phase Grid-Tie Fuel Cell Power Conditioning System," in *Proceedings of IEEE APEC*, Anaheim, CA, February 2007, pp. 1010 – 1016.

5. S. Moon, S. Park, C. Liu, and J.-S. Lai, "Solid Oxide Fuel Cell Current Ripple Impact and Reduction Techniques," in *Proc. of IEEE PESC*, Jeju, Korea, June 2006, pp. 2037–2042.

References

1. R. Teodorescu, F. Blaabjerg, U. Borup, and M. Liserre, "A new control structure for grid-connected LCL PV inverters with zero steady-state error and selective harmonic compensation," *Proc. of IEEE APEC*, Anaheim, CA, March 2004, pp. 580–586.

2. C.-L. Chen, S.-Y. Park, J.-S. Lai and S. Moon, "Admittance Compensation in Current Loop Control for a Grid-Tie LCL Fuel Cell Inverter," to be appeared in *Proc. of IEEE Power Electronics Specialists Conference*, Orlando, FL, June 2007.

IV. SECA RESEARCH & DEVELOPMENT

D. Modeling & Simulation

IV.D.1 SOFC Modeling at PNNL

Mohammad A. Khaleel (Primary Contact), Brian J. Koeppel, Kurt P. Recknagle, Xin Sun, Elizabeth V. Stephens, Wenning Liu and Ba Nghiep Nguyen
Pacific Northwest National Laboratory (PNNL)
902 Battelle Blvd.
Richland, WA 99352
Phone: (509) 375-2438; Fax: (509) 375-4392
E-mail: moe.khaleel@pnl.gov

DOE Project Manager: Travis Shultz
Phone: (304) 285-1370
E-mail: Travis.Shultz@netl.doe.gov

Objectives

- Develop and validate multi-physics modeling tools to simulate solid oxide fuel cell (SOFC) stack performance.
- Utilize computational techniques for the mitigation of performance degradation and optimization of modular SOFC stack and system designs.
- Obtain necessary material properties to support the development and optimization of SOFC designs through modeling.
- Disseminate/transfer modeling tools to Solid State Energy Conversion Alliance (SECA) industry teams and Core Technology Program (CTP) members.

Accomplishments

- Developed a finite element-based code, called SOFC-Multi Physics (SOFC-MP), to solve the coupled flow, electrochemistry, and heat transfer solution in fuel cell stacks under steady-state conditions.
- Co-developed with MSC Software a stack design tool, called Mentat-Fuel Cell (Mentat-FC), for SOFC model generation, integration/solution with SOFC-MP, and structural analysis using the MARC finite element mesh and modeling capabilities.
- Provided training for SOFC modeling tools and techniques through a demonstration seminar at the April 2005 SECA workshop, comprehensive technical programs hosted at PNNL covering the full suite of SOFC modeling tools, individual student training and collaboration at PNNL, and individual telephone/email support.
- Distributed the SOFC-MP and Mentat-FC software packages to multiple industry teams and CTP university researchers for modeling and development of SOFC stacks.
- Established a methodology to assess glass-ceramic seal failure. A continuum damage mechanics model based on the experimental stress/strain response was developed for G18 sealing glass. The damage model was implemented in MSC MARC and used for SOFC stack stress analysis to predict accumulated damage and failure of the seals under thermal-mechanical loading. The methodology was extended to predict seal damage accumulation in stacks due to thermal cycling processes.
- Developed a probabilistic-based component design methodology for the SOFC stack. This method takes into account the randomness in SOFC material properties as well as stresses arising from different manufacturing and operating conditions.
- Developed an integrated modeling/experimental framework to predict the life of SOFC interconnect materials. Oxide scale properties were evaluated experimentally and the effects of interconnect oxide growth on interfacial structural integrity during isothermal cooling was studied.
- Initiated a design basis document in collaboration with the American Society of Mechanical Engineers (ASME) and Oak Ridge National Laboratory (ORNL) to provide industry teams with technical guidance on materials characterization, constitutive models, modeling techniques, failure analyses, and software usage to support SOFC design and development efforts.
- Developed modeling methodologies and constitutive models based on experimental characterizations to evaluate the time-dependent mechanical response of stack components. The models can quantify the effect of creep in metallic components and glass-ceramic seals on stack deformations and cell component stresses during operation and shutdown. A homogenization model to predict glass-ceramic seal properties as a function of composition was developed and implemented.
- Established a methodology to assess interconnect scale growth and effect of the associated electrical resistance increase on stack performance. The capability enables evaluation of the long term behavior of prospective interconnect materials with respect to thermal and electrical stack performance.
- Supported development of a standardized SOFC cell geometry for use in the SECA program to evaluate materials and technologies within a common testing platform.

Introduction

In order to efficiently develop and optimize planar SOFC stacks to meet technical performance targets, it is desirable to experiment numerically with the effects of geometry, material properties, operational parameters, and thermal-mechanical loading. The computations with representative baseline designs, validated by experimental data, have been used to develop better understanding of the stack behavior while avoiding costly and time-consuming experiments. In order to model the coupled physics associated with an SOFC stack, the simulation tool SOFC-MP was developed. This modeling tool combines the versatility of a commercial multi-physics code and a validated electrochemistry calculation routine to predict the gas flow distributions, current distribution, temperature field, and power output for stack-level simulations. The fundamental building blocks of the modeling and simulation tools are electrochemical models, heat and mass transfer simulations, computational mechanics, and experimental data.

The multi-physics modeling tools developed were then used in studying a wide range of design criteria as well as current material development and degradation challenges. A probabilistic-based component design methodology was developed, which takes into account the randomness in SOFC material properties as well as stresses arising from different manufacturing and operating conditions. For SOFC materials and stack development, the time-dependent mechanical response of seal and interconnect components were considered to predict the impact on stack performance and component stresses. Interconnect scale growth was evaluated for both its mechanical durability to resist growth-induced spallation as well as its influence on the cell electrochemistry. The modeling tools were also used to evaluate issues expected to be problematic for cell scale-up such as high stresses and loss of contact in the stack. The developed design methodology and stack analytical procedures are currently being incorporated into a design basis document for distribution within the SECA program.

Approach

The following technical approach has been taken in the modeling task to meet program goals:

- Maintain, enhance, and provide guidance for the integrated modeling tools developed under the SECA CTP for evaluating fuel cell stack design concepts by the industry teams.
- Investigate the effects of materials degradation on cell performance and life.
- Investigate the effects of cell geometric design, material property distributions, and operating conditions on SOFC reliability.
- Perform material experiments for property data essential to constitutive and numerical model development.

Results

Increased Usage of Modeling Tools

The modeling tools and techniques developed at PNNL played a greater role in continued support of SOFC technology development for the SECA industry and university team members:

- The SOFC-MP and Mentat-FC modeling tools were delivered to GE Energy, Delphi, and West Virginia University with accompanying technical support for usage and operation.
- The developed modeling tools were used for collaboration with the University of Cincinnati to study the performance of their glass sealant in a realistic SOFC cell. Other university participants from West Virginia University, Carnegie Mellon University, and Georgia Tech will participate in summer internships to learn about SOFC modeling.
- The modeling tools were used for design of the SECA test cell. The pressure drop analysis showed that a serpentine geometry had small air pressure drop <10" H_2O for 4-cm tests cells, but was excessive if used for realistic cells sizes. In contrast, a non-serpentine channel design could be used for up to a 30-cm cell with comparable pressure drops. The thermal analysis for the serpentine and cross-flow geometries showed that the entire structure was nearly isothermal, and the structural analysis is now in progress.
- PNNL has co-led the development of the design basis document which will serve as a modeling and analysis guide for SECA members. Contributions regarding document objectives, modeling approaches, modeling tool usage, and failure analyses have been incorporated, and detailed modeling descriptions continue to be added to the analysis sections.

Modeling of Time-Dependent Material Properties

The use of time-dependent creep and stress-relaxation behaviors of cell materials was investigated and found to have a great influence on the stress predictions for the components.

- For the ferritic interconnect, modeling of the stack deformation during long periods of operation were simulated. The coefficient of thermal expansion (CTE) mismatches were found to cause cell

bowing which changed with time and contributed to changes in the gas channel heights (Figure 1); however, significant beneficial reduction in positive electrode/electrolyte/negative electrode (PEN) and seal stresses were also observed.

- The effect of oxide scale growth over time on the scale strength and stress state was quantified using indentation tests and simulations.
- For the G18 sealant, experimental creep tests were performed to determine the secondary creep strain rate dependency on stress and temperature (Figure 2). The data was implemented into the previously developed continuum damage mechanics model to predict the material response at different strain rates, and the effects of creep/relaxation on cell stresses were evaluated for different operating and shutdown durations.
- The glass-ceramic constitutive model was also extended to include material property predictions for the homogenized sealant behavior based on the volume fractions and properties of the ceramic and glassy phases. The model can be used to evaluate the effect of different seal material properties on stack stresses during operation and shutdown.

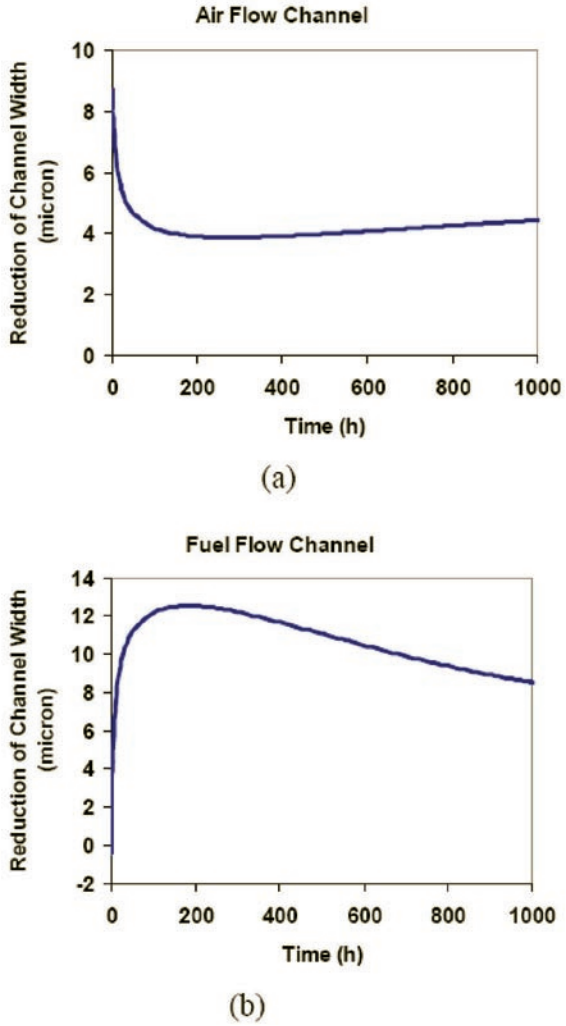

FIGURE 1. Effect of Interconnect Creep on Flow Channel Heights for 1,000 Hours Operating Duration

Modeling for Issues Related to Scale-Up

The desired use of SOFCs in megawatt-scale power applications using coal-based fuels provided motivation to study scale-up of cell dimensions. Larger cells are expected to have greater issues with thermal management for mechanical reliability, electrochemical variability across the cell, and maintenance of the electrical contact path. The modeling tool capabilities were extended to evaluate these issues:

- Cell sizes of 10-20-cm were evaluated for co-, counter- and cross-flow configurations, where the average stack temperature was kept constant by varying the inflow gas temperatures. The results (Table 1) indicated that the temperature difference increased by 70-100 K and peak stresses in the anode were significantly increased.

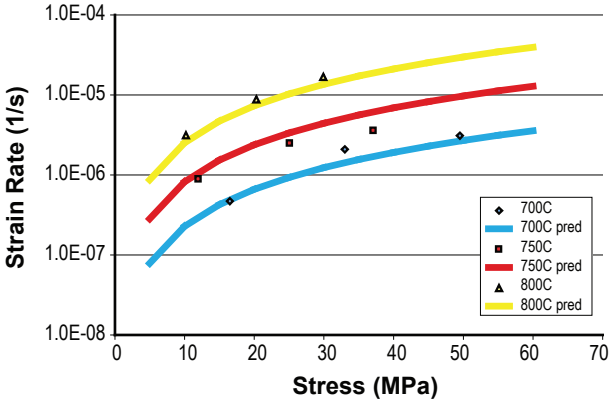

FIGURE 2. Secondary Creep Strain Rate for 4-hour Heat Treated G18 Glass-Ceramic as a Function of Stress and Temperature

TABLE 1. Predicted Temperatures, Peak Anode Principal Stress, and Peak Interconnect von Mises Stress for Cells of Different Sizes and Flow Configurations

Variables	Co-flow		Counter-flow		Cross-flow	
	10x10	20x20	10x10	20x20	10x10	20x20
Max T (°K)	1049	1120	1054	1155	1051	1170
Min T (°K)	970	898.5	967.1	847.9	970.3	857.3
σ_{IC} (MPa)	20.95	36.03	20.83	63.21	20.23	50.39
σ_{anode} (MPa)	10.30	36.06	13.67	63.87	9.612	51.0

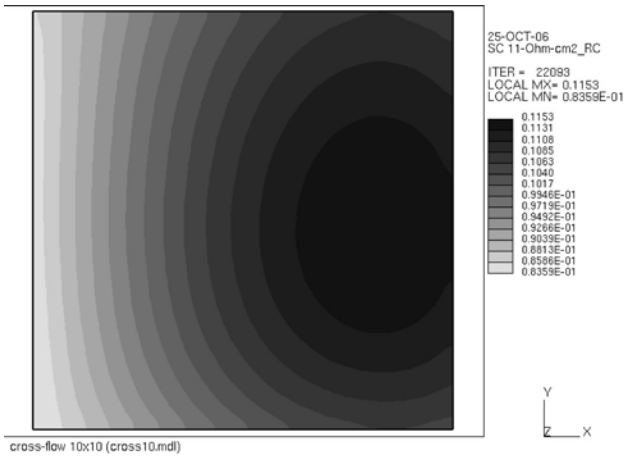

FIGURE 3. Predicted Cathode-Side Interconnect Electrical Resistance Distribution (Ω-cm^2) for a Stack Operated at 750°C, 0.6 A/cm^2 for 10,000 Hours

- The greater range of operating temperatures in a large cell are expected to affect the rate of thermally driven mechanisms such as scale growth. The growth of the interconnect scale and corresponding increase in the electrical resistance was simulated, and it was found that the local area specific resistance (ASR) varied from 0.83-0.12 Ω-cm^2 across the active area (Figure 3) with an increase of 26°C in the cell temperature difference after 10,000 hours of operation.
- Each cell in the stack must maintain electrical contact with the interconnect by a combination of mechanical bonding and compressive loading. Loss of contact through deformations or debonding and the corresponding impact on performance due to greater ohmic losses was simulated by modeling the stack electric field. The modeling capability was used to quantify a cell's total ohmic loss due to different corrugated interconnect geometries and loss of cathode contact due to mechanical bowing of the PEN.

Conclusions and Future Directions

In the last year, the modeling tools had greater usage and were enhanced with additional capabilities to address durability issues. Future modeling activities will continue to focus on reliability, degradation, time-dependent response, and scale-up issues:

- Continue to improve the modeling tools to meet the needs of the SECA program. Continue to increase the usage of the tools by the industry and academic teams.
- Continue to add improved material models and numerical procedures to the modeling tools for simulation of time-dependent response and reliability.
- Continue modeling to improve bond strengths of the oxide and protective coating layers for ferritic stainless steel interconnects.
- Evaluate thermal management needs, influence of high pressure electrochemistry, and reliability of seal/cell structures during cell scale-up.
- Continue to support development of a robust test cell design.
- Evaluate the mechanical requirements for successful fabrication using refractory glass sealants and low-temperature sintering of cathode contact materials for reliable interconnection during operation and shutdown.
- Continue to develop seal property predictions via homogenization methods to identify reliable composite seal structures and compositions for stacks.
- Develop analytical methods to evaluate the time-dependent mechanical behavior (creep, thermal fatigue, loss of interconnect contact) of fuel cell stacks/components and corresponding influence on electrochemical performance.

FY 2007 Publications/Presentations

1. MA Khaleel, KP Recknagle, X Sun, BJ Koeppel, EV Stephens, BN Nguyen, KI Johnson, VN Korolev, JS Vetrano, and P Singh, "Recent Development of Modeling Activities at PNNL," presented at the SECA Core Technology Program Peer Review, Philadelphia, PA, September 12–14, 2006.

2. KP Recknagle, BJ Koeppel, X Sun, JS Vetrano, ST Yokuda, DL King, P Singh, and MA Khaleel, "Analysis of Percent On-Cell Reformation of Methane in SOFC Stacks and the Effects on Thermal, Electrical, and Mechanical Performance," presented at the Fuel Cell Seminar 2006, Honolulu, HI, November 13–17, 2006.

3. X Sun, W Liu, J Vetrano, G Yang, MA Khaleel and M Cherkaoui, "Life Prediction of Ferritic Stainless Steel Interconnect under Thermal Stress and Oxide Growth Stress," presented at the Fuel Cell Seminar 2006, Honolulu, HI, November 13–17, 2006.

4. W Liu, X Sun, and MA Khaleel, "Fracture Failure Criteria of SOFC PEN Structure," presented at the 31st International Conference on Advanced Ceramics and Composites, Daytona Beach, FL, January 21–26, 2007.

5. BN Nguyen, BJ Koeppel, and MA Khaleel, "Design of a Glass-Ceramic Seal for Solid Oxide Fuel Cell Applications by Means of a Homogenization Approach," presented at the ASME Applied Mechanics and Materials Conference, Austin, TX, June 3–7, 2007.

6. X Sun, W Liu, and MA Khaleel, "Effects of Interconnect Creep on Long-Term Performance of a One-Cell Stack," PNNL–16342, Pacific Northwest National Laboratory, Richland, WA, 2007.

IV.D.2 Interfacial Strength and Interconnect Life Quantification Using an Integrated Experimental/Modeling Approach

Mohammad A. Khaleel (Primary Contact), Xin Sun, Wenning Liu, Elizabeth Stephens, Kurt Recknagle and Brian Koeppel
Pacific Northwest National Laboratory (PNNL)
902 Battelle Blvd.
Richland, WA 99352
Phone: (509) 375-2438; Fax: (509) 375-4392
E-mail: moe.khaleel@pnl.gov

DOE Project Manager: Travis Shultz
Phone: (304) 285-1370
E-mail: Travis.Shultz@netl.doe.gov

Objectives

- To develop a systematic methodology for quantifying the interfacial strength between oxide scale and interconnect substrate.
- To report the quantified interfacial strength developed by the combined experimental/modeling technique.
- To predict possible debonding/delamination and subsequent spallation at the scale/substrate interface for Crofer 22 APU, therefore indicating the possible interconnect life under isothermal cooling or thermal cycling conditions.

Accomplishments

- Identified the driving force for delaminations during indentation tests.
- Developed a coupled experimental/analytical approach for quantifying oxide/substrate interfacial strength.
- Applied the developed interfacial strength quantification method in predicting interconnect life upon isothermal cooling.

Introduction

Interconnects (IC) in solid oxide fuel cells (SOFCs) provide cell-to-cell electrical connection and also serve as gas separator for the separation of the fuel (anode) from the oxidant (cathode). Recently, Solid State Energy Conversion Alliance (SECA) funded interconnect materials development has been mostly focusing on ferritic stainless steels. Compared to chromium-based alloys, iron-based alloys have advantages in terms of high ductility, good workability and low-cost [1]. By far, iron-based alloys, especially Cr-Fe-based alloy, e.g. Crofer 22 APU, are the most attractive metallic interconnect material for SOFCs [2, 3].

It should be noted that the oxidation reaction of the metallic interconnect in the SOFC working environments is unavoidable. Appearance and growth of the oxide scale will cause growth stress in the oxide scale [2, 3]. In addition, thermal expansion coefficient mismatch between the oxide and the substrate creates stresses in the scale and on the scale/substrate interface during cooling [4], leading to scale delamination/buckling and eventual spallation. The interfacial strength between the oxide scale and substrate is therefore crucial to the reliability and durability of the metallic interconnect in SOFC operating environments. The objectives of the current work are: 1) to develop a methodology for quantifying the interfacial strength between oxide scale and interconnect substrate; 2) to report the quantified interfacial strength developed by the combined experimental/modeling technique; and 3) to predict possible delamination and subsequent spallation at the scale/substrate interface therefore indicating the possible interconnect life under isothermal cooling or thermal cycling conditions.

Approach

First, finite element fracture mechanics analyses of the micro-indentation test are performed with preexisting cracks at the oxide scale/Crofer substrate interface for various crack length, location and scale thickness. It is found that the interfacial crack tips are mainly mode II dominant, with very low ratios of K_I/K_{II}. From these results, one can conclude that the interfacial shear stress can indeed be considered the driving force for interfacial failure, and that this strength-based failure criterion is similar in many ways to the conventionally used fracture toughness criterion. The critical shear strength of the interface is then quantified by an integrated experimental/analytical approach. The predicted interfacial strength along with the predicted interfacial shear stress generated during the isothermal cooling process is used to determine the critical oxide scale thickness. The critical oxide scale thickness is next used in conjunction with the experimentally determined oxidization kinetics law for bare Crofer to predict IC life under normal operating temperature of 800°C.

Results

Evolution of Interfacial Shear Stress during Indentation

Figure 1 shows the cross-sectional microstructures of Crofer 22 APU after oxidation at 800°C for 1,200 hours. The thickness of the oxide scale is assumed uniform in the analyses. Temperature dependent material property is used for Crofer 22 APU. Taking advantage of the structural symmetry of an indentation test, an axisymmetric model is used. The total thickness of the substrate and its scale is kept constant at 0.5 mm. Figure 2 shows the predicted stress distribution in the scale during indentation process. It shows that a field of very high shear stress is generated by the indentation process, at the interface of the scale/substrate, right outside the contact radius of the indenter with the scale. The location and magnitude of the maximum shear stress on the interface evolve with the indentation depth and the thickness of the oxide scale. This high interfacial shear stress can be considered as the driving force for interfacial failure.

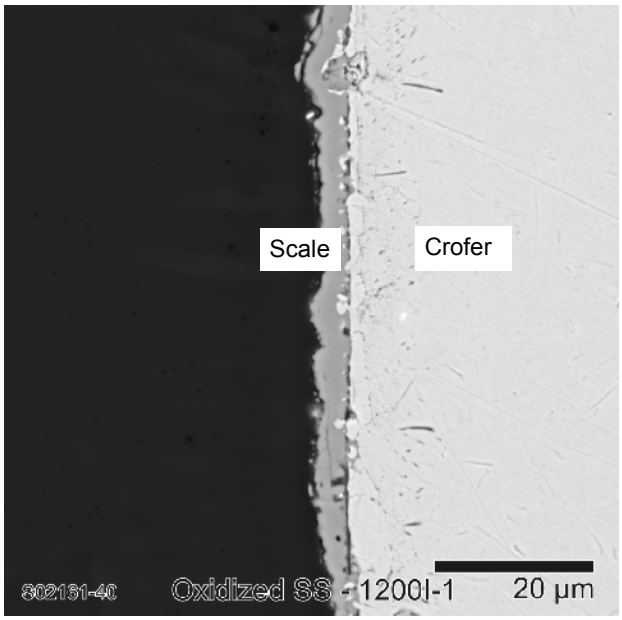

FIGURE 1. Cross-Sectional Microstructures of Crofer 22 APU after Oxidation at 800°C for 1,200 Hours

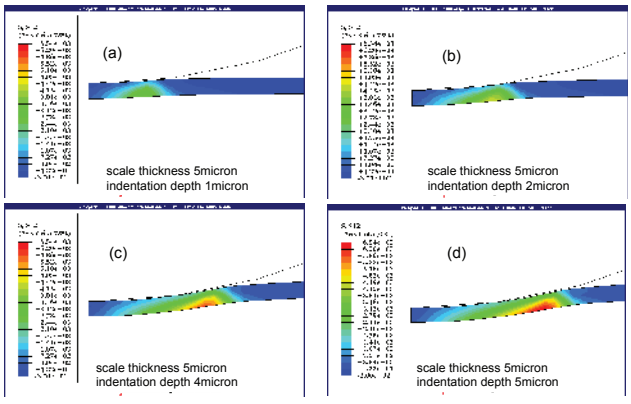

FIGURE 2. Development of Shear Stress Contours in 5-micron Thick Scale during Indentation

Crack Tip Mode Mixture for Pre-Existing Interfacial Crack during Indentation

In order to verify that interfacial shear stress is the driving force for delamination, finite element fracture mechanics analyses of the micro-indentation test are performed with preexisting cracks at the oxide scale/Crofer substrate interface for various crack length, location and scale thickness. Figure 3 shows the schematic of axisymmetric model for the indentation test. A Brale-C indenter with 0.2 mm tip radius is used. The indenter tip angle is 120°. A preexisting interfacial crack with length a is placed on the scale/substrate interface at distance L from the center of the indenter. The predicted stress intensity factor ratio, K_I/K_{II}, is plotted over the entire indentation depth of 10 microns for different initial crack length and different scale thickness. See Figure 3 for example of scale thickness of 5 microns. For all the scale thicknesses examined, the results clearly indicate that the interfacial crack tips have much higher stress intensity factor K_{II} than K_I. In other words, the interfacial crack tips are mostly mode II dominant. This is true for both the left and the right crack tips.

Experimental Indentation Test

Room temperature indentation tests were then performed on oxidized Crofer specimens in quantifying the interfacial strength between the oxide scale and the Crofer substrate. A hardness tester was used to apply the load utilizing a Rockwell 1/16”-diameter ball indenter to penetrate the oxide scale on the Crofer material. The loads were stair-stepped between 60 kgf and 150 kgf to determine the load that spallation occurred on each specimen. When spallation was observed, the load was typically reduced and the indentation repeated, continually increasing the load with each indent until failure was observed again. The load that spallation occurred along with the corresponding oxide scale thickness measured were inputted into the model to determine the interfacial shear strength of the interface.

Seven specimens oxidized at varying lengths of time were tested. All specimens were oxidized at 800°C. Metallography was performed to determine the oxide scale thickness for each specimen. Visual inspection was used to determine whether a specimen spalled after indenting. Typically, in the specimens with a

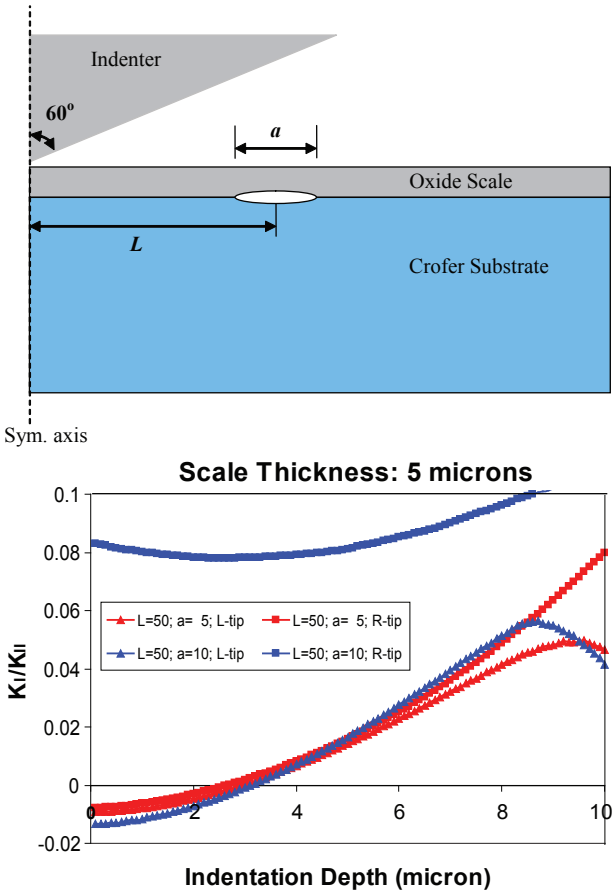

FIGURE 3. Schematic of the Indentation Test and Predicted K_I/K_{II} during Indentation

thicker scale layer, a full radial debonding of the scale was observed where as in specimens with a thinner oxide scale only partial flaking was observed. At a particular scale thickness, the number of spalled samples increases with indentation load. On the other hand, under a specific indentation load, more spalled samples are observed with increasing oxide scale thickness. Generally speaking, the results are quite consistent with some exceptions due to the statistical nature of the oxide layer thickness as well as the pre-existing interfacial flaws.

Quantification of Interfacial Strength

Summarizing the results from indentation tests, Figure 4 illustrates the numbers of non-spalled samples and spalled samples with increasing indentation load for the sample with oxide scale thickness of 2.41 microns. The sample was oxidized at 800°C for 1,500 hours. Clearly, with the resolution of the indentation load used, the critical indentation force to cause scale spallation is 100 kgf.

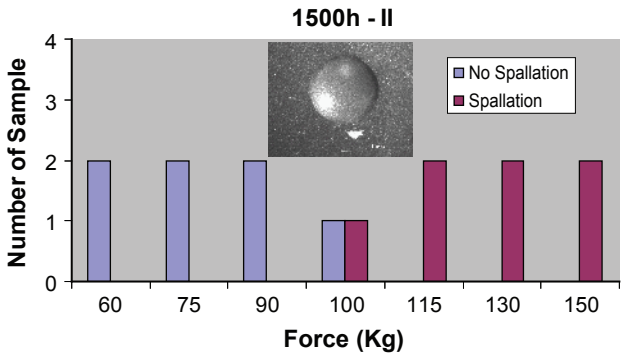

FIGURE 4. Number of Spalled and Non-Spalled Samples versus Indentation Force

Finite element simulation of the corresponding Rockwell 1/16"-diameter ball indentation test on 2.41-micron oxide scale/substrate system is then performed to quantify the interfacial shear stress at the critical indentation load of 100 kgf. The characteristic mesh size at the location for maximum shear stress is around 3 microns. At the critical applied force of 100 kgf, the corresponding maximum interface shear stress is 455 MPa. Therefore, the interfacial shear strength is quantified as 455 MPa for the oxide scale/substrate interface.

IC Life Prediction under Isothermal Cooling

In PNNL Report 15794 [4], it was reported that the interfacial shear stress will be generated during isothermal cooling from the operating temperature to room temperature, and the predicted cooling induced interfacial shear stress increases with the growth of the oxide scale thickness. The interfacial strength quantified can now be used to quantify the critical oxide scale thickness at which interfacial fracture/delamination will occur during isothermal cooling. For example, the critical oxide thickness corresponding to shear stress of 455 MPa is 14.2 microns under isothermal cooling for a 0.5 mm thick IC plate.

The critical oxide thickness can then be used together with the typical oxide growth kinetics law to estimate the interconnect life under normal operating temperature of 800°C. For example, the oxide growth kinetics for bare Crofer 22 APU can be expressed as the following experimental oxidation measurements: $h(\text{in micron}) = 0.15455 \cdot t^{1/2}(\text{in hour}) + 0.751$. Taking the critical oxide thickness as 14.2 microns, the lifetime for the bare Crofer is calculated as 7,570 hours.

Conclusions and Future Directions

In this report, we first use finite element fracture mechanics analysis to correlate the mode II dominance of interfacial crack tip, to the high shear stress levels at the interface between oxide/substrate during indentation process. A simplified, critical shear stress-based interfacial failure criterion is then proposed. The shear strength of the oxide/substrate interface is quantified using a combined experimental/analytical approach. Stair-stepping indentation tests are performed to quantify the critical indentation loads at which scale spallation occurs, for various scale thickness. Corresponding finite element indentation tests are then performed, to calculate the interfacial shear strength, at the critical indentation load. As an illustrative example, the interfacial strength is then compared to the shear stress predicted during isothermal cooling to determine the critical oxide scale thickness at which spallation will occur. The IC life is then determined using the oxide growth kinetics for bare Crofer.

It should be mentioned that the proposed approach is a deterministic approach, and it does not consider the statistical nature of the oxide thickness, as well as the interfacial flaw size and distribution. In addition, the critical shear strength quantified by this approach depends on the finite element mesh size used in the indentation simulation. In our analyses, we use equivalent mesh size in the subsequent isothermal cooling simulation, such that the influence of mesh size on predicted critical scale thickness, therefore IC life can be minimized.

In addition, the stair-stepping indentation tests, and the corresponding finite element indentation simulations are performed under room temperature. Therefore, high temperature interfacial strength quantification remains the subject for future study. Furthermore, we assumed that the interfacial strength is constant for various scale thickness. This will be subjected to further validations. Our future work will include identifying the delamination location, and quantifying the interfacial strength, for the spinel coating/oxide scale/Crofer substrate tri-layer system.

FY 2006 Publications/Presentations

1. Sun X, Liu W, Vetrano J, Yang ZG, Recknagle K and Khaleel MA, *Effects of Oxide Thickness on Scale and Interface Stresses under Isothermal Cooling and Micro-Indentation for Ferritic Stainless Steel Interconnect,* Poster Presentation at Fuel Cell Seminar 2006, Hawaii.

2. Sun X, Liu W, Stephens EV, Khaleel MA, *Interfacial Strength and IC Life Quantification using an Integrated Experimental/Modeling Approach,* PNNL Topical Report 16610, Pacific Northwest National Laboratory, Richland, WA 99354, May 2007.

References

1. J. W. Fergus, Metallic interconnects for solid oxide fuel cells. *Materials Science & Engineering A (Structural Materials: Properties, Microstructure and Processing)*, 397(1-2), pp. 271-83, 2005.

2. Z. Yang, G. Xia, and J.W. Stevenson, Mn1.5Co1.5O4 spinel protection Layers on ferritic stainless steels for SOFC interconnect applications. *Electrochemical and Solid-State Letters*, 8(3), pp. 168-70, 2005.

3. Z. Yang, J.S. Hardy, M.S. Walker, G. Xia, S.P. Simner and J.W. Stevenson, Structure and Conductivity of Thermally Grown Scales on Ferritic Fe-Cr-Mn Steel for SOFC Interconnect Applications, *Journal of The Electrochemical Society*, 151(11), A1825-A1831, 2004.

4. X. Sun, W.N. Liu, P. Singh and M.A. Khaleel, *Effects of Oxide Thickness on Scale and Interface Stresses under Isothermal Cooling and Micro-Indentation*, PNNL Report 15794, Pacific Northwest National Laboratory, Richland, WA 99354, May 2006.

IV. SECA RESEARCH & DEVELOPMENT

E. Balance of Plant

IV.E.1 Hybrid Ceramic/Metallic Recuperator for SOFC Generator

Anthony F. Litka (Primary Contact)
and Norm Bessette
Acumentrics Corporation
20 Southwest Park
Westwood, MA 02090
Phone: (800) 332-0277; Fax: (781) 461-1261
E-mail: tlitka@acumentrics.com

DOE Project Manager: Briggs White
Phone: (304) 285-5437
E-mail: Briggs.White@netl.doe.gov

Subcontractor:
Blasch Precision Ceramics, Albany, NY

Objectives

- Enable the use of inexpensive metallic alloys in a solid oxide fuel (SOFC) exhaust recuperator through the use of a ceramic heat exchange section in the high temperature region.
- Design and develop methods to mechanically integrate the ceramic and metallic sections into a recuperator assembly.
- Evaluate and characterize the performance of a hybrid ceramic/metallic recuperator under typical SOFC operating conditions.
- Demonstrate the performance and durability of the hybrid recuperator through both long-term steady-state and thermal cycle testing.

Accomplishments

- Demonstrated that a ceramic monolith recuperator can be integrated into a multi-pass cross-flow assembly with additional metallic recuperator sections, while maintaining adequate gas sealing at the ceramic/metallic interface.
- Designed a hybrid recuperator assembly which successfully managed the differing thermal expansion properties of the ceramic and metallic sections.
- Validated the thermal model created for the ceramic core using empirical data collected during testing.
- Achieved sufficient heat exchange in the high temperature ceramic section reducing exhaust temperatures observed by the subsequent metallic sections to a level where lower grade alloys may be employed (target <750ºC).
- Proved that a hybrid ceramic/metallic recuperator can achieve a heat exchange effectiveness of greater than 80% when operating at conditions typical of an SOFC generator.
- Subjected the hybrid recuperator to a multitude of thermal cycles with no observed change in performance or mechanical integrity.

Introduction

Acumentrics Corporation continues to focus on the development of efficient, reliable, and low-cost solid oxide fuel cell generators. A key component of the SOFC generator is the heat exchanger, or recuperator, which preheats the incoming cathode air using available heat in the exhaust stream. Typical exhaust temperatures of an SOFC generator are in the range of 800 to 1,000ºC. While the use of full metallic recuperators requires expensive high-alloy metals for oxidation resistance, these operating temperatures are well within the capabilities of lower cost ceramic and refractory materials.

A proof-of-concept hybrid (ceramic/metallic) recuperator was designed, manufactured and tested. The hybrid design includes a ceramic monolith heat exchanger combined with additional metallic recuperator sections. This configuration takes advantage of the high temperature, low fouling capability of the ceramic section, while enabling the use of lower grade metallic alloys in the medium-to-low temperature regions. Results to date have shown that a ceramic monolith recuperator can be successfully integrated with additional metallic recuperator sections to achieve an overall heat exchange effectiveness required for use with an SOFC generator. These advances show significant promise that a recuperator capable of withstanding the severe operation conditions of an SOFC can be manufactured, while at the same time achieving significant cost reduction of the component.

Approach

Acumentrics worked closely with Blasch to design and manufacture a single pass cross-flow ceramic core, made of silicon carbide, as shown in Figure 1. A method of plenum attachment was devised and the ceramic core was combined with two standard metallic fin cores supplied by T.RAD to produce a three-pass cross-flow hybrid recuperator assembly. A model of the assembled recuperator depicting the multi-pass cross-flow arrangement is provided in Figure 2.

A test rig, shown in Figure 3, was constructed, instrumented and commissioned specifically for the

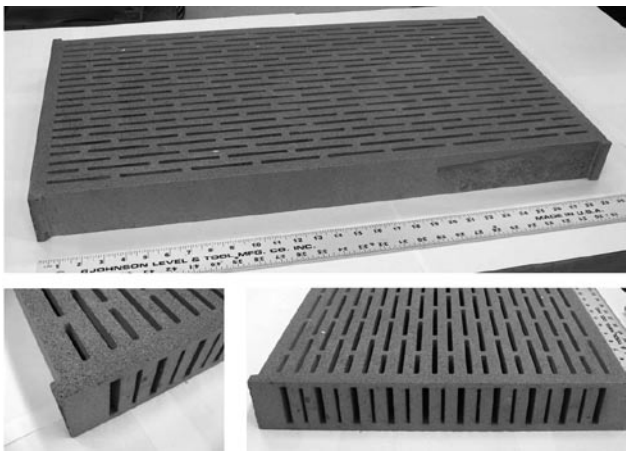

FIGURE 1. Single-Pass Cross-Flow Ceramic Recuperator Core

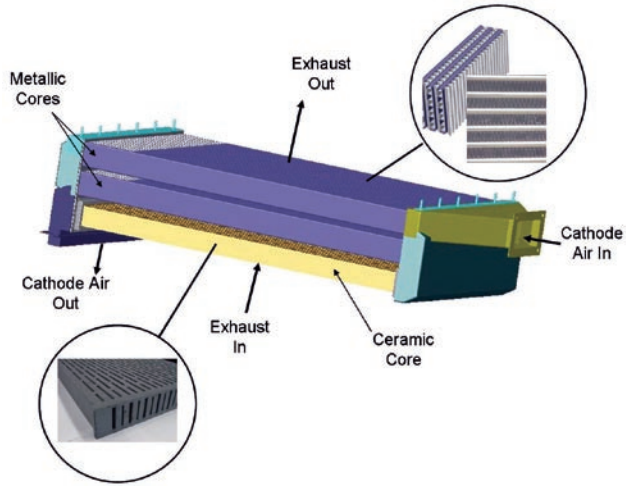

FIGURE 2. Hybrid Recuperator Assembly

FIGURE 3. Recuperator Test Rig

purposes of recuperator testing. The test rig was designed to enable the operator to simulate a variety of conditions typical of SOFC generator operation. Both the cathode air flow and exhaust flow could be regulated independently, and the inlet exhaust temperature was adjustable to enable simulation of operating points typical of start-up, steady-state and shutdown operation of an SOFC. Combined with measured flow rates, temperatures measured in the air and exhaust streams enabled a detailed analysis of recuperator effectiveness and performance characteristics of the hybrid assembly. Data collected during operation of a standard metallic 3-pass cross-flow recuperator, currently used on Acumentrics 5 kW SOFC generators, provided a baseline for comparison.

Results

Empirical data collected during the testing of the hybrid recuperator was analyzed and compared against the original spreadsheet-based thermal model created for the ceramic core. A strong correlation between the model data and that collected experimentally was observed. The graph in Figure 4 depicts the actual performance of the ceramic core against the curves generated by the model while operating at conditions typical of an Acumentrics 5 kW fuel cell generator.

The performance of the three-pass hybrid assembly (one ceramic core + two metallic cores) was evaluated at a variety of operating conditions. The recuperator consistently operated at an effectiveness of greater than 80%, reaching over 85% at some conditions. During testing at maximum exhaust inlet temperatures (approximately 850ºC) the ceramic core was capable of reducing the exhaust temperature observed by the subsequent metallic section to below 725ºC, allowing the

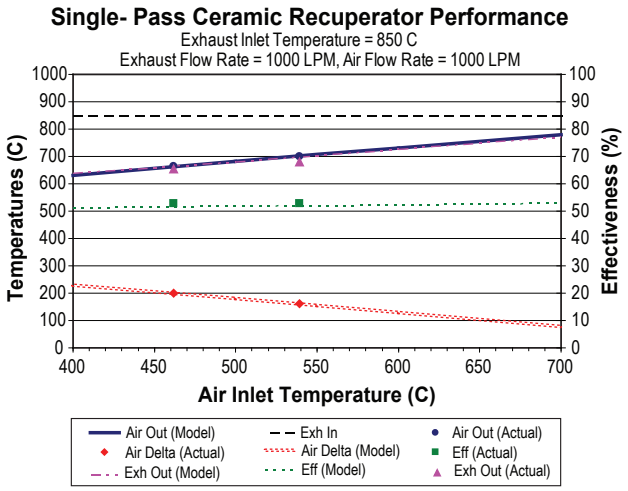

FIGURE 4. Ceramic Core Performance – Exhaust Temperature = 850ºC

use of lower grade alloys in the metallic sections. Air outlet temperatures of greater than 700ºC were achieved, thereby meeting the system requirements. The table provided below summarizes some proof-of-concept operational data collected during testing.

Air/Exhaust Flow	Exhaust Inlet Temp	Air Outlet Temp	Effectiveness
(kg/hr)	(°C)	(°C)	%
80.4	586	516	87.3
55.4	596	520	86.4
48	753	631	83.2
83.7	849	727	85.2
64.5	952	810	83.7
Air Inlet Temperature = 24°C			

Pressure drops measured on both the air and exhaust side were lower than those observed on the standard 3-pass metallic recuperator for the same temperature and flow conditions. This indicates that additional work may be conducted to enhance the heat exchange capabilities of the ceramic core by possibly reducing the dimensions of the flow passages to increase flow velocities, or by introducing ceramic inserts to promote turbulent flow and thereby increase the heat exchange in the ceramic core.

Following over 500 hours of operation at temperature and over 10 full thermal cycles, the ceramic core showed no signs of degradation after operating in the highly oxidizing environment. The core did not exhibit any cracking due to thermal stresses it may have been subjected to during operation in the hybrid configuration. Leakage tests were conducted following 500 hours of operation by statically pressurizing the air side of the recuperator and monitoring leakage flow rates through the material. There was no change in leakage flow rates when compared to the results of leakage testing which was performed in the as-manufactured state. Leakage rates at pressures typical of operation on an Acumentrics 5 kW SOFC were less than 2% of full cathode air flow rates.

Additional testing was conducted with an alternate hybrid configuration of one ceramic core and one metallic core. Although the ceramic core was able to drop the exhaust temperatures to levels below 750ºC, air outlet temperatures were slightly below 700ºC. The overall effectiveness of this arrangement was slightly below 80%. Future work to enhance the effectiveness of the ceramic recuperator may enable the 1+1 hybrid configuration to meet the required performance criteria for use on a 5 kW SOFC generator while significantly reducing the cost, parts count and weight of this component.

Conclusions and Future Directions

Acumentrics Corporation, in conjunction with Blasch Precision Ceramics, has successfully integrated a ceramic monolith into a multi-pass cross-flow recuperator and obtained greater than 80% effectiveness. The thermal model that was created for the ceramic core has been validated by empirical data, enabling the engineering team to use the model to accurately assess the effects of design changes to the ceramic core geometries prior to commitment of funds for new molds. Temperatures measured at intermediate stages in the recuperator during testing show that targets have been met for the use of lower grade alloys in the metallic sections. The initial steps to determine the feasibility of a hybrid ceramic/metallic recuperator have been successfully completed.

Future work will see the design, construction, and testing of pre-production hybrid recuperators. The following is a summary of future technical objectives:

- Evaluate ceramic component manufacturing techniques to optimize the ceramic core heat transfer rates.
- Design and manufacture custom molds for ceramic cores optimized to meet the performance and integration requirements of a hybrid recuperator suitable for volume production.
- Finalize a detailed hybrid recuperator design package incorporating all knowledge acquired regarding sealing and support techniques and integrated system performance.
- Manufacture several pre-commercial prototypes for testing and evaluation of construction techniques.
- Conduct both long term steady-state and thermal cycle testing to verify the performance and durability of the hybrid recuperator.
- Evaluate a combined cross-flow ceramic/counter-flow metallic hybrid configuration which may provide synergistic benefits in size, performance and cost for systems such as large scale coal-based power plants, or sub-1 kW portable generators.

IV.E.2 Advanced Control Modules for Hybrid Fuel Cell/Gas Turbine Power Plants

Hossein Ghezel-Ayagh (Primary Contact) and S. Tobias Junker
FuelCell Energy, Inc.
3 Great Pasture Road
Danbury, CT 06813
Phone: (203) 825-6048; Fax: (203) 825-6273
E-mail: hghezel@fce.com

DOE Project Manager: Travis Shultz
Phone: (304) 285-1370
E-mail: Travis.Shultz@netl.doe.gov

Subcontractors:
- National Fuel Cell Research Center (NFCRC), Irvine, CA
- Carnegie Mellon University (CMU), Pittsburgh, PA
- Pennsylvania State University (PSU), State College, PA

Objectives

The overall project goal is to develop advanced and intelligent control algorithms for hybrid fuel cell/gas turbine (FC/T) power plants. The specific objectives are:

- Establish a dynamic modeling environment to facilitate simulation studies, as well as development and testing of control algorithms.
- Increase reliability and availability to extend service life of the components in the hybrid FC/T power plant.
- Develop robust controllers that maintain stable operation and high performance in the presence of disturbances.
- Develop optimal control strategies to improve performance and to accommodate fast response during rapid transients.
- Accommodate measurement errors, as well as sensor and actuator faults to reduce the number of unplanned shutdowns.
- Integrate robust and optimal controllers into an overall supervisory framework.

Accomplishments

- Completed development of modular dynamic models for internally reforming carbonate fuel cells (Direct FuelCell®, DFC®) and solid oxide fuel cells (SOFCs) as well as balance-of-plant equipment including a micro-turbine generator. The models were based on the MATLAB®/Simulink® programming environment.
- Completed integration of sub-MW hybrid DFC®/T and SOFC/T simulation programs.
- Developed control strategies for fuel cell stack temperature, gas turbine operation, and fuel feed rate during start-up and power ramps.
- Completed input/output pairing ensuring stable plant operation and minimal interactions among control loops.
- Designed and validated decentralized multi-loop feedforward-feedback control structure.
- Completed off-line optimization studies for eighteen ramp and step load profiles while maximizing efficiency.
- Developed an inferential control strategy for adjusting fuel flow rate via estimation of disturbances in fuel composition.
- Developed a centralized linear quadratic regulator including state estimation via Kalman filtering that led to improved control of stack temperature and cell voltage.
- Developed and trained a neural network suitable for online control supervision based on the results from the control optimization studies.
- Improved prediction accuracy of the fundamental model by augmenting it with a neural network.

Introduction

The control system for FC/T hybrid power plants plays an important role in achieving synergistic operation of subsystems, improving reliability of operation, and reducing frequency of maintenance and downtime. The control strategy plays a significant role in system stability and performance as well as ensuring the protection of equipment for maximum plant life. Figure 1 shows a simplified process diagram of an

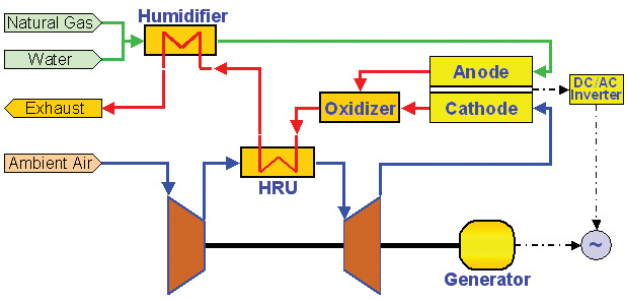

FIGURE 1. Conceptual Process Flow Diagram for SOFC/T System

internally reforming SOFC/T system, which is being studied for development of advanced control algorithms. The system is based on an indirectly heated Brayton cycle. The anode exhaust, which contains unreacted fuel, is mixed with the cathode exhaust in a catalytic oxidizer, where oxidation of fuel is completed. The oxidizer exhaust passes through a heat recovery unit in which it preheats the compressed air before entering the turbine. The hot compressed air is expanded through the turbine section, driving an electric generator.

Dynamic simulation has proven to be a powerful design tool to study the transient behavior of fuel cell/gas turbine hybrid systems. Development of an advanced control strategy is facilitated by using a dynamic model both as a simulation test bed and as part of the controller itself. Components of the advanced control module include a neural network supervisor, robust feedback controllers, and predictive system models. These advanced control components are used in the development and demonstration of an innovative algorithm that optimally and robustly controls hybrid power systems. The algorithm can easily be adapted to the type of fuel used, whether natural gas, coal gas, or digester gas.

Approach

The advanced control module shown in Figure 2 is based on a feedforward/feedback structure. It consists of a combined robust controller and a neural network supervisor that together manipulate the actuators to optimally control the hybrid system during load ramps. The feedforward controller will provide optimal dynamic scheduling based on the prescribed load profile and trends. Because the optimization routines are computationally too intensive for real-time application, they are carried out off-line. The resulting data is then used to train a neural network supervisor. The feedforward controller performance depends strongly on the accuracy of the model employed to tune it. A feedback control strategy is utilized to compensate for setpoint deviations caused by imperfect feedforward control moves and to counteract process disturbances such as variations in fuel composition and ambient temperature. The feedback controller will be designed to be robust to modeling errors and process disturbances.

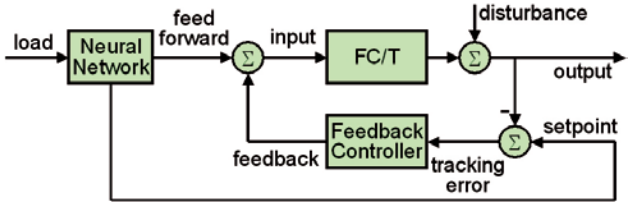

FIGURE 2. Advanced Control Module Comprising Neural Network Supervisor and Robust Feedback Controller

Results

A nonlinear dynamic model was developed and linearized. Optimal input/output pairing was determined via analysis of the relative gain array (RGA). A decentralized control structure comprising proportional and proportional-plus-integral control as well as feed-forward control and cascade control was developed and performance was confirmed. RGA analysis indicated that independent control loops of the hybrid system are coupled at time scales greater than one second.

To improve control performance, a centralized linear quadratic regulator (LQR) including state estimation via Kalman filtering (KF) was developed [1]. The controller was augmented by local turbine speed control and integral system power control. This control structure offers improved control of fuel cell temperature and improved rejection of variations in fuel composition when compared to the decentralized controller (Figure 3). However, the decentralized controller achieved better control of the oxidizer temperature. Because rejection of fuel variations and maintenance of cell temperature are more important than tight control of the oxidizer temperature the new controller is an improvement over the current state of the art.

A neural network (NN) supervisor was developed that mimics the function of the nonlinear dynamic optimization function block in generating setpoint profiles and feedforward (FF) control inputs. To avoid the high computational cost, the dynamic optimization could be replaced with a NN for fast on-line computations. Based on structural considerations, a diagonal recurrent neural network structure [2] was

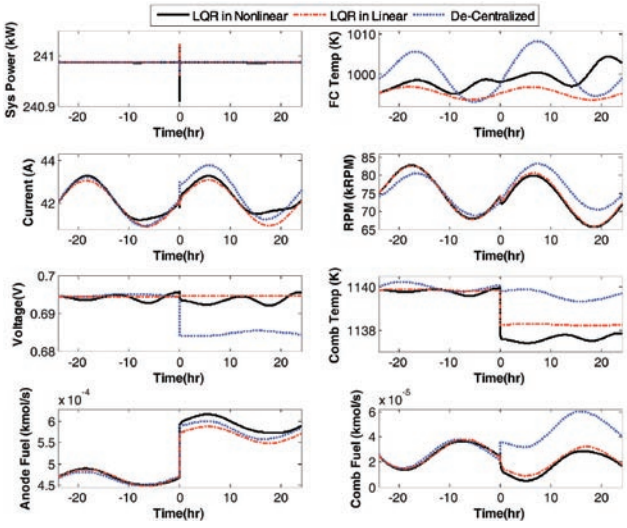

FIGURE 3. Performance Comparison of Centralized LQR Controller (using Linear and Nonlinear Models) with Previously Developed Decentralized Controller

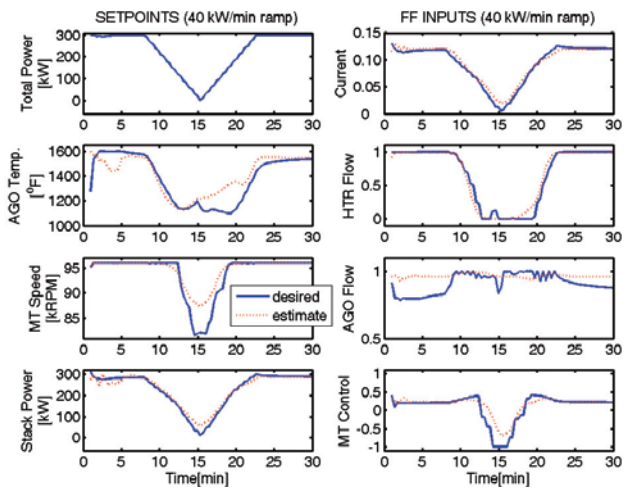

FIGURE 4. Neural Network Performance Evaluation for a 40 kW/min Power Ramp

developed for prediction of the optimal setpoint and FF inputs.

It was observed that dividing the supervisor into two separate NNs, one for setpoints, and one for FF inputs, resulted in better predictions. Several NN structures were tested to find an optimal structure for the available data. It was demonstrated, as shown in Figure 4, that the NN supervisor is suitable to generate outputs for an arbitrary load, even though the load was not used for the network training.

Conclusions and Future Directions

Summary and conclusions of results obtained this year include:

- Control of stack temperature and fuel cell voltage of the SOFC/T plant was improved via development of a centralized controller with state estimation.
- Compared to the previously developed decentralized controller, this controller takes all inputs/outputs and their interactions into account.
- Optimal control results were successfully modeled and predicted by means of a NN supervisor. This facilitates optimal feedforward control moves and setpoints under varying process conditions.
- Prediction of the original neural network supervisor was further improved by training the neural network with dynamic data including feedback of delayed outputs.
- The fundamental dynamic model was improved via a neural network compensator. This hybrid fundamental/NN model achieves better prediction of experimental data than is possible via the fundamental model by itself.

Overview of future work includes:

- Develop fuzzy logic fault detection and fault accommodation techniques.
- Integrate the developed control strategies into the simulation environment for extensive testing of the algorithms for their stability and robustness.

FY 2007 Publications/Presentations

1. R. Roberts, J. Brouwer, F. Jabbari, T. Junker, and H. Ghezel-Ayagh. *Control design of an atmospheric solid oxide fuel cell/gas turbine hybrid system: Variable versus fixed speed gas turbine operation*, Journal of Power Sources 161(1), pp. 484–491, October 2006.

2. F. Mueller, F. Jabbari, J. Brouwer, S. T. Junker, and H. Ghezel-Ayagh. *Linear Quadratic Regulator for a Bottoming Solid Oxide Fuel Cell Gas Turbine Hybrid System*, Proceedings of the 7th International Colloquium on Environmentally Preferred Advanced power Generation (ICEPAG), Newport Beach, CA, Paper No. ICEPAG2006-24018, September 5–8, 2006.

3. S. Kameswaran, L. T. Biegler, S. T. Junker, and H. Ghezel-Ayagh. *Optimal off-line trajectory planning of hybrid fuel cell/gas turbine power plants*, AIChE Journal, 53(2), 460–474 (2007).

4. F. Mueller, F. Jabbari, J. Brouwer, R. Roberts, S. T. Junker, and H. Ghezel-Ayagh. *Control Design for a Bottoming Solid Oxide Fuel Cell Gas Turbine Hybrid System,* Accepted for Publication in the Journal of Fuel Cell Science and Technology, scheduled for May 2007.

5. T.-I. Choi, K. Y. Lee, S. T. Junker, and H. Ghezel-Ayagh. *Neural Network Supervisor for Hybrid Fuel Cell/Gas Turbine Power Plants*, IEEE Power Engineering Society (PES) General Meeting, Tampa, FL, June 24–28, 2007.

References

1. S. Skogestad and I. Postlethwaite, *Multivariable Feedback Control – Analysis and Design*, John Wiley & Sons, New York, 1996.

2. C. C. Ku and K. Y. Lee, *Diagonal Recurrent Neural Network for Dynamic Systems Control*, IEEE Transactions on Neural Networks, 6:144-156, January 1995.

IV.E.3 Hot Anode Recirculation Blower for SOFC Systems

Dr. Mark C. Johnson
Phoenix Analysis & Design Technologies (PADT)
7755 S. Research Dr., Suite 110
Tempe, AZ 85284
Phone: (480) 813-4884; Fax: (480) 813-4807
E-mail: mark.johnson@padtinc.com

DOE Project Manager: Charles Alsup
Phone: (304) 285-5432
E-mail: Charles.Alsup@netl.doe.gov

Objectives

- Develop configuration that can pump anode gas at 750°C.
- Develop thermal choke design and component test at full temperature (750°C).
- Verify bearing/seal selection and design.
- Integrate and evaluate controller/motor.
- Develop low-cost integrated assembly to provide required performance and offer low cost in high volume.
- Develop technology that will service FutureGen requirements.

Accomplishments

- Completed pump head configuration study and down selected final low cost pumphead design. This pumphead is novel and is currently being reviewed for a patent application.
- Developed two bearing rigs and initiated endurance testing. Goal is 40,000 hours of life. Additionally, a novel bearing system has been developed that is intended to help meet this very long life requirement.
- Developed method for protecting motor components from process flow while operating at high-speed (20,000 RPM).
- Completed design suitable for servicing FutureGen configurations up to 1 MW in size. Conducted design review with Department of Energy (DOE) personnel.
- Participated in Commercialization Assistance Program with Dawnbreaker to help insure the marketability of the final product.

Introduction

The thrust of this research and development (R&D) effort is to develop technology that serves the solid oxide fuel cell (SOFC) industry and helps developers in this industry to succeed. The starting point for success rests with understanding the needs of the companies involved and this has been done through substantial discussions with these companies and the development of specifications with them. The designs that are now emerging can service some of the FutureGen requirements for SOFCs. Additionally, a derivative design is being developed that will service the smaller SOFC requirement.

The challenge is to develop a blower that is durable and can survive in a very harsh environment. Unlike proton exchange membrane fuel cell (PEMFC) systems, SOFC systems operate at very high temperatures (~850°C). Depending on system architecture, the proposed pump may very well be exposed to these extreme conditions (or close to it). Yet, the electric motor, controller, and bearings in the system must be kept at much cooler temperatures than the process flow. Therefore, the focus of this project is to develop an innovative approach to pump this hot process flow while providing cool temperatures for the sensitive pump components. Additionally, innovation is required to provide this capability and maintain low costs in high-volume production.

Approach

The approach used to develop this pump emphasizes design iterations with a reduction to working prototypes in rapid succession. Because of the complexities involved, side testing is used extensively. Side testing implies a test of some sub-system, or even a component, to ensure suitability. Finite element analysis is used liberally whenever detailed analysis can provide insight into design tradeoffs.

Additionally, the success of this project will be dependent on close collaboration between PADT and SOFC developers. The requirements for the developers is changing continually and to glean the most out of the prototypes we build, regular feedback is needed. We are conducting design reviews with likely users of hot anode recycle blower (HARB) technology. Lastly, for some of the applications we are looking to service, partnership with high volume manufacturers will be required to achieve the DOE cost objectives.

Results

Unfortunately, many of the most important results of our recent work are either PADT proprietary information or proprietary to our customers. Therefore, we can only provide high level summaries here.

One high-level accomplishment was the successful testing of our proof-of-concept blower. This blower, shown in Figure 1, was tested to almost 600°C. Still, the sensitive motor and bearing components were kept well under 80°C. This testing has provided a proof-of-concept for our thermal management approach.

A second major accomplishment of the last years' effort is the down selection and design of a novel aerodynamic solution to the specifications we have been receiving. This has lead to a pumphead investigation that included the following options:

- Regenerative, or side channel pumphead. We looked at many variations here.
- Cast centrifugal pumphead.
- Multistage options.

The results of this effort has lead us to the lowest cost solution that can still meet the durability and aerodynamic specifications required by our customers. We are now manufacturing a prototype with this pumphead style. Unfortunately, we cannot show any details regarding this solution because of proprietary issues. A patent is now being evaluated.

A third important result of our effort deals with bearing life. To support this work, we have constructed two bearing rigs and mule motor, which are now running as much as possible with various bearing options. The bearing rigs are shown in Figure 2. These tools have provided us with much early bearing data. This data

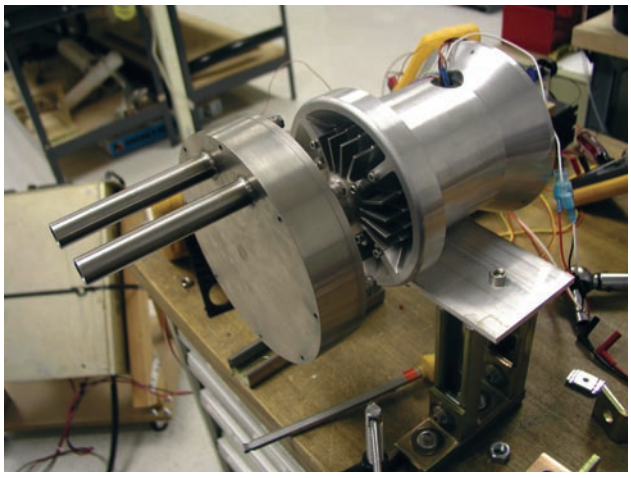

FIGURE 1. PADT HARB Prototype

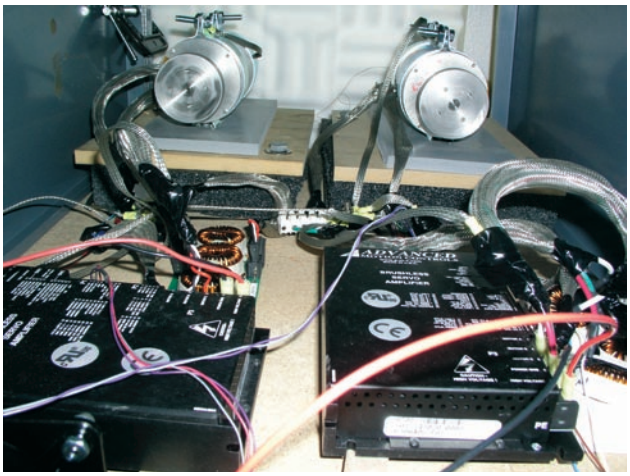

FIGURE 2. Bearing Rigs for Life Evaluation and Extension

along with expert consultation has lead to a very long life bearing system which is now incorporated in our HARB baseline blower. Again, we cannot show a cross-section of the bearing system because of proprietary issues. Also, we are investigating the patentability of this design.

Two other important results include:

1. Development of a motor and controller system that is integrated with the blower housing but protected from the process flow.
2. Build up of clear understanding of customer requirements in both the FutureGen effort and the smaller (3 kW – 10 kW) SOFC effort.

Conclusions and Future Directions

The work we have done so far has led us to the conclusion that we really need two types of blower solutions: one for FutureGen and one for small SOFC power plants. Fortunately, the technologies for the pumphead, bearing life, and thermal management will support both requirements. Additionally, we have concluded that close interaction with SOFC developers and manufacturing partners will be important for overall commercial success of our efforts.

Future work will now focus on demonstrating the durability and performance of the designs we have developed. We anticipate a number of endurance tests will be run and some of these blowers will be tested at customer's facilities.

FY 2007 Publications/Presentations

1. We are planning a presentation for the upcoming SECA Workshop in San Antonio.

IV.E.4 Foil-Bearing Supported High-Speed Centrifugal Cathode Air Blower

Giri Agrawal (Primary Contact), Bill Buckley, Dennis Burr, Sam Rajendran
R&D Dynamics Corporation
15 Barber Pond Road
Bloomfield, CT 06602
Phone: (860) 726-1204; Fax: (860) 726-1206
E-mail: agragiri@rddynamics.com
Website: www.rddynamics.com

DOE Project Manager: Charles Alsup
Phone: (304) 285-5432
E-mail: Charles.Alsup@netl.doe.gov

Objective

Design a foil-bearing supported high-speed centrifugal cathode air blower (CAB) meeting all the technical requirements of the Solid State Energy Conversion Alliance (SECA) members and develop a process to reduce manufacturing cost of CABs to $100 per unit based upon a production volume of 50,000 units/year.

Accomplishments

- Preliminary design for a low cost high efficiency cathode air blower was completed.
- A cost model targeting $100 was developed.
- Breadboard testing was conducted to prove structural integrity of plastic impellers.
- Feasibility of program was shown.

Introduction

The goal of SECA is to develop commercially-viable ($400/kW) 3 to 10 kW solid oxide fuel cell (SOFC) systems by year 2010. SOFC power generation systems are attractive alternatives to current technologies in diverse stationary, mobile, and military applications. SOFC systems are very efficient, from 40 to 60 percent in small systems and up to 85 percent in larger co-generation applications. The electrochemical conversion in a SOFC takes place at a lower temperature (650 to 850ºC) than combustion-based technologies, resulting in decreased emissions – particularly nitrogen oxides, sulfur oxides, and particulate matter. These systems all offer fuel flexibility, as they are compatible with conventional fuels such as hydrogen, coal, natural gas, gasoline, or diesel. Despite these advantages, advances in balance of plant (BOP) component design must be developed before the SECA program goals can be realized.

SOFC systems require blowers to provide motive force to incoming atmospheric air, in order to overcome the pressure drop in the various valves and heat exchangers, and in the fuel cell stack. The energy required to drive this component is typically one of the largest parasitic loads for the SOFC system; consequently, high blower efficiency is paramount to high system efficiency. Furthermore, blower reliability is critical to ensure safe long-term system operation.

Approach

- In Phase I, a CAB was conceptualized and designed. A process using DFMA (Design for Manufacturing and Assembly) techniques was developed for reducing manufactured cost of CABs to $100 per unit, based upon a production volume of 50,000 units per year.
- In Phase II, a detailed design of CABs will be completed and a prototype manufactured and tested using cost reduction techniques identified in Phase I.
- Phase III will start the commercialization phase of the project. CAB field demonstrations will be initiated with SECA members and other potential OEM manufacturers. Distributors will be identified and contacted.

Results

A preliminary design has been performed. The CAB has been designed as a centrifugal compressor running at 80,500 rpm. In order to meet high reliability, the rotating assembly will be supported on foil air bearings.

The CAB is driven by a brushless permanent magnet DC motor and controlled by a sensorless controller. Such motors have shown high efficiency and high reliability for the power range required for the CAB.

An existing fuel processor blower (FPS) developed at R&D Dynamics Corporation was used as a baseline to develop and reduce the cost of the CAB. The existing FPS blower was previously designed, manufactured and successfully tested for a proton exchange membrane (PEM) fuel processor and was built by R&D Dynamics for UTC Fuel Cells under a DOE funded project. A cross-section of the CAB is shown in Figure 1. An innovative low cost split housing was designed to reduce manufacturing and assembly cost of the CAB. Figure 2 shows the split housing design. Plastic impellers were tested for structural integrity to be used in CABs which will reduce blower cost. Figure 3 shows the

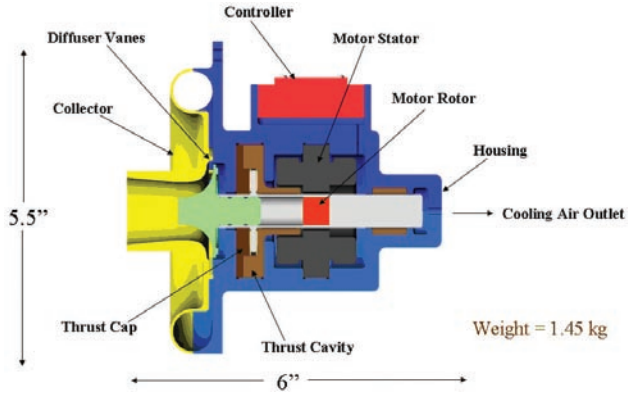

FIGURE 1. Cross-Section of CAB

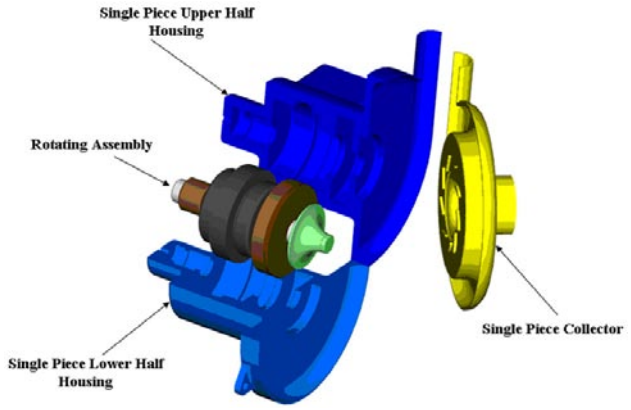

FIGURE 2. Split Housing Design of CAB

plastic impeller installed in the high speed test rig ready for testing.

The CAB is affordable, efficient, reliable, small, light weight, and meets turndown requirements.

The FPS blower was used to develop the first cost model using DFMA tools. From the first cost model of the FPS blower, cost components were identified. From the cost components and lessons learned, the CAB was designed. A final cost model was developed for the CAB. Part count was reduced from a total number of 113 parts for the existing FPS blower to a part count of 16 for the CAB. The CAB estimated cost is $105.11, which is close to the DOE target of $100 at a production rate of 50,000 units/year. Additional DFMA analysis could further reduce the cost.

Technical Requirements

A blower specification was selected from the requirements provided by DOE and discussions with SECA members. It was understood that once this blower is developed, it can be scaled to meet specific requirements of various SECA members. The specific

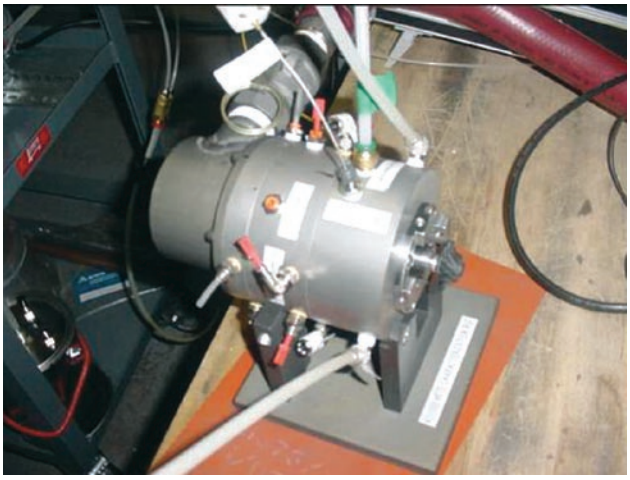

FIGURE 3. Plastic Impeller Installed in Test Rig

blower requirements selected to design the CAB are as follows:

- Process Gas Air
- Inlet Pressure 1.01 Bar (14.7 psia)
- Outlet Pressure 1.22 Bar (17.64 psia)
- Pressure Ratio 1.2
- Inlet Temperature 20°C (68 °F)
- Outlet Temperature 40.7°C (105.4 °F)
- Volume Flow Rate 1500 slpm
- Mass Flow Rate 1.8 kg/min (3.98 lbm/min)
- Turn Down Ratio 5:1
- Isentropic Power 474 watt

Technical Summary of CAB (Design Point)

The technical summary of the blower design is as follows:

- Blower Type Centrifugal
- Mechanical Speed 80,500 rpm
- Weight 1.45 kg (3.2 lbm)
- Bearings Foil Gas Bearings
- Motor Type Permanent Magnet Motor
- Controller Type Sensorless Controller
- Input Electric Power 769 watt
- Isentropic Efficiency 75%
- Total Blower Cost $105.11 [@ 50,000 units/year]
- Life >40,000 hrs

Conclusions and Future Directions

Phase I research work was highly successful in meeting all the requirement of SECA members and proved the feasibility of the project. Phase I work opened venues for further development to

manufacture the designed blower and test successfully to commercialize the technology for SOFC system applications to meet the goals of SECA members, which will be done in Phase II of this project.

FY 2007 Publications/Presentations

1. "Project Review Presentation" March 5, 2007, DOE NETL- Morgantown,WV 26507.

IV.E.5 Foil Gas Bearing Supported High-Speed Centrifugal Anode Gas Recycle Blower

Giri Agrawal (Primary Contact),
Bill Buckley, Dennis Burr, Ali Shakil
R&D Dynamics Corporation
15 Barber Pond Rd.
Bloomfield, CT 06002
Phone: (860) 726-1204; Fax: (860) 726-1206
E-mail: agragiri@rddynamics.com

DOE Project Manager: Charles Alsup
Phone: (304) 285-5432
E-mail: Charles.Alsup@netl.doe.gov

Objectives

Demonstrate the feasibility of using a high-speed centrifugal foil bearing supported anode gas recycle blower (FBS-AGRB) to help members of the Solid State Energy Conversion Alliance (SECA) meet their solid oxide fuel cell (SOFC) goal of higher efficiency and lower overall system cost.

Accomplishments

- Substantial progress has been made, and a prototype FBS-AGRB unit has been designed and built meeting all SECA member requirements. The unit has the following features:
  - Low-cost design which incorporates "design for manufacturing and assembly" concepts
  - High temperature capability: >850°C
  - High-efficiency high-speed motor and centrifugal blower
  - Oil-free gas bearings
  - Compact
  - Scalability to larger sizes
  - No gas, sulfur, silica or heavy metal leakage
  - No purge gas required
  - No parasitic cooling required
  - Mechanical type seals were not required
  - Explosion-proof design
  - No corrosion/carbon deposition
  - 40,000-hour lifetime
  - Maintenance free
- The prototype FBS-AGRB unit is ready for testing at elevated temperatures.
- Initiated cost-reduced design. Conical gas bearing design and manufacturing is in progress for low-cost, high temperature capability and efficiency.

Introduction

The goal of the SECA is to develop commercially-viable ($400/kW) 3- to 10-kW SOFC systems by 2010. SOFC power generation systems are attractive alternatives to current technologies in diverse stationary, mobile, and military applications. SOFC systems are very efficient, from 40 to 60 percent in small systems and up to 85 percent in larger co-generation applications. The electrochemical conversion in a SOFC takes place at a lower temperature (650 to 850ºC) than combustion-based technologies, resulting in decreased emissions – particularly nitrogen oxides, sulfur oxides, and particulate matter. These systems all offer fuel flexibility, as they are compatible with conventional fuels such as hydrogen, coal, natural gas, gasoline, or diesel. Despite these advantages, advances in balance-of-plant component design must be developed before the SECA program goal can be realized.

SOFC systems that incorporate some recycling of the anode exhaust gas, which is mixed with incoming fresh fuel prior to entering the pre-reformer, have a higher efficiency and offer the potential for lower overall system cost. An anode gas recycle blower (AGRB) is an attractive solution to perform this task.

Approach

R&D Dynamics has focused on the design and development of a FBS-AGRB to achieve the goals set by SECA members. An innovative, cost-reduced, compact, high-temperature, high-speed centrifugal blower has been designed and built. The FBS-AGRB rotating assembly is supported on state-of-the-art proven foil gas bearing technology. The foil gas bearing technology and the high-speed permanent magnet (PM) motor design make the FBS-AGRB very promising for meeting the technical targets and cost. The integration of conical foil bearings into the FBS-AGRB will further drive down the blower cost.

The FBS-AGRB has been designed and built to meet the requirements of SOFC systems. The FBS-AGRB advances progress toward the goal of making economically viable and efficient SOFC systems because of its potential for:

- Low cost using simple design and materials.
- High temperature capability (>850°C) using foil gas bearings, and advanced high temperature magnets for PM motor.
- Highest blower efficiency via high-speed centrifugal impeller, foil gas bearings, PM motor and sensor-less controller.
- Contamination-free using oil-free foil gas bearings.
- High reliability requires no maintenance.
- Compactness and light weight.

Results

The FBS-AGRB has been designed and built for an inlet temperature of 600 to 850°C, atmospheric pressure, pressure rise of 4-10 inches of water, and a flow of 100 standard liters per minute (slpm), which is nominally composed of 46 slpm H_2O, 27 slpm CO_2, 20 slpm H_2 and 7 slpm CO. Overall efficiency exceeds 40% under aforementioned operating conditions. The unit has a variable speed control with a flow turndown ratio of 5 to 2. The blower unit will have a design life of >40,000 hours, with a 100% duty cycle and 10,000 hour maintenance interval. The unit will be able to tolerate at least 30 thermal cycles between operating and room temperatures over its design life. The unit cost of the blower for production rates of >50,000 units was estimated to be $100.

Design points for the FBS-AGRB are as follows:

Shaft speed	98,000 rpm
Pressure Ratio	1.025
Pressure Rise	25.4 cm of water (10 inches of water)
Inlet Pressure	1.01 bar (14.69 psia)
Outlet Pressure	1.08 bar (15.06 psia)
Inlet Temperature	850°C (1562°F)
Outlet Temperature	857.3°C (1575.2°F)
Gas Constant	0.369 J/Kg °C (68.64 ft-lbf/lbm R)
Specific Heat Ratio	1.274
Mass Flow	1.54 g/s (0.204 lbm/min)
Volume Flow	100 slpm
Impeller Isentropic Power	15.6 Watt

Figures 1 and 2 show the cut-section view and the manufactured blower assembly, respectively. Figure 3 shows the manufactured shaft assembly.

Key technologies were incorporated into the blower design, including state-of-the-art aerodynamics, foil gas bearings, PM magnet motor using advanced high temperature magnets, innovative fan design with fins mounted on the shaft assembly, thermal choke to separate the hot side from the cold side, and sensor-

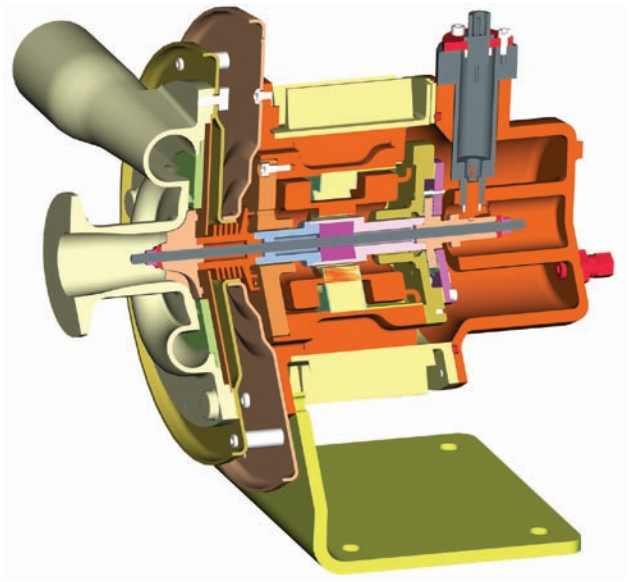

FIGURE 1. Cut-Section View of AGRB

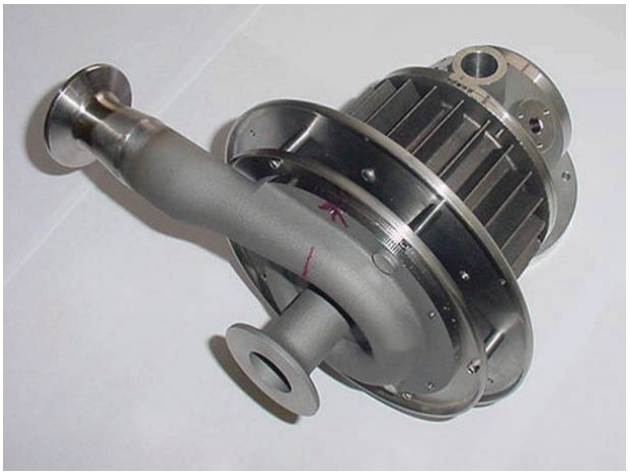

FIGURE 2. View of the Manufactured FBS-AGRB Prototype Unit

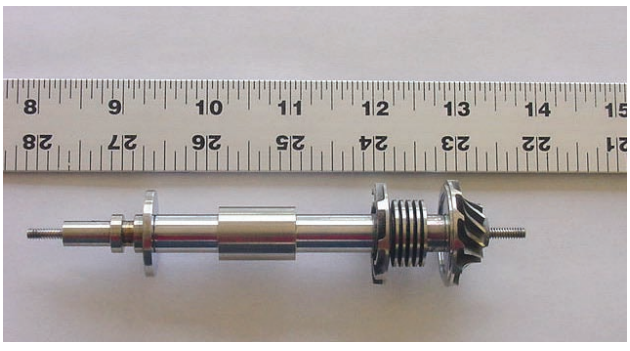

FIGURE 3. View of the Manufactured Shaft Assembly

less controller. Design analysis included performance prediction maps; preliminary design; finite element analysis including thermal, vibration and stress; computational fluid dynamics analysis; rotor dynamics analysis; cooling flow analysis; detailed design and drawings. Tests performed on AGRB components were load deflection on journal and thrust bearings, back electromotive force testing on motor rotor and stator, etc. A furnace will be used to heat the gas to 850°C for elevated temperature testing of the FBS-AGRB. The blower is ready for testing.

Technical feasibility of the conical bearing, proven in Phase I, has been extended to the manufacturing of the bearing and the test rig. The designed test rig is capable of testing many combinations of conical bearings at loads and speeds while measuring friction.

Conclusions and Future Directions

- Key blower technologies were proven by extensive design and analysis.
- A prototype unit has been designed and built which is ready for testing.
- The high-temperature blower design evolved to be a successful design which can achieve SECA goals.
- The blower cost was estimated to be $100 at a production volume of 50,000 units/year.

Phase II is in progress. Work needs to be continued in Phase II as follows:

- Test blower at high temperature conditions.
- Incorporate rigorous “design for manufacturing and assembly” techniques to further reduce cost.
- Build conical bearing rig, test bearings and incorporate bearings into blower design.
- Demonstrate blower to SECA members.
- Test blower in SECA member’s fuel cell systems.

FY 2007 Publications/Presentations

1. “Foil Bearing Supported High Speed Centrifugal Blower” Progress Report Period 08/07/06 - 04/20/07, April 2007.

2. “Foil Bearing Supported High Speed Centrifugal Blower” Project Review Presentation, DOE NETL - Morgantown, WV, March 05, 2007.

3. “Foil Bearing Supported High Speed Centrifugal Blower” Progress Report Period 08/07/06 - 12/07/06, December 2006.

IV.E.6 Low-Cost, High-Temperature Recuperators for SOFC Fabricated from Titanium Aluminum Carbide (Ti_2AlC)

Detlef Westphalen (Primary Contact), John Dieckmann, Anant Singh and Tyson Lawrence
TIAX LLC
15 Acorn Park
Cambridge, MA 02140
Phone: (617) 498-5821; Fax: (617) 498-7206
E-mail: westphalen.d@tiaxllc.com

DOE Project Manager: Charles Alsup
Phone: (304) 285-5432
E-mail: Charles.Alsup@netl.doe.gov

Subcontractor:
3-ONE-2 LLC
4 Covington Place, Voorhees, NJ 08043

Objectives

- Verify technical feasibility of solid oxide fuel cell (SOFC) recuperators made of titanium aluminum carbide (Ti_2AlC) through analysis and testing.
- Develop and validate fabrication approach for SOFC recuperators using Ti_2AlC.
- Establish limited-run production capability for SOFC recuperators for systems of 3 to 10 kW net power.

Accomplishments

Initial work in a Phase I small business innovative research (SBIR) project has resulted in the following accomplishments.

- Tested a recuperator core sample, demonstrating suitability of Ti_2AlC for this application.
- Demonstrated feasibility for key manufacturing issues: molding of fins with sufficiently thin dimensions, bonding of components for final assembly, and cost estimates for fabrication consistent with recuperator cost targets.
- Sized recuperator for SOFC system of target power level (3-10 kW).

Introduction

Achieving low system cost for SOFC technology requires novel approaches to the materials used for the air preheat recuperator. The recuperator is needed to heat up large quantities of air (~6 to 7 times in excess of stoichiometric requirements). The cost of existing recuperator designs is high primarily because of the high cost of the materials used. Heat resistant metal alloys tolerant of gas temperatures up to 1,000°C such as the Inconel-series metal alloys are typically used. These alloys are expensive, difficult to machine and form, and cannot be cast into near-net shape, leading to bulky heat exchanger designs. Further, the recuperator surfaces exposed to air need to be aluminized to prevent chromia poisoning of the cathode. The aluminizing further increases cost.

A new class of machinable, easily fabricated ceramic materials with good high temperature properties has been discovered. The example of this material class that is best suited for the recuperator application is Ti_2AlC. This material has excellent high temperature mechanical and thermal properties, high temperature stability, and good manufacturability, making this an ideal material for high temperature recuperators, specifically for air preheaters for SOFCs. Extensive testing has been carried out by our subcontractor in environments similar to that of a SOFC recuperator to provide assurance that the material is compatible with this application. The material forms a strong protective alumina layer which adheres well to the base material because of the very close match between the coefficients of thermal expansion of alumina and Ti_2AlC.

Fabrication with Ti_2AlC involves the following steps: preparation of a powder of the material, combining with organic binders, heating to a modest temperature level, injection molding, cooldown, soaking in water to partially dissolve the binders, and sintering at high temperature (and perhaps simultaneously joining separately molded parts). Follow-up processing can include machining and subsequent joining.

Approach

TIAX is developing an approach for net-shape (or near net-shape) fabrication of SOFC recuperators with machinable ceramic (Ti_2AlC) using counterflow plate-fin heat exchanger configurations. During the Phase I work, we first assessed key manufacturability attributes of the material and our design approach, including molding of thin fins, bonding of component parts of a Ti_2AlC recuperator, and estimated cost for volume production. A small proof-of-concept recuperator core sample was designed, fabricated, and successfully tested. Testing included heat transfer performance testing and thermal

cycling. Analysis was carried out for sizing of a full-scale recuperator for a 3 to 10 kW SOFC system.

Results

Manufacturability test work included mold experiments to verify that fins with sufficiently thin dimensions can be fabricated, tests of diffusion bonding of pre-sintered parts, and tests of simultaneous diffusion bonding and sintering.

Small fin dimensions will enable high heat transfer performance with a compact lightweight recuperator. Fins of thickness from 0.5 to 2 mm were fabricated using a dedicated mold. Examples of the molded fins are shown in Figure 1. The molding and sintering work showed that fins with optimized dimensions can be fabricated using this approach.

The ability to use diffusion bonding to connect Ti_2AlC parts makes fabrication of complex structures much easier and eliminates the use of a separate bonding material, whose compatibility with the SOFC recuperator environment would have to be proven. Bond testing was carried out first for presintered parts machined to mimic fins and a plate to which the fins would be attached with connection between the fin tips and the plate. The parts bonded securely with no evidence of gaps at the bond interfaces. Additional work was carried out with unsintered parts to test simultaneous sintering and bonding. Two parts bonded in this fashion are shown in Figure 2. The high level of continuity of the material across the interface of the formerly separated parts shows the success of this joining technique.

Testing was carried out with a proof-of-concept core sample of the Ti_2AlC recuperator. The core sample is shown in Figure 3. The sample was machined out of a block of Ti_2AlC, and hence has somewhat coarser

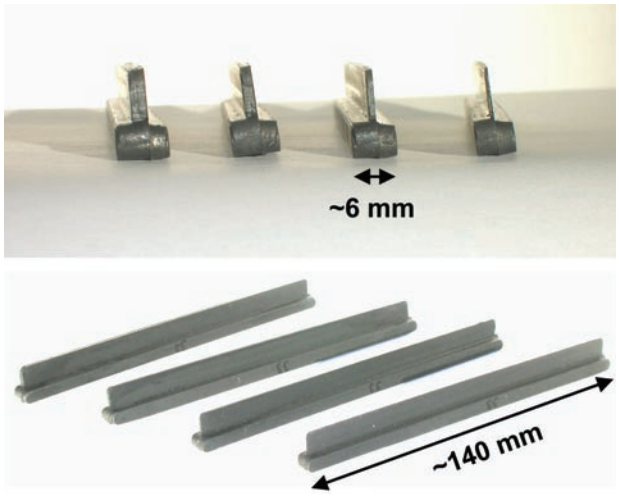

FIGURE 1. Molded Fins Prior to Sintering

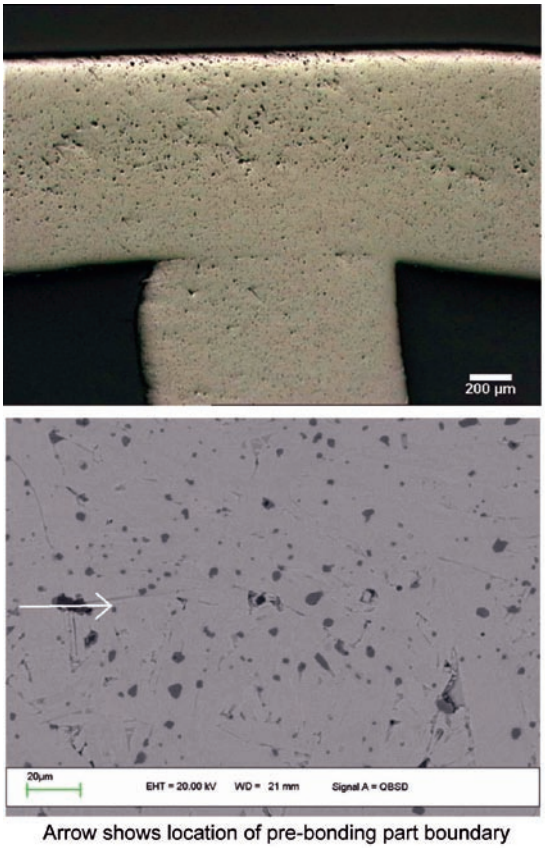

FIGURE 2. Closeup and Scanning Electron Microscope Image of Simultaneously Sintered and Bonded Ti_2AlC

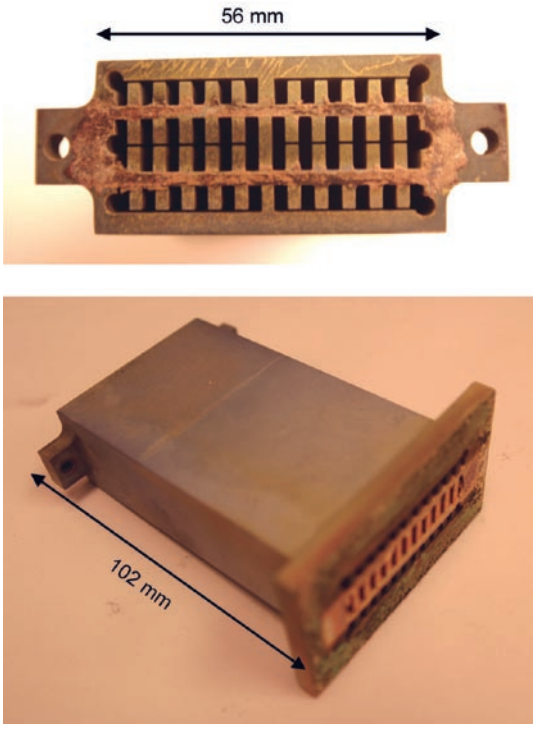

FIGURE 3. Recuperator Core Sample after Testing

dimensions than desired for a full-scale recuperator and plain fins, rather than enhanced fins which will be implemented in a more mature design. The core sample is intended to represent a portion of a recuperator in that it does not provide the full level of effectiveness required for the SOFC application. Roughly four of these sections in series would be required to achieve the desired level of recuperator effectiveness. Testing was carried out with the core sample representing a different portion of a complete counterflow recuperator for each test. Air inlet temperatures were selected accordingly. Test results for one of the tests are shown in Figure 4. The effectiveness measured for the core sample ranged from roughly 40% to 60%, with lower effectiveness for the lower test temperatures. The results compared well with predicted effectiveness levels for the lower test temperatures and exceeded the predictions at higher temperatures.

Transient testing was also carried out with the core sample to determine whether the material is susceptible to thermal gradients and thermal shock. The core was heated up to a high temperature with the hot gas inlet temperature close to 1,000°C and then allowed to cool. Tests were done with peak cooldown rates for measured air temperatures up to 45°C/min. Total test time for the core sample, including both steady-state performance tests and transient tests, was 67 hours. The sample showed no indications of damage after testing.

Analysis was carried out to design a recuperator for the SBIR Topic Description requirements, which were as follows.

- Pressure drop:
  - 6 to 10 in w.c. (1.5 to 2.5 kPa) on the air side
  - 3 to 5 in w.c. (0.75 to 1.25 kPa) on the stack exhaust side
- Effectiveness: 85% to 90%
- Flow rate: 1,500 standard liters/min (53 std ft^3/min or 108 kg/hr)

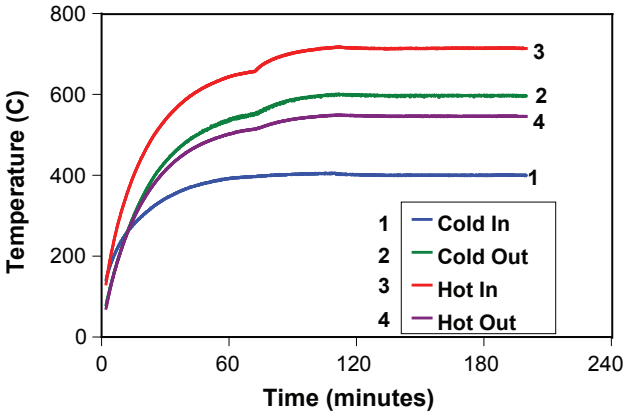

FIGURE 4. Example Data for Core Sample Testing

Based on these parameters, the recuperator uninsulated size including manifold passages is 15 inches long x 6 inches wide x 7 inches high. Its weight is roughly 25 lb (11.4 kg). Manufacturing cost analysis was carried out for the recuperator design for a production volume of 50,000 units per year for a production process which has been proposed but must be validated in the next phase of the work. The analysis made use of TIAX's activity-based manufacturing cost analysis tools, used extensively for a wide range of products from appliances to fuel cells (e.g. Reference 1). The cost calculated for the recuperator is roughly $200, 58% of which represents raw material costs. This is based on a future cost scenario for titanium powder, one of the key raw materials. The assumed cost scenario is consistent with predictions of References 2 and 3.

Conclusions and Future Directions

The work carried out during the Phase I SBIR project supports the feasibility of the proposed approach for manufacture of low-cost, high-performance recuperators for SOFC fuel cells using Ti_2AlC. Two of the key manufacturing issues have been tested with subscale fabrication tests. A proof-of-concept recuperator core sample was fabricated and successfully tested. Thermal and manufacturing cost analyses were carried out, thus defining the size of a recuperator for SOFCs in the 3 to 10 kW range and showing that the recuperators can be low-cost in volume production.

Next steps will include verification of full-scale manufacturing and a series of environmental tests for the Ti_2AlC material to assure compatibility with the SOFC exhaust gas in the anticipated recuperator operating environment. The work will lead towards fabrication and testing of a full-scale recuperator prototype and set up for limited production of the prototype after successful testing.

FY 2007 Publications/Presentations

1. SBIR Phase I final presentation made to DOE/NETL project management, March 20, 2007.

2. SBIR Phase I final report has been finalized and will be submitted in July 2007.

References

1. "Conceptual Design of POX / SOFC 5kW Net System", presentation to DOE/NETL, prepared by Arthur D. Little, Inc., January 2001.

2. Crowley, G., "Low-Cost Titanium", *Advanced Materials & Processes,* November 2003.

3. Camanoe Associates, "The Role of Titanium in the Automobile: Understanding the Economic Implication of Three Emerging Technologies", report prepared for the Northwest Alliance for Transportation Technology, July 2002.

IV.E.7 Feasibility of a SOFC Stack Integrated Optical Chemical Sensor

Michael A. Carpenter
College of Nanoscale Science and Engineering
University at Albany – SUNY
Albany, NY 12203
Phone: (518) 437-8667; Fax: (518) 437-8603
E-mail: mcarpenter@uamail.albany.edu

DOE Project Manager: Heather Quedenfeld
Phone: (412) 386-5781
E-mail: Heather.Quedenfeld@netl.doe.gov

Objectives

- Design of thermally stable nano-cermets using radio frequency magnetron sputtering techniques.
- Synthesis of nano-cermets with a narrow particle diameter distribution.
- Probe Au nanoparticle surface plasmon resonance (SPR) properties and Pd-YSZ (yttria-stablized zirconia) optical properties as a function of temperature and chemical exposure.

Approach

- Synthesis of Au-YSZ nano-cermets using physical vapor deposition techniques.
- Characterize Au nanoparticles using optical and microstructural analytical techniques.
- Testing of thermal stability (500-1,000°C) of nano-cermets and their corresponding optical properties.
- Determine the thermal and chemical stability (CO, NO_2, hydrogen) of nano-cermets and the corresponding optical properties.

Accomplishments

- The detection of H_2 with a detection limit of 100 ppm using all-optical techniques was demonstrated at an operating temperature of 500°C in the presence of an air carrier gas.
- The detection of NO_2 with a detection limit of 5 ppm using all-optical techniques was demonstrated at an operating temperature of 500°C in the presence of an air carrier gas.
- Performed initial sensor testing studies for the detection of ethanol (as a representative hydrocarbon target gas) at an operating temperature of 500°C in the presence of an air carrier gas. Easily detect 150 ppm of ethanol with no obvious carbon contamination.

Future Directions

- Evaluate the long term stability of the Au-YSZ films towards both temperature and CO, H_2 and NO_2 exposures. Increase detection selectivity between the target gases
- Evaluate the sensing properties of the Au-YSZ tailored nanocomposite films for the detection of sulfur compounds

Introduction

The Department of Energy is investigating the feasibility of harsh environment compatible chemical sensors based on monitoring the surface plasmon resonance (SPR) bands of metal nanoparticle doped YSZ nano-cermets, as a function of changes in its chemical environment (e.g. exposures to CO, H_2, NO_2 and hydrocarbons) and changes in temperature (500-900°C). In particular, Au nanoparticles exhibit a strong SPR band whose shape and spectral position is not only highly dependent on the refractive index of the host medium but also on chemical reactions at the interface between the metal and the surrounding environment [1].

Approach

The Au-YSZ nanocomposite films are deposited using dual target confocal physical vapor deposition, with the metal and metal oxide sputtering gun deposition rates tuned to achieve the desired metal to metal oxide composition. Thermal annealing in argon at temperatures above their respective operating temperatures is used both to thermally stabilize the films and also to grow nanoparticles of a given size. Materials characterization of the films using scanning electron microscopy (SEM), Auger spectroscopy, Rutherford backscattering spectroscopy (RBS) and X-ray diffraction (XRD) analyses is used to determine the microstructural and composition properties. Ex-situ optical characterization using ultraviolet-to-visable (UV-Vis) absorption spectroscopy and spectro-ellipsometric analysis is used to correlate the material properties with the resulting optical properties. *In situ* Uv-Vis spectroscopy utilizing a charge coupled device (CCD) based detection system as a function of both temperature and chemical exposure is used to determine the gas sensing properties with a time resolution on the seconds scale. Test gases include, CO, NO_2, hydrogen and hydrocarbons which will provide a range of reducing and oxidizing environments whose absorption

spectra effects combined with theoretical calculations will help deconvolute changes in both the dielectric and the chemical environment surrounding the bimetallic and metallic nanoparticles.

Results

From our previous work we have determined that O_2 at high temperatures reacts to form O_2- which then occupy the oxygen vacancies in the YSZ matrix. In doing so, electrons are removed from the gold nanoparticle causing a redshift in the SPR band. Highlights of the last year has included further studies of the CO reaction but much of the effort this current year has included H_2, NO_2 and ethanol sensing studies. As the reaction of CO with the bound O_2- is a prerequisite for the oxidation of CO, it is likely that H_2 will interact in a similar manner with O_2- and form water as the reaction product, while donating electrons back to the gold nanoparticle, as per the following reaction scheme:

$$H_2 + O^{2-}/Au^{2+} / YSZ \rightarrow H_2O + Au / YSZ$$

The hydrogen exposure experiments we have performed cause a blue shift and a narrowing of the SPR band in support of the above reaction mechanism. The data analysis of these reactions was performed in a similar manner as done for the CO studies. The H_2 sensing signal is shown in Figure 1 and has a response time of ~40 s, while the recovery time has only one stage and is comparable to the response time.

We have also studied the temperature dependence of the H_2 reaction and as shown in Figure 2 for 1% hydrogen in air exposures there is no change in the SPR band at room temperature upon exposure to the hydrogen gas mixture. The reaction onset appears at a lower temperature than observed for the CO reactions at ~200°C, which is still consistent with the onset of

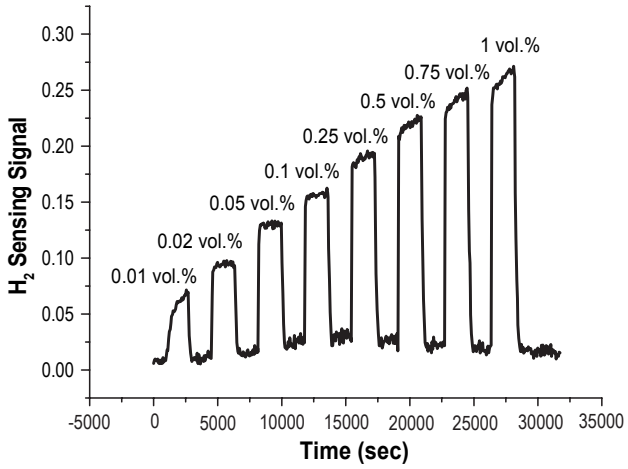

FIGURE 1. H_2 Sensing Signal as a Function of Rime for Repeated 0.01, 0.02, 0.05, 0.1, 0.25, 0.5, 0.75 and 1% H_2 in Air Exposures at 500°C

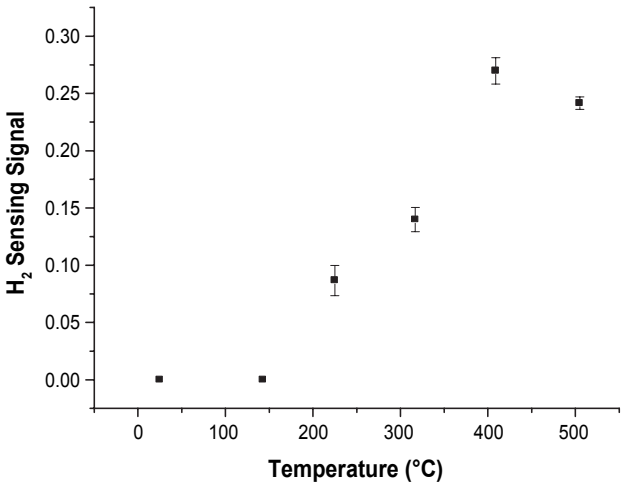

FIGURE 2. Sensing Signal Dependence on Temperature for 1% H_2 in Air Exposures

the O^{2-} formation on YSZ matrices. The H_2 sensing signal change appears to saturate at 400 and 500°C. Furthermore, the sensing signal was also dependent on the presence of oxygen as hydrogen was not detectable for H_2 mixtures in pure nitrogen at any of the operating temperatures, thus further supporting the proposed sensing mechanism.

NO_2 Sensing Studies

We have performed a series of exposure studies which demonstrate the reversible detection of NO_2 which show a detection limit of 5 ppm at 500°C in the presence of air. The reaction of NO_2 on the Au-YSZ matrix is significantly different than the H_2 and CO studies. While H_2 and CO require a reaction with O^{2-} to induce a sensing signal, NO_2 catalytically reacts on hot gold particles forming NO and O atoms. The O atoms then subsequently react at the tri-phase boundary forming O^{2-} ions and remove electrons from the Au nanoparticles causing a red shift in the SPR band similar to that observed for O_2 reacting with the Au-YSZ matrix. A series of NO_2 exposure experiments were performed at

$$NO_2 + Au / YSZ \rightarrow O^{2-} + NO + Au^{2+} / YSZ$$

an operating temperature of 500°C with NO_2 concentrations from 1 ppm to 100 ppm as shown in Figure 3 which displays signal change vs. time. The NO_2 detection limit as seen in this figure is 5 ppm with reversible signal changes observed over the entire three day experiment. As indicated in the above reaction scheme NO_2 would not require any oxygen to be present in order to induce a signal change in the SPR band. In fact, the extra oxygen present in the Au-YSZ matrix would likely cause the detection limit for NO_2 to be lower as the matrix is nearly saturated with O^{2-} ions. Initial oxygen titration experiments with oxygen at 5 and

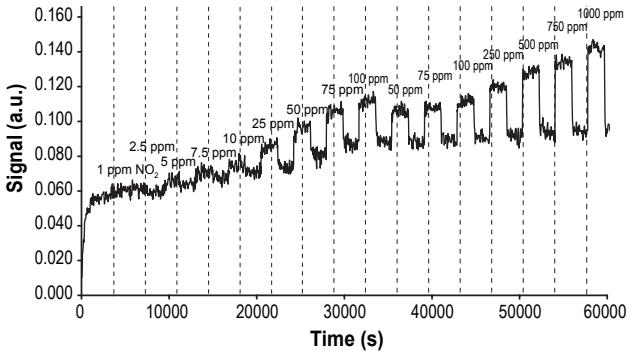

FIGURE 3. Signal Change vs. Time for NO_2 Exposures in Air at 500°C

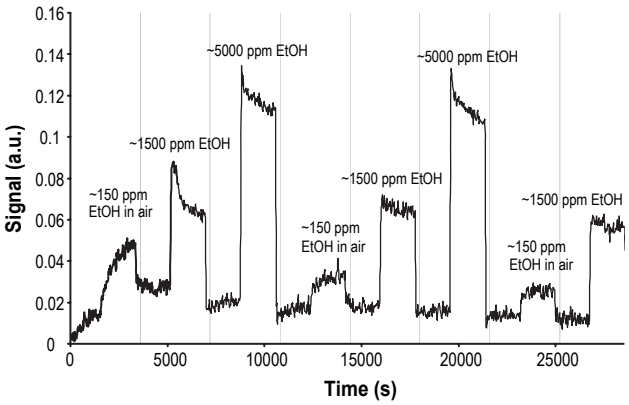

FIGURE 4. Signal Change vs. Time for Ethanol Exposures in Air at 500°C

10 vol% levels has determined that at all NO_2 levels the signal change is greater with less oxygen present in the gas mixture.

Hydrocarbon Detection – Ethanol at 500°C

The last portion of the work we have performed this year has been focused on the detection of hydrocarbons at elevated temperatures, which served as a prelude to the detection of sulfur containing hydrocarbons. Ethanol was our test hydrocarbon and its vapors were picked up and mixed into the gas stream through the use of a bubbler pick-up source. By varying the volumetric split of flow through the bubbler we are able to deliver ethanol exposures of 150, 1,500 and 5,000 ppm for these experiments. Figure 4 displays the change in sensing signal vs. time for these ethanol exposures and it is clear that we are able to reversibly detect ethanol under these conditions. Analysis of the change in the SPR band's peak position and full width at half maximum indicate that the characteristic blue shift and narrowing of the SPR band upon reaction with O^{2-}, leading to electron donation back to the gold nanoparticles is the reaction mechanism for the detection of ethanol. We have performed a total of 20 hours of ethanol exposure experiments to date and at this point the detection of 150 ppm of ethanol as seen in the figures has quite a bit of contrast which should allow for future studies and development of more sensitive Au-YSZ films for the detection of hydrocarbons. However, of particular interest to the studies is that the Au-YSZ films have no obvious problems with carbon buildup due to the catalytic reaction of ethanol which should produce CO_2 and water as the by-products of this reaction. As ethanol produces a strong change in the SPR band, it is likely that we will not be able to distinguish sulfur containing hydrocarbons from non-sulfur containing hydrocarbons without extra treatments to our sensing materials. These are efforts that are currently being investigated so as to increase the selectivity of our materials set.

Conclusions

- Was able to demonstrate the detection of hydrogen with a detection limit of 100 ppm at an operating temperature of 500°C in the presence of air.
- The detection of NO_2 was achieved with a detection limit of 5 ppm and the sensing mechanism does not require the presence of O^{2-} ions.
- Tested the Au-YSZ nanocomposite for the detection of ethanol. The sensing mechanism is the same as that for CO and H_2. No obvious problems with carbon contamination were evident after a 20 hr exposure experiment.
- Future work would entail further development of Au-YSZ materials which provide a selective response to the target gas.

FY 2007 Publications/Presentations

1. "Development and Characterization of Au-YSZ Surface Plasmon Resonance Based Sensing Materials: High Temperature Detection of CO", George Sirinakis, Rezina Siddique, Ian Manning, Philip H. Rogers, Michael A. Carpenter, J. Phys. Chem. B, 110, 13508 (2006).

References

1. Kreibig, U.; Vollmer, M.; Optical Properties of Metal Clusters; Springer, New York, 1995.

V. ADVANCED RESEARCH

V.1 Proton Conducting Solid Oxide Fuel Cell

S. (Elango) Elangovan (Primary Contact),
J. Hartvigsen and B. Heck
Ceramatec, Inc.
2425 South 900 West
Salt Lake City, UT 84119-1517
Phone: (801) 978-2162; Fax: (801) 972-1925
E-mail: Elango@ceramatec.com

DOE Project Manager: Lane Wilson
Phone: (304) 285-1336
E-mail: Lane.Wilson@netl.doe.gov

Objectives

- Identification of dopant type and concentration in a perovskite host to achieve high proton conductivity and high protonic transference number under solid oxide fuel cell (SOFC) operating conditions.
- Selection of dopant type and concentration in a perovskite host to provide resistance to reactivity towards CO_2 and H_2O.
- Evaluation of electrode materials using symmetric cells and full cells in button cell configuration.
- Test button cells using selected perovskite compositions.

Approach

- Select an appropriate B-site dopant in a perovskite matrix by evaluating protonic conductivity and transference number in SOFC relevant atmospheres.
- Investigate stability of compositions in syngas.
- Select a composition and evaluate in button cell tests.

Accomplishments

- Dopant type was identified to achieve a high protonic conductivity of 3 x 10^{-3} S/cm.
- Selected compositions were found to be less prone to formation of $BaCO_3$ in the presence of CO_2.
- High ionic transference number was demonstrated as indicated by open circuit voltage in button cells.
- A proton transference number of 0.7 was estimated at 800°C.
- Potential for high efficiency operation using a proton conductor-based SOFC relative to oxygen conductor-based SOFC was shown.

Future Directions

- Optimization of electrode compositions and electrode application techniques to improve cell performance.
- Evaluation of performance in button cell and stack tests using syngas fuel.

Introduction

One of the prime attractions of fuel cells is the possibility of realizing higher energy conversion efficiencies than are possible with thermal cycle systems. The basis of this difference is that thermal cycle system efficiencies are bounded by Carnot cycle thermodynamics, whereas fuel cell efficiencies are determined by chemical equilibrium thermodynamics and non-equilibrium force-flux relationships that govern charge, mass, momentum and energy transport. Materials have been developed which function as high temperature solid electrolytes in fuel cell applications. Two of the most widely considered materials are yttria doped ZrO_2 (YSZ) which transports oxygen ions and gadolinium doped $BaCeO_3$ which transports protons [1].

The thermodynamic difference between proton and oxygen ion cells is manifest in reversible potential variation with reactant utilization as a function of product water location. Excess air flow, used to remove the heat generated by cell operation, results in a lower water concentration in the cathode stream of a proton cell than in the anode stream of an O^{2-} cell.

Reversible potential variation with fuel utilization is shown for both proton and oxygen ion cells in Figure 1. The proton cell has a substantially higher reversible

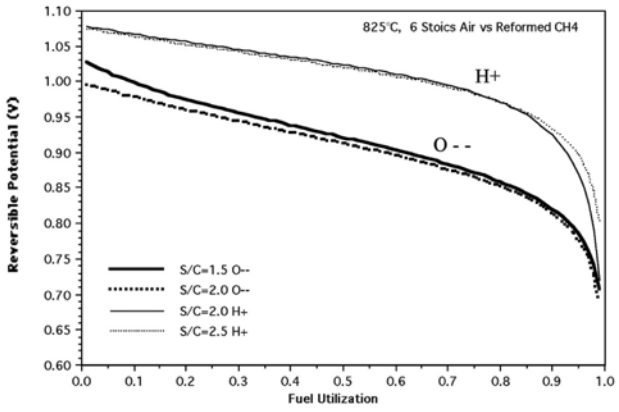

FIGURE 1. Comparison of Reversible Cell Potential

potential across the full range of fuel utilization. An interesting observation is that steam ratios greater than stoichiometric (S/C=2) increase the high utilization potential of a proton cell while oxygen ion cell potentials are uniformly higher with sub-stoichiometric steam ratios. This is due to the use of carbon monoxide via the shift reaction. The oxygen ion cell generates water in the anode stream so inlet compositions can be water deficit (high potential) and still have sufficient water to drive the shift reaction as utilization increases. The proton cell, on the other hand, must have sufficient or even excess water at the inlet to drive the shift reaction at high utilizations. However, water in the anode stream does not directly enter in the calculation of proton cell potentials and thus has little effect on the potential until higher utilizations where shift produced hydrogen is important. Thus, high temperature proton conductors have a thermodynamic advantage over oxygen ion conductors.

Comparable electrolyte ionic conductivities are required to take practical advantage of the thermodynamic benefit. Applications driven by maximizing efficiency at the expense of power density would favor proton cells. Thus, the opportunity for very high efficiency operation is one of the primary motivating factors for investigating proton conducting solid oxide fuel cells (P-SOFC). However, to date the research work on P-SOFCs has lagged far behind the well-known YSZ-based oxygen conducting solid oxide fuel cells (O-SOFC). The challenges that have been encountered in P-SOFC systems are discussed below.

Proton Conductivity

As mentioned earlier, the differences in electrolyte ionic conductivity may be greater than differences in the driving force and must be included in any comparison of an operating cell at a fixed current density. In general, the protonic conductivity of commonly known perovskite materials, such as doped $SrCeO_3$ and $BaCeO_3$, are considerably lower than the oxygen ion conductivity of YSZ. The proton conductivity ranges from 5×10^{-3} to 2×10^{-2} S/cm at 800°C [1-5]. While the high end of this range is comparable to the oxygen conductivity of 8-YSZ, the perovskite materials also possess some level of oxygen ion conductivity and electronic conductivity at various temperatures. Thus, the protonic transference number varies as a function of temperature. While the doped $BaCeO_3$ composition functions as an effective electrolyte, an increase in hydrogen conductivity is preferable to fully exploit the benefit of high efficiency with high power density.

Stability

One of the biggest technical challenges lies in maintaining the chemical stability of the perovskite in the presence of CO_2 and moisture; both are present in a typical hydrocarbon fuel. Numerous studies have confirmed the instability of the perovskite compositions.

It has been shown [1] that partial replacement of the B-site dopant with Zr completely eliminates this reaction. A similar improvement in stability in moist conditions was also reported with Zr substitution [1]. However, the stability improvement is at the expense of protonic conductivity. The proton conductivity was found to decrease monotonically with increasing Zr content [1, 2, 3].

Thus, what is required for successful development of a P-SOFC is an electrolyte material that has high proton conductivity to achieve a low area specific resistance, high protonic transference number relative to oxygen transference number to realize high efficiency, and stability in CO_2 and H_2O without compromising protonic conductivity for cell operation using practical hydrocarbon fuels.

Approach

Perovskite compositions that are known to exhibit protonic conductivity were evaluated for dopant study. The B-site dopants, typcially rare earth metals, have been shown to increase the proton conductivity of perovskites such as $BaCeO_3$. Several dopants and dopant levels were screened to identify compositions that have high conducivity and stability. Selected compositions were evaluated in button cell tests.

Results

A variety of B-site dopants were evaluated for their effect in total ionic conductivity and proton transference number. Protonic conductivities as high as 0.015 S/cm at 700°C and 0.02 to 0.03 S/cm at 800°C were measured. In addtion, the estimated protonic transference number ranged from 0.6 to 0.7 at 800°C, while the total ionic transference number was around 0.9.

$BaCeO_3$-type perovskite materials are known to be difficult to achieve good sintered density. A small amount of a sintering aid was added to achieve a sintered density in excess of 98%. The addition of the sintering aid did not affect the ionic conduction properties of the material. Micrographs of sintered $BaCeO_3$ are shown in Figure 2. As can be seen, the addtion of the sintering aid improves densification to achieve the needed denisty for an electrolyte.

Selected compositions, baseline and modified perovskites, were also exposed to syngas at 800°C. Comparison of powder X-ray diffraction patterns showed a significant reduction in the $BaCeO_3$ for certain modified compositions relative to the baseline material as shown in Figure 3.

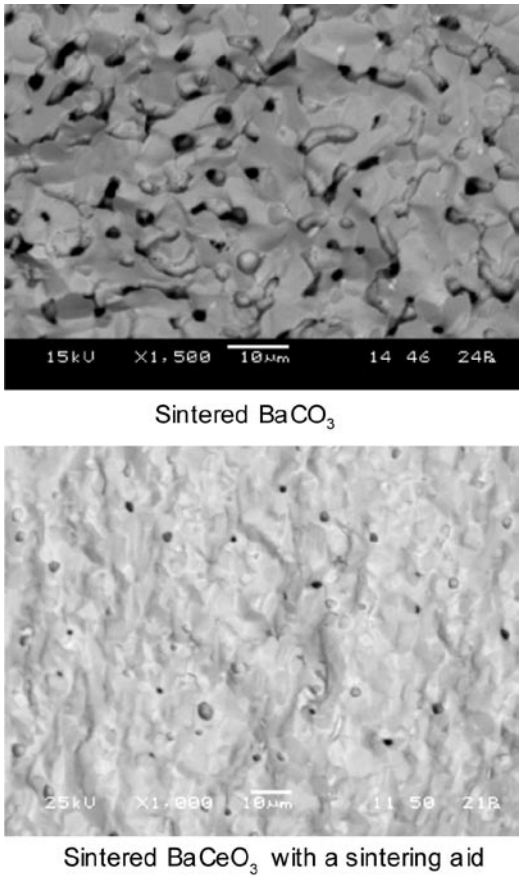

FIGURE 2. Comparsion of Sintered Density With and Without the Addition of a Sintering Aid

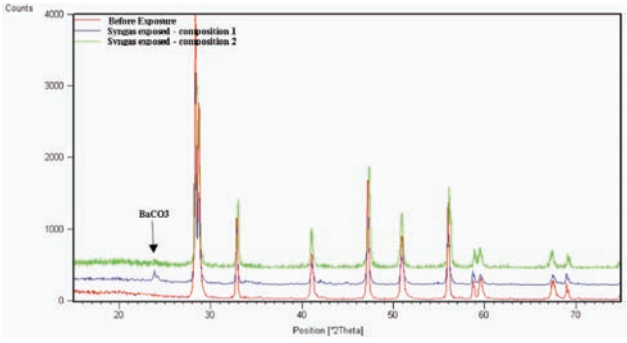

FIGURE 3. Powder X-ray Diffraction Patterns of 800°C Syngas Exposed Baseline and Modified Compositions

Button cell tests with 500 µm thick doped $BaCeO_3$ pellets were conducted. The cell performance was somewhat low. Post-test examination showed poor anode bonding to the electrolyte. However, comparison of proton and oxygen conducting electrolyte fuel gas potential as a function of cell current density, as measured by independent reference electrodes, showed the high efficiency potential for the proton SOFCs. This is shown in Figure 4.

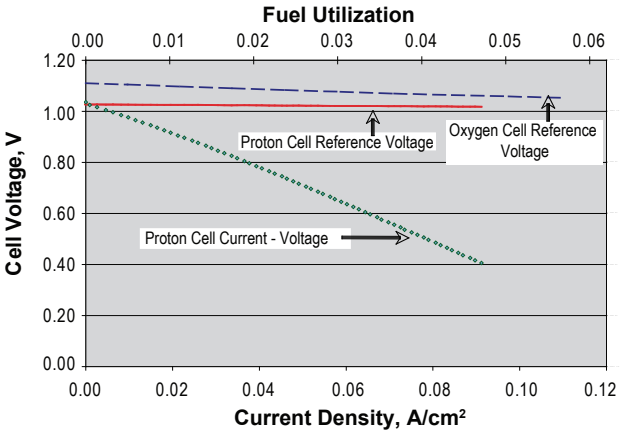

FIGURE 4. Comparison between Proton SOFC and Oxygen SOFC: Fuel Potential as a Function of Fuel Utilization

Comparison of the reference voltage trace provides several interesting points.

- First, at open circuit the proton open circuit voltage (OCV) is lower than that of oxygen OCV. This again is a confirmation of pure ionic conduction of zirconia electrolyte providing near theoretical Nernst potential. The lower OCV of the proton cell is indication of the ionic transference number, t_{ion}, being less than one, in this case about 0.96.
- As a function of utilization however, the driving potential of the oxygen cell drops more steeply than the proton cell again confirming the benefit of the proton cell in maintaining higher driving force.
- Because of t_{ion} being less than 1, the true benefit of the proton cell does not manifest until the cell reaches much higher utilization. The driving potential in this case will cross over at about 10 to 15% fuel utilization. It is theoretically possible to achieve very high utilization at a higher operating voltage with a proton cell.
- Finally, while high efficiency operation is clearly possible with the proton cell, the cell resistance must be lowered by a factor of 10 to fully realize the benefits of the proton cell in terms of cost/kW as well as specific weight and volume. Improvements to electrode compositions and electrode application technique as well as the use of thin electrolytes are expected to provide the necessary performance improvement.

Conclusions and Future Directions

The project results reconfirm the high efficieny potential for proton conductor-based SOFCs. By proper B-site doping very high proton conductivity, comarable to that of the oxygen ion conductivity of yttria-doped zirconia can be achieved to enable high performance cell operation. The inherent oxygen and electron

conductivities in the $BaCeO_3$-type of material limit the efficiency benefit to some extent depending on the operating conditions. When the cell is operated at high utlization, significantly higher electrochemical efficieny can be realized compared to an oxygen ion conductor-based SOFC. Electrode improvements and process development for fabrication of thin supported electrolyte cells need to the research focus for realizing the full capability of proton SOFC systems.

References

1. Iwahara, H., Hibino, T., and Yamada, M., Proc. 3rd International Symosium on Solid Oxide Fuel Cells, p 137, Singhal and Iwahara eds., Honolulu, Hawaii, 1993.

2. H. Iwahara, T. Esaka, H. Uchida, N. Maeda, Solid State Ionics 3/4, 359 (1981).

3. H. Iwahara, H. Uchida, N. Maeda, J. Power Sources 7, 193 (1982).

4. H. Iwahara, H. Uchida, I. Yamasaki, Int. J. Hydrogen Energy 12, 73 (1987).

5. H. Iwahara, Solid State Ionics 28–30, 573 (1988).

6. N. Bonanos, K.S. Knight, B. Ellis, Solid State Ionics 79 (1995) 61.

7. T.R. Armstrong et al., "Stability of Perovskite Hydrogen Separation Membranes," AR Materials Conference, Baltimore, MD, April 2003.

8. N. Taniguchi et al., "Endurance against moisture for protonic conductors of perovskite-type ceramics and preparation of practical conductors," Solid State Ionics 145, 349–355 (2001).

9. K.H. Ryu and S.M. Haile "Chemical Stability and Proton Conductivity of Doped Perovskite Oxides in the BaCeO3-BaZrO3 System," Solid State Ionics 125 (1999) 355–367.

10. K Katahira, Y. Kohchi, T. Shimura, H. Iwahara, "Protonic Conduction in Zr-substituted BaCeO3", Solid State Ionics, 138, 91–98 (2000).

11. S. Wienströer and H.-D. Wiemhöfer, "Investigation of the influence of zirconium substitution on the properties of neodymium-doped barium cerates," Solid State Ionics 101–103, 1113–1117 (1997).

V.2 Photo-Activated Low Temperature, Micro Fuel Cell Power Source

Professor Harry L. Tuller
Department of Materials Science and Engineering
Massachusetts Institute of Technology
77 Massachusetts Ave. 13-3126
Cambridge, MA 02139
Phone: (617) 253-6890; Fax: (617) 258-5749
E-mail: tuller@mit.edu

DOE Project Manager: Lane Wilson
Phone: (304) 285-1336
E-mail: Lane.Wilson@netl.doe.gov

Objectives

- Assemble and test unique Microprobe Thin Film Test Chamber for *in situ* characterization of thin film solid oxide fuel cell (SOFC) components.
- Prepare model electrode materials system over range of compositions in thin film form.
- Demonstrate that model electrode system exhibits expected properties and can be configured and operated as model cathode material.
- Test potential of illumination in enhancing electrode performance.

Accomplishments

- Assembly of Microprobe Thin Film Test Chamber completed with demonstrated ability to measure complex impedance and work function with high precision in controlled temperature and atmosphere and under illumination.
- $SrTi_{1-x}Fe_xO_3$ (STF) model electrode films (x=0.05, 0.35 and 0.50) were prepared by pulsed laser deposition (PLD) and ink jet printing and their measured crystal structures and electrical properties agreed with expected properties based on earlier studies of bulk specimens.
- STF model microelectrodes were demonstrated to exhibit typical electrode characteristics and scaling with area confirming mixed ionic-electronic conducting properties.
- Demonstration of as much as a factor of 73% reduction in electrode impedance of $SrTi_{1-x}Fe_xO_3$ ($x = 0.35$) model electrode under low intensity illumination confirming ability to modulate electrode impedance by illumination of a model electrode-electrolyte interface.

Introduction

Fuel cells convert the chemical energy stored in hydrogen or hydrocarbon fuels to electrical energy via electrochemical reactions at the anode and cathode. They offer higher efficiency and reduced emissions of greenhouse gases such as CO_2 compared to conventional combustion processes. SOFCs, in particular, offer unrivaled energy conversion efficiency and fuel flexibility and therefore are expected to play a key role in the forthcoming hydrogen economy era. At present, however, SOFCs are too expensive for commercial applications. The high cost of this technology is largely due to the use of expensive refractory materials that need to operate at temperatures as high as 1,000°C in conventional SOFC designs. These high temperatures are required to reduce the ohmic resistance of the oxygen-ion electrolyte (typically yittria-stabilized zirconia, YSZ) in large-scale SOFCs. The use of thinner electrolytes (~10 μm) in intermediate temperature (IT)-SOFCs and thin film electrolytes (<<1 μm) in micro-SOFCs, currently being examined as alternative power sources for portable electronic devices, however, ensure short diffusion paths and correspondingly low ohmic resistances, thereby putting the burden of performance largely on the electrodes. Finding methods to increase the electrochemical performance of the electrodes is thus a key enabling technology for high performance micro-SOFCs designed to operate at moderate temperatures. Achieving improvements in electrode kinetics is important, as well, for increasing the power output of IT-SOFCs of traditional size scales. Unfortunately, despite many years of research, much remains unclear regarding the dominant loss mechanisms and limiting reaction steps at the electrodes. Therefore, it has been difficult to develop new electrodes that meet the demands for high electrochemical performance at reduced operation temperatures.

Approach

Many research efforts are directed towards finding solutions that would enable operation at reduced temperatures (<600°C) by adding special catalysts, by investigating new or modified materials and by attempting to enhance the reaction zone at the three phase boundaries between electrode, electrolyte, and gas phase. While these efforts are showing some success, progress is spotty and often not reproducible between different R&D groups. We take a multifaceted approach which addresses the need to a) work with well defined and reproducible electrode structures and model

electrode compositions thereby enabling conclusions to be made about the rate limiting mechanisms controlling electrode performance, b) utilize measurement techniques, including illumination, Kelvin probe and impedance spectroscopy, which provide the ability to isolate the contributions of e.g. gas adsorption, charge transfer and diffusive kinetics towards the overall electrode impedance and c) offer prototype structures demonstrating reduced temperature operation and the potential advantages of illumination.

Results

A number of model electrode structures were prepared including interdigitated electrodes and spherical microelectrodes with varying diameter. Examples of the latter are shown in Figure 1. In this case, thin films of our model electrodes based on STF, were prepared for electrical and electrochemical characterization.

Thin films (thickness between 60 and 200 nm) of the model electrode STF35 were deposited by PLD on Al_2O_3 (sapphire) and MgO substrates and were shown, via X-ray diffraction (XRD) and atomic force microscopy (AFM), to be polycrystalline (grain size ≤100 nm) and of the expected perovskite structure with a degree of preferential orientation along the (110) direction. Their chemical composition, examined by Rutherford backscattering spectrometry, was found to be commensurate with the composition of the target material. Electrical characterization was largely consistent with our earlier studies of bulk STF ceramics. Additionally, STF films (x=0.1, 0.35) were deposited onto single crystal YSZ (100) or (111) substrates by thermal ink-jet (TIJ) printing, given its convenience for depositing and screening ternary or quaternary ceramic compounds. Following firing at 1,100°C for 3 hours in air, XRD patterns confirmed, as well, the formation of the perovskite phase.

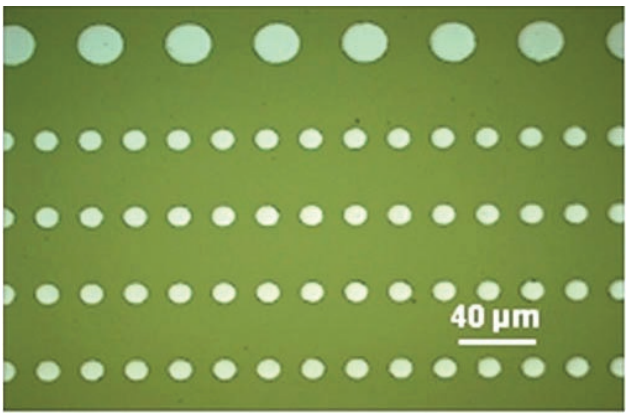

FIGURE 1. STF35 Films on MgO Substrates with Pt Electrodes Sputtered onto the Surface of the Films in a Microcontact Electrode Configuration

Impedance studies of STF electrodes (x=0.05, 0.35 and 0.50) on YSZ resulted in typical spectra expected for cathodes (see e.g. Figures 2 and 3) and so demonstrate the utility of our selection of the STF model system. The equivalent circuit elements were examined as functions of temperature and pO_2 and corresponding activation energies and pO_2 dependencies derived. At low temperatures, a Warburg signature spectrum is obtained pointing to a diffusion controlled process. These parameters are now being studied as functions of STF composition, bias and illumination and in concert with work function studies. Results confirm that the impedance decreases with increasing area rather than increasing perimeter of the electrode, consistent with the mixed ionic-electronic conductor (MIEC) nature

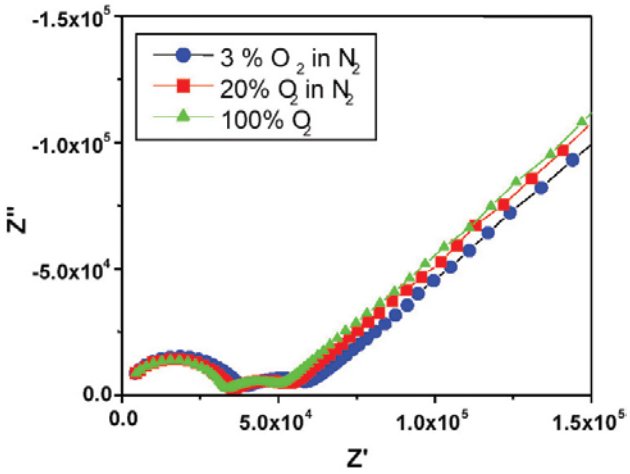

FIGURE 2. Impedance spectra of symmetrical STF35-YSZ cells at 400°C. Oxygen partial pressure as indicated.

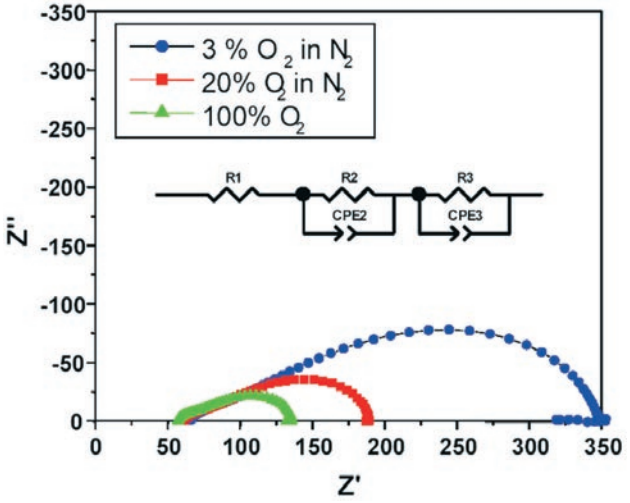

FIGURE 3. Impedance spectra of symmetrical STF35-YSZ cells at 900°C. Oxygen partial pressure as indicated. Inset: equivalent circuit used for data fitting.

of STF. Preliminary studies examining the effect of illumination were previously shown to result in as much as a 73% reduction under illumination which is equal to ~30-60 mW. More systematic studies of the effects of illumination on electrode impedance are under way.

The Kelvin probe, non-invasive, yet extremely sensitive to changes in the top-most atomic layer, as reflected in measured changes in work function (WF), provides the opportunity to examine surface processes such as chemisorption and oxygen incorporation into electrode. The instrument installed in our microprobe system, based on the McAllister KP-6500 Kelvin probe, was modified by us in collaboration with McAllister personnel to allow for a) high-temperature measurements (up to ca. 800°C), and b) for surface photovoltage spectroscopy (SPS) measurements by incorporating a light-guide.

WF measurements were initiated on both on LSC30 and STF35. The changes in contact potential difference (CPD), the difference in WF between the specimen and the reference electrode, in response to changes in pO_2 were large, rapid and reversible. Figure 4 shows CPD data for STF 35 under periodic pO_2 changes at 410°C. Here the CPD changed by ~200 mV, in concert with period changes in pO_2. These data also show our ability to examine the influence of broad band illumination while performing the CPD measurements under controlled temperature and pO_2. In other measurements, not shown, the ability to resolve changes in WF on the order of 10 mV were demonstrated. Also, decreasing WF with increasing temperature was observed as expected for corresponding enhanced levels of oxygen desorption. Initial rapid increases in WF with increasing pO_2 were followed by a much slower decreases which is attributed to initial rapid changes in chemisorption followed by slower changes in stoichiometry as predicted by Nowotny et al [1].

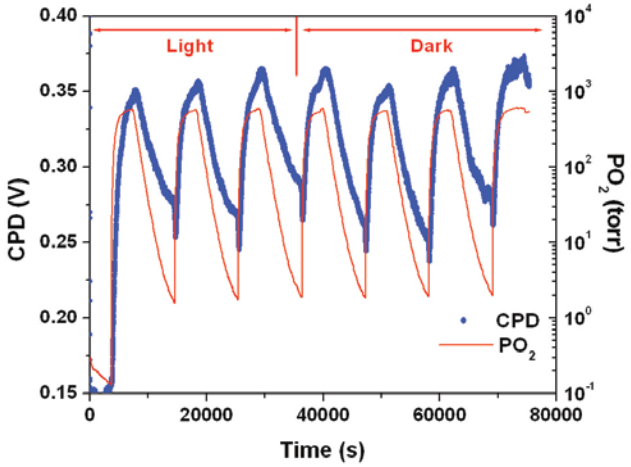

FIGURE 4. CPD of $SrTi_{0.65}Fe_{0.35}O_3$ as Function of Time at 410°C Under Periodic pO_2 Changes Both in the Dark and Under Illumination

Conclusions and Future Directions

In order to identify electrodes that will make it possible to significantly reduce the operating temperature of micro-SOFC and thin film-based SOFCs, the following objectives are pursued:

- Identify key rate limiting steps limiting presently utilized electrodes from performing at reduced temperatures.
- Investigate use of optical as opposed to thermal energy as a means for photocatalyzing electrode reactions and enabling reduced operating temperatures.

Towards this end, we initiated a multifaceted approach to address the need by:

- Demonstrated ability to prepare and characterize well-defined and reproducible electrode structures (microelectrodes) and model electrode compositions (STF).
- Utilized measurement techniques, including Kelvin probe and impedance spectroscopy, under controlled temperature, atmosphere and illumination, in a uniquely designed microprobe measurement system. This showed ability to deconvolute chemisorption from stoichiometry effects and electrode from bulk effects.
- Demonstrated ability of illumination to enhance electrode performance.

Future goals are to systematically investigate: 1) illumination as a means of enhancing electrode performance, 2) surface chemical effects which a) enhance chemisorption and insertion reactions, or b) degrade performance, and 3) the role of varying MIEC and band structure in the model STF system on electrode performance. The further goal is to fabricate and characterize prototype SOFC cells and optimize their electrochemical and photoelectrochemical performance at reduced temperature utilizing insights gained from the efforts applied towards the first three goals.

Special Recognitions & Awards/Patents Issued

1. Prof. Tuller was inducted into the World Academy of Ceramics.

2. Prof. Tuller, Plenary Lecturer, International Symposium on Electroceramics, Seoul Korea, May 2007.

3. Prof. Tuller was selected to give the 2007 Edward Orton Jr. Memorial Lecture of the American Ceramic Society.

FY 2007 Publications/Presentations (Invited talks)

1. Micro-Ionics: Pros and Cons of Nanotechnology, ECS, Chicago, Illinois, May 6–9, 2007.

2. Ibid, Energy Center, KIST, Seoul, Korea, May 14.

3. Prospects for Micro-fuel cells and Micro-sensor Arrays, Bosch R&D, Stuttgart, Germany, June 12, 2007.

4. Challenges and Opportunities for Integration of Sensor and Power Functions into Miniature Electroceramic Devices, Workshop on Integrated Electroceramic Functional Structures, Berchtesgaden, Germany, June 14–15, 2007.

5. Ibid, R&D Center, Siemens, Munich, Germany, June 13, 2007.

References

1. J. Nowotny, T. Bak, and C.C. Sorrell, "Charge transfer at oxygen/zirconia interface at elevated temperatures - Part 8", *Advances in Applied Ceramics*, ***104*** (2005), 200-205.

V.3 A High Temperature (400 to 650°C) Secondary Storage Battery Based on Liquid Sodium and Potassium Anodes

Greg Tao (Primary Contact), Neill Weber, and Anil Virkar
Materials and Systems Research, Inc. (MSRI)
5395 West 700 South
Salt Lake City, UT 84104
Phone: (801) 530-4987; Fax: (801) 530-4820
E-mail: gtao@msrihome.com

DOE Project Manager: Heather Quedenfeld
Phone: (412) 386-5781
E-mail: Heather.Quedenfeld@netl.doe.gov

Subcontractor:
University of Utah, Salt Lake City, UT

Objectives

- Develop an energy storage device based on an alkali metal ion conducting beta" alumina solid electrolyte (BASE) (high temperature battery).
- Investigate materials for suitable electrochemical couples.
- Fabricate both tubular and planar BASE possessing high strength, high conductivity, and high moisture-resistance.
- Design and construct planar batteries.
- Evaluate the charge/discharge and freeze/thaw capability of batteries at elevated temperatures.

Accomplishments

- Both Na-BASE and K-BASE discs and tubes have been successfully fabricated using MSRI's patented vapor phase process. Ionic conductivity measurements showed that Na-BASE had higher conductivity than K-BASE. At 500°C, Na-BASE conductivity is 0.36 S/cm. The activation energy is 22.58 kJ/mol.
- $CuCl_2$, $FeCl_2$, $ZnCl_2$, and AgCl were identified as suitable materials for electrochemical couples used for Na-metal salt batteries from thermochemical data. Further open circuit voltage (OCV) measurements matched these deduced from the thermochemical data.
- Tubular cells with $CuCl_2$ as the cathode and Na as the anode were constructed. It was discovered that $CuCl_2$ was somewhat corrosive and dissolved iron, an element of the cathode compartment.
- $FeCl_2$ and $ZnCl_2$ were acquired as the potential cathodes for Na-metal salt batteries for delivering high specific energies.
- Planar cells were designed. Na-$FeCl_2$ and Na-$ZnCl_2$ batteries were constructed and tested between 400 and 650°C. Charge/discharge characteristics showed these as the most promising types of batteries. Charge/discharge cycles were performed as many as 27 times, and the current was as high as 500 mA. No failure was detected after 50 hours tests.
- Freeze-thaw cycling tests were carried out and the survival was remarkably good for planar BASE disks fabricated by MSRI's patented vapor phase process.

Introduction

The solid oxide fuel cell (SOFC) is an energy conversion device, which efficiently converts chemical energy of hydrocarbon fuels directly into electricity at a high efficiency without the need for moving parts, except those for auxiliary pumps and blowers. As an electricity generator, its most efficient, practical and realistic use is in combination with an efficient energy storage device for electric-power generation and distribution application, particularly for utility load leveling and peak shaving. However, the associated energy storage devices of the integrated energy conversion-storage system must be capable of a very high roundtrip efficiency. Suitable batteries and reversible SOFC (or so-called solid oxide electrolysis cell – SOEC) could be the candidates serving as the energy storage devices in different energy forms, which are electrical energy and chemical energy carried by hydrogen, respectively. Due to the inherent limitations, such as hydrogen gas storage and parasitical losses, the SOEC doesn't have high enough roundtrip efficiency. In addition, the high cost of hydrogen storage and infrastructure also confines the reversible SOFC application. Instead, load leveling batteries (such as the sodium-sulfur battery, a.k.a. NAS), which have been under development widely outside of U.S., are capable of achieving a high roundtrip efficiency. An advanced high-temperature energy storage battery, based on an alkali metal ion conducting BASE and a non-corrosive metal salt, is proposed in this project to demonstrate a roundtrip efficiency in excess of 90%. The similar applications of BASE is NAS batteries, with as large as 8 MW power rating (64 MWh capacity), have been developed and installed by NGK Insulators, Ltd. and

Tokyo Electric Power Company (TEPCO) in Japan, and have demonstrated life in excess of 7 years with projected cost less than $140/kWh for annual installed capacity of >3,200 MWh. The NAS battery is by all indications close to commercialization.

An alkali metal-metal salt battery to be developed in the project comprises an alkali metal ion conducting BASE sandwiched between an alkali metal as the anode and a metal salt as the cathode. At elevated temperatures, during discharge, the alkali metal is oxidized at the anode forming metal ions, which migrate through the alkali metal ion conducting BASE and react with the metal salt at the cathode. Consequently, electrical power is generated by the battery. During charge, the above processes are reversed, and electrical power is stored in the battery. In addition to the inherent advantage of its high roundtrip efficiency, the high-temperature battery to be developed can be thermally integrated with intermediate temperature SOFC (IT-SOFC) stacks, forming an economical, compact, lightweight hybrid system with very high system efficiency.

Approach

This project is directed toward the development of a planar, high temperature (400~650°C) secondary storage battery based on alkali metal – metal salt battery technology. Both Na-BASE and K-BASE were fabricated using the methods of cold isostatic-pressing and tape-casting of α-Al_2O_3 + 8YSZ for tubes and planar discs, respectively, followed by MSRI's patented vapor phase process. Packing powders for conversion of K-BASE and Na-BASE were prepared in-house and could be reused each time by replenishing the K_2O and $NaAlO_2$ contents. Material properties of BASE were qualified by measuring the density and the ionic conductivity at various temperatures. Microstructures of the discs were characterized using a scanning electron microscopy (SEM) to determine the morphology of BASE before/after conversion.

Electrochemical couples comprised of an alkali metal (Na and K) and a transition metal salt were investigated through literature search on thermochemical data. Open circuit voltages and specific energies were calculated based on the thermochemical data over temperatures from 350°C to 700°C to determine prospective couples suitable for electrodes of the proposed battery. Dissolution tests of iron, an element of electrode compartments, were carried out for metal salts to exclude any corrosive salt from the candidates. Phase diagrams of the metal salt and the alkali metal salt were also studied to assist the choice of the cathode, thus ensuring excellent mass transport in the liquid cathode and allowing for a greater depth of discharge. OCVs of the interested electrochemical couples were measured in BASE tubes at elevated temperatures. Planar cells were designed, and correlative cell components, including electrode compartments, seals and wicks, were identified and acquired. Planar cells in two sizes, either with 2.5 cm^2 or 10 cm^2 active areas, were constructed in the partially discharged state. The planar battery characteristic tests of the charge/discharge cycles and thermal cycles were conducted in an oxygen-free and moisture-free glove box over a range of temperatures between 400 and 650°C. After tests, batteries were dissembled and inspected for any potential damage to BASE, electrode compartments, and seals. 1 kWh battery designs and BASE optimization designs were proposed for further development, and preliminary investigations were also carried out.

Results

Important results and accomplishments were summarized in what follows.

1. From the standpoint of high specific energy and open circuit voltage, the prospective cathodes were $FeCl_2$, $ZnCl_2$ and AgCl, listed in the order of preference from high to low. In addition, they were not corrosive and the corresponding eutectic temperatures were lower than the working temperatures ensuring a greater depth of discharge. OCV measurements of the Na/$FeCl_2$ and Na/AgCl electrochemical couples between 350 and 700°C, as presented in Figure 1, show excellent agreements with these deduced from the thermochemical data.
2. A tape-casting method was developed to fabricate planar cells. Green tapes were laser-cut into desired shapes, either in a circular or in a square shape. Tubes were fabricated in a specially designed mold with a steel mandrel followed by a cold-isostatic

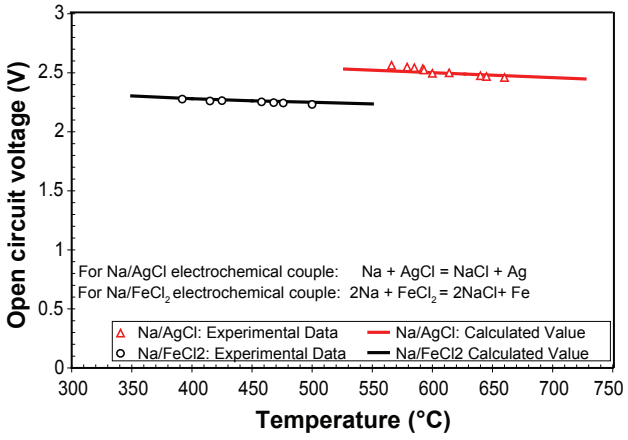

FIGURE 1. OCV measurements for Na/AgCl and Na/$FeCl_2$ electrochemical couples. Symbols are experimental data. The lines are calculations based on thermodynamic data. Note excellent agreement between measurements and calculations.

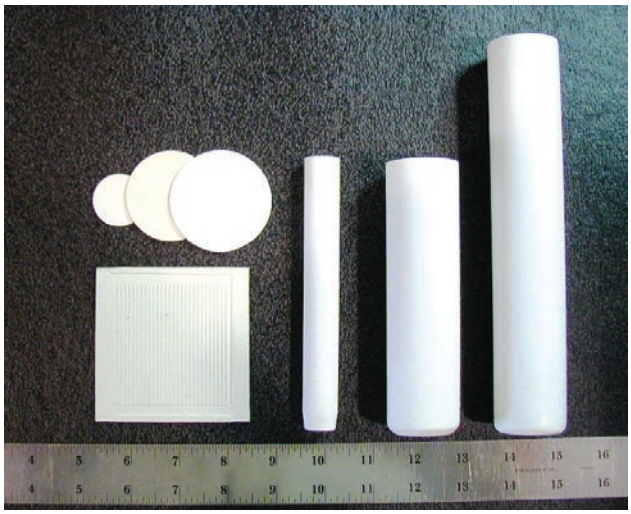

FIGURE 2. A Photograph of Several BASE Tubes and Discs Made by MSRI's Patented Vapor Phase Process

press at 30,000 psi. Figure 2 is a photograph of the BASE tubes and disks made by the MSRI patented vapor phase process. BASE tubes were made as long as 20 cm, and disks were as large as 6 cm in diameter, or plates 9 cm in length. Typical BASE tubes fabricated by the conventional process for use in NAS batteries were well in excess of 1 to 1.5 mm in thickness leading to a high ohmic area specific resistance (ASR). In contrast, the BASE made by MSRI's novel, patented process exhibits excellent properties, unmatched by BASE made using conventional processes.

3. Ionic conductivities of Na-BASE and K-BASE were measured using AC impedance method at elevated temperatures. The experimental results showed that Na-BASE had higher ionic conductivity than K-BASE, consistent with the literature. At 500°C, Na-BASE conductivity is 0.36 S/cm, which is more than 20 times higher than 8YSZ electrolyte used for SOFC at 800°C. The activation energy of Na-BASE is 22.58 kJ/mol. Microstructures of the discs after thermally etching were characterized using the SEM to determine the morphology of BASE before/after converting into Na-BASE and K-BASE. Unique textured microstructures, which were developed during the conversion process and played an important role in the attainment of good conductivity of the BASE, were observed.
4. Planar batteries were designed. Stainless steel cups were acquired as the electrode compartments. Cathodes, in a partially discharged state at a eutectic composition of $FeCl_2$+NaCl or $ZnCl_2$+NaCl, were fabricated by the impregnation method. In order to provide reactants/products to/from the electrochemical reaction sites, and to make good contacts with the BASE and the metal compartments, steel wool and copper wool were used as the wick for the cathode and anode, respectively. Copper gaskets were used as the seals for both the anode and cathode. The final assembly of the batteries was carried out in the glove box. Compression was applied by low thermal expansion bolts over two end plates. Figure 3 is a photograph of a battery assembly.
5. Planar single-cell batteries were tested over the temperature range between 400°C and 650°C. Figure 4 shows the Na-$FeCl_2$ battery voltage characteristics obtained at 500°C and 104 mA constant current. The discharge voltage limit was set to 2.157 V, 96% of OCV (2.254 V). The charge voltage limit was set to 2.302V, 102% of OCV. The roundtrip efficiency was about 94%. No obvious degradation was observed after 6 cycles over 7 hours of testing. Na-$FeCl_2$ batteries were also

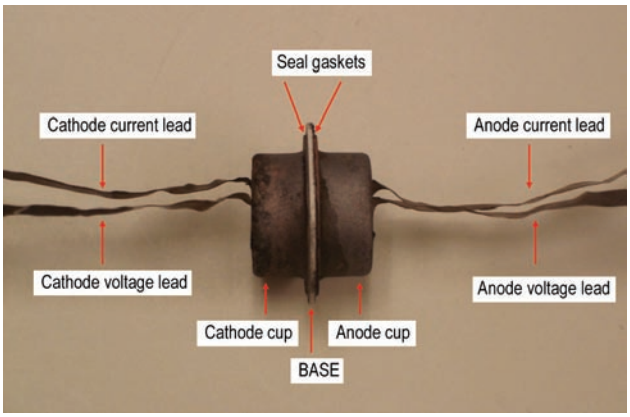

FIGURE 3. A Photograph of a Na-$FeCl_2$ Battery Assembly

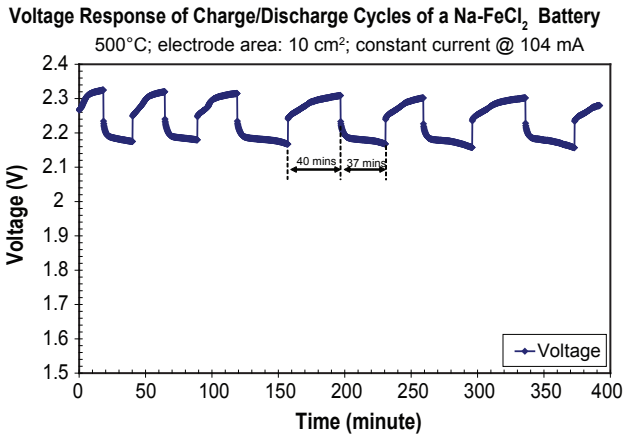

FIGURE 4. Voltage characteristics of a Na-$FeCl_2$ single-cell battery tested at 500°C and 104 mA constant current. The cell was charged/discharged with a round trip efficiency of ~94%.

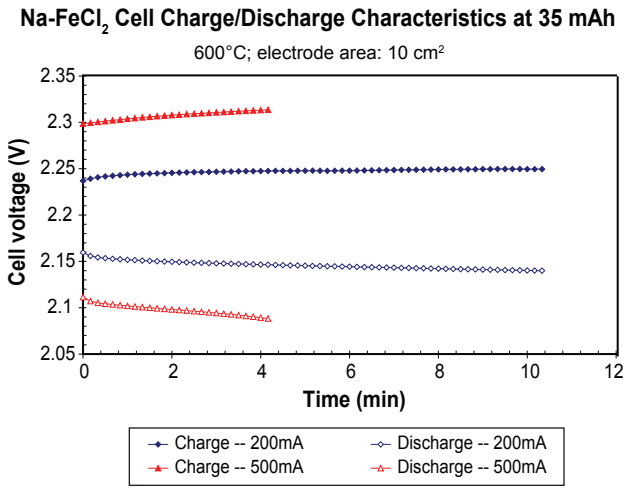

FIGURE 5. Voltage characteristics of a Na-$FeCl_2$ single-cell battery tested at 600°C and 35 mAh capacity. The charge/discharge currents were 200 mA and 500 mA.

tested at 600°C, and the typical charge/discharge characteristics at a fixed 35 mAh capacity are shown in Figure 5 at 200 mA and 500 mA constant currents. The roundtrip efficiency was estimated to be 95%.

Conclusions and Future Directions

- Both Na-BASE and K-BASE discs and tubes were made using MSRI's patented vapor phase process. The BASE is free of moisture and CO_2 attack. Impendence measurements showed that Na-BASE had much higher ionic conductivity than K-BASE. Therefore, Na-BASE electrolyte favors batteries for delivering high specific energy.
- Due to its very high OCV and high specific energy, $CuCl_2$ is a promising cathode and investigation of $CuCl_2$ cathode is proposed to be performed in Phase II by using suitable coating technologies.
- Na/$FeCl_2$ and Na/$ZnCl_2$ electrochemical couples were identified as the prospective electrodes from the standpoint of high specific energy, high OCV, and none dissolution of electrode compartments. OCV measurements of the identified electrochemical couples matched these deduced from the thermochemical data.
- Planar cells were designed, constructed, and tested successfully between 400 and 650°C. The roundtrip efficient was demonstrated as high as 95%.
- Charge/discharge cycles were conducted as many as 27 times without failures after 50 hours of testing on the Na-$ZnCl_2$ battery at 425°C, which was performed by the subcontractor under a separate DOE-funded project.
- Freeze-thaw survival was remarkably good after numerous thermal cycling tests for planar BASE disks fabricated by MSRI's patented vapor phase process.
- Preliminary studies of BASE optimization and the 1 kWh battery design were applicable to high specific energy batteries.

FY 2007 Publications/Presentations

1. G. Tao, N. Weber, A. Virkar and P. Parthasarathy, "A secondary battery based on liquid anode for energy storage", 16th International Conference on Solid State Ionics, July 1-6, 2007, Shanghai, China.

V.4 A Thin Film, Anode-Supported Solid Oxide Fuel Cell Based on High Temperature Proton Conducting Membrane for Operation at 400 to 700°C

Joon-Ho Koh (Primary Contact) and Feng Zhao
Materials and Systems Research, Inc.
5395 West 700 South
Salt Lake City, UT 84104
Phone: (801) 530-4987 Ext. 18; Fax: (801) 530-4820
E-mail: jkoh@msrihome.com

DOE Project Manager: Lane Wilson
Phone: (304) 285-1336
E-mail: Lane.Wilson@netl.doe.gov

Subcontractor: Dr. Anil V. Virkar
The University of Utah, Salt Lake City, UT

Objectives

- Fabricate high-temperature proton conductor (HTPC), anode-supported solid oxide fuel cell (SOFC) button cells and measure performance on hydrogen/air up to a maximum of 700°C.
- Demonstrate successful thermal cycling of cells.

Accomplishments

- Fabricated anode-supported thin film HTPC cells using various electrolyte materials including BCY ($BaCe_{1-y}Y_yO_{3-\delta}$), SCYb ($SrCe_{1-y}Yb_yO_{3-\delta}$), and KBZY (K-doped and Y-doped $BaZrO_3$).
- Demonstrated satisfactory performance on anode-supported thin film HTPC-SOFCs at 650~700°C with a maximum power density of ~0.5 W/cm².
- Demonstrated excellent stability upon repeated thermal cycling, showing no degradation after 3~4 thermal cycles.
- Fabricated large-area cells of HTPC electrolyte on Ni+YSZ anode support successfully for both planar (4"×4" active area) and tubular designs.

Introduction

SOFCs typically employ oxygen-ion-conducting membranes as a solid electrolyte. Alternatively, HTPC solid oxide membranes (analogous to the low temperature polymer electrolyte membrane fuel cells) can be used wherein protons transport from the anode through the electrolyte membrane to the cathode, where they react with oxygen molecules and electrons to form water vapor at the cathode. One advantage of SOFCs based on a proton conducting membrane over an oxygen ion conducting membrane is that with hydrogen as the fuel, there is no fuel dilution, allowing for operation at high fuel utilization, and thus at high overall system efficiency. SOFCs based on high temperature proton conducting membranes also offer important advantages over low-temperature proton exchange membrane fuel cells (PEMFCs), namely: (i) Higher operating temperature allows for the use of non-noble metal catalysts, thus lowering cost; (ii) The catalysts are not poisoned by CO due to high operating temperatures; and, (iii) Highly efficient thermal integration with fuel processors and other balance-of-plant components is possible unlike lower temperature PEM.

In this project, we demonstrated fully fabricated anode-supported HTPC cells which exhibited good performance. We also demonstrated that the fabricated cells can be subjected to repeated thermal cycles without a significant loss of performance, a key requirement for virtually any application. Further, we have demonstrated that Ni+YSZ as the anode support is ideally suited for many solid electrolytes, including HTPC. All these indicate that HTPC-SOFCs can be operated stably at very high fuel utilization, thus allowing for attaining high system efficiency, and further reduce green house gas emission per kWh produced.

Approach

The best known materials for application in HTPC-SOFCs are B-site doped $BaCeO_3$ and $SrCeO_3$. These materials exhibit high proton conductivity, with values reported as high as ~10^{-2} S/cm at 700°C. However, the stability of the materials must be demonstrated, especially for application in SOFCs, because these materials are known to exhibit sensitivity to H_2O and CO_2 at relatively low temperatures (below 600°C), but are known to be stable at higher temperatures. The reactivity with CO_2 is not a major consideration in fuel cells, since the possible interaction will be limited only on the surface of electrolyte, and does not affect stability. The reactivity with H_2O is an issue for stability, since water vapor dissolves into the lattice, which is required for conduction. There is no reactivity of $BaCeO_3$ and $SrCeO_3$ at the SOFC operating temperature (above 600°C), but there is the potential for reaction at lower temperatures, for example if the SOFC is idling in humid atmospheres at low temperatures. The following approach was used to achieve and demonstrate stability of HTPC-SOFCs: (i) Fabrication of anode-supported thin film HTPC-SOFCs; (ii) Optimization of materials

and microstructure for high performance; and (iii) Operation under conditions such that the SOFC is not exposed to too high a humidity at low temperatures, especially not to liquid water. Prior work has shown that HTPC materials remain stable in water vapor even at low temperatures, and are only affected by liquid water [1]. In this project, HTPC-SOFCs were subjected to several thermal cycles.

Results

Anode-supported thin film HTPC-SOFCs were successfully fabricated. Button cells were fabricated in several steps to have four or five distinct layers: (i) porous anode support; (ii) porous anode interlayer; (iii) dense thin film electrolyte; (iv) porous cathode interlayer; and/or (v) porous cathode current collector. The cathode area was approximately 2 cm², which was used as the basis for the current density calculation. Three different HTPC materials were used: Y-doped $BaCeO_3$ (BCY), Yb-doped $SrCeO_3$ (SCYb), and K-doped and Y-doped $BaZrO_3$ (KBZY). Micrographs showing the cross-section of those cells are given in Figure 1. Note that the HTPC electrolytes are fully dense and the electrolyte thickness is in the range of 8 to 15 μm. Both the anode and cathode exhibit fine porous microstructures.

Work done to date has shown that $BaZrO_3$ or BCN18 ($Ba_3Ca_{1.18}Nb_{1.82}O_{9-d}$) are generally more stable in water vapor and liquid water compared to BCY and SCYb. Their stability has been demonstrated by heat-treating them in an autoclave at temperatures as high as 500°C and water vapor pressures as high as 180 bars [2]. In addition, it has been demonstrated that $BaZrO_3$ and BCN18 can be boiled in water without any reaction. Proton conductivities of these materials are, however, lower than $BaCeO_3$ and $SrCeO_3$-based materials, due to their lower basicity (the affinity towards water vapor). Doping on the A-site of $BaZrO_3$ with an alkali ion is expected to increase affinity for water vapor by increasing basicity. The reason for doping on the A-site is because of the comparable size of monovalent alkali ions (Na, K, etc.) to those of divalent alkaline earth ions (Ba, Sr, etc.). For this reason, the fabrication of KBZY cells was tried using fine powders made in-house, and cells were successfully fabricated as shown in Figure 1.

Of all the perovskite type materials investigated to date, rare earth ion-doped $BaCeO_3$ exhibits the highest proton conductivity, followed by rare earth ion-doped $BaThO_3$ and $SrCeO_3$. For this reason, much work has been conducted on $BaCeO_3$ and $SrCeO_3$. For the same reason, thin film anode-supported HTPC-SOFC button cells with Y-doped $BaCeO_3$ (BCY) and Yb-doped $SrCeO_3$ (SCYb) were tested over the temperature range 600~800°C using hydrogen or syngas as the fuel. In these cells, the electrolyte was BCY or SCYb, and the anode support was Ni+BCY or Ni+SCYb. Figure 2 shows the current-voltage and power density curves for a typical BCY cell with LSC as the cathode material. The performance is satisfactory, showing ~0.45 W/cm² at 0.7 V (700°C). For HTPC-based cells, this is an excellent result, especially with non-optimized anode.

Even though $BaCeO_3$ or $SrCeO_3$ are thermodynamically unstable at low temperatures (below 600°C) [3,4], work conducted in the present work showed that the cells fabricated using these materials can be operated stably under repeated thermal cycles. In the solid state, both $BaCeO_3$ and $SrCeO_3$ are kinetically stable over a wide temperature range. This is due to slow solid-state diffusion at low temperatures. At room

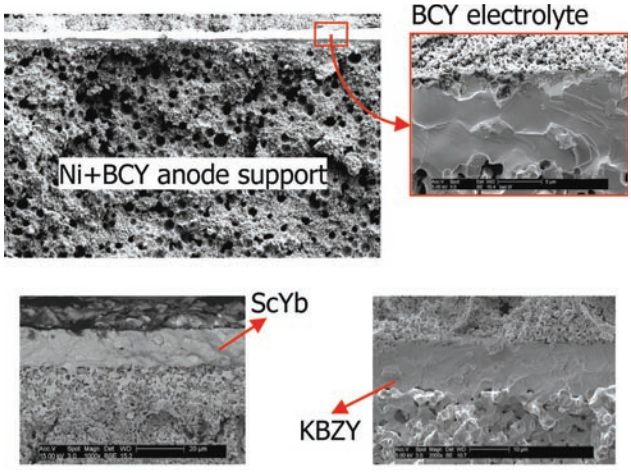

FIGURE 1. Micrographs of typical anode-supported thin film HTPC-SOFCs, using three different electrolytes (BCY, SCYb, and KBZY). Anode-support materials were Ni+HTPC, and cathode materials were LSCM, LSM, LSC, or Ag.

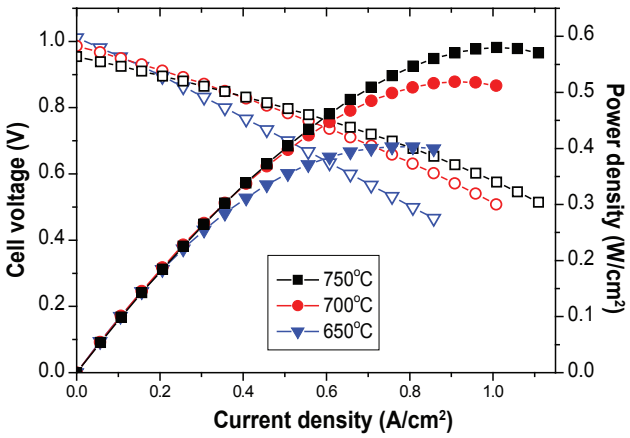

FIGURE 2. I-V curves of a BCY cell with LSC cathode tested between 650 and 750°C using hydrogen as the fuel (without humidification) and air in the cathode. Anode-support = Ni+BCY, anode interlayer = Ni+BCY, electrolyte = BCY, cathode interlayer = BCY+LSC, cathode = LSC.

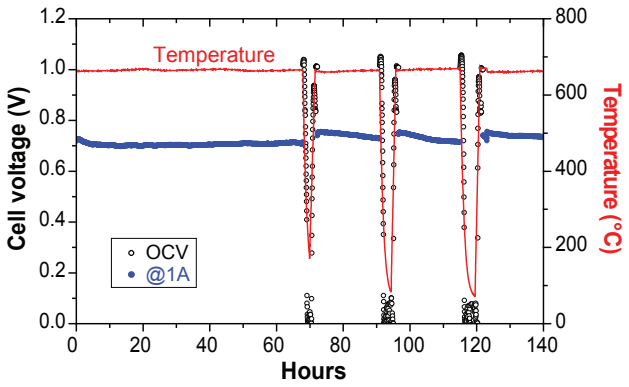

FIGURE 3. The test results of thermal cycling with a BCY-electrolyte cell. The discharge current was 1.0 A (0.5 A/cm²) at 650°C. Open circuit voltages are also shown in the plot (open circle). Both the anode and cathode gases were not humidified externally. Anode-support = Ni+BCY, anode interlayer = Ni+BCY, electrolyte = BCY, cathode interlayer = BCY+LSC, cathode = LSC.

temperature, both $BaCeO_3$ and $SrCeO_3$ maintain their stability indefinitely. At higher temperatures (above 800°C), the materials are thermodynamically stable. It is anticipated that an SOFC stack/system will be subjected to several thermal cycles during the operating life. Thus, it is imperative that stability under the conditions of thermal cycling be evaluated via experiments. For these reasons, many cells were subjected to several thermal cycles under various conditions. The key to the stable thermal cycling of HTPC-SOFCs is to maintain dry gas conditions during thermal cycle. High-temperature operation mode can be either humidified or dry fuel for the anode and either humidified or dry air for the cathode. Cool-down and re-heating mode should be dry fuel for the anode and dry air for the cathode. The objective was to minimize any possibility of BCY and SCYb decomposing. Figure 3 shows the results of thermal cycling of a BCY cell with LSC as the cathode material. The open circuit voltages are larger than 1.0 V as shown in the figure. The performance was excellent (~0.35 W/cm² at 0.7 V, 650°C) and very stable between thermal cycles. This is an important milestone demonstrating the practical viability of HTPC solid oxide fuel cells in terms of both high performance and stability.

For any practical application, it is imperative that SOFC stacks withstand several hundred to even several thousand thermal cycles. This means all possible steps should be taken to make the cells as robust as possible. To this end, a new approach of using the proven Ni+YSZ anode support was developed. Since Ni+YSZ is a proven anode support (and anode) in YSZ-based SOFC, it was reasoned that it should also be a viable support for other electrolytes, including HTPC, as long as the electrolyte and anode are compatible and do not react. In order to explore this possibility, we also fabricated HTPC-based cells with Ni+YSZ anode support.

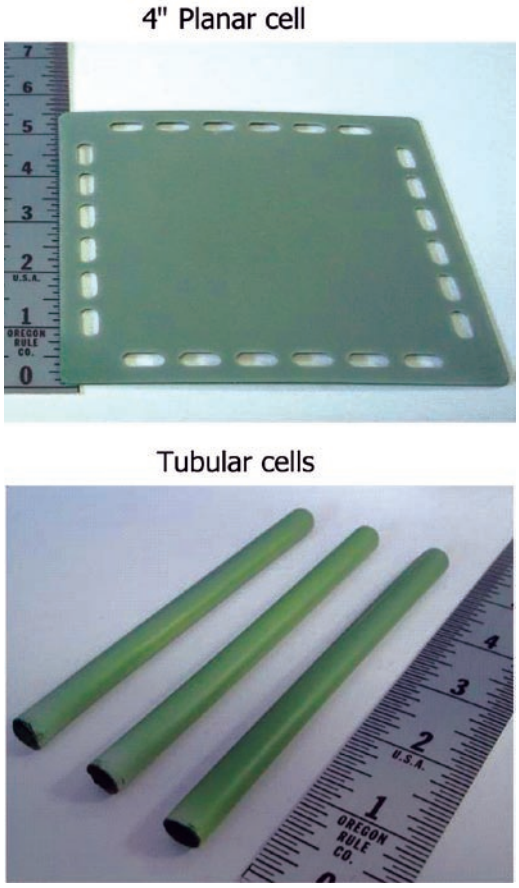

FIGURE 4. Photos of 4"×4" (cathode area) planar cells and tubular cells. Both types of cells have BCY electrolyte on Ni+YSZ support and were sintered at 1,450°C.

Assuming success, this also opens other options for the cathode. That is, the general approach developed is to use the established anodes and cathodes for SOFCs, but make a suitable choice of the electrolyte, in the present case an HTPC. The feasibility of Ni+YSZ anode-supported, HTPC electrolyte cell was demonstrated from a button cell test using SCYb as electrolyte in our recent experiment. Based on that result, it was recognized that cells of practical size need to be demonstrated. Therefore we fabricated a couple of 4"×4" planar BCY cells on Ni+YSZ anode support as shown in Figure 4. Tubular cells, being another practically important SOFC technology, were also fabricated using Ni+YSZ support tubes and BCY electrolyte layers as shown in Figure 4.

Conclusions and Future Directions

Thin film anode-supported HTPC-SOFCs were successfully fabricated and their high performance was demonstrated. Stable operation with repeated thermal cycles was demonstrated as well. In the future, larger planar cells (*e.g.* 100 cm² active area) and tubular cells of up to 10 inches long need to be fabricated. Short stacks

of both planar cells and tubular cells need to be tested and their performance needs to be analyzed. A kW-scale stack demonstration will prove practical applicability.

References

1. S.V. Bhide, A.V. Virkar, "Stability of $BaCeO_3$-Based Proton Conductors in Water-Containing Atmospheres", *Journal of the Electrochemical Society*, 146(6) (1999) 2038–2044.

2. S. Gopalan, A.V. Virkar, "Thermodynamic Stabilities of $SrCeO_3$ and $BaCeO_3$ Using a Molten Salt Method and Galvanic Cells", *Journal of the Electrochemical Society*, 140(4) (1993) 1060–1065.

3. K.H. Ryu, S.M. Haile, "Chemical stability and proton conductivity of doped $BaCeO_3$-$BaZrO_3$ solid solutions", *Solid State Ionics*, 125 (1999) 355–367.

4. C.W. Tanner, A.V. Virkar, "Instability of $BaCeO_3$ in H_2O-Containing Atmospheres", *Journal of the Electrochemical Society*, 143(4) (1996) 1386–1389.

V.5 SECA Coal-Based Systems Core Research – Montana State University

Lee H. Spangler (Primary Contact),
Richard Smith, Yves Idzerda, Hugo Schmidt,
Hashem Nehrir, Steven Shaw, Stephen Sofie,
Max Diebert and Hongwei Gao
Montana State University
207 Montana Hall
Bozeman, MT 59717-2460
Phone: (406) 994-4399; Fax: (406) 994-2893
E-mail: spangler@montana.edu

DOE Project Manager: Heather Quedenfeld
Phone: (412) 386-5781
E-mail: Heather.Quedenfeld@netl.doe.gov

Subcontractor:
Arcomac Surface Engineering, Bozeman, MT

Objectives

- Develop thin corrosion resistant physical vapor deposition (PVD) coatings on steel interconnect plates that exhibit: good electronic conductivity; long-term thermal stability; barrier capacity against outward diffusion of Fe and Cr from the interconnect plate; and barrier capacity against inward transport of oxygen from the gas phase.
- Investigate Cr poisoning processes in solid oxide fuel cells (SOFCs) through quantitative measurements of (1) Cr volatility rates from coated/uncoated steel surfaces, and (2) oxygen diffusion and surface exchange rates for electrolyte and cathode materials with surface impurities.
- Construct and use apparatus for measuring gas flow and tortuosity in SOFC electrodes.
- Develop low coefficient of thermal expansion (CTE) anode blends through the addition of electrochemically inert ceramic oxide additives to the Ni/YSZ-based anode system.
- Optimize the freeze tape casting system for the fabrication of engineered Ni/YSZ functionally graded porous anodes and contrast the performance of freeze cast anodes against traditional porous anodes.
- Develop a suitable process under both vacuum and inert atmospheres for the application of a noble metal-free copper-based for the robust sealing of SOFCs.
- Develop a DC/DC converter of 96% efficiency and $40/kW cost for fuel cell residential power systems.
- Develop a load sharing control strategy for modularly designed DC/AC inverters in large-scale fuel cell power systems to ensure the load sharing error among the modules is less than 5%.
- Validate SOFC dynamic model developed at Montana State University (MSU).
- Demonstrate fuel cell reference simulator using an SOFC under transient conditions.
- Explore electrically induced degradation under electrical conditions that might occur in stacks under both static and dynamic conditions.

Accomplishments

- Demonstrated PVD coatings on ferritic steels with excellent corrosion-resistance, high electronic conductivity and negligible Cr volatility.
- Determined that TiCrAlY oxide coated 430 stainless steel was thermally stable for times up to 270 hours at 800°C, and exhibited a negligible Cr volatility rate after a burn-in time of about 70 hours. Area specific resistance (ASR) for this coating was too high for interconnect use, but could be reduced to acceptable levels with additional Co and Mn doping.
- Derived replacement for Butler-Volmer equation that predicts physically reasonable current density *vs*. activation polarization behavior in SOFCs and solid oxide electrolysis cells.
- Developed procedures and equipment to carry out measurements of oxygen diffusion and surface exchange in electrolyte and cathode materials using nuclear reaction analysis, and ^{18}O exposures near atmospheric pressure and 800°C using an evacuated tube furnace.
- Determined with X-ray photoelecton spectroscopy (XPS) that chromia deposits on yttria-stabilized zirconia (YSZ) surfaces at 800°C in air were not stable, and desorbed from the surface. This suggests that Cr poisoning is most likely occurring at the cathode, or only with the influence of the electrochemical potential present at the triple phase boundary.
- Demonstrated the measurement of volatility of Si from the walls of a quartz tube with flowing moist air at 800°C setting the stage for rapid, quantitative, extremely sensitive measurements of volatility of Si and other elements heavier than carbon, such as found in SOFC insulation or sealing materials.
- Established the effective use of aluminum titanate and zirconium aluminum titanate filler compounds to effectively reduce anode CTE by 10% and improve flexural strength with addition of ~ 5 wt% filler.
- Identified the appropriate organic binders for the synthesis of suitable copper braze pastes

for SOFC sealing in both inert and vacuum atmospheres. Significantly improved performance and repeatability of brazing processes with the setup of a new brazing furnace and fabricated a testing apparatus for pressure testing brazed joints.

- Demonstrated a robust, hermetic braze joint that surpassed the strength of the bulk YSZ when subjected to failure.
- Developed a DC/DC converter of 96% efficiency and $40/kW cost for fuel cell residential power systems.
- Developed a load sharing control strategy for modularly designed DC/AC inverters in large-scale fuel cell power systems to ensure the load sharing error among the modules is less than 5%.
- The steady-state response of MSU's SOFC model was compared with GE data.
- Model reference simulator control circuitry was finalized and a printed circuit board was designed, fabricated and tested using InDEC cells under dynamic conditions.
- Preliminary results were obtained showing electrically induced SOFC degradation, consistent with theoretical predictions.

Introduction

Interconnects and CR Volatility. The requirements of low-cost and high-temperature corrosion resistance for bipolar interconnect plates in SOFC stacks has directed attention to the use of steel plates with more oxidation resistant compositions. However, volatile Cr species from these steels find their way to the triple-phase boundary, leading to rapid degradation of fuel cell performance. Coatings can slow oxidation rates, and act as diffusion barriers for the Cr-derived species from the steel, slowing the degradation process. We have also developed a relatively quick, quantitative procedure using Rutherford backscattering spectroscopy (RBS) to measure the time evolution of various elemental vaporization rates.

Sulfer Poisoning. One disadvantage of using currently available fuels is their naturally occurring, or artificially added, contaminants content such as hydrogen sulfide (H_2S), which is known to have detrimental effects on SOFC performance. The results presented here reveal that H_2S promotes nickel migration and can compromise the percolating nickel network in nickel/ceramic anodes, thereby destroying their electrical conductivity.

Electrode Development. A prominent factor in SOFC failure is related to thermal cycling and hence thermal stresses within the cell/stack. While all-ceramic mixed conducting anodes yield good CTE matching, performance is still poor at best. Ni/YSZ persists as the most reliable and heavily used anode, therefore, to minimize difficulties in system integration of anode supported cell technology the most effective near term approach is the modification of the current materials set.

Engineered Pore Structures and Tortuosity. Research activities examining the effects of concentration polarization under high current densities suggest that gas diffusion through thick pore structures can limit the performance of SOFCs. Typical electrode structures are fabricated with techniques that yield highly tortuous paths through the electrode, thus impeding the exchange of steam at the interface with fresh hydrogen. New processing techniques for graded pore structure are required to fabricate porous supports specialized for SOFC application.

Metallic Brazed Seals. Traditional approaches to SOFC sealing have been focused on compliant and/or rigid glass or glass/ceramic seals, however, the metallic braze seal may yield a more robust, chemically bound, and true hermetic seal. While a key goal for cost effective implementation is the elimination of noble metals, additional concerns with metallic seals include the use of inert/vacuum environments; the potential shorting of the cell due to the electrical conductivity of braze; oxidation resistance of non-noble metal base materials; metal/ceramic bonding; and substantial thermal expansion mismatch.

Power Electronics. Modular design is an option for design of the inverter in a large-scale fuel cell power system. Such design requires a control strategy for the inverter modules to ensure the modules share load evenly.

The model reference simulator is an electrical device that can be connected between a short stack or a single cell and full-size, full-power (3 kW) electrical loads and associated control circuitry. This device simplifies effort needed to characterize the full dynamic and nonlinear behavior of a cell in order to predict its potential. This is especially important given that power-conditioning electronics will generally present the stack with a negative incremental resistance, which means that dynamics interactions, if any, would tend to be under damped.

The concern relative to electrically induced degradation is that a stack of slightly different cells, particularly a stack with series and parallel connections, individual cells may be exposed to unintuitive electrical terminal conditions. As an example, a cell with an abnormally high Thevenin equivalent resistance may actually be reverse-biased in the stack, a situation which would never occur if that cell were removed from the stack and connected to a resistive load.

Approach

Interconnects and Cr Volatility. Corrosion resistant coatings were deposited on 430 stainless steel by screen printing and electroplating at MSU and filtered arc deposition and hybrid filtered arc-assisted electron beam evaporation at Arcomac, LLC [1]. High-temperature furnace systems at MSU are used for corrosive exposures, with before and after analyses performed using state-of-the-art surface and cross section analytical tools, e.g., scanning electron microscopy (SEM), energy dispersive X-ray spectroscopy, electron backscattered diffraction, X-ray diffraction and RBS. ASR is measured *in situ* using a standard 4-point probe setup with porous Pt paste or cathode material for electrical contact. For the Cr volatility measurements, Cr-containing vapors from the steel coupons in a tube furnace at 800ºC were transported with various flow rates of humid air to a Si wafer at ~110ºC near the end of the quartz tube in the furnace, where the vapors adsorbed on the Si surface were subsequently analyzed using Rutherford backscattering.

Sulfur Poisoning. We performed XPS and X-ray absorption spectroscopy (XAS) on the conducting and insulating parts of the anode before and after H_2S exposure.

Electrode Development. Ultra-low CTE additives (0.5 – 2.0 ppm/°C) were synthesized and mechanically mixed into 66 wt% NiO/34 wt% YSZ anode powders. Anode blend bars were sintered at 1,400°C for 2 hours and evaluated by dilatometry, 4-wire DC conductivity, and 3-point Modulus of Rupture tests.

Engineered Pore Structures and Tortuosity. A novel freeze-tape casting ceramic processing technique is being optimized that can create ordered pore structures with tortuosities approaching unity, without the additions of thermal fugitives that are based on commercially available technologies. Varying of solids loading, freezing rate, and organic additives are used to tailor the porosity, morphology, and shrinkage.

Metallic Brazed Seals. A copper-based active braze alloy has been evaluated for sealing SOFCs and processed via vacuum, inert, and reducing conditions. The braze employs a titanium dopant to facilitate chemical bonding with YSZ and aluminum dopant to improve the oxidation resistance of the copper base.

Power Electronics. We have used scalable design to reduce the cost of the DC/DC converter, maximized the duty ratio of the converter to reduce the conduction loss, and employed soft-switching technique to reduce the switching loss.

We continued our work on the development of a physically-based dynamic model for a 5-kW tubular SOFC. The model steady-state power response was compared with the laboratory steady-state data from a 40-cell SOFC stack, reported by GE at the 2006 DOE-SECA Workshop, September 2006.

The model reference simulator circuitry was constructed, and the instrumented was tested under dynamic conditions using an InDEC SOFC in the modular test stand. To test electrically induced degradation, we conducted an experiment that reproduced conditions outlined by Anil Virkar [2, 3]. We believe that some sub-set of Virkar's conditions may occur in a stack. The experimental procedure was to characterize the cell in the normal operating range, briefly create the degradation conditions, re-characterize in the normal range until some electrical evidence of degradation was observed. Then the cell was removed to determine if any physical evidence of degradation could be found.

Results

Interconnects and Cr Volatility. Significantly improved SOFC interconnect performance has been realized using protective coatings developed by our group. This includes a dramatic improvement in long-term surface stability, increased electronic conductivity, and substantial Cr volatility reduction. Quantified results include: the essential absence of physical or chemical changes within the coating for over 1,000 hours at 800°C in air through several thermal cycles; stable ASR values of <50 mΩ•cm^2 for over 1,000 hours in 800°C air with LSM contact paste; and, negligible Cr volatility compared with uncoated 430SS.

Figure 1 shows the Cr volatility for 430 steel with and without the TiCrAlY coating calculated from RBS measurements on the Si wafer condenser as a function of exposure time for humid air flowing through the tube

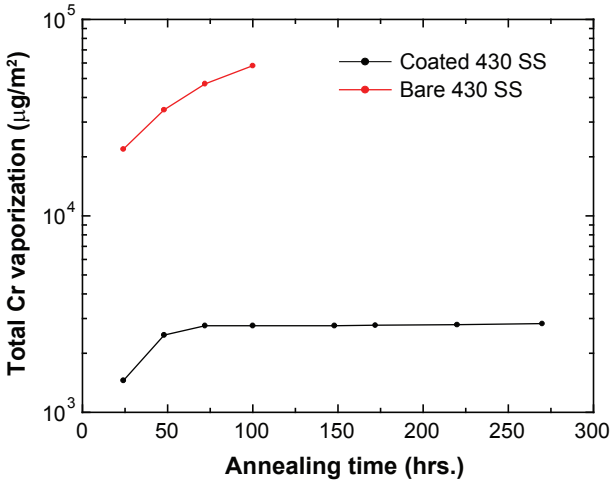

Figure 1. Total Cr Evolved from the Coated and Bare Steel Surface as a Function of Annealing Time at 800°C in Humid Air

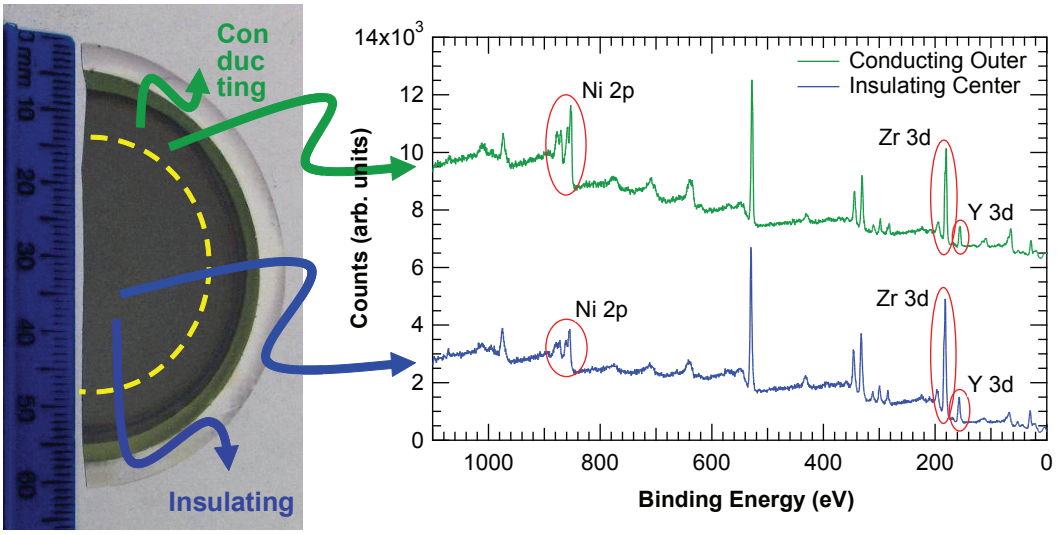

Figure 2. XPS spectra taken from the Ni/YSZ anode of a tested cell. The upper spectrum was taken on the outer, conducting part of the cell and the lower spectrum was taken in the center of the anode, which was insulating after completion of the cell test which included H_2S exposure and failure of the cell.

furnace at 800°C. The volatility rate is negligibly small after the initial 70 hour anneal.

Sulfur Poisoning. Atomic elemental analysis showed that the nickel-to-ceramic ratio was reduced by a factor of two. The spectra and regions of acquisition of those spectra are illustrated in Figure 2. We found that the insulating parts were severely depleted in nickel. At such low concentrations the conductive percolating nickel network is compromised that the anode becomes non-conductive.

Engineered Pore Structures and Tortuosity. We extended our previous gas flow analysis based on molecular and Knudsen diffusion processes to include permeation flux from convective flow. SOFC $V(i)$ curves found from our model agree quite well with experiment [4]. This model replaces the Butler-Volmer $i(V_{act})$ expression with one that does not incorrectly predict infinite i if infinite V_{act} is applied, as in the high-applied-V limit in the solid oxide electrolysis cell mode.

Metallic Brazed Seals. Significantly improved brazing results have been achieved using the new polypropylene carbonate binder system, braze paste extruder, and dedicated vacuum brazing furnace. Figure 3 shows a macro-defect free joint between stainless steel and 8 mol% YSZ using the copper-based braze bead. The braze is well wetted and chemically bound to the YSZ layer and subsequent prying of the joint yield failure of the bulk YSZ. A key benefit of this braze is the high solidus temperature above 960°C, which should extend the operational range of this composition up to the 850°C range.

Power Electronics. Development of the DC/DC converter is under way. Simulation shows that the load sharing control strategy can yield a less than 5% load sharing error among the modules.

The power density characteristic obtained from the MSU's 5-kW SOFC stack model compares well with the GE's laboratory data for a 40-cell SOFC stack. The overloading capability of SOFC is mainly affected by its dynamic characteristics in the short time scale (msec) and medium time scale (sec).

The fuel cell reference simulator was successfully demonstrated in a dynamic test with good fidelity between fuel cell and load terminals. The electrically induced degradation test appeared to result in an irreversible change in the current-voltage characteristic of the cell (InDEC). A significant change was achieved after approximately 10 minutes of electrical conditions predicted to induce degradation, see Figure 4. Optical and SEM examination of the cell revealed massive

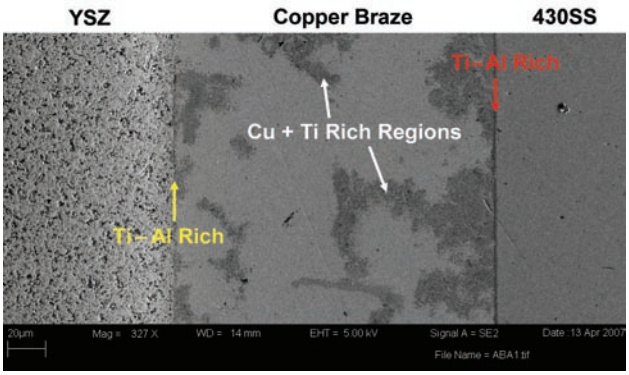

Figure 3. Copper Braze Joint Under Medium Vacuum Environment (10-4 mb)

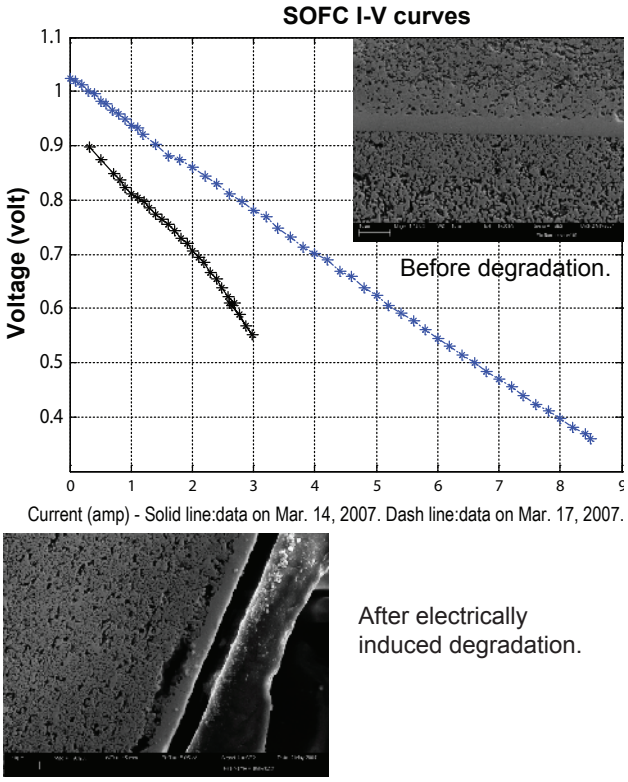

Figure 4. I-V Curves Before and After Degradation Tests

changes in the structure, including cracks, fissures, and apparent changes in the density gradient of the active anode region near the electrolyte.

Conclusions and Future Directions

Interconnects and Cr Volatility. The TiCrAlY coatings characterized to date have good oxidation resistance, low Cr volatility, but relatively high ASR. Doping with Co and/or Mn should improved the electron conductivity of the coated interconnect. In general, our future measurements include the following: (1) measurements of corrosion resistance, Cr volatility, and thermal stability for additional coatings with improved electrical conductivity; (2) measurements of elemental volatility from glass seals and metal brazes being used for the SOFC stack, and consideration of the impact of these volatile elements on SOFC operation; and (3) measurements of surface exchange and diffusion coefficients for oxygen transport in YSZ, with controlled exposure to poisoning elements from SOFC components, or from synthetic coal gas on testing coatings in operating SOFC short stacks.

Sulfur Poisoning. MSU has developed the means to test, analyze, and characterize the mechanistic effects of H_2S impurities on SOFCs. In addition to aiding in the development of sulfur resistance anode materials, these analyses and testing capabilities will be further applied to examine alternate anode gas impurities including phosphorous, arsenic, etc.

Electrode Development. Aluminum titanate has been shown to effectively reduce CTE, while dramatically improving strength at low quantities.

Engineered Pore Structures and Tortuosity. Freeze cast anode supported cells have been successfully fabricated and comparative tests (both electrochemical and passive) are underway to establish the real benefits of graded anodes. Our gas flow equation based on molecular and Knudsen diffusion and laminar flow will be applied to SOFCs, to our future opposing-gas-flow and tortuosity results, and to flow-nuclear magnetic resonance tortuosity measurements made by another MSU group.

Metallic Brazed Seals. Copper-based brazes have shown to form a robust joint between stainless steel and YSZ. YSZ discs will be brazed to a stainless steel fixtures to be pressure tested at both room temperature and operating temperature to evaluate the leakage and failure modes of the braze. The durability of this joint may yield the potential to pursue pressurized SOFC cell/stack development.

Power Electronics. The new DC/DC converter has the potential to reach 96% efficiency and $40/kW cost and the load sharing control strategy has the potential to yield a less than 5% load sharing error. We will verify the developed DC/DC converter through simulation and experimental work. We will further develop the control software to implement the developed load sharing control strategy.

The steady-state power density curve obtained from the MSU's dynamic SOFC model compares well with that reported by GE.

The fuel cell reference simulator appears to be ready for experimental use on real system integration problems with fuel cells. The electrically induced degradation result appears consistent with the largely theoretical predictions in Virkar's papers but we have not had an opportunity to establish repeatability.

Special Recognitions & Awards/Patents Issued

1. The 2005 paper, "Dynamic Models and Model Validation for PEM Fuel Cells using Electrical Circuits", C. Wang, M.H. Nehrir, and S.R. Shaw, IEEE Transactions on Energy Conversion, received the EDPG Technical Committee Prize Paper Award in 2007 for its impact.

2. Uni-Cell: High Performance, Textured, Electrolyte Supported Solid Oxide Fuel Cell, patent pending.

3. S. R. Shaw was invited to write a special topic essay on fuel cell technology for a popular introductory chemistry text.

FY 2007 Publications/Presentations (Selected from 27 total)

1. P.E. Gannon, "Advanced PVD Nanocomposite Protective Coatings for SOFC Metallic Interconnects", Invited Presentation - TMS Annual Meeting; February 25–March 1, 2007; Orlando, FL.

2. A. Kayani, R. J. Smith, S. Teintze, M. Kopczyk, P. E. Gannon, M. C. Deibert, V. I. Gorokhovsky, V. Shutthanandan, "Oxidation Studies of CrAlON Nanolayered Coatings on Steel Plates", Surface and Coatings Technology, **201** (2006), 1685–1694.

3. A. Kayani, T.L. Buchanan, M. Kopczyk, C. Collins, J. Lucas, K. Lund, R. Hutchison, P.E. Gannon, M.C. Deibert, R.J. Smith, D.-S. Choi, and V.I. Gorokhovsky, "Oxidation Resistance at 800°C for Magnetron-Sputtered CrAlN Coatings on 430 Steel", Surface and Coatings Technology, **201** (2006), 4460–4466.

4. C. Collins, J. Lucas, T.L. Buchanan, M. Kopczyk, A. Kayani, P.E. Gannon, M.C. Deibert, R. J. Smith, D.-S. Choi, V.I. Gorokhovsky, "Chromium Volatility of Coated and Uncoated Steel Interconnects for SOFCs", Surface and Coatings Technology, **201** (2006), 4467–4470.

5. S.W. Sofie and J.M. Buscher, "Copper Based Braze for Robust Sealing of Planar Solid Oxide Fuel Cells," Submitted to the 31st International Cocoa Beach Conference & Exposition on Advanced Ceramics and Composites, January 2007.

6. S.W. Sofie and D.R. Taylor, "Controlled Thermal Expansion Anode Compositions with Improved Strength for Use in Anode Supported SOFC's," 31st International Cocoa Beach Conference on Advanced Ceramics and Composites, January 2007.

7. Alternative Energy System Modeling and Control, invited presentation, given at the College of Electrical Engineering at Chongqing University, China, April 24, 2007.

References

1. V. Gorokhovsky, US Patent No. 6,663,7552.

2. Anil V. Virkar, "Theoretical Analysis of Solid Oxide Fuel Cells with Two-layer, Composite Electrolytes: Electrolyte Stability", J. Electrochemical Soc., Vol. 138, No. 5, May 1991.

3. Anil V. Virkar, J. Nachlas, A. Joshi, J. Diamond, "Internal Precipitation of Molecular Oxygen and Electromechanical Failure of Zirconia Solid Electrolytes", Journal of the American Ceramic Society, 73 [11], 3382-90, 1990.

4. Y. Jiang and A.V. Virkar, "Fuel Composition and Diluent Effect on Gas Transport and Performance of Anode-Supported SOFCs", J. Electrochem. Soc. **150**, A942-A951 (2003).

V.6 Advanced Fuel Cell Development

Randall Gemmen
National Energy Technology Laboratory
3610 Collins Ferry Rd.
Morgantown, WV 26507
Phone: (304) 285-4536
E-mail: Randall.Gemmen@netl.doe.gov

Subcontractors:
- The Georgia Institute of Technology, Atlanta, GA
- University of West Virginia, WV
- Carnegie Mellon University, PA
- University of Pittsburgh, PA

Objectives

- Evaluate Department of Energy (DOE)-sponsored solid oxide fuel cell (SOFC) systems to ensure progress in meeting DOE goals.
- Measure response of SOFCs to coal contaminates and develop analysis tools to understand SOFC performance on coal syngas.
- Assess the dynamic performance of SOFC components and systems, and determine control requirements for these advanced systems.
- Develop new coating methods for low-cost fuel cell metallic components.

Accomplishments

- Successfully installed and operated the Solid State Energy Conversion Alliance (SECA) Phase I Prototype units made by FuelCell Energy/Versa Power Systems and Acumentrics to verify performance versus SECA Phase I requirements.
- Measured the effects of arsine and phosphine on SOFC performance, and applied detailed transport models to predict SOFC performance on coal syngas.
- Performed system analysis for coal-based fuel cell and gas turbine hybrid systems. Experimentally characterized hybrid plant response for purpose of control method development, and derived a control method using advanced control theory.
- Experimentally measured the performance of advanced electroplated interconnect coatings.

Introduction

The U.S. DOE is supporting the development of solid oxide fuel cells through the SECA program so that future coal-based power plants will achieve the highest possible fuel efficiency while protecting our environment. It is expected that coal gasification will be employed for these future plants. Therefore, to achieve future coal-based operation will require new understanding of how to integrate the fuel cell with the gasifier technology, and how gasified coal (syngas) will affect the operation of a SOFC. In addition, because of concerns for CO_2 within the environment, these systems must also perform carbon capture and sequestration. The work performed here accomplishes all these by: 1) developing test capability for the evaluation of SOFC systems and components; 2) measuring the effects of coal syngas on cell performance; 3) applying advanced analysis tools for the purpose of understanding solid oxide fuel cell operation on coal syngas; and 4) developing low-cost manufacturing options for metal materials used in SOFCs.

Approach

Systems Test and Evaluation Capability–The U.S. DOE National Energy Technology Laboratory established a fuel cell test facility for evaluating the performance of prototype fuel cell systems developed by government sponsored fuel cell developers. The goal of this work is to provide additional and confirmation testing of the developer units. This testing allows the government to independently evaluate a given unit's performance, and establish whether or not the unit is able to meet expected requirements. The facility is configured to handle fuel cell systems running on natural gas or methane with a nominal power rating of 3 to 10 kW.

Hybrid System Studies–A hybrid experimental simulator is used to investigate the dynamic performance of, and control methods for, fuel cell gas turbine hybrid systems. Here we employ a 'hardware-in-the-loop' approach whereby an experimental gas turbine is coupled to necessary hardware components (i.e., pipe volumes) that simulate the presence of a fuel cell via a real-time dynamic fuel cell model. This experimental capability shows, for example, the extent at which perturbations in the compressor/turbine system can propagate through the piping/hardware and be present in the fuel cell. If pressure waves of significant amplitude reach the fuel cell, risk to failure is possible.

Also important is to develop the time-scales for different process events and control actions. Such information is important to control design/development.

Coal Syngas Operation–Both thermodynamic and experimental work are under way to help us understand the effects of trace syngas species on the operation of solid oxide fuel cells. Because of the numerous trace elements existing in coal, a large number of species could, in principle, be formed during the gasification process. The concern for the fuel cell is that these species can react unfavorably with the fuel cell to cause performance loss or failure. To reduce the scope of the experimental work, thermodynamic models have been applied to help us understand the relative potential of the different species in surviving any of the clean-up stages of the system. A priority in the examination of the likely trace species can then be developed, and experimental focus can be applied to those species with the greatest potential of reaching and reacting with the cell. This year, experimental focus has been given to Cl, As, and P element effects on cell operation, and some of those results are given here.

Coatings for Metallic SOFC Components–Low cost coating methods for applying protective layers on iron alloy steels are needed to provide an effective solution for preventing chromium attack on SOFC cathodes. The approach taken in this portion of our work is to investigate electroplating methods. Such methods have an advantage in regards to their ability to deposit coatings on potentially intricate metallic components (components that have machined or stamped features to allow improved operation of the fuel cell). This year we have studied 'full cell' performances using interconnects having three different coatings, two with electroplated cobalt layers, and one with electroplated bi-layers of Co and Mn.

Results

Systems Test and Evaluation Capability–FuelCell Energy/Versa Power Systems (FCE/VPS) provided the first unit tested this past year for independent evaluation. The second unit was provided by Acumentrics Corporation. The FCE/VPS unit was operated on pipeline natural gas, and the Acumentrics unit was operated on bottled methane. In short, both units were able to meet the minimum requirements for the SECA program of >35% efficiency, <2% degradation per 500 hours, and <1% degradation after 10 transients. The testing of both units provided needed information that was able to independently assure SECA program management that progress is being made to achieve program goals.

Dynamic System and Component Studies–Results for work that determined the timescales present in hybrid systems are given here. Frequency modulation tests were conducted in FY 2007 that yielded dynamic transfer function models that allow for control stability analysis. Figure 1 shows the response of several hybrid system process variables due to modulation of fuel, which is a control variable for the plant. The peak response of the heat exchanger temperature as a function of the modulated frequency of turbine combustor fuel valve is characteristic of the transport delay of the recuperator falling into phase with the previous cycle to yield a resonant feedback within the cycle. This characteristic frequency is consistent with previously observed 90 second step response of the heat exchangers with the energy balance between turbine exhaust heat and compressor air flow back work. The method of modulation and analysis for phase and amplitude of process data has allowed the fully integrated system to be characterized, quantitatively, for time scales that are attributed to the physical parameters of turbine inertia, heat exchanger thermal mass and transfer rates.

Coal Syngas Operation–From thermodynamic analysis using the FACTSAGE commercial software package, it was concluded that Sb, As, Cd, Pb, Hg, P, and Se elements will form the volatile compounds that will potentially interact with the SOFC anode. Specific to a nickel reaction, the elements, Sb, As, and P were found to form secondary phases. To begin to examine these elements, experimental studies of HCl, AsH_3, and PH_3 were performed on single button cells. Our approach is to individually inject such elements (in the forms that they exist under post syngas clean-up conditions) into the fuel gas passing over an SOFC button cell. Because future cleanup systems have not been fully identified, these tests are performed over a range of temperatures and specie concentrations. The results for the effect of arsine for one of the conditions tested are shown in Figure 2. Results show that (for relatively short term studies, ca. 100 hours) arsenic does not affect the performance of the fuel cell for concentrations less than 1 ppm. Longer term studies with 0.1 ppm arsine (ca. 800 hours) did show gradual decay in fuel cell performance, however, by about 10%. In coordination with other research by other organizations we will be able to confirm these results,

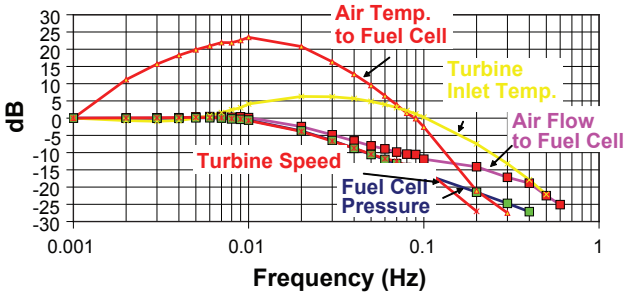

FIGURE 1. Frequency Response of Hybrid System Components Due to Fuel Valve Modulation

and if so confirmed will provide the needed information to researchers developing cleanup technology as to target levels for SOFC applications. Finally, in further support of this investigation into trace specie effects on SOFC operation, the detailed design of a portable test rig capable of testing multiple (~12) cells simultaneously is completed, and hardware is now being constructed. This unit will be taken to gasification facilities to determine more directly the effect of actual syngas on cell performance. The results from that study will be related to those from our individual specie studies to determine the unique behavior that reactant-to-reactant conditions provide.

Coatings for Metallic SOFC Components–The results of short term testing full cells using a coated interconnect of Crofer APU 22 showed that both Co and Co/Mn (as bi-layer) could be effective in preventing chromium from being evolved from the interconnect substrate, and provide stable operation of a SOFC. Results from a case using a 15 μm coating of Co are shown in Figure 3. Only the degradation information shown in the figure is relevant (not the absolute performance) given the fact that a 20 μm electrolyte cell is used for this test. As is evident, there is a conditioning period which is followed by a stable performance of the cell. Post test analysis showed a relatively small concentration of Cr in the outer coating layer, and no Cr was seen in the cross-sections of the cathode. X-ray diffraction (XRD) data showed that the Co formed a protective Co_3O_4 spinel as expected, and also showed the $CoCr_2O_4$ spinel phase. While longer tests need to be completed, these results favorably suggest that electroplated coatings will operate effectively in SOFC applications.

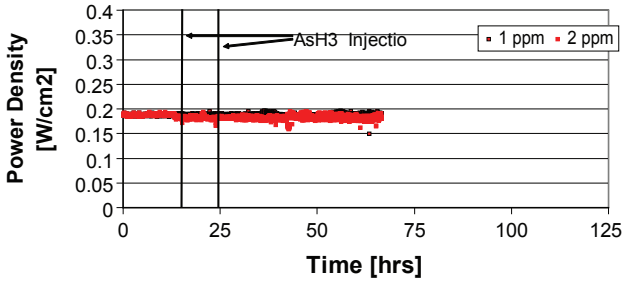

FIGURE 2. SOFC Power Density Operating at 750°C and 0.25 Acm^{-2} with AsH_3 Concentrations of 1 and 2 ppm

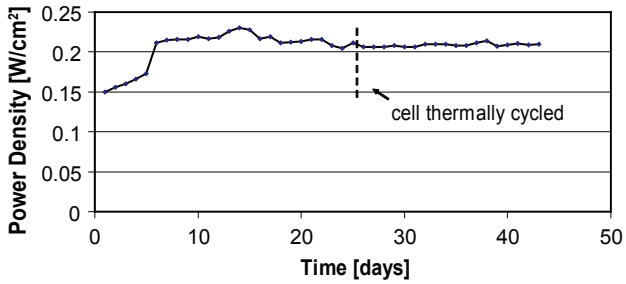

FIGURE 3. SOFC Cell Power Density as a Function of Time Using Anode Supported Cell with a 20 μm Thick Electrolyte and Co_3O_4 Coating on Crofer APU 22 Substrate

Conclusions and Future Directions

The DOE Fuel Cell Test Facility has completed evaluation of the SECA Phase I prototype units, and the important finding is that developers are presently meeting program requirements. Beginning in FY 2007, the major level of our work is focused on investigating coal-based fuel cell systems, and in particular the effects of trace species on fuel cell operation. Testing to date shows that certain trace species (e.g., HCl) behave very closely to what has been seen for H_2S, and similar clean-up requirements are expected. As shown in this report, AsH_3, on the other hand, is likely to require lower concentration requirements based on the presently available data. Tests for the effects of Sb-, Cd-, Hg-, and Pb-based compounds on fuel cell performance remains to be completed. While these basic technical studies will be the main focus of our work, we also anticipate the need to improve our understanding of these future coal-based systems via steady and dynamic modeling investigations in order to be assured that proposed hybrid systems will operate safely at peak efficiency. Finally, progress has been shown in achieving low-cost interconnect coatings suitable for SOFC conditions, and future work will now examine the effects of coal syngas contaminants on these materials.

FY 2007 Publications/Presentations

1. Christopher Johnson, Xingbo Liu, Caleb Cross. Proceedings of Material Science & Technology 2006 Conference and Exhibition, Materials and Systems: Volume I, October 15-19, 2006, Cinergy Center, Cincinnati, OH.

2. Christopher D. Johnson, Junwei Wu, Xingbo Liu, Randall S. Gemmen, "Solid oxide fuel cell performance using metallic interconnects coated by electroplating methods," ASME Fuel Cell Science, Engineering and Technology Conference, June 18-20, 2007, New York, NY.

3. J.P. Trembly, R.S. Gemmen, D.J. Bayless, "The effect of coal syngas containing HCl on the performance of solid oxide fuel cells: Investigations into the effect of operational temperature and HCl concentration," J. Power Sources 169, 2007, pp. 347-354.

4. J.P. Trembly, R.S. Gemmen, D.J. Bayless, "The effect of trace As, Cl, P, and Se coal cyngas species on the performance of a planar solid oxide fuel cell," ASME Fuel Cell Science, Engineering and Technology Conference, June 18-20, 2007, New York, NY.

5. J.P. Trembly, R.S. Gemmen, D.J. Bayless, "The effect of IGFC warm gas cleanup system conditions on the gas-solid partitioning and form of trace species in coal syngas and their interactions with SFOC anodes," J. Power Sources 163, 2007, pp. 986-996.

6. J.P. Trembly, R.S. Gemmen, D.J. Bayless, "The effect of coal syngas containing AsH_3 on the performance of SOFCs: Investigation into the effect of operational temperature, current density and AsH_3 concentration," accepted for publication in J. Power Sources, 2007.

7. D. Tucker, J. VanOsdol, E. Liese, L. Lawson, S. Zitney, R. Gemmen, J.C. Ford, C. Haynes, "Evaluation of methods for thermal management in a coal-based SOFC turbine hybrid through numerical simulation," Proceedings of the 7th International Colloquium on Environmentally Preferred Advanced Power Generation, September 5-8, Irvine, CA.

V.7 Component Manufacturing and Optimization of Protonic SOFCs

Matthew M. Seabaugh (Primary Contact), Michael Beachy, Sergio Ibanez, and Michael J. Day
NexTech Materials, Ltd.
404 Enterprise Drive
Lewis Center, OH 43035
Phone: (614) 842-6606; Fax: (614) 842-6607
Website: www.nextechmaterials.com

DOE Project Manager: Lane Wilson
Phone: (304) 285-1336
E-mail: Lane.Wilson@netl.doe.gov

Subcontractor: Dr. Sossina Haile
Professor of Materials Science and
of Chemical Engineering
California Institute of Technology, Pasadena, CA

Objectives

- Demonstrate protonic solid oxide fuel cell (p-SOFC) performance of 125 mW/cm^2 at 600°C, using scalable manufacturing approaches and improved cell electrodes.
- Demonstrate enhanced cell electrode performance through compositional and microstructural tailoring. Demonstrate (cathode + anode) contributions of <0.5 Ω-cm^2 to cell ASR at 600°C.
- Establish tape casting and sintering routes to produce conventional electrolyte supports and electrolyte components at the button cell and 10 x 10 cm cell size. Minimize cell membrane thickness, with a target of ASR of <1.0 Ω-cm^2.
- Produce of Zn-modified BYZ $Ba(Zr_{1-X}Y_X)O_{3-\delta}$ electrolyte powders at the 600 g batch size, using scalable preparation routes, and demonstrate that these powders in tape cast forms can be sintered to densities of more than 95% ρ_{th} at temperatures of less than 1,400°C.

Accomplishments

- Manufactured $Ba(Zr_{0.6}Ce_{0.4})_{0.8}Y_{0.2}O_{2.9}$ with ZnO (BYZC-Zn) doping by a solid state synthesis route.
- Densified $Ba(Zr_{0.6}Ce_{0.4})_{0.8}Y_{0.2}O_{2.9}$ with ZnO doping material to 97% of expected theoretical density at 1,550°C.
- Demonstrated significantly improved conductivity over standard BYZ-Zn powder.

Introduction

Protonic solid oxide fuel cells (p-SOFCs) offer unique characteristics compared to competing technologies. In a p-SOFC, protons diffuse from the anode to the cathode through a thin membrane layer, generating power from the electrochemical reaction. P-SOFCs are characterized by their potential for high fuel utilization without steam diffusion limitation, and their intermediate operating temperatures (450-600°C). P-SOFCs avoid steam formation at the anode (experienced by SOFCs), maintaining high fuel concentration over the anode, allowing high fuel utilization and the high efficiency operation. The cells operate at temperatures that increase the reaction kinetics compared to proton exchange membrane (PEM) fuel cells, but low enough to offer the potential for metal interconnects without corrosion. If operating temperatures can be kept at the lower end of this range (using thin membranes and efficient electrodes) conventional high temperature seals may become practicable, avoiding a design issue of SOFC systems.

To date, p-SOFC development has been hampered by processing difficulties associated with ceramic proton-conductors. In this project, NexTech and Caltech will collaboratively advance the materials science and manufacturing technology for ceramic p-SOFCs. Using materials processing strategies for $Ba(Zr_{0.8}Y_{0.2})O_{2.9}$ identified by Caltech, NexTech will fabricate its thin-membrane electrolyte-supported cells using proprietary designs well suited to the BZY material set. This demonstration will require the transition of demonstrated laboratory processes to commercially viable approaches. Caltech will assist this transition and use the resultant cell platform to optimize p-SOFC electrodes. The successful completion of this program will shift p-SOFC development from electrolyte development to electrode optimization and the large cell demonstration.

Approach

Researchers at Caltech have developed a chemical approach in which a sintering aid is used to enhance grain growth and enable densification at reduced temperatures [1]. From a comprehensive screening of transition metal oxides, it was determined that ZnO enhances sintering without generating deleterious intermediate phases or introducing excessive electronic conductivity.

NexTech has developed cost-effective manufacturing processes for a range of state-of-the-art SOFC cell designs. These efforts have revealed the manufacturing and performance strengths and weaknesses of various cell manufacturing approaches. Based on this experience, NexTech developed target specifications for an optimized solid oxide fuel cell, a planar cell component with a thin (≤50 µm) electrolyte, a 30-50 µm thick anode (to improve fuel oxidation kinetics) and a 30-50 µm thick cathode (to minimize oxygen diffusion limitations). The cell should be mechanically robust and have a dense periphery to simplify sealing.

The cell developed by NexTech offers an excellent demonstration platform for protonic electrolyte and fuel cell research. The principal manufacturing step for the cell platform are tape casting and co-sintering. The processing routes developed at Caltech have been demonstrated with glycine-nitrate produced powders having surface area values (5-8 m^2/g), ideal for tape casting approaches. In this project, NexTech will tailor this process for scaled-up powder production, and validate its utility in tape casting and cell fabrication experiments.

Results

ZnO-doped $Ba(Zr_{0.6}Ce_{0.4})_{0.8}Y_{0.2}O_{2.9}$ (BYZC-Zn) material was synthesized by a solid state route and subsequently cast into thin tapes consisting of ~74 microns in thickness. Laminates of the cast tape were hot pressed into sheets measuring 400 microns thick. The sheets were cut into button cell shapes. The button cells were fabricated into two designs, the standard circular disc with no texture and a thin (~50 micron) membrane design. The button cells were sintered at various temperatures, up to 1,450ºC. This allowed for dense, non-porous parts while preventing unwanted surface reaction with the surrounding sacrificial powder. Cells were sent to Caltech for electroding and subsequent performance tests. Measurements resulted in 4 mW/cm^2, which is nominal to the performance seen with BYZ-Zn based substrates.

Figure 1 demonstrates the sintering curve of the BYZC-Zn materials. The densification data on pressed pellets indicates that BYZC-Zn samples can densify as low as 1,250ºC. However, upon firing tape casted parts, densification behavior required increased temperatures to 1,450ºC most likely due to changes in geometrical design of the part.

In addition, Figure 2 shows results of conductivity values as measured by AC Impedance of the BYZC-Zn pellets sintered at 1,550ºC. The results demonstrated a 115% increase in conductivity over BYZ-Zn powders measured at 600ºC. Although promising,

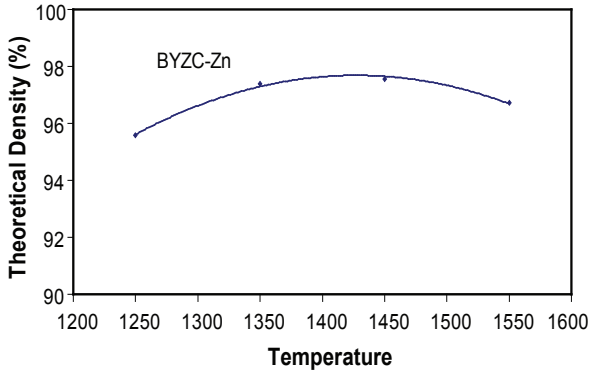

FIGURE 1. Sintering Study for BYZC-Zn Synthesized by Solid State Route

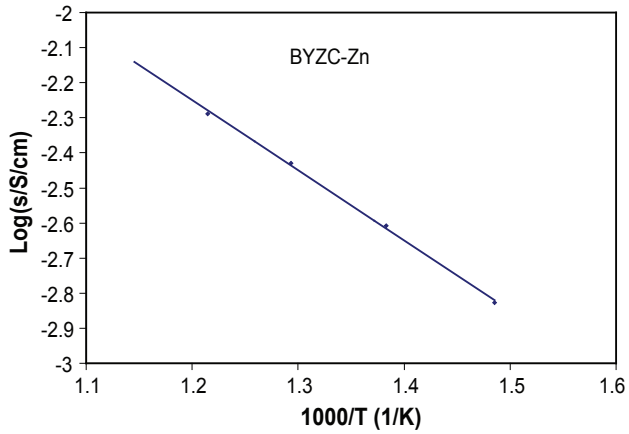

FIGURE 2. Conductivity Measurements for BYZC-Zn Synthesized by Solid State Route

the conductivity of 5.15 mS/cm is still a below that of equivalent oxygen ion conductor ceramics for the fuel cell industry.

Conclusions and Future Directions

NexTech has been able to demonstrate manufacture of BYZC-Zn doped ceramics that demonstrate 115% more conductivity over BYZ-Zn powders. Button cell size discs have been fabricated by a low cost synthesis route and fired at reasonable sintering temperatures while demonstrating dense parts. The improved conductivity should provide better performance in fuel cell and other electrochemical reactors.

References

1. Babilo, P., and Haile, S.M., *J. Am. Ceram. Soc.*, 88 (9), 2362-2368 (2005).

V.8 High Temperature Fuel Cells for Co-Generation of Chemicals and Electricity

Scott A. Barnett (Primary Contact),
Manoj Pillai and David Bierschenk
Northwestern University
Department of Materials Science and Engineering
Evanston, IL 60208
Phone: (847) 491-2447; Fax: (847) 491-7820
E-mail: s-barnett@northwestern.edu

DOE Project Manager: Heather Quedenfeld
Phone: (412) 386-5781
E-mail: Heather.Quedenfeld@netl.doe.gov

Objectives

- Determine the thermal self-sustainability, temperature gradients, electrical output, product composition, efficiency, and syngas productivity of a methane electrochemical partial oxidation (EPOx) reactor.
- Develop methods to avoid coking, and prove that excellent stability against coking can be achieved during long-term operation.
- Explore the use of alternative anode materials in order to eliminate coking with methane and other hydrocarbons and also allow redox cycling.
- Evaluate the technical and economic viability of the proposed technology based on the above information.

Accomplishments

- Showed that stability and coke-free direct-methane solid oxide fuel cell (SOFC) operation is promoted by the addition of small amounts of CO_2 or air to the fuel stream.
- The operation range for coke-free operation is greatly increased by replacing the thin nickel yttria-stabilized zirconia (Ni-YSZ) anode support with a ceramic support, including segmented-in-series stacks.
- Stable coke-free operation in natural gas was achieved by using a ceramic-anode-supported SOFC.
- Demonstrated current interruptions of up to 8 minutes in methane with no permanent coking or change in cell performance.
- EPOx operation was demonstrated at 750°C that yielded 0.9 W/cm^2 and a syngas production rate of 30 sccm/cm^2, with reaction product composition close to equilibrium during the early stages of cell testing.
- The stability of methane conversion was improved via the addition of a reforming catalyst to the SOFC anode.

Introduction

In the second year of this Phase I project, we have further studied direct-methane and direct-natural-gas operation of SOFCs. It was demonstrated that SOFCs can simultaneously produce high electrical power density and high-quality syngas. A new issue with poor reforming stability of the Ni-YSZ anode/catalyst was discovered, and the initial solution of adding a catalyst material was demonstrated.

Combined generation of electricity and syngas has significant potential economic advantages. That is, when SOFCs become cost-effective for electricity generation, the syngas becomes a low-cost by-product. This could provide an important new route to low-cost hydrogen and gas-to-liquid fuels. From another perspective, the ability to sell both electricity and chemicals increases the value of the SOFCs, improving their prospects for commercialization.

Approach

Extensive electrical testing of anode-supported SOFCs with methane and simulated natural gas fuel were done in combination with gas chromatograph and mass spectrometer measurements of reaction products for a range of conditions. While these were single-cell tests, the cell area and current were large enough to achieve partial oxidation stoichiometry ($O^{2-}/CH_4 \approx 1$) for reasonable fuel flow rates. Cell stability was tested versus additions of H_2O/CO_2 to the methane, barrier layers, and for ceramic-anode-supported cells.

Detailed modeling was carried out in collaboration with Colorado School of Mines, providing detailed predictions of gas composition gradients within the anode and anode flow field. The work focused on the effect of anode barrier layers on overall cell/stack performance and changes in the gas composition within the Ni-YSZ anode that influence anode coking. Most model input parameters were quantitatively established by structural evaluation of the SOFCs and barriers combined with calibration experiments performance on the SOFCs prior to methane testing.

Results

In order to demonstrate EPOx in a larger-area multiple-cell configuration, a segmented-in-series (SIS)-SOFC module was operated directly with methane under EPOx conditions. The segmented-in-series modules can produce a total of 8 W at 800°C in humidified hydrogen, corresponding to ~650 mW/cm^2 [1]. These devices consist of thick-film SOFC layers on a ceramic (partially-stabilized zirconia) anode support. For the EPOx experiments, a Ru-CeO_2 catalyst material was applied to the inner surfaces of the SIS-SOFC tube that was operated at 750°C. Stack power density was 325 mW/cm^2 at 750°C and 600 mW/cm^2 at 800°C, similar to the values obtained for the same stack with hydrogen fuel. Mass spectrometer exhaust gas measurements at 750°C with an O^{2-}/CH_4 ratio of ≈1 showed very good methane conversion of ~90% with the primary products being CO and H_2 with a small amount of CO_2.

We have tested direct-methane stability in SOFCs with (Sr,La)TiO_3 (SLT) ceramic anode supports. A series of methane stability tests were carried out at different current densities. Figure 1 shows the result in dry methane at 800°C. The current density was first maintained at 0.5 A/cm^2, and then decreased by 0.1 A/cm^2 and stability tested again for >8 hours. The cell was stable at the lowest current density tested, 0.1 A/cm^2. For comparison, Ni-YSZ-supported cells were not stable unless the current density was at least 1.0 A/cm^2. That is, the SLT-supported cells showed a much wider stability range than conventional SOFCs (even with barrier layers). This dramatic increase in the stability range is presumably due to the relatively thin Ni-containing active layer in these cells, combined with the thick SLT support layer that acts as a built-in barrier layer.

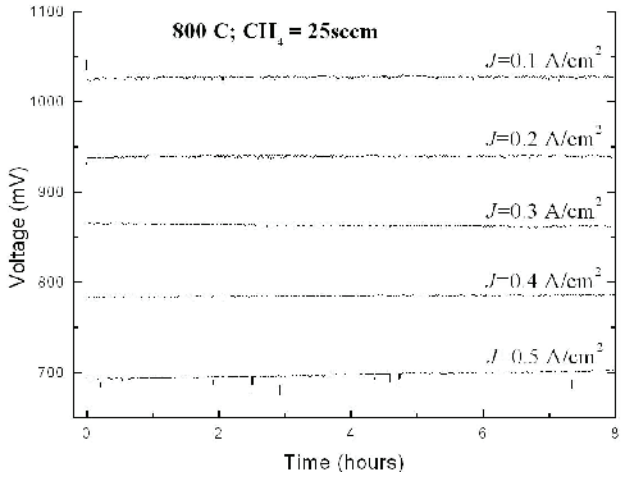

FIGURE 1. Measured Product Composition versus Time from an EPOx SOFC Reactor Showing a Gradual Decrease in Methane Conversion to Syngas over 35 Hours

An SLT-supported SOFC was tested in the "worst-case" natural gas mixture of 85% methane, 10% ethane, and 5% propane. The cell was stable over 72 hours. Figure 2 shows an image of this cell showing the Ni-YSZ active layer (bottom), dense YSZ electrolyte layer (middle), and the LSM-YSZ/LSM cathode layer (top). There was no coking observed on the active layer. Images from other areas of the anode support showed a SLT structure similar to that in Figure 2, with no evidence of coking. Furthermore, ceramic-supported SOFCs with thin Ni-based active layers have shown excellent redox stability, such that it would be possible to clean any carbon from the SOFC anode and anode compartment by periodically exposing to air. The ceramic-supported SOFCs are very similar to conventional Ni-YSZ anode-supported cells; thus, they could easily be substituted into conventional planar stacks.

Although our results have shown that SOFCs are stable during steady-state operation at a reasonable current density, it was not clear what would happen if there was a break in stack current. Thus, studies of the effects of different current interruption cycles on single SOFCs were carried out. Figure 3 shows a typical interruption test. After the cell reached steady-state operating on pure methane at 750°C, the current was abruptly stopped for 1.5 mins, and then abruptly increased back to 1.8 A/cm^2. The voltage returned to its initial steady-state value after briefly being higher than the original value. A similar result was obtained with a subsequent 6-min interruption. However, when the

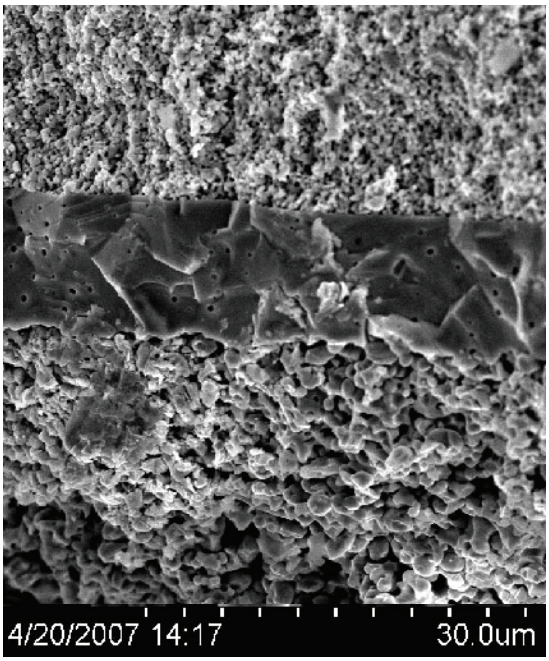

FIGURE 2. Cross Sectional SEM Image of the Active Region of the SLT-supported SOFC after Operation in Synthetic Natural Gas at 700°C

interruption time was increased to 10 mins, the voltage remained ~15 mV lower than before the interruption. These results suggest that although coking occurs when the cell is at open circuit, the early stage coking does not cause any permanent damage. Resumption of cell current actually etches carbon from the anode, returning the cell to its initial condition and performance. On the other hand, for a ≥10-min interruption, carbon buildup continues to a point where the carbon fills and then begins to expand anode pore cavities. The result is irreversible structural damage to the anode. The bottom line is that direct-methane SOFCs can survive several minutes without current, such that methane could be flushed from the cell prior to any damage.

Gas chromatography measurements have shown that the initial product gas composition closely approximates that expected from equilibrium calculations with >90% methane conversion. Figure 4 shows an example of the syngas output experimentally measured from a SOFC versus the O^{2-}/CH_4 ratio (varied by changing the SOFC current). The measurements were done during the early stages of operation, there was no barrier layer, and pure methane was the fuel. Also shown on the plot are the predicted equilibrium gas compositions. The measured gas composition is quite close to the equilibrium prediction. Furthermore, at a near-optimal O^{2-}/CH_4 ratio of 1.2, only ≈5% methane remains in the fuel stream and 2.4 moles of syngas are produced per mole of methane, very near the ideal ratio of 3. That is, the SOFC acts as a near-ideal partial oxidation reactor.

Figure 5 shows a plot that helps illustrate the efficacy of the SOFC as a dual electricity/syngas generator. In this case, the methane flow rate and oxygen ion current were varied together in order to maintain a constant O^{2-}/CH_4 ratio = 1.2. The plot shows the output power density and syngas production rate versus the methane flow and cell current. The syngas production rate increased linearly with the methane inlet flow rate. The power density curve shows the normal dependence on cell current density, with at peak power at 0.92 W/cm^2. This figure shows that it is possible to obtain ~0.9 W/cm^2 power output from the SOFC while producing a syngas output of ~30 sccm/cm^2. The power density is similar to state-of-the-art SOFCs operated at 750°C, whereas the syngas rate is comparable to the best ceramic membrane reactors, although these are typically operated at a higher temperature of 900°C [2, 3].

It is important to note that the data in Figures 4 and 5 were obtained during the early stages of SOFC

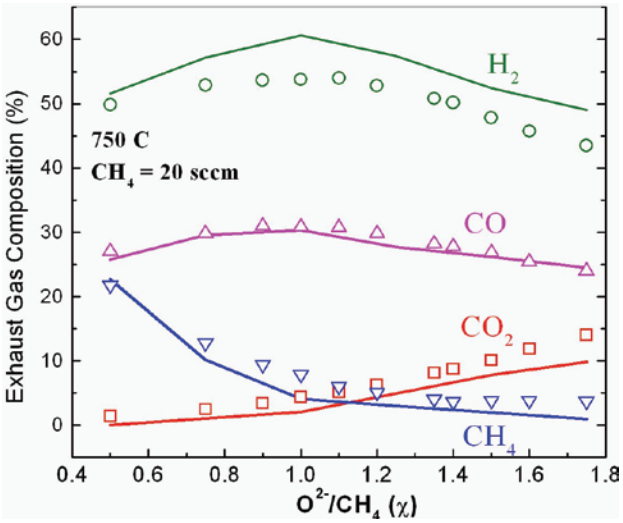

FIGURE 4. Measured Product Gas Composition (Data Points) and Equilibrium Values (Curves) versus Oxygen to Methane Ratio

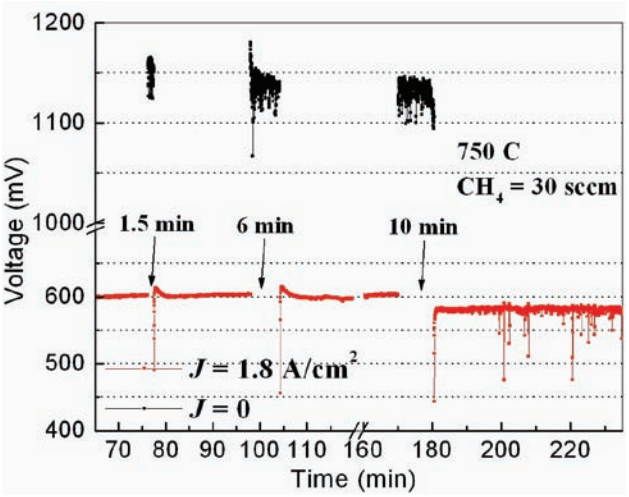

FIGURE 3. Effect of Current Interruptions on the Performance of a SOFC at 750°C on Methane Fuel

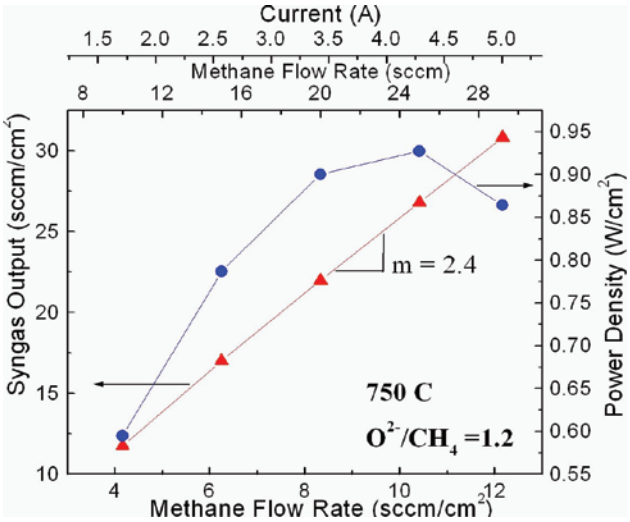

FIGURE 5. Syngas Output and Power Density versus Methane Flow Rate (and Cell Current) with the Ratio O^{2-}/CH_4 Maintained Constant at 1.2

operation. The methane conversion to syngas was found to decrease gradually with increasing operation time. That is, the amounts of methane, steam, and CO_2 in the exhaust increased, while CO and H_2 decreased. This occurred even while the SOFC was stable and the O^{2-}/CH_4 ratio was constant. This indicates that the reforming activity of the Ni-YSZ anode was decreasing with time, in agreement with recent results from David King's group at Pacific Northwest National Laboratory (see presentations at the Solid State Energy Conversion Alliance Review meeting, Fall 2006, Philadelphia). Note that reforming is necessary because the SOFC products are primarily H_2O and CO_2 – these must reform CH_4 in order to produce syngas. The Ni anodes have been thoroughly tested for carbon, so it is clear that the catalyst was not deactivated by coking.

Based on the above, the addition of catalysts to the SOFC anodes was investigated. Initial work with Rh-alumina catalysts applied directly to the SOFC anode showed much better product stability than the SOFC with no catalyst. More work is needed on catalyst testing to demonstrate the desired long-term stability. The prospects of finding an appropriate catalyst are good, since stable catalyst systems have already been developed for other types of methane reforming.

Conclusions and Future Directions

The above results demonstrate that direct-methane SOFCs can very effectively produce electricity while converting methane to syngas. Cell stability testing has continued to show ways to increase the stable operation range for SOFCs with methane fuel; a particularly important example is the ceramic-anode-supported SOFC, which shows excellent stability in both methane and natural gas. It was also found that SOFCs can survive current interruptions of several minutes without any damage.

A key area for future work is clearly to develop catalyst systems that provide stable long-term reforming activity and thus stable syngas production. To test this, stability tests of several hundred hours will be carried out. The tests will increasingly focus on (Sr,La)TiO_3-anode-supported single SOFCs and segmented-in-series SOFCs. Simulation work will continue in order to obtain more accurate predictions of gas composition and temperature gradients within the anodes of these ceramic-supported SOFCs, to help explain the stability results.

FY 2007 Publications/Presentations

1. Zhu, H., Colclasure, A.M., Kee, R.J., Lin, Y. & Barnett, S.A., Anode barrier layers for tubular solid-oxide fuel cells with hydrocarbon fuel streams. *J. Power Sources* **161**(1), 413-419 (2006).

2. Zhan, Z., Lin, Y., Pillai, M., Kim, I. & Barnett, S.A., High-rate electrochemical partial oxidation of methane in solid oxide fuel cells. *Journal of Power Sources* **161**(1), 460-465 (2006).

3. Huayang Zhu, Andrew M. Colclasure, Robert J. Kee, Yuanbo Lin, Scott A. Barnett, "Tubular solid-oxide fuel cells using either anode recycle or barrier layers," 7th European Solid Oxide Fuel Cell Forum, Edited by Ulf Bossel.

4. Scott A. Barnett, "Hydrocarbon reforming processes internal to solid oxide fuel cells" Hydrocarbon Resources Gordon Conference, Ventura, CA, January 2007.

5. Manoj Pillai, Yuanbo Lin and Scott A. Barnett, Huayang Zhu, Andrew M. Colclasure, and Robert J. Kee, Effect of Anode Barrier Layer and Hydrocarbon Fuel Composition On Solid Oxide Fuel Cell Stability, American Ceramic Society Conference, Daytona Beach, FL, January 2007.

References

1. Pillai, M.R., Gostovic, D., Kim, I. & Barnett, S.A., Short-period segmented-in-series solid oxide fuel cells on flattened tube supports. Journal of Power Sources **163**(2), 960-965 (2007).

2. Sundmacher, K., Rihko-Struckmann, L.K. & Galvita, V., Solid electrolyte membrane reactors: Status and trends. Catalysis Today **104**(2-4), 185-199 (2005).

3. Bouwmeester, H.J.M., Dense ceramic membranes for methane conversion. Catalysis Today **82**(1-4), 141-150 (2003).

V.9 SECA Coal-Based Systems Core Research

Larry R. Pederson (Primary Contact),
Olga A. Marina, Xiao-Dong Zhou,
Yeong-Shyung Chou, Gregory W. Coffey,
Christopher A. Coyle, Benjamin P. McCarthy,
Carolyn D. Nguyen, and Edwin C. Thomsen

Pacific Northwest National Laboratory
902 Battelle Blvd., P.O. Box 999
Richland, WA 99352
Phone: (509) 375-2731; Fax: (509) 375-2167
E-mail: larry.pederson@pnl.gov

DOE Project Manager: Heather Quedenfeld
Phone: (412) 386-5781
E-mail: Heather.Quedenfeld@netl.doe.gov

Subcontractors:
- Montana State University, Bozeman, MT
- University of Florida, Gainesville, FL

Objectives

- Determine how contaminants found in coal gas will affect the performance of nickel-based solid oxide fuel cell (SOFC) anodes, with an emphasis on those contaminants expected to form secondary solid phases with nickel. This information is needed to help establish clean-up criteria for coal gas intended to fuel large SOFC systems.
- Establish the role of pressure on SOFC electrode activity and stability. Pressures in the range of 1 to 15 bar are emphasized, which are most relevant to SOFC integration with gasifier and turbine technology.
- Develop contact paste compositions and forms aimed at providing a more reliable electrical connection between the cathode and interconnect plate, and can be processed at temperatures less than 1,000°C.

Accomplishments

- Irreversible losses in SOFC performance of approximately 10 percent per 100 hours were observed when exposed to low concentrations of phosphine (PH_3) in simulated coal gas and in humidified hydrogen. Phosphine, expected to be present at about 2 ppm in coal gas following warm gas clean-up, interacts strongly with Ni in the anode to form stable secondary phases such as Ni_3P and Ni_5P_2. In contrast, sulfur forms no secondary phases with Ni at similar concentrations. No interactions of phosphorus-containing species with either zirconia or ceria were observed.
- Low concentrations of arsine (AsH_3) in simulated coal gas also led to irreversible losses in SOFC performance of approximately 10 percent per 100 hours, similar to results obtained for phosphine. Arsine concentrations of approximately 0.6 ppm are expected in coal gas following warm gas clean-up. Like phosphorus, arsenic reacts to form stable, secondary phases with nickel (primarily Ni_5As_2). No interactions with either zirconia or ceria were observed.
- The performance of lanthanum strontium manganite (LSM) and LSM-ceria composite electrodes were shown to improve considerably with increased pressure up to at least 100 bar. For LSM electrodes, polarization losses decreased as the square root of the oxygen partial pressure, which was shown by electrochemical impedance spectroscopy (EIS) to be dominated by gas adsorption processes. More active LSM-ceria composite electrodes also improved with increased pressure but more slowly due to a greater contribution of charge transfer processes.
- Enhanced densification of LSM was induced by thermal and oxygen partial pressure, at temperatures hundreds of degrees lower than typical processing temperatures. Enhanced sintering is the result of the creation of transient oxygen vacancies by thermal and oxygen partial pressure cycles, which interact with metal vacancies already present in LSM. This behavior potentially offers a way to densify LSM-based cathode contact pastes at low temperatures.

Introduction

The purpose of this project is to address key barrier issues of relevance to the operation of solid oxide fuel cells on gasified coal, in support of the Solid State Energy Conversion Alliance (SECA) Coal-Based Systems Program. The interaction of contaminants known to be present in gasified coal with nickel-based SOFC anodes is being investigated, with an emphasis on those contaminants that are expected to form secondary phases with anode components. This information is needed to help establish criteria for coal gas cleanup. Because integration of SOFC stacks with gasifiers and turbines may require operation at elevated pressures, this project is evaluating how the activity and stability of SOFC electrodes are affected by high pressure. Contributions to electrode losses include charge transfer,

gas adsorption, and concentration polarization, all of which show pressure dependence. High steam partial pressures on the anode side are expected to affect the stability of the nickel electrode. Finally, contact paste compositions and forms are being developed to provide a more reliable electrical connection between the porous cathode and the interconnect plate. To minimize degradation of metallic components during stack assembly, it is considered essential that the contact pastes be processed at temperatures less than 1000°C.

Approach

This project is addressing three principal topics: (1) interaction of SOFC anodes with coal gas contaminants, (2) the influence of elevated pressures on SOFC electrode performance, and (3) electrical contact paste development. Coal gas contaminant studies emphasize those trace species expected to remain after warm gas cleanup and possibly form secondary phases with nickel, following the results of a recent study by Trembly, Gemmen, and Bayless [1], as summarized in Table 1. The tendency for adsorption and second phase formation was evaluated using zirconia test coupons, onto which anode materials were screen-printed, which were exposed to contaminants of interest in a coal gas matrix. Anode-supported button cells were similarly exposed, and changes in performance evaluated by direct and alternating current methods. Post-test analyses were conducted with analytical electron microscopy and surface electron spectroscopies to evaluate the extent of adsorption and secondary phase formation. To evaluate the effect of pressure on SOFC electrode performance, a high-pressure cell was constructed that is capable of operation to 950°C and 130 bar. Cells with thick (~2 mm) electrolytes were employed, which enabled an embedded reference electrode to be used. Electrode performance under cathodic and anodic polarization was evaluated by direct and alternating current methods. LSM and LSM composite electrodes were emphasized in initial studies. Contact paste compositions that were considered include the layered calcium cobaltites and LSM. Layered calcium cobaltates exhibit a misfit layered structure, consisting of an oxygen octahedral layer and a Co-O layer. These materials yield an unusually stable electrical conductivity over a wide temperature regime, a good thermal expansion match to other fuel cell components, and a favorable processing temperature. Oxygen partial pressure cycling was employed to lower the sintering temperature of LSM, effective because of the unique defect structure of that material.

TABLE 1. Trace Species in Coal Gas Expected to Affect SOFC Performance and Concentrations Following Warm Gas Cleanup (from Trembly, Gemmen, and Bayless [1]).

Component	Concentration, ppmv
Antimony	0.07
Arsenic	0.6
Cadmium	0.011
Lead	0.26
Mercury	0.025
Phosphorus	1.9
Selenium	0.15

Results

Coal Gas Contaminant Studies: In this study, SOFC operation on simulated coal gas was evaluated in the presence of certain impurities that are expected to remain in low concentration after warm gas cleanup. Phosphorus, arsenic and antimony compounds were emphasized because of their ability to form secondary phases with Ni in the SOFC anode in low concentration.

It was found that the SOFC did not show immediate degradation upon exposure to PH_3 or AsH_3. After 30-50 hours of exposure, cell area specific resistances (ASR) began to increase at the rate of 10-20%/100 hours, as shown in Figure 1 for PH_3 exposure. This process was irreversible and returning to moist hydrogen without contaminants in the stream did not lead to a decrease in the ASR. Post-mortem microstructural and surface analysis revealed secondary nickel phase formation, mainly on the metal nickel current collecting grid on the Ni/YSZ anode. Depending on the time of exposure and proximity to the gas channel, Ni was partially or entirely converted either into nickel phosphides or nickel arsenide. Scanning electron microscopy/energy dispersive spectrometer (SEM/EDS) identified the presence of only one form of the arsenide, Ni_5As_2, while several forms of nickel phosphides, Ni_3P, Ni_5P_2 and Ni_2P, were found. Although conductive, nickel phosphides have much lower melting temperature than metallic

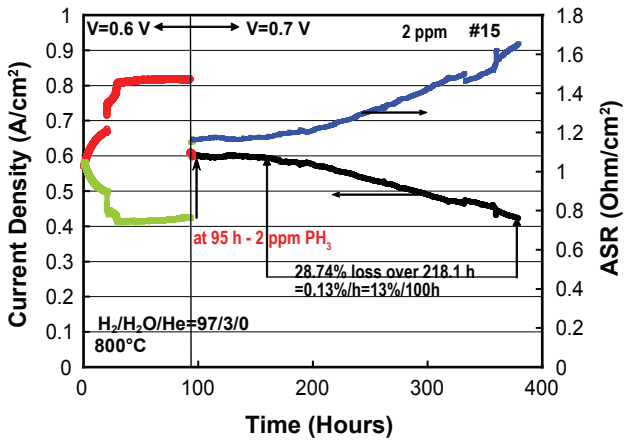

FIGURE 1. Anode Supported Cell Performance at 800°C When Exposed to 2 ppm PH_3 in Hydrogen/Steam

Ni. This resulted in the current collector surface reorganization followed by densification.

It is suggested that phosphorus and arsenic adsorb immediately on the Ni surface, both in hydrogen and the coal gas. Because of the strong Ni-P and Ni-As interactions, the main changes occurred on the surface and not in the anode bulk. At the same time, x-ray photoelectron spectroscopy (XPS) and transmission electron microscopy (TEM) analyses revealed gradients in P and As from the top of the anode to the anode/electrolyte interface, as is shown in Figure 2. In particular, after the test at 800°C in the presence of 5 ppm of PH_3, Ni_3P was observed up to 70 μm from the top. Nickel secondary phases at the electrode/electrolyte interface were not detectable by the techniques used. Thus, cell degradation could be ascribed to changes in the current collector (the mass transport limitations because of the current collector densification and perhaps the difference in conductivities of Ni and Ni_3P).

Pressure Dependence of Cathode Performance: The performance of LSM and LSM/ceria composite electrodes was found to improve substantially with increases in pressure. Polarization curves for an LSM electrode in both cathodic and anodic directions are given in Figure 3 at different oxygen partial pressures, and show typical Tafel behavior with two electrons transferred in the rate-limiting step. Exchange currents for LSM electrodes, calculated from polarization curves, were found to increase as the square root of the oxygen partial pressure to at least 100 bar, as is shown in Figure 4. Two principal features were observed in the EIS spectra for LSM electrodes: a dominant low frequency arc associated with gas adsorption processes and a much smaller arc at high frequency associated with charge transfer processes. These results suggest rate control by a dissociative oxygen adsorption mechanism, and show that the surface of LSM is not saturated with oxygen adatoms even to very high pressures. In contrast, platinum electrodes do become saturated with oxygen adatoms below 1 bar, and actually become less active with further increases in pressure.

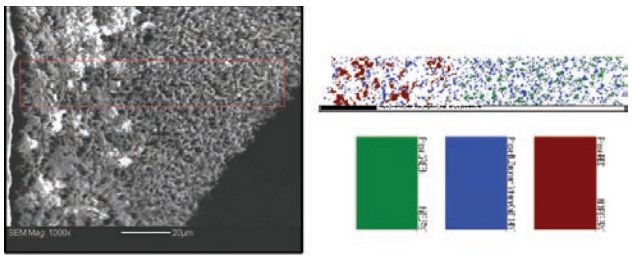

FIGURE 2. Electron backscatter diffraction (EBD) characterization of the Ni/YSZ anode after the SOFC test at 800°C in $H_2/H_2O=97/3$ with 5 ppm of PH_3 for 166 hours. Left side is the top part of the anode (closest to the fuel channels). Red is Ni_3P, blue is YSZ, green is Ni.

LSM-ceria composite electrodes also improved with increased pressure but more slowly, the results of which are also included in Figure 4. The composite electrode is a mixed electron and ion conductor, and more active than LSM alone. At 850°C, a clear change in slope was apparent at higher pressures. For oxygen pressures less than 10 bar, exchange currents followed a square root of pressure dependence, while a $P^{1/4}$ dependence was followed for pressures greater than that value. A $P^{1/4}$ oxygen partial pressure dependence is expected for dissociative charge transfer-limited reactions, where surface sites are not saturated. Electrochemical impedance results for the composite electrode again showed two principal features, dominated by a high frequency charge transfer feature, in agreement with the observed pressure dependence. This is the first such investigation of SOFC cathode performance at elevated pressures conducted with a DC bias, and shows that significant improvements in SOFC performance may

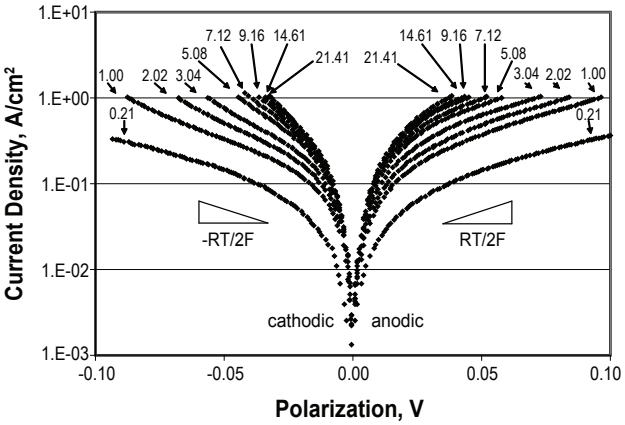

FIGURE 3. Polarization Curves for an LSM-20 Cathode on Yttria-Zirconia at 850°C at the Indicated Oxygen Partial Pressures, Determined Using Current Interrupt Methods

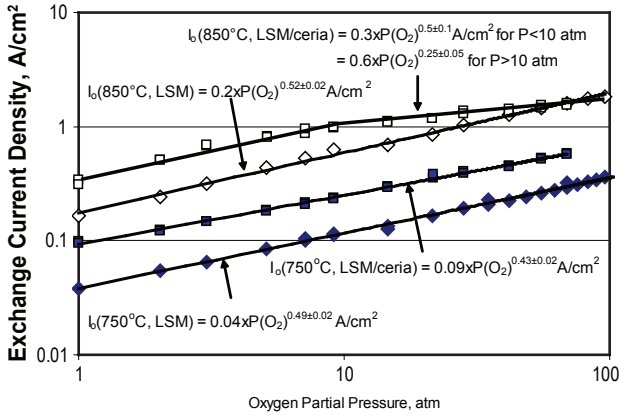

FIGURE 4. Relation of Exchange Current Density to Oxygen Partial Pressure for an LSM-20 Cathode and for an LSM-20/Ceria Composite Cathode

be expected when operated at greater than atmospheric pressure.

Enhanced Sintering of LSM by Oxygen Partial Pressure Cycling: Exposure of $(La_{0.90}Sr_{0.10})_{0.98}MnO_{3+\delta}$ (LSM-10) to repeated oxygen partial pressure cycles (air/10 ppm O_2) resulted in enhanced densification rates, similar to behavior shown previously due to thermal cycling. Shrinkage rates in the temperature range of 700 to 1,000°C were orders of magnitude higher than Makipirtti-Meng model estimations based on stepwise isothermal dilatometry results at high temperature, as is shown in Figure 5. A maximum in enhanced shrinkage due to oxygen partial pressure cycling occurred at 900°C. Shrinkage was greatest when LSM-10 bars that were first equilibrated in air were exposed to gas flows of lower oxygen fugacity than in the reverse direction. The former creates transient cation and oxygen vacancies well above the equilibrium concentration, resulting in enhanced mobility. These vacancies annihilate as Schottky equilibria is re-established, whereas the latter condition does not lead to excess vacancy concentrations.

These principles were applied in developing a method to densify LSM-based contact pastes at low temperatures. Figure 6 provides fracture strengths for two spinel-coated Crofer 22 coupons bonded together with an LSM slurry. Two sets of samples were evaluated: the first was held in air at 900°C (control) and the second was subjected to alternating air/10 ppm O_2 cycles. The control set developed no significant bond strength, while the second gave fracture strengths of several MPa. LSM is a preferred contact paste composition because of relatively good stability and compatibility with other fuel cell components, however

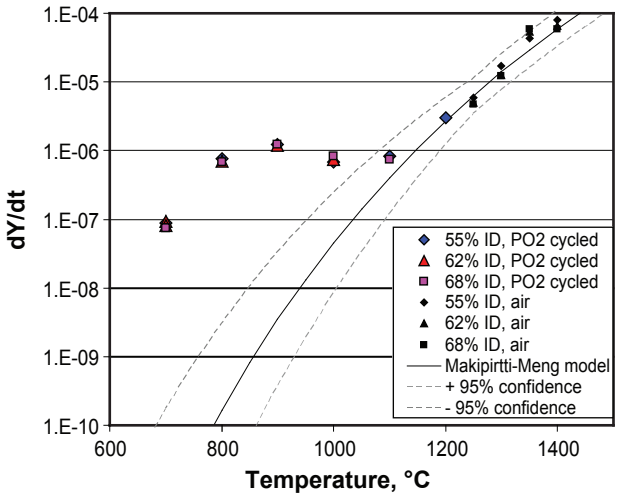

FIGURE 5. Volumetric shrinkage rate for LSM-10 as a function of temperature for samples with initial densities (ID) ranging from 52 to 68 percent of theoretical. Air/10 ppm O_2 cycles resulted in a significant increase in sintering rate compared to sintering in air alone.

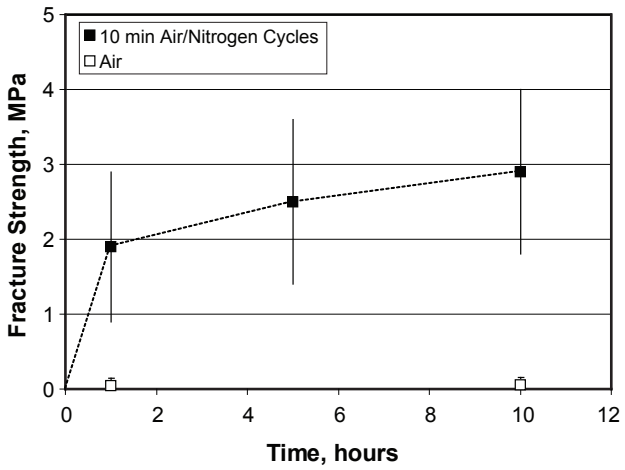

FIGURE 6. Fracture strength of two coated Crofer 22 plates that had been bonded together with an LSM-10 contact paste. Samples exposed to air/10 ppm O_2 cycles developed substantially greater fracture strengths than those exposed only to air at 900°C.

its high sintering temperature limits its use in stacks with metallic interconnects. Though considerable work remains to be done to optimize contact paste compositions and bonding schedules, this work demonstrates that low temperature processing of LSM contact pastes is possible.

Conclusions and Future Directions

- Exposure of nickel-based SOFC anodes to phosphorus and arsenic compounds of 1 to 5 ppm in a coal gas matrix led to irreversible performance losses of ~10 percent per 100 hours. Secondary phases were formed with both these coal gas contaminants, particularly involving the nickel-based current collector paste. Future studies will address degradation reactions involving these and other high priority coal gas contaminants, as well as synergistic effects.
- Elevated pressures, which may be necessary when integrating SOFCs with gasifiers and turbines, were shown to lead to significantly improved cathode performance. The improvement followed a $P^{1/2}$ dependence for LSM, which is dominated by dissociative oxygen adsorption reactions. Mixed electronic and ionic conductors such as an LSM/ceria composite improved more slowly with increased pressure, reflecting a greater dependence on charge transfer reactions. Future work will address the role of pressure on anode reaction kinetics and stability.
- Densification of LSM was accomplished in a cyclical oxygen partial pressure environment at temperatures hundreds of degrees lower than typical processing temperatures, an outgrowth of the unique

defect structure of LSM. Using these principles, a processing schedule for LSM contact pastes was developed that provided fracture strengths between two Crofer 22 coupons of several MPa in a matter of hours. Future work will be directed towards optimizing contact paste compositions and processing conditions.

FY 2007 Publications/Presentations

1. Zhou XD, Pederson LR, Cai Q, Yang J, Scarfino BJ, Kim M, Yelon WB, James WJ, Anderson HU, Wang C. "Structural and magnetic properties of $LaMn_{1-x}Fe_xO_3$ ($0 < x < 1.0$)." *J. Appl. Phys* 99 (8): Art. No. 08M918 2006.

2. Pederson LR, Singh P, and Zhou XD. ""Application of vacuum deposition methods to solid oxide fuel cells – a review." *Vacuum* 80: 1066–1083 (2006).

3. Marina OA, Pederson LR, Williams MC, Coffey GW, Meinhardt KD, Nguyen CD, and Thomsen EC. "Electrode Performance in Reversible Solid Oxide Fuel Cells." *J. Electrochem. Soc*., 154 (5): B452–B459 2007.

4. McCarthy BP, Pederson LR, Anderson HU, Zhou XD, Singh P, Coffey GW, and Thomsen EC. "Enhanced Shrinkage of Lanthanum Strontium Manganite ($La_{0.90}Sr_{0.10}MnO_{3+\delta}$) Resulting from Thermal and Oxygen Partial Pressure Cycling." *J. ACerS 2007 (in press)*.

5. Zhou XD and Pederson LR. "Solid State Materials for Energy Conversion." Presented by Xiao-Dong Zhou (Invited Speaker) at 53rd Midwest Solid State Physics Conference, Kansas City, Missouri, October 6–8, 2006.

6. McCarthy BP, Pederson LR, Anderson HU, Zhou XD, and Coffey GW. "Anomalous Shrinkage of Strontium Doped Lanthanum Manganite." Presented at Materials Science & Technology Conference, Cincinnati, OH, October 15–19, 2006.

7. Zhou XD, Thomsen EC, Nie Z, Coffey GW, and Pederson LR. "Oxide Thermoelectric Materials and Devices ." Presented at Materials Science & Technology Conference, Cincinnati, OH, October 15–19, 2006.

8. Zhou XD, Thomsen EC, McCarthy BP, Nie Z, Senor DJ, Coffey GW, Simner SP, and Pederson LR. "Processing and characterization of Calcium Cobaltates." Presented at Materials Science & Technology Conference, Cincinnati, OH, October 15–19, 2006.

9. Zhou XD, Xia GG, Yang Y, Thomsen EC, Coffey GW, Stevenson JW, and Pederson LR. "High Temperature thermoelectric power and electrical conductivity in perovskites and spinels." Presented at Materials Science & Technology Conference, Cincinnati, OH, October 15–19, 2006.

10. Marina OA, Pederson LR, Thomsen EC, Simner SP, Templeton JW, and Andersen M. "Performance of Single Cell Reversible SOFCs under Various Operating Conditions." Presented at 4th International Symposium on Solid Oxide Fuel Cells (SOFC), Daytona Beach, FL on January 23, 2007.

11. Zhou XD and Pederson LR. "Oxides for Direct Thermal-to-Electric Energy Conversion." Presented at Materials Research Society Spring Meeting, San Francisco, CA, April 9–13, 2007.

12. Pederson LR, Singh P, and Zhou XD. "Application of Vacuum Deposition Methods to Solid Oxide Fuel Cells." Presented at International Conference on Metallurgical Coatings and Thin Films, San Diego, CA on April 24, 2007 (invited).

13. Zhou XD and Pederson LR. "Size Dependence of Electrical and Thermal Transport Properties in Oxides." US-Korea Nanotechnology Forum, Honolulu, HI, April 26–27, 2007.

References

1. Trembly JP, Gemmen RS, Bayless RJ. "The effect of IGFC warm gas cleanup system conditions on the gas-solid partitioning and form of trace species in coal syngas and their interactions with SOFC anodes." *J. Power Sources* 163,986(2007).

V.10 Effect of Coal Contaminants on Solid Oxide Fuel System Performance and Service Life

Gopala N. Krishnan (Primary Contact) and Palitha Jayaweera
SRI International
333 Ravenswood Ave.
Menlo Park, CA 94025
Phone: (650) 859-2627; Fax: (650) 859-2111
E-mail: gopala.krishnan@sri.com

DOE Project Manager: Briggs White
Phone: (304) 285-5437
E-mail: Briggs.White@netl.doe.gov

Subcontractor: RTI International

Objectives

- Determine the sensitivity of solid oxide fuel cell (SOFC) performance to trace level contaminants present in coal-derived gas streams.
- Assess the catastrophic damage risk and long-term cumulative effect of trace level contaminants.
- Assess the life expectancy of solid oxide fuel cell systems fed with coal-derived gas streams.

Accomplishments

- Conducted a critical review of literature which indicated that Ni-cermet based SOFCs are vulnerable to degradation in the presence of contaminants that are expected to be present in a coal-derived fuel gas stream.
- Performed thermodynamic calculations to determine the speciation of various contaminants at SOFC operating temperatures.
- Assembled and tested several Ni-cermet SOFCs under varying conditions with select contaminants (HCl, CH_3Cl, and volatile species of As, P, Hg, Zn, Cd, and Sb) in a simulated coal-derived gas stream.

Introduction

SOFCs have high fuel-to-electricity conversion efficiency, environmental compatibility (low NO_x production), and modularity. They operate in the temperature range 700-1,000°C and can use fuel streams containing both H_2 and CO. Thus, they are ideal candidates to be integrated with a gas stream from an advanced coal gasifier. However, impurities containing virtually every element in the periodic table are present in coal (Clarke and Sloss, 1992) and many become constituents of coal-derived gas. The distribution of trace level contaminants between gaseous and solid phases depends on the individual gasification processes. The contaminants associated with the gaseous phase have deleterious effects on the performance and lifetime of coal-derived gas fed SOFCs.

The well-known impurities in the coal-derived gas stream include H_2S, NH_3, and HCl vapors; volatile metals such as Zn, Cd, and Hg; and metalloids such as As, P, and Sb; and transition metals such as Ni, Cr, and V, and Mn (Pigeaud and Helble, 1994). Some of these contaminants such as H_2S are removed by several methods. This project addresses the effect of the key impurities such as HCl, methyl chloride, zinc, mercury, arsenic, phosphorous on the efficiency and lifetime of SOFCs.

Approach

The research project includes a literature review, thermodynamic calculations, and a comprehensive experimental and analytical study to assess the impact of trace contaminants on SOFC performance.

1. A review of the scientific literature provided a preliminary assessment of the effect of trace level contaminants on the performance of the SOFC.
2. Thermodynamic equilibrium calculations allowed the identification of the chemical nature of the trace contaminants as they pass through the gas cleanup system from the coal gasifier and enter the SOFC anode.
3. A well-defined experimental program was designed to substantiate the preliminary assessment based on thermodynamic calculations and literature data.

In the second year of the project, the SOFC anodes (Ni-cermet) were exposed to a simulated coal gas containing individual contaminants at the operating temperature range of the SOFC (700 to 850°C) for an extended period of time. During such exposure, the electrical performance of the SOFC is monitored to determine the performance degradation. After the exposure period, the anodes are analyzed for the accumulation of the contaminants.

Results

The results of the literature review and thermodynamic calculations were summarized in the 2006 annual report. Also included in that report was the performance of the SOFC during exposure to a simulated coal-derived gas containing ~40 ppm of HCl or CH_3Cl vapors. In Table 1 of this report, the performance of the SOFC on exposure to other contaminants such as As, P, Hg, Zn, Cd, and Sb is summarized.

The various contaminants in the coal-derived gas exiting the gasifier can be removed by several well-known processes such as Selexol or Rectisol. These processes also remove essentially all the fly ash particles from the gas stream. Many gaseous contaminants are also reduced to sub-ppm levels. Hence, long-term data (>1,000 h) of SOFC performance were obtained with selected impurities at sub-ppm levels. However, during upset conditions, the impurity levels may be higher than those found at steady-state operating conditions. Thus, short-term data (~100 h) were also collected with impurity levels ranging from 5 to 40 ppm.

For short and long term tests, solid oxide Ni-cermet fuel cell samples from InDec B. V., Netherlands (4.5 cm^2 active area) were used. They have an electrolyte layer of dense yttria-stabilized zirconia (YSZ) of 4 to 6 μm in thickness, porous anode layer of 5 to 10 μm, porous anode support layer of 520 to 600 μm, and a porous lanthanum strontium manganite - yttria-stabilized zirconia (LSM-YSZ) cathode layer of 30 to 40 μm thick. The cells were operated at 750º to 850ºC with syngas (30% CO, 30.6% H_2, 11.8% CO and 27.6% H_2O) under 1 A load. After stabilization in the simulated coal-derived gas mixture without known contaminants, the cell was exposed to a low level of the select contaminant (0.5 to 50 ppmv) by adding them into the simulated gas mixture.

Figure 1 shows the performance of a cell on exposure to the simulated coal-derived gas stream containing 7 ppm mercury vapor. Even at this high level, Hg vapor did not have an effect on the power density of the cell. Similar results were obtained at 750 and 850°C both at 0.18 and 7 ppm levels. Because of its volatility, Hg vapor is difficult to remove from the gas stream and the results from these tests show that Hg vapor need not be reduced to sub-ppm levels for use in the SOFC.

TABLE 1. Effect of Trace Level Impurities on SOFC Output Power

		Observed Degradation (%) after 100 h at		
Contaminant	**Exposure Level**	**750°C**	**800°C**	**850°C**
HCl(g)	40	<1	<1	
Hg(g)	7	<1	<1	
Sb (SbO(g))	8	<1	<1	<1
Zn(g)	10		<1	<1
Cd (g)	5		<1	8
CH_3Cl (g)	40		<1	4
As (As_2(g))	10	10	15	
P (HPO_2(g))	40	7.5	10	

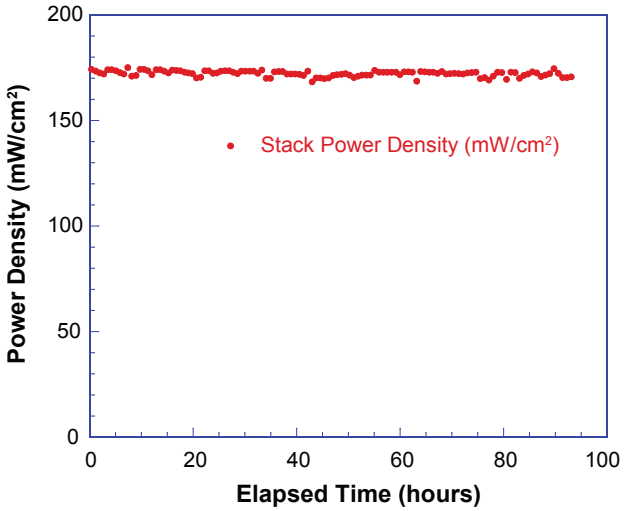

FIGURE 1. The Variation of the Power Density of a Cell at 800°C during Exposure to Simulated Coal-Derived Gas Containing 7 ppm Hg Vapor

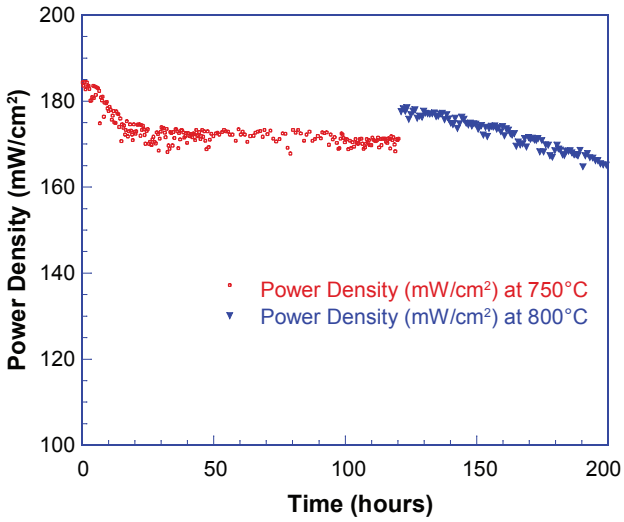

FIGURE 2. The Variation of the Power Density of a Cell at 750° and 800°C during Exposure to Simulated Coal-derived Gas Containing 40 ppm HPO_2 Vapor

Figure 2 shows the performance of a cell on exposure to a phosphorous-containing vapor (HPO_2(g)). Thermodynamic equilibrium calculations showed that in the presence of steam and the temperature range 750 to 850°C, phosphorous compounds such as PH_3 that are stable at near-ambient temperatures will be converted to HPO_2(g). At high levels, the vapor phase phosphorous compound appears to have a deleterious effect on the output power of the SOFC. We are planning to conduct tests at sub-ppm levels with PH_3 in the near future to establish the tolerance limit.

Volatile arsenic compounds such as AsH_3 may also be present at trace levels in the coal-derived gas even after treatment with Selexol. Short-term (100 h) tests with As_2(g) showed that the As compounds at a level of 10 ppm also degrade the SOFC performance at 750° and 800°C. However, when the concentration of As vapor (AsH_3) was reduced to 0.5 ppm, no degradation was observed even after 1,000 h (Figure 3). Additional tests are underway to determine the tolerance limit of SOFC for AsH_3.

The short term tests indicated that many of the potential trace level impurities do not have a significant effect on the output power density in the temperature range 750° to 850°C even at relatively high levels of the impurity. However, volatile impurities such as As and P vapor compounds exhibited observable degradation in the 100 h tests.

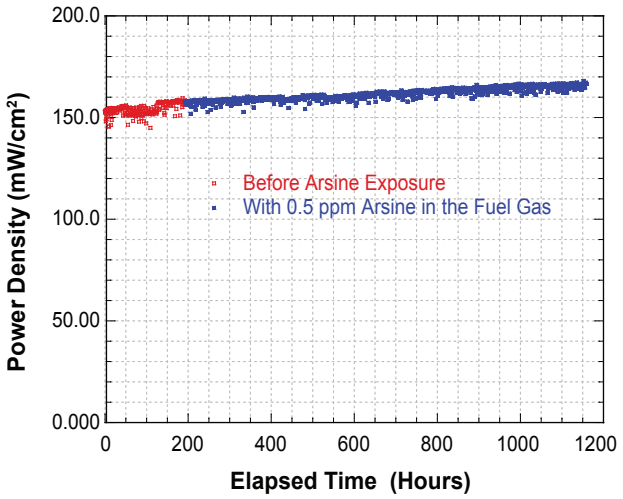

FIGURE 3. The Variation of the Power Density of a Cell at 750°C during Exposure to Simulated Coal-Derived Gas Containing 0.5 ppm AsH_3 Vapor

Conclusions and Future Directions

- Several potential trace level contaminants (HCl, Sb, Zn, and Hg) at relatively high levels (5 to 40 ppm) do not have a significant effect on the performance of SOFC coupons under short-term exposure conditions.
- Volatile species of As and P at relatively high levels (10 and 40 ppm, respectively) appear to degrade the power output of SOFC in 100 h.
- AsH_3 at 0.5 ppm level did not degrade the performance of an SOFC coupon even after 1,000 h of exposure indicating that this contaminant when present at sub-ppm levels may not have a significant effect.
- In future experiments, we will expose SOFC coupons to simulated coal-derived gas streams containing several contaminants (H_2S, PH_3, AsH_3) and determine their effect on long-term performance (1,000 h) of the cells.

FY 2007 Publications/Presentations

1. Effect of Coal Contaminants on Solid Oxide Fuel System Performance and Service Life, Quarterly Technical Progress Report 2 covering the period October 1, 2006 through December 31, 2006.

2. Effect of Coal Contaminants on Solid Oxide Fuel System Performance and Service Life, Paper presented at the 7th Annual SECA Review Meeting, Philadelphia, September 12-14, 2006.

3. Effect of Coal Contaminants on Solid Oxide Fuel System Performance, Presentation at West Virginia University Symposium, March 21, 2007.

References

1. Clarke, L. B. and L. L. Sloss (1992). Trace Elements – Emissions from Coal Combustion and Gasification, IEA Coal Research, London.

2. Pigeaud, A. E., and J. J. Helble (1994). "Trace Species Emissions for IGFC," Proceedings of the Coal-Fired Power Systems 94 – Advances in IGCC and PFBC Review Meeting, Eds. H. M. McDaniel, R. H. Staubly, and V. K. Venkataraman, DOE/METC-94/1008.

V.11 Techno-Economic Feasibility of Highly Efficient Cost Effective Thermoelectric-SOFC Hybrid Power Generation Systems

Jifeng Zhang (Primary Contact) and Jean Yamanis
United Technologies Research Center
411 Silver Lane MS 129-89
East Hartford, CT 06108
Phone: (860) 610-7461; Fax: (860) 660-8442
E-mail: ZhangJ@utrc.utc.com

DOE Project Manager: Heather Quedenfeld
Phone: (412) 386-5781
E-mail: Heather.Quedenfeld@netl.doe.gov

Subcontractor: Lon Bell
BSST LLC, Irwindale, CA

Objectives

Phase I

- Create innovative integrated solid oxide fuel cell-thermoelectric (SOFC-TE) technical concepts meeting the requirements of 65% electric efficiency and $400/kWe.
- Develop techno-economic models to assess the feasibility of the created concepts using trade studies
- Create specifications for the optimal system and identify the barriers/technology gaps.

Phase II

- Present the detailed technology/issue/solution to be matured that lead the concept going beyond a feasibility analysis in Phase I.

Accomplishments

- Identified the best system configuration with an ambient pressure stack, which serves as an intermediate step in technology maturation toward the optimal pressurized SOFC-TE system to meet the project goals for high-efficiency, coal-based central power plants.
- Created the specifications for the optimal systems, including both the pressurized SOFC-TE and the ambient-pressure SOFC-TE systems.
- Identified the barriers and technology gaps for the deployment of the hybrid systems.
- Created a conceptual framework for Phase II work.

Future Work

Complete the Phase I report and Phase II proposal.

Introduction

A TE material can generate power directly when it is conducting heat from a hot fluid to a cold one, known as the Seebeck effect. In a SOFC, the exhaust fluid leaving the stack and its afterburner typically has a temperature around 800°C. In today's SOFC design, the exhaust heat is usually recovered in a heat exchanger or preheater, to preheat the fuel or air entering the stack. A TE generator can be used for heat recovery as well as converting part of the heat to electricity directly.

This study is concerned with the trade-off between the performance and cost in reaching the overall system performance and cost targets. During the first year of the project, the best system configuration was identified as a pressurized SOFC-TE system. The project focus for the second year includes the product cost and performance specifications for the optimal concept, as well as the evaluation of the technology and identification of cost barrier and enablers.

Approach

A road map was created that shows the intermediate stages from a proof-of-concept unit at 1 kW scale to the ultimate, optimized hybrid system in multi-megawatt coal power plants. Ambient-pressure systems were found to be one of the intermediate stages in the development and maturity roadmap. The optimal ambient-pressure configuration was obtained based on system modeling.

Based on the modeling results, system specifications were created for both the optimal pressurized and the ambient-pressure systems. The technology and cost barriers were evaluated for the deployment of the hybrid system. While the SOFC stack using coal gas as the fuel and the TE technology require development by themselves, the barriers and enablers analysis here focuses on the integration of the SOFC and TE. The plan for Phase II work is being framed and includes the building and testing of a proof-of-concept lab unit.

Results

Optimal Ambient-Pressure SOFC-TE

Due to the fact that the ambient-pressure system does not have a turbine, the exhaust gas leaving the SOFC burner has a temperature of more than 800°C and is higher by approximately 300°C than in the pressurized case. This can be used for power generation with a high stage TE in addition to the TE in a pressurized system. The system diagram is shown in Figure 1.

The system efficiency results are shown in Figure 2. Major parameters affecting the system efficiency include ZT, the figure of merit of the TE materials, and the cold gas flow rate in the low stage TE. The cold gas flow rate at the high stage TE is determined by the SOFC stack. It is approximately equal to the hot gas flow rate and cannot be changed arbitrarily. Today's state-of-the-art ZT value with high technology readiness level, i.e., in production, is at about 1 at mid-range temperatures [1]. Higher ZT of 3.2 has been achieved in Lincoln Lab [2] but the technology readiness level is low. The electricity generated by the two TE contributes close to 6% points of the overall 51% system efficiency for the ambient-pressure SOFC-TE system.

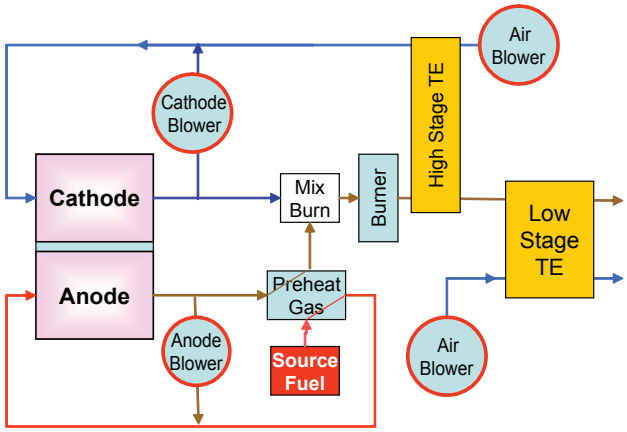

FIGURE 1. Diagram for the Optimal Ambient-Pressure SOFC-TE System

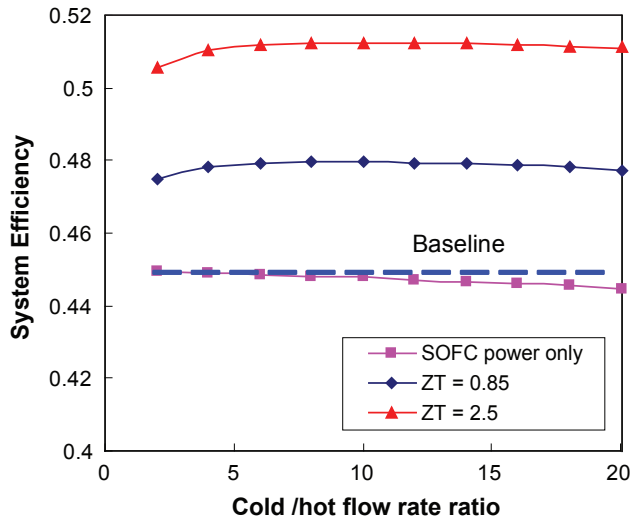

FIGURE 2. Ambient-Pressure System Efficiency at Different Cold Flow Rate and ZT

Cost and Performance Specifications for the Selected Concepts

For this task, the system working principles were described first. The system operation includes five modes: start-up, steady operation, load transition, shut-down and idle.

Major system design requirements are: 1) overall performance requirements, such as system efficiency, overall capacity; 2) transient requirement, mainly the time for start-up, load transition and shut-down; 3) system control, allowing the system to operate in different modes with proper transition and logic control of fuel and air supply; and 4) subsystem or replacement requirements, i.e., time for a component or subsystem replacement.

Based on the system requirements, the components design requirements were defined. Major component requirements are performance specifications such as heat exchanger capacity and fan efficiency. The life of major components was listed and a replacement schedule was created, as shown in Table 1. The factory manufacturing cost specifications were then obtained based on the cost modeling. The cost specifications considered the market size or production volume effect.

Technology Gaps/Cost and Performance Barriers

The major technology gaps to reach the goal of 60% or higher system efficiency arise from the stack, the TE and the system integration. Although development of the standalone SOFC stack and the TE generator are important, the focus of this study is conceptual system definition, modeling and integration. Major cost and performance barriers include:

1) The cathode recycle blower that can withstand the >800°C exhaust temperature.
2) The anode blower that can withstand the same high temperature but with the flow rate 35 times smaller than the cathode blower. An ejector may serve this function but needs to be developed.
3) The air preheater that should have long life, low cost and can resist 800-1,000°C hot gas.
4) The control of coupled turbo-compressor and the stack.
5) Possible carbon deposit due to metastability of the (H_2 + CO) mixture in the fuel supply pipe.

TABLE 1. Replacement Schedule for the Proposed SOFC-TE Optimal Configuration

Component	Life		Replacement or Overhaul Schedule																		
	Years	0	1	2	3	4	5	6	7	8	9	10	11	12	13	14	15	16	17	18	19	20
SOFC stack	5	1					1					1					1					1
Cathode Blower	2.5	1			1		1			1		1			1		1			1		1
Anode Blower	2.5	1			1		1			1		1			1		1			1		1
Turbine	5	1					1					1					1					1
Air compressor	3	1			1			1			1			1			1			1		
Pressure vessel	3	1			1			1			1			1			1			1		
Air preheater	5	1					1					1					1					1
PCS	5	1					1					1					1					1
BOP	10	1										1										1
Control	10	1										1										1
Insulation	10	1										1										1
Burner	5						1					1					1					1
TE blower	5	1					1					1					1					1
TE	20	1																				

6) A 200 kW SOFC-TE system requires a turbo-compressor of 50-60 kW of net power. Small turbines tend to increase the cost per kilowatt. If multiple SOFC stacks share one turbo-compressor for higher efficiency and low cost, the control between the sharing stacks needs to be coordinated. The piping should be able to resist 800-1,000°C hot gas and have a small pressure drop and good insulation.
7) The power conditioning system (PCS) that can handle the power generated by the SOFC and TE. The components generate DC power at different current and voltage levels. The PCS constitutes about 1/3 of the system cost. A cost-effective solution, e.g., using a plant DC bus, may be a good option.

Phase II Planning

A step-by-step development approach is proposed from today's feasibility study in Phase I to the ultimate application in coal-based central power plants. The conceptual roadmap is shown in Figure 3. This conceptual roadmap involves product development and introduction commensurate with technology maturity. Earlier products generate revenues, a fraction of which can be invested to develop the next and more capital intensive technology.

The first stage of the SOFC-TE development roadmap is a 1 kW scale proof-of-concept unit, which is proposed as part of the Phase II work. This is an ambient-pressure system with moderate technical risks but demonstrates the integration capabilities of the distinct, SOFC and TE, electrical generators while providing the opportunity for, at least, partial validation of system models. The second stage is the development, demonstration, and product design of 1-10 kW units that can be used in residential or defense applications. Process development for cost optimization and reduction would be an important activity starting with this stage. The third stage is the development of units on the order of 100 kW that can be used for commercial building applications, such as large box stores, supermarkets, office buildings, hospitals and schools. The last stage is the coal-based power plant application, where the technology for the key SOFC and TE components is matured, scaled-up, and effectively integrated to convert the heat content of coal gas to electricity efficiently and cost-effectively reaching the capital cost target of $400/kWe.

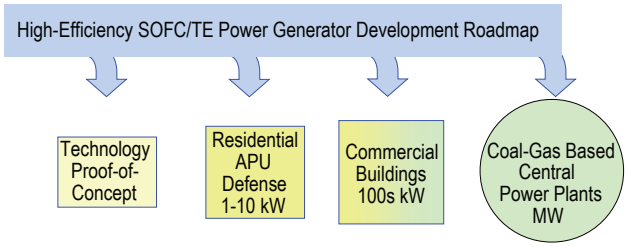

FIGURE 3. Roadmap from Today's Feasibility Study to Multi-MW Coal Power Plant Application

Conclusions

- An ambient-pressure SOFC-TE with 51% system efficiency is identified as a proof-of-concept system demonstrator toward the ultimate SOFC-TE central power plant systems.
- Performance and cost specifications for the optimal systems were created based on modeling.
- Technology and cost barriers were identified.
- A step-by-step approach is being proposed to progressively develop and mature the hybrid SOFC-TE system technology from the Phase II feasibility study to the central power plant application technology readiness level.

FY 2007 Presentations

1. Jifeng Zhang, Benoit Olsommer, Jean Yamanis, Douglas Crane, Lon Bell and Robert Collins, "Techno-Economic Analysis of SOFC-TE Hybrid Power Generation Systems", Presented at the Direct Thermal-to-Electrical Energy Conversion (DTEC) Program Review and Workshop, Coronado, CA, August 29-September 1, 2006.

2. Jifeng Zhang, Benoit Olsommer, Jean Yamanis, Douglas Crane, Lon Bell and Robert Collins, "Techno-Economic Feasibility of Highly Efficient Cost-Effective Thermoelectric-SOFC Hybrid Power Generation Systems", Presented at the 7th Annual Solid State Energy Conversion Alliance (SECA) Workshop and Peer Review, Philadelphia, PA, September 12-14, 2006.

References

1. H. Bottner, "Micropelt Miniaturized Thermoelectric Devices: Small Size, High Cooling Power Densities, Short Response Time", ICT 2005, Clemson, SC.

2. Robert F. Service, "Temperature Rises for Devices That Turn Heat Into Electricity", Science 29 October 2004 306: 806-807.

V.12 SECA Coal-Based Systems Core Research - University of Florida

Eric D. Wachsman
University of Florida
Gainesville, FL 32611-6400
Phone: (352) 846-2991; Fax: (352) 846-0326
E-mail: ewach@mse.ufl.edu

DOE Project Manager: Heather Quedenfeld
Phone: (412) 386-5781
E-mail: Heather.Quedenfeld@netl.doe.gov

Objectives

- Apply computational approach to develop fundamental understanding of ionic transport and heterogeneous electrocatalysis in solid oxide fuel cells (SOFCs).
- Develop high resolution characterization techniques to quantify electrode microstructures.
- Combine heterogeneous catalysis, electrochemistry, and microstructure characterization techniques to deconvolute contributions to electrode polarization.

Accomplishments

- Utilized *ab initio* and molecular dynamic simulations to calculate defect and defect cluster formation energies and effect on ionic transport.
- Computationally and experimentally determining thermo-mechanical properties based on fundamental thermodynamic/bond-energy constants.
- Used atomic-level simulation methods to elucidate the effects of non-stoichiometry and temperature on the elastic properties of CeO_{2-x}.
- Determined adsorption and absorption energies for O on and in $LaFeO_3$ (110) using first principles, electronic structure calculations.
- Developed high resolution scanning electron microscopy (SEM) - focused ion beam (FIB) characterization technique and applied to SOFC cathodes to quantify 3D microstructure.
- Determined effect of sintering temperature on lanthanum strontium manganate (LSM) and lanthanum strontium cobalt ferrite (LSCF) cathode microstructures.
- Established first direct relationship between charge transfer and area normalized triple phase boundary length and between adsorption polarization resistance and volume normalized pore surface area.
- Developed a kinetic model that correctly predicts the relationship between experimentally obtained charge transfer polarization resistance and triple phase boundary length.
- Developing unique electrocatalytic techniques to determine fundamental oxygen exchange kinetics (k/D) on cathode surfaces based on O-isotope exchange as a function of applied voltage/current.
- Identified O_2 reduction mechanism steps on LSM and LSCF using O-isotope exchange.
- Demonstrated greater catalytic activity of LSCF versus LSM.

Introduction

To fully achieve the tremendous socio-economic benefits of electrochemical energy conversion and power generation, fundamental scientific breakthroughs in the transport of ionic species through electrolyte/membranes and reaction rates at electrode surfaces are necessary. Therefore, the mission of this project is to develop a fundamental understanding of ionic transport in, and electrocatalytic (electrochemical catalysis) phenomena on the surface of, ion conducting materials. The research spans the range from first-principles calculations and molecular dynamic simulations of ionic transport and gas-solid interactions of novel ion conducting materials and electrocatalysts to development of advanced technology devices for efficient energy utilization:

SOFCs – Increasing the ionic conductivity and electrode reaction rates results in higher power density cells at lower operating temperature. These higher power density cells will dramatically reduce the cost of fuel cell technology, thus, overcoming the final hurdle (cost) to widespread commercial deployment.

Membranes – Membrane reactors are a major component of the FutureGen Initiative. Improving the transport of ions through the membrane and reaction rates at the membrane surface will help achieve dramatic breakthroughs in industrial energy efficiency and cost of hydrogen production.

Sensors – By developing a fundamental understanding of the gas-solid reactions that occur on sensor electrodes we will be able to develop sensors that are highly sensitive and selective to specific gaseous pollutants. These sensors will allow more accurate control of combustion resulting in greater fuel economy and reduced air pollution.

Approach

Our computational research focuses first on gaining insight into mechanisms of ion transport and heterogeneous electrocatalysis, and then on applying this fundamental knowledge to the design of new materials. Using electronic structure calculations and large-scale atomic-level simulation on cluster parallel computers we are elucidating the fundamental processes of ion transport in various electrolyte and electrode materials. Among the effects being explored are the effect of defects and defect clustering on the mechanical behavior and on ionic transport. The effect of grain boundary interfaces is being determined from simulations of ionic transport in polycrystalline materials. The insights gained from these simulations will help guide the development of higher conductivity electrolyte and electrode materials.

In addition, we are using similar calculations to develop a fundamental understanding of heterogeneous electrocatalytic phenomena at the surface of ion conducting ceramics. Because cathode polarization limits the performance of SOFCs at low temperature, the insights gained from this study will lead to the development of lower polarization SOFC cathodes at lower temperatures. In addition, these computational methods will be used to determine the mechanisms responsible for the cathode performance degradation.

We are developing high-resolution, quantitative, microstructural characterization techniques based on a FIB/SEM. This includes development of mathematical techniques to create a 3D reconstruction of the entire porous electrode structure as well as quantify electrode microstructural features (e.g., triple phase boundary length, porosity and tortuosity). In addition, we are using the FIB/SEM to prepare samples for high resolution transmission electron microscope (HRTEM) analysis of specific interfaces for analysis of issues such as tertiary phase formation, cathode degradation, etc.

Finally, using heterogeneous catalysis techniques–temperature programmed desorption (TPD), reaction (TPR), and oxygen-isotope exchange–combined with electrochemistry techniques–impedance spectroscopy, I-V, and conductivity relaxation–and the microstructural characterization and computational approach (above), we are deconvoluting the various contributions to electrode polarization to obtain a more fundamental understanding and develop a methodology to design improved performance electrodes in the future.

Results

Computational – Previously, we showed that there is considerable elastic softening with increasing oxygen deficiency in CeO_{2-x}. By simulating a series of different systems, we have shown that this elastic softening arises mainly from the decreased electrostatic interactions in the system rather than from the free volume associated with the oxygen vacancies themselves. By comparing systems with corresponding expansions, we have determined that the chemical expansion has a much larger softening effect on the elastic properties than the corresponding expansion arising from thermal effects alone. We have also established that the lattice parameter and elastic moduli both depend essentially linearly on the ionic radii of aliovalent dopants and on their concentration. Simulations on the oxygen vacancy diffusion mechanism are underway.

In addition, we have used a combination of *ab initio* and thermodynamics to determine the surface energies of different low miller index planes of $LaFeO_3$ under varying oxygen partial pressure and temperature. Among the various low-miller index planes, weakly polar (010) and (101) planes have lower surface energies than the strongly polar (111), (110) and (011) planes. Guided by this result, we have continued our adsorption and absorption calculations of oxygen ions on the (010) plane of $LaFeO_3$ that has either LaO or FeO_2 terminations. In particular, we have considered several adsorption sites with and without oxygen vacancies. The LaO-terminated surface is predicted to have a lower oxygen-adsorption energy than the FeO_2-terminated surface. This is because the oxygen adatom preferentially bonds with the two La surface atoms on the LaO-terminated surface. In contrast, in the case of the FeO_2-terminated surface, the adatom is only able to bond with one Fe surface atom. These calculations are continuing now with oxygen molecules. Additionally, calculations on the $La_{1-x}Sr_xFeO_3$ and $LaCo_{1-x}Fe_xO_3$ surfaces are in progress to elucidate the effect of dopants on adsorption and absorption of oxygen ions and molecules.

Microstructural Characterization – Ongoing work involves a FEI Strata 235 dual beam FIB/SEM in reconstructing porous SOFC cathodes. Current studies are being conducted on LSCF and LSM of various isochronal sintering temperatures. FIB/SEM serial sectioning and imaging is conducted at ~20 nm intervals. The resulting two-dimensional (2D) images are stacked and aligned with the aid of fiducial marks. Amira Resolve RT software is then utilized to reconstruct a three-dimensional (3D) triangular mesh to represent the serially sectioned area of interest. The reconstruction's voxel (3D equivalent of pixel in 2D) dimensions are on the order of 3 nm X 4 nm X 20 nm thus making it possible to have ~100 nm particle resolution in the 3D reconstruction. This reconstruction is then used to quantify microstructural properties of the porous cathode such as average particle size, average pore size, closed porosity, open porosity, tortuosity, pore surface area, porosity grading, and triple phase boundary length (L_{TPB}).

Figure 1 shows an example of this technique for an LSCF cathode. First, a series of SEM images were obtained. Then they were integrated and reconstructed into a virtual 3D structure. Finally, that reconstructed 3D structure was analyzed to quantify microstructural features. In this case the phase fraction of yttria-stabilized zirconia (YSZ), LSCF, and pores were determined as a function of distance from the YSZ/LSCF interface.

Deconvolution of Electrode Polarization and Comparison of Microstructure with Electrochemical Performance – Symmetric LSM on YSZ samples were fabricated for electrochemical-microstructural comparison. Microstructural features (porosity, volume normalized pore surface area, L_{TPB}, and tortuosity) were modified by varying the sintering temperature and time used during fabrication. We evaluated the effects of sintering temperature on both electrochemical and microstructural characteristics of these LSM on YSZ symmetric cells. All microstructural quantities were influenced by sintering temperature with the most dynamic changes occurring at temperatures near and above 1,200°C.

Electrochemical impedance spectroscopy (EIS), using a Solartron 1260 frequency response analyzer, was performed on the symmetrical samples prior to their analysis by the FIB/SEM. From the obtained impedance profiles charge transfer, dissociative adsorption, and gas diffusion related processes were identified. It was found that polarization resistance for both charge transfer and dissociative adsorption increase with sintering temperature. This corresponded to a decrease in specific microstructural features, L_{TPB} and pore surface area (normalized per unit volume - S_V), with increasing sintering temperature as quantified by the FIB/SEM.

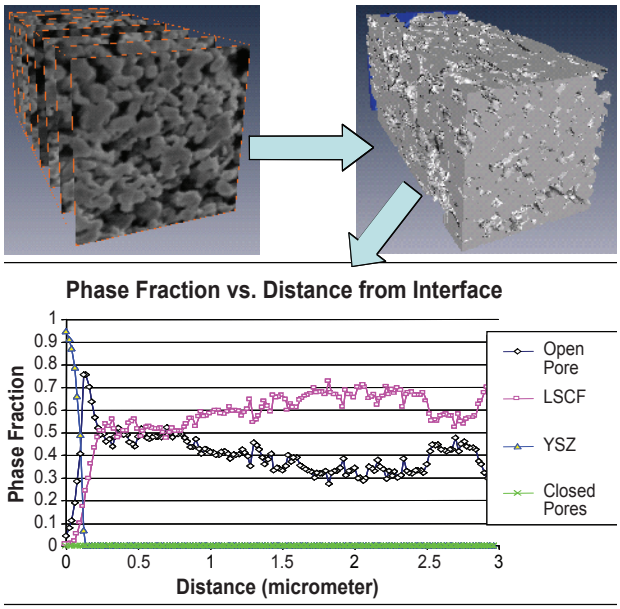

FIGURE 1. Progression from serially sectioned FIB/SEM images, reconstruction into a 3D representative structure; used to quantify the porous microstructure, in this case graded porosity.

Relating the microstructural and electrochemical results revealed that charge transfer polarization resistance (R_{CT}) decreased as L_{TPB} increased and polarization due to dissociative adsorption (R_{DA}) decreased as S_V increased. Excellent power law fits were obtained for both microstructural-polarization relationships (Figure 2):

$$R_{CT} = 2.93(L_{TPB})^{-3.5} \quad (1)$$

$$R_{DA} = 1025(S_V)^{-1.8} \quad (2)$$

These, first ever reported, direct relationships between microstructure and electrochemical performance can now start to be used to develop fundamental cathode polarization mechanisms.

The basic oxygen reduction reaction is

$$1/2O_2 + V_o^{\bullet\bullet} + 2e' \rightarrow O_o^x \quad (3)$$

We have shown that a power law dependence for R_{CT} on L_{TPB} can be obtained from this reaction (1).

$$R_{CT} = (RT/(nF)^2 k_f)([e'](\omega_{TPB}/A)_{e'})^{-m} ([O_2](\omega_{TPB}/A)_{O2})^{-n} ([V_o^{\bullet\bullet}](\omega_{TPB}/A)_{Vo\bullet\bullet})^{-p} \bullet (L_{TPB})^{-(n+m+p)} \quad (4)$$

In chemical reactions, the reaction order is given by the coefficients in the balanced chemical equation. Using the reaction order coefficients in Equation (3), the exponential quantity (n+m+p) is -3.5, resulting in $R_{CT} \propto L_{TPB}^{-3.5}$ which is exactly what we observed.

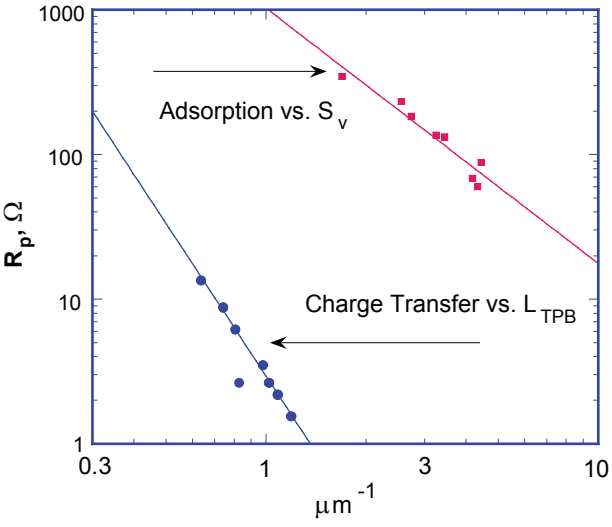

FIGURE 2. Effect of LSM microstructure on cathode polarization; dissociative adsorption as a function of pore surface area, and charge transfer polarization as a function of triple phase boundary length; at 800°C in air.

The next step in deconvolution of the cathode polarization is to determine the fundamental oxygen reduction mechanisms and rate constants of LSM and LSCF. In order to do this, we used the heterogeneous catalysis techniques of TPD and TPR, as well as oxygen-isotope exchange.

Oxygen Exchange Kinetics – Temperature programmed isotope exchange on SOFC cathode materials can elucidate the surface exchange mechanisms as well as characterize reactivity towards the oxygen reduction reaction. For these experiments, ~3,000 ppm $^{18}O_2$ balanced in He is flowed over a small amount of cathode powder, the temperature is ramped 30˚C/min, and the reactor effluent recorded by mass spectrometry. Since the oxide is made of ^{16}O, and $^{18}O_2$ is only found in the gas phase, we can determine what happens to the oxygen. If it goes into the lattice, a decrease in the mass 36 signal is seen. If dissociation occurs and there is a buildup of surface intermediates, the scrambled product $^{16}O^{18}O$ (mass 34) will be detected. Oxygen coming out of the lattice in large quantities will be seen as $^{16}O_2$, or mass 32. From these experiments, the mechanisms and kinetics of oxygen incorporation are being studied *in situ*.

As seen from the surface-area normalized (0.26 m^2) plots in Figure 3, LSM20 (Nextech) shows very little activity compared with LSCF6428 (Praxair) for the same given temperature. Surface exchange, producing $^{16}O^{18}O$, does not occur until about 350˚C for LSM but begins as early as 150˚C for LSCF. This indicates LSCF is a better catalyst for oxygen dissociation and would be better than LSM as an intermediate temperature SOFC cathode material. At higher temperatures, the $^{18}O_2$ and $^{16}O^{18}O$ signal completely disappears from the LSCF spectrum, indicating that the incorporation step is much faster than the dissociation step. Looking at the $^{16}O_2$ signal at higher temperature (400-600˚C) shows the material becomes oxygen deficient. The kinetics of the desorption process is much faster than that of incorporation. Additional isothermal experiments will be performed to study the effect of temperature and oxygen partial pressure on the rate law that governs oxygen exchange on these cathode materials.

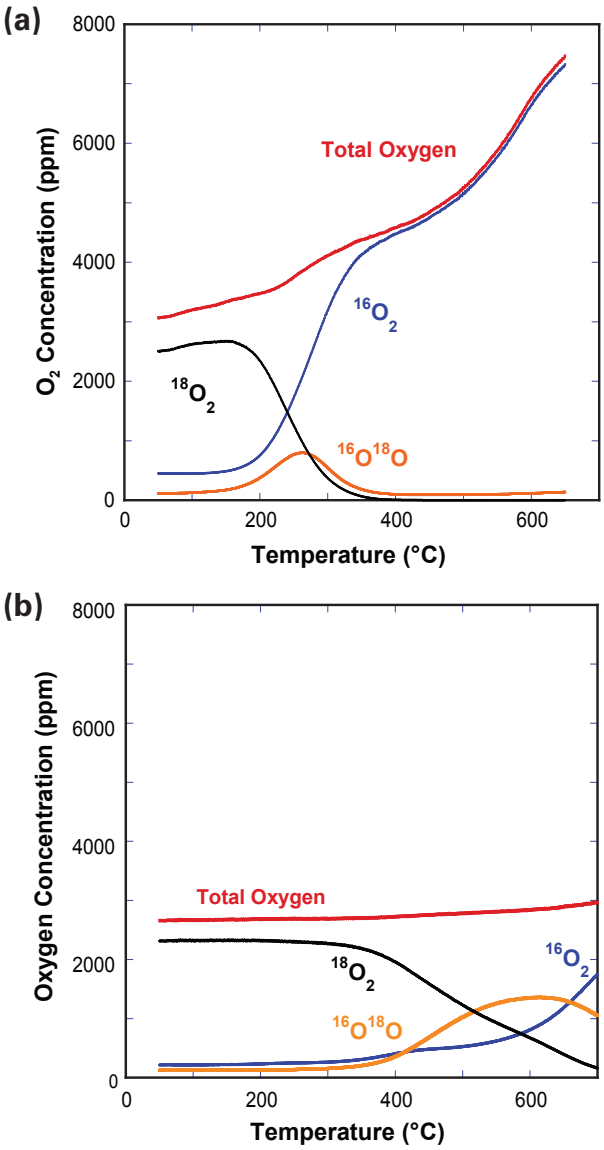

FIGURE 3. Oxygen Isotope Exchange of (a) LSCF and (b) LSM.

Conclusions and Future Directions

- Demonstrated with computational simulations that the mechanical properties of CeO_{2-x} are dominated by the electrostatic interactions between the ions.
- Computationally determined adsorption and absorption energies for O on/in $LaFeO_3$ (110) cathodes, and established with electronic structure calculations that oxygen preferentially adsorbs on the LaO-terminated surface of $LaFeO_3$ rather than the FeO_2-terminated surface.
- Developed high resolution SEM/FIB characterization technique and applied to SOFC cathodes. Demonstrated that results can be used to produce 3D reconstructions. Quantified LSM and LSCF cathode microstructures as a function of sintering.
- Combined microstructural characterization of LSM cathodes with impedance spectroscopy results to deconvolute polarization mechanisms and quantify effect of microstructure on electrode polarization.
- Determined direct relationship between charge transfer resistance and triple phase boundary length ($R_{CT} \sim L_{TPB}^{-3.5}$) in LSM cathodes. These experiments will continue and will be applied to LSCF cathodes for comparison.

- Demonstrated ability of O-isotope exchange to elucidate oxygen reduction mechanism and further demonstrated greater catalytic activity of LSCF than LSM using this approach.
- Additional isotope experiments will be conducted to fully investigate the mechanism of oxygen surface exchange. Steady-state isotopic-transient kinetic analysis (SSITKA) will be used to study *in situ* oxygen surface exchange kinetics and intermediates. This method is based on the isothermal switching of the feed stream between lines containing oxygen isotope $^{16}O_2$ and $^{18}O_2$. This switch introduces a traceable isotopic step without perturbing the steady state oxygen concentration, pressure and flow rate. Monitoring changes in the various isotope concentrations with time will yield valuable information towards understanding the surface exchange mechanism and the effective rate constant for surface exchange. By understanding which surface step(s) limit performance in intermediate temperature SOFCs, better cathodes can be engineered to counteract the natural loss in performance at lower temperatures.
- These kinetic experiments should result in specific rate constants and P_{O2} dependencies of the basic cathode materials, LSM and LSCF. When combined with deconvoluted impedance data and quantified LSM and LSCF cathode microstructures, a fundamental and quantifiable understanding of cathode performance should finally be achieved.

FY 2007 Publications/Presentations

1. "Evaluation of the Relationship Between Cathode Microstructure and Electrochemical Behavior for SOFCs," J.R. Smith, A. Chen, D. Gostovic, D. Hickey, D. Kundinger, K.L. Duncan, R.T. DeHoff, K.S. Jones and E.D. Wachsman, Solid State Ionics, submitted.

2. "3D Reconstruction of LSCF Cathodes," D. Gostovic, J.R. Smith, K.S. Jones and E.D. Wachsman, Electrochemical and Solid State Letters, submitted.

3. "Deconvolution of SOFC Cathode Polarization," E.D. Wachsman, *Solid Oxide Fuel Cells X, ECS Transactions*, K. Eguchi, S.C. Singhal, H. Yokokawa, and J. Mizusaki, Ed, **7-1**, 1051 – 1054 (2007).

4. "Oxygen Diffusion Mechanism in δ-Bi_2O_3 Using Molecular Dynamics Simulations", D. S. Aidhy, S. B. Sinnott, E. D. Wachsman and S. R. Phillpot, 31st International Cocoa Beach Conference & Exposition on Advanced Ceramics & Composites, Daytona Beach, 21–26 January, 2007.

5. "Mechanical Properties of Ceria by Molecular Dynamics Simulation", H. Xu, R. K. Behera, Y. Wang, F. Ebrahimi, E. D. Wachsman, S. B. Sinnott and S. R. Phillpot, 31st International Cocoa Beach Conference & Exposition on Advanced Ceramics & Composites, Daytona Beach, 21–26 January, 2007.

6. "Chemical Properties of $LaFeO_3$ from First Principles Calculations: Implications for Use as SOFC Cathodes", C. Lee, E. D. Wachsman, S. R. Phillpot and S. B. Sinnott, 31st International Cocoa Beach Conference & Exposition on Advanced Ceramics & Composites, Daytona Beach, 21–26 January, 2007.

V.13 A High Temperature Electrochemical Energy Storage System Based on Sodium Beta Alumina Solid Electrolyte (BASE)

Anil V. Virkar
University of Utah
Department of Materials Science & Engineering
122 S. Central Campus Drive
Salt Lake City, UT 84112
Phone: (801) 581-5396; Fax: (801) 581-4816
E-mail: anil.virkar@m.cc.utah.edu

DOE Project Manager: Lane Wilson
Phone: (304) 285-1336
E-mail: Lane.Wilson@netl.doe.gov

Objectives

Phase I:

- To synthesize planar, thin, strong BASE using a patented vapor phase process.
- To fabricate metal end caps and the associated hardware for the construction of planar BASE-based electrochemical energy storage systems.
- To construct electrochemical cells comprising of sodium anode, BASE, and selected cathodes.
- To electrochemically test cells (discharge-charge) over a range of temperatures and up to the highest possible depths of discharge.
- To conduct theoretical analysis of the electrochemical energy storage system from the standpoint of maximum possible capacity, efficiency, and integrability with power generation systems.

Phase II:

- To construct a planar stack of 10 Na/BASE/optimized cathode cells.
- To operate a stack for a minimum of 100 charge-discharge cycles.
- To thermally cycle the stack between the operating temperature and room temperature.
- To disassemble the stack and conduct post-mortem analysis.

Approach

- To fabricate BASE discs by the method of die pressing or tape casting and BASE tubes by the method of slip casting using a vapor phase process.
- To investigate the effect of microstructure on the kinetics of conversion.
- To fabricate BASE discs with porous BASE surface layers for enhanced electro catalysis.
- To measure the conductivity of BASE tubes by assembling a symmetric cell with a zinc chloride-sodium chloride eutectic mixture.
- To conduct ion exchange experiments in prospective cathodes of $ZnCl_2$, $SnCl_2$, and SnI_4.
- To construct tubular and planar electrochemical cells that could be assembled in three different states: discharged state, charged state, and partially charged at eutectic composition.
- To conduct experiments to test the electrochemical working of tubular cells and to analyze the voltage response of the charge-discharge cycles.
- To construct planar cells and to test the electrochemical working of the same by analyzing the voltage response of the charge-discharge cycles.
- To conduct several freeze-thaw cycles on the planar cells and to test the performance of the same after undergoing the thermal cycles.
- Assemble a two cell planar stack and test.
- To conduct electrochemical tests in an aqueous media: Cu/Zn couple.
- To assemble a five cell stack.

Accomplishments

- BASE discs were successfully fabricated by tape casting, sintering and vapor phase treatment.
- BASE tubes were successfully fabricated by slip casting, sintering and vapor phase treatment.
- α-alumina + yttria-stabilized zirconia (YSZ) samples of differing grain sizes were fabricated by varying sintering temperature/time.
- Preliminary work on the kinetics of conversion was conducted.
- Electrochemical cells were designed, constructed, and tested.
- No incorporation of zinc within the BASE structure was observed, suggesting that BASE is stable in the battery environment. No incorporation of Sn^{4+} was observed suggesting BASE is stable in Sn^{4+} salts. However, ion exchange did occur in $SnCl_2$, indicating BASE is not stable in the presence of Sn^{2+} salts.
- Planar cells were designed, assembled and successfully tested. Cells were subjected to several charge-discharge and freeze-thaw cycles.
- Freeze-thawing of planar cells were done a couple of times followed by several charge-discharge cycles

without the failure of electrolyte. These tests were conducted at an operating temperature of 350°C. Cells were also tested at 425°C.
- A two cell planar stack was successfully discharged.
- A five cell stack has been assembled.

Future Directions

- To test the five cell stack.
- To investigate additional cathodes. They include $CuCl_2$, SnI_4, and AgCl.
- To incorporate high conductivity BASE with porous surface layers into cells.
- To construct a 10-cell, 200 Wh (100 W with 2 hour discharge) stack with high specific energy and high specific power.
- Integration of the high temperature energy storage system based on BASE with a power generation system such as a solid oxide fuel cell (SOFC).

Introduction

The demand for electricity varies depending upon the time of the day: low demand during night and high demand during day. All power plants are designed for peak power which leads to the underutilization of excess capacity during off peak periods. One of the main reasons for the emergence of electrochemical energy storage devices such as batteries is that power plants can be designed for average demand. This will augment the capacity of power plants as the excess energy during off peak periods will be stored for use later during high peak demands. This strategy is expected to lower the capital cost. In high temperature batteries, the most advanced batteries are Na-S. NGK in Japan has demonstrated 8 MW (64 MWh – 8 hour discharge) Na-S batteries (NAS), connected to the local grid for load leveling. The roundtrip efficiency of the NAS battery is ~90%. Other batteries using BASE currently under development include the ZEBRA battery which utilizes $NiCl_2$ or $FeCl_2$ as the cathode.

Both the NAS and ZEBRA batteries use conventional BASE, which is not strong and is not water-resistant. It needs to be stored in dry atmospheres before incorporating it into batteries. The corrosive nature of the cathode (sulfur or $NiCl_2$) necessitates the use of tubular geometry, to minimize seal area. In the NAS battery, containers are protected by an expensive protective coating. Also, expensive graphite is required in the cathode. In the ZRBRA battery, to minimize corrosion, the cathode is placed inside the BASE tube. This lowers the specific energy and specific power. It is not possible with either of the two batteries to construct planar cells. The main objective of this work is to use a high strength vapor phase processed BASE (patented process) to make planar cells, and use alternate cathodes to increase both specific energy and specific power.

Approach

BASE discs were fabricated using the method of tape casting and die-pressing. For tape-casting, the dispersant used was KD1. BASE tubes were fabricated by the method of slip casting with Darvan C as the deflocculent. The conductivity of the BASE tubes was measured by assembling symmetric cells. Ion exchange experiments were conducted in molten $ZnCl_2$, $SnCl_2$, and SnI_4 for up to 24 hours. The objective was to determine if Na^+ can be replaced by Zn^{2+}, Sn^{2+}, and Sn^{4+} ions. Na/BASE/$ZnCl_2$ cells were assembled in the fully charged, fully discharged, and partially charged-discharged states. Steel wool was used in both the cathode and the anode compartments. The cells were operated up to 425°C - the temperature at which Zn is in a molten state. Samples of α-alumina + zirconia were die pressed and sintered at various temperatures, ranging between 1,500 and 1,800°C and up to 4 hours. The objective was to vary the grain size. Subsequently, samples were packed in BASE powder and heated to 1,450°C. The conversion thickness was measured as a function of time. This yielded the conversion rate. A two cell planar stack of Na/BASE/$ZnCl_2$ + NaCl + Zn was constructed and tested. A five cell stack has been assembled. Disc samples of BASE with porous surface BASE layers were fabricated. The objective was to determine if porous surface layers lower cell resistance. Preliminary experiments were conducted in aqueous media by constructing electrochemical cells of the type Cu + $CuCl_2$ + NaCl/BASE/Zn + $ZnCl_2$ + NaCl. The cells were subjected to numerous charge-discharge cycles.

Results

1. Several BASE discs and tubes were fabricated. Figure 1(a) is a photograph of the BASE discs. Figure 1(b) is a photograph of a BASE tube.
2. The mechanism of α-alumina + zirconia conversion into BASE + zirconia was investigated. The mechanism involves coupled transport of O^{2-} ions through zirconia and Na^+ ions through BASE. The kinetics were noted to be linear in time. Figure 2(a) shows a schematic of the conversion process. Figure 2(b) shows plots of conversion thickness vs. time at various temperatures.
3. Fabrication of α-alumina + YSZ of differing grain sizes by varying sintering conditions was conducted. Figure 3(a) shows a scanning electron microscope (SEM) micrograph of a sample sintered at 1,500°C for 1 hour. The grain size is ~0.5 μm.

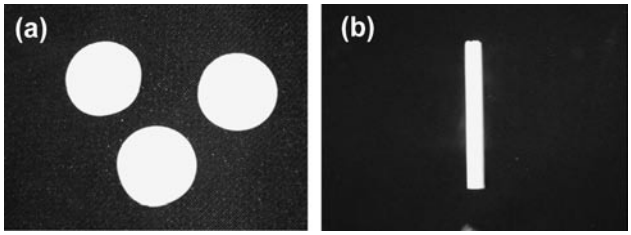

FIGURE 1. (a) A Photograph of BASE Discs and (b) a Photograph of a BASE Tube

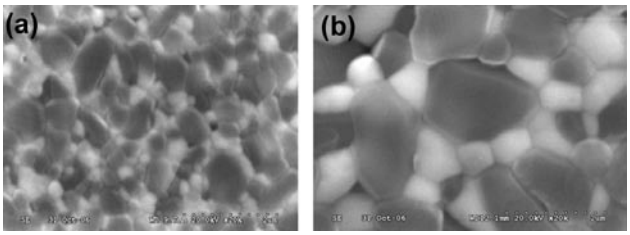

FIGURE 3. (a) Microstructure of α-alumina + Zirconia Sintered at 1,500°C/1 Hour and (b) Microstructure of α-alumina + Zirconia Sintered at 1,600°C/4 Hours

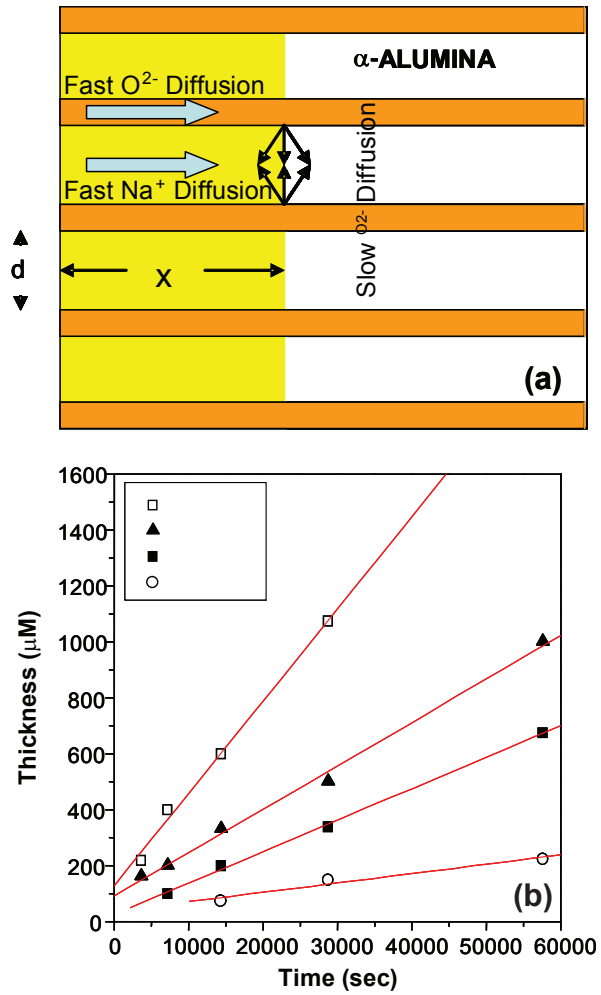

FIGURE 2. (a) A Schematic Showing the Mechanism of Conversion and (b) Experimental Data on Conversion Kinetics

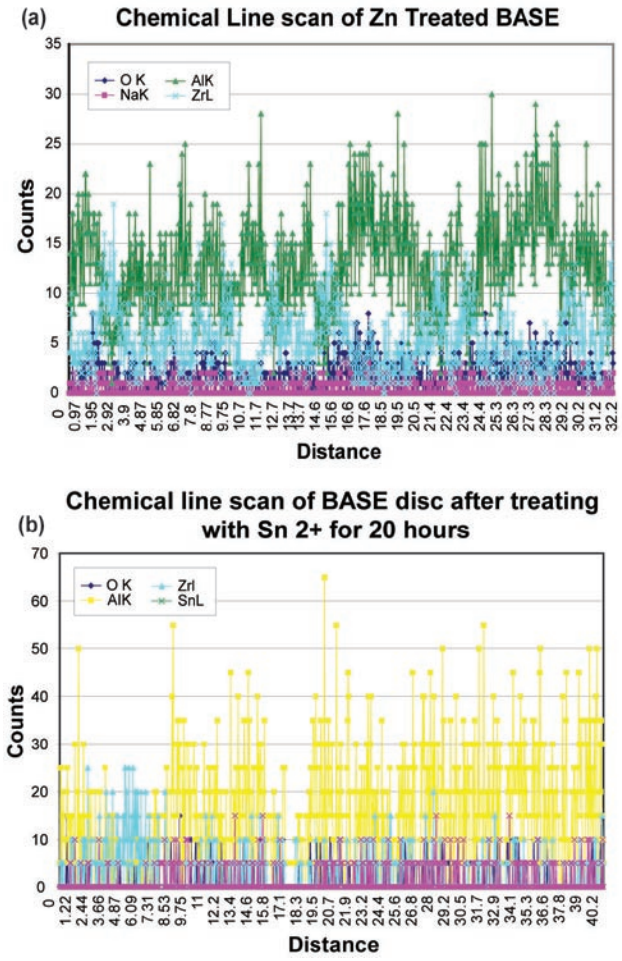

FIGURE 4. (a) EDS Trace of a Sample Treated in Molten $ZnCl_2$ and (b) EDS Trace of a Sample Treated in $SnCl_2$

The conversion rate was ~0.23 μm/s. Figure 3(b) shows a SEM micrograph of a sample sintered at 1,600°C for 4 hours. The grain size is ~1.24 μm. The conversion rate was ~0.12 μm/s.

4. No ion exchange occurred in $ZnCl_2$. Figure 4(a) shows an energy dispersive spectroscope (EDS) trace. Ion exchange did occur in $SnCl_2$. Figure 4(b) shows an EDS trace.
5. Planar Na/BASE/Zn + $ZnCl_2$ + NaCl cells were made. Figure 5 shows components of a planar cell.
6. The cell was subjected to several charge-discharge cycles and freeze-thaw cycles. Figure 6 shows the results of testing at 425°C which is above the melting point of zinc.
7. A five cell stack has been assembled. Figure 7 shows a photograph of a five cell stack.

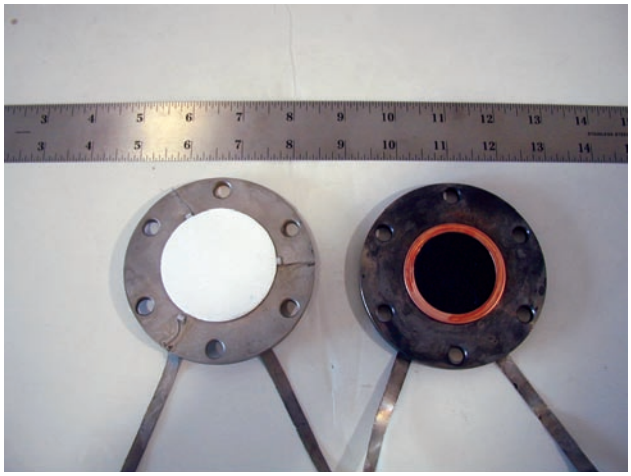

FIGURE 5. Components of a Planar Cell

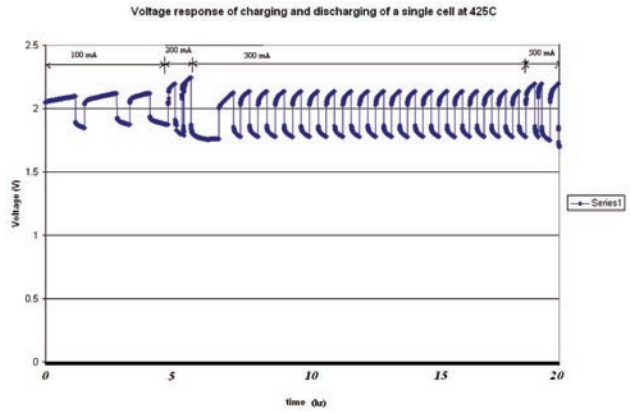

FIGURE 6. Results of Charge-Discharge at 425°C

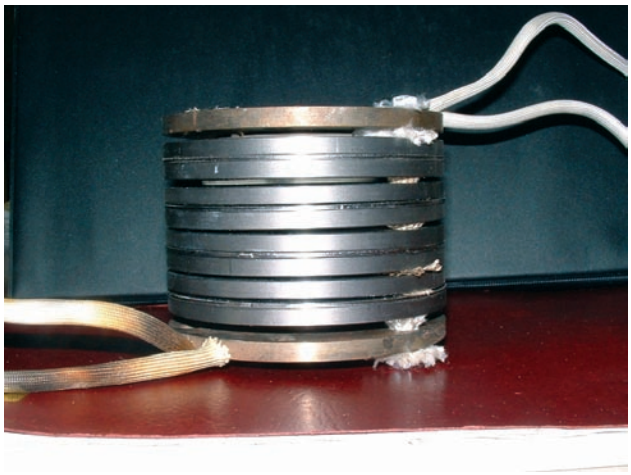

FIGURE 7. A Photograph of a Five Cell Stack

8. BASE samples with porous surface layers exhibited half the resistance of BASE without porous surface layers.

Conclusions

1. Thin BASE discs were fabricated by tape casting and die-pressing and BASE tubes were successfully made by slip casting.
2. Samples of BASE with different grain sizes were made. It is expected that samples with larger grain size will exhibit greater conductivity.
3. The conversion kinetics were linear. This suggests the kinetics to be interface controlled, where interface control arises due to diffusion parallel to the reaction front.
4. No ion exchange occurred in $ZnCl_2$ and SnI_4. Thus, both of these are viable cathodes.
5. Electrochemical cells were successfully charge/discharged and subjected to freeze-thaw cycling. Na/BASE/Zn + $ZnCl_2$ + NaCl could be successfully operated at a high temperature (425°C), indicating it should be possible to integrate with an SOFC as a hybrid unit.
6. Planar cell stacks could be assembled.

V.14 Direct Utilization of Coal Syngas in High Temperature Fuel Cells

Ismail Celik (Primary Contact), Richard Bajura
Mechanical and Aerospace Engineering Department
West Virginia University
PO Box 6106
Morgantown, WV 26505
Phone: (304) 293-3111 x 2325; Fax: (304) 293-6689
E-mail: ismail.celik@mail.wvu.edu

DOE Project Manager: Briggs White
Phone: (304) 285-5437
E-mail: Briggs.White@netl.doe.gov

Objectives

- Characterize the effects of major trace contaminants in coal syngas on solid oxide fuel cell (SOFC) performance.
- Identify the fundamental mechanisms through which these impurities affect performance.
- Develop novel materials to minimize impact of contaminants.
- Propose remedies for adverse effects of contaminants on fuel cell performance.

Accomplishments

- Identified from the available literature the levels of trace elements usually found in coal-syngas that cause performance degradation in solid oxide fuel cells.
- Built two test stands and began initial performance testing and material characterization.
- Purchased material processing equipment and attained capability to make/manufacture fuel cells in our laboratories.
- Initiated modeling activities at the atomistic, molecular, and continuum levels.

Introduction

This project is supported under the Department of Energy (DOE) Experimental Program to Stimulate Competitive Research (EPSCoR), a program designed to enhance the capabilities of EPSCoR states in energy research and economic development through the support of advanced research at academic institutions. Our vision is to establish an internationally recognized, sustainable fuel cell research center for coal-based clean power generation which serves as a technology resource for the emerging fuel cell industry in West Virginia. Under the present project, we will develop a laboratory infrastructure, solidify interactive working relationships, and attain national recognition for the work conducted by the center in the area of coal-based clean power generation via fuel cells. Our project will be conducted in collaboration with the National Energy Technology Laboratory (NETL). Our three-year project started in December 2006.

Approach

The research plan uses a multi-scale, multi-disciplinary approach that is supported by nine faculty members in four departments at West Virginia University (WVU). The work is organized under four integrated projects: (1) anode material development and experimental characterization of fuel cell anodes, (2) sub-micro-scale modeling, (3) multi-scale continuum modeling, and (4) laboratory testing of individual fuel cells and fuel cell systems. At the end of three years, we anticipate four outcomes. First, we will have identified the fundamental processes characterizing the operation of SOFC anodes from the atomic level to the level of the operating fuel cell. Second, strategies will be developed for constructing SOFCs that exhibit stable operation with coal syngas. Third, the research infrastructure (equipment for analysis and for cell fabrication, computers for modeling) and collaborations across disciplines and departments at WVU will be well developed for future research on fuel cells. Fourth, a program of educating and training future energy researchers will be established.

Results

Identification of Contaminants: Data was obtained from the literature on the effects of coal syngas on fuel cell components to identify possible contaminants in coal syngas and their typical concentrations. Coal syngas contains CO, H_2, CO_2, H_2O, CH_4 and N_2 in the majority and trace amounts of many naturally occurring elements [1]. Experimental results (Krishnan [2], [3]) show the effect of HCl, CH_3Cl, Zn, P, As, Cd and Hg found in syngas on SOFC performance. Our literature review [4] provides insight into the effects of coal syngas contaminants on the performance of an SOFC. Based on this knowledge, our initial testing will be performed with syngas containing As and P. Literature was also reviewed on the effects of sulfur. There are two primary sulfur-degradation mechanisms for the anode materials: (1) physical absorption of sulfur that blocks the hydrogen reaction sites and (2) chemical reaction that forms nickel sulfide. The results of our review will appear in *Journal of Power Sources*.

Anode Materials Development and Characterization: This research task seeks to investigate the electro-chemical and structural degradation of SOFC anode materials due to the effect of impurities in coal syngas and to develop new materials that would reduce or eliminate such degradation. We have designed and built a unique button cell testing apparatus (Figure 1a) that is capable of half cell or full cell testing including EIS (electrochemical impedance spectroscopy) and ASR (anelastic strain recovery) measurements. This testing apparatus includes three main components: (a) testing, (b) mass-flow-control (MFC) and (c) furnace assembly. This computer-automated rig can control the temperature and the gas flow through programming. Figure 1b shows EIS curves for a half cell measured by the system at different temperatures.

A second furnace is constructed (Figure 2a) for *in situ* surface deformation monitoring of the anode side of the button cell subjected to attack by impurities in a coal syngas stream. Most likely, the structural degradation will only occur on the surface, which may cause a change in the structural mechanical properties. We shall apply suitable pressure loading to the button cell to "amplify" the state of surface structural degradation coupled with the simultaneous EIS and ASR measurements to correlate the linkage between mechanical and electro-chemical degradation under operating conditions.

A fuel cell manufacturing lab has been set up with a total area of 280 ft^2. The following equipment has been purchased: tape caster with single-blade (TTC-1200, Richard E. Mistler Inc.), jar-mill (755RMV, U.S. Stoneware); spin-coater (KW4A, Chemat Technology Inc.), screen printer (3230B, Aremco), and low-temperature furnace (Carbolite). Figure 2b shows some of the button cells manufactured in our lab. Cells are being tested with different levels of contaminant exposure; results will be available soon.

(a)

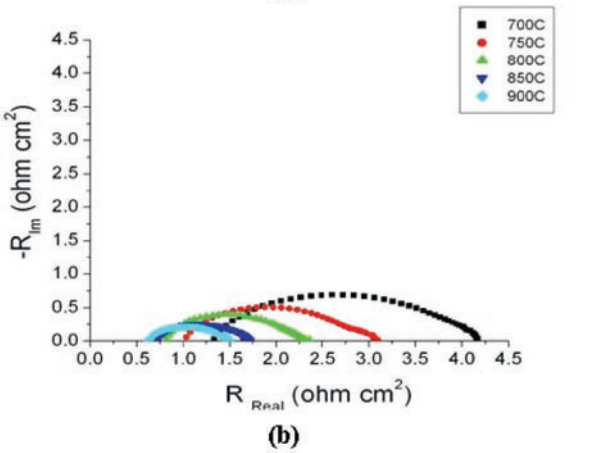

(b)

FIGURE 1. EIS Measurement (a) Layout of the Experimental Setup (b) Sample Result

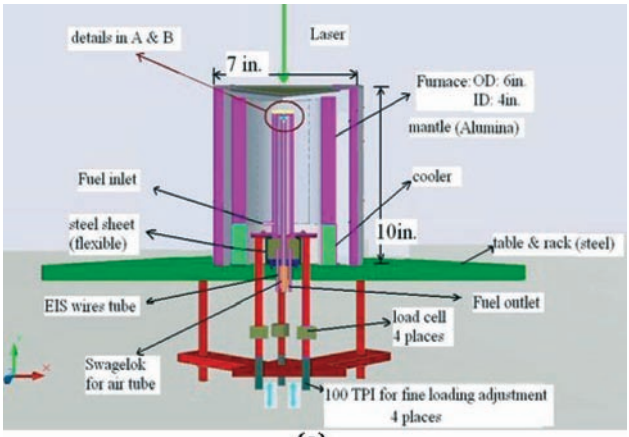

(a)

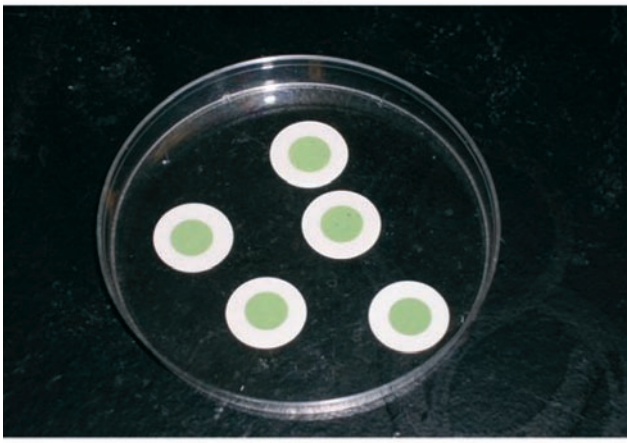

(b)

FIGURE 2. Button Cell Testing (a) Schematic of Apparatus Designed for *In Situ* Electrochemical and Structural Measurements (b) Button SOFCs Manufactured at WVU

Sub-Micro-Scale Modeling: Virtual modeling efforts progressed in two fronts: (1) atomistic level and (2) molecular level modeling. Using *ab initio* FP-LMTO techniques based on density functional theory, we calculated the electronic structures for a hydrogen atom adsorbed on the Ni (1,0,0) surface (Figure 3a). Detailed analysis reveals the properties and features of chemical bonding, charge transfer, and Ni surface electronic states. This knowledge helps us to understand the fuel consumption and nickel catalytic mechanisms. It will also serve as a comparison basis to analyze the bonding mechanisms of trace elements on catalysts in our future work. We have also developed an *ab initio* tight-binding parameter base for Ni/S/H, which will be used in tight-binding based molecular dynamics simulations involving larger scale and longer time.

Molecular dynamics modeling will provide enough statistical data to retrieve macroscopic properties of the substance, such as effective diffusion coefficient, thermal expansion coefficients and heat capacities, as well as molecular kinetic parameters of importance for determining reaction rates. So far, a literature review has been performed and the necessary hardware and software for this task have been procured and tested. The work on the first C++ prototype of the sequential simulation code has been initiated. The implementation of the essential classes is underway, which include: (a) Atom: to represent indivisible atomic species, e. g., H, O, C, S, Ni. (b) Molecule: to represent chemical compounds, such as H_2, O_2, H_2O, H_2S, CO_2. Figure 3b shows a computer simulation of crystal bonding structure which can be used to analyze the effect of lattice defects and lattice deformations caused by doping elements.

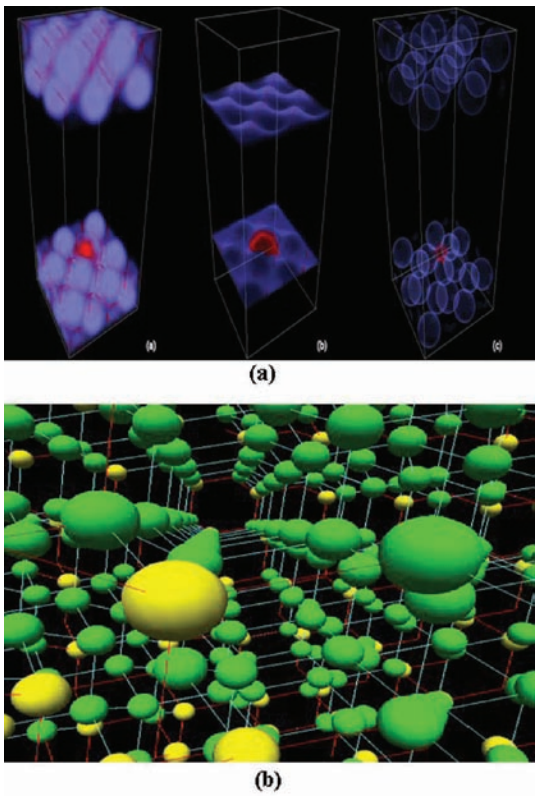

FIGURE 3. Sub micro-scale modeling - 3-D visualizations of results obtained using FP-LMTO techniques: Section (a) - (a) the total charge density distribution, (b) the surface states, and (c) Ni-H chemical bond. A 2x2x2 (32 atom) Ni supercell is used. Section (b) Computer simulation of crystal bonding structure which can be used to analyze the effect of lattice defects and lattice deformations caused by doping elements.

Multi-Scale Continuum Modeling: Preliminary results were obtained from modeling of a small button cell, similar to those to be tested in our laboratory, using an in house code DREAM SOFC. Figure 4a shows the calculated temperature distribution on the top (anode) and bottom (cathode) surfaces of the button cell with prescribed H_2 and O_2 concentrations on the anode and cathode sides, respectively.

Two models for multi-component molecular diffusion transport inside a typical anode were tested. These models are the Stefan Maxwell Model including the Knudsen diffusion and Fick's law using an effective multi component diffusion coefficient. Based on our results using both models, the simpler Fick's model performed sufficiently well that it can be used for future calculations. Transient mass transport calculations for a typical coal syngas operated anode revealed that chemical kinetics play a critical role in cell performance. This model will be expanded to include the trace species with detailed reaction mechanisms. Laboratory conditions will be simulated as closely as possible to provide feedback to the experimental work.

Cell and System Laboratory Testing: A survey of chemical literature was done for relevant information on measurements of electron transfer kinetics. A complete impedance spectroscopy set up (Solartron Model 1287 potentiostat, Model 1252 frequency response analyzer, ZPlot and ZView software for electrochemical impedance spectroscopy and CorrWare and CorrView software for other electrochemical measurements) was installed in our lab and concerned personnel developed expertise with the hardware and software using model electrochemical cells. This system is capable of performing the three electrochemical methods: (1) electrochemical impedance spectroscopy, (2) cyclic voltammetry, and (3) current-interrupt measurements. An SOFC test stand (Figure 4b) is also made

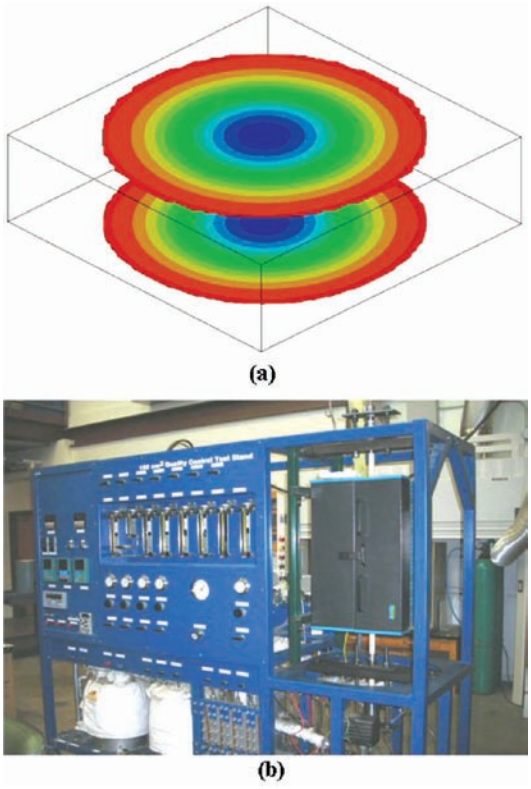

FIGURE 4. (a) Temperature distribution on top and bottom surfaces of a button cell calculated using DREAM SOFC. Red color indicates hotter region and blue indicates colder region. (b) SOFC test stand.

operational. Cell testing with standard yttria-stabilized zirconia (YSZ) material is currently underway.

Conclusions and Future Directions

- The operation of the cell test stand will be verified using the commercially available fuel cells using pure hydrogen fuel as a baseline. A variety of operating conditions will be tried so that the experimental capabilities of the test stand can be established before testing the fuel cell performance in the presence of contaminants.
- Electrochemical characterization (impedance spectroscopy, cyclic voltammetry, current-interrupt measurements) of the commercial fuel cells will be undertaken soon. In particular, scanning electron microscopy and X-ray diffraction will be utilized to establish baseline characterization techniques and to gain familiarity with the testing procedures.
- Cell manufacturing capability will be perfected and new types of materials will be tried.
- Atomistic and molecular dynamics modeling will first focus on sulfur mechanisms to validate our approach against literature, and then mechanisms for contaminants such As and P will be investigated.
- Continuum modeling will proceed towards full simulation of conditions being tested in the laboratory.

FY 2007 Publications/Presentations

1. M. Gong, X. Liu, J. Trembly, C. Johnson: Sulfur-Tolerant Anode Materials for Solid Oxide Fuel Cell Application, Accepted J. of Power Sources (2007).

2. X. Liu, C. Johnson, C. Li, J. Xu, C. Cross: Developing TiAlN Coatings for Intermediate Temperature SOFC Interconnects Applications, submitted, Int. J. of Hydrogen Energy (2007).

3. R. Dastane, C. Johnson, X. Liu: Degradation of SOFC Metallic Interconnect in Coal Syngas, abstract submitted to Materials Science & Technology 2007 conference.

4. J. Wu, Y. Jiang, C. Johnson, M. Gong, X. Liu: Pulse Plating of Manganese-Cobalt Alloys for SOFC Interconnect Application, abstract submitted to Materials Science & Technology 2007 conference.

5. S. R. Pakalapati, F. Elizalde-Blancas, I. Celik (2007): Numerical Simulation of SOFC Stacks: Comparison between a Reduced Order Pseudo Three-dimensional Model and a Multidimensional Model, abstract submitted to the Fifth Int. Fuel Cell Sci., Eng. and Tech. Conference, June 18-20, NY.

6. N. Cayan, M. Zhi, S. R. Pakalapati, I. Celik, N. Wu: Coal Syngas Contaminants and Their Effect on Operation of SOFC: a Literature Review, in preparation.

References

1. Trembly, J.P., Gemmen, R.S. and Bayless, D.J. (2007), "The effect of IGFC warm gas cleanup system conditions on the gas-solid partitioning and form of trace species in coal syngas and their interactions with SOFC anodes", vol. 163, pp. 986-996.

2. Krishnan, G. (2006), 7th Annual SECA Review Meeting September 12–14, Philadelphia, PA.

3. Dr. Gopala N. Krishnan (2007), Private communication, Seminar presentation at National Research Center for Coal and Energy (NRCCE) at WVU, March 21.

4. N. Cayan, M. Zhi, S. R. Pakalapati, I. Celik, N. Wu: Coal Syngas Contaminants and Their Effect on Operation of SOFC: a Literature Review, in preparation.

VI. Acronyms & Abbreviations

°C	Degrees Celsius
°C/min	Degrees Celsius per minute
°F	Degrees Fahrenheit
°K	Degrees Kelvin
2D	Two-dimensional
3-D	Three-dimensional
3DP	Three-dimensional printing
μg	Microgram(s)
$\mu g/m^2$	Microgram(s) per square meter
μm	Micrometer(s), micron(s)
$\mu m/m^2$	Micron(s) per square meter
Ω	Ohm(s)
Ωcm_2, $\Omega–cm^2$	Ohm(s) centimeter squared
A	Ampere(s), amp(s)
Å	Angstrom(s)
ABO_3	Perovskite type materials
A/cm^2	Amp(s) per square centimeter
AC	Alternating current
AC	Activated carbon
ACerS	Advanced Ceramics and Composites
AcerSoc	American Ceramic Society
ACS	American Chemical Society
AFM	Atomic force microscope
Ag	Silver
AgCl	Silver chloride
AGRB	Anode gas recycle blower
AIChE	American Institute of Chemical Engineers
Al	Aluminum
Al_2O_3	Alumina, aluminum oxide, sapphire
Am.	American
ANL	Argonne National Laboratory
APEC	Applied Power Electronics Conference
Appl.	Applied
APS	Atmospheric plasma spray
APU	Auxiliary power unit
As	Arsenic
AsH_3	Arsine
Ar	Argon
ASE	Arcomac Surface Engineering, LLC
ASM	ASM International, formerly American Society for Metals
ASME	American Society of Mechanical Engineers
ASR	Anelastic strain recovery
ASR	Area specific resistance
ASTM	American Society for Testing and Materials
ASU	Air separation unit
ATI	Allegheny Technologies, Inc.
atm	Atmosphere(s)
Au	Gold
a.u.	Arbitrary units
AUTOCAD	Automated computer aided design
B	Boron
B_2O_3	Boron (III) oxide
Ba	Barium
BaO	Barium oxide
$BaCeO_3$	Barium cerate
$BaCO_3$	Barium carbon oxide
$BaCrO_4$	Barium chromium oxide
BASE	Beta alumina solid electrolyte
$BaThO_3$	Barium thorate
$BaZrO_3$	Barium zirconate
Be	Beryllium
BET	Braunauer-Emmett-Teller
BC&T	Building, commissioning and testing
BCN	$Ba_3Ca_{1+x}Nb_{2-x}O_{9-\delta}$
BCY	Yttrium-doped barium cerate
BN	Boron Nitride
BOP	Balance of plant
BTU	British thermal unit
BYZ	Barium zirconium yttrium oxide
BYZC-Zn	Zinc oxide doped barium zirconium yttrium oxide
C	Carbon
C	Celsius
C++	A computer program language
cBOP	Cold balance of plant
C-C	Carbon to carbon
Ca	Calcium
CA	California
CAB	Cathode air blower
CAD	Computer aided design
CARB	California Air Resources Board
CCD	Charge coupling device
Cd	Cadmium
Ce	Cerium

$CeCrO_3$	Cerium chromium trioxide
CeO_2	Ceric oxide
Ceram.	Ceramics
CH_3Cl	Methyl chloride
CH_4	Methane
Cl	Chlorine
cm	Centimeter(s)
cm^2	Square centimeter(s)
cm^3	Cubic centimeter(s)
CMU	Carnegie Mellon University
CO	Carbon monoxide
CO	Colorado
Co	Cobalt
CO_2	Carbon dioxide
Co_3O_4	Cobalt oxide
$CoCr_2O_4$	Cobalt chromium oxide
CPD	Contact potential difference
CPG	Cummins Power Generation
CPOX, CPOx	Catalytic partial oxidation
Cr	Chromium
CRADA	Cooperative research and development agreement
CrAlYO	Chromium aluminum yttrium oxide
CrO_2	Chromium dioxide
$CrNbO_4$	Chromium niobium oxide
Cr_2O_3	Chromic oxide
CrO_3	Chromium trioxide (chromic acid)
CSC	Convection syngas cooler
CSU	Catalyst screening unit
CT	Connecticut
CTE	Coefficient of thermal expansion
CTP	Core Technology Program
Cu	Copper
$CuCl_2$	Copper (II) chloride
DARPA	Defense Advanced Research Projects Agency
dB	Decibel
DC	Direct current
DC	District of Columbia
DC/AC	Direct current to alternating current
DC/DC	Direct current to direct current
deg	Degree
DF#1	Number 1 diesel fuel
DF#2	Number 2 diesel fuel
DFC	Direct Fuel Cell
DFMA	Design for manufacturing and assembly
DFT	Density functional theory
DMS	Dimethyl sulfide
DOE	U.S. Department of Energy
DPI	Drexel Plasma Institute
DTEC	Direct thermal to electrical energy conversion
DVD	Digital video disk
E	Energy
e^-	Electron
E-BRITE®	Fe-26Cr-1Mo alloy
EBPVD	Electron beam physical vapor deposition
ECS	The Electrochemical Society
EDAX	Electron spectroscopy for chemical analysis
EDPG	Explosive-driven power generator
EDS	Energy dispersive spectroscopy
EDTA	Ethylenediamine tetraacetic acid
EDX	Energy dispersive x-ray
EELS	Electron energy loss spectroscopy
EIS	Electrochemical impedance spectroscopy
EMI	Electromagnetic interference
EPOx	Electrochemical partial oxidation
EPRI	Electric Power Research Institute
EPSCOR	Experimental Program to Stimulate Competitive Research
eV	Electron volt(s)
F	Fluorine
FAPSID	Filtered arc plasma source ion deposition
FBS-AGRB	Foil gas bearing supported anode gas recycle blower
FC	Fuel cell
FCE	FuelCell Energy, Inc.
FC/T	Hybrid fuel cell/gas turbine
F.C.	Flow Controller
Fe	Iron
$FeCl_2$	Iron chloride
$FeCrO_4$	Iron chromium oxide
FeCrAlY	Iron chromium aluminum yttrium
FEA	Finite element analysis
FeO_2	Iron oxide
FF	Feedforward
FIB	Focused ion beam
FL	Florida
F.M.	Flow Meter
FPU	Fuel processing unit
fs	Femtosecond(s)
FSS	Ferritic stainless steel

ft	Foot (feet)
Ft-lbf/ lbm	Foot-pound(s) force per pound mass
FTIR, FT-IR	Fourier transform infrared spectroscopy
FY	Fiscal year
(g)	Gas
g	Gram(s)
GA	Georgia
g/m^2	Gram(s) per cubic meter
GC	Gas chromatograph
GCO	Multilayered gadolinium: ceric oxide
Gd	Gadolinium
GDC	Gadolinia-doped ceria
GE	General Electric
GT	Gas turbine
GT	Georgia Tech
GTO	Gate turnoff thyristor
H230	Haynes 230
h	Hour(s)
H_2	Diatomic hydrogen
H_2S	Hydrogen sulphide
HARB	High-temperature anode recirculation blower
HCl	Hydrogen chloride
He	Helium
Hg	Mercury
HHV	Higher heating value
HI	Hawaii
H_2O	Water
H_2S	Hydrogen sulfide
HPD	High power density
HRTEM	High resolution transmission electron microscope
hr	Hour(s)
hrs	Hours
HTPC	High temperature proton conductor
HV	High voltage
Hz	Hertz
I	Current
IAPG	Interagency Power Group
IC	Interconnection, interconnect
ICM	Integrated component manifold
ICT	International Conference on Thermoelectrics
i.e.	*id est*, that is
IEA	International Energy Agency
IEEE	Institute of Electrical and Electronics Engineering
IGBT	Insulated gate bipolar transistor
IGCC	Integrated gasification combined cycle
IGCT	Integrated gate commutated thyristor
IGFC	Integrated gasification fuel cell
IL	Illinois
in	Inch(es)
Inc.	Incorporated
InDEC	InDEC B.V (Innovative Dutch Electro Ceramics), a Dutch energy technology company
ISBN	International Standard Book Number
IT-SOFC	Intermediate-temperature solid oxide fuel cell
ITM	Ion transport membrane
I-V	Current-voltage
J	Joule
J.	Journal
J/kg	Joule(s) per kilogram
J/m	Joule(s) per meter
K	Kelvin
K	Potassium
K-BASE	Potassium based beta alumina solid electrode
KBZY	Potassium-doped and yttrium-doped barium zirconate
kcal	Kilocalories
kcal/mol	Kilocalories per mole
kg	Kilogram(s)
kgf	Kilogram(s) of force
kg/h	Kilogram(s) per hour
kg/min	Kilogram(s) per minute
kHz	Kilohertz
KIST	Korea Institute of Science and Technology
kJ	Kilojoule(s)
kJ/mole, kJ/mol	Kilojoule(s) per mole
KF	Kalman filtering
KP	Kelvin probe
KrF	Krypton fluoride
kRPM	Kilo revolutions per minute (thousand revolutions per minute)
kV	Kilovolt(s)
kVA	Kilovolt-ampere(s)
kW	Kilowatt(s)
kW/min	Kilowatt(s) per minute
kWe	Kilowatt(s) electric
kWh	Kilowatt-hour(s)

l	Liter(s)
La	Lanthanum
$LaAlO_3$	Lanthanum aluminum oxide
$LaCoO_3$	Lanthanum cobalt oxide
$LaCrO_3$	Lanthanum chromite
LAFAD	Large area filtered arc deposition
$LaFeO_3$	Lanthanum iron oxide
$LaMnO_3$	Lanthanum manganite
LAO	Lanthanum aluminum oxide
lb	Pound(s)
lb/h	Pound(s) per hour
lbm	Pound(s) mass
lbm/min	Pound(s) mass per minute
LBNL	Lawrence Berkeley National Laboratory
LC	$LaCrO_3$, Lanthanum chromite
LHV	Lower heating value
LLC	Limited Liability Company
LM	$LaMnO_3$, Lanthanum manganite
LMT	Titanium doped lanthanum manganite
LNC	Niobium-doped lanthanum chromite
LPG	Liquefied petroleum gas
LQR	Linear quadratic regulator
LSC	Lanthanum strontium cobaltite
LSCF	Lanthanum strontium cobalt ferrite
LSF	Lanthanum strontium ferrite
LSGM	Strontium and magnesium doped lanthanum gallate
LSM	Lanthanum strontium manganite, strontium doped lanthanum manganite, (lanthanum strontium manganese oxide)
L_{TPB}	Triple phase boundary length
m	Meter(s)
m^2	Square meter(s)
m^2/g	Square meter(s) per gram
MA	Massachusetts
mA	Milliampere(s)
mA/cm^2	Milliampere(s) per square centimeter
mAh	Milliampere(s)-hour
MATLAB	A computer programming environment
MD	Maryland
MD	Molecular dynamics
METC	Morgantown Energy Technology Center
MEP	Minimum-energy path
MFC	Mass-flow control
mg	Milligram(s)
mg/cm^2, $mg.cm^2$	Milligram(s) per square centimeter
Mg	Magnesium
MgO	Magnesium oxide
MHz	Megahertz
MI	Michigan
MIEC	Mixed ionic electronic conductors, mixed ionic electronic conducting
min	Minute(s)
ml	Milliliter(s)
mm	Millimeter(s)
Mn	Manganese
MN	Minnesota
$MnCr_2O_4$	Manganese chromium spinel
$MnCo_2O_4$	Manganese cobalt spinel
MnO_3	Manganese oxide
MO	Missouri
mΩ	Milli-ohm(s)
$mOhm.cm^2$, $m\Omega{\cdot}cm^2$	Milli-ohm square centimeter
MOSFET	Metal-oxide-semiconductor field effect transistors
MPa	Megapascal(s)
msec	Millisecond(s)
MS	Mail stop
MS&T	Materials Science and Technology
MSRI	Materials and Systems Research, Inc.
MSU	Montana State University
MT	Montana
mV	Millivolt(s)
MW	Megawatt(s)
mW	Milliwatt(s)
mW/cm^2	Milliwatt(s) per square centimeter
MWe	Megawatt(s) electric
MWh	Megawatt-hour(s)
N	Nitrogen
N/mm^2	Newtons per square millimeter
N_2	Diatomic nitrogen
Na	Sodium
NaCl	Sodium chloride (salt)
Na-BASE	Sodium-based beta alumina solid electrolyte
NAS	Sodium silicon batteries
NASA	National Aeronautics and Space Administration
Nb	Niobium
$NdGaO_3$	Neodymium gallium oxide
NE	Northeast
NETL	National Energy Technology Laboratory

NFCRC	National Fuel Cell Research Center
NGK	NGK Insulators Ltd., a Japanese manufacturer and supplier of electric power related equipment
NGO	Neodymium gallium oxide
NH_3	Hydrogen nitride (ammonia)
Ni	Nickel
Ni_3S_2	Nickel sulfide
Ni_3S_4	Nickel sulfide
Ni_5As_2	Nickel arsenide
NiO	Nickel monoxide, nickel oxide
Ni_3P	Nickel phosphide
Ni_5P_2	Nickel phosphide
Ni_2P	Nickel phosphide
NiS	Nickel sulfide
NiS_2	Nickel sulfide
NIST	National Institute for Standards and Technology
Ni-YSZ	Nickel-yttria-stabilized zirconia
nm	Nanometer(s)
NM	New Mexico
NN	Neural network
No.	Number
NO_2	Nitrogen dioxide
NOx	Oxides of nitrogen
NRCCE	National Research Center for Coal and Energy
NW	Northwest
NY	New York
O	Oxygen
O-O	Oxygen to oxygen
O_2	Diatomic oxygen
O/C	Oxygen to carbon ratio
OEM	Original equipment manufacturer
$Ohm.cm^2$	Ohm square centimeter
OCRC	Ohio Coal Research Center
OCV	Open circuit voltage
OH	Ohio
OH	Oxyhydroxide
ON	Ontario
OR	Oregon
ORNL	Oak Ridge National Laboratory
O-SOFC	Oxygen conduction solid oxide fuel cell
P	Phosphorous
P	Pressure
pO_2	Partial pressure of oxygen
p-SOFC	Protonic solid oxide fuel cell
P-SOFC	Proton conducting solid oxide fuel cell
PA	Pennsylvania
PADT	Phoenix Analysis and Design Technologies
Pb	Lead
PBCO	$PrBaCo_2O_{5+x}$, Praseodymium barium cobalt oxide
PCS	Power conditioning system
Pd	Palladium
PDPA	Phase Doppler particle analyzer
PEN	Positive-electrolyte-negative (cathode-electrolyte-anode)
PEM	Proton exchange membrane
PEMFC	Proton exchange membrane fuel cell
PGM	Platinum group metal
pH	A measure of acidity
PH_3	Phosphine
PhD	Doctor of philosophy
Phys.	Physics
PI	Proportional-integral
PI	Principal investigator
PLD	Pulsed laser deposition
PLL	Phase-locked loop
PNNL	Pacific Northwest National Laboratory
PO	Post office
PPH	Pound(s) per hour
ppm	Part(s) per million
ppm/°C	Part(s) per million per degree Celsius
ppmv	Part(s) per million by volume
ppmw	Part(s) per million by weight
Pr	Praseodymium
PR	Proportional resonant
psi	Pound(s) per square inch
psia	Pound(s) per square inch absolute
psig	Pound(s) per square inch gauge
p-SOFC	Protonic solid oxide fuel cell
P-SOFC	Proton conducting solid oxide fuel cell
PSOFC/GT	Pressurized solid oxide fuel cell gas turbine
PSU	Pennsylvania State University
Pt	Platinum
P-V	Pressure-volume
PVB	Polyvinyl butyral
PVD	Physical vapor deposition
Q1	First quarter
Q3	Third quarter
Q4	Fourth quarter

QC	Quantum chemistry
QMD	Quantum molecular dynamics
R&D	Research and development
RBS	Rutherford backscattering spectroscopy
Rd.	Road
RDF	Radial distribution function
RGA	Relative gain array
Rh	Rhodium
RPM	Revolution(s) per minute
RSC	Radiant syngas cooler
Ru	Ruthenium
s	Second(s)
S	Sulfur
S-Ni	Sulfur-nickel
SAED	Selected area electron diffraction
Sb	Antimony
SBIR	Small Business Innovation Research
S/C	Steam to carbon ratio
S/cm, Scm^{-1}	Siemen(s) per centimeter
S/cm^2	Siemen(s) per square centimeter
SC	South Carolina
Sci.	Science
sccm	Standard cubic centimeter(s) per minute
SCYb	Ytterbium doped strontium cerate
SDC	Samaria-doped ceria
Se	Selenium
sec	Second(s)
SECA	Solid State Energy Conversion Alliance
SEM	Scanning electron microscope
SEM/EDS	Scanning electron microscopy/energy dispersive spectroscopy
SFC	Stationary Fuel Cells (Siemens Power Generation)
Si	Silicon
SiC	Silicon carbide
SIMS	Secondary ion mass spectrometry
SiO_2	Silicon dioxide
SIS	Segmented-in-series
slpm	Standard liter(s) per minute
SLT	Strontium lanthanum titanate
SMA	Shape memory alloy
Sn	Tin
SnI_4	Tin iodide
$SnCl_2$	Tin chloride
Soc.	Society
SOEC	Solid oxide electrolysis cell
SOFC	Solid oxide fuel cell
SOFC-MP	Solid oxide fuel cell multi physics
SOFC-TE	Solid oxide fuel cell thermoelectric
SOx	Oxides of sulfur (e.g., SO_2)
SPR	Surface plasmon resonance
SPS	Surface photovoltage spectroscopy
Sr	Strontium
$SrCrO_4$	Strontium chromium oxide
$SrCeO_3$	Strontium cerate
SrO	Strontium oxide (strontia)
$SrTiO_3$	Strontium titanate
SS, ss	Stainless steel
SSC	Strontium samarium cobalt oxide
SSITKA	Steady state isotopic transient kinetic analysis
ST	Steam turbine
St.	Street
STF	$SrTi_{1-x}Fe_xO_3$
Std ft^3/min	Standard cubic feet/minute
STF05	$SrTi_{1-x}Fe_xO_3$with x=0.05
STF35	$SrTi_{1-x}Fe_xO_3$with x=0.35
STO	Strontium titanate
SUNY	State University of New York
S_v	Surface area normalized per unit volume
SW	Southwest
T	Temperature
TE	Thermoelectric
Tech.	Technology
TEM	Transmission electron microscopy or tunneling electron microscopy
Tg	Glass transition temperature
TGO	Thermally-grown chromium oxide
Th	Thorium
THD	Total harmonic distortion
Ti	Titanium
Ti_2AlC	Titanium aluminum carbide
TiCrAlY	Titanium chromium aluminum yttrium
TiCrAlYO	Titanium chromium aluminum yttrium oxide
TIJ	Thermal ink jet
TiNiHf	Titanium nickel hafnium
TiO_3	Titanate
t_{ion}	Ionic transference number
TMS	The Metallurgical Society
TN	Tennessee
TOMMI	Temperature optical-mechanical measuring instrument

TPB	Triple-phase boundary, three-phase boundary
TPD	Temperature-programmed desorption
TPO	Temperature-programmed oxidation
TPR	Temperature-programmed reaction
TSC	Tape casting, Screen printing, and Co-firing
TX	Texas
ug/m^2	Microgram(s) per square meter
um	Micrometer(s)
UMR	University of Missouri - Rolla
UBM	Unbalanced magnetron
UCRC	University Cooperative Research Center
US, U.S.	United States
USA	United States of America
USC	University of South Carolina
USPTO	United States Patent and Trademark Office
UT	Utah
UTC	United Technologies Corporation
UTSA	University of Texas at San Antonio
Uv	Ultraviolet
Uv-vis	Ultraviolet to visible
V	Vanadium
V	Volt(s)
VA	Virginia
VIM	Vacuum induction melting
$V_{O,}V_O$	Oxygen vacancy
vol	Volume
vol%	Volume percent
VPS	Versa Power Systems
W	Watt(s)
w.c.	Water column
W/cm^2	Watt(s) per square centimeter
Wh	Watt hour(s)
WHSV	Weight hourly space velocity
W	Tungsten
WA	Washington
WF	Work function
wt	Weight
wt%	Weight percent
WV	West Virginia
WVU	West Virginia University
XANES	X-ray absorption near edge spectroscopy
XAS	X-ray absorption spectroscopy
XPS	X-ray photoelectron spectroscopy
XRD	X-ray diffraction
Y	Yttrium
Yb	Ytterbium
YBCO	$Y_xBaCe_{1-x}O_3$
YDC	$Y_{0.2}Ce_{0.8}O_{1.9}$
Y_2O_3	Yttrium oxide (yttria)
YSZ	Yttria-stabilized zirconia
Zn	Zinc
$ZnCl_2$	Zinc chloride
ZnO	Zinc oxide
Zn_2SiO_4	Zinc silicate
ZrO_2	Zirconium oxide
Zr	Zirconium
ZrO_2	Zirconium dioxide (zirconia)
ZT	Thermoelectric figure of merit

VII. Primary Contact Index

Y

Z

VIII. Organization Index

IX. Contract Number Index

X. Index of Previous Projects

Projects Discontinued in FY 2007

Contract Number	Performer	Project Topic
FEAA067	Oak Ridge National Laboratory	Power Electronics for Solid Oxide Fuel Cells
FWP49100	Argonne National Laboratory	Technology Development in Support of SECA
34139	Siemens Power Generation	High Temperature Solid Oxide Fuel Cell Development
40798	FuelCell Energy, Inc.	Direct Fuel Cell/Turbine Power Plant
41562	University of Florida	Determination of Electrochemical Performance and Thermo-Mechanical-Chemical Stability of SOFCs from Defect Modeling
41566	University of Washington	Advanced Measurement and Modeling Techniques for Improved SOFC Cathodes
41569	Ceramatec, Inc.	Metal Interconnect for Solid Oxide Fuel Cell Power Systems
41571	Georgia Institute of Technology	An Integrated Approach to Modeling and Mitigating SOFC Failure
41574	[1]University of Illinois at Chicago [2]Ceramatec Inc. [3]Virginia Tech [4]Oak Ridge National Laboratory [5]Pacific Northwest National Laboratory	An Investigation of Resolve the Interaction between Fuel Cell, Power Conditioning System and Application Load
41575	NexTech Materials, Ltd.	Continuous Process for Low-Cost, High-Quality YSZ Powder
41578	University of Pittsburgh	Fundamental Studies of the Durability of Materials for Interconnects in Solid Oxide Fuel Cells
41915	Southern University and A&M College	Dense Membranes for Anode Supported All-Perovskite IT-SOFCs
41959	University of Florida	Electrocatalytically Active High Surface Area Cathodes for Low Temperature SOFCs
41960	University of Houston	New Cathode Materials for Intermediate Temperature Solid Oxide Fuel Cells
42222	Chevron Energy Research and Technology Company	Development of Ni-Based Sulfur-Resistant Catalyst for Diesel Reforming
42228	Connecticut Global Fuel Cell Center University of Connecticut	Low-Cost Integrated Composite Seal for SOFC: Materials and Design Methodologies
42514	Franklin Fuel Cells, Inc.	Novel Cathodes Prepared by Impregnation Procedures
42515	Georgia Institute of Technology Center for Innovative Fuel Cell and Battery Technologies	Quantitative Characterization of Chromium Poisoning of Cathode Activity
42517	University of Michigan	Desulfurization of High-Sulfur Jet Fuels by Adsorption and Ultrasound-Assisted Sorbent Regeneration
73138	Ceramatec, Inc.	Advanced Net-Shape Insulation for Solid Oxide Fuel Cells
83528	NexTech Materials, Ltd.	Highly Textured Glass Composite Seals for Intermediate-Temperature SOFCs
84387	FuelCell Energy, Inc.	Diesel Plasma Reformer
84212	Spinworks, LLC	Low-Cost/High-Temperature Heat Exchanger for SOFCs Using Near-Net-Shape Ceramic Powder Forming Process

Projects Discontinued in FY 2006

Contract Number	Performer	Project Topic
FE09	Los Alamos National Laboratory	Diesel Reforming for Solid Oxide Fuel Cell Auxiliary Power Units
40779	General Electric	SOFC Hybrid System for Distributed Power Generation
41539	Boston University	Materials System for Intermediate-Temperature SOFC
41602	University of Utah	Active Cathodes for Super-High Power Density SOFC Through Space Change Effects
41631	California Institute of Technology	Enhanced Power Stability for Proton-Conducting Solid Oxide Fuel Cells
41801	Virginia Tech	Modeling and Design for a Direct Carbon Fuel Cell with Entrained Fuel and Oxidizer
41803	University of Akron	Carbon-based Fuel Cell
41804	Duke University	Carbon Ionic Conductors for Use in Novel Carbon-Ion Fuel Cells
83212	Ceramatec, Inc.	Lanthanum Gallate Electrolyte Based Intermediate-Temperature Solid Oxide Fuel Cell Development

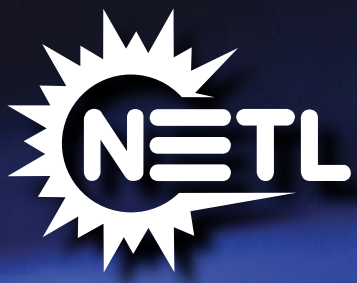

National Energy Technology Laboratory

1450 Queen Avenue SW
Albany, OR 97321-2198
541-967-5892

2175 University Avenue South
Suite 201
Fairbanks, AK 99709
907-452-2559

3610 Collins Ferry Road
P.O. Box 880
Morgantown, WV 26507-0880
304-285-4764

626 Cochrans Mill Road
P.O. Box 10940
Pittsburgh, PA 15236-0940
412-386-4687

One West Third Street, Suite 1400
Tulsa, OK 74103-3519
918-699-2000

Wayne A. Surdoval
Technology Manager, Fuel Cells
412-386-6002
wayne.surdoval@netl.doe.gov

Visit the NETL website at:
www.netl.doe.gov

Customer Service:
1-800-553-7681

U.S. Department of Energy
Office of Fossil Energy

Printed in the United States on recycled paper

August 2007